

Portofoliu TIPERCIUC BRINDUSA

Tiperciuc Brîndușa Georgeta

Articol 1 – pag 2

Fodor A., **Tiperciuc B.**, Login C., Orasan O., Lazar A., Buchman C., Hanghichel P., Sitar-Taut A., Suharoschi R., Vulturar R., Cozma A., Endothelial Dysfunction, inflammation and oxidative stress in COVID-19, Mechanisms and therapeutic targets, *Oxidative Medicine and Cellular Longevity*, 2021, 2021

Articol 2 – pag 17

Hanganu D., Benedec D., Olah N.K., Ranga F., Mirel S., **Tiperciuc B.**, Oniga I., Research on enzyme inhibition potential and phenolic compounds from *Origanum Vulgare* SSP., *Farmacia*, 2020, 68(6),

Articol 3 pag. 23

Stana, A; Vodnar, DC; Marc, G; Benedec, D; **Tiperciuc, B**; Tamaian, R; Oniga, O, Antioxidant activity and antibacterial evaluation of new thiazolin-4-one derivatives as potential tryptophanyl-tRNA synthetase inhibitors, *Journal of Enzyme Inhibition and Medicinal Chemistry*, 2019, 34(1):898-908,;

Articol 4 pag 35

Login, CC; Baldea, I; **Tiperciuc, B**; Benedec, D; Vodnar, DC; Decea, N; Suci, S, A Novel Thiazolyl Schiff Base: Antibacterial and Antifungal Effects and In Vitro Oxidative Stress Modulation on Human Endothelial Cells, *Oxidative Medicine and Cellular Longevity*, 2019, 2019

Articol 5 pag 52

Nastasa, C; Tamaian, R; Oniga, O; **Tiperciuc, B**, 5-Arylidene(chromenyl-methylene)-thiazolidinediones: Potential New Agents against Mutant Oncoproteins K-Ras, N-Ras and B-Raf in Colorectal Cancer and Melanoma, *Medicina-Lithuania*, 2019, 55(4)

Articol 6 pag 64

Nastasa, C; Vodnar, DC; Ionut, I; Stana, A; Benedec, D; Tamaian, R; Oniga, O; **Tiperciuc B.**, Antibacterial Evaluation and Virtual Screening of New Thiazolyl-Triazole Schiff Bases as Potential DNA-Gyrase Inhibitors, *Int. J. Mol. Sci.* 2018, 19(1), 222

Articol 7 pag 83

Ionuț I, **Tiperciuc B.**, Oniga O, Lipophilicity Evaluation of Some N1-Arylidene-Thiosemicarbazones and 1,3,4-Thiadiazolines with Antimicrobial Activity., *J Chromatogr Sci.* 2017 55(4), 411-416,

Articol 8 pag. 88

Stana A, Vodnar D, Tamaian R, Pîrnau A, Vlase L, Ionut I, Oniga O, **Tiperciuc B.**, Design, Synthesis and Antifungal Activity Evaluation of New Thiazolin-4-ones as Potential Lanosterol 14alpha-Demethylase Inhibitors, *Int. J. Mol. Sci.*, 2017, 18, 177

Articol 9 pag.114

D. Benedec, D. Hanganu, L. Filip, I. Oniga, **B. Tiperciuc**, N-K Olah, A-M Gheldiu, O. Raita, L. Vlase, Chemical, antioxidant and antibacterial studies of romanian *Heracleum Sphondylium*, *Farmacia*, 2017, 65(2), 252-256

Articol 10 pag 119

Stana, A, Enache, A, Vodnar, DC, Nastasa, C, Benedec, D, Ionut, I, Login, C, Marc, G, Oniga, O, **Tiperciuc B.**, New Thiazolyl-triazole Schiff Bases: Synthesis and Evaluation of the Anti-Candida Potential, *Molecules*, 2016, 21(11):1595,

Articol 11 pag 137

Tamaian, Radu; Mot, Augustin; Silaghi-Dumitrescu, Radu; Ionut, Ioana; Stana, Anca; Oniga, Ovidiu; Nastasa, Cristina; Benedec, Daniela; Tiperciuc, Brindusa, Study of the Relationships between the Structure, Lipophilicity and Biological Activity of Some Thiazolyl-carbonyl-thiosemicarbazides and Thiazolyl-azoles, *Molecules*, 20, 12, 22188-201, 2015,

Articol 12 pag 152

Tiperciuc B., Pârnu A., Tamaian R., Nastasa C., Ionut I., Oniga O. New Anti-inflammatory Thiazolyl-carbonyl-thiosemicarbazides and Thiazolyl-azoles with Antioxidant Properties as Potential iNOS Inhibitors *Arch. Pharm. Res.* 36:702-714, 2013,

Articol 13 pag 167

Maties R., Szefer R., Ionut I., **Tiperciuc B.**, QSPR Study on the Chromatographic Behavior of a Set of Thiazole Derivatives by Auto-Correlation Analysis, *Studia UBB Chemia*, 7, 4, 121 –135, 2012,

Articol 14 pag 180

Tiperciuc B., Zaharia V., Colosi I., Moldovan C., Crisan O., Parnau A., Vlase L., Duma M., Oniga O. , Synthesis and evaluation of antimicrobial activity of some new hetaryl-azoles derivatives obtained from 2-aryl-4-methylthiazole-5-carbohydrazides and isonicotinic acid hydrazide. *J. Het.Chem*, 49, 6, 1407–1414, 2012,

Articol 15 pag 188

Benedec D., Vlase L., Oniga I., Toiu A., Tamas M., **Tiperciuc B.**, Isoflavonoids from *Glycyrrhiza* sp. and *Ononis spinosa*, *Farmacia*, 60, 5, 615-20, 2012,

Articol 16 pag 194

Tiperciuc B., Zaharia V., Campean R., Curticapean M., Costescu A., Diudea M. V., A QSAR Study on Antimicrobial Activity of Some New Sulfonhydrylthiazoles, *Match Communications in Mathematical and in Computer Chemistry*, 60, 3, 985-996, 2008,

Articol 17 pag 201












Tiperciuc B., Sârbu C., Prediction of the Chromatographic Retention (Lipophilicity) of Some New Methyl-Thiazole-Oxadiazoline Derivatives by Multivariate Regression Methods, *Journal of Liquid Chromatography and Related Technologies*, 29, 15, 2257-2270, 2006,

Articol 18 pag 207

Sârbu C., **Tiperciuc B.**, Modeling, by multivariate regression methods, of the chromatographic retention (Lipophilicity) of new oxadiazoline derivatives, *JPC - Journal of Planar Chromatography - Modern TLC*, 19, 111, 342-347, 2006,

Review Article

Endothelial Dysfunction, Inflammation, and Oxidative Stress in COVID-19—Mechanisms and Therapeutic Targets

Adriana Fodor ¹, **Brandusa Tiperciuc** ², **Cezar Login** ³, **Olga H. Orasan** ⁴,
Andrada L. Lazar ⁵, **Cristina Buchman** ⁶, **Patricia Hanghichel** ⁷, **Adela Sitar-Taut** ⁴,
Ramona Suharoschi ⁸, **Romana Vulturar** ⁹, and **Angela Cozma** ⁴

¹Clinical Center of Diabetes, Nutrition, and Metabolic Diseases, “Iuliu Hațieganu” University of Medicine and Pharmacy, 400012 Cluj-Napoca, CJ, Romania

²Department of Pharmaceutical Chemistry, “Iuliu Hațieganu” University of Medicine and Pharmacy, 400012 Cluj-Napoca, Romania

³Department of Physiology, “Iuliu Hațieganu” University of Medicine and Pharmacy, 400012 Cluj-Napoca, CJ, Romania

⁴Internal Medicine Department, 4th Medical Clinic “Iuliu Hațieganu” University of Medicine and Pharmacy, 400012 Cluj-Napoca, Romania

⁵Department of Dermatology, “Iuliu Hațieganu” University of Medicine and Pharmacy, 400006 Cluj-Napoca, Romania

⁶Department of Oncology, “Iuliu Hațieganu” University of Medicine and Pharmacy, 400015 Cluj-Napoca, Romania

⁷Department of Neurology, “Iuliu Hațieganu” University of Medicine and Pharmacy, 400012 Cluj-Napoca, Romania

⁸Department of Food Science, University of Agricultural Science and Veterinary Medicine, 400372 Cluj-Napoca, Romania

⁹Department of Molecular Sciences, “Iuliu Hațieganu” University of Medicine and Pharmacy, 400012 Cluj-Napoca, Romania

Correspondence should be addressed to Olga H. Orasan; hildaolgaorasan@gmail.com

Received 26 June 2021; Accepted 7 August 2021; Published 25 August 2021

Academic Editor: Vladimir Jakovljevic

Copyright © 2021 Adriana Fodor et al. This is an open access article distributed under the Creative Commons Attribution License, which permits unrestricted use, distribution, and reproduction in any medium, provided the original work is properly cited.

The outbreak of the COVID-19 pandemic represents an ongoing healthcare emergency responsible for more than 3.4 million deaths worldwide. COVID-19 is the disease caused by SARS-CoV-2, a virus that targets not only the lungs but also the cardiovascular system. COVID-19 can manifest with a wide range of clinical manifestations, from mild symptoms to severe forms of the disease, characterized by respiratory failure due to severe alveolar damage. Several studies investigated the underlying mechanisms of the severe lung damage associated with SARS-CoV-2 infection and revealed that the respiratory failure associated with COVID-19 is the consequence not only of acute respiratory distress syndrome but also of macro- and microvascular involvement. New observations show that COVID-19 is an endothelial disease, and the consequent endotheliopathy is responsible for inflammation, cytokine storm, oxidative stress, and coagulopathy. In this review, we show the central role of endothelial dysfunction, inflammation, and oxidative stress in the COVID-19 pathogenesis and present the therapeutic targets deriving from this endotheliopathy.

1. Introduction

The SARS-CoV-2 virus, responsible for COVID-19 disease, can evolve with a wide range of clinical manifestations, from mild forms manifesting as fever, dyspnea, cough, and loss of smell and taste to severe forms, especially in the elderly with comorbidities, characterized by respiratory failure due to severe alveolar damage [1]. In the extremely severe forms

of the disease, rapidly progressive multiple organ failure occurs, which manifests through complications such as shock, acute cardiac injury, acute respiratory distress syndrome (ARDS), disseminated intravascular coagulopathy (DIC), and acute kidney injury, which may ultimately prove fatal [2]. Recent studies have demonstrated that respiratory failure occurring in COVID-19 is due not only to acute respiratory distress syndrome but also to macro- and

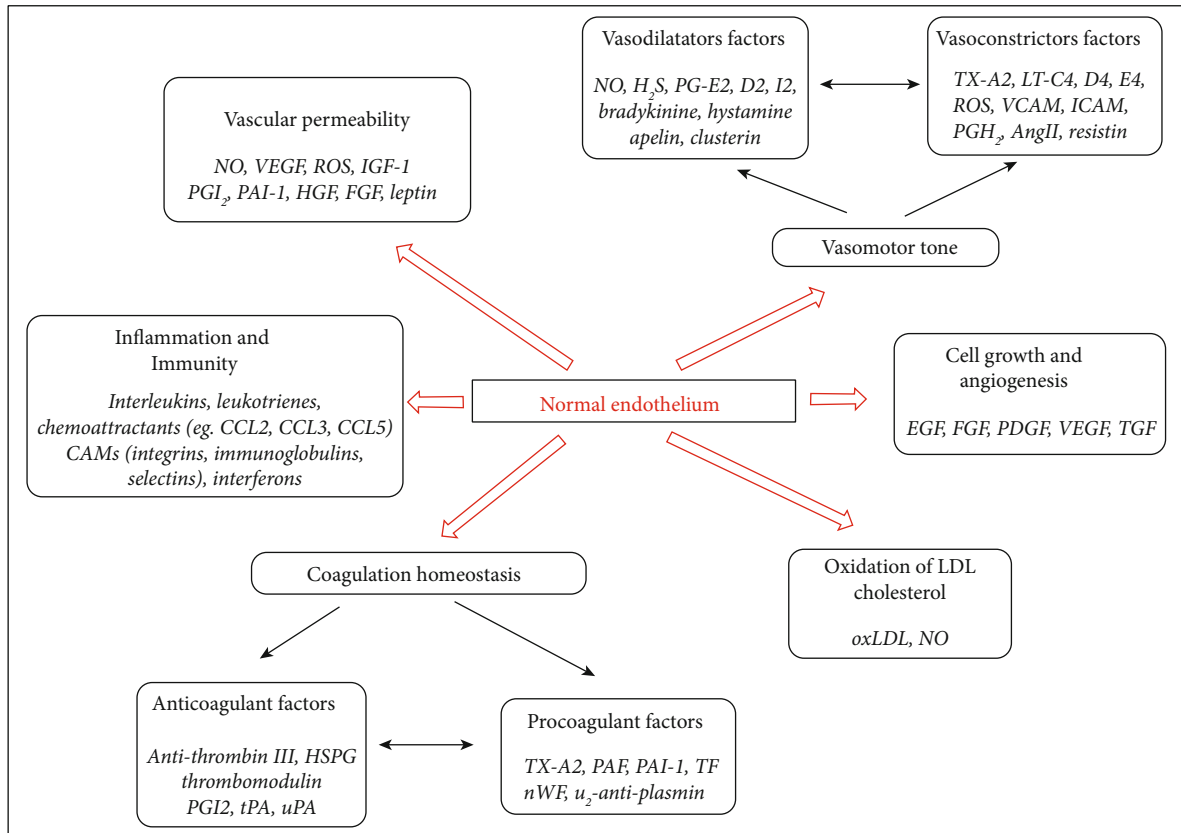


FIGURE 1: Functions of vascular endothelium. Endothelium cells produced some vascular mediators/factors that accomplished the six major functions of normal endothelium (modulation of vascular permeability and vasomotor tone modulation, coagulation homeostasis, inflammation and immunity regulation, cell growth regulation, and oxidation of LDL cholesterol) by which the vascular homeostasis is maintained (adapted after [9]).

microvascular involvement [3–5], a particular role being played by vascular endothelial damage [6, 7]. New observations show that COVID-19 is an endothelial disease [8] and that endotheliopathy is responsible for inflammation, cytokine storm, oxidative stress, and coagulopathy. An argument of this theory is the fact that patients who have endothelial dysfunction due to various comorbidities (obesity, hypertension, and diabetes) develop more severe forms of COVID-19, explained by an additional alteration of the already dysfunctional vascular endothelium [7].

In this review, we show the central role of endothelial dysfunction, inflammation, and oxidative stress in the development of complications of SARS-CoV-2 infection and their pathophysiological consequences, and examine the main therapeutic targets deriving from this endotheliopathy.

The endothelium, one of the largest organs of the human body, is capable of producing a wide variety of molecules, with effects that are often contradictory, with a role in maintaining homeostasis, such as vasodilator and vasoconstrictor, procoagulant and anticoagulant, inflammatory and anti-inflammatory, fibrinolytic and antifibrinolytic, and oxidant and antioxidant substances [9].

The normal endothelium regulates vascular homeostasis through six major functions: (1) modulation of vascular permeability, (2) modulation of vasomotor tone, (3) mod-

ulation of coagulation homeostasis, (4) regulation of inflammation and immunity, (5) regulation of cell growth, and (6) oxidation of LDL cholesterol (Figure 1). These functions are achieved through numerous mediators, of which the most studied is nitric oxide (NO) [9].

Nitric oxide is the most important vasodilator substance produced by endothelial cells. NO also has an antithrombotic action, inhibiting the fibrotic properties of angiotensin II and endothelin I by downregulating the receptors for these molecules. NO is synthesized in endothelial cells from L-arginin under the action of the endothelial NO synthase (eNOS) [10]. This reaction requires the presence of molecular oxygen and certain cofactors, including calmodulin, tetrahydrobiopterin (THB4), NADPH (adenine dinucleotide phosphate), flavin adenine dinucleotide, and flavin mononucleotide. From this reaction, L-citrulline as a by-product results [11].

Endothelial dysfunction is defined as a reduction in the bioavailability of vasodilator substances, especially NO, and an increase in vasoconstrictor substances.

The reduction of NO bioavailability can be due to a decrease in eNOS production (lack of cofactors necessary for eNOS synthesis) on the one hand, and to an increase in excessive NO degradation or inactivation by reactive oxygen species (ROS), on the other hand [12]. The increase in the

production of ROS, such as superoxide anion (O_2^-), hydrogen peroxide (H_2O_2), hydroxyl radical (HO^\bullet), hypochlorous acid (HOCl), and lipid superoxide radical, represents the main cause of the decrease in NO bioavailability in cardiovascular diseases [13]. Under physiological conditions, ROS production is controlled by an effective system of antioxidants, molecules that are capable of neutralizing ROS, thus preventing oxidative stress. In tissues, natural enzymatic antioxidants, such as superoxide dismutase (SOD), glutathione peroxidase, and catalase, play an important role in the conversion of ROS to oxygen and water. In pathological conditions, ROS can be present in excess relatively to the existing antioxidant capacity. This alteration of the balance in favor of oxidation termed “oxidative stress” may have negative effects on cell and tissue function [9].

Endothelial cells (EC) possess a number of mechanisms that reduce local oxidative stress. When subjected to shear stress, the endothelium produces SOD, which eliminates ROS [14]. The endothelial cell can also express glutathione peroxidase, which can mitigate oxidative stress [15]. Similarly, haem-oxygenase provides another mechanism by which the endothelial cell can resist to local oxidative stress [16, 17].

In contrast, proinflammatory cytokines can stimulate endothelial cells to mobilize NADPH-oxidase that generates superoxide anions, amplifying local oxidative stress [18, 19].

2. COVID-19-Associated Endotheliopathy and Oxidative Stress

Endothelial dysfunction or endotheliopathy is an important pathological characteristic in COVID-19 [20]. Electron microscopy of blood vessels in autopsy samples from patients with COVID-19 revealed the presence of endothelial cell degradation and apoptosis [21, 22]. Endothelial dysfunction biomarkers, such as thrombomodulin, von Willebrand factor (vWF), angiopoietin 2, and PAI-1, are frequently increased in patients with COVID-19 compared to healthy persons and seem to have prognostic significance, being associated with more severe forms of the disease and high mortality [23, 24]. Endothelial dysfunction is an important factor in the pathophysiology of thrombotic complications associated with COVID-19, including myocardial infarction and stroke [23, 24].

At present, it is uncertain whether endotheliopathy associated with COVID-19 is the result of direct endothelial cell viral infection, as reported in some autopsy studies [21, 25] or is a consequence of the inflammatory response induced by the virus.

Many pathophysiological mechanisms have been described which explain the implication of endothelial dysfunction in the occurrence of microvascular involvement in COVID-19 infection. Microvascular cerebral involvement in COVID-19 as a result of age-related endothelial dysfunction is an important challenge for research [20]. Overactivation of poly-(ADP-ribose) polymerase 1, as can be observed in viral infections, can lead to NAD⁺ depletion and subsequent endothelial dysfunction [26, 27]. In addition, the dysfunction of the nuclear factor erythroid 2-related factor 2

(NRF2) antioxidant defense pathway in endothelial cells might also play a role in the COVID-19 associated endotheliopathy [28]. The pharmacological activators of NRF2 were proposed as potential treatment options for COVID-19 [29]. NRF2 has strong anti-inflammatory and antiapoptotic effects in endothelial cells. It should be noted that NRF2 dysfunction exacerbates the deleterious effect of hypertension and diabetes on the endothelium, conditions known for the increase in the COVID-19-related risk of death [29].

Oxidative stress is generated by high Ang II concentrations and low Ang 1-7 concentrations (Figure 2). These ROS can oxidize cysteine residues in the peptidase domain of receptors ACE2 and RBD of proteins SARS-CoV and SARS-CoV-2, maintaining them in oxidized forms (disulfide), unlike reduced forms (thiol) [30]. It is possible that oxidation of these thiols to disulfides, through an oxidative stress mechanism, may increase the affinity of proteins SARS-CoV and SARS-CoV-2 S for ACE2 receptors and, consequently, increase the severity of COVID-19 infection [31].

The relationship between Ang II and NADPH-oxidase was investigated using murine smooth vascular muscle cells. When the cells were exposed to Ang II, the researchers observed an increased activity of NADPH-oxidase, as well as an increased production of superoxide anions. The exact mechanisms for the stimulation of NADPH-oxidase are complex, genetically mediated, at transcriptional and post-transcriptional level, and involve numerous signaling molecules and scaffolding proteins/platforms [32]. Inactive NADPH-oxidase contains two subunits: glycoprotein (gp) 91phox and p22phox. In the presence of Ang II, NADPH-oxidase is activated through the involvement of additional subunits p67phox, p47phox, p40phox, and Rac1. Activated NADPH-oxidase can generate superoxide anions. Studies in mice have shown that increased NADPH-oxidase activity can be found even in the absence of ACE2 [33, 34]. Since binding of SARS-CoV-2 to ACE2 receptor inhibits the catalytic activity of the enzyme, i.e., the conversion of Ang II to Ang 1-7, the activity of NADPH-oxidase increases in patients with SARS-CoV-2, subsequently leading to an increase in oxidative stress [35].

In a recently published study [36], the long-term effects of SARS-CoV-2 virus on oxidative stress and vascular endothelium were discussed. Thus, it was proposed that SARS-CoV-2, by inducing mitochondrial dysfunction and oxidative stress, can initiate a feedback loop promoting a chronic state of inflammation and endothelial dysfunction even after the viral particles have been eliminated from the body. In this proposed mechanism, SARS-CoV-2 first induces activation of NADPH-oxidase, which produces superoxide (O_2^-), a ROS that is involved in reactions which deteriorate the electron transport chain (ETC) [32, 37].

Increased oxidative stress and inflammation resulting from this mitochondrial dysfunction subsequently initiate a feedback loop that perpetuates NADPH-oxidase activation, mitochondrial dysfunction, inflammatory cytokine production and loss of identity of EC [36]. Considering these hypothetical long-term consequences of SARS-CoV-2 infection on blood vessels, the treatment of chronic oxidative stress

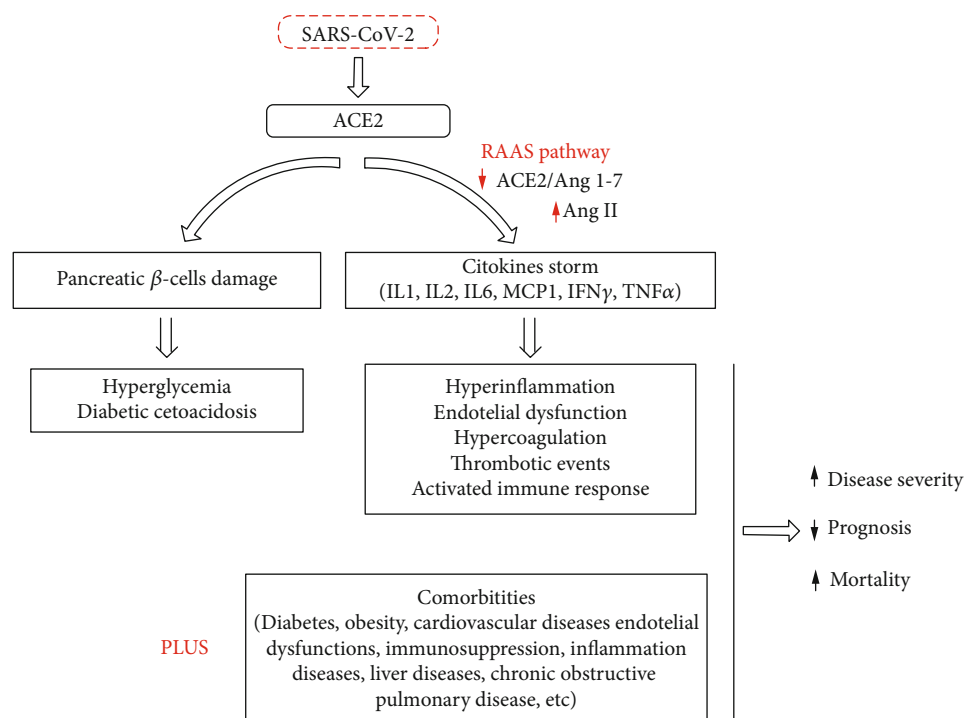


FIGURE 2: SARS-CoV-2 enters the human body by binding to ACE2. Activation of RAAS produced a cytokine storm, resulting in the secretion of proinflammatory cytokines/chemokines such as interleukins (ILs), interferon-gamma (IFN- γ), monocyte chemoattractant protein-1 (MCP1), and tumor necrosis factor-alpha (TNF- α). This storm produces a pleiades of phenomena which is associated with preexistent comorbidities that lead to an increase in disease severity (adapted after [31]).

and inflammation in EC can be essential in preventing future complications among millions of persons currently diagnosed with COVID-19 [38].

3. COVID-19 Endotheliitis

Numerous postmortem histopathological examinations in patients who died of COVID-19 not only revealed the presence of endotheliitis in the key organs affected by SARS-CoV-2, but also demonstrated the presence of viral structures within the endothelial cells by electron microscopy [21, 25, 39, 40]. By analyzing samples from the transplanted kidney in a COVID-19 patient who developed multiorgan failure, Varga et al. [25] demonstrated the capacity of the virus to invade endothelial cells. In the same patient, histological findings showed the inflammatory infiltrate of the endothelium and the morphological changes that occur during apoptosis in the heart, small bowel, and lungs. Furthermore, they proved the presence of endotheliitis in the lung, heart, kidney, liver, and small intestine of two other COVID-19 patients by postmortem analysis [25]. The wide distribution of ACE2 receptor in endothelial cells explains the multiorgan affinity of the virus, confirmed once more in a study by Puelles et al. The presence of viral particles in the pharynx, lungs, heart, blood, liver, kidneys, and brain was established despite the level of viral load [39].

The electron microscopy studies performed by Ackermann et al. [21] proved the presence of SARS-CoV-2 within the endothelial cells and in the extracellular space; furthermore, ultrastructural injury of the endothelium was also

present. The authors of the aforementioned study compared the histological changes that occur in the lungs of SARS-CoV-2 patients with those occurring in acute respiratory distress syndrome caused by influenza A (H1N1) and ten uninfected control lungs. The results revealed that the lungs of COVID-19 patients presented disseminated alveolar injury associated with necrosis, lymphocytic inflammation, and microthrombosis. In addition, the expression of angiotensin-converting enzyme 2 (ACE2) investigated by immunohistochemical analysis was present in lymphocytes only in the COVID-19 and influenza groups [21].

The postmortem electron microscopy analysis of the kidney tissue of 26 patients with COVID-19 from China revealed the presence of coronavirus-like particles in the renal tissue. Furthermore, the SARS-CoV-2 receptor ACE2 was upregulated in these patients. This study conducted by Su et al. confirms once more the virus tropism for kidney tissue [40].

Menter et al. identified in patients who died with COVID-19 the presence of capillaritis and microthrombi in the lungs, and showed diffuse vascular damage in other organs highly suggestive of vascular dysfunction [41].

Cutaneous biopsies from the skin lesions associated with SARS-CoV-2 were also performed. The optical microscopy findings of a biopsy from a chilblain-like lesion in a 23-year-old patient diagnosed with coronavirus disease revealed the presence of inflammatory infiltrate, consisting especially of lymphocytes, which were “tightly cuffing the vessels” [42]. Kanitakis et al. accomplished histological,

immunofluorescence, and immunohistochemical studies in seventeen cases of acral chilblain-like skin lesions in patients with suspected, but not confirmed, coronavirus disease, and endotheliitis was present in 65% of cases [43]. The association of COVID-19 with chilblain-like skin lesions is still conflicting. Initially, acral lesions were thought to be related to SARS-CoV-2 infection, but more recent case studies could not sustain an association between them [43, 44].

All data collected from the autopsies indicate that changes in the endothelium are not limited to the lungs and suggest that COVID-19 is a whole-body disease.

Numerous symptoms of SARS-CoV-2-positive patients could be assigned to multiorgan endotheliitis and subsequent endothelial dysfunction.

As mentioned above, tropism for the kidneys, lungs, and cardiovascular system of the novel coronavirus was demonstrated. This explains the respiratory and cardiocirculatory events associated with the disease. Several hypotheses were proposed in order to explain other organ specific symptoms. The early neurological manifestations (hyposmia, anosmia, dysgeusia, or hypogeusia) which have been frequently described in these patients together with life threatening events such as stroke and intracerebral or subarachnoid hemorrhage could represent a consequence of endotheliitis [45]. In a short communication, Bengler et al. made a detailed analysis of 5 patients with COVID-19 and intracerebral hemorrhage. They suggest that endothelial damage and endotheliitis along with a prothrombotic state and proinflammatory cytokine production are responsible for intracerebral hemorrhage, which occurred in younger individuals. Hemorrhage affected the anterior cerebral circulation [46].

In addition to the detrimental effect on blood vessels, the heart also represents a target for SARS-CoV-2. The main cardiovascular manifestations of COVID-19 are cardiac arrhythmias, caused by the inflammation of the myocardium and metabolic dysregulation [47]. It has been suggested that both direct and indirect viral injury is responsible for COVID-19-associated myocarditis [48].

The emerging evidence recognizes the endothelium as a key factor in the pathophysiological chain in COVID-19 [49]. Therefore, arterial and venous thrombosis, pulmonary embolism [49], central nervous system acute hemorrhagic events, and multiorgan failure associated with SARS-CoV-2 infection [50] might be the aftermath of subsequent endotheliitis and endothelial dysfunction associated with a procoagulant state. Endothelial cell damage together with endotheliitis also explains the predisposition for severe manifestations of the disease in patients with preexisting endothelial dysfunction caused by chronic pathologies such as hypertension [47].

While the major role of endothelial cells in the pathophysiology of COVID-19 is a compelling subject for ongoing research projects, the hypothesis according to which the endothelium could represent a therapeutic target in critically ill patients is intensely analyzed [49].

4. COVID-19-Renin-Angiotensin System

The role of the renin-angiotensin-aldosterone system (RAAS) in COVID-19 infection has been taken into consid-

eration from the beginning of the pandemic, since one of the first known facts was that ACE2 (angiotensin-converting enzyme 2) is the receptor that allows SARS-CoV-2 to enter human cells.

RAAS is a natural protective mechanism for maintaining circulatory volume. Renal hypoperfusion stimulates renin release from the juxtaglomerular apparatus. Renin cleaves angiotensinogen to angiotensinogen I, and ACE hydrolyzes Ang I to Ang II. Ang II binds to angiotensin II type 1 receptor (AT1R) and promotes aldosterone production, leading to sodium retention, water reabsorption, and vasoconstriction. On the other arm of the cascade, ACE2 is maintaining the equilibrium by converting Ang II to angiotensin 1-7. Angiotensin 1-7 binds to the Mas receptor and mediates anti-inflammatory, antioxidative, and vasodilatory effects. In the case of insufficient ACE2, Ang II binding AT1R prevails and exerts vasoconstrictive and proinflammatory effects [51].

Angiotensin-converting enzyme 2 (ACE2) is expressed in the human vascular endothelium, respiratory epithelium, and other types of cells, and represents a primary mechanism for the entry and infection of SARS-CoV-2 virus. In a physiological state, ACE2 through the activity of carboxypeptidase generates angiotensin fragments (Ang 1-9 and Ang 1-7) and plays an essential role in the renin-angiotensin system (RAS), which is an important regulator of cardiovascular homeostasis. SARS-CoV-2 through its surface glycoprotein interacts with ACE2 and invades the host cells.

For SARS-CoV-2 infection, in addition to ACE2, one or more proteases including transmembrane protease serine 2 (TMPRSS2), basigin (also known as CD147), and potentially cathepsin B or cathepsin L are required [52].

ACE2 is expressed as a transmembrane protein whose active site is exposed at the extracellular surface and resides in the lung alveolar epithelial cells, heart, kidneys, vessels, and gastrointestinal system [53]. ACE2 can be cleaved and circulates in small amounts in the blood stream, but its role is uncertain [54–57].

While ACE2 is clearly responsible for facilitating cell insertion, it may also be the cause of individual variation in disease severity. The polymorphism of ACE2 in the population could impact the affinity for the virus's spike protein and make the infection more likely or more severe [57]. Also, the ACE2 gene is X-linked, and this could explain the slight protective effect in the female sex observed in COVID-19. Besides these genetic variations, ACE2 gene expression is increased in diabetes, CVD, and hypertension [58]. Several researches indicate that RAAS-modulating drugs could also modulate ACE2 expression and activity in various ways. Animal model studies have shown that ACE inhibitors (ACEIs) and angiotensin II receptor blockers (ARBs) upregulate ACE2 cell expression, and ARBs and mineralocorticoid receptor antagonists (MRA) increase ACE2 activity, [59, 60]. However, simultaneously, ACEIs reduce Ang II synthesis, and consequently, in the absence of excess Ang II, AT1R is thought to interact with ACE2 [61]. This interaction could reduce the affinity of COVID S protein to ACE2 and then reduce COVID-19 viral entry [61].

SARS-CoV-2 spike protein binding to ACE2 in alveolar epithelial cells downregulates ACE2 expression. Without ACE2 to lead Ang II to angiotensin 1-7, Ang II binds to AT1R, leading to a hyperaldosteronism state, materialized as hypokalemia in severe cases of COVID-19 infection [62], vasoconstriction, fibrosis, and inflammatory cell proliferation [63]. Murine studies proved that loss of ACE2 expression enhances vascular permeability, increases lung edema and neutrophil accumulation, and hence worsening lung function [64].

One of the earliest researches of Chinese scientists empowers the theory that excessive Ang II leads to a bad outcome. Liu et al. observed in a small cohort of COVID-19 patients that the plasma concentrations of Ang II were significantly higher than in healthy individuals and also that Ang II levels in COVID-19 patients were correlated with viral load and lung injury [65].

Besides exacerbated inflammation and hypoxemia through vasoconstriction in small pulmonary vessels, Ang II induces plasminogen activator inhibitor-1 (PAI-1) expression in endothelial cells via the AT1 receptor. PAI-1 leads to unresolved fibrin deposits in the alveoli of patients with both SARS and COVID-19 infection [51]. Also, excessive Ang II can be metabolized to angiotensin IV [66], which enhances thrombosis development [67, 68]; since hypercoagulability has been noticed in many severe cases, it can be hypothesized that a reduction in ACE2 contributes to increasing thrombotic risk.

Since ACE2 has been recognized as the gate of SARS-CoV-2, worldwide medical boards raised the question if RAAS modulators—ACEIs and ARBs—increase the risk of developing severe forms of COVID-19 infection. The rationale behind this concern was based on some experimental animal models which have shown increasing numbers of ACE2 after intravenous infusion of ACEIs and ARBs [59].

In order to establish whether RAAS modulators are harmful or not, scientists firstly compared the outcomes of COVID-19 patients with arterial hypertension and different treatments. Shyh et al. found that those on ARBs are significantly less likely to develop COVID-19, while ACEIs did not show a similar effect, considering that they do not directly affect ACE2 activity [69]. On the other hand, patients taking calcium channel-blockers (CCBs) had a significantly increased risk of manifesting symptoms of COVID-19.

Several other retrospective multicenter studies [63, 70] looked for an association between in-hospital use of ACEIs/ARBs and all-cause mortality of COVID-19 among patients with hypertension. Their results show that COVID-19 hypertensive patients treated with ACEIs/ARBs had a better outcome than COVID-19 patients without ACEIs/ARBs or treated with a different class of other antihypertensive agents. On a molecular basis, they identified that patients on ACEIs/ARBs had lower levels of IL-6, decreased cytokine production, and decreased viral load during hospitalization, and peripheral T cells were significantly higher than in the non-ACEI/ARB group [70].

Researchers' restless work not only offered substantial information about the role of ACE2 in COVID-19 infection,

but also brought up several potential therapeutic approaches: spike protein-based vaccine, inhibition of transmembrane protease serine 2 (TMPRSS2-human proteinase which facilitates viral spike protein binding to ACE2) activity, blocking ACE2 receptor, and delivering an excessive soluble form of ACE2 [71]. It was postulated that delivering excessive soluble ACE2 would capture most of the viral load, restricting their fixation on cell membrane ACE2, and therefore limit the infection and also keep the balance of the 2 RAAS arms, preventing severe inflammatory tissue lesions [72, 73]. Most of these theories are based on animal model or in vitro studies and, needless to say, require extensive research and trials before becoming available therapies.

5. Cytokine Storm Associated with SARS-CoV-2 Infection

About 5% of the patients infected with SARS-CoV-2 develop critical disease forms manifesting by respiratory failure, shock, or multiple organ failure [74]. The presence of these disease forms does not seem to be correlated with viral load. Although these patients have a high viral load, the same load is found in patients having mild forms of the disease and even in asymptomatic persons [75]. Thus, the hypothesis was advanced that abnormal immune response, manifesting as a "cytokine storm," is the main determining factor of disease severity [76].

Cytokine storm associated with COVID-19 is similar to other clinical entities, such as cytokine release syndrome observed following CAR-T cell therapy [77], primary or secondary hemophagocytic lymphohistiocytosis (HLH), sepsis caused by Herpesviridae and other pathogens [78], and macrophage activation syndrome that occurs in various autoimmune diseases [79].

This progressive systemic inflammation leads to the loss of vascular tone clinically manifesting by a decrease in blood pressure, vasodilatory shock, and progressive organ failure. In the context of cytokine storms associated with highly pathogenic viruses such as SARS-CoV-2, SARS-CoV, and MERS-CoV, the greatest impact is on the lungs, where acute respiratory distress syndrome (ARDS) occurs which is the main cause of death. The effects are not limited to the lungs; cardiac, renal, and central nervous system damage is also involved [80].

After receptor binding and complex internalization, the viral RNA is released into the cell cytosol, replicated, and finally removed by exocytosis.

Intracellular viral RNA is identified by the recognition mechanisms of the innate immune response through specific receptors: PRRs (pattern recognition receptors), TLRs (toll-like receptors), and NLRs (NOD-like receptors). The recognition of viral RNA by these receptors determines the activation of intracellular signaling pathways, such as NF- κ B and IRF 3/7. NF- κ B stimulates the transcription of proinflammatory cytokines such as TNF-alpha, IL-6, and IL-1 and activates the immune response mediated by T helper 1 and 17 lymphocytes. IRF 3/7 stimulates the production of type 1 IFN, which induces activation of the JAK1/TYK2-STAT1/2 pathway, the effect being the transcription

of interferon-stimulated genes (ISG), with a role in the secretion of cytokines and the activation of other immune system components to stop viral replication [81, 82].

Previous studies have shown that in some cases, coronaviruses can delay type I IFN response through various mechanisms, the result being a more severe form of the disease caused by ineffective viral replication control and paradoxical hyperinflammation caused by type I IFN. In the case of SARS-CoV-2, an altered response of type I IFN seems to occur. A study showed that serum IFN activity was significantly lower in patients with severe or critical forms of the disease compared to those with mild-moderate forms. Moreover, serum ISG and type I IFN values in patients who subsequently developed ARDS with the need for invasive ventilation indicated that a mitigated type I IFN response precedes clinical deterioration [83].

This abnormal response of interferon leads to a massive inflow of neutrophils and monocytes, which are a major source of proinflammatory cytokines, apoptosis of T lymphocytes, and epithelial and endothelial cells [81].

Lymphopenia occurs in about 80% of the patients infected with SARS-CoV-2 and is more marked in the severe forms of the disease. There are many causal hypotheses explaining this process. Firstly, the virus can directly infect T lymphocytes but cannot replicate inside these, thus leading to cell death through apoptosis, necrosis, or pyroptosis. Secondly, the first wave of cytokines released, described above, includes anti-inflammatory cytokines such as TNF- α and IL-10, which cause apoptosis, exhaustion, and inhibition of TL proliferation. Not the least, lymphopenia could be the result of redistribution in the lungs and lymphoid organs [81, 84].

In the most severe disease cases, a sudden and rapid clinical deterioration occurs, which is associated with increased levels of acute phase reactants, coagulopathy, and cell lysis, and high proinflammatory cytokine levels, suggesting a second wave of cytokines, responsible for the so-called cytokine storm [81].

The triggering factor of the cytokine storm seems to be immunodeficiency caused by the decrease in the number and the dysfunction of T lymphocytes. Although other innate immunity hyperactivation mechanisms are supposed to be responsible, the cytokine storm is much more likely to occur as a result of a delayed response of innate immunity, followed by persistent hypercytokinemia and an abnormal response of the acquired immune system through T lymphocytes. The result is the failure to eliminate apoptotic cells or macrophages migrated to the site of inflammation and continuous antigenic stimulation by failure of viral clearance. These cells will continue to secrete proinflammatory cytokines, of which the most important are IL-18 and IFN- γ , which restimulate macrophage activation. Thus, a vicious circle is created which culminates in cytokine secretion, hemophagocytosis, coagulopathy, and ARDS [82, 85].

5.1. Cytokines and the Correlation with the Severity of the Disease. The first evidence of this correlation comes from the study conducted by Huang et al. in a sample of 41 patients who had the plasma levels of several cytokines and

chemokines measured. The authors observed that the initial plasma levels of IL-1B, IL-1RA, IL-7, IL-8, IL-9, IL-10, FGF, GCSF, GMCSF, IFN- γ , IP-10, MCP1, MIP1A, MIP1B, PDGF, TNF- α , and VEGF were higher in all COVID-19 patients compared to healthy persons, the plasma concentrations of IL-5, IL-12p70, IL-15, eotaxin, and RANTES were similar in patients infected with SARS-CoV-2 and healthy persons, and the levels of IL-2, IL-7, IL-10, GCSF, IP-10, MCP1, MIP1A, and TNF- α were significantly higher in patients with severe forms of the disease requiring intensive therapy compared to those with mild or moderate forms [86]. Since then, many studies have been conducted in the attempt to elucidate the pathogenic mechanisms of the exacerbated immune response associated with SARS-CoV-2 infection and in the attempt to identify laboratory markers that correlate with the severity and prognosis of the disease in order to achieve a stratification of patients for adequate management based on early therapeutic intervention.

A recently published meta-analysis of 50 studies showed statistically significantly higher values of IL-2, IL-2R, IL-4, IL-6, IL-8, IL-10, TNF- α , and INF- γ in patients with severe forms of the disease compared to the others. In contrast, there were no significant differences between IL-17 and IL-1 β values. As it can be seen, in some cases, there is an excessive production of proinflammatory as well as anti-inflammatory cytokines (IL-2R, IL-10), which highlights the dual pathogenic mechanism responsible for the occurrence of the cytokine storm [87]. Another meta-analysis and extensive systematic analysis shows that in patients with severe forms of the disease, lymphocytopenia (decreased CD3, CD4, and CD8 T lymphocytes), leukocytosis, high values of ESR, procalcitonin, LDH, and ALT occur more frequently. The levels of inflammatory cytokines, especially IL-6, 8, 10, and 2R and TNF- α , were significantly increased [88].

Regarding the profile of leukocytes, both meta-analyses evidenced a significant decrease in CD4 and CD8 T lymphocytes in the group of patients with severe disease forms [87, 88].

The most studied interleukin is perhaps IL-6, given that tocilizumab, a monoclonal antibody directed against the IL-6 receptor, can be used as therapy for COVID-19 patients who present signs of hyperinflammation. Mojtabavi et al. show in their analysis of 11 studies that IL-6 values are significantly higher in patients with severe forms of COVID-19 compared to those with mild or moderate forms [89]. Furthermore, Laguna-Goya et al. elaborated a model for predicting the risk of mortality in hospitalized COVID-19 patients based on IL-6 values. This includes 5 parameters: FiO₂/SatO₂ ratio, neutrophil/lymphocyte ratio, IL-6 value, LDH value, and age. This model might help to stratify patients into more uniform groups from a clinical and biological point of view before their inclusion in randomized clinical trials evaluating the efficacy of tocilizumab or other drugs. Until completion of clinical trials, this model could be used to select patients that would benefit the most from immunomodulatory therapy [90].

The prognostic value of IL-6 was also demonstrated in another study, where it was incorporated along with

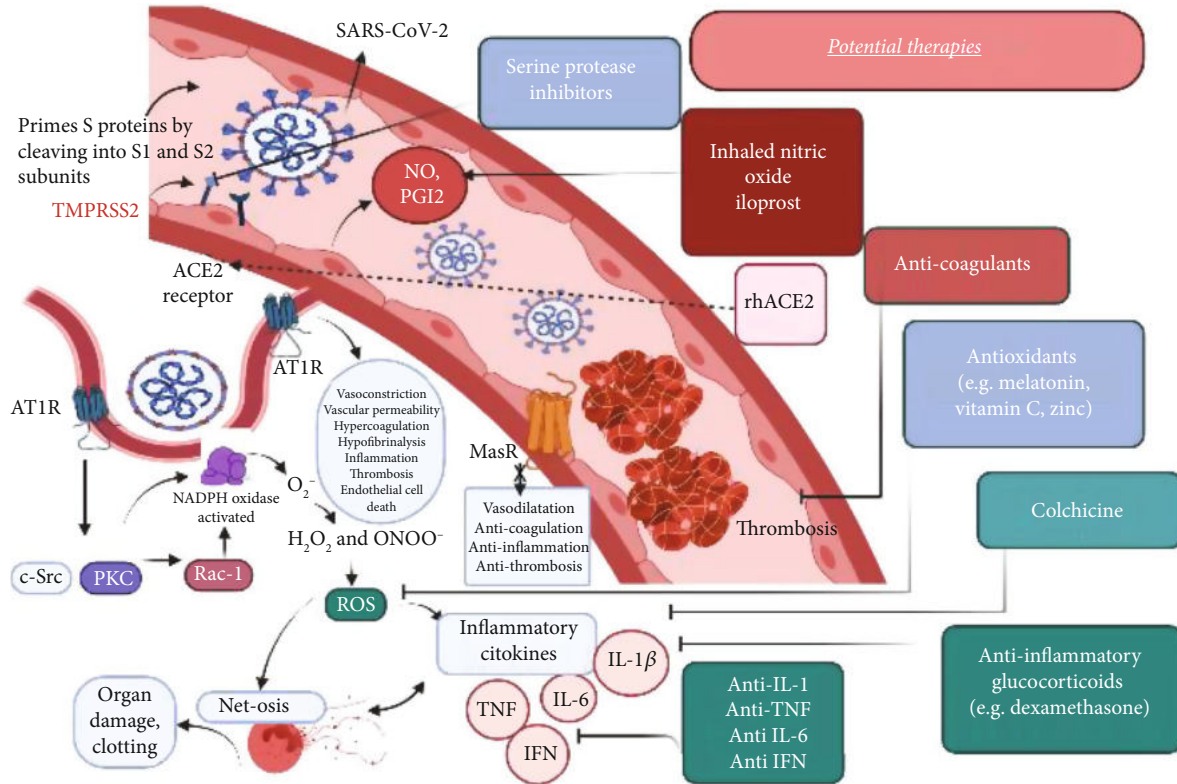


FIGURE 3: Mechanisms of endothelial dysfunction, inflammation, oxidative stress, and therapeutic targets in SARS-CoV-2 infection. SARS-CoV-2 infection begins when its peak proteins are proteolytically prepared by TMPRSS2, allowing them to bind to ACE2 and initiate viral endocytosis in the EC. This increases the amount of binding of Ang II to AT1R, which in turn activates NADPH-oxidase and subsequently induces an increased production of ROS. These excess ROS mediate signaling pathways that increase the production of inflammatory cytokines (such as IL-1 β , IL-6, and TNF), decrease the bioavailability of NO and PGI2, and induce endothelial cell apoptosis, leading to endothelial damage and dysfunction. Furthermore, the release of proinflammatory and prothrombotic factors can lead to vascular inflammation, platelet aggregation, and thrombosis. These interactions increase the risk of thrombosis and lung damage in people infected with SARS-CoV-2. ROS also induce an overflow of NETs. There may be several positive feedback loops between cytokines (TNF- α , IL-1 β) and ROS production as well as between cytokines (TNF- α , IL-1 β) and NET formation. ROS, NETs, and proteolytic enzymes released by activated neutrophils also contribute to organ damage and clotting in vessels. Therapeutic targets address SARS-CoV-2-induced feedback loops in EC. Although there have been many therapies proposed to stop the spread of the coronavirus pandemic, those described here address feedback loops involving endothelial dysfunction, oxidative stress, and inflammation. TMPRSS2: transmembrane protease, serine 2; ACE2: angiotensin-converting enzyme 2; AT1R: angiotensin type 1 receptor; ROS: reactive oxygen species; c-Src: protooncogene tyrosine-protein kinase Src; PKC: protein kinase C; IL: interleukin; TNF: tissue necrosis factor; NO: nitric oxide; PGI2: prostaglandin I2 (also known as prostacyclin).

CD8+ TL into a prognostic model. The authors of the study showed that IL-6 values > 20 pg/mL and CD8 + TL values < 165 cells/ μ L are correlated with mortality, being a better indicator of in-hospital mortality than the CURB-65 score [91].

Other cytokines were studied in the attempt to identify the prognostic factors of disease severity and prove their usefulness. An example is represented by IL-2R, included in several prognostic models such as the IL-2R/lymphocyte ratio, as demonstrated in the study conducted by Hou et al. [92], or the model developed by another group which incorporates IL-2R, the values of neutrophils, lymphocytes, and thrombocytes [93]. Another study proposes to monitor IP-10 and MCP-3 values early during the course of the disease in order to identify patients at risk for hyperinflammation and implicitly for more severe forms of the disease [94].

6. Therapeutic Targets for the Treatment of COVID-19

Numerous therapeutic targets (Figure 3) have been proposed taking into consideration the various mechanisms of action of SARS-CoV-2 on the endothelium. Regarding the key role of oxidative stress, endotheliopathy, and inflammatory mediators in the COVID-19 pathogenesis [8], we will further present the therapies that counteract the SARS-CoV-2-induced disturbances.

6.1. Interleukin-6 Inhibitors. As shown above, IL-6 plays an extremely important role in the occurrence and maintenance of the cytokine storm associated with COVID-19 and is correlated with disease severity, and thus it is an important therapeutic target. In addition, the inhibitors of IL-6 or its receptor proved to be effective in the treatment of other

similar syndromes such as HLH associated with Still's disease [95] or in the cytokine storm secondary to CAR-T cell therapy [96]. Regarding their use in COVID-19 patients, only data from case-control studies or case reports are currently available. It should be taken into consideration that these studies were extremely heterogeneous, performed on small samples, with divergent results concerning the monitored indicators (e.g., the need for invasive ventilation and the length of hospital stay). With respect to mortality, the majority showed an increase in survival or at least a favorable trend. Currently, many clinical trials are in progress to evaluate the efficacy and safety of using IL-6 inhibitors in this context. Experimental studies have shown that IL-6 can have a dual effect, both facilitating and suppressing viral replication [23], so that the optimal time of administration is another question that these clinical trials should answer [82, 97–100].

Tocilizumab, sarilumab, and siltuximab are Food and Drug Administration- (FDA-) approved IL-6 inhibitors evaluated for the management of patients with COVID-19 who have systemic inflammation. Tocilizumab is a recombinant humanized anti-IL-6 receptor monoclonal antibody that is approved by the FDA for use in patients with rheumatologic disorders and cytokine release syndrome (CRS) induced by chimeric antigen receptor T cell (CAR-T cell) therapy. Tocilizumab in combination with dexamethasone are indicated in certain hospitalized patients who are exhibiting rapid respiratory decompensation due to COVID-19 [101]. Further findings from REMAP-CAP and the RECOVERY study justify the use of tocilizumab in certain hospitalized patients with rapid respiratory decompensation due to COVID-19 [102].

Sarilumab is a recombinant humanized anti-IL-6 receptor monoclonal antibody that is approved by the FDA for use in patients with rheumatoid arthritis. It is available as an SQ formulation and is not approved for the treatment of CRS [101]. Preliminary efficacy results from REMAP-CAP for sarilumab were similar to those for tocilizumab. Compared to placebo, sarilumab reduced both mortality and time to ICU discharge, and increased the number of organ support-free days; however, the number of participants who received sarilumab in this trial was relatively small, limiting the conclusions and implications of these findings [102].

Siltuximab is a recombinant human-mouse chimeric monoclonal antibody that binds IL-6 and is approved by the FDA for use in patients with multicentric Castleman's disease. Siltuximab prevents the binding of IL-6 to both soluble and membrane-bound IL-6 receptors, inhibiting IL-6 signaling. Siltuximab is dosed as an IV infusion [103]. There are limited data describing the efficacy of siltuximab in patients with COVID-19 [104].

6.2. Interleukin-1 Inhibitors. Anakinra is a recombinant IL-1 receptor antagonist, currently approved in the treatment of a number of autoimmune diseases induced by excessive IL-1 secretion, with the aim of reducing inflammation and complications such as ARDS [105].

Starting from the data obtained from the use of anakinra in other similar syndromes such as secondary HLH or mac-

rophage activation syndrome [105] and taking into consideration the high values of this interleukin reported in persons infected with SARS-CoV-2, it was supposed that IL-1 could be an important target in the management of the cytokine storm associated with SARS-CoV-2 as well. A retrospective study showed a clinical improvement in 72% of COVID-19 and ARDS patients treated with this drug [106]. Several randomized clinical trials that test anakinra in COVID-19 patients are underway.

Aside from anakinra, canakinumab, a high-affinity human monoclonal antibody [101], and rilonacept, a soluble IL-1 trap, represent therapeutic options for IL-1 inhibition [107].

Canakinumab counteracts the activity of IL-1 by blocking the interaction between IL-1 β and its receptor [108]. The beneficial effect of canakinumab for COVID-19 patients results from the improvement of clinical status and reduction of invasive mechanical ventilation needed in these patients together with a prompt amelioration and maintenance in oxygenation levels [109, 110]. Furthermore, canakinumab ameliorates the prognosis of COVID-19 patients and prevents the clinical degradation by blocking the cytokine storm [110].

6.3. Anti-TNF- α . TNF- α is another cytokine with important inflammatory effects, whose increased serum values were also demonstrated in COVID-19 patients. Opinions diverge on the usefulness of anti-TNF- α monoclonal antibodies in this context. Infliximab, adalimumab, etanercept, certolizumab, and golimumab are the 5 most commonly prescribed TNFs inhibitors. On the one hand, TNF- α inhibition decreases IL-6 and IL-1 concentrations and reduces capillary permeability [111], and studies on animals have shown that the inhibition of this cytokine confers protection against SARS-CoV-2 infection. On the other hand, studies in which TNF- α inhibitors were used in syndromes similar to the cytokine storm have reported divergent results, some of them even demonstrating an aggravation of the disease [112].

6.4. Type I IFN. Considering the key role of IFN in antiviral response and its immunomodulatory effect, type I IFN seems to be an important potential therapeutic target. Type I IFN was studied both in vivo and in vitro, as monotherapy or in combination with antiviral drugs, in the treatment of SARS-CoV and MERS-CoV infection. Although interferon treatment was demonstrated to be efficient in vitro and in some studies on animals, in human studies the results were divergent. These results can be explained by the limited number of patients included and the heterogeneity of the studies, by the different inhibition mechanisms of the IFN signaling pathway used by the two viruses, as well as by the difficulty in assessing whether the clinical benefit observed was due to IFN or to the drugs with which it was used as part of combined therapy [113].

Another explanation for these results could be the subtype of IFN used as a therapeutic target. Compared to IFN- α , IFN- β seems to be a much more potent inhibitor of coronaviruses [114]. The time of administration seems to be an important element. Early administration was

associated with favorable results, while late administration was associated with significant adverse reactions without an effect on viral replication [115]. In addition, *in vitro* studies report viral replication inhibition by administration of prophylactic IFN in the case of SARS-CoV-2, while the same strategy is ineffective in the case of SARS-CoV and MERS-CoV [116–118]. A prospective study conducted in China on a sample of 2944 persons working in the health care system showed that interferon administered as a nasal spray is effective in the prophylaxis of SARS-CoV-2 infection [119].

Starting from the information obtained from previous studies on SARS-CoV and MERS-CoV and from the data regarding the pathology of SARS-CoV-2 infection, a number of clinical trials are in progress to test the efficacy of type I IFN in patients infected with SARS-CoV-2.

6.5. Inhibitor of Synthetic Serine Protease. Transmembrane protease serine 2 (TMPRSS2) represents the cornerstone in the SARS-CoV-2 S protein interaction with the endothelial cell [120]. TMPRSS2 is a protease that proved its capacity of preventing the cell invasion by SARS-CoV-2 *in vitro* [52].

Camostat mesylate, an inhibitor of synthetic serine protease infection, could block SARS-CoV-2 spreading in human tissue [120]. Taking into consideration the desirable effects in COVID-19 patients, TMPRSS2 has been approved for clinical use [52].

6.6. Recombinant Human ACE2 Protein (rhACE2). Taking into consideration that SARS-CoV-2 infection induces the depletion of ACE2 receptors, which contributes to systemic and especially pulmonary inflammation, the hypothesis was advanced that administration of recombinant human ACE2 protein can represent a therapeutic target. The causal mechanisms of immune dysfunction and hyperinflammation are multiple, so that the use of rhACE2 as monotherapy is probably insufficient, as demonstrated in patients infected with SARS-CoV in 2017 [76]. There is currently a clinical trial that studies the therapeutic efficacy of this molecule in COVID-19 patients.

6.7. JAK Inhibitors. The activated type I IFN JAK1/TYK2-STAT1/2 intracellular signaling pathway plays an important role in cytokine production, so that its inhibition might have a therapeutic effect in the cytokine storm associated with SARS-CoV-2.

Baricitinib is an inhibitor of JAK kinase currently used in the treatment of rheumatoid arthritis, which by selective and reversible binding to JAK receptors disrupts the transduction of the intracellular signal mediated by cytokines and thus attenuates the inflammatory response [121]. In addition, this compound is supposed to inhibit AAK1 receptor, required for viral endocytosis, also inhibiting in this way the entrance of the virus into the host cell [122].

At present, there are several ongoing clinical trials that investigate the efficacy of different JAK inhibitors in COVID-19 patients. An important aspect should be taken into account: the fact that SARS-CoV-2 infection predisposes to coagulopathy and formation of thrombi, and treat-

ment with JAK inhibitors has been associated with an increase in thromboembolic risk [123].

6.8. Nitric Oxide. Inhaled nitric oxide (NO) proved its antiviral effects against various coronavirus strains together with the pulmonary vasodilation activity. Of great interest is the ability of NO in the prevention of the development of severe forms of the disease, if administered at the proper time, at the early stage of COVID-19 [101].

6.9. Iloprost. The prostacyclin (PGI₂) analogue, iloprost, showed beneficial effects in COVID-19 patients. Iloprost might represent a valuable therapeutic option for respiratory performance improvement [124]. Synthesized in the vascular endothelium, PGI₂ plays a role not only in the endothelial barrier homeostasis and platelet aggregation, but it also has anti-inflammatory and vasodilatory effects. [125, 126].

In COVID-19 patients, iloprost could prevent the associated thrombotic events through its protective effects on the endothelium and the antithrombotic activity [124].

6.10. The Glycosaminoglycans. Another valuable therapeutic approach is represented by the glycosaminoglycans (GAGs), taking into consideration the double role they play in COVID-19 pathogenesis, their interaction with the chemokines, and the SARS-CoV-2 coreceptor function. Thus, the chemokine interaction with GAGs together with SARS-CoV-2 GAG-mediated cell entry might represent important targets in COVID-19 therapy [127].

6.11. Chemokine Receptor 5 Antagonism. The chemokine receptor 5 (CCR5) is a transmembrane structure expressed by several cells, including the endothelial cells [128], and it might be implicated in the SARS-CoV-2 invasion of the endothelial cells. By preventing the SARS-CoV-2 from entering the cell, the CCR5 antagonism could represent a valuable tool in preventing the severe inflammatory response characteristic for COVID-19-associated acute respiratory distress syndrome (ARDS) [127]. CCR5 antagonists proved their efficiency for preventing HIV-1 entry into the cells [129]. Maraviroc, a CCR5 antagonist, blocks the SARS-CoV-2 fusion with other cells (via S protein) and prevents its multiplication [130]. Leronlimab is a monoclonal IgG4 antibody which also has CCR5 as a therapeutic target. Leronlimab successfully reduced the IL-6 levels in patients with severe COVID 19 manifestations [131]. Taking into consideration the role of CCR5 in the COVID-19 pathogenesis and their expression by the endothelial cells, the CCR5 antagonism might represent a therapeutic option in the treatment of SARS-CoV-2-induced endotheliopathy.

6.12. The CXCL-8 Pathway. CXCL-8/IL-8 is an inflammatory chemokine that promotes the angiogenesis on endothelial cells via VEGF [132, 133]. The implication of the CXCL-8 pathway in SARS-CoV-2 infection pathogenesis results from its increased circulating levels identified in COVID-19 patients [134]. CXCL-8 is a powerful neutrophil chemoattractant factor [135] and its high serum levels in COVID-19 patients might explain the associated neutrophilia. The neutralizing IL-8 antibody therapy and CXCL-8 receptor

(CXCR-2) antagonists might represent a therapeutic option for hospitalized COVID-19 patients [127].

7. Conclusions

This review summarized the relationship between COVID-19, endothelial dysfunction, inflammation, and oxidative stress. The implication of endothelium in SARS-CoV-2 pathogenesis remains a subject of interest which is intensely researched in current studies. Even though several studies place the endothelial dysfunction and oxidative stress as the main factors responsible for microvascular COVID-19-associated complications, the direct invasion of endothelial cells by SARS-CoV-2 remains disputable. An explanation for the severe COVID-19 manifestations in patients suffering from cardiovascular and metabolic comorbidities might be the endothelial dysfunction associated with the aforementioned conditions; thus, those patients are at high risk for developing pulmonary and extrapulmonary complications. The central role of endothelium in the COVID-19 pathogenesis remains of great interest particularly for its role as a valuable therapeutic target for the prevention and/or treatment of vascular complications in SARS-CoV-2 patients. With a plethora of physiopathological mechanisms, the SARS-CoV-2-induced endotheliopathy appears to play a central role in COVID-19 pathogenesis.

Conflicts of Interest

The authors declare that there is no conflict of interest regarding the publication of this paper.

Authors' Contributions

The authors Adriana Fodor, Brandusa Tiperciuc, and Cezar Login have equal contribution.

References

- [1] X. Yang, Y. Yu, J. Xu et al., "Clinical course and outcomes of critically ill patients with SARS-CoV-2 pneumonia in Wuhan, China: a single-centered, retrospective, observational study," *The Lancet Respiratory Medicine*, vol. 8, no. 5, pp. 475–481, 2020.
- [2] Y. Deng, W. Liu, K. Liu et al., "Clinical characteristics of fatal and recovered cases of coronavirus disease 2019 in Wuhan, China: a retrospective study," *Chinese Medical Journal*, vol. 133, no. 11, pp. 1261–1267, 2020.
- [3] C. Magro, J. J. Mulvey, D. Berlin et al., "Complement associated microvascular injury and thrombosis in the pathogenesis of severe COVID-19 infection: a report of five cases," *Translational Research*, vol. 220, pp. 1–13, 2020.
- [4] Z. Magyar, A. Molnar, D. B. Nachmias et al., "Impact of groin flap ischemia-reperfusion on red blood cell micro-rheological parameters in a follow-up study on rats," *Clinical Hemorheology and Microcirculation*, pp. 1–11, 2017.
- [5] M. Oudkerk, H. R. Büller, D. Kuijpers et al., "Diagnosis, prevention, and treatment of thromboembolic complications in COVID-19: report of the National Institute for Public Health of the Netherlands," *Radiology*, vol. 297, no. 1, pp. E216–E222, 2020.
- [6] F. Jung, A. Krüger-Genge, R. P. Franke, F. Hufert, and J. H. Küpper, "COVID-19 and the endothelium," *Clinical Hemorheology and Microcirculation*, vol. 75, no. 1, pp. 7–11, 2020.
- [7] R. Amraei and N. Rahimi, "COVID-19, renin-angiotensin system and endothelial dysfunction," *Cells*, vol. 9, no. 7, 2020.
- [8] P. Libby and T. Luscher, "COVID-19 is, in the end, an endothelial disease," *European Heart Journal*, vol. 41, no. 32, pp. 3038–3044, 2020.
- [9] R. J. Esper, R. A. Nordaby, J. O. Vilariño, A. Paragano, J. L. Cacharrón, and R. A. Machado, "Endothelial dysfunction: a comprehensive appraisal," *Cardiovascular Diabetology*, vol. 5, 2006.
- [10] S. Moncada, R. M. J. Palmer, and E. A. Higgs, "Nitric oxide: physiology, pathophysiology, and pharmacology," *Pharmacological Reviews*, vol. 43, no. 2, pp. 109–142, 1991.
- [11] B. Y. Wang, H. K. Ho, P. S. Lin et al., "Regression of atherosclerosis: role of nitric oxide and apoptosis," *Circulation*, vol. 99, no. 9, pp. 1236–1241, 1999.
- [12] H. Cai and D. G. Harrison, "Endothelial dysfunction in cardiovascular disease: the role of oxidant stress," *Circulation Research*, vol. 87, no. 10, pp. 840–844, 2000.
- [13] N. R. Maadanchi, A. Vendrov, and M. S. Runge, "Oxidative stress and cardiac disease," *The American Journal of Medicine*, vol. 25, pp. 29–38, 2005.
- [14] M. A. Gimbrone and G. García-Cardeña, "Endothelial cell dysfunction and the pathobiology of atherosclerosis," *Circulation Research*, vol. 118, no. 4, pp. 620–636, 2016.
- [15] E. Lubos, N. J. Kelly, S. R. Oldebeken et al., "Glutathione Peroxidase-1 Deficiency Augments Proinflammatory Cytokine-induced Redox Signaling and Human Endothelial Cell Activation," *Journal of Biological Chemistry*, vol. 286, no. 41, pp. 35407–35417, 2011.
- [16] E. Nagy, J. W. Eaton, V. Jeney et al., "Red cells, hemoglobin, heme, iron, and atherogenesis," *Arteriosclerosis, Thrombosis, and Vascular Biology*, vol. 30, no. 7, pp. 1347–1353, 2010.
- [17] S. Quan, L. Yang, N. G. Abraham, and A. Kappas, "Regulation of human heme oxygenase in endothelial cells by using sense and antisense retroviral constructs," *Proceedings of the National Academy of Sciences*, vol. 98, no. 21, pp. 12203–12208, 2001.
- [18] S. Pennathur and J. W. Heinecke, "Oxidative stress and endothelial dysfunction in vascular disease," *Current Diabetes Reports*, vol. 7, pp. 257–264, 2007.
- [19] L. A. Teuwen, V. Geldhof, A. Pasut, and P. Carmeliet, "COVID-19: the vasculature unleashed," *Nature Reviews Immunology*, vol. 20, no. 7, pp. 389–391, 2020.
- [20] S. X. Gu, T. Tyagi, K. Jain et al., "Thrombocytopeny and endotheliopathy: crucial contributors to COVID-19 thromboinflammation," *Nature Reviews Cardiology*, vol. 18, no. 3, pp. 194–209, 2021.
- [21] M. Ackermann, S. E. Verleden, M. Kuehnel et al., "Pulmonary vascular endothelialitis, thrombosis, and angiogenesis in COVID-19," *New England Journal of Medicine*, vol. 383, no. 2, pp. 120–128, 2020.
- [22] J. M. O'Sullivan, D. M. Gonagle, S. E. Ward, R. J. S. Preston, and J. S. O'Donnell, "Endothelial cells orchestrate COVID-19 coagulopathy," *The Lancet Haematology*, vol. 7, no. 8, pp. e553–e555, 2020.
- [23] G. Goshua, A. B. Pine, M. L. Meizlish et al., "Endotheliopathy in COVID-19-associated coagulopathy: evidence from a

- single-centre, cross-sectional study,” *The Lancet Haematology*, vol. 7, no. 8, pp. e575–e582, 2020.
- [24] A. B. Pine, M. L. Meizlish, G. Goshua et al., “Circulating markers of angiogenesis and endotheliopathy in COVID-19,” *Pulmonary Circulation*, vol. 10, no. 4, p. 204589402096654, 2020.
- [25] Z. Varga, A. J. Flammer, P. Steiger et al., “Endothelial cell infection and endotheliitis in COVID-19,” *Lancet*, vol. 395, no. 10234, pp. 1417–1418, 2020.
- [26] T. Kiss, P. Balasubramanian, M. N. Valcarcel-Ares et al., “Nicotinamide mononucleotide (NMN) treatment attenuates oxidative stress and rescues angiogenic capacity in aged cerebrovascular endothelial cells: a potential mechanism for the prevention of vascular cognitive impairment,” *Geroscience*, vol. 41, no. 5, pp. 619–630, 2019.
- [27] S. Tarantini, A. Yabluchanskiy, T. Csipo et al., “Treatment with the poly(ADP-ribose) polymerase inhibitor PJ-34 improves cerebrovascular endothelial function, neurovascular coupling responses and cognitive performance in aged mice, supporting the NAD⁺ depletion hypothesis of neurovascular aging,” *Geroscience*, vol. 41, no. 5, pp. 533–542, 2019.
- [28] Z. Ungvari, S. Tarantini, Á. Nyúl-Tóth et al., “Nrf2 dysfunction and impaired cellular resilience to oxidative stressors in the aged vasculature: from increased cellular senescence to the pathogenesis of age-related vascular diseases,” *Geroscience*, vol. 41, no. 6, pp. 727–738, 2019.
- [29] J. M. McCord, B. M. Hybertson, A. Cota-Gomez, K. P. Geraci, and B. Gao, “Nrf2 activator PB125[®] as a potential therapeutic agent against COVID-19,” *Antioxidants*, vol. 9, no. 6, 2020.
- [30] J. Nordberg and E. S. Arnér, “Reactive oxygen species, antioxidants, and the mammalian thioredoxin system¹,” *Free Radical Biology & Medicine*, vol. 31, no. 11, pp. 1287–1312, 2001.
- [31] S. Hati and S. Bhattacharyya, “Impact of thiol-disulfide balance on the binding of COVID-19 spike protein with angiotensin-converting enzyme 2 receptor,” *ACS Omega*, vol. 5, no. 26, pp. 16292–16298, 2020.
- [32] A. Nguyen Dinh Cat, A. C. Montezano, D. Burger, and R. M. Touyz, “Angiotensin II, NADPH oxidase, and redox signaling in the vasculature,” *Antioxidants & Redox Signaling*, vol. 19, no. 10, pp. 1110–1120, 2013.
- [33] H. Xia, S. Suda, S. Bindom et al., “ACE2-mediated reduction of oxidative stress in the central nervous system is associated with improvement of autonomic function,” *PLoS One*, vol. 6, no. 7, article e22682, 2011.
- [34] J. Wysocki, D. I. Ortiz-Melo, N. K. Mattocks et al., “ACE2 deficiency increases NADPH-mediated oxidative stress in the kidney,” *Physiological Reports*, vol. 2, no. 3, article e00264, 2014.
- [35] S. Suhail, J. Zajac, C. Fossum et al., “Role of oxidative stress on SARS-CoV (SARS) and SARS-CoV-2 (COVID-19) infection: a review,” *The Protein Journal*, vol. 39, no. 6, pp. 644–656, 2020.
- [36] R. Chang, A. Mamun, A. Dominic, and N. T. Le, “SARS-CoV-2 mediated endothelial dysfunction: the potential role of chronic oxidative stress,” *Frontiers in Physiology*, vol. 11, 2021.
- [37] X. Li, P. Fang, J. Mai, E. T. Choi, H. Wang, and X. F. Yang, “Targeting mitochondrial reactive oxygen species as novel therapy for inflammatory diseases and cancers,” *Journal of Hematology & Oncology*, vol. 6, no. 1, 2013.
- [38] E. Petersen, M. Koopmans, U. Go et al., “Comparing SARS-CoV-2 with SARS-CoV and influenza pandemics,” *The Lancet Infectious Diseases*, vol. 20, no. 9, pp. e238–e244, 2020.
- [39] V. G. Puelles, M. Lütgehetmann, M. T. Lindenmeyer et al., “Multiorgan and renal tropism of SARS-cov-2,” *The New England Journal of Medicine*, vol. 383, no. 6, pp. 590–592, 2020.
- [40] H. Su, M. Yang, C. Wan et al., “Renal histopathological analysis of 26 postmortem findings of patients with COVID-19 in China,” *Kidney International*, vol. 98, no. 1, pp. 219–227, 2020.
- [41] T. Menter, J. D. Haslbauer, R. Nienhold et al., “Postmortem examination of COVID19 patients reveals diffuse alveolar damage with severe capillary congestion and variegated findings of lungs and other organs suggesting vascular dysfunction,” *Histopathology*, vol. 77, no. 2, pp. 198–209, 2020.
- [42] A. Kolivras, F. Dehavay, D. Delplace et al., “Coronavirus (COVID-19) infection-induced chilblains: a case report with histopathologic findings,” *JAAD Case Reports*, vol. 6, no. 6, pp. 489–492, 2020.
- [43] J. Kanitakis, C. Lesort, M. Danset, and D. Jullien, “Chilblain-like acral lesions during the COVID-19 pandemic (“COVID toes”): Histologic, immunofluorescence, and immunohistochemical study of 17 cases,” *Journal of the American Academy of Dermatology*, vol. 83, no. 3, pp. 870–875, 2020.
- [44] J. Roca-Ginés, I. Torres-Navarro, J. Sánchez-Arráez et al., “Assessment of acute acral lesions in a case series of children and adolescents during the COVID-19 pandemic,” *JAMA Dermatology*, vol. 156, no. 9, pp. 992–997, 2020.
- [45] G. C. Román, P. S. Spencer, J. Reis et al., “The neurology of COVID-19 revisited: a proposal from the Environmental Neurology Specialty Group of the World Federation of Neurology to implement international neurological registries,” *Journal of the Neurological Sciences*, vol. 414, article 116884, 2020.
- [46] M. Benger, O. Williams, J. Siddiqui, and L. Sztrihai, “Intracerebral haemorrhage and COVID-19: clinical characteristics from a case series,” *Brain, Behavior, and Immunity*, vol. 88, pp. 940–944, 2020.
- [47] T. J. Guzik, S. A. Mohiddin, A. Dimarco et al., “COVID-19 and the cardiovascular system: implications for risk assessment, diagnosis, and treatment options,” *Cardiovascular Research*, vol. 116, no. 10, pp. 1666–1687, 2020.
- [48] B. Siripanthong, S. Nazarian, D. Muser et al., “Recognizing COVID-19-related myocarditis: the possible pathophysiology and proposed guideline for diagnosis and management,” *Heart Rhythm*, vol. 17, no. 9, pp. 1463–1471, 2020.
- [49] S. Pons, S. Fodil, E. Azoulay, and L. Zafrani, “The vascular endothelium: the cornerstone of organ dysfunction in severe SARS-CoV-2 infection,” *Critical Care*, vol. 24, no. 1, 2020.
- [50] S. Zaim, J. H. Chong, V. Sankaranarayanan, and A. Harky, “COVID-19 and multiorgan response,” *Current Problems in Cardiology*, vol. 45, no. 8, p. 100618, 2020.
- [51] B. M. Henry, J. Vixse, S. Benoit, E. J. Favaloro, and G. Lippi, “Hyperinflammation and derangement of renin-angiotensin-aldosterone system in COVID-19: a novel hypothesis for clinically suspected hypercoagulopathy and microvascular immunothrombosis,” *Clinica Chimica Acta*, vol. 507, pp. 167–173, 2020.
- [52] M. Hoffmann, H. Kleine-Weber, S. Schroeder et al., “SARS-CoV-2 cell entry depends on ACE2 and TMPRSS2 and is

- blocked by a clinically proven protease inhibitor,” *Cell*, vol. 181, no. 2, pp. 271–280.e8, 2020.
- [53] A. J. Turner, J. A. Hiscox, and N. M. Hooper, “ACE2: from vasopeptidase to SARS virus receptor,” *Trends in Pharmacological Sciences*, vol. 25, no. 6, pp. 291–294, 2004.
- [54] D. W. Lambert, N. M. Hooper, and A. J. Turner, “Angiotensin-converting enzyme 2 and new insights into the renin-angiotensin system,” *Biochemical Pharmacology*, vol. 75, no. 4, pp. 781–786, 2008.
- [55] J. Lan, J. Ge, J. Yu et al., “Structure of the SARS-CoV-2 spike receptor-binding domain bound to the ACE2 receptor,” *Nature*, vol. 581, no. 7807, pp. 215–220, 2020.
- [56] Y. Wan, J. Shang, R. Graham, R. S. Baric, and F. Li, “Receptor recognition by the novel coronavirus from Wuhan: an analysis based on decade-long structural studies of SARS coronavirus,” *Journal of Virology*, vol. 94, no. 7, 2020.
- [57] T. C. Hanff, M. O. Harhay, T. S. Brown, J. B. Cohen, and A. M. Mohareb, “Is there an association between COVID-19 mortality and the renin-angiotensin system? A call for epidemiologic investigations,” *Clinical Infectious Diseases*, vol. 71, no. 15, pp. 870–874, 2020.
- [58] M. Vaduganathan, O. Vardeny, T. Michel, J. J. V. McMurray, M. A. Pfeffer, and S. D. Solomon, “Renin-angiotensin-aldosterone system inhibitors in patients with COVID-19,” *The New England Journal of Medicine*, vol. 382, no. 17, pp. 1653–1659, 2020.
- [59] C. M. Ferrario, J. Jessup, M. C. Chappell et al., “Effect of angiotensin-converting enzyme inhibition and angiotensin II receptor blockers on cardiac angiotensin-converting enzyme 2,” *Circulation*, vol. 111, no. 20, pp. 2605–2610, 2005.
- [60] M. A. Chamsi-Pasha, Z. Shao, and W. H. Tang, “Angiotensin-converting enzyme 2 as a therapeutic target for heart failure,” *Current Heart Failure Reports*, vol. 11, no. 1, pp. 58–63, 2014.
- [61] M. R. Deshotels, H. Xia, S. Sriramula, E. Lazartigues, and C. M. Filipeanu, “Angiotensin II mediates angiotensin converting enzyme type 2 internalization and degradation through an angiotensin II type I receptor-dependent mechanism,” *Hypertension*, vol. 64, no. 6, pp. 1368–1375, 2014.
- [62] G. Lippi, A. M. South, and B. M. Henry, “Electrolyte imbalances in patients with severe coronavirus disease 2019 (COVID-19),” *Annals of Clinical Biochemistry*, vol. 57, no. 3, pp. 262–265, 2020.
- [63] P. Zhang, L. Zhu, J. Cai et al., “Association of inpatient use of angiotensin-converting enzyme inhibitors and angiotensin II receptor blockers with mortality among patients with hypertension hospitalized with COVID-19,” *Circulation Research*, vol. 126, no. 12, pp. 1671–1681, 2020.
- [64] K. Kuba, Y. Imai, and J. M. Penninger, “Angiotensin-converting enzyme 2 in lung diseases,” *Current Opinion in Pharmacology*, vol. 6, pp. 271–276, 2006.
- [65] Y. Liu, Y. Yang, C. Zhang et al., “Clinical and biochemical indexes from 2019-nCoV infected patients linked to viral loads and lung injury,” *Science China. Life Sciences*, vol. 63, no. 3, pp. 364–374, 2020.
- [66] G. Wolf, U. Wenzel, K. J. M. Assmann, and R. A. K. Stahl, “Renal expression of aminopeptidase A in rats with two-kidney, one-clip hypertension,” *Nephrology, Dialysis, Transplantation*, vol. 15, no. 12, pp. 1935–1942, 2000.
- [67] A. Mogielnicki, E. Chabielska, R. Pawlak, J. Szemraj, and W. Buczko, “Angiotensin II enhances thrombosis development in renovascular hypertensive rats,” *Thrombosis and Haemostasis*, vol. 93, no. 6, pp. 1069–1076, 2005.
- [68] E. Y. Senchenkova, J. Russell, C. T. Esmon, and D. N. Granger, “Roles of coagulation and fibrinolysis in angiotensin II-enhanced microvascular thrombosis,” *Microcirculation*, vol. 21, no. 5, pp. 401–407, 2014.
- [69] G. I. Shyh, J. J. Nawarskas, and A. Cheng-Lai, “Angiotensin-converting enzyme inhibitors and angiotensin receptor blockers in patients with coronavirus disease 2019,” *Cardiology in Review*, vol. 28, no. 4, pp. 213–216, 2020.
- [70] J. Meng, G. Xiao, J. Zhang et al., “Renin-angiotensin system inhibitors improve the clinical outcomes of COVID-19 patients with hypertension,” *Emerging Microbes & Infections*, vol. 9, no. 1, pp. 757–760, 2020.
- [71] H. Zhang, J. M. Penninger, Y. Li, N. Zhong, and A. S. Slutsky, “Angiotensin-converting enzyme 2 (ACE2) as a SARS-CoV-2 receptor: molecular mechanisms and potential therapeutic target,” *Intensive Care Medicine*, vol. 46, no. 4, pp. 586–590, 2020.
- [72] K. Kuba, Y. Imai, S. Rao et al., “A crucial role of angiotensin converting enzyme 2 (ACE2) in SARS coronavirus-induced lung injury,” *Nature Medicine*, vol. 11, no. 8, pp. 875–879, 2005.
- [73] D. Batlle, J. Wysocki, and K. Satchell, “Soluble angiotensin-converting enzyme 2: a potential approach for coronavirus infection therapy?,” *Clinical Science*, vol. 134, no. 5, pp. 543–545, 2020.
- [74] Z. Wu and J. M. McGoogan, “Characteristics of and important lessons from the coronavirus disease 2019 (COVID-19) outbreak in China,” *JAMA*, vol. 323, no. 13, pp. 1239–1242, 2020.
- [75] Y. Liu, L. M. Yan, L. Wan et al., “Viral dynamics in mild and severe cases of COVID-19,” *The Lancet Infectious Diseases*, vol. 20, no. 6, pp. 656–657, 2020.
- [76] R. H. Manjili, M. Zarei, M. Habibi, and M. H. Manjili, “COVID-19 as an acute inflammatory disease,” *Journal of Immunology*, vol. 205, no. 1, pp. 12–19, 2020.
- [77] J. Garcia Borrega, P. Gödel, M. A. Rüger et al., “In the eye of the storm: immune-mediated toxicities associated with CAR-T cell therapy,” *Hema*, vol. 3, no. 2, article e191, 2019.
- [78] E. Karakike and E. J. Giamarellos-Bourboulis, “Macrophage activation-like syndrome: a distinct entity leading to early death in sepsis,” *Frontiers in Immunology*, vol. 10, 2019.
- [79] F. Caso, L. Costa, P. Ruscitti et al., “Could Sars-coronavirus-2 trigger autoimmune and/or autoinflammatory mechanisms in genetically predisposed subjects?,” *Autoimmunity Reviews*, vol. 19, no. 5, article 102524, 2020.
- [80] N. Mangalmurti and C. A. Hunter, “Cytokine storms: understanding COVID-19,” *Immunity*, vol. 53, no. 1, pp. 19–25, 2020.
- [81] S. Jensen and A. R. Thomsen, “Sensing of RNA viruses: a review of innate immune receptors involved in recognizing RNA virus invasion,” *Journal of Virology*, vol. 86, no. 6, pp. 2900–2910, 2012.
- [82] Y. Jamilloux, T. Henry, A. Belot et al., “Should we stimulate or suppress immune responses in COVID-19? Cytokine and anti-cytokine interventions,” *Autoimmunity Reviews*, vol. 19, no. 7, article 102567, 2020.
- [83] J. Hadjadj, N. Yatim, L. Barnabei et al., “Impaired type I interferon activity and inflammatory responses in severe COVID-19 patients,” *Science*, vol. 369, no. 6504, pp. 718–724, 2020.

- [84] B. Diao, C. Wang, Y. Tan et al., "Reduction and functional exhaustion of T cells in patients with coronavirus disease 2019 (COVID-19)," *Frontiers in Immunology*, vol. 11, 2020.
- [85] R. Channappanavar, A. R. Fehr, R. Vijay et al., "Dysregulated type I interferon and inflammatory monocyte-macrophage responses cause lethal pneumonia in SARS-CoV-infected mice," *Cell Host & Microbe*, vol. 19, no. 2, pp. 181–193, 2016.
- [86] C. Huang, Y. Wang, X. Li et al., "Clinical features of patients infected with 2019 novel coronavirus in Wuhan, China," *The Lancet*, vol. 395, no. 10223, pp. 497–506, 2020.
- [87] H. Akbari, R. Tabrizi, K. B. Lankarani et al., "The role of cytokine profile and lymphocyte subsets in the severity of coronavirus disease 2019 (COVID-19): a systematic review and meta-analysis," *Life Sciences*, vol. 258, article 118167, 2020.
- [88] R. Mulchandani, T. Lyngdoh, and A. K. Kakkar, "Deciphering the COVID-19 cytokine storm: systematic review and meta-analysis," *European Journal of Clinical Investigation*, vol. 51, no. 1, article e13429, 2021.
- [89] H. Mojtavavi, A. Saghazadeh, and N. Rezaei, "Interleukin-6 and severe COVID-19: a systematic review and meta-analysis," *European Cytokine Network*, vol. 31, no. 2, pp. 44–49, 2020.
- [90] R. Laguna-Goya, A. Utrero-Rico, P. Talayero et al., "IL-6-based mortality risk model for hospitalized patients with COVID-19," *Journal of Allergy and Clinical Immunology*, vol. 146, no. 4, pp. 799–807.e9, 2020.
- [91] M. Luo, J. Liu, W. Jiang, S. Yue, H. Liu, and S. Wei, "IL-6 and CD8+ T cell counts combined are an early predictor of in-hospital mortality of patients with COVID-19," *JCI Insight*, vol. 5, no. 13, article e139024, 2020.
- [92] H. Hou, B. Zhang, H. Huang et al., "Using IL-2R/lymphocytes for predicting the clinical progression of patients with COVID-19," *Clinical & Experimental Immunology*, vol. 201, no. 1, pp. 76–84, 2020.
- [93] F. Wang, H. Hou, T. Wang et al., "Establishing a model for predicting the outcome of COVID-19 based on combination of laboratory tests," *Travel Medicine and Infectious Disease*, vol. 36, p. 101782, 2020.
- [94] Y. Yang, C. Shen, J. Li et al., "Plasma IP-10 and MCP-3 levels are highly associated with disease severity and predict the progression of COVID-19," *J Allergy Clin Immunol*, vol. 146, no. 1, pp. 119–127.e4, 2020.
- [95] E. Watanabe, H. Sugawara, T. Yamashita, A. Ishii, A. Oda, and C. Terai, "Successful tocilizumab therapy for macrophage activation syndrome associated with adult-onset Still's disease: a case-based review," *Case Reports in Medicine*, vol. 2016, Article ID 5656320, 7 pages, 2016.
- [96] C. Kotch, D. Barrett, and D. T. Teachey, "Tocilizumab for the treatment of chimeric antigen receptor T cell-induced cytokine release syndrome," *Expert Rev Clin Immunol.*, vol. 15, no. 8, pp. 813–822, 2019.
- [97] L. Velazquez-Salinas, A. Verdugo-Rodriguez, L. L. Rodriguez, and M. V. Borca, "The role of interleukin 6 during viral infections," *Frontiers in Microbiology*, vol. 10, p. 1057, 2019.
- [98] X. Xu, M. Han, T. Li et al., "Effective treatment of severe COVID-19 patients with tocilizumab," *Proceedings of the National Academy of Sciences of the United States of America*, vol. 117, no. 20, pp. 10970–10975, 2020.
- [99] P. Luo, Y. Liu, L. Qiu, X. Liu, D. Liu, and J. Li, "Tocilizumab treatment in COVID-19: a single center experience," *Journal of Medical Virology*, vol. 92, no. 7, pp. 814–818, 2020.
- [100] K. Ghazvini, M. Karbalaei, and M. Keikha, "What are the clinical benefits of tocilizumab for COVID-19 patients? Evidence from available case-control studies," *Le Pharmacien Hospitalier & Clinicien*, vol. 56, no. 2, pp. 217–221, 2021.
- [101] J. Robinson, "Everything you need to know about the COVID-19 therapy trials," *Pharmaceutical Journal*, 2021.
- [102] REMAP-CAP Investigators, A. C. Gordon, P. R. Mouncey et al., "Interleukin-6 receptor antagonists in critically ill patients with COVID-19," *The New England Journal of Medicine*, vol. 384, no. 16, pp. 1491–1502, 2021.
- [103] S. Sarosiek, R. Shah, and N. C. Munshi, "Review of siltuximab in the treatment of multicentric Castleman's disease," *Therapeutic Advances in Hematology*, vol. 7, no. 6, pp. 360–366, 2016.
- [104] A. M. Johnson, R. Barigye, and H. Saminathan, "Perspectives on the use and risk of adverse events associated with cytokine-storm targeting antibodies and challenges associated with development of novel monoclonal antibodies for the treatment of COVID-19 clinical cases," *Human Vaccines & Immunotherapeutics*, vol. 11, pp. 1–17, 2021.
- [105] L. A. Monteagudo, A. Boothby, and E. Gertner, "Continuous intravenous anakinra infusion to calm the cytokine storm in macrophage activation syndrome," *ACR Open Rheumatology*, vol. 2, no. 5, pp. 276–282, 2020.
- [106] G. Cavalli, G. de Luca, C. Campochiaro et al., "Interleukin-1 blockade with high-dose anakinra in patients with COVID-19, acute respiratory distress syndrome, and hyperinflammation: a retrospective cohort study," *The Lancet Rheumatology*, vol. 2, no. 6, pp. e325–e331, 2020.
- [107] E. A. Dubois, R. Rissmann, and A. F. Cohen, "Rilonacept and canakinumab," *British Journal of Clinical Pharmacology*, vol. 71, no. 5, pp. 639–641, 2011.
- [108] A. X. Goh, S. Bertin-Maghit, S. Ping Yeo et al., "A novel human anti-interleukin-1 β neutralizing monoclonal antibody showing in vivo efficacy," *MAbs*, vol. 6, no. 3, pp. 764–772, 2014.
- [109] D. Generali, G. Bosio, F. Malberti et al., "Canakinumab as treatment for COVID-19-related pneumonia: a prospective case-control study," *International Journal of Infectious Diseases*, vol. 104, pp. 433–440, 2021, Epub 2020 Dec 29.
- [110] F. Katia, D. P. Myriam, C. Ucciferri et al., "Efficacy of canakinumab in mild or severe COVID-19 pneumonia," *Immunity, Inflammation and Disease*, vol. 9, no. 2, pp. 399–405, 2021, Epub 2021 Jan 19.
- [111] J. E. McDermott, H. D. Mitchell, L. E. Gralinski et al., "The effect of inhibition of PP1 and TNF α signaling on pathogenesis of SARS coronavirus," *BMC Systems Biology*, vol. 10, no. 1, pp. 1–12, 2016.
- [112] A. Stern, R. Riley, and L. Buckley, "Worsening of macrophage activation syndrome in a patient with adult onset Still's disease after initiation of etanercept therapy," *JCR: Journal of Clinical Rheumatology*, vol. 7, no. 4, pp. 252–256, 2001.
- [113] L. J. Stockman, R. Bellamy, and P. Garner, "SARS: systematic review of treatment effects," *PLoS Medicine*, vol. 3, no. 9, pp. e343–1531, 2006.
- [114] E. Sallard, F. X. Lescure, Y. Yazdanpanah, F. Mentre, and N. Peiffer-Smadja, "Type 1 interferons as a potential treatment against COVID-19," *Antiviral Research*, vol. 178, p. 104791, 2020.
- [115] R. Channappanavar, A. R. Fehr, J. Zheng et al., "IFN-I response timing relative to virus replication determines

- MERS coronavirus infection outcomes,” *The Journal of Clinical Investigation*, vol. 129, no. 9, pp. 3625–3639, 2019.
- [116] K. G. Lokugamage, A. Hage, M. de Vries et al., “Type I interferon susceptibility distinguishes SARS-CoV-2 from SARS-CoV,” *Journal of Virology*, vol. 94, no. 23, 2020.
- [117] T. P. Sheahan, A. C. Sims, S. R. Leist et al., “Comparative therapeutic efficacy of remdesivir and combination lopinavir, ritonavir, and interferon beta against MERS-CoV,” *Nature Communications*, vol. 11, no. 1, p. 222, 2020.
- [118] V. Thiel and F. Weber, “Interferon and cytokine responses to SARS-coronavirus infection,” *Cytokine & Growth Factor Reviews*, vol. 19, no. 2, pp. 121–132, 2008.
- [119] Z. Meng, T. Wang, L. Chen et al., “An experimental trial of recombinant human interferon alpha nasal drops to prevent coronavirus disease 2019 in medical staff in an epidemic area,” *MedRxiv*, vol. 2020, no. 4, 2020.
- [120] T. Iba, J. M. Connors, and J. H. Levy, “The coagulopathy, endotheliopathy, and vasculitis of COVID-19,” *Inflammation Research*, vol. 69, no. 12, pp. 1181–1189, 2020.
- [121] M. C. Genovese, J. Kremer, O. Zamani et al., “Baricitinib in patients with refractory rheumatoid arthritis,” *The New England Journal of Medicine*, vol. 374, no. 13, pp. 1243–1252, 2016.
- [122] R. Lu, X. Zhao, J. Li et al., “Genomic characterisation and epidemiology of 2019 novel coronavirus: implications for virus origins and receptor binding,” *Lancet*, vol. 395, no. 10224, pp. 565–574, 2020.
- [123] H. Chugh, A. Awasthi, Y. Agarwal, R. K. Gaur, G. Dhawan, and R. Chandra, “A comprehensive review on potential therapeutic interventions for COVID-19,” *European Journal of Pharmacology*, vol. 890, article 173741, 2021.
- [124] A. Filippini, C. Bnà, R. Bellosta et al., “COVID-19 acute respiratory distress syndrome: can iloprost have a role for the treatment?,” *Respiratory Medicine Case Reports*, vol. 32, p. 101358, 2021.
- [125] P. D’Amelio, M. A. Cristofaro, L. D’Amico et al., “Iloprost modulates the immune response in systemic sclerosis,” *BMC Immunol*, vol. 11, no. 1, 2010.
- [126] A. A. Birukova, T. Wu, Y. Tian et al., “Iloprost improves endothelial barrier function in lipopolysaccharide-induced lung injury,” *European Respiratory Journal*, vol. 41, no. 1, pp. 165–176, 2013.
- [127] A. Pum, M. Ennemoser, T. Adage, and A. J. Kungl, “Cytokines and chemokines in SARS-CoV-2 infections—therapeutic strategies targeting cytokine storm,” *Biomolecules*, vol. 11, no. 1, p. 91, 2021.
- [128] G. Li, G. Zhu, Y. Gao et al., “Neferine inhibits the upregulation of CCL5 and CCR5 in vascular endothelial cells during chronic high glucose treatment,” *Inflammation*, vol. 36, no. 2, pp. 300–308, 2013.
- [129] O. S. Latinovic, M. Reitz, and A. Heredia, “CCR5 inhibitors and HIV-1 infection,” *J AIDS HIV Treat*, vol. 1, no. 1, pp. 1–5, 2019.
- [130] K. H. Risner, K. V. Tieu, Y. Wang et al., “Maraviroc inhibits SARS-CoV-2 multiplication and S-protein mediated cell fusion in cell culture,” *BioRxiv*, 2020.
- [131] N. Agresti, J. P. Lalezari, P. P. Amodeo et al., “Disruption of CCR5 signaling to treat COVID-19-associated cytokine storm: case series of four critically ill patients treated with leronlimab,” *Journal of Translational Autoimmunity*, vol. 4, article 100083, 2021.
- [132] D. Martin, R. Galisteo, and J. S. Gutkind, “CXCL8/IL8 Stimulates Vascular Endothelial Growth Factor (VEGF) Expression and the Autocrine Activation of VEGFR2 in Endothelial Cells by Activating NFκB through the CBM (Carma3/Bcl10/Malt1) Complex,” *Journal of Biological Chemistry*, vol. 284, no. 10, pp. 6038–6042, 2009.
- [133] J. Heidemann, H. Ogawa, M. B. Dwinell et al., “Angiogenic Effects of Interleukin 8 (CXCL8) in Human Intestinal Microvascular Endothelial Cells Are Mediated by CXCR2,” *The Journal of Biological Chemistry*, vol. 278, no. 10, pp. 8508–8515, 2003.
- [134] D. M. del Valle, S. Kim-Schulze, H. H. Huang et al., “An inflammatory cytokine signature predicts COVID-19 severity and survival,” *Nature Medicine*, vol. 26, no. 10, pp. 1636–1643, 2020.
- [135] S. de Oliveira, C. C. Reyes-Aldasoro, S. Candel, S. A. Renshaw, V. Mulero, and Á. Calado, “Cxcl8 (IL-8) mediates neutrophil recruitment and behavior in the zebrafish inflammatory response,” *The Journal of Immunology*, vol. 190, no. 8, pp. 4349–4359, 2013.

RESEARCH ON ENZYME INHIBITION POTENTIAL AND PHENOLIC COMPOUNDS FROM *ORIGANUM VULGARE* SSP. *VULGARE*

DANIELA HANGANU^{1,#}, DANIELA BENEDEC^{1*}, NELI-KINGA OLAH², FLORICA RANGA³, SIMONA MIREL^{1,#}, BRÎNDUȘA TIPERCIUC^{1,#}, ILIOARA ONIGA¹

¹"Iuliu Hațieganu" University of Medicine and Pharmacy, 8 V. Babeș Street, RO-400010, Cluj-Napoca, Romania

²"Vasile Goldiș" Western University of Arad, 94 Revoluției Avenue, Arad, Romania

³University of Agricultural Science and Veterinary Medicine, 3-5 Mănăștur Street, Cluj-Napoca, Romania

*corresponding author: dani_67ro@yahoo.com

#Authors with equal contribution

Manuscript received: December 2019

Abstract

This study assessed for the first time, the enzyme inhibitory properties of the *Origanum vulgare* ssp. *vulgare* extract. The main compounds were analysed chromatographically and spectrophotometrically. The enzymatic inhibitory potential was evaluated *in vitro*, against enzymes that play key roles in different diseases: acetylcholinesterase, urease, tyrosinase, trypsin and xanthine oxidase. A specific phenolic profile was evidenced, with large amounts of rosmarinic acid and luteolin 7-*O*-glucuronide; two phenolic diterpenes (rosmanol and rosmadial) were identified for the first time in this species. The oregano extract exhibited significant urease, tyrosinase and xanthine oxidase inhibitory effects, in line with the phenolic content. As a result of this study, new potential biological activities have been described for *Origanum vulgare* extract, which can be further studied and used in the pharmaceutical field.

Rezumat

În acest studiu se evaluează pentru prima dată potențialul inhibitor enzimatic al extractului de *Origanum vulgare* ssp. *vulgare* (șovârf). Principalii compuși chimici au fost analizați prin metode cromatografice și spectrofotometrice. Capacitatea inhibitorie a fost evaluată *in vitro*, asupra unor enzime implicate în anumite afecțiuni: acetilcolinesteraza, ureaza, tirozinaza, tripsina și xantin-oxidaza. În ceea ce privește profilul fenolic al extractului, s-au pus în evidență cantități mari de acid rozmarinic și luteolin-7-*O*-glucuronidă; două diterpene fenolice (rosmanol și rosmadial) au fost identificate pentru prima dată în această specie. Extractul de șovârf a inhibat semnificativ ureaza, tirozinaza și xantin-oxidaza, în concordanță cu conținutul mare de compuși polifenolici. Prin acest studiu s-au semnalat noi activități biologice potențiale ale extractului de *Origanum vulgare*, care deschid noi perspective de interes științific în domeniul farmaceutic.

Keywords: *Origanum vulgare* ssp. *vulgare*, polyphenols, enzyme inhibition

Introduction

Origanum vulgare L. (*Lamiaceae* family) is used worldwide for its flavour as a spice, having a long history of use in gastronomy and traditional medicine [10, 28]. At the same time, oregano is considered a medicinal plant due to its complex chemical composition which includes: essential oil, polyphenols, diterpenoids, triperpenoids. It is known as antimicrobial, antiviral, hepatoprotective, antidiabetic, antiinflammatory, anti-oxidant, antispasmodic, antiurolithic, antiproliferative, neuroprotective agent, to mention some of the scientifically proven therapeutic actions [6-8, 11, 23, 25, 26]. Natural herbal products are increasingly used in many fields: pharmaceutical, food and cosmetics. In recent years, interest in this plant, as well as the enzymatic activities of plant extracts involved in the protection of human health, have increased. The purpose of this study was to analyse the chemical composition and to evaluate the enzymatic inhibition

of *O. vulgare* ssp. *vulgaris* ethanolic extract, in order to be used in the design of new formulations with therapeutic applications in Alzheimer's disease, ulcer, gout, or hyperpigmentation.

Materials and Methods

The aerial parts of *O. vulgare* ssp. *vulgare* were harvested from Beliș (Cluj, Romania), during the blooming period (July 2018) and a voucher specimen (no. 96) was deposited in the Herbarium of the Department of Pharmacognosy, Faculty of Pharmacy, Cluj-Napoca, Romania. The extract was prepared in 70% vol. ethanol and the ratio between the vegetal material and the solvent was 1:10 (m/v) [2, 5, 32].

Chemicals, HPLC chromatographic conditions and quantitative analysis

Chemicals were obtained from Merck, Alfa-Aesar and Roth (Germany).

The HPLC analysis was performed using an Agilent HPLC system series 1200 with quaternary pump, solvent degassing system, auto-sampler, DAD spectrophotometric detector and single quadruple MS detector type Agilent 6110 (Agilent Technologies, CA, USA). The separation was performed on an Eclipse XDB C18 column, 4.6 x 150 mm with particles of 5 μ m (Agilent Technologies, USA), at 25°C, in gradient elution. The mobile phases were water: 0.1% acetic acid in acetonitrile (99:1) (solvent A) and 0.1% acetic acid in acetonitrile (solvent B) at a flow of 0.5 mL/min. The gradient applied was as follows: % B = 5% (0 - 2 min), from 5% to 40% (2 - 18 min), from 40% to 90% (18 - 20 min), then isocratic 4 min and decrease from 90% to 5% (24 - 25 min). The MS was used in ESI positive mode, in the following scanning conditions: capillary voltage at 3.000 V, temperature at 300°C, nitrogen flow at 8 L/min, m/z ranges from 100 to 1000, full-scan mode. The DAD spectrophotometric detection was performed at 340 nm. The data acquisition and the results processing were performed using ChemStation software from Agilent Technologies, USA. The identification was performed by comparison of obtained MS spectra with the ones from the library, meanwhile for the quantitative determination was used the DAD detection [3].

Determination of total polyphenols content

The total polyphenols content (TPC) was determined using the Folin-Ciocalteu method, with a calibration curve of gallic acid ($R^2 = 0.999$), and the results were expressed as mg of gallic acid equivalents (GAE)/g dry plant material [2, 4, 14, 32].

Enzyme inhibitory activity

Urease inhibition assay. This assay is based on ammonia quantification after urea hydrolysis in the presence of urease. Briefly, 0.2 mL urease (0.1 mg/mL) were treated with 4 mL Tris-HCl acid buffer (pH 8), 0.2 mL urea (60 mM) and 0.02 mL extract. The mixture was incubated at 30°C, for 20 min and then the reaction was stopped by addition of 1 mL 10% trichloroacetic acid. The ammonia content was evaluated by using 0.5 mL Nessler reagent. Absorbance was determined at 436 nm. Thiourea (200 μ g/mL) was used as a standard inhibitor [24].

Tyrosinase inhibition assay. The activity of this enzyme was spectrometrically evaluated using L-DOPA as a substrate. To 0.4 mL tyrosinase (250 UI/mL), 7.4 mL phosphate buffer (pH 7) and 0.04 mL extract were added; then the mixture was incubated 15 minutes at 30°C. At the end 0.2 mL 10 mM L-DOPA was added. Absorbance was determined at 475 nm and the ascorbic acid (340 μ g/mL) was used as standard [13, 20].

Acetylcholinesterase inhibition assay. The extract (1 μ L) was treated with 6 mL Tris-HCl buffer (pH 8) and with 0.05 mL acetylcholinesterase (6 UI/mL), then the mixture was incubated 15 minutes at 30°C. Subsequently, 0.1 mL 5,5-dithiobis-2-nitrobenzoic acid (3 mM) and 0.1 mL acetylthiocholine iodide

(15 mM) were added. The hydrolysis of the substrate was monitored by the formation of 5-thio-2-nitrobenzoate anion as the result of the reaction of 5,5-dithiobis-2-nitrobenzoic acid with thiocholine, released by enzymatic hydrolysis of acetyl thiocholine iodide. Absorbance was measured at 405 nm and galantamine (1.5 mg/mL) was used as a standard [20, 30, 31].

Trypsin inhibition assay. The assay was based on the spectrophotometric evaluation of trypsin inhibition using bovine serum albumin as a sub-substrate. To 0.1 mL extract, 0.2 mL trypsin (0.05%) were added and the mixture was incubated at 37°C, for 20 min. Then, 2 mL bovine serum albumin (10 mg/mL) and 4 mL phosphate buffer (pH 7.6) were added. The reaction was stopped by adding 2 mL trichloroacetic acid (10%). The mixture was treated with 1 mL alkaline cupric reagent and 0.1 mL phosphomolybdenic reagent. The absorbance was measured at 750 nm. Salicylic acid (5 mg/mL) was used as standard [12, 16, 21, 29].

Xanthine oxidase inhibition assay. To 0.15 mL extract, 3.9 mL phosphate buffer (pH 7.4) and 0.6 mL xanthine oxidase (0.2 UI/mL) were added and then the mixture was incubated 10 minutes at 25°C. Finally, 4.5 mL 0.15 mM xanthine was added and this was followed by 30 min incubation at 25°C. Allopurinol (0.3 mg/mL) was used as standard [1, 18, 22].

For all assays the standards and the control samples were prepared in the same manner. The inhibition potency (I%) was calculated in all cases with the following formula:

$$I\% = [1 - A_{\text{sample}}/A_{\text{control}}] \times 100,$$

where A_{sample} is the absorbance for sample (with the extract or standard) and A_{control} is the absorbance for control (without the extract or standard).

Statistical analysis. The samples were analysed in triplicate; the average and the relative SD were calculated using the Excel software package.

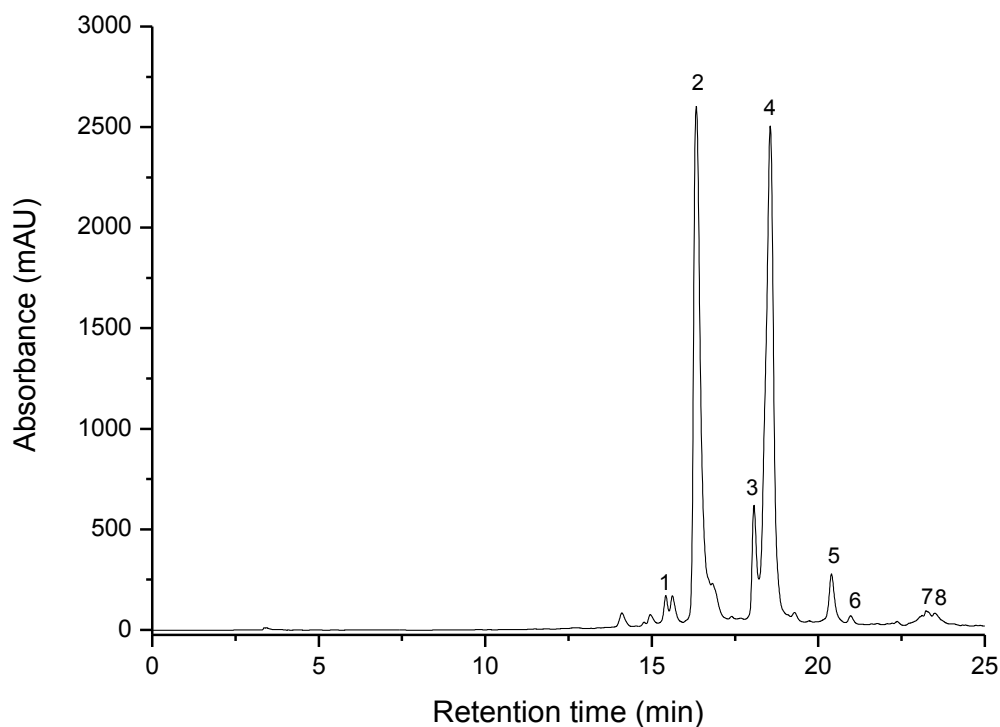
Results and Discussion

In the *Origanum* ethanolic extract a high content of total polyphenols (89.21 ± 2.79 mg GAE/g dry plant material) was determined. The results were similar to those previously obtained [6, 23].

With respect to HPLC analysis, Table I and Figure 1 show the phenolic compounds found in the ethanolic extract of *O. vulgare* ssp. *vulgare*, meaning 8 main phenolic compounds: 5 flavonoids of which 3 glycosides: of quercetin (rutin form), luteolin (glucuronide form) and kaempferol (glucoside form), and 2 free aglycons (luteolin and kaempferol). Rosmarinic acid was found in a large quantity, in accordance with similar results presented by other authors [6, 23, 28]. Two phenolic lactones diterpenes, rosmanol and rosmadial, were determined for the first time in the oregano extract. These antioxidant diterpenic compounds have been also identified in rosemary [9, 27].

Table IHPLC analysis of the phenolic compounds from *O. vulgare* ssp. *vulgare*

Compounds	m/z value	R _t (min)	Peak No.	Concentration (mg/g plant product)
Rutin (quercetin-3- <i>O</i> -rutinoside)	611	15.42	1	0.67 ± 0.02
Luteolin 7- <i>O</i> -glucuronide	463	16.03	2	15.20 ± 0.70
Kaempferol- <i>O</i> -glucoside	448	18.07	3	2.58 ± 0.42
Rosmarinic acid	361	18.55	4	16.89 ± 0.11
Rosmanol	347	20.39	5	1.79 ± 0.02
Luteolin	287	21.57	6	0.55 ± 0.06
Rosmadial	345	22.98	7	0.45 ± 0.04
Kaempferol	287	23.49	8	0.62 ± 0.08

**Figure 1.**HPLC chromatograms for *Origanum vulgare* extract

Chromatographic conditions were as given in the Material and Methods section. The identified compounds: 1. Rutin; 2. luteolin 7-*O*-glucuronide; 3. kaempferol-*O*-glucoside; 4. rosmarinic acid; 5. Rosmanol; 6. Luteolin; 7. Rosmadial; 8. kaempferol

In order to determine the enzyme inhibitory activity, our extract was tested against urease, tyrosinase, acetylcholinesterase, trypsin and xanthine oxidase (Table II).

There were correlated the total polyphenols content with the individual polyphenols concentrations. The Figure 2 shows that the main identified polyphenols are the rosmarinic acid respectively the luteoline-7-

O-glucuronide, representing 18.9 respectively 17 % from the total polyphenols content, while the others have less than 3 %. These polyphenols induce to the *O. vulgare* extract more antioxidant effect, that lead us to foresee mostly an inhibition on oxidative enzymes, like xanthinoxidase or tyrosinase, and less inhibition on hydrolytic enzymes, like acetylcholinesterase or trypsin.

Table IIEnzyme inhibition activity of *O. vulgare* ssp. *vulgare* extract

Sample	URE inhibition (%)	TYRE inhibition (%)	AChE inhibition (%)	TRY inhibition (%)	XO inhibitory (%)
<i>O. vulgare</i> extract	90.47 ± 6.07	58.63 ± 8.60	40.67 ± 3.00	17.1 ± 0.09	85.19 ± 5.10
Standards	Thi	Aa	Ga	Sa	Al
	93.26 ± 5.85	96.53 ± 5.14	99.83 ± 1.52	90.2 ± 0.13	91.05 ± 2.35

Each value is the mean ± SD of three independent measurements. URE: urease; α-CHYM: α-chymotrypsin; TYRE: tyrosinase; AChE: acetylcholinesterase; TRY: trypsin; XO: xanthine oxidase. Thi: thiourea; Aa: ascorbic acid; Ga: galantamine; Sa: salicylic acid; Al: allopurinol

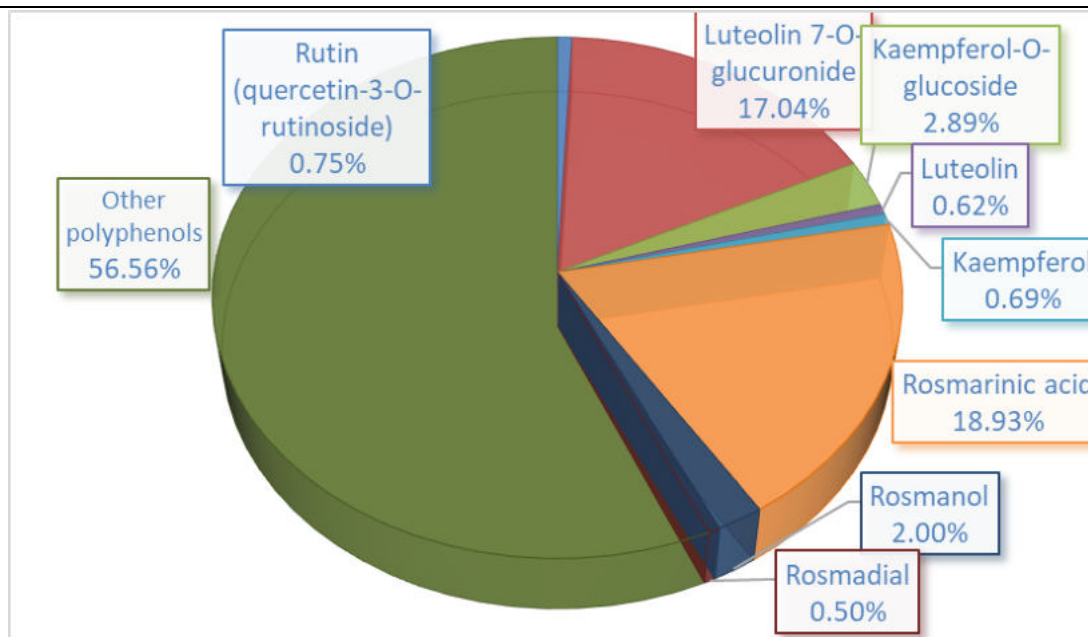


Figure 2.

Percentage distribution of individual polyphenols from total polyphenol content

Data on the enzymatic inhibitory properties of the ethanolic extract obtained from spontaneous *O. vulgare* ssp. *vulgare* are limited. Our results confirm the foresee upon the phytochemical profile, a better inhibition being obtained on oxidative enzymes, xanthinoxidase and tyrosinase, 85.19 respectively 58.63 %.

Urease is a Ni-containing enzyme related to gastro-duodenal diseases (gastric and peptic ulcers). It catalyses the hydrolysis of urea to ammonia and carbonic acid, and allows bacteria like *Helicobacter pylori* to survive at low pH values of the stomach [19, 24]. The results of this study suggest that at the tested dose, *O. vulgare* extract revealed a strong *in vitro* urease inhibitory activity (90.47%), very close to inhibition of the standard (Thi: 93.26% at 200 µg/mL). So, the oregano extract can be a potential anti-ulcer agent because of the polyphenolic compounds that are involved in the inhibition of *Helicobacter pylori* [19, 24].

Tyrosinase is an oxidase that converts L-tyrosine to L-DOPA and oxidizes DOPA to dopaquinone, which induces melanin biosynthesis. Tyrosinase inhibitors can control the melanin synthesis and could be useful in therapy (in hyperpigmentation, age spots etc.). In addition, polyphenols structurally similar to DOPA and tyrosine could block the synthesis of melanin. In the same time the lack of dopamine, obtained from L-DOPA, is involved in the pathogenesis of Parkinson's disease. Recently the tyrosinase inhibitors were tested to prevent or lower the evolution of this neuro-degenerative disease [17]. The tested extract of *O. vulgare* ssp. *vulgare* showed moderate tyrosinase inhibition activity (58.63%). Other authors have reported

similar anti-tyrosinase activity and rosmarinic acid is probably involved in this effect [13, 15].

Cholinesterase inhibition has become the most widely employed clinical approach for treating the symptoms of Alzheimer's disease [31]. In our study, the *O. vulgare* extract had a moderate inhibition activity on AChE (40.67%). Other authors have achieved comparable results [15].

Trypsin plays an important role in the virulence of many human, plant and insect pathogens. The trypsin inhibitors of plant origin have been reported widely from many plant species. *O. vulgare* extract exhibited low trypsin inhibition activity (17.1%). Naturally occurring trypsin inhibitors are proteins and this could explain the low activity of the ethanolic extract [12].

A good xanthine oxidase inhibition effect may be associated with a decrease in the production of uric acid. Our extract showed a good xanthine oxidase inhibitory activity (85.19%), so *O. vulgare* extract can provide encouraging premise for new anti-hyperuricemic natural products [18].

Conclusions

This study is the first attempt to evaluate the inhibitory action of ethanolic extracts of the indigenous species *Origanum vulgare* ssp. *vulgare* on some key enzymes involved in chronic diseases. A specific phenolic profile was highlighted by the presence of rosmarinic acid and luteolin-7-*O*-glucuronide, as well as rosmanol and rosmadial, two phenolic diterpenes, which are reported for the first time. Our results showed that *O. vulgare* extract revealed a good urease, xanthine oxidase and tyrosinase *in vitro* inhibitory activity. These preliminary results could be useful for future

experimental studies, in order to define the efficiency of the *O. vulgare* extract in the treatment of different diseases.

Conflict of interest

The authors declare no conflict of interest.







References

- Alam MN, Bristi NJ, Rafiqzaman M, Review on *in vivo* and *in vitro* methods evaluation of antioxidant activity. *Saudi Pharm J.*, 2013; 21: 143-152.
- Andriamadio JH, Rasoanaivo LH, Benedec D, Vlase L, Gheldiu AM, Duma M, Toiu A, Raharisololalao A, Oniga I, HPLC/MS analysis of polyphenols, antioxidant and antimicrobial activities of *Artabotrys hildebrandtii* O. Hffm. extracts. *Nat Prod Res.*, 2015; 29: 2188-96.
- Badalica-Petrescu M, Dragan S, Ranga F, Fetea F, Socaciu C, Comparative HPLC-DAD-ESI(+)MS Fingerprint and quantification of phenolic and flavonoid composition of aqueous leaf extracts of *Cornus mas* and *Crataegus monogyna*, in relation to their cardiotoxic potential. *Not Bot Horti Agrobo.*, 2014; 42: 9-18.
- Benedec D, Danganu D, Filip L, Oniga I, Tiperciuc B, Olah NK, Gheldiu AM, Raita O, Vlase L, Chemical, antioxidant and antibacterial studies of Romanian *Heracleum sphondylium*. *Farmacia*, 2017; 65(2): 253-256.
- Benedec D, Hanganu D, Oniga I, Filip L, Bischin C, Silaghi R, Tiperciuc B, Vlase L, *Achillea schurii* flowers: chemical, antioxidant and antimicrobial investigations. *Molecules*, 2016; 21(8): 1-12.
- Benedec D, Hanganu D, Oniga I, Tiperciuc B, Olah N, Raita O, Bischin C, Silaghi R, Vlase L, Assessment of rosmarinic acid content in six *Lamiaceae* species extracts and their antioxidant and antimicrobial potential. *Pak J Pharm Sci.*, 2015; 28: 2297-2303.
- Benedec D, Oniga I, Cuius F, Sevastre B, Stiuftuc G, Duma M, Hanganu D, Iacovita C, Stiuftuc R, Lucaciu CM, *Origanum vulgare* mediated green synthesis of biocompatible gold nanoparticles simultaneously possessing plasmonic, antioxidant and antimicrobial properties. *Int J Nanomedicine*, 2018; 13: 1041-1058.
- Benedec D, Oniga I, Kozma-Imre A, Hanganu D, Ţărmure V, Bodoki E, Determination of rosmarinic acid by HPTLC-image analysis in medicinal teas and their biological properties. *Farmacia*, 2017; 65(4): 605-609.
- Bunghuz F, Rotar MA, Pop RM, Romanciuc F, Csernatonu F, Fetea F, Diaconeasa Z, Socaciu C, Comparative phenolic fingerprint and LC-ESI+QTOF-MS composition of oregano and rosemary hydrophilic extracts in relation to their antibacterial effect. *Bull UASVM Food Sci Technol.*, 2015; 72: 33-40.
- Chishti S, Kaloo ZA, Sultan PJ, Medicinal importance of genus *Origanum*: a review. *Pharmacognosy Phytother.*, 2013; 5: 170-177.
- Chishti S, Sultan P, Kaloo ZA, Wani BA, Sheikh MA, Antibacterial activity and DPPH scavenging antioxidant potential in *Origanum vulgare* L. *Int J Adv Res Biol Sci.*, 2014; 1: 15-21.
- Divya C, Sreejina Sreedharan K, Punathum Parambath B, Meethal V, Identification of plant extracts expressing trypsin inhibitor. *Acta Biologica Indica*, 2014; 3: 522-526.
- Doveci E, Tel-Cavan G, Duru ME, Phenolic profile, antioxidant, anticholinesterase, and anti-tyrosinase activities of the various extracts of *Ferula elaeochoytris* and *Sideritis stricta*. *Int J Food Prop.*, 2018; 21: 771-783.
- Epure A, Oniga I, Benedec D, Hanganu D, Gheldiu AM, Toiu A, Vlase L, Chemical analysis and antioxidant activity of some rooibos tea products. *Farmacia*, 2019; 67(6): 963-966.
- Gonçalves S, Moreira E, Grosso C, Paula BA, Valentão P, Romano A, Phenolic profile, antioxidant activity and enzyme inhibitory activities of extracts from aromatic plants used in Mediterranean diet. *J Food Sci Technol.*, 2017; 54: 219-227.
- Hade S, Joshi P, Pilley H, Wadeaonkar V, Wadeaonkar P, Evaluation of *Crataeva nurvala* extracts as antioxidant, antiproteolytic and cytotoxic against hepato-carcinoma and mouse melanoma cell line. *J Appl Pharm Sci.*, 2016; 6: 189-196.
- Hasegawa T, Tyrosinase-expressing neuronal cell line as *in vitro* model of parkinson's disease. *Int J Mol Sci.*, 2010; 11: 1082-1089.
- Hudaib MM, Tawaha KA, Mohammad MK, Assaf AM, Issa AY, Alali FQ, Aburjai TA, Bustanji YK. Xanthine oxidase inhibitory activity of the methanolic extracts of selected Jordanian medicinal plants. *Pharmacogn Mag.*, 2011; 7: 320-324.
- Lin YT, Kwon YI, Labbe RG, Shetty K, Inhibition of *Helicobacter pylori* and associated urease by oregano and cranberry phytochemical synergies. *Appl Environ Microbiol.*, 2005; 71: 8558-64.
- Neagu E, Paun G, Albu C, Radu GL, Assessment of acetylcholinesterase and tyrosinase inhibitory and antioxidant activity of *Alchemilla vulgaris* and *Filipendula ulmaria* extracts. *J Taiwan Inst Chem Eng.*, 2015; 52: 1-6.
- Nile SH, Park SW, Optimized methods for *in vitro* and *in vivo* anti-inflammatory assays and its applications in herbal and synthetic drug analysis. *Mini-Rev Med Chem.*, 2013; 13: 95-100.
- Noro T, Oda Y, Miyase T, Ueno A, Fukushima S, Inhibitors of xanthine oxidase from the flowers and buds of *Daphne genkwa*. *Chem Pharm Bull.*, 1983; 31: 3984-3987.
- Oniga I, Puşcaş C, Silaghi-Dumitrescu R, Olah NK, Sevastre B, Marcus R, Marcus I, Sevastre-Berghian AC, Benedec D, Pop CE, Hanganu D, *Origanum vulgare* ssp. *vulgare*: Chemical composition and biological studies. *Molecules*, 2018; 23(8): 1-14.
- Paun G, Litescu SC, Neagu E, Tache A, Radu GL, Evaluation of *Geranium* spp., *Helleborus* spp. and *Hyssopus* spp. polyphenolic extracts inhibitory activity against urease and α -chymotrypsin. *J Enzyme Inhib Med Chem.*, 2014; 29: 28-34.
- Păduraru DN, Coman F, Ozon EA, Gherghiceanu F, Andronic O, Ion D, Stănescu M, Bolocan A, The use of nutritional supplement in Romanian patients - Attitudes and beliefs. *Farmacia*, 2019; 67(6): 1060-1065.
- Pezzani R, Vitalini S, Iriti M, Bioactivities of *Origanum vulgare* L.: an update. *Phytochem Rev.*, 2017; 16: 1253-1268.

27. Razboršek MI, Vončina DB, Doleček V, Voncina E, Determination of major phenolic acids, phenolic diterpenes and triterpenes in rosemary (*Rosmarinus officinalis* L.) by gas chromatography and mass spectrometry. *Acta Chim Slov.*, 2007; 54: 60-67.
28. Shekarchi M, Hajimehdipour H, Saeidnia S, Gohari AR, Hamedani MP, Comparative study of rosmarinic acid content in some plants of *Labiatae* family. *Pharmacogn Mag.*, 2012; 8: 37-41.
29. Tandon M, Tandon P, Barthwal J, Bhalla TN, Bhargava KP, Anti-inflammatory and antiproteolytic activities of newer indolyl isoquinolones. *Drug Res.*, 1982; 32: 1233-1235.
30. Topcu G, Kusman T, *Lamiaceae* Family plants as a potential anticholinesterase source in the treatment of Alzheimer's disease. *Bezmialem Science*, 2014; 1: 1-25.
31. Vladimir-Knežević S, Blažeković B, Kind M, Vladić J, Lower-Nedza AD, Brantner AH, Acetylcholinesterase inhibitory, antioxidant and phytochemical properties of selected medicinal plants of the *Lamiaceae* family. *Molecules*, 2014; 19: 767-782.
32. xxx - European Pharmacopoeia, 8th edition, Council of Europe, 2014.

Research Article

A Novel Thiazolyl Schiff Base: Antibacterial and Antifungal Effects and *In Vitro* Oxidative Stress Modulation on Human Endothelial Cells

Cristian Cezar Login ¹, Ioana Bâldea ¹, Brîndușa Tipericiuc ², Daniela Benedec ³,
Dan Cristian Vodnar ⁴, Nicoleta Decea ¹, and Șoimița Suciu¹

¹Department of Physiology, Iuliu Hațieganu University of Medicine and Pharmacy, 1 Clinicilor Street, 400006 Cluj-Napoca, Romania

²Department of Pharmaceutical Chemistry, Iuliu Hațieganu University of Medicine and Pharmacy, 41 Victor Babeș Street, 400012 Cluj-Napoca, Romania

³Department of Pharmacognosy, Iuliu Hațieganu University of Medicine and Pharmacy, 12 Ion Creangă Street, 400010 Cluj-Napoca, Romania

⁴Department of Food Science, University of Agricultural Sciences and Veterinary Medicine, 3-5 Mănăstur Street, 400372 Cluj-Napoca, Romania

Correspondence should be addressed to Ioana Bâldea; baldeaioana@gmail.com and Brîndușa Tipericiuc; brandu32@yahoo.com

Received 5 April 2019; Revised 13 July 2019; Accepted 5 September 2019; Published 10 October 2019

Guest Editor: Birke Bartosch

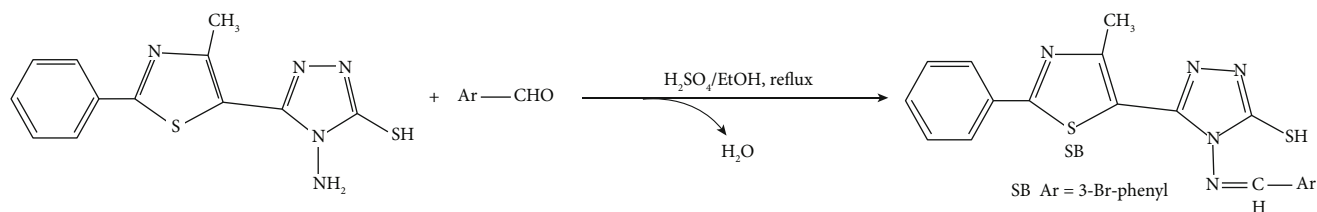
Copyright © 2019 Cristian Cezar Login et al. This is an open access article distributed under the Creative Commons Attribution License, which permits unrestricted use, distribution, and reproduction in any medium, provided the original work is properly cited.

Schiff bases (SBs) are chemical compounds displaying a significant pharmacological potential. They are able to modulate the activity of many enzymes involved in metabolism and are found among antibacterial, antifungal, anti-inflammatory, antioxidant, and antiproliferative drugs. A new thiazolyl-triazole SB was obtained and characterized by elemental and spectral analysis. The antibacterial and antifungal ability of the SB was evaluated against Gram-positive and Gram-negative bacteria and against three *Candida* strains. SB showed good antibacterial activity against *L. monocytogenes* and *P. aeruginosa*; it was two times more active than ciprofloxacin. Anti-*Candida* activity was twofold higher compared with that of fluconazole. The effect of the SB on cell viability was evaluated by colorimetric measurement on cell cultures exposed to various SB concentrations. The ability of the SB to modulate oxidative stress was assessed by measuring MDA, TNF- α , SOD1, COX2, and NOS2 levels *in vitro*, using human endothelial cell cultures exposed to a glucose-enriched medium. SB did not change the morphology of the cells. Experimental findings indicate that the newly synthesized Schiff base has antibacterial activity, especially on the Gram-negative *P. aeruginosa*, and antifungal activity. SB also showed antioxidant and anti-inflammatory activities.

1. Introduction

Aerobic organisms have antioxidant defense systems against reactive oxygen species- (ROS-) induced damage produced in various stress conditions. ROS are also involved in the innate immune system and have an important role in the inflammatory response; they attract cells, by chemotaxis, to the inflammation site. Nitric oxide (NO) is another important intracellular and intercellular signaling molecule involved in the regulation of multiple physiological and pathophysiological mechanisms. It acts as a biological modulator.

NO is able to regulate vascular tone and can function as a host defense effector. Also, it can act as a cytotoxic agent in inflammatory disorders. NO synthase (NOS) enzyme family catalyzes NO production. Inhibition of inducible NOS (iNOS) might be beneficial in the course of treatment of certain inflammatory diseases [1]. The reactions between NO and ROS, such as superoxide radicals ($O_2^{\cdot-}$), lead to the production of a potent prooxidant radical (peroxynitrite), thus inducing endothelial and mitochondrial dysfunction. The major cellular defense against peroxide and peroxynitrite radicals are the superoxide dismutases (SODs) that catalyzes



SCHEME 1: Synthesis of the Schiff base (SB).

the transformation of peroxide radicals into hydrogen peroxide (H_2O_2), which is further transformed by catalase into water and molecular oxygen. Also, SODs play an important role in preventing peroxynitrite formation [2]. All isoforms have in their catalytic site a transition metal, such as copper and manganese [3].

Recent studies showed that exogenous NO, produced by bacterial NOS, protects Gram-positive and Gram-negative bacteria (*Pseudomonas aeruginosa*, *Staphylococcus aureus*, etc.) against oxidative stress and increases bacterial resistance to a broad spectrum of antibiotics [4]. Fungal resistance to antimycotic treatment is one of the consequences of the emergence of resistant strains, but more and more, in the last years, fungal resistance is due to the capacity of fungal strains to form biofilms, which are considered critical in invasive fungal infections, associated with high mortality. Certain studies showed that only a few antimycotics are effective against fungal biofilms. All of them have the capacity to induce ROS formation in fungal biofilm cells [5]. In this context, finding bioactive substances capable to reduce NO synthesis in bacteria or able to induce ROS synthesis in fungal biofilms could represent new directions in the development of new antimicrobial drugs. Thiazoles, triazoles, and their derivatives are found among antibacterial and anti-inflammatory drugs [6–9].

Schiff bases (SBs) are chemical structures that have a significant pharmacological potential. SBs contain an azomethine group obtained through the condensation of primary amines with carbonyl compounds [10]. The pharmacophore potential of this group is due to their ability to form complex compounds with bivalent and trivalent metals located in the active center of numerous enzymes involved in metabolic reactions. The relationship between a chemical structure and biological activity (SAR) underlines the importance of the azomethine group for the synthesis of new compounds with antibacterial, antifungal, and even antitumor activities [11–13].

Multiple studies showed the ability of SBs to act as antiproliferative and antitumoral agents [14–16]. The azomethine pharmacophore is used in developing new bioactive molecules [17]. The discovery of selective cytotoxic drugs influenced oncological therapy. However, completely satisfactory answers for metastasis onset have not yet been found. Due to the increased prevalence of neoplasia and to the existence of various cellular tumor lines resistant to cytotoxic therapy, the research of new active agents is justified [18, 19].

The current study is aimed at testing a newly synthesized heterocyclic SB in terms of antimicrobial activity against Gram-positive and Gram-negative bacteria and antifungal

effects against *Candida* strains [20, 21], as well as to evaluate the biocompatibility of the SB *in vitro* on human endothelial cells and the ability of this SB to modulate oxidative stress, by assessing enzymes involved in cellular antioxidant defense.

2. Materials and Methods

2.1. Synthesis of the Schiff Base. All reagents and solvents used were purchased from Sigma-Aldrich and were used without further purification. The starting compound was previously reported and was synthesized by us according to methodologies described in the literature [21].

The synthesis of Schiff base (SB) 4-(3-bromobenzylideneamino)-5-(4-methyl-2-phenylthiazol-5-yl)-4H-1,2,4-triazole-3-thiol was made using a general procedure (Scheme 1) [21]. 2 mmol (0.578 g) of 4-amino-5-(4-methyl-2-phenylthiazol-5-yl)-4H-1,2,4-triazole-3-thiol was suspended in 10 mL of absolute ethanol. The resulting suspension was added with an alcoholic solution of 2 mmol of 3-bromobenzaldehyde in 5 mL of absolute ethanol and 2–3 drops of concentrated H_2SO_4 , as a catalyst. The reaction mixture was refluxed for 6 h. The obtained precipitate was filtered hot and washed with absolute ethanol, and then, it was dried and recrystallized from dimethyl sulfoxide (DMSO).

2.2. In Vitro Antibacterial and Antifungal Screening

2.2.1. Preparation of Sample Solution. SB was dissolved in DMSO, at a final concentration of 100 $\mu\text{g}/\text{mL}$. Sample solution was stored at 4°C [22, 23].

2.2.2. Inhibition Zone Diameter Measurements. Antimicrobial activity was tested *in vitro* using the agar disk diffusion method through the measurement of the inhibition zone diameters. Agar plates were inoculated with a standardized inoculum of the test microorganisms: two Gram-negative bacterial strains—*Salmonella enteritidis* ATCC 14028 and *Escherichia coli* ATCC 25922, two Gram-positive bacterial strains—*Listeria monocytogenes* ATCC 19115 and *Staphylococcus aureus* ATCC 49444, and a fungal strain—*Candida albicans* ATCC 10231. Petri plates with Mueller Hinton Agar (20.0 mL) were used for all bacterial tests. Mueller-Hinton medium supplemented with 2% glucose (providing adequate growth of yeasts) and 0.5 g/L methylene blue (providing a better definition of the inhibition zone diameter) was used for antifungal testing. Each paper disk was impregnated with 10 μL of solution (100 μg compound/disk). The filter paper disks were placed on Petri dishes previously seeded “in layer” with the tested bacterial strain inoculums. Then, Petri dishes were maintained at room temperature to ensure the equal

diffusion of the compound in the medium, and afterwards, the dishes were incubated at 37°C for 24 hours. Inhibition zones were measured after 24 hours of incubation. Assessment of the antimicrobial effect was realized by measuring the diameter of the growth inhibition zone. Ciprofloxacin (10 µg/well) and fluconazole (25 µg/well) were used as *standard* antibacterial and antifungal *drugs*. DMSO was used for comparison, as a negative control, for all experiments, and it did not inhibit the growth of microorganisms (diameter = 6 mm). The clear halos with a diameter larger than 10 mm were considered positive results [22, 23]. Tests were performed in triplicate, and values are presented as the average value ± standard deviation.

2.2.3. Determination of Minimum Inhibitory Concentrations (MICs), Minimum Bactericidal Concentrations (MBCs), and Minimum Fungicidal Concentrations (MFCs). Minimum inhibitory concentrations (MICs), minimum bactericidal concentrations (MBCs), and minimum fungicidal concentrations (MFCs) were determined by an agar dilution method. Strains of microorganisms used were as follows: *Salmonella enteritidis* ATCC 14028, *Escherichia coli* ATCC 25922, *Listeria monocytogenes* ATCC 19115, *Staphylococcus aureus* ATCC 49444, *Candida albicans* ATCC 10231, *Candida albicans* (ATCC 18804), and *Candida krusei* (ATCC 6258) [22–26]. For the experiment, 100 µL nutrient broths were placed in a 96-well plate, and sample solution at high concentration (100 µg/mL) was added into the first rows of the microplates. 10 µL of culture suspensions was inoculated into all the wells. The plates were incubated at 37°C for 16–24 hours (48 hours for fungi). The reference drugs, ciprofloxacin and fluconazole, were used in the same concentrations.

2.3. Determination of Antioxidant Activity by DPPH (2,2-Diphenyl-1-picrylhydrazyl) Bleaching Assay. The DPPH antioxidant activity assay was done as previously described, with minor modification. SB was dissolved in DMSO (1 mg/mL). DPPH• radical was dissolved in methanol (0.25 mM). Equal volumes (1.0 mL) of methanolic DPPH solution and sample solution (or standard) in methanol at different concentrations have been used. The mixtures were incubated for 30 min at 40°C in a thermostatic bath; absorbance was measured at 517 nm. The percent DPPH scavenging ability was calculated as follows: $\text{DPPH scavenging ability} = (A_{\text{control}} - A_{\text{sample}}) / A_{\text{control}} \times 100$, where A_{control} is the absorbance of DPPH radical and methanol (containing all reagents, except the sample) and A_{sample} is the absorbance of the mixture of DPPH radical and sample. A curve of % DPPH scavenging ability versus concentration was plotted, and IC_{50} values were calculated. The IC_{50} value is the sample concentration required to scavenge 50% of DPPH free radicals. The lesser the IC_{50} value, the stronger the antioxidant capacity. Thus, if $IC_{50} \leq 50 \mu\text{g/mL}$, the sample shows a high antioxidant capacity; if $50 \mu\text{g/mL} < IC_{50} \leq 200 \mu\text{g/mL}$, the sample has a moderate antioxidant capacity; if $IC_{50} > 200 \mu\text{g/mL}$, the sample has poor or no activity. BHT (butylated hydroxytoluene)

and trolox (6-hydroxy-2,5,7,8-tetramethylchroman-2-carboxylic acid) were used as positive controls [20, 27–30].

2.4. Assessment of the Ability of the SB to Modulate Inflammatory Response and Oxidative Stress on Cell Cultures

2.4.1. Cell Source. Human umbilical vein endothelial cells (HUVECs, Promocell, Hamburg, Germany) were used. The cells were grown in RPMI medium supplemented with 5% fetal calf serum, 50 µg/mL gentamycin, and 5 ng/mL amphotericin (Biochrom Ag, Berlin, Germany). Cell cultures in the 13rd to 15th passages were used. SB was diluted in DMSO (Biochrom Ag, Berlin, Germany) to obtain a stock solution of 1 mg/mL. The stock solution was used to make further dilutions in complete cell growth medium, immediately prior to the experiments. The final DMSO concentration was lower than 0.05%, a nontoxic concentration for the cells [31].

2.4.2. Cell Viability Testing. Cells cultured at a density of 10^4 /well on ELISA 96-well plaques (TPP, Switzerland) were settled for 24 hours, then exposed to different concentrations of the substance ranging from 0.001 to 200 µg/mL. Viability was measured by the colorimetric measurement of a colored compound—formazan, generated by viable cells using the CellTiter 96® Aqueous Non-Radioactive Cell Proliferation Assay (Promega Corporation, Madison, USA). Readings were done at 540 nm, using an ELISA plate reader (Tecan, Mannedorf, Austria). Results were presented as OD_{540} . All experiments were performed in triplicate. Untreated cultures were used as controls [32].

2.4.3. Experimental Design. Four groups were made: (1) control cells treated only with medium, (2) cells exposed to a high-glucose (4.5 g/L) medium, (3) cells treated with SB 0.001 µg/mL, and (4) cells concomitantly exposed to high glucose and SB (0.001 µg/mL). All groups were treated for 24 hours. Afterwards, cells were used for the assessment of cytoskeleton modifications—phalloidin staining (fluorescence microscopy), oxidative stress (Western blot measurement of SOD1, COX2, and inducible NOS2 and spectrophotometric measurement of MDA), and inflammation (ELISA measurement of TNF-α).

2.4.4. Cell Lysis. The cell lysates used in the following experiments were prepared as previously described [33]. Protein concentrations were determined by the Bradford method, according to the manufacturer's specifications (Bio-Rad, Hercules, California, USA) and using bovine serum albumin as standard. For all assays, the lysates were corrected by total protein concentration.

2.4.5. Oxidative Stress and Inflammation Assessment. Quantification of malondialdehyde (MDA) a marker for the peroxidation of membrane lipids was performed by spectrophotometry, as previously described [34]. All reagents were purchased from Sigma-Aldrich. Data were expressed as nM/mg protein [35]. Following viability testing and following the assessment of the MDA level, cells used in further experiments were treated with a concentration of 0.001 µg/mL.

TNF- α ELISA Immunoassay kit from R&D Systems, Inc. (Minneapolis, USA) was used. Cell supernatants were treated according to the manufacturer's instructions; readings were done at 450 nm with correction wavelength set at 540 nm, using an ELISA plate reader (Tecan) [33].

Lysates (20 μ g protein/lane) were separated by electrophoresis on SDS PAGE gels and transferred to polyvinylidene difluoride membranes, using a Bio-Rad Miniprotean system (Bio-Rad). Blots were blocked and then incubated with antibodies against superoxide dismutase 1 (SOD1), cyclooxygenase 2 (COX2), and inducible nitric oxide synthase 2 (NOS2), then further washed and incubated with corresponding secondary peroxidase-linked antibodies. All antibodies were acquired from Santa Cruz Biotechnology. Proteins were detected using Supersignal West Femto Chemiluminescent substrate (Thermo Fisher Scientific, Rockford IL, USA) and a Gel Doc Imaging system equipped with a XRS camera and Quantity One analysis software (Bio-Rad). Glyceraldehyde 3-phosphate dehydrogenase (GAPDH, Trevigen Biotechnology, Gaithersburg, MD (Maryland), USA) was used as a protein loading control.

Phalloidin-FITC 50 μ g/mL (Sigma-Aldrich, St. Louis, MO, USA) a marker for actin myofilaments (green) was used, according to the manufacturer's instructions. Cells were seeded in chamber slides at a density of 5×10^4 /chamber, allowed to settle for 24 hours, and then exposed to high glucose and SB as described above. Treated cells were then stained with phalloidin-FITC. Images of cells were documented at a magnification of 20x, using an inverted microscope Olympus BX40 equipped with an Olympus CKX-RFA fluorescent lamp and an E330 camera (Olympus, Hamburg, Germany).

2.5. Statistical Analysis. The statistical significance of the differences between the control group and the treated groups was assessed with the nonparametric Kruskal-Wallis test for multiple groups, followed by a post hoc analysis using the Conover test. Correlation coefficients between parameters have been calculated using Spearman's correlation coefficient for ranks (ρ). Statistical tests were performed using MedCalc version 18.11.3 and GraphPad Prism Software version 8.0.2. The results were considered statistical significant at $p < 0.05$.

3. Results

3.1. Chemical Characterization of the SB. The SB structure was confirmed by elemental analysis and on the basis of its mass spectrum (MS), infrared spectrum (IR), and nuclear magnetic resonance (^1H NMR and ^{13}C NMR) spectra [21].

4-(3-Bromobenzylideneamino)-5-(4-methyl-2-phenylthiazol-5-yl)-4H-1,2,4-triazole-3-thiol. Yield 80.3% (0.366 g); m.p. 268-270°C; light yellow powder; Anal. Calcd for $\text{C}_{19}\text{H}_{14}\text{BrN}_5\text{S}_2$ (456.38): C, 49.89; H, 3.06; N, 15.33; S, 14.02; Found: C, 50.1; H, 3.07; N, 15.33; S, 14.07; IR (ATR, cm^{-1}): 3104 (ν $\text{NH}_{\text{triazole}}$), 1618 (ν -N=CH-), 1274 (ν C=S); 1055 (ν C-Br); ^1H NMR (500 MHz, $\text{DMSO-}d_6$, δ/ppm): 14.18 (s, 1H, NH), 9.52 (s, 1H, -N=CH-), 7.97-8.06

TABLE 1: Inhibition zone diameters on tested microorganisms.

Samples	Diameter of the inhibition zone (mm)				
	SA	LM	EC	ST	CA
<i>Schiff base</i>	14	14	14	18	18
Ciprofloxacin	28	18	27	22	—
Fluconazole	—	—	—	—	25

SA: *Staphylococcus aureus*; LM: *Listeria monocytogenes*; EC: *Escherichia coli*; ST: *Salmonella typhimurium*; CA: *Candida albicans*.

(d, 2H, ArH), 7.92 (s, 1H, ArH), 7.77 (d, 1H, ArH), 7.59 (d, 1H, ArH), 7.47-7.54 (m, 4H, ArH), 2.41 (s, 3H, CH_3); ^{13}C NMR (125 MHz, $\text{DMSO-}d_6$, δ/ppm): 170.12 (C=S), 159.15 (C), 157.66 (CH=N), 153.81 (C), 151.07 (C), 143.96 (C), 135.16 (C), 134.51 (C), 131.21 (CH), 130.93 (2CH), 130.29 (CH), 129.29 (2CH), 128.94 (CH), 128.68 (C), 127.36 (CH), 127.14 (CH), 15.92 (CH_3); MS (EI, 70 eV) m/z (%): 457 (M+1).

3.2. Antimicrobial Activity. Results obtained by measuring the diameters of growth inhibition zones of the tested microorganisms, compared to ciprofloxacin and fluconazole, used as standard reference drugs, are presented in Table 1.

MIC, MBC, and MFC values of the new compound are presented in Tables 2 and 3. The results showed that MIC values ranged from 1.95 (*Listeria monocytogenes*) to 62.5 $\mu\text{g/mL}$, MBC values were between 3.9 and 125 $\mu\text{g/mL}$, and MFC scores ranged between 62.5 and 125 $\mu\text{g/mL}$.

3.3. In Vitro Antioxidant Capacity. The antioxidant capacity of the SB was determined by the DPPH bleaching method, and BHT and trolox were used as positive controls. The results are displayed in Table 4. The new compound showed a very low IC_{50} value (16.10 $\mu\text{g/mL}$), similar to that of BHT (16.39 $\mu\text{g/mL}$).

3.4. Cell Viability. SB did not lead to significant changes in HUVEC viability for doses lower than 0.1 $\mu\text{g/mL}$ (Figure 1). Higher concentrations led to a dose-dependent viability decrease, compared with control.

3.5. Assessment of the Ability of the SB to Modulate Inflammatory Response and Oxidative Stress on HUVECs. Lipid peroxidation level (MDA), the ability to modulate inflammatory response (TNF- α , COX2), and the activity of enzymes involved in the prooxidant/antioxidant equilibrium (SOD1, NOS2) were appreciated. The ability of the SB to modulate oxidative stress was tested *in vitro* on HUVECs, using a glucose-enriched medium [36-38]. A SB concentration of 0.001 $\mu\text{g/mL}$ was used for all experiments.

The effect of the newly synthesized compound on lipid peroxidation (MDA level) was assessed. SB administration decreased the MDA level compared with both control and glucose-enriched medium, thus reducing the lipid peroxidation in endothelial cells (Figure 2).

The TNF- α level was quantified through ELISA for the same SB concentration (Figure 3). Glucose-enriched medium slightly increased the TNF- α level. SB also increased the TNF- α level both alone and in combination with glucose.

TABLE 2: Minimum inhibitory concentrations (MIC).

Samples	Minimum inhibitory concentration (MIC ($\mu\text{g}/\text{mL}$))					
	SA	LM	PA	ST	CA (ATCC 10231)	CA (ATCC 18804)
Schiff base	31.25	1.95	1.95	62.5	62.5	31.25
Ciprofloxacin	1.95	3.9	3.9	0.97	—	—
Fluconazole	—	—	—	—	62.5	62.5

SA: *Staphylococcus aureus*; LM: *Listeria monocytogenes*; PA: *Pseudomonas aeruginosa*; ST: *Salmonella typhimurium*; CA: *Candida albicans*.

TABLE 3: Minimum bactericidal (MBC) and minimum fungicidal concentrations (MFC).

Samples	MBC ($\mu\text{g}/\text{mL}$)				MFC ($\mu\text{g}/\text{mL}$)		
	SA	LM	PA	ST	CA (ATCC 10231)	CA (ATCC 18804)	CK (ATCC 6258)
Schiff base	62.5	3.9	3.9	125	125	62.5	62.5
Ciprofloxacin	3.9	7.8	7.8	1.95	—	—	—
Fluconazole	—	—	—	—	125	125	125

SA: *Staphylococcus aureus*; LM: *Listeria monocytogenes*; PA: *Pseudomonas aeruginosa*; ST: *Salmonella typhimurium*; CA: *Candida albicans*; CK: *Candida krusei*.

TABLE 4: Antioxidant capacity using the DPPH method.

Samples	IC ₅₀ ($\mu\text{g}/\text{mL}$)
Schiff base	16.10 \pm 1.2
BHT	16.39 \pm 0.9
Trolox	11.98 \pm 0.4

The same SB concentration (0.001 $\mu\text{g}/\text{mL}$) was used to further test its effect on the protein level of the enzymes involved in the oxidant/antioxidant equilibrium and in the inflammatory response (SOD1, NOS2, and COX2).

An inflammatory marker (COX2) and antioxidant enzyme (constitutive SOD1 and inducible NOS2) expression was quantified by Western Blot (Figure 4).

COX2, an inflammatory marker, significantly decreased after both glucose and SB treatments, compared to control. Combined exposure (SB+G) strongly decreased the protein level of COX2 (Figure 4(b)). This finding is consistent with MDA levels and may be due to the antioxidant effect of the SB in this experimental setting. Interestingly, it is not consistent with TNF- α , a fact which might be explained by a different mechanism than oxidative stress that triggers an increase of TNF- α . Exposure to glucose-enriched medium significantly decreased SOD1. SB slightly decreased SOD1 activity compared with the control group, but SOD1 activity was maintained at a significantly higher level, compared with glucose ($p < 0.05$). Combination (SB+G) treatment significantly decreased SOD1 compared with both glucose and control (Figure 4(c)). Exposure to glucose increased significantly NOS2. The SB drastically decreased the NOS2 level compared with both the control and glucose groups (Figure 4(d)).

Correlation analysis, using Spearman's coefficient for rank correlation (Table 5), revealed statistically significant positive correlations between MDA and enzyme (COX2, SOD1, and NOS2) levels. On the other hand, the TNF- α level negatively correlates with both MDA and all enzymes measured.

Cell morphology does not seem to be affected by exposure to the Schiff base compared to control. When exposed to high-glucose concentration, cells had a tendency to conglomerate and to form multilayered spherical bodies, with alteration of the actin filament disposition. The aspect of the cells receiving combination treatment was similar to those of controls (Figure 5).

4. Discussion

The structure of the Schiff base was established by elemental analysis and on the basis of its mass spectrum (MS), infrared spectrum (IR), and nuclear magnetic resonance (^1H -NMR and ^{13}C -NMR) spectra. The results of the C, H, N, S quantitative elemental analysis were in agreement with the calculated values, within $\pm 0.4\%$ of the theoretical values. The spectral data confirmed the formation of the SB. The recorded mass spectrum revealed the correct molecular ion peak ($M + 1$), as suggested by the molecular formula. The absence of the NH_2 asymmetric and symmetric stretching vibrations at 3281 cm^{-1} and 3186 cm^{-1} , and the presence of $\text{N}=\text{CH}$ stretch absorption bands at 1618 cm^{-1} in the IR spectrum of the final compound provided strong evidences for the formation of the SB. The ^1H -NMR spectrum of the starting compound was recorded a signal characteristic for the amino protons, as a singlet, at 5.73 ppm. The absence of this signal from the ^1H -NMR spectrum of the newly synthesized compound and the presence of a singlet characteristic to the $\text{N}=\text{CH}$ proton at 9.52 ppm further confirmed the condensation between the 4-amino-5-(4-methyl-2-phenylthiazol-5-yl)-4H-1,2,4-triazole-3-thiol and the 3-bromo-phenyl-carbaldehyde. The ^{13}C -NMR spectrum of the newly synthesized compound was consistent with the proposed structure.

The aim of the present study was to evaluate the antibacterial and antifungal activity of a new SB as well as its ability to modulate oxidative stress.

The new thiazolyl SB exerted moderate to good antibacterial activity against tested strains (Tables 1–3). The inhibition of bacterial growth was more pronounced in Gram-negative bacteria, especially in *Pseudomonas aeruginosa* strain, where

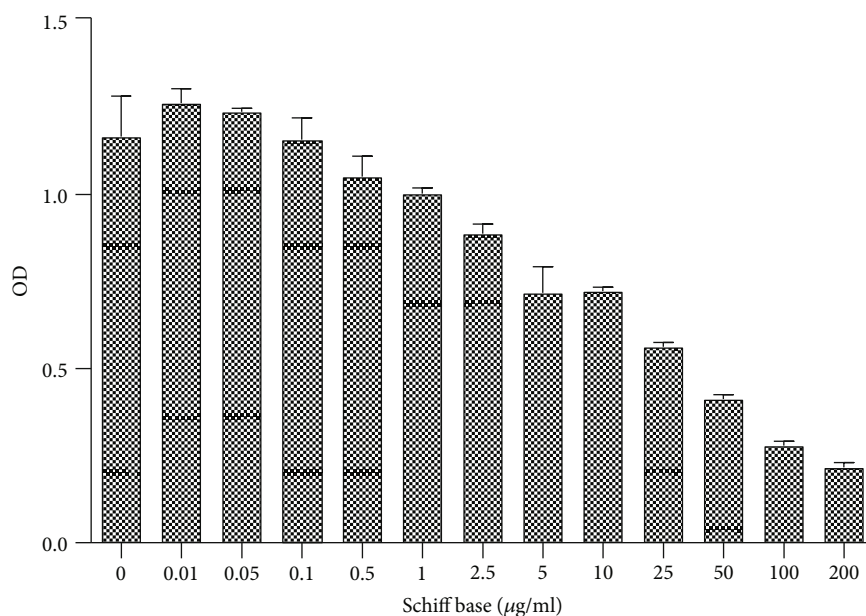


FIGURE 1: Cell viability testing. Schiff base (SB) was tested for multiple concentrations (0.01-200 µg/mL). Cell viability is presented as OD 540 nm (mean values ± standard deviation at 540 nm, $n = 3$).

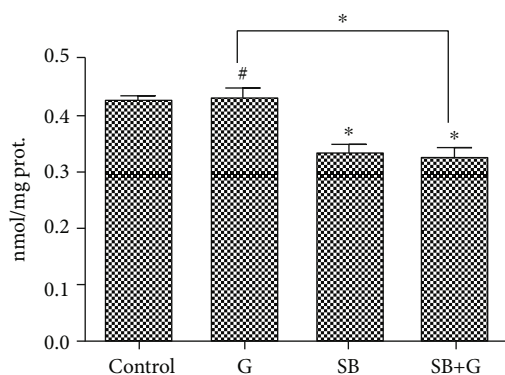


FIGURE 2: Lipid peroxidation levels (MDA) in endothelial cells exposed to medium (control), glucose (G), Schiff base (SB), and combination treatment (SB+G). Each bar represents the mean ± standard deviation ($n = 3$). #Not significant. * $p < 0.05$.

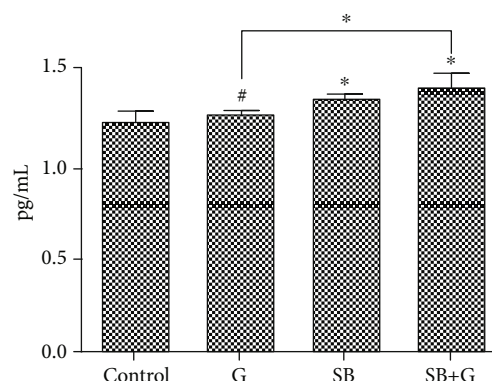


FIGURE 3: TNF-α levels in endothelial cells exposed to medium (control), glucose (G), Schiff base (SB), and combination treatment (SB+G). Each bar represents the mean ± standard deviation ($n = 3$). #Not significant. * $p < 0.05$.

the SB showed better activity compared with ciprofloxacin, used as the reference drug. Regarding antifungal activity, the compound showed a better anti-*Candida* effect than fluconazole, used as the reference drug. Previous studies showed that SBs have the ability to modulate oxidative stress [17, 39]. This ability can be exploited in order to use them as antibacterial drugs and/or as potential oxidative stress modulators in medicine. The SB was tested on endothelial cells exposed to a glucose-enriched environment.

High-carbohydrate intake, impaired glucose tolerance, and diabetes mellitus lead to hyperglycemia and chronic inflammatory status. Endothelial lesions are often involved in the pathology of these conditions [40]. During inflammatory episodes, such as response to injury, nitric oxide (NO) is released in order to modulate vascular tone. Since glycocalyx

plays an important role in transducing the fluid stress to the cytoskeleton of the endothelial cells, vasodilator substance production is stimulated [40–42]. High-glucose concentration increases oxidative stress and influences the structure of the cytoskeleton. Exposure to high-glucose hyperosmolar medium induces, using an AQP1-dependent mechanism, remodeling of the F-actin and cytoskeleton [43]. Our results are consistent with these findings (Figure 5). A high-glucose level led to mitochondrial dysfunction and increased production of ROS [44, 45].

A glucose-enriched environment also triggers the release of proinflammatory cytokines, such as tumor necrosis factor alpha (TNF-α), by the cells involved in immune reactions [46, 47], along with other proinflammatory molecules, such as CRP, interleukin 6, intercellular adhesion molecule 1, and VCAM-1. In diabetic patients, TNF-α was related with

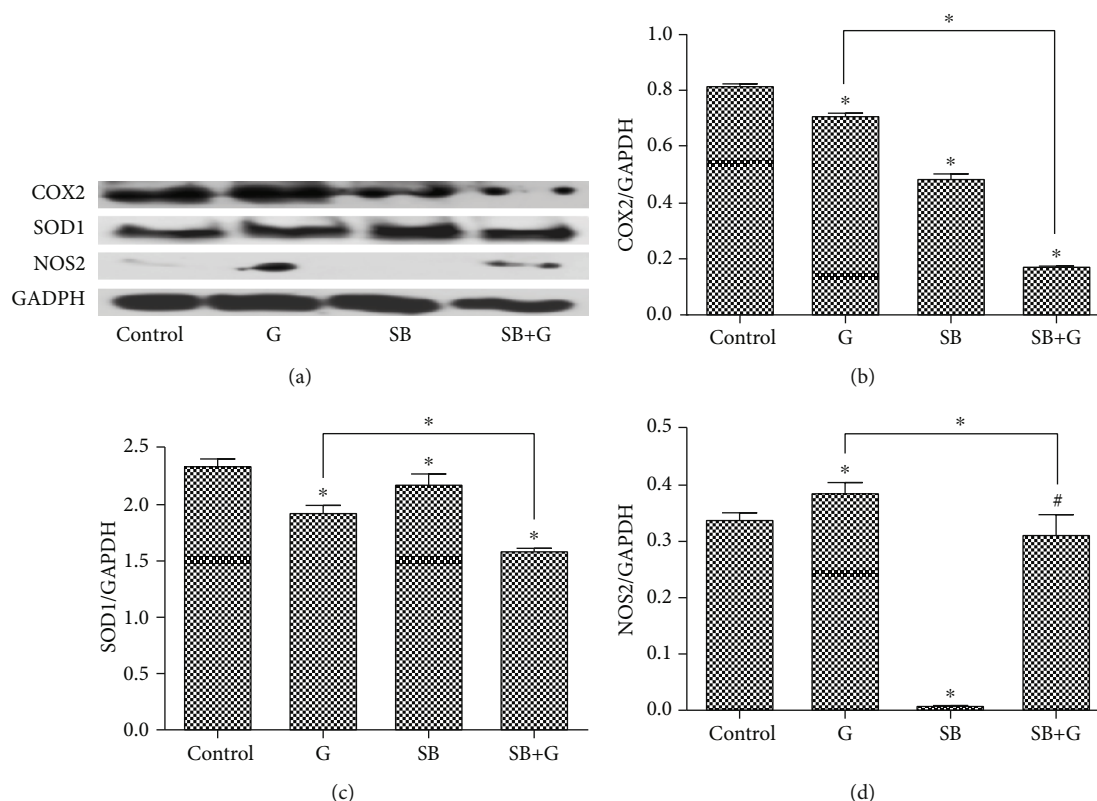


FIGURE 4: Protein levels of COX2, SOD1, and NOS2 in endothelial cells exposed to medium (control), glucose (G), Schiff base (SB), and combination treatment (SB+G). Comparative Western blot images showing expressions of COX2, SOD1, and NOS2 in HUVECs (b, c, d). Image analysis of Western blot bands (a) was performed by densitometry; results were normalized to GAPDH. Each bar represents the mean \pm standard deviation ($n = 3$). #Not significant. * $p < 0.05$.

an atherogenic profile and with vascular complications [48]. A similar effect was obtained in our study, where higher levels of TNF- α were observed after hyperglycemia exposure. This effect was also seen after SB treatment and was augmented by the combined SB and high-glucose concentration. However, TNF- α production was negatively correlated with MDA and antioxidant enzymes (Table 5). This suggests that the increased TNF- α was not produced through enhanced oxidative stress, but through a different mechanism. Its clarification requires further studies. Since TNF- α acts as a promoter of leucocyte adhesion to the endothelium, the SB might be beneficial as antimicrobial, local immune response, and oxidative status modulator in the treatment of infectious diseases.

The results obtained by the DPPH study showed that the SB exhibited antioxidant activity. The low IC₅₀ value, similar to the positive control (BHT), reflects a strong antioxidant activity *in vitro*. The new compound showed radical scavenging activity according to the DPPH method, the presence of the -SH group being probably responsible of the radical scavenging activity [49–51]. The effect of the SB on the oxidative stress was also tested *in vitro* on cell cultures (HUVECs), by assessing the MDA level, a marker of lipid peroxidation and the expression of two enzymes involved in the oxidative equilibrium (SOD1 and NOS2). The results showed that, at the tested concentration (0.001 $\mu\text{g}/\text{mL}$), SB decreased lipid peroxidation (MDA) and the protein level of certain enzymes

TABLE 5: Spearman's coefficient of rank correlation (ρ) between the oxidative stress and inflammation markers in HUVECs.

	MDA	TNF- α	COX2	SOD1	NOS2
MDA	1.00	-0.776**	0.699*	0.462	0.595*
TNF- α		1.00	-0.818**	-0.566	-0.455
COX2			1.00	0.755**	0.431
SOD1				1.00	-0.144
NOS2					1.00

* $p < 0.05$, ** $p < 0.01$.

involved in the modulation of oxidative stress and inflammatory response (COX2 and NOS2). These changes are consistent with the DPPH result and suggest an anti-inflammatory effect of the tested SB, mostly by interfering with the prooxidant mediators.

The ability of the SB, in low concentrations, to decrease lipid peroxidation, might be explained by its capacity to form complexes with the bivalent and trivalent metal ions located in the active center of the enzymes involved in the onset of the oxidative stress or in the scavenging of the prooxidant molecules [52–57]. The antioxidant effect on the human cells (Figures 2 and 4) is also consistent with the absence of morphological changes of the cells observed in the present study (Figure 5).

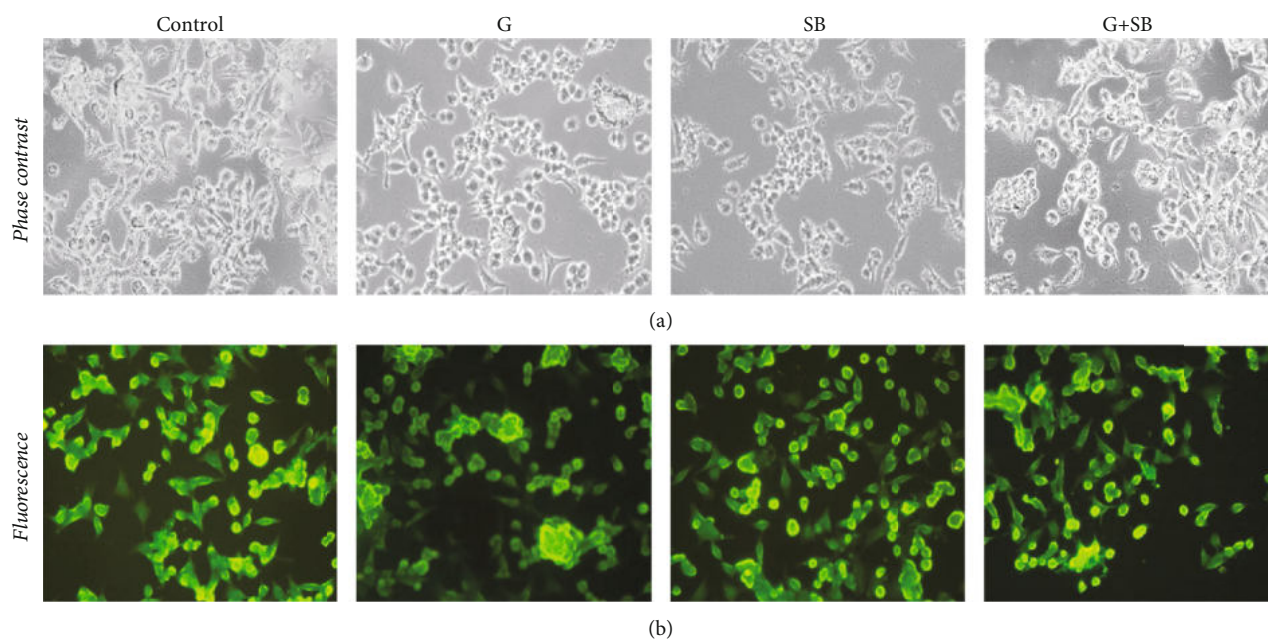


FIGURE 5: Images of HUVECs treated with medium (control), glucose (G), Schiff base (SB), and combination treatment (SB+G), stained with phalloidin-FITC; the same microscopic field is presented as phase contrast images (a) and fluorescence images (b) for comparison (pictures taken through an Olympus BX inverted microscope, original magnification 20x).

Considering antibacterial activity, especially against *Pseudomonas aeruginosa*, the decrease of the NOS2 protein level in HUVECs after SB exposure, it might be possible that the synthesis of NO by bacteria could also be reduced. One of the many proposed roles of NO in bacteria is to help protect the bacteria from host cell antibiotic-induced oxidative stress; therefore, the inhibition of bacterial nitric oxide synthase has been identified as a promising antibacterial strategy, especially for resistant bacteria [58].

Nitric oxide synthase (NOS) inhibitor NO-donating drugs were reported to inhibit IL-1 β production, modulate PGE₂ production, and protect against apoptosis in human endothelial cells and human monocytes [59]. In type 2 diabetes, hyperglycemia stimulates endothelial cell migration in the retina, leading to retina neoangiogenesis and visual impairment by CXC receptor-4 stimulation and activation of the PI3K/Akt/eNOS signaling pathway. Therefore, SB modulation of the NOS2 might be beneficial for the endothelial dysfunction in hyperglycemia [60, 61].

Recent studies showed that the antibacterial and antifungal activity in general and antibiofilm activity of some newly identified classes seem to correlate with their ability to induce ROS synthesis [5]. The SB showed an anti-*Candida* effect, with a twofold increased activity compared with the consecrated antifungal fluconazole (Tables 2 and 3). Also, the results showed that SB reduced the SOD1 level and increased the activity of the proinflammatory cytokine (TNF- α). The antifungal effect could also be explained by the ability of the tested SB to form complexes between the azomethine group and the metal from the active center of the enzymes and also by its capacity to induce ROS production, similar with some antifungal azoles (e.g., miconazole) [5].

Additional studies are needed in order to clarify the effect of such compounds as SB and their role as adjuvant antioxidant, antimicrobial, and local immune response modulators (TNF- α) in the treatment of infectious diseases.

5. Conclusions

The new Schiff base exhibited antibacterial effects on both Gram-positive and Gram-negative bacteria, as well as antifungal activity against *Candida albicans*. The results of the present study show that the new SB plays a role in the prooxidant/antioxidant equilibrium. In the tested dose, SB does not change endothelial cell morphology, has an antioxidant effect, as demonstrated by the DPPH test, decreased lipid peroxidation (MDA), and decreased the inducible NOS2 level. Therefore, it can be considered a potential candidate with promising antioxidant properties that may be used as an adjuvant therapy in diseases caused by excessive free radical production. The decrease in COX2 and NOS2 levels also might suggest an anti-inflammatory action. A possible mechanism for the antibacterial activity on Gram-negative bacilli could include the decrease of the bacterial NOS level and the formation of complexes with metals located in the active center of certain bacterial enzymes. Also, the SB might potentially act as an antifungal agent, through ROS production in fungal biofilm cells. Its clarification requires further studies.

Data Availability

The data used to support the findings of this study are included within the article.

Conflicts of Interest

The authors declare that there is no conflict of interest regarding the publication of this paper.

Authors' Contributions

Cristian Cezar Login, Şoimiţa Suci, Ioana Bâldea, and Brînduşa Tipericiu conceived and planned the experimental design. Brînduşa Tipericiu performed the chemical synthesis and the characterization of the compounds. Dan Cristian Vodnar performed the antibacterial and antifungal investigation. Daniela Benedec performed the *in vitro* assessment of the antioxidant activity. Ioana Bâldea performed the *in vitro* testing on cell cultures. Nicoleta Decea performed the biochemical assessment of some oxidative stress markers. Cristian Cezar Login and Ioana Bâldea performed the statistical analysis. Cristian Cezar Login, Ioana Bâldea, Brînduşa Tipericiu, Daniela Benedec, and Şoimiţa Suci analyzed the data and wrote the paper. Cristian Cezar Login, Brînduşa Tipericiu, Ioana Bâldea, and Daniela Benedec equally contributed to this work.

Acknowledgments

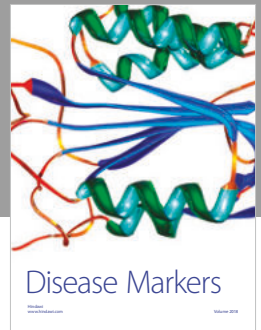
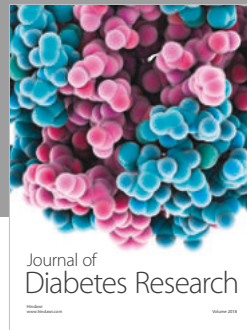
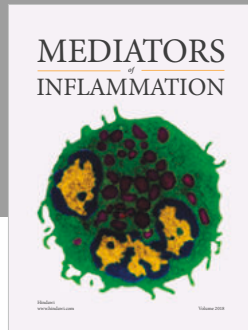
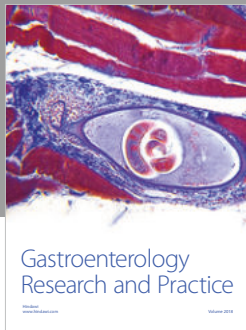
This research was funded by "Iuliu Haţieganu" University of Medicine and Pharmacy Cluj-Napoca internal research grant No. 4944/23/08.03.2016 (Cristian Cezar Login).

References

- [1] F. Aktan, "iNOS-mediated nitric oxide production and its regulation," *Life Sciences*, vol. 75, no. 6, pp. 639–653, 2004.
- [2] W. Droge, "Free radicals in the physiological control of cell function," *Physiological Reviews*, vol. 82, no. 1, pp. 47–95, 2002.
- [3] T. Fukai and M. Ushio-Fukai, "Superoxide dismutases: role in redox signaling, vascular function, and diseases," *Antioxidants & Redox Signaling*, vol. 15, no. 6, pp. 1583–1606, 2011.
- [4] B. D. McCollister, M. Hoffman, M. Husain, and A. Vázquez-Torres, "Nitric oxide protects bacteria from aminoglycosides by blocking the energy-dependent phases of drug uptake," *Antimicrobial Agents and Chemotherapy*, vol. 55, no. 5, pp. 2189–2196, 2011.
- [5] N. Delattin, B. P. Cammue, and K. Thevissen, "Reactive oxygen species-inducing antifungal agents and their activity against fungal biofilms," *Future Medicinal Chemistry*, vol. 6, no. 1, pp. 77–90, 2014.
- [6] L. Balanean, C. Braicu, I. Berindan-Neagoe et al., "Synthesis of novel 2-methylamino-4-substituted-1,3-thiazoles with antiproliferative activity," *Revista de Chimie-Bucharest*, vol. 65, pp. 1413–1417, 2014.
- [7] R. Tamaian, A. Moş, R. Silaghi-Dumitrescu et al., "Study of the relationships between the structure, lipophilicity and biological activity of some thiazolyl-carbonyl-thiosemicarbazides and thiazolyl-azoles," *Molecules*, vol. 20, no. 12, pp. 22188–22201, 2015.
- [8] Y. Ünver, K. Sancak, F. Çelik et al., "New thiophene-1,2,4-triazole-5(3)-ones: highly bioactive thiosemicarbazides, structures of Schiff bases and triazole-thiols," *European Journal of Medicinal Chemistry*, vol. 84, pp. 639–650, 2014.
- [9] G. Y. Nagesh, K. Mahendra Raj, and B. H. M. Mruthyunjayaswamy, "Synthesis, characterization, thermal study and biological evaluation of Cu(II), Co(II), Ni(II) and Zn(II) complexes of Schiff base ligand containing thiazole moiety," *Journal of Molecular Structure*, vol. 1079, pp. 423–432, 2015.
- [10] E. M. Zayed and M. A. Zayed, "Synthesis of novel Schiff's bases of highly potential biological activities and their structure investigation," *Spectrochimica Acta. Part A, Molecular and Biomolecular Spectroscopy*, vol. 143, pp. 81–90, 2015.
- [11] K. P. Rakesh, H. M. Manukumar, and D. C. Gowda, "Schiff's bases of quinazolinone derivatives: synthesis and SAR studies of a novel series of potential anti-inflammatory and antioxidants," *Bioorganic & Medicinal Chemistry Letters*, vol. 25, no. 5, pp. 1072–1077, 2015.
- [12] N. Parmar, S. Teraiya, R. Patel, H. Barad, H. Jajda, and V. Thakkar, "Synthesis, antimicrobial and antioxidant activities of some 5-pyrazolone based Schiff bases," *Journal of Saudi Chemical Society*, vol. 19, no. 1, pp. 36–41, 2015.
- [13] M. Yıldız, Ö. Karpuz, C. T. Zeyrek et al., "Synthesis, biological activity, DNA binding and anion sensors, molecular structure and quantum chemical studies of a novel bidentate Schiff base derived from 3,5-bis(trifluoromethyl)aniline and salicylaldehyde," *Journal of Molecular Structure*, vol. 1094, pp. 148–160, 2015.
- [14] N. El-wakiel, M. El-keiy, and M. Gaber, "Synthesis, spectral, antitumor, antioxidant and antimicrobial studies on Cu(II), Ni(II) and Co(II) complexes of 4-[(1H-benzimidazol-2-ylimino)-methyl]-benzene-1,3-diol," *Spectrochimica Acta. Part A, Molecular and Biomolecular Spectroscopy*, vol. 147, pp. 117–123, 2015.
- [15] S. A. Al-Harbi, M. S. Bashandy, H. M. Al-Saidi, A. A. A. Emar, and T. A. A. Mousa, "Synthesis, spectroscopic properties, molecular docking, anti-colon cancer and anti-microbial studies of some novel metal complexes for 2-amino-4-phenylthiazole derivative," *Spectrochimica Acta. Part A, Molecular and Biomolecular Spectroscopy*, vol. 145, pp. 425–439, 2015.
- [16] R. Selwin Joseyphus, C. Shiju, J. Joseph, C. Justin Dhanaraj, and D. Arish, "Synthesis and characterization of metal complexes of Schiff base ligand derived from imidazole-2-carboxaldehyde and 4-aminoantipyrine," *Spectrochimica Acta. Part A, Molecular and Biomolecular Spectroscopy*, vol. 133, pp. 149–155, 2014.
- [17] N. Turan, M. F. Topçu, Z. Ergin et al., "Pro-oxidant and anti-proliferative effects of the 1,3,4-thiadiazole-based Schiff base and its metal complexes," *Drug and Chemical Toxicology*, vol. 34, no. 4, pp. 369–378, 2011.
- [18] S. Gupta, A. Roy, and B. S. Dwarakanath, "Metabolic cooperation and competition in the tumor microenvironment: implications for therapy," *Frontiers in Oncology*, vol. 7, p. 68, 2017.
- [19] K. Zhao, D. Li, W. Xu et al., "Targeted hydroxyethyl starch prodrug for inhibiting the growth and metastasis of prostate cancer," *Biomaterials*, vol. 116, pp. 82–94, 2017.
- [20] C. Nastasă, B. Tipericiu, M. Duma, D. Benedec, and O. Oniga, "New hydrazones bearing thiazole scaffold: synthesis, characterization, antimicrobial, and antioxidant investigation," *Molecules*, vol. 20, no. 9, pp. 17325–17338, 2015.
- [21] A. Stana, A. Enache, D. Vodnar et al., "New thiazolyl-triazole Schiff bases: synthesis and evaluation of the anti-Candida potential," *Molecules*, vol. 21, no. 11, p. 1595, 2016.
- [22] C. Nastasă, D. Vodnar, I. Ionuţ et al., "Antibacterial evaluation and virtual screening of new thiazolyl-triazole Schiff bases as

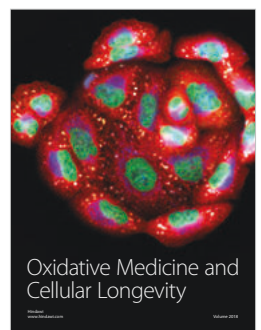
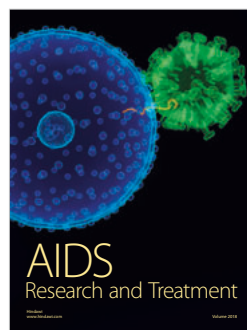
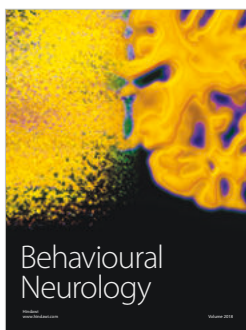
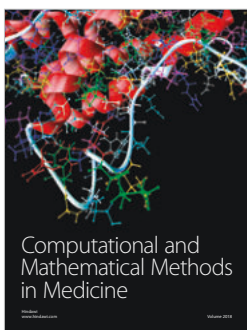
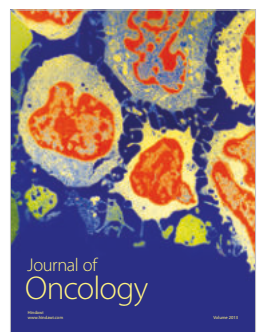
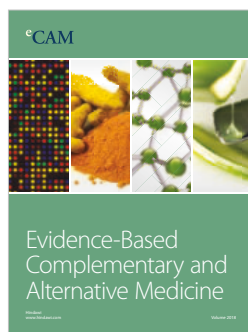
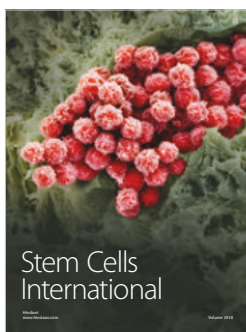
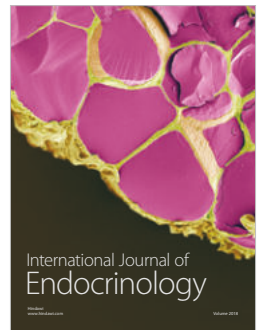
- potential DNA-gyrase inhibitors,” *International Journal of Molecular Sciences*, vol. 19, no. 1, p. 222, 2018.
- [23] A. Stana, D. Vodnar, R. Tamaian et al., “Design, synthesis and antifungal activity evaluation of new thiazolin-4-ones as potential lanosterol 14 α -demethylase inhibitors,” *International Journal of Molecular Sciences*, vol. 18, no. 1, p. 177, 2017.
- [24] M. A. Hassan, A. M. Omer, E. Abbas, W. M. A. Baset, and T. M. Tamer, “Preparation, physicochemical characterization and antimicrobial activities of novel two phenolic chitosan Schiff base derivatives,” *Scientific Reports*, vol. 8, no. 1, p. 11416, 2018.
- [25] M. Krátký, M. Dzurková, J. Janoušek et al., “Sulfadiazine salicylaldehyde-based Schiff bases: synthesis, antimicrobial activity and cytotoxicity,” *Molecules*, vol. 22, no. 9, p. 1573, 2017.
- [26] C. T. Zeyrek, B. Boyacıoğlu, M. Yıldız et al., “Synthesis, characterization, and evaluation of (E)-methyl 2-((2-oxonaphthalen-1(2H)-ylidene)methylamino)acetate as a biological agent and an anion sensor,” *Bioorganic & Medicinal Chemistry*, vol. 24, no. 21, pp. 5592–5601, 2016.
- [27] Y. Ünver, S. Deniz, F. Çelik, Z. Akar, M. Küçük, and K. Sancak, “Synthesis of new 1,2,4-triazole compounds containing Schiff and Mannich bases (morpholine) with antioxidant and antimicrobial activities,” *Journal of Enzyme Inhibition and Medicinal Chemistry*, vol. 31, no. sup3, pp. 89–95, 2016.
- [28] W. Yehye, N. Abdul Rahman, O. Saad et al., “Rational design and synthesis of new, high efficiency, multipotent Schiff base-1,2,4-triazole antioxidants bearing butylated hydroxytoluene moieties,” *Molecules*, vol. 21, no. 7, p. 847, 2016.
- [29] E. S. Lima, A. C. S. Pinto, K. L. Nogueira et al., “Stability and antioxidant activity of semi-synthetic derivatives of 4-nerolidylcatechol,” *Molecules*, vol. 18, no. 1, pp. 178–189, 2013.
- [30] D. Benedec, L. Vlase, I. Oniga et al., “Polyphenolic composition, antioxidant and antibacterial activities for two Romanian subspecies of *Achillea distans* Waldst. et Kit. ex Willd.,” *Molecules*, vol. 18, no. 8, pp. 8725–8739, 2013.
- [31] I. Baldea, G. E. Costin, Y. Shellman et al., “Biphasic pro-melanogenic and pro-apoptotic effects of all-trans-retinoic acid (ATRA) on human melanocytes: time-course study,” *Journal of Dermatological Science*, vol. 72, no. 2, pp. 168–176, 2013.
- [32] I. Baldea, D. E. Olteanu, P. Bolfa et al., “Efficiency of photodynamic therapy on WM35 melanoma with synthetic porphyrins: role of chemical structure, intracellular targeting and antioxidant defense,” *Journal of Photochemistry and Photobiology. B*, vol. 151, pp. 142–152, 2015.
- [33] D. Tudor, I. Nenu, G. A. Filip et al., “Combined regimen of photodynamic therapy mediated by Gallium phthalocyanine chloride and metformin enhances anti-melanoma efficacy,” *PLoS One*, vol. 12, no. 3, p. e0173241, 2017.
- [34] M. L. Hu, “[41] Measurement of protein thiol groups and glutathione in plasma,” *Methods in Enzymology*, vol. 233, pp. 380–385, 1994.
- [35] A. Filip, D. Daicovicu, S. Clichici, T. Mocan, A. Muresan, and I. D. Postescu, “Photoprotective effects of two natural products on ultraviolet B-induced oxidative stress and apoptosis in SKH-1 mouse skin,” *Journal of Medicinal Food*, vol. 14, no. 7–8, pp. 761–766, 2011.
- [36] J. Shen, M. Liu, J. Xu, B. Sun, H. Xu, and W. Zhang, “ARL15 overexpression attenuates high glucose-induced impairment of insulin signaling and oxidative stress in human umbilical vein endothelial cells,” *Life Sciences*, vol. 220, pp. 127–135, 2019.
- [37] R. Chibber, P. A. Molinatti, and E. M. Kohner, “Intracellular protein glycation in cultured retinal capillary pericytes and endothelial cells exposed to high-glucose concentration,” *Cellular and Molecular Biology (Noisy-le-Grand, France)*, vol. 45, no. 1, pp. 47–57, 1999.
- [38] R. J. Esper, J. O. Vilariño, R. A. Machado, and A. Paragano, “Endothelial dysfunction in normal and abnormal glucose metabolism,” *Advances in Cardiology*, vol. 45, pp. 17–43, 2008.
- [39] J. Joseph and G. B. Janaki, “Copper complexes bearing 2-aminobenzothiazole derivatives as potential antioxidant: synthesis, characterization,” *Journal of Photochemistry and Photobiology. B*, vol. 162, pp. 86–92, 2016.
- [40] N. W. Hansen, A. J. Hansen, and A. Sams, “The endothelial border to health: mechanistic evidence of the hyperglycemic culprit of inflammatory disease acceleration,” *IUBMB Life*, vol. 69, no. 3, pp. 148–161, 2017.
- [41] J. A. Florian, J. R. Kosky, K. Ainslie, Z. Pang, R. O. Dull, and J. M. Tarbell, “Heparan sulfate proteoglycan is a mechanosensor on endothelial cells,” *Circulation Research*, vol. 93, no. 10, pp. e136–e142, 2003.
- [42] S. Mochizuki, H. Vink, O. Hiramatsu et al., “Role of hyaluronic acid glycosaminoglycans in shear-induced endothelium-derived nitric oxide release,” *American Journal of Physiology. Heart and Circulatory Physiology*, vol. 285, no. 2, pp. H722–H726, 2003.
- [43] R. Madonna, Y. J. Geng, H. Shelat, P. Ferdinandy, and R. de Caterina, “High glucose-induced hyperosmolarity impacts proliferation, cytoskeleton remodeling and migration of human induced pluripotent stem cells via aquaporin-1,” *Biochimica et Biophysica Acta*, vol. 1842, no. 11, pp. 2266–2275, 2014.
- [44] W. Zhu, Y. Yuan, G. Liao et al., “Mesenchymal stem cells ameliorate hyperglycemia-induced endothelial injury through modulation of mitophagy,” *Cell Death & Disease*, vol. 9, no. 8, p. 837, 2018.
- [45] A. Pallag, G. A. Filip, D. Olteanu et al., “Equisetum arvense L. extract induces antibacterial activity and modulates oxidative stress, inflammation, and apoptosis in endothelial vascular cells exposed to hyperosmotic stress,” *Oxidative Medicine and Cellular Longevity*, vol. 2018, 14 pages, 2018.
- [46] R. D. Martinus and J. Goldsbury, “Endothelial TNF- α induction by Hsp60 secreted from THP-1 monocytes exposed to hyperglycaemic conditions,” *Cell Stress & Chaperones*, vol. 23, no. 4, pp. 519–525, 2018.
- [47] I. Castellano, P. di Tomo, N. di Pietro et al., “Anti-inflammatory activity of marine ovothiol A in an *in vitro* model of endothelial dysfunction induced by hyperglycemia,” *Oxidative Medicine and Cellular Longevity*, vol. 2018, 12 pages, 2018.
- [48] D. Tousoulis, N. Papageorgiou, E. Androulakis et al., “Diabetes mellitus-associated vascular impairment: novel circulating biomarkers and therapeutic approaches,” *Journal of the American College of Cardiology*, vol. 62, no. 8, pp. 667–676, 2013.
- [49] M. Kumar, T. Padmini, and K. Ponnuvel, “Synthesis, characterization and antioxidant activities of Schiff bases are of cholesterol,” *Journal of Saudi Chemical Society*, vol. 21, pp. S322–S328, 2017.
- [50] C. Aswathanarayanappa, E. Bheemappa, Y. D. Bodke, P. S. Krishnegowda, S. P. Venkata, and R. Ningegowda, “Synthesis and evaluation of antioxidant properties of novel 1,2,4-

- triazole-based schiff base heterocycles,” *Arch Pharm (Weinheim)*, vol. 346, no. 12, pp. 922–930, 2013.
- [51] N. Revathi, M. Sankarganesh, J. Rajesh, and J. D. Raja, “Biologically active Cu(II), Co(II), Ni(II) and Zn(II) complexes of pyrimidine derivative Schiff base: DNA binding, antioxidant, antibacterial and in vitro anticancer studies,” *Journal of Fluorescence*, vol. 27, no. 5, pp. 1801–1814, 2017.
- [52] M. Hajrezaie, S. Golbabapour, P. Hassandarvish et al., “Acute toxicity and gastroprotection studies of a new schiff base derived copper (II) complex against ethanol-induced acute gastric lesions in rats,” *PLoS One*, vol. 7, no. 12, p. e51537, 2012.
- [53] V. A. Daier, E. Rivière, S. Mallet-Ladeira, D. M. Moreno, C. Hureau, and S. R. Signorella, “Synthesis, characterization and activity of imidazolate-bridged and Schiff-base dinuclear complexes as models of Cu,Zn-SOD. A comparative study,” *Journal of Inorganic Biochemistry*, vol. 163, pp. 162–175, 2016.
- [54] Q. Wei, J. Dong, P. Zhao et al., “DNA binding, BSA interaction and SOD activity of two new nickel(II) complexes with glutamine Schiff base ligands,” *Journal of Photochemistry and Photobiology. B*, vol. 161, pp. 355–367, 2016.
- [55] C. Palopoli, G. Gómez, A. Foi et al., “Dimerization, redox properties and antioxidant activity of two manganese(III) complexes of difluoro- and dichloro-substituted Schiff-base ligands,” *Journal of Inorganic Biochemistry*, vol. 167, pp. 49–59, 2017.
- [56] P. Zhao, S. Zhai, J. Dong et al., “Synthesis, structure, DNA interaction, and SOD activity of three nickel(II) complexes containing L-phenylalanine Schiff base and 1,10-phenanthroline,” *Bioinorganic Chemistry and Applications*, vol. 2018, 16 pages, 2018.
- [57] S. Maghraoui, S. Clichici, A. Ayadi et al., “Oxidative stress in blood and testicle of rat following intraperitoneal administration of aluminum and indium,” *Acta Physiologica Hungarica*, vol. 101, no. 1, pp. 47–58, 2014.
- [58] J. K. Holden, M. C. Lewis, M. A. Cinelli et al., “Targeting bacterial nitric oxide synthase with aminoquinoline-based inhibitors,” *Biochemistry*, vol. 55, no. 39, pp. 5587–5594, 2016.
- [59] J. N. Sharma, A. Al-Omran, and S. S. Parvathy, “Role of nitric oxide in inflammatory diseases,” *Inflammopharmacology*, vol. 15, no. 6, pp. 252–259, 2007.
- [60] M. Botta, E. Distrutti, A. Mencarelli et al., “Anti-inflammatory activity of a new class of nitric oxide synthase inhibitors that release nitric oxide,” *ChemMedChem*, vol. 3, no. 10, pp. 1580–1588, 2008.
- [61] S. Hamed, B. Brenner, Z. Abassi, A. Aharon, D. Daoud, and A. Roguin, “Hyperglycemia and oxidized-LDL exert a deleterious effect on endothelial progenitor cell migration in type 2 diabetes mellitus,” *Thrombosis Research*, vol. 126, no. 3, pp. 166–174, 2010.



Hindawi

Submit your manuscripts at
www.hindawi.com



Article

5-Arylidene(chromenyl-methylene)-thiazolidinediones: Potential New Agents against Mutant Oncoproteins K-Ras, N-Ras and B-Raf in Colorectal Cancer and Melanoma

Cristina Nastasă^{1,*} , Radu Tamaian^{2,3,*} , Ovidiu Oniga¹ and Brîndușa Tipericiu¹ 

- ¹ Department of Pharmaceutical chemistry, Faculty of Pharmacy, “Iuliu Hațieganu” University of Medicine and Pharmacy, 41 Victor Babeș Street, RO-400012 Cluj-Napoca, Romania; onigao65@yahoo.com (O.O.); brandu32@yahoo.com (B.T.)
- ² National Research and Development Institute for Cryogenics and Isotopic Technologies, ICSI Analytics, 4th Uzinei Street, RO-240050 Râmnicu Vâlcea, Romania
- ³ SC Biotech Corp SRL, 4th Uzinei Street, RO-240050 Râmnicu Vâlcea, Romania
- * Correspondence: cmoldovan@umfcluj.ro (C.N.); radu.tamaian@gmail.com (R.T.); Tel.: +40-745-264-393 (C.N.)

Received: 18 December 2018; Accepted: 28 March 2019; Published: 31 March 2019



Abstract: *Background and objectives:* Cancer represents the miscommunication between and within the body cells. The mutations of the oncogenes encoding the MAPK pathways play an important role in the development of tumoral diseases. The mutations of KRAS and BRAF oncogenes are involved in colorectal cancer and melanoma, while the NRAS mutations are associated with melanoma. Thiazolidine-2,4-dione is a versatile scaffold in medicinal chemistry and a useful tool in the development of new antitumoral compounds. The aim of our study was to predict the pharmacokinetic/pharmacodynamic properties, the drug-likeness and lead-likeness of two series of synthetic 5-arylidene(chromenyl-methylene)-thiazolidinediones, the molecular docking on the oncoproteins K-Ras, N-Ras and B-Raf, and to investigate the cytotoxicity of the compounds, in order to select the best structural profile for potential anticancer agents. *Materials and Methods:* In our paper we studied the cytotoxicity of two series of thiazolidine-2,4-dione derivatives, their ADME-Tox properties and the molecular docking on a mutant protein of K-Ras, two isoforms of N-Ras and an isoform of B-Raf with 16 mutations. *Results:* The heterocyclic compounds strongly interact with K-Ras and N-Ras right after their posttranslational processing and/or compete with GDP for the nucleotide-binding site of the two GTPases. They are less active against the GDP-bound states of the two targets. All derivatives have a similar binding pattern in the active site of B-Raf. *Conclusions:* The data obtained encourage the further investigation of the 5-arylidene(chromenyl-methylene)-thiazolidinediones as potential new agents against the oncoproteins K-Ras, N-Ras and B-Raf.

Keywords: thiazolidine-2,4-dione; K-Ras; N-Ras; B-Raf; cytotoxicity; ADME-Tox; molecular docking

1. Introduction

Cancers are a group of diseases which can be perceived as miscommunications between the cells and within the cells. One of the most dangerous triggers that leads to cancers is the mutation of genes. Oncogenes are genes that encode proteins able to induce cancer via various metabolic pathways. Somatic mutations in genes encoding the mitogen-activated protein kinase (MAPK) pathways components occur frequently in various tumors, making them critical turning points in the development of human cancer [1]. Oncogenic mutations in MAPK signaling pathways frequently

affect the Ras proteins and the serine/threonine-protein kinase B-Raf (B-Raf) in the extracellular signal-regulated kinase pathway [1–3]. In this respect, the most common somatic mutations of Kirsten Rat Sarcoma Viral Oncogene Homolog KRAS and BRAF oncogenes are known to play an important role in the advance and progression of both colorectal cancer (CRC) and melanoma [1,2,4–11]. Moreover, Neuroblastoma Rat Sarcoma Viral Oncogene Homolog NRAS mutations also have a crucial role in the development of melanoma [7,9,12] and are becoming an emerging threat in CRC [13]. In a very recent review, Cicenias and collaborators suggested that the mutated oncoproteins of KRAS, NRAS and BRAF oncogenes could skip the normal activation stage [7].

Clinical studies revealed that the prevalence of KRAS mutations in codons 12 and 13 in the tumors of patients with metastatic CRC range from 35% to 42% [4,6,14], meanwhile the three most common mutations (G12D, G12V and G13D) account for approximately 75% of all KRAS mutations [6]. KRAS undergoes alternative splicing, resulting in two isoforms of GTPase KRas (K-Ras) that differ only in the C-terminal region [15,16] and both isoforms (K-Ras4A and K-Ras4B) are oncogenic when gene is mutated [5,15–17].

Mutations of NRAS appear in codons 12, 13 and 61 and arise in 15%–20% of all melanomas and the mutant GTPase NRas (N-Ras) has been associated with aggressive clinical behavior and poor prognosis [12].

The products of KRAS and NRAS genes (K-Ras and N-Ras isoforms) belong to the Ras proteins family [7,11,15,18] and are both small GTPases, having a 189 amino acids (AAs) length. Both GTPases are involved in cellular signal transduction, having a crucial role in the regulation of cell proliferation, differentiation and survival through various pathways. K-Ras and N-Ras act as molecular switches by cycling between their guanosine-5'-triphosphate bound (GTP-b) active state and their guanosine 5'-imidotriphosphate bound (GDP-b) inactive state [15,18]. Recently, a 20 AAs length isoform of N-Ras was found to be expressed in an aggressive cell phenotype of melanoma [19]. This 5th isoform of Ras proteins doesn't have GTPase activity and probably binds to another protein(s), to increase the aggressiveness of melanoma cells.

BRAF gene encodes B-Raf, a protein belonging to the protein kinase superfamily, the tyrosine-kinase like (TKL) serine/threonine-protein kinase family, and the RAF subfamily [7,8]. B-Raf plays an important role in regulating the MAP kinase/ERKs signaling pathway, which affects cell division, differentiation, and secretion. BRAF mutations have been associated with various cancers, somatic missense mutations appearing in 66% of malignant melanomas [8].

The conventional chemotherapy, due to its lack of action selectivity, has many adverse effects. The research conducted in the last years has aimed to achieve a better understanding of the mechanism of genesis and progression of malignant tumors, from where it is outlined the necessity of targeted therapies [20]. Discovering efficient gene inhibitors has become a valuable direction in fighting cancer. Some of the inhibitors may act as covalent binders [21–26]. 2,4-Thiazolidinedione (TZD) proved to be a very versatile scaffold in medicinal chemistry; the heterocycle itself or combined with other rings is a highly studied tool in cancer therapy. TZDs act mainly as agonist of the nuclear receptor PPAR γ . During recent years, numerous studies have been performed to understand their anticancer mechanism of action. It seems that TZDs exert PPAR γ -independent effects on a broad spectrum of signaling targets: Wnt signal transduction pathways, Raf/MEK/ERK and PI3K/Akt signaling pathway, DNAs and RNAs dependent interaction, PIM kinases inhibitor pathways, in producing antiproliferative or apoptotic activity in various cell lines [27–31]. The derivatives substituted with 5-arylidene/5-chromenyl-methylene and 3-benzylidene groups seem to express higher activity [27].

Based on our team's experience in the virtual screening, molecular docking, chemical synthesis and biological investigation of different heterocyclic-based compounds [32–34], we present here the investigation of the cytotoxicity of two series of 5-arylidene (chromenyl-methylene)-thiazolidine-2,4-diones, their ADME-Tox profiling and the molecular docking on K-Ras, N-Ras and B-Raf proteins.

2. Materials and Methods

2.1. Virtual Screening

VS carried out in this paper used two cheminformatics tools to accomplish its aim: an ADME-Tox predictor and a docking software.

Ligands: prior to VS, an academic license of MarvinSketch was used for drawing, displaying of 2D structure and 3D optimization of all ligands and generation of the required input files for ADME-Tox predictions (SDF files) and docking (Tripos MOL2 files), MarvinSketch 16.10.24.0, 2016, ChemAxon (<https://www.chemaxon.com>) [35].

Prediction of the ADME-Tox properties: was done with FAF-Drugs3 [36].

The previously generated SDF files were formatted accordingly FAF-Drugs3's requirements using the files formatter submodule—Bank Formatter. For the estimation of the lipophilicity and of the derived ADME-Tox descriptors, we used XLOGP3 [37], due to its high prediction precision [38]. A series of FAF-Drugs3's build-in filters for lead-likeness, drug-likeness, detection of non-peptidic inhibitors of protein-protein interactions (PPIs) [39], detection of undesirable moieties and substructures (UMSs) involved in toxicity problems [40–50], covalent inhibitors [51,52], Pan-Assay Interference Compounds (PAINS) [53,54] and a series of customized filters for safety profiling [44,55–57] were exploited for the ADME-Tox screening.

The Lead-Like Soft filter uses descriptors for lead-likeness [58–61], meanwhile the Drug-Like Soft filter is built on physico-chemical, molecular properties and bioavailability data, commonly encountered in the development of new drugs [58,62–65]. These soft filters use a build-in statistical analysis of drugs [36] from the e-Drugs3D library [65] for the threshold values of the computed parameters.

PPIs are required in a normal, healthy life, while the abnormal PPIs may lead to diseases. In consequence, they may be considered important targets in medicinal chemistry [66]. For this, FAF-Drugs3 uses a decision tree [39,67] built on two trained Dragon descriptors, Ui and RDF070m [68].

The detection of UMSs involved in toxicity was possible due to FAF-Drugs3 build-in filters, based on the literature data. Also, for identifying the covalent inhibitors (CIs), FAF-Drugs3 build-in filters were applied. Three filters (A, B and C) [36,53,69] were used in order to discover PAINS [45,46].

We investigated the safety profiling according to the GSK 4/400 rule [57], the Pfizer 3/75 rule [56], the estimation of phospholipidosis induction (PhI) [55], the MedChem rules [44] and the golden triangle (GT) rule [70]. The MedChem rules allow the identification of the molecules that may disturb the biological assays, allowing their removal from the screening. We used the MedChem rules in our screening process with the regular settings, involving a 100-demerit cutoff.

2.2. Molecular Docking

Targets: docking demands the 3D structure of a target, which contains its spatial coordinates, and for the target identification process it was necessary to cross-reference 3 on-line databases to identify the most adequate targets with a high-resolution 3D structure—a resolution higher than 2.0 Å being advised for the docking computations [71]: The Human Gene Database—GeneCards® (<http://www.genecards.org>) [72], The Universal Protein Resource—UniProt (<http://www.uniprot.org>) [73] and RCSB Protein Data Bank—RCSB-PDB (<http://www.rcsb.org>) [74]. The targets selected were: one of the most common mutants of K-Ras [6], the two isoforms of N-Ras (the canonical form and the short isoform) and an oncogenic B-Raf isoform with 16 mutations (Table 1).

Table 1. Targets selected for docking—3D structural data.

Protein	3D Structure Data	
	PBD ID (Mutation)	Resolution * (Å)
K-Ras	4DSU (G12D) [75]	1.70
N-Ras	3CON [TPB]	1.65
	2N9C ^{20AAs} [19]	NA
B-Raf	5ITA (I543A, I544S, I551K, Q562R, L588N, K630S, F667E, Y673S, A688R, L706S, Q709R, S713E, L716E, S720E, P722S, K723G) [76]	1.95

*: resolution is available only for 3D structures determined by X-ray crystallography; the term is not applicable for structures determined by Nuclear Magnetic Resonance (NMR) spectroscopy; ^{20AAs}: the 20 AAs length isoform of N-Ras (N-Ras isoform 5), expressed in an aggressive cell phenotype of melanoma; NA: not applicable; TPB: to be published, according to the RCSB-PDB site: <http://www.rcsb.org/pdb/explore/explore.do?structureId=2N9C>.

Docking set-up: all ligands were docked against the selected targets (Table 1), in separate runs, with PyRx—Python Prescription 0.9.5 [77] AutoDock Vina was used as the docking algorithm [78]. AutoDock Vina automatically calculates the grid maps [78] based on a scoring function, inspired by an X-score [79] and tuned with PDBbind data set [80,81], to predict noncovalent binding and clusters the results. The renderings of resulting 3D images were performed with the help of The Visualization ToolKit (VTK—Kitware, Inc. USA) (<http://www.kitware.com>) [82]—an embedded module of PyRx 0.9.5. Supplementary, Molegro Molecular Viewer 2.5 (Molegro, A CLC bio company, Aarhus N, Denmark) was performed for more advanced extraction of data and high resolution renderings of the individual poses. Docking runs against the corresponding PDB IDs (4DSU and 3CON) were carried out twice: with and without the GDP molecule bound in its pocket. Separate single docking runs were carried out for the N-Ras isoform 5 (2N9C) and for B-Raf (5ITA). The docking runs were realized setting an extended search space to completely cover the target, with a volume higher than 27.0 Å³, meanwhile the exhaustiveness was manually expanded 10 times from the default value (8), to increase the precision of all predictions [78,83].

2.3. Cytotoxicity

The murine cancer cell lines B16 (mouse melanoma) and CT26 (colorectal carcinoma) (Thermo Fisher Scientific, Waltham, MA, USA) were grown in Dulbecco's modified essential medium (DMEM). This was supplemented with 10% fetal bovine serum, 2 mM L-glutamine, 100 U/mL penicillin and 100 µg/mL streptomycin. The growing cancer cells were plated onto 96-well plates, at 5000 cells/well, in 200 µL DMEM. After 24 h, the cells were exposed, for 48 h, to dimethylsulfoxide (DMSO) and to the compounds' solutions, respectively. Stock solutions of compounds (10 mM) were diluted, in order to obtain solutions of different concentrations (100 µM, 50 µM, 25 µM, 12.5 µM, 6.25 µM and 3.125 µM) [34]. The MTT (1-(4,5-dimethylthiazol-2-yl)-3,5-diphenyltetrazolium) test was used to assess the viability of the cells. The number of the living cells, after 72 h of culture, directly proportional to the intensity of the blue color, was spectrophotometrically measured, at 562 nm, by a microplate reader (BioKinetics Reader EL340, Fisher Bioblock Scientific, Illkirch, France) [84]. Control cells were used and they were exposed to 1% DMSO. The experiments were repeated three times. The results obtained were quantified as the inhibitory concentrations for 50% of cells (IC₅₀), for a 48 h exposure time.

3. Results

3.1. Chemistry

The thiazolidinedione derivatives investigated for their cytotoxicity were previously synthesized, with the exception of compound 26, which was obtained according to the technique [85]:

5-((6-chloro-4-oxo-4H-chromen-3-yl)methylene)-3-(2-(4-methoxyphenyl)-2-oxoethyl)thiazolidine-2,4-dione (26): Yield 75%. Yellow powder, mp: 300 °C. ¹H NMR (DMSO-*d*₆, 500 MHz, ppm): δ 3.06 (s, 3H, -CH₃);

5.23 (s, 2H, -CH₂-); 7.12 (d, 2H, phenyl); 7.65 (d, 1H, C8-chromone-H); 7.71 (dd, 1H, C7-chromone-H); 7.75 (s, 1H, C = CH); 7.94 (s, 1H, C5-Chromone-H); 8.06 (d, 2H, phenyl); 8.95 (s, 1H, C2-chromone-H). Anal. Calcd. (%) for C₂₂H₁₄ClNO₆S (455.87): C, 57.96; H, 3.10; N, 3.07; S, 7.03. Found: C, 57.92; H, 3.09; N, 3.06; S, 7.05. MS (EI, 70 eV): m/z: 456.80 [M + 1].

3.2. Virtual screening (VS)—ADME-Tox predictions

A potential drug candidate has to correspond to some important drug features, such as: oral absorption, body distribution, metabolism, excretion, low toxicity, beside its pharmacological activity. This is why the virtual screening is extremely important in drug development, allowing the prediction of these parameters (ADME-Tox predictions), with the help of specialized software, before the effective lab synthesis. In our case, a license of MarvinSketch was involved in drawing and generating the 2D structures, 3D optimization of all ligands, and also for creating the input SDF files for the ADMET profiling and Tripos MOL2 files for docking (MarvinSketch 17.6.0, 2017, ChemAxon, Budapest, Hungary) [35]. Table 2 summarizes the results of the ADME-Tox screening carried out with FAF-Drugs3, for the lead-likeness and drug-likeness criteria.

Table 2. Virtual screening done with FAF-Drugs3, for lead-likeness and drug-likeness.

ID	MW (Da)	LogP	H _{BA}	H _{BD}	Tpsa (Å ²)	RtB	RiB	R _s	M _x S	C _s	HA	H/C	Crg	T _{Crg}	SC
DLS _{IV}	100–600	−3–6	≤12	≤5	≤180	≤11	≤30	≤6	≤18	3–35	1–15	0.1–1.1	≤3	−2–2	–
LLS _{IV}	150–400	−3–4	≤7	≤4	≤160	≤9	≤30	≤4	≤18	3–35	1–15	0.1–1.1	≤3	−2–2	≤2
1	457.36	5.29	4	0	103.81	4	25	4	6	20	7	0.35	0	0	0
2	457.36	5.29	4	0	103.81	4	25	4	6	20	7	0.35	0	0	0
3	457.36	5.29	4	0	103.81	4	25	4	6	20	7	0.35	0	0	0
4	394.47	4.25	5	1	124.04	4	25	4	6	20	7	0.35	0	0	0
5	394.47	4.25	5	1	124.04	4	25	4	6	20	7	0.35	0	0	0
6	394.47	4.25	5	1	124.04	4	25	4	6	20	7	0.35	0	0	0
7	412.91	5.23	4	0	103.81	4	25	4	6	20	7	0.35	0	0	0
8	412.91	5.23	4	0	103.81	4	25	4	6	20	7	0.35	0	0	0
9	447.36	5.86	4	0	103.81	4	25	4	6	20	8	0.40	0	0	0
10	447.36	5.86	4	0	103.81	4	25	4	6	20	8	0.40	0	0	0
11	447.36	5.86	4	0	103.81	4	25	4	6	20	8	0.40	0	0	0
12	423.46	4.43	7	0	149.63	5	27	4	6	20	9	0.45	0	0	0
13	423.46	4.43	7	0	149.63	5	27	4	6	20	9	0.45	0	0	0
14	408.49	4.57	5	0	113.04	5	25	4	6	21	7	0.33	0	0	0
15	408.49	4.57	5	0	113.04	5	25	4	6	21	7	0.33	0	0	0
16	290.36	2.48	4	0	103.81	3	18	3	6	13	6	0.46	0	0	0
17	321.74	2.64	5	0	92.89	1	20	2	10	14	7	0.50	0	0	0
18	335.76	3.00	5	0	92.89	2	20	2	10	15	7	0.47	0	0	0
19	348.31	1.06	7	2	135.98	2	22	2	10	15	9	0.60	0	0	0
20	301.32	2.38	5	0	92.89	1	20	2	10	15	6	0.40	0	0	0
21	307.71	2.46	5	1	101.68	1	20	2	10	13	7	0.54	0	0	0
22	431.06	3.21	5	1	101.68	1	20	2	10	13	8	0.62	0	0	0
23	291.25	1.93	5	1	101.68	1	20	2	10	13	7	0.54	0	0	0
24	287.29	2.19	5	1	101.68	1	20	2	10	14	6	0.43	0	0	0
25	342.15	3.08	5	1	101.68	1	20	2	10	13	8	0.62	0	0	0
26	455.87	4.02	7	0	119.19	5	27	3	10	22	9	0.41	0	0	0
27	490.31	4.65	7	0	119.19	5	27	3	10	22	10	0.45	0	0	0
28	460.29	4.68	6	0	109.96	4	27	3	10	21	9	0.43	0	0	0

DLS_{IV}: threshold values of the *Drug-Like Soft* filter; LLS_{IV}: threshold values of the *Lead-Like Soft* filter; MW: molecular weight (in Daltons); LogP: the logarithm of the partition coefficient between n-octanol and water; H_{BA}: hydrogen bond acceptors; H_{BD}: hydrogen bond donors; tPSA: topological Polar Surface Area; RtB: number of rotatable bonds; RiB: number of rigid bonds; R_s: number of the smallest set of smallest rings; M_xS: maximum size of the biggest ring system; C_s: number of carbon atoms; HA: number of heteroatoms; H/C: the ratio between the number of non-carbon atoms and the number of carbon atoms; Crg: number of charged groups; T_{Crg}: formal total charge of the compound; SC: stereo centers (– computed only for leads) **bold & italic values**: violation of RO5, but do not overpass the threshold values of drug-likeness filters; underlined values: overpass the thresholds for lead-likeness filters.

For a drug, a good oral bioavailability is a desired characteristic. The predictors used for this property are: a good intestinal absorption, a reduced molecular flexibility, low polar surface area and the hydrogen-bonding ability.

Thiazolidinediones 1–3 and 7–11 have a higher value of LogP, in terms of the drug-likeness filters (LogP > 5), and only compounds 16–25 respect the lead-like criteria (LogP < 4). Thiazolidinedione derivatives 1–3 and 26–28 also have bad predictions for the molecular weight (MW). All molecules have values of tPSA inferior to 160 Å², passing the criteria requested for the gastro-intestinal absorption,

after an oral administration. The studied substances have less than 9 rotatable bonds (RtB) and no chirality center (SC); in consequence, exhibiting low conformational flexibility. All compounds validate all other filters for drug-likeness and also, for lead-likeness (Table 2).

The ADME-Tox profiling also provides a helpful guidance on acute and later toxicity (Table 3).

Table 3. ADME-Tox profiling—risks and safety concerns.

ID	PPIs	UMSs	CIs	PAINS Filters			GSK 4/400 Rule	Pfizer 3/75 Rule	PhI	Med Chem	GT Rule
				A	B	C					
1	yes	halogenure thioester	UC	ND	ND	ND	bad	warning	not	thioester	out
2	yes	halogenure thioester	UC	ND	ND	ND	bad	warning	not	thioester	out
3	yes	halogenure thioester	UC	ND	ND	ND	bad	warning	not	thioester	out
4	yes	thioester	UC	ND	ND	ND	good	warning	not	thioester	out
5	yes	thioester	UC	ND	ND	ND	good	warning	not	thioester	out
6	yes	thioester	UC	ND	ND	ND	good	warning	not	thioester	out
7	yes	halogenure thioester	UC	ND	ND	ND	bad	warning	not	thioester	out
8	yes	halogenure thioester	UC	ND	ND	ND	bad	warning	not	thioester	out
9	yes	halogenure thioester	UC	ND	ND	ND	bad	warning	not	thioester	out
10	yes	halogenure thioester	UC	ND	ND	ND	bad	warning	not	thioester	out
11	yes	halogenure thioester	UC	ND	ND	ND	bad	warning	not	thioester	out
12	yes	nitro thioester	UC	ND	ND	ND	bad	warning	not	thioester	out
13	yes	nitro thioester	UC	ND	ND	ND	bad	warning	not	thioester	out
14	yes	thioester	UC	ND	ND	ND	bad	warning	not	thioester	out
15	yes	thioester	UC	ND	ND	ND	bad	warning	not	thioester	out
16	no	thioester	ND	ND	ND	ND	good	good	not	thioester	in
17	no	halogenure thioester	UC	ND	ND	ND	good	good	not	thioester	in
18	no	halogenure thioester	UC	ND	ND	ND	good	warning	not	thioester	in
19	no	thioester	UC	ND	ND	ND	good	good	not	thioester	in
20	no	thioester	UC	ND	ND	ND	good	good	not	thioester	in
21	no	halogenure thioester thiazolidinedione	UC	ND	ND	ND	good	good	not	thioester	out
22	no	halogenure thioester thiazolidinedione	UC	ND	ND	ND	good	warning	not	thioester	out
23	no	thioester thiazolidinedione	UC	ND	ND	ND	good	good	not	thioester	in
24	no	thioester thiazolidinedione	UC	ND	ND	ND	good	good	not	thioester	in
25	no	halogenure thioester thiazolidinedione	UC	ND	ND	ND	good	warning	not	thioester	in
26	yes	halogenure thioester	UC	ND	ND	ND	bad	warning	not	thioester	out
27	yes	halogenure thioester	UC	ND	ND	ND	bad	warning	not	thioester	out
28	yes	halogenure thioester	UC	ND	ND	ND	bad	warning	not	thioester	out

PPIs: protein-protein interactions; underlined values: high risk UMSs; Cis: covalent inhibitors; UC: α , β -unsaturated carbonyl (a covalent inhibitor moiety); PAINS: Pan-Assay Interference Compounds; ND: none detected (compound is free of problematic substructures for the corresponding risk criteria); PhI: phospholipidosis induction.

The risk and safety concern profiling for the studied molecules revealed that these are not phospholipidosis non-inducers. They are free of PAINS. All the lead-like compounds (16–25) were detected as not being PPIs friendly and, with the exception of 16, the rest of all the investigated compounds were flagged as possible covalent inhibitors, due to the presence of the α , β -unsaturated carbonyl [40,86,87].

It can be observed that thiazolidinedione, a high risk UMSs [36], was detected in the structure of 21–25 (Table 3), meanwhile all the other compounds have in their structure other low risk UMSs, like nitro in compounds 12 and 13 [40,42,43], halogenure in 1-3, 7–11, 17, 18, 20, 21, 25–28 and thioester [44]. Moreover, the thioester moiety (present in all compounds) is also considered a liability by the MedChem rules, due to being potentially reactive or promiscuous [44].

The screening revealed that GSK 4/400 rule, the Pfizer 3/75 rule and the GT rule placed the compounds 16, 17, 19, 20, 23 and 24, under the most favorable ADME-Tox predictions.

3.3. Molecular Docking

The results of the molecular docking runs on the mutant K-Ras, N-Ras or B-Raf isoforms are presented in Table 4 as binding affinity (BA) for the best poses, at root-mean-square deviation (RMSD)

equal to zero. The detailed binding patterns and the total energetic interactions are showed in Supplementary Table S1. The graphical depiction of the docking results is illustrated in Figures 1–5.

Table 4. The binding affinity (BA) expressed by the thiazolidinedione derivatives 1–28.

Ligand ID	BA (kcal/mol)					
	<i>K-Ras</i>		<i>N-Ras</i>		<i>B-Raf</i>	
	4DSU	4DSU ^{GDP-b}	3CON	3CON ^{GDP-b}	2N9C	5ITA
1	-8.00	-7.80	-8.70	-6.10	-5.80	-9.10
2	-9.00	-8.00	-8.50	-6.20	-6.30	-9.70
3	-8.10	-7.60	-8.70	-5.90	-6.20	-8.90
4	-8.00	-7.70	-8.40	-6.50	-5.70	-9.10
5	-8.70	-7.70	-9.50	-6.30	-5.80	-9.40
6	-9.40	-7.80	-8.40	-6.30	-6.10	-9.10
7	-8.40	-7.90	-8.50	-6.40	-6.20	-9.30
8	-8.60	-7.80	-8.90	-6.20	-6.30	-9.10
9	-8.10	-8.20	-8.70	-6.50	-6.20	-9.40
10	-8.00	-7.70	-8.70	-6.00	-6.20	-9.40
11	-8.30	-7.40	-8.70	-6.20	-5.90	-9.20
12	-10.00	-7.90	-9.50	-6.70	-6.40	-9.70
13	-8.50	-7.40	-9.30	-6.20	-5.90	-9.80
14	-8.40	-7.80	-8.50	-6.20	-5.80	-9.20
15	-8.70	-7.60	-8.60	-6.20	-5.80	-9.10
16	-8.00	-6.20	-7.80	-5.50	-4.80	-7.90
17	-8.50	-6.70	-7.80	-5.80	-5.20	-8.20
18	-7.90	-6.60	-7.50	-5.80	-5.10	-8.10
19	-8.70	-6.90	-8.70	-6.10	-5.00	-8.20
20	-8.70	-6.90	-8.00	-6.10	-5.20	-8.90
21	-8.30	-6.80	-8.20	-6.00	-5.20	-9.00
22	-8.60	-6.90	-8.20	-5.60	-5.00	-8.60
23	-8.60	-7.20	-8.40	-6.30	-5.30	-9.50
24	-8.60	-7.00	-8.50	-6.20	-5.30	-9.30
25	-8.90	-6.80	-8.50	-5.90	-5.10	-9.00
26	-8.70	-7.50	-8.90	-6.60	-5.80	-10.40
27	-9.10	-7.50	-10.00	-6.60	-5.90	-10.20
28	-8.80	-7.40	-8.60	-6.40	-6.20	-10.30

GDP^{-b}: GDP-bound state of GTPases; **bold** values: the strongest interaction with the target chosen.

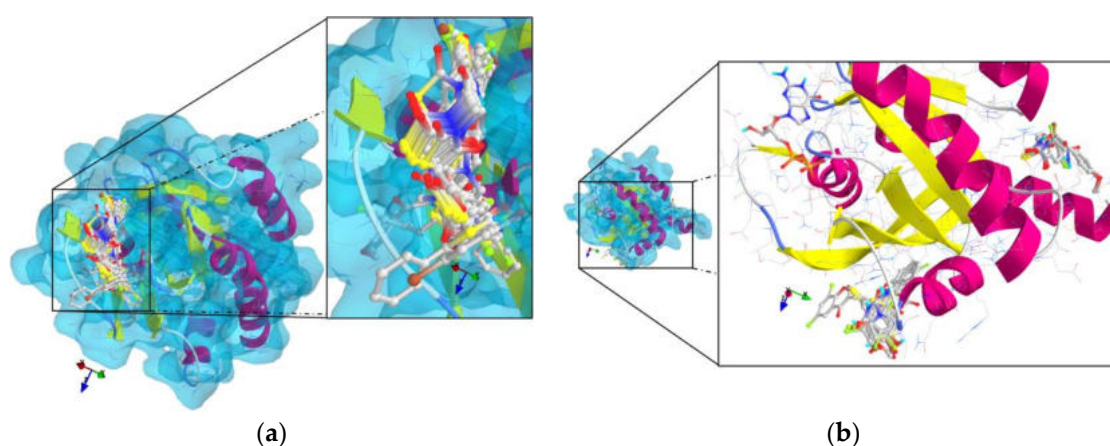


Figure 1. General views and details of the docking poses in the active site of K-Ras (target is presented as thin sticks with secondary structure drawn as cartoon backbone and transparent light blue molecular surface, meanwhile ligands are figured as ball-and-stick—image rendered with VTK/PyRx 0.9.5). (a) The docking results for K-Ras without GDP bound in the pocket; (b): The docking poses from the simulation against the GDP-bound state of K-Ras (top-left: GDP; central-bottom: 1–16, 23, 28; top-right: 17–22, 24–27).

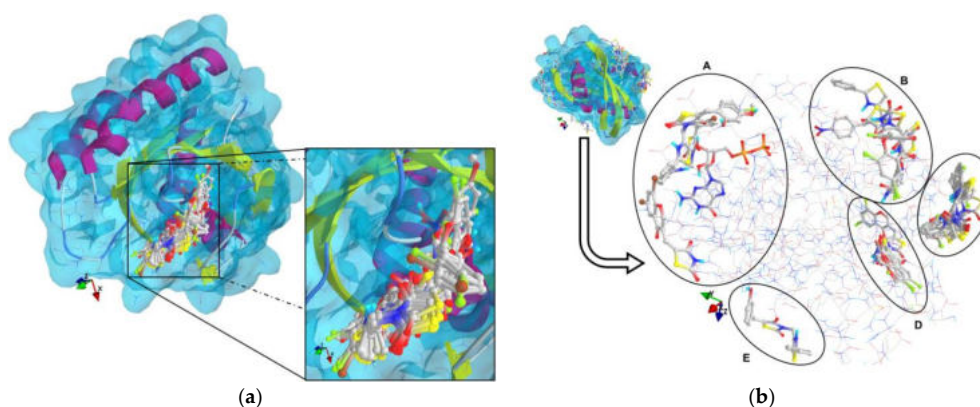


Figure 2. General views and details of the docking poses in the active site of N-Ras (the target is presented as thin sticks with secondary structure drawn as cartoon backbone and transparent light blue molecular surface; the ligands are depicted as ball-and-stick—image rendered with VTK/PyRx 0.9.5). (a): The docking results for N-Ras without GDP bound in the pocket; (b): The docking poses from the simulation against the GDP-bound state of N-Ras (A: GDP, 3–4; 6, 8, 15, 22; B: 13, 16, 23, 28; C: 1–2, 7, 9–12, 14, 18–20; D: 15, 21, 24–27; E: 5).

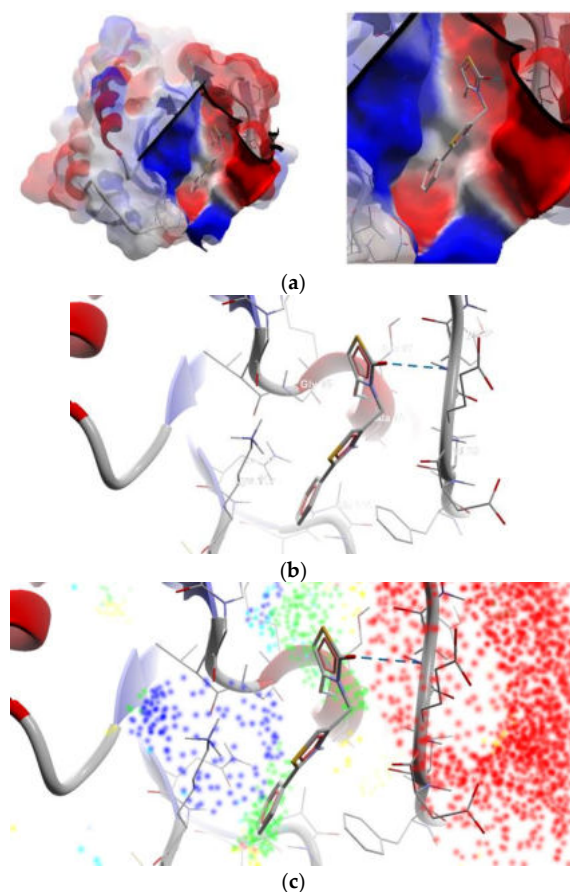


Figure 3. Best pose of compound 16 in the active site of the canonical isoform of N-Ras without GDP bound in the pocket (the target is presented as thin sticks with secondary structure drawn as cartoon backbone; the ligand is drawn as sticks; the H-bonds are in dashed blue lines—image rendered with Molegro Molecular Viewer 2.5). (a) General view and detail: ligand is presented buried in the nucleotide-binding pocket (molecular surface of target is depicted as electrostatic potential molecular surface); (b) Detail: hydrogen bonds formation with Ala18 and Tyr32; (c) Detail: energy grid depiction (green—steric favorable; light blue—hydrogen acceptor favorable; yellow—hydrogen donor favorable; orange to red and dark blue—electrostatic interactions).

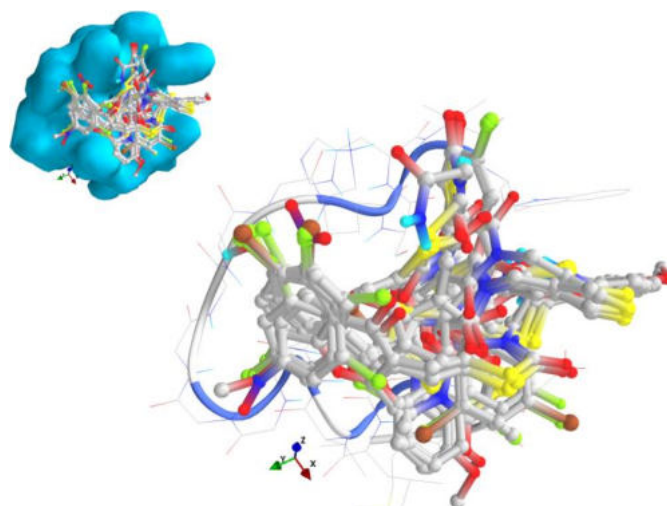


Figure 4. General view and detail of the docking poses in the active site of N-Ras isoform 5 (the target is presented as thin sticks with secondary structure drawn as cartoon backbone and solid light blue molecular surface; the ligands are drawn as ball-and-stick—image rendered with VTK/PyRx 0.9.5).

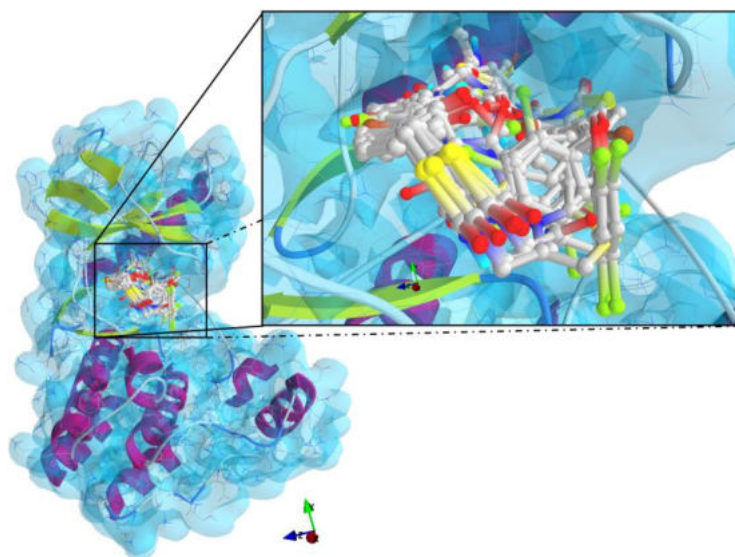


Figure 5. General view and detail of the docking poses in the active site of B-Raf (the target is presented as thin sticks with secondary structure drawn as cartoon backbone and transparent light blue molecular surface; the ligands are drawn as ball-and-stick - image rendered with VTK/PyRx 0.9.5).

The strongest interaction with the targets chosen was that of compound 12, bearing a nitro moiety: the binding affinity for the mutant isoform of K-Ras was -10 kcal/mol, respectively for N-Ras isoforms, -6.70 kcal/mol and -6.40 kcal/mol. Compound 26 proved to be a strong binder of B-Raf (-10.40 kcal/mol) and compound 27, of N-Ras (-10 kcal/mol). The substances which passed the lead-like filter in the ADME-Tox predictions (16–25) have good binding affinities to the targets, but do not display the strongest interaction. From Table 4 it could be observed that the safer lead-like compound, 16 (the non-covalent binder—Figure 3) is a weak binder of K-Ras and B-Raf, and slightly more potent than 19 against the canonical isoform of N-Ras. All compounds are less active against the N-Ras isoform 5 (which doesn't have GTPase activity and is responsible for an aggressive phenotype of melanoma) and interact with the alpha-helix (Supplementary Table S1 and Figure 4).

The thiazolidinedione derivatives studied bound more weakly to the GDP-bound state of the GTPases (Figures 1 and 2).

The thiazolidinediones studied have a similar binding pattern in the active site of B-Raf (Figure 5) from the protein kinase domain, between Ile463 and Gly596 (Supplementary Table S1).

3.4. Cytotoxicity

Genetic alterations in the MAPK pathway (including the mutation of KRAS, NRAS and BRAF genes) can cooperate in the development of B16 melanomas [88,89] and CT26 colorectal carcinoma [90,91]. Considering this aspect, we investigated the cytotoxicity of the compounds on B16 and CT26 murine cell lines. The results obtained are presented in Table 5.

Table 5. The cytotoxicity of the thiazolidinedione derivatives.

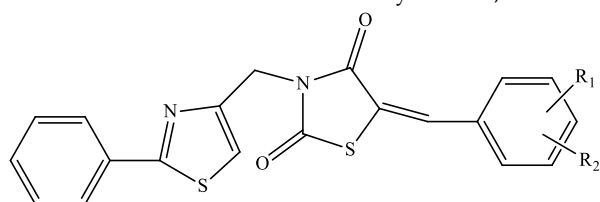
Compound	IC50 (µM)	
	B16	CT26
1	82.794	27.227
2	45.394	29.923
3	17.061	>100
4	74.131	>100
5	53.407	57.544
6	52.481	29.444
7	30.2	>100
8	69.502	81.846
9	37.931	>100
10	>100	>100
11	49.888	>100
12	87.297	>100
13	66.834	40.832
14	62.373	67.298
15	>100	>100
16	>100	>100
17	28.314 [34]	>100 [34]
18	66.374 [34]	>100 [34]
19	56.624	>100
20	69.823 [34]	62.951 [34]
21	40.272 [34]	33.651 [34]
22	42.17 [34]	52.481 [34]
23	72.277 [34]	73.451 [34]
24	85.114 [34]	67.608 [34]
25	NT	NT
26	NT	NT
27	NT	NT
28	NT	NT

Bold values: good inhibitory activity; *bold & italic values*: the best inhibitory activity; NT: not tested.

The best inhibitory effect of the B16 cells was registered for the compound 3 (IC50 = 17.061 µm), bearing a 4-Br-benzylidene fragment in its structure. The weakest activity was that of derivatives 10, 15 and 16, with IC50 > 100 µm. Regarding the effect against the CT26 cells, it can be observed that compound 1, with a 2-Br-benzylidene moiety, had the lowest IC50 (27.227 µm), and therefore had the best inhibitory activity. The weakest effect was displayed by the thiazolidinediones 3, 4, 7, 9–12, 15–19 (IC50 > 100 µm).

4. Discussion

The thiazolidinedione derivatives belong to two structural profiles: 5-arylidene-*N*-(phenyl-thiazolyl-methylene)-2,4-thiazolidinediones 1–16 (Table 6) [33] and 5-chromenyl-methylene-2,4-thiazolidinediones 17–28 (Table 7) [34,85,92].

Table 6. Chemical structures of the *N*-substituted 5-arylidene-2,4-thiazolidinediones 1–16.


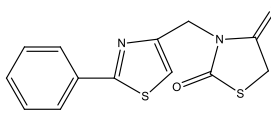
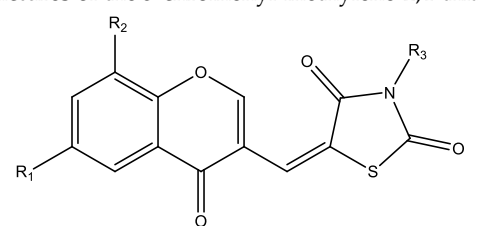
Compound	R ₁	R ₂
1	2-Br	H
2	3-Br	H
3	4-Br	H
4	2-OH	H
5	3-OH	H
6	4-OH	H
7	3-Cl	H
8	4-Cl	H
9	2-Cl	3-Cl
10	2-Cl	4-Cl
11	2-Cl	6-Cl
12	3-NO ₂	H
13	4-NO ₂	H
14	3-OCH ₃	H
15	4-OCH ₃	H
16		

Table 7. Chemical structures of the 5-chromenyl-methylene-2,4-thiazolidinediones 17–28.


Compound	R ₁	R ₂	R ₃
17	Cl	H	CH ₃
18	Cl	H	C ₂ H ₅
19	F	H	CH ₂ -CO-NH ₂
20	CH ₃	H	CH ₃
21	Cl	H	H
22	Br	Br	H
23	F	H	H
24	CH ₃	H	H
25	Cl	Cl	H
26	Cl	H	CH ₂ -CO-C ₆ H ₄ -OCH ₃ (p)
27	Cl	Cl	CH ₂ -CO-C ₆ H ₄ -OCH ₃ (p)
28	Cl	Cl	CH ₂ -CO-C ₆ H ₅

Virtual screening (VS) proved to be a highly useful tool for drug discovery, being able to select the most promising chemical profiles as drug candidates, before the lab synthesis. This adds value to a targeted, more environmental-friendly obtention process, with a considerable reduction of the work time and a remarkable increase in efficiency.

A good oral bioavailability represents a very important characteristic of a bioactive substance. In our case, all the investigated compounds complied with the drug-likeness filters. Even if molecules 1–3 and 7–11 had higher values of LogP, since there was only one violation of Lipinski's "Rule of 5" (RO5) [93], the estimation of the oral bioavailability was good. Regarding the lead-likeness predictions, only compounds 16–25 can be considered good lead-like molecules, meanwhile all the rest of the investigated structures fail in terms of the logarithm of the partition coefficient between *n*-octanol and water (LogP). All thiazolidinedione derivatives complied with Veber's rule [94] and with Egan's rule [95] on the molecular properties with impact on the oral bioavailability. Topological polar surface area (tPSA), a descriptor that correlates well with the transport through membranes, including the blood-brain barrier, had values inferior to 140 Å², suggesting that the compounds pass the criteria required for a good gastro-intestinal absorption, after an oral administration. Supplementary, all derivatives were predicted to have a reduced blood-brain barrier transport (tPSA > 90 Å²). This aspect presents a high significance due to the reduced or totally absent possible side effects on the central nervous system.

In drug development, the investigation of both acute and later toxicity is mandatory: a drug must be pharmacologically active, but also very well tolerated, without side effects. The software-based predictions of the safety and risks profiling are very useful tools in medicinal chemistry, providing many advantages, such as: the availability of the specialized software, the rapidity of the data obtention, the possibility of selecting multiple parameters and filters and the major ethical advantage of reducing the number of the lab animals sacrificed in the classical toxicity assays. The screening performed on our compounds showed that these are not inducers of phospholipidosis, which is a disorder manifested by the accumulation of phospholipids in tissues and a sign of molecules' toxicity. All substances seemed to be free of PAINS (structures or substructures predicted not to interfere with the biological assays) and PPIs friendly, therefore successfully complying with these safety criteria.

The ADME-Tox profiling identified some low risk problematic moieties in the structure of the compounds, like thiazolidinedione, halogenure, nitro or thioester. MedChem rules considered the thioester fragment as potentially reactive or promiscuous. Considering this observation, the lead-like compounds 16–20 should be placed on the short list of possible hits for further structural optimization in a drug development project. Applying the GSK 4/400 rule, the Pfizer 3/75 rule and the GT rule, we could select the derivatives 16, 17, 19, 20, 23 and 24 as the best candidates, with an optimal permeability (low clearance) and a good metabolic stability [70].

The ADME-Tox data revealed that the studied thiazolidinedione derivatives display good pharmacokinetic properties, but with some limitations. All compounds pass the drug-likeness criteria, while only compounds 16–25 pass the lead-likeness filter. Further structural optimization might be helpful in achieving better ADME-Tox properties.

Molecular docking represents a modern, useful tool in drug discovery. Based on computation methods, it aims to give a prediction of a ligand-receptor complex, therefore suggesting a mechanism of action for the compounds studied.

In our paper, the binding patterns and the binding affinities of the compounds suggest that the substances may strongly interact with K-Ras and N-Ras right after their posttranslational processing and/or compete with GDP for the nucleotide-binding site of the two GTPases. Moreover, all the investigated molecules are less active against the GDP-bound states of the two targets, being weak binders. The compounds interact with the G domain of K-Ras and N-Ras in the bordering region of the nucleotide-binding pocket, in the absence of GDP molecule, acting as a competitor of GDP for its binding pocket. In the presence of GDP in the binding pocket, the compounds not only are weaker binders, but the binding patterns also indicate less pharmacological relevance.

However, AutoDock Vina cannot evaluate the covalent binding capacity of which derivatives are capable (with the exception of **16**), as resulted from the ADME-Tox predictions.

The binding pattern in the active site of B-Raf from the protein kinase domain, similar for all thiazolidinediones investigated, suggests that the tested compounds may also interact with the

other members of TKL serine/threonine-protein kinase family, since the interaction region is highly conserved—especially for the RAF subfamily [7,8].

The evaluation of the cytotoxicity is a mandatory step in drug development. For this, we evaluated in vitro the viability of the B16 (mouse melanoma), respectively CT26 (colorectal carcinoma) murine cell lines growth, in an MTT assay. Analyzing the data obtained, we could say that compounds 2, 3, 7, 9, 11, 17, 21 and 22 manifested a good inhibitory effect ($IC_{50} < 50 \mu\text{M}$), against the B16 cells. From these, the derivative 3, with a 4-Br-benzylidene fragment in position 5 of the thiazolidinedione ring, displayed the lowest value of IC_{50} . The proliferation of CT26 cells was effectively impeded by compounds 1, 2, 6, 13, 21. The strongest activity was manifested by the thiazolidinedione derivative 1, bearing the 2-Br-benzylidene fragment bound to the heterocycle. The good inhibitory effect expressed by the two molecules with bromine, confirm the impact of this halogen on the cytotoxic activity, in total agreement with the literature data [27].

5. Conclusions

The cytotoxicity assay realized on the two series of 5-arylidene-*N*-(phenyl-thiazolyl-methylene)-2,4-thiazolidinediones and 5-chromenyl-methylene-2,4-thiazolidinediones, respectively, revealed that the compounds expressed good inhibitory effects against the B16 and CT26 cell lines as well. The strongest activity was manifested by the derivatives with a Br-benzylidene fragment in the structure. All the investigated compounds complied with the drug-likeness filters, while substances 16–25 could be considered as lead-like molecules. The thiazolidine-2,4-diones were less active against the GDP-bound states of the K-Ras and N-Ras isoforms chosen as targets, acting as competitors of GDP for its binding pocket. The binding pattern in the active site of B-Raf was common to all the investigated compounds and was highly conserved. All data obtained encourage us to continue work in the field of the thiazolidinedione heterocyclic derivatives with therapeutic properties.

Supplementary Materials: The following are available online at <http://www.mdpi.com/1010-660X/55/4/85/s1>, Table S1: Binding patterns and total energetic interactions of the thiazolidine-2,4-dione derivatives.

Author Contributions: Conceptualization, C.N. and B.T.; Methodology, O.O.; Software, R.T.; Validation, C.N., B.T., O.O. and R.T.; Investigation, C.N.; Writing—Original Draft Preparation, C.N. and R.T.; Writing-Review & Editing, B.T., C.N. and R.T.; Supervision, O.O.

Funding: This study was funded by “Iuliu Hațieganu” University of Medicine and Pharmacy Cluj-Napoca internal research grant No. 4944/7/08.03.2016 (C.N.) and conducted also by the The Executive Agency for Higher Education Research Development and Innovation Funding—UEFISCDI, Romania, on the Contract 210/2014—Project PN-II-PT-PCCA-2013-4-2075 (R.T.).

Conflicts of Interest: The authors declare no conflict of interest.

References

1. Dhillon, A.S.; Hagan, S.; Rath, O.; Kolch, W. MAP kinase signalling pathways in cancer. *Oncogene* **2007**, *26*, 3279–3290. [[CrossRef](#)]
2. Fernández-Medarde, A.; Santos, E. Ras in cancer and developmental diseases. *Genes Cancer* **2011**, *2*, 344–358. [[CrossRef](#)]
3. Masliah-Planchon, J.; Garinet, S.; Pasmant, E. RAS-MAPK pathway epigenetic activation in cancer: miRNAs in action. *Oncotarget* **2015**, *7*, 38892–38907. [[CrossRef](#)] [[PubMed](#)]
4. Baldus, S.E.; Schaefer, K.-L.; Engers, R.; Hartleb, D.; Stoecklein, N.H.; Gabbert, H.E. Prevalence and Heterogeneity of KRAS, BRAF, and PIK3CA Mutations in Primary Colorectal Adenocarcinomas and Their Corresponding Metastases. *Clin. Cancer Res.* **2010**, *16*, 790–799. [[CrossRef](#)]
5. Tan, C.; Du, X. KRAS mutation testing in metastatic colorectal cancer. *World J. Gastroenterol.* **2012**, *18*, 5171–5180.
6. Neumann, J.; Zeindl-Eberhart, E.; Kirchner, T.; Jung, A. Frequency and type of KRAS mutations in routine diagnostic analysis of metastatic colorectal cancer. *Pathol. Res. Pract.* **2009**, *205*, 858–862. [[CrossRef](#)]

7. Cicenás, J.; Tamosaitis, L.; Kvederaviciute, K.; Tarvydas, R.; Staniute, G.; Kalyan, K.; Meskinyte-Kausiliene, E.; Stankevicius, V.; Valius, M. KRAS, NRAS and BRAF mutations in colorectal cancer and melanoma. *Med. Oncol.* **2017**, *34*, 26. [[CrossRef](#)] [[PubMed](#)]
8. Davies, H.; Bignell, G.R.; Cox, C.; Stephens, P.; Edkins, S.; Clegg, S.; Teague, J.; Woffendin, H.; Garnett, M.J.; Bottomley, W.; et al. Mutations of the BRAF gene in human cancer. *Nature* **2002**, *417*, 949–954. [[CrossRef](#)] [[PubMed](#)]
9. Ekedahl, H.; Cirenajwis, H.; Harbst, K.; Carneiro, A.; Nielsen, K.; Olsson, H.; Lundgren, L.; Ingvar, C.; Jönsson, G. The clinical significance of BRAF and NRAS mutations in a clinic-based metastatic melanoma cohort. *Br. J. Dermatol.* **2013**, *169*, 1049–1055. [[CrossRef](#)] [[PubMed](#)]
10. Fedorenko, I.V.; Gibney, G.T.; Sondak, V.K.; Smalley, K.S.M. Beyond BRAF: Where next for melanoma therapy? *Br. J. Cancer* **2014**, *112*, 217–226. [[CrossRef](#)]
11. Prior, I.A.; Lewis, P.D.; Mattos, C. A comprehensive survey of Ras mutations in cancer. *Cancer Res.* **2012**, *72*, 2457–2467. [[CrossRef](#)]
12. Johnson, D.B.; Puzanov, I. Treatment of NRAS-Mutant Melanoma. *Curr. Treat. Options Oncol.* **2016**, *16*, 15. [[CrossRef](#)] [[PubMed](#)]
13. Meriggi, F.; Vermi, W.; Bertocchi, P.; Zaniboni, A. The Emerging Role of NRAS Mutations in Colorectal Cancer Patients Selected for Anti-EGFR Therapies. *Rev. Recent Clin. Trials* **2014**, *9*, 35–39. [[CrossRef](#)]
14. Cejas, P.; López-Gómez, M.; Aguayo, C.; Madero, R.; de Castro Carpeño, J.; Belda-Iniesta, C.; Barriuso, J.; Moreno García, V.; Larrauri, J.; López, R.; et al. KRAS Mutations in Primary Colorectal Cancer Tumors and Related Metastases: A Potential Role in Prediction of Lung Metastasis. *PLoS ONE* **2009**, *4*, e8199. [[CrossRef](#)] [[PubMed](#)]
15. Ostrem, J.; Shokat, K. Direct small-molecule inhibitors of K-Ras: from structural insights to mechanism-based design. *Nat. Rev. Drug Discov.* **2016**, *15*, 771–785. [[CrossRef](#)]
16. Tsai, F.D.; Lopes, M.S.; Zhou, M.; Court, H.; Ponce, O.; Fiordalisi, J.J.; Gierut, J.J.; Cox, A.D.; Haigis, K.M.; Phillips, M.R. K-Ras4A splice variant is widely expressed in cancer and uses a hybrid membrane-targeting motif. *Proc. Natl. Acad. Sci. USA* **2015**, *112*, 779–784. [[CrossRef](#)]
17. Hunter, J.C.; Manandhar, A.; Carrasco, M.A.; Gurbani, D.; Gondi, S.; Westover, K.D. Biochemical and Structural Analysis of Common Cancer-Associated KRAS Mutations. *Mol. Cancer Res.* **2015**, *13*, 1325–1335. [[CrossRef](#)]
18. Cox, A.D.; Fesik, S.W.; Kimmelman, A.C.; Luo, J.; Der, C.J. Drugging the undruggable RAS: Mission Possible? *Nat. Rev. Drug Discov.* **2014**, *13*, 828–851. [[CrossRef](#)]
19. Markowitz, J.; Mal, T.K.; Yuan, C.; Courtney, N.B.; Patel, M.; Stiff, A.R.; Blachly, J.; Walker, C.; Eisfeld, A.K.; De La Chapelle, A.; et al. Structural characterization of NRAS isoform 5. *Protein Sci.* **2016**, *25*, 1069–1074. [[CrossRef](#)] [[PubMed](#)]
20. Căinap, S.S.; Nagy, V.; Căinap, C. Chemotherapy-induced cardiotoxicity in oncology drugs involved and clinical assessment. *Farmacia* **2016**, *64*, 487–492.
21. Ostrem, J.M.; Peters, U.; Sos, M.L.; Wells, J.A.; Shokat, K.M. K-Ras(G12C) inhibitors allosterically control GTP affinity and effector interactions. *Nature* **2013**, *503*, 548–551. [[CrossRef](#)]
22. Hunter, J.C.; Gurbani, D.; Ficarro, S.B.; Carrasco, M.A.; Lim, S.M.; Choi, H.G.; Xie, T.; Marto, J.A.; Chen, Z.; Gray, N.S.; et al. In situ selectivity profiling and crystal structure of SML-8-73-1, an active site inhibitor of oncogenic K-Ras G12C. *Proc. Natl. Acad. Sci. USA* **2014**, *111*, 8895–8900. [[CrossRef](#)]
23. Zhou, S.; Chan, E.; Duan, W.; Huang, M.; Chen, Y.-Z. Drug Bioactivation, Covalent Binding to Target Proteins and Toxicity Relevance. *Drug Metab. Rev.* **2005**, *37*, 41–213. [[CrossRef](#)]
24. Johnson, D.S.; Weerapana, E.; Cravatt, B.F. Strategies for discovering and derisking covalent, irreversible enzyme inhibitors. *Future Med. Chem.* **2010**, *2*, 949–964. [[CrossRef](#)]
25. Mah, R.; Thomas, J.R.; Shafer, C.M. Drug discovery considerations in the development of covalent inhibitors. *Bioorg. Med. Chem. Lett.* **2014**, *24*, 33–39. [[CrossRef](#)]
26. London, N.; Miller, R.M.; Krishnan, S.; Uchida, K.; Irwin, J.J.; Eidam, O.; Gibold, L.; Cimermančič, P.; Bonnet, R.; Shoichet, B.K.; et al. Covalent docking of large libraries for the discovery of chemical probes. *Nat. ChemBio* **2014**, *10*, 1066–1072. [[CrossRef](#)] [[PubMed](#)]
27. Asati, V.; Mahapatra, D.K.; Bharti, S.K. Thiazolidine-2,4-diones as multi-targeted scaffold in medicinal chemistry: Potential anticancer agents. *Eur. J. Med. Chem.* **2014**, *87*, 814–833. [[CrossRef](#)] [[PubMed](#)]

28. Jung, K.-Y.; Samadani, R.; Chauhan, J.; Nevels, K.; Yap, J.L.; Zhang, J.; Worlikar, S.; Lanning, M.E.; Chen, L.; Ensey, M.; et al. Structural modifications of (Z)-3-(2-aminoethyl)-5-(4-ethoxybenzylidene)thiazolidine-2,4-dione that improve selectivity for inhibiting the proliferation of melanoma cells containing active ERK signalling. *Org. Biomol. Chem.* **2013**, *11*, 3706–3732. [CrossRef] [PubMed]
29. Shao, J.; Sheng, H.; DuBois, R.N. Peroxisome Proliferator-activated Receptors Modulate K-Ras-mediated Transformation of Intestinal Epithelial Cells. *Cancer Res.* **2002**, *62*, 3282–3288. [PubMed]
30. Huang, W.C.; Chio, C.C.; Chi, K.H.; Wu, H.M.; Lin, W.W. Superoxide anion-dependent Raf/MEK/ERK activation by peroxisome proliferator activated receptor gamma agonists 15-deoxy-delta(12,14)-prostaglandin J(2), ciglitazone, and GW1929. *Exp. Cell Res.* **2002**, *277*, 192–200. [CrossRef] [PubMed]
31. Kole, L.; Sarkar, M.; Deb, A.; Giri, B. Pioglitazone, an anti-diabetic drug requires sustained MAPK activation for its anti-tumor activity in MCF7 breast cancer cells, independent of PPAR- γ pathway. *Pharmacol. Rep.* **2016**, *68*, 144–154. [CrossRef] [PubMed]
32. Stana, A.; Enache, A.; Vodnar, D.C.; Nastasă, C.; Benedec, D.; Ionuț, I.; Login, C.; Marc, G.; Oniga, O.; Tipericiu, B. New Thiazolyl-triazole Schiff Bases: Synthesis and Evaluation of the Anti-Candida Potential. *Molecules* **2016**, *21*, 1595. [CrossRef] [PubMed]
33. Nastasă, C.; Tipericiu, B.; Pârvu, A.; Duma, M.; Ionuț, I.; Oniga, O. Synthesis of New N-Substituted 5-Arylidene-2,4-thiazolidinediones as Anti-Inflammatory and Antimicrobial Agents. *Arch. Pharm.* **2013**, *346*, 481–490. [CrossRef] [PubMed]
34. Nastasă, C.; Duma, M.; Marie, C.; Scherman, D.; Tipericiu, B.; Oniga, O. New N-substituted 5-chromenyl-thiazolidinediones as antimicrobial and antiproliferative agents. *Dig. J. Nanomater. Bios.* **2013**, *8*, 1079–1087.
35. ChemAxon. Available online: <https://chemaxon.com> (accessed on 24 March 2015).
36. Lagorce, D.; Sperandio, O.; Baell, J.B.; Miteva, M.A.; Villoutreix, B.O. FAF-Drugs3: a web server for compound property calculation and chemical library design. *Nucleic Acids Res.* **2015**, *43*, W200–W207. [CrossRef] [PubMed]
37. Cheng, T.; Zhao, Y.; Li, X.; Lin, F.; Xu, Y.; Zhang, X.; Li, Y.; Wang, R.; Lai, L. Computation of octanol-water partition coefficients by guiding an additive model with knowledge. *J. Chem. Inf. Model.* **2007**, *47*, 2140–2148. [CrossRef]
38. Delaney, J.S. ESOL: estimating aqueous solubility directly from molecular structure. *J. Chem. Inf. Comput. Sci.* **2004**, *44*, 1000–1005. [CrossRef]
39. Reynès, C.; Host, H.; Camproux, A.-C.; Laconde, G.; Leroux, F.; Mazars, A.; Deprez, B.; Fahraeus, R.; Villoutreix, B.O.; Sperandio, O. Designing Focused Chemical Libraries Enriched in Protein-Protein Interaction Inhibitors using Machine-Learning Methods. *PLoS Comput. Biol.* **2010**, *6*, e1000695. [CrossRef] [PubMed]
40. Enoch, S.J.; Ellison, C.M.; Schultz, T.W.; Cronin, M.T.D. A review of the electrophilic reaction chemistry involved in covalent protein binding relevant to toxicity. *Crit. Rev. Toxicol.* **2011**, *41*, 783–802. [CrossRef] [PubMed]
41. Blagg, J. Structural Alerts for Toxicity. In *Burger's Medicinal Chemistry and Drug Discovery*; Abraham, D.J., Ed.; John Wiley & Sons, Inc.: Hoboken, NJ, USA, 2010; pp. 301–334.
42. Benigni, R.; Bossa, C. Mechanisms of Chemical Carcinogenicity and Mutagenicity: A Review with Implications for Predictive Toxicology. *Chem. Rev.* **2011**, *111*, 2507–2536. [CrossRef]
43. Stepan, A.F.; Walker, D.P.; Bauman, J.; Price, D.A.; Baillie, T.A.; Kalgutkar, A.S.; Aleo, M.D. Structural alert/reactive metabolite concept as applied in medicinal chemistry to mitigate the risk of idiosyncratic drug toxicity: A perspective based on the critical examination of trends in the top 200 drugs marketed in the United States. *Chem. Res. Toxicol.* **2011**, *24*, 1345–1410. [CrossRef]
44. Bruns, R.F.; Watson, I.A. Rules for Identifying Potentially Reactive or Promiscuous Compounds. *J. Med. Chem.* **2012**, *55*, 9763–9772. [CrossRef]
45. Rishton, G.M. Nonleadlikeness and leadlikeness in biochemical screening. *Drug Discov. Today* **2003**, *8*, 86–96. [CrossRef]
46. Cumming, J.G.; Davis, A.M.; Muresan, S.; Haerberlein, M.; Chen, H. Chemical predictive modelling to improve compound quality. *Nat. Rev. Drug Discov.* **2013**, *12*, 948–962. [CrossRef] [PubMed]
47. NIH Molecular Libraries-Small Molecule Repository. Available online: <https://ncats.nih.gov/smr> (accessed on 3 April 2015).

48. Horvath, D.; Lisurek, M.; Rupp, B.; Kühne, R.; Specker, E.; von Kries, J.; Rognan, D.; Andersson, C.D.; Almqvist, F.; Elofsson, M.; et al. Design of a General-Purpose European Compound Screening Library for EU-OPENSREEN. *ChemMedChem* **2014**, *9*, 2309–2326. [[CrossRef](#)] [[PubMed](#)]
49. Smith, G.F. Designing drugs to avoid toxicity. *Prog. Med. Chem.* **2011**, *50*, 1–47. [[PubMed](#)]
50. Pearce, B.C.; Sofia, M.J.; Good, A.C.; Drexler, D.M.; Stock, D.A. An empirical process for the design of high-throughput screening deck filters. *J. Chem. Inf. Model.* **2006**, *46*, 1060–1068. [[CrossRef](#)] [[PubMed](#)]
51. Potashman, M.H.; Duggan, M.E. Covalent modifiers: An orthogonal approach to drug design. *J. Med. Chem.* **2009**, *52*, 1231–1246. [[CrossRef](#)]
52. Roberts, D.W.; Natsch, A. High Throughput Kinetic Profiling Approach for Covalent Binding to Peptides: Application to Skin Sensitization Potency of Michael Acceptor Electrophiles. *Chem. Res. Toxicol.* **2009**, *22*, 592–603. [[CrossRef](#)]
53. Baell, J.B.; Holloway, G.A. New substructure filters for removal of pan assay interference compounds (PAINS) from screening libraries and for their exclusion in bioassays. *J. Med. Chem.* **2010**, *53*, 2719–2740. [[CrossRef](#)]
54. Mok, N.Y.; Maxe, S.; Brenk, R. Locating Sweet Spots for Screening Hits and Evaluating Pan-Assay Interference Filters from the Performance Analysis of Two Lead-like Libraries. *J. Chem. Inf. Model.* **2013**, *53*, 534–544. [[CrossRef](#)]
55. Przybylak, K.R.; Alzahrani, A.R.; Cronin, M.T.D. How Does the Quality of Phospholipidosis Data Influence the Predictivity of Structural Alerts? *J. Chem. Inf. Model.* **2014**, *54*, 2224–2232. [[CrossRef](#)]
56. Hughes, J.D.; Blegg, J.; Price, D.A.; Bailey, S.; Decrescenzo, G.A.; Devraj, R.V.; Ellsworth, E.; Fobian, Y.M.; Gibbs, M.E.; Gilles, R.W.; et al. Physicochemical drug properties associated with in vivo toxicological outcomes. *Bioorg. Med. Chem. Lett.* **2008**, *18*, 4872–4875. [[CrossRef](#)]
57. Gleeson, M.P. Generation of a set of simple, interpretable ADMET rules of thumb. *J. Med. Chem.* **2008**, *51*, 817–834. [[CrossRef](#)] [[PubMed](#)]
58. Oprea, T.I.; Davis, A.M.; Teague, S.J.; Leeson, P.D. Is There a Difference between Leads and Drugs? A Historical Perspective. *J. Chem. Inf. Model.* **2001**, *41*, 1308–1315. [[CrossRef](#)]
59. Workman, P.; Collins, I. Probing the probes: Fitness factors for small molecule tools. *Chem. Biol.* **2010**, *17*, 561–577. [[CrossRef](#)] [[PubMed](#)]
60. Baell, J.B. Broad Coverage of Commercially Available Lead-like Screening Space with Fewer than 350,000 Compounds. *J. Chem. Inf. Model.* **2013**, *53*, 39–55. [[CrossRef](#)]
61. Brenk, R.; Schipani, A.; James, D.; Krasowski, A.; Gilbert, I.H.; Frearson, J.; Wyatt, P.G. Lessons Learnt from Assembling Screening Libraries for Drug Discovery for Neglected Diseases. *ChemMedChem* **2008**, *3*, 435–444. [[CrossRef](#)] [[PubMed](#)]
62. Lipinski, C.A.; Lombardo, F.; Dominy, B.W.; Feeney, P.J. Experimental and computational approaches to estimate solubility and permeability in drug discovery and development settings. *Adv. Drug Deliv. Rev.* **2001**, *46*, 3–26. [[CrossRef](#)]
63. Oprea, T.I. Property distribution of drug-related chemical databases. *J. Comput. Aided. Mol. Des.* **2000**, *14*, 251–264. [[CrossRef](#)]
64. Irwin, J.J.; Shoichet, B.K. ZINC—a free database of commercially available compounds for virtual screening. *J. Chem. Inf. Model.* **2004**, *45*, 177–182. [[CrossRef](#)] [[PubMed](#)]
65. Pihan, E.; Colliandre, L.; Guichou, J.-F.; Douguet, D. e-Drug3D: 3D structure collections dedicated to drug repurposing and fragment-based drug design. *Bioinformatics* **2012**, *28*, 1540–1541. [[CrossRef](#)] [[PubMed](#)]
66. Domling, A. *Protein-Protein Interactions in Drug Discovery*; Mannhold, R., Kubinyi, H., Folkers, G., Eds.; WILEY-VCH Verlag GmbH: New York, NY, USA, 2013; p. 56.
67. Sperandio, O.; Reynès, C.H.; Camproux, A.-C.; Villoutreix, B.O. Rationalizing the chemical space of protein-protein interaction inhibitors. *Drug Discov. Today* **2010**, *15*, 220–229. [[CrossRef](#)] [[PubMed](#)]
68. Todeschini, R.; Consonni, V. *Handbook of Molecular Descriptors*; Mannhold, R., Kubinyi, H., Timmerman, H., Eds.; WILEY-VCH Verlag GmbH: New York, NY, USA, 2008.
69. Lagorce, D.; Sperandio, O.; Galons, H.; Miteva, M.A.; Villoutreix, B.O. FAF-Drugs2: Free ADME/tox filtering tool to assist drug discovery and chemical biology projects. *BMC Bioinformatics* **2008**, *9*, 396. [[CrossRef](#)]
70. Johnson, T.W.; Dress, K.R.; Edwards, M. Using the Golden Triangle to optimize clearance and oral absorption. *Bioorg. Med. Chem. Lett.* **2009**, *19*, 5560–5564. [[CrossRef](#)]

71. Varnek, A.; Tropsha, A. *Cheminformatics Approaches to Virtual Screening*; Varnek, A., Tropsha, A., Eds.; Royal Society of Chemistry: Cambridge, London, UK, 2008.
72. Gene Database–GeneCards®. Available online: <http://www.genecards.org> (accessed on 20 February 2015).
73. The Universal Protein Resource–UniProt. Available online: <http://www.uniprot.org> (accessed on 20 February 2015).
74. RCSB Protein Data Bank–RCSB-PDB. Available online: <http://www.rcsb.org> (accessed on 20 February 2015).
75. Maurer, T.; Garrenton, L.S.; Oh, A.; Pitts, K.; Anderson, D.J.; Skelton, N.J.; Fauber, B.P.; Pan, B.; Malek, S.; Stokoe, D.; et al. Small-molecule ligands bind to a distinct pocket in Ras and inhibit SOS-mediated nucleotide exchange activity. *Proc. Natl. Acad. Sci. USA* **2012**, *109*, 5299–5304. [[CrossRef](#)]
76. Karoulia, Z.; Wu, Y.; Ahmed, T.A.; Xin, Q.; Bollard, J.; Krepler, C.; Wu, X.; Zhang, C.; Bollag, G.; Herlyn, M.; et al. An Integrated Model of RAF Inhibitor Action Predicts Inhibitor Activity against Oncogenic BRAF Signaling. *Cancer Cell* **2016**, *30*, 501–514. [[CrossRef](#)]
77. Dallakyan, S.; Olson, A.J. Small-molecule library screening by docking with PyRx. *Methods Mol. Biol.* **2015**, *1263*, 243–250. [[PubMed](#)]
78. Trott, O.; Olson, A.J. AutoDock Vina: Improving the speed and accuracy of docking with a new scoring function, efficient optimization, and multithreading. *J. Comput. Chem.* **2010**, *31*, 455–461. [[CrossRef](#)]
79. Wang, R.; Lai, L.; Wang, S. Further development and validation of empirical scoring functions for structure-based binding affinity prediction. *J. Comput. Aided. Mol. Des.* **2002**, *16*, 11–26. [[CrossRef](#)] [[PubMed](#)]
80. Wang, R.; Fang, X.; Lu, Y.; Wang, S. The PDBbind database: Collection of binding affinities for protein-ligand complexes with known three-dimensional structures. *J. Med. Chem.* **2004**, *47*, 2977–2980. [[CrossRef](#)]
81. Wang, R.; Fang, X.; Lu, Y.; Yang, C.-Y.; Wang, S. The PDBbind database: methodologies and updates. *J. Med. Chem.* **2005**, *48*, 4111–4119. [[CrossRef](#)]
82. The Visualization ToolKit. Available online: <http://www.kitware.com> (accessed on 20 February 2015).
83. Feinstein, W.P.; Brylinski, M. Calculating an optimal box size for ligand docking and virtual screening against experimental and predicted binding pockets. *J. Cheminform.* **2015**, *7*, 18. [[CrossRef](#)]
84. Kalhor-Monfared, S.; Beauvineau, C.; Scherman, D.; Girard, C. Synthesis and cytotoxicity evaluation of aryl triazolol derivatives and their hydroxymethine homologues against B16 melanoma cell line. *Eur. J. Med. Chem.* **2016**, *122*, 436–441. [[CrossRef](#)] [[PubMed](#)]
85. Nastasă, C.M.; Duma, M.; Pîrnău, A.; Vlase, L.; Tîperciuc, B.; Oniga, O. Development of new 5-(chromene-3-yl) methylene-2,4-thiazolidinediones as antimicrobial agents. *Clujul Med.* **2016**, *89*, 122–127.
86. Kalgutkar, A.; Gardner, I.; Obach, R.; Shaffer, C.; Callegari, E.; Henne, K.; Mutlib, A.; Dalvie, D.; Lee, J.; Nakai, Y.; et al. A Comprehensive Listing of Bioactivation Pathways of Organic Functional Groups. *Curr. Drug Metab.* **2005**, *6*, 161–225. [[CrossRef](#)]
87. Pérez-Garrido, A.; Helguera, A.M.; López, G.C.; Cordeiro, M.N.D.S.; Escudero, A.G. A topological substructural molecular design approach for predicting mutagenesis end-points of α , β -unsaturated carbonyl compounds. *Toxicology* **2010**, *268*, 64–77. [[CrossRef](#)]
88. Melnikova, V.O.; Bolshakov, S.V.; Walker, C.; Ananthaswamy, H.N. Genomic alterations in spontaneous and carcinogen-induced murine melanoma cell lines. *Oncogene* **2004**, *23*, 2347–2356. [[CrossRef](#)] [[PubMed](#)]
89. Zaidi, S.; Blanchard, M.; Shim, K.; Ilett, E.; Rajani, K.; Parrish, C.; Boisgerault, N.; Kottke, T.; Thompson, J.; Celis, E.; et al. Mutated BRAF Emerges as a Major Effector of Recurrence in a Murine Melanoma Model After Treatment With Immunomodulatory Agents. *Mol. Ther.* **2015**, *23*, 845–856. [[CrossRef](#)] [[PubMed](#)]
90. Castle, J.C.; Loewer, M.; Boegel, S.; de Graaf, J.; Bender, C.; Tadmor, A.D.; Boisguerin, V.; Bukur, T.; Sorn, P.; Paret, C.; et al. Immunomic, genomic and transcriptomic characterization of CT26 colorectal carcinoma. *BMC Genomics* **2014**, *15*, 190. [[CrossRef](#)] [[PubMed](#)]
91. Ebert, P.J.R.; Cheung, J.; Yang, Y.; McNamara, E.; Hong, R.; Moskalenko, M.; Gould, S.E.; Maecker, H.; Irving, B.A.; Kim, J.M.; et al. MAP Kinase Inhibition Promotes T Cell and Anti-tumor Activity in Combination with PD-L1 Checkpoint Blockade. *Immunity* **2016**, *44*, 609–621. [[CrossRef](#)] [[PubMed](#)]
92. Bozdağ-Dündar, O.; Evranos, B.; Daş-Evcimen, N.; Sarıkaya, M.; Ertan, R. Synthesis and aldose reductase inhibition activity of some new chromonyl-2,4-thiazolidinediones. *Eur. J. Med. Chem.* **2008**, *43*, 2412–2417. [[CrossRef](#)] [[PubMed](#)]

93. Lipinski, C.A.; Lombardo, F.; Dominy, B.W.; Feeney, P.J. Experimental and computational approaches to estimate solubility and permeability in drug discovery and development settings. *Adv. Drug Deliv. Rev.* **2012**, *64*, 4–17. [[CrossRef](#)]
94. Veber, D.F.; Johnson, S.R.; Cheng, H.-Y.; Smith, B.R.; Ward, K.W.; Kopple, K.D. Molecular Properties That Influence the Oral Bioavailability of Drug Candidates. *J. Med. Chem.* **2002**, *45*, 2615–2623. [[CrossRef](#)] [[PubMed](#)]
95. Egan, W.J.; Merz, K.M.; Baldwin, J.J. Prediction of Drug Absorption Using Multivariate Statistics. *J. Med. Chem.* **2000**, *43*, 3867–3877. [[CrossRef](#)]



© 2019 by the authors. Licensee MDPI, Basel, Switzerland. This article is an open access article distributed under the terms and conditions of the Creative Commons Attribution (CC BY) license (<http://creativecommons.org/licenses/by/4.0/>).



Antioxidant activity and antibacterial evaluation of new thiazolin-4-one derivatives as potential tryptophanyl-tRNA synthetase inhibitors

Anca Stana, Dan C. Vodnar, Gabriel Marc, Daniela Benedec, Brîndușa Tipericiuc, Radu Tamaian & Ovidiu Oniga

To cite this article: Anca Stana, Dan C. Vodnar, Gabriel Marc, Daniela Benedec, Brîndușa Tipericiuc, Radu Tamaian & Ovidiu Oniga (2019) Antioxidant activity and antibacterial evaluation of new thiazolin-4-one derivatives as potential tryptophanyl-tRNA synthetase inhibitors, *Journal of Enzyme Inhibition and Medicinal Chemistry*, 34:1, 898-908, DOI: [10.1080/14756366.2019.1596086](https://doi.org/10.1080/14756366.2019.1596086)

To link to this article: <https://doi.org/10.1080/14756366.2019.1596086>



© 2019 The Author(s). Published by Informa UK Limited, trading as Taylor & Francis Group.



[View supplementary material](#)



Published online: 02 Apr 2019.



[Submit your article to this journal](#)




[View Crossmark data](#)

RESEARCH PAPER



Antioxidant activity and antibacterial evaluation of new thiazolin-4-one derivatives as potential tryptophanyl-tRNA synthetase inhibitors

Anca Stana^{a*} , Dan C. Vodnar^b, Gabriel Marc^{a*}, Daniela Benedec^c, Brîndușa Tiperciuc^{a*}, Radu Tamaian^{d,e} and Ovidiu Oniga^a

^aDepartment of Pharmaceutical Chemistry, “Iuliu Hațieganu” University of Medicine and Pharmacy, Cluj-Napoca, Romania; ^bDepartment of Food Science and Technology, University of Agricultural Sciences and Veterinary Medicine, Cluj-Napoca, Romania; ^cDepartment of Pharmacognosy, “Iuliu Hațieganu” University of Medicine and Pharmacy, Cluj-Napoca, Romania; ^dICSI Analytics Department, National Research and Development Institute for Cryogenics and Isotopic Technologies - ICSI Rm. Vâlcea, Râmnicu Vâlcea, Romania; ^eSC Biotech Corp SRL, Râmnicu Vâlcea, Romania

ABSTRACT

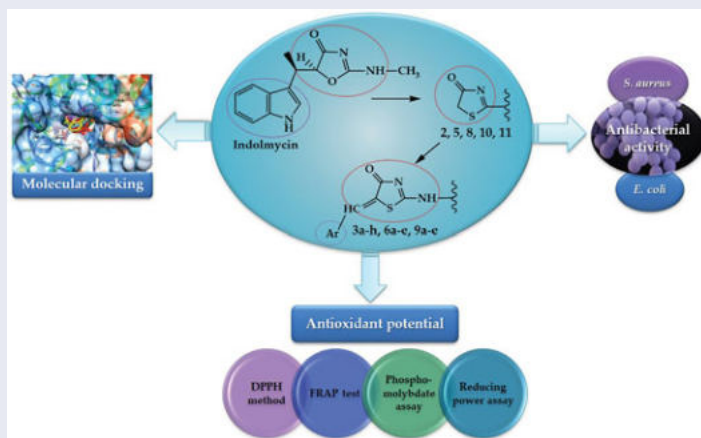
The rapid emergence of bacterial resistance to antibiotics currently available for treating infectious diseases requires effective antimicrobial agents with new structural profiles and mechanisms of action. Twenty-three thiazolin-4-one derivatives were evaluated for their antibacterial activity by determining the growth inhibition zone diameter, the minimum inhibitory concentration (MIC), and the minimum bactericidal concentration (MBC), against gram-positive and gram-negative bacteria. Compounds **3a–c**, **3e–h**, **6b–c** and **9a–c** expressed better MIC values than moxifloxacin, against *Staphylococcus aureus*. Compounds **3h** and **9b** displayed similar effect to indolmycin, a tryptophanyl-tRNA ligase inhibitor. Due to their structural analogy to indolmycin, all compounds were subjected to molecular docking on tryptophanyl-tRNA synthetase. Compounds **3a–e**, **6a–e**, **8** and **9a–e** exhibited better binding affinities towards the target enzymes than indolmycin. The antioxidant potential of the compounds was evaluated by four spectrophotometric methods. Thiazolin-4-ones **3e**, **6e** and **9e** presented better antiradical activity than ascorbic acid, trolox and BHT, used as references.

ARTICLE HISTORY

Received 6 January 2019
Revised 27 February 2019
Accepted 11 March 2019

KEYWORDS



Thiazolin-4-one; antibacterial activity; antioxidant activity; tryptophanyl-tRNA synthetase; docking




1. Introduction

Thiazoles, in general, and their derivatives, thiazolin-4-ones, in particular, are an important class of heterocyclic compounds, with a remarkable medicinal value. They have been associated with a large variety of significant pharmacological activities, such as antifungal^{1–3}, antibacterial^{4,5}, antitumor^{3,4,6}, antiviral⁷, antioxidant^{6,8}, neuroprotective⁹, analgesic, anti-inflammatory^{4,10} and anticonvulsant⁹.

The significant progress of medicinal chemistry, represented by the discovery of antibiotics, during the past decades led to major improvements in the diagnosis, prognosis and therapy of infections. Despite the numerous antibacterial agents approved for the treatment of infectious diseases, the continuously developing resistance of bacteria to most common classes of antibiotics and the emerging difficulties in dealing with infections outcome in

CONTACT Dan C. Vodnar  dan.vodnar@usamvcluj.ro  Department of Food Science and Technology, University of Agricultural Sciences and Veterinary Medicine, 3-5 Manăștur Street, Cluj-Napoca, RO-400372, Romania

*These authors contributed equally to this work.

 Supplemental data for this article can be accessed [here](#).

© 2019 The Author(s). Published by Informa UK Limited, trading as Taylor & Francis Group.

This is an Open Access article distributed under the terms of the Creative Commons Attribution License (<http://creativecommons.org/licenses/by/4.0/>), which permits unrestricted use, distribution, and reproduction in any medium, provided the original work is properly cited.

hospitalised patients or in patients with impaired immune system¹¹, drew the scientists' attention towards the discovery of effective antimicrobial agents, with new structural profiles and mechanisms of action.

The aminoacyl-tRNA synthetases, also called aminoacyl-tRNA ligases, are a class of validated enzymatic targets that remain underexploited and that play an important role in RNA translation, the expression of genes to create proteins. Aminoacyl-tRNA synthetases are responsible for the precision of ribosomal protein biosynthesis by ensuring that amino acids are correctly esterified to their corresponding tRNA molecules. In general, there is a specific aminoacyl-tRNA synthetase available for each amino acid¹². Compounds that can selectively inhibit these bacterial enzymes without interfering with their mammalian analogues are therefore potential candidates for antimicrobial agents. There have been reported several natural aminoacyl-tRNA synthetase inhibitors, like indolmycin (a tryptophanyl-tRNA synthetase (TrpRS) inhibitor), granaticin (a leucyl-tRNA synthetase inhibitor), mupirocin (a isoleucyl-tRNA synthetase inhibitor, clinically used as a topical antibacterial agent), and ochratoxin A (a phenylalanyl-tRNA synthetase inhibitor)¹³.

Indolmycin is a natural antibiotic that was first isolated in 1960 and that competitively inhibits the bacterial TrpRS, due to its analogy to L-tryptophan (Figure 1). This enzyme activates L-tryptophan for translation by forming a tryptophyladenylate intermediate and then it links this activated amino acid to the corresponding tRNA molecule (tryptophanyl-tRNA). Although potent antibacterial activity against bacteria like *Helicobacter pylori*, *Escherichia coli*, *Bacillus subtilis*, and mupirocin and methicillin-resistant *Staphylococcus aureus* was reported for indolmycin, because of its insufficient activity against common pathogenic bacteria, the development of indolmycin for chemotherapeutic use was abandoned^{14,15}. Better antibacterial potential was reported against gram-positive bacteria due to a higher

intracellular uptake of indolmycin by the uptake systems for tryptophan. A poorer antibacterial activity on gram-negative bacteria was attributed to the lower penetrability of indolmycin through the hydrophilic barrier of the outer membrane, due to its increased hydrophobicity¹⁶.

The excess of reactive oxygen and nitrogen species causes oxidative stress, that has been increasingly recognised in the last decades as an important contributing factor in the pathogenesis of many serious diseases, such as atherosclerosis, heart failure, myocardial infarction, diabetes and its complications, several neurodegenerative diseases, cancer and cirrhosis of the liver¹⁷. Some phenolic synthetic antioxidants, like butylhydroxytoluene and butylhydroxyanisole, widely used as antioxidants and preservatives in the food industry, pharmaceutical preparations, and cosmetic formulations are anticipated to be tumour promoters, based on reported evidence of carcinogenicity from studies in experimental animals¹⁸. Therefore, there is a great demand for the discovery of new potent antioxidant therapeutics, with a better pharmaco-toxicological profile. Compounds bearing chromone, thiazole, thiazolin-4-one, or phenol moieties^{8,19,20} have been reported to possess antioxidant activities.

There is also an increased need for the discovery of novel antibacterial agents, especially for the treatment of chronic infections such as mucoviscidosis, a genetic disease that is frequently associated with infections caused by drug-resistant pathogens and epithelial damage due to pulmonary oxidative stress. In these situations, it would be useful to develop bioactive compounds that have antioxidant and antibacterial properties combined in the same molecule. A better therapeutic solution for treating complex multigenic diseases like the one mentioned above would be the development of new dual-active antibacterial-antioxidant agents²¹.

Based on the various biological activities of the thiazoline-4-ones that have been reported in the literature, we present herein

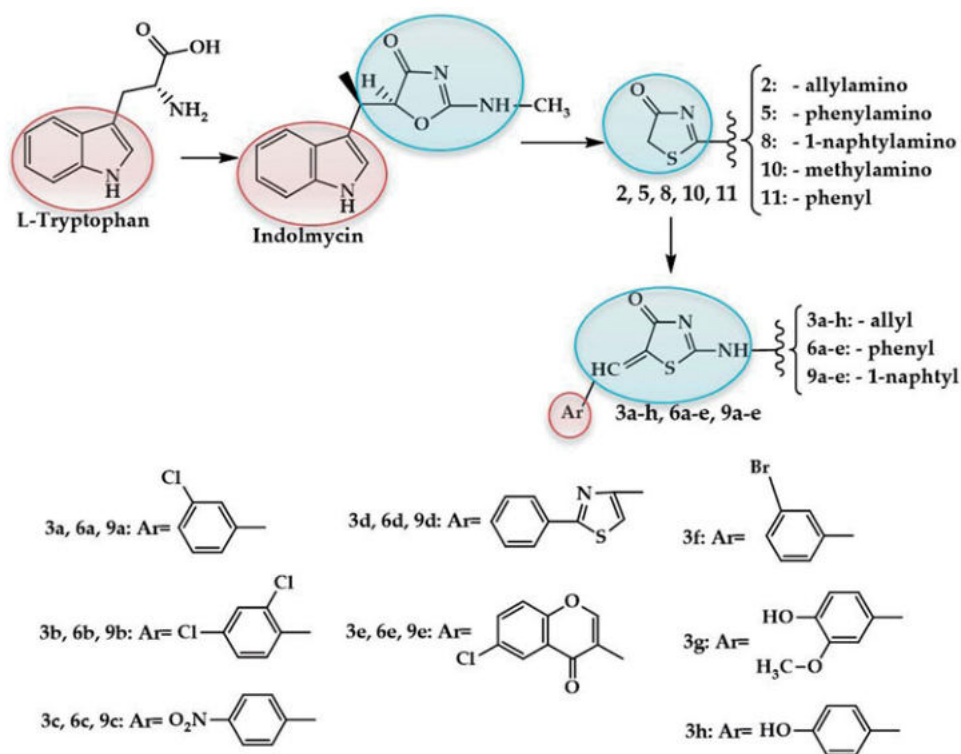


Figure 1. The study design and the chemical structures of the synthesized compounds.

the antibacterial and antioxidant activity evaluation of previously synthesized thiazoline-4-ones² diversely substituted in positions 2 and 5. In order to establish the compounds potential mechanism of action, due to their structural analogy to indolmycin (Figure 1), the previously reported thiazolin-4-one derivatives² were docked against two bacterial tryptophanyl-tRNA ligases and their affinities towards these biological targets were assessed. As some of the compounds have other chromophores in their structure, like the chromone, thiazole and phenol moiety, with proven antioxidant activity^{8,19,20}, the antioxidant potential of the compounds was evaluated by assessing the DPPH• radical scavenging activity, the ferric reducing antioxidant power (FRAP), the reducing power and the total antioxidant capacity (TAC).

2. Materials and methods

2.1. Antibacterial activity assays

Stock solutions (1 mg/mL) were prepared by dissolving the test compounds (the thiazolin-4-one derivatives and indolmycin) and the reference antibacterial agent (moxifloxacin) in sterile dimethyl sulfoxide (DMSO). Moxifloxacin and DMSO were purchased from Merck (Darmstadt, Germany) and indolmycin was purchased from Toronto Research Chemicals (North York, Canada).

The microorganisms used for the antimicrobial activity evaluation were obtained from the University of Agricultural Sciences and Veterinary Medicine Cluj-Napoca, Romania. The inhibition zone diameters, the minimum inhibitory concentration (MIC) and minimum bactericidal concentration (MBC) values were determined against cultures of gram-positive bacteria *S. aureus* ATCC 49444 and gram-negative bacteria *E. coli* ATCC 25922.

2.1.1. Determination of inhibition zone diameters

The *in vitro* antimicrobial activity was determined using the cup-plate agar diffusion method according to the Clinical and Laboratory Standards Institute (CLSI) guidelines²².

For antibacterial testing, Mueller–Hinton agar medium and 0.5 mg/mL methylene blue (providing a better definition of the inhibition zone diameter) were used. The inoculum was prepared by suspending five representative colonies, obtained from an 18–24 h culture on nonselective nutritive agar medium, in sterile distilled water. The cell density was adjusted to the density of a 0.5 McFarland standard by measuring the absorbance in a spectrophotometer at a wavelength of 530 nm and adding sterile distilled water as required (corresponding to a population of $1\text{--}5 \times 10^3$ CFU/mL). A sterile swab was soaked in suspension and then the Mueller–Hinton agar plates were inoculated by streaking the entire surface. After drying for 10–15 min, six-millimeter diameter wells were cut from the agar using a sterile cork-borer, and a volume of 20 μ L of each compound solution (1 mg/mL in DMSO) was delivered into the wells (20 μ g/well). Moxifloxacin (20 μ g/well) was used as standard drug. The controls were performed with only sterile broth, overnight culture and 20 μ L of DMSO. The plates were incubated at 35 °C. Zone diameters were measured to the nearest whole millimeter, at a point in which there was no visible growth after 24–48 h. Results were obtained in triplicate. The solvent used for the preparation of each compound stock solution (1 mg/mL), DMSO exhibited no inhibitory activity against the tested bacterial strains.

2.1.2. Determination of MIC and MBC values

Antibacterial activity was tested by the broth microdilution method according to the Clinical and Laboratory Standard Institute (CLSI) guidelines²³, following a previously reported protocol²⁴. The growth control, sterility control and control of antibacterial compounds were used. The MIC was defined as the lowest concentration required for arresting the growth of bacteria. The MBC was defined as the lowest concentration of the agent at which no colonies are observed. All MIC and MBC assays were repeated three times.

2.2. Antioxidant activity assays

1 mg/mL stock solutions of the tested compounds (**2**, **3a–h**, **5**, **6a–e**, **8**, **9a–e**, **10** and **11**) were prepared by dissolving the solid powders in DMSO.

Overlapping of the absorption spectra of the compounds in the region 430–700 nm (Figure S1 in Supplementary Materials) was realised using a UV-VIS spectrophotometer Jasco V-530 (Jasco International Co., Tokyo, Japan) and 2.5 mL cuvettes of poly(methyl methacrylate) with a 10 mm light path. None of the tested compounds have absorption peaks near the wavelengths where the antioxidant and antiradical assays were performed (517 nm, 593 nm, 695 nm, and 700 nm). All the assays were performed in triplicate, mean values of different measurements being reported.

Analytical grade methanol and DMSO were purchased from Sigma (St. Louis, MO), DPPH•, ascorbic acid, trolox and dibutylhydroxytoluene (BHT) were purchased from Alfa-Aesar (Karlsruhe, Germany).

2.2.1. The DPPH• scavenging activity

The antioxidant potential of the synthesized compounds was assessed on the basis of their radical scavenging effect of the stable 2,2-diphenyl-1-picrylhydrazyl (DPPH•) following a previously described method in the literature with a few minor modifications^{25,26}. The samples were dissolved in DMSO or absolute methanol according to the compound's solubility to give a stock solution of 5 mg/mL. For the most active compounds (**3e**, **6e**, **9e**), dilutions were made to obtain a stock solution of 0.2 mg/mL. To different volumes (0.25 mL, 0.50 mL, 0.75 mL, 1 mL, 1.25 mL, 1.50 mL, 1.75 mL, 2 mL) of each compound's stock solution, methanol was added in order to obtain 2 ml of sample solution and subsequently, 2 ml of DPPH• solution in methanol (0.1 mg/mL) was added. The mixture was shaken vigorously and left to stand in dark for 30 min in a water bath at 40 °C, and then the absorbance at 517 nm was read using a UV-VIS spectrophotometer Jasco V-530 (Jasco International Co.), against a blank solution. Ascorbic acid, trolox, and BHT were used as standard antioxidants. The ability to inhibit the free radicals of DPPH• was calculated according to the formula:

$$\text{Inhibition ratio}\% = [(A_0 - A_5)/A_0] \times 100$$

A_0 is the absorbance of DPPH• methanol solution and A_5 is the absorbance of sample after 30 min. The radical scavenging ability was measured as a decrease in the absorbance of DPPH•. Lower absorbance of the reaction mixture has indicated higher free radical scavenging activity.

Subsequently, the ability to neutralise the DPPH• radicals was evaluated as a percentage, through its graphic representation according to the concentration, which allowed calculation of the EC₅₀ values, the test compound's concentration at which 50% of

the DPPH[•] radicals are scavenged. The EC₅₀ value is correlated to the antioxidant capacity of the compound. The smaller this value is, the higher is the antioxidant activity of the compound. All determinations were performed in triplicate and the average thereof was the final value.

2.2.2. The FRAP test

The reducing power of the tested compounds was determined by the FRAP assay, according to a modified method, initially proposed by Benzie and Strain^{27–29}. 50 µL of each compound's solution (1 mg/mL in DMSO) was mixed with 1000 µL of FRAP reagent^{27,29} and the resulted mixture were vigorously shaken for 30 min. Their absorbance was measured at $\lambda = 593$ nm, compared to a blank sample, where 50 µL of DMSO and 1000 µL of FRAP reagent were taken. The reducing power was compared to trolox, BHT and ascorbic acid, used as standard antioxidants and expressed as percent of control's reducing power, based on the following formula:

$$\% \text{ of control ferric reducing power} = \frac{[(\text{sample absorbance}) / (\text{control absorbance})] \times 100}$$

A calibration curve ($R^2 = 0.9993$) was made using an aqueous 1 mM ferrous sulfate solution, with concentrations ranging from 0.1 to 1.0 mM, tested in the same way as the test compounds. The resulted absorbance of each tested compound was interpolated to give the equivalent Fe²⁺ amount, generated by the reduction of ferric ions.

2.2.3. The phosphomolybdate assay for TAC

To determine the TAC of the tested compounds, we used a previously reported procedure^{29–31}, with slight modifications. To 100 µL of each compound's solution (1 mg/mL in DMSO), 1 mL reagent²⁹ was added in test tubes, then they were well mixed and incubated for 90 min in a water bath at 95 °C. After cooling at room temperature, the absorbance of the samples was measured against blank at $\lambda = 695$ nm. The TAC of compounds was expressed as percent of standard antioxidant power.

$$\% \text{ of control antioxidant power} = \frac{[(\text{sample absorbance}) / (\text{control absorbance})] \times 100}$$

2.2.4. The reducing power assay

In this assay, the tested compound reduces the ferric ions from potassium ferricyanide and the resulted ferrocyanide forms a blue complex in the presence of ferric ions. The principle driving this method is based on increasing the absorbance in the final test tubes. An increase in the antioxidant activity is correlated with an increase in the absorbance. The current assay was adapted to a semi-microscale based on previous literature reports²⁹. 0.1 mL of the stock solutions of compounds **2**, **3a–h**, **5**, **6a–e**, **8**, **9a–e**, **10** and **11** subjected to testing, was mixed with 1 mL of DMSO, 0.4 mL of phosphate buffer (0.2 M, pH = 6.6) and 0.4 mL of K₃[Fe(CN)₆] (1% w/v). The mixture was incubated in a water bath at 50 °C for 20 min. After cooling at room temperature, 0.5 mL of trichloroacetic acid (10% w/w) was added. The resulting mixture was left to rest for 30 min, for eventually resulting precipitates to deposit on the bottom of the test tubes. 0.25 mL of the solution was collected carefully and mixed with 0.14 mL of FeCl₃ (0.1% w/v) and 0.75 mL of distilled water. The absorbance was measured at $\lambda = 700$ nm

against a blank sample. Results were calculated using the formula:

$$\% \text{ of control reducing power} = \frac{[(\text{sample absorbance}) / (\text{control absorbance})] \times 100}$$

2.3. Molecular docking studies

The three-dimensional structures of compounds **2**, **3a–h**, **5**, **6a–e**, **8**, **9a–e**, **10**, **11** and indolmycin, considered as ligands in the molecular docking study, were prepared based on a previously reported protocol³² following the drawing and energy minimisation, carefully observing the double bond isomerism in position 5 of the thiazolin-4-one nucleus and subsequently converting to pdbqt file using OpenBabel 2.3.2³³ and Python preparation ligand script version 4 from AutoDockTools 1.5.6³⁴.

Two structures of TrpRS were used as targets in the molecular docking study: 5V0I and P67592_1I6K. The structure 5V0I, isolated from *E. coli*, was taken as it is from Protein Data Bank (<http://www.rcsb.org>), while P67592_1I6K was built by homology modelling, due to the lack of deposited high-resolution structures of TrpRS isolated from *S. aureus*. Based on the amino acid sequence of the *S. aureus* enzyme taken from Uniprot (P67592 sequence) and the PDB 1I6K as template, the P67592_1I6K structure was modelled using the SWISS-MODEL service^{35,36}.

In the target file structures, polar hydrogen atoms were added, nonpolar were removed, ligands and other additional molecules removed, and Gasteiger charges were defined using AutoDockTools 1.5.6. Both proposed structures as targets were subjected to an analysis with BLASTP 2.6.1 service³⁷, which detected conserved domains in our structures and confirmed the membership of the two structures to the PRK12282 superfamily. More, the active residues in the catalytic sites of both proteins were identified and are depicted with red in Figures S2 and S5 (in Supplementary Materials) generated after sequence alignments using EMBOSS Stretcher (<https://www.ebi.ac.uk>). Analysis of the pockets in the catalytic sites of the enzymes was performed using DoGSiteScorer³⁸.

For both enzymes, search space was configured, taking care that all amino acids presented as important in the catalytic site were included. Search space sides were set to $x=y=z=60$ for both targets and the centre of the search space was defined as $x=15.898$, $y=6.481$, $z=9.892$ for 5V0I and $x=55.048$, $y=21.595$, $z=40.051$ for P67592_1I6K. Fifty conformations were generated for each molecular docking study, clustered in 2 Å cluster tolerance. Based on the computed binding affinity (BA) energy (ΔG), inhibition constants (K_i) were calculated using the formula:

$$K_i = e^{\frac{\Delta G \times 1000}{R \times T}}$$

where R represents the Regnault constant = $1.98719 \frac{\text{kcal}}{\text{K} \times \text{mol}}$ and $T = 298.15$ K.

Visualisation and analysis of the docking results were performed using Chimera 1.10.2³⁹ and AutoDockTools 1.5.6. Hydrophobicity surface representations were generated with transparency set to 50%.

3. Results and discussion

3.1. Antibacterial activity

3.1.1. Determination of inhibition zone diameters

All the synthesized compounds were initially subjected to *in vitro* antimicrobial screening using the cup-plate agar diffusion method,

Table 1. The inhibition zone diameters of the synthesized thiazolin-4-one derivatives^a.

Compound	<i>S. aureus</i> ATCC 49444		<i>E. coli</i> ATCC 25922	
	Diameter (mm)	%AI	Diameter (mm)	%AI
2	6	33.3	14	51.8
3a	14	77.7	14	51.8
3b	16	88.8	14	51.8
3c	16	88.8	14	51.8
3d	12	66.6	14	51.8
3e	18	100	16	59.2
3f	18	100	20	74.1
3g	18	100	16	59.2
3h	18	100	16	59.2
5	6	33.3	14	51.8
6a	12	66.6	16	59.2
6b	14	77.7	16	59.2
6c	16	88.8	16	59.2
6d	12	66.6	16	59.2
6e	14	77.7	16	59.2
8	6	33.3	18	66.6
9a	20	111.1	16	59.2
9b	20	111.1	22	81.4
9c	18	100	14	51.8
9d	14	77.7	14	51.8
9e	16	88.8	18	66.6
10	8	44.4	22	81.4
11	6	33.3	14	51.8
Indolmycin	20	111.1	14	51.8
Moxifloxacin	18	100	27	100

^aAll determinations were performed in triplicate ($n=3$) and the average thereof was the final value. The values obtained for the most active compounds are marked in bold. %AI: percentage activity index [(Inhibition zone diameter of synthetic compound/Inhibition zone diameter of moxifloxacin) \times 100].

against a gram-negative bacterial strain (*E. coli* ATCC 25922) and a gram-positive bacterial strain (*S. aureus* ATCC 49444).

The results of the antimicrobial activity testing of the 2-substituted-thiazolin-4-ones **2**, **5**, **8**, **10**, **11**, of the 2-(allyl/aryl-amino)-5-arylidene-thiazolin-4-ones **3a–h**, **6a–e**, **9a–e**, and indolmycin, in comparison with those of the reference compound used (moxifloxacin) are given in Table 1.

All the tested compounds were active and showed moderate to good inhibitory activity against gram-positive and gram-negative bacteria. All the synthesized compounds and indolmycin were active, recording a moderate antibacterial activity against *E. coli* ATCC 25922 (14–22 mm inhibition zone diameters), lower than the reference antibiotic. Although no major differences were observed between the compounds' inhibitory activities against the gram-negative bacterial strain used for testing, the thiazolin-4-ones **3f**, **8**, **9b**, **9e** and **10** were slightly more active than the rest of the compounds.

The synthesized thiazolin-4-ones and indolmycin were also active against *S. aureus* ATCC 49444, showing modest to good inhibitory activity. Of these, compounds **3e–h**, **9a–c** and indolmycin exhibited similar or better antibacterial activities than moxifloxacin. The 2-(1-naphthylamino)-5-arylidene-thiazolin-4-ones **9a–e** were, in general, more active against *S. aureus* ATCC 49444 than the thiazolin-4-ones **3a–e** and **6a–e**, suggesting that the presence of a voluminous fragment, the α -naphthyl-amine, in position 2 of the thiazolin-4-one ring is more favourable to the antibacterial activity against the gram-positive bacterial strain, than the presence of an allylamine or phenylamine fragment, probably as a result of some differences regarding the compounds' intracellular uptake. The 2-(allyl/aryl-amino)-thiazolin-4-ones **2**, **5** and **8** presented lower inhibitory activities than the 5-substituted derivatives, indicating that the introduction of an arylidene rest in position 5 of the thiazolin-4-one moiety

Table 2. Minimum inhibitory concentration – MIC (in $\mu\text{g}/\text{mL}$) and minimum bactericidal concentration – MBC (in $\mu\text{g}/\text{mL}$) of thiazolin-4-one derivatives^a.

Samples	<i>S. aureus</i> ATCC 49444			<i>E. coli</i> ATCC 25922		
	MIC	MBC	MBC/MIC ratio	MIC	MBC	MBC/MIC ratio
2	62.5	62.5	1	62.5	125	2
5	62.5	125	2	62.5	125	2
8	62.5	125	2	15.62	31.25	2
10	62.5	125	2	7.81	15.62	2
11	62.5	125	2	62.5	125	2
3a	31.25	62.5	2	62.5	62.5	1
3b	31.25	62.5	2	62.5	62.5	1
3c	31.25	31.25	1	62.5	62.5	1
3d	62.5	125	2	62.5	62.5	1
3e	15.62	31.25	2	62.5	62.5	1
3f	7.81	15.62	2	31.25	62.5	2
3g	31.25	31.25	1	62.5	125	2
3h	0.97	1.95	2	62.5	125	2
6a	62.5	125	2	62.5	125	2
6b	31.25	62.5	2	62.5	125	2
6c	31.25	62.5	2	62.5	125	2
6d	62.5	62.5	1	62.5	125	2
6e	62.5	125	2	62.5	125	2
9a	3.9	7.81	2	62.5	125	2
9b	0.97	1.95	2	15.62	15.62	1
9c	31.25	62.5	2	62.5	125	2
9d	125	250	2	125	250	2
9e	62.5	62.5	1	62.5	125	2
Indolmycin	0.97	1.95	2	31.25	62.5	2
Moxifloxacin	31.25	62.5	2	1.95	3.9	2
Inoculum	+++	+++	–	+++	+++	–
control						
Broth control	No growth	No growth	–	No growth	No growth	–

The values obtained for the most active compounds are marked in bold.

– indicates no inhibitory activity; +++ indicates growth in all concentrations.

^aAll determinations were performed in triplicate ($n=3$) and the average thereof was the final value.

significantly increases the antibacterial potential against *S. aureus* ATCC 49444.

Also, the fact that compound **3f** (having a 3-bromobenzylidene moiety in its structure) was more active than compound **3a** (with a 3-chlorobenzylidene rest) against both bacterial strains tested, suggested that the presence of a more voluminous halogen atom, like bromine, in position 3 of the benzene ring enhances the antibacterial properties of the compound. Supplementary, compounds bearing two chlorine atoms were generally more active than the compounds with only one chlorine atom (compounds **b** vs. compounds **a**), suggesting that the presence of more halogen atoms in the molecule is favourable to the antibacterial activity (probably due to an increase in compound's lipophilicity that enhances the intracellular uptake of the compound by the bacteria).

3.1.2. Determination of MIC and MBC values

Prompted by the results obtained in the antimicrobial screening using the agar diffusion method, MICs and MBCs were determined, employing the broth microdilution method. All the synthesized compounds and indolmycin were tested against the same bacteria strains used in the previous study (*S. aureus* ATCC 49444 and *E. coli* ATCC 25922). Moxifloxacin was used as positive control for antibacterial activity. The results are depicted in Table 2.

The MIC values against *S. aureus* ranged from 0.97 $\mu\text{g}/\text{mL}$ (compounds **3h**, **9b** and indolmycin) to 125 $\mu\text{g}/\text{mL}$ (compound **9d**) and the MBC values ranged from 1.95 $\mu\text{g}/\text{mL}$ (compounds **3h** and **9b**) to 250 $\mu\text{g}/\text{mL}$ (compound **9d**). Against *E. coli*, the compounds' MIC values ranged from 7.81 $\mu\text{g}/\text{mL}$ (compound **10**) to 125 $\mu\text{g}/\text{mL}$ (compound **9d**) and the MBC values ranged from 15.62 $\mu\text{g}/\text{mL}$

(compounds **10** and **9b**) to 250 µg/mL (compound **9d**). Analyzing the results obtained, it can be seen that the growth inhibitory activity was more pronounced against *S. aureus*, where 12 compounds exhibited similar or higher MIC values than moxifloxacin and 15 compounds presented similar or higher MBC values than moxifloxacin. The strain of *E. coli* was less sensitive to the activity of thiazolin-4-one derivatives, which displayed lower MIC and MBC values than the antibacterial used as a reference, in agreement with the inhibitory zone diameters.

All the synthesized thiazolin-4-ones presented moderate to good antibacterial properties. Overall, the compounds were more active against the gram-positive bacterial strain than against the gram-negative bacterial strain used in the antibacterial activity assays. The thiazolin-4-one derivatives **3h** and **9b** displayed the best antibacterial activity against *S. aureus*, similar to indolmycin and 32 fold better than that of moxifloxacin. The most active compounds against *E. coli* were the thiazolin-4-ones **8**, **10** and **9b**, which presented similar or better antibacterial activity than indolmycin, but lower than moxifloxacin. The calculated MBC/MIC ratio suggested a bactericidal effect for these compounds.

3.2. Antioxidant activity

One of the bacterial mechanisms of resistance to antibiotics is the ability to form biofilms. Oxidative stress was recently reported to be a potential contributing factor for the selection of resistant bacterial strains, since reactive oxygen species were incriminated in the selection of pro-biofilm variants selection⁴⁰, thus the need for discovery of agents with both antibacterial and antioxidant activities.

3.2.1. The DPPH* scavenging activity

The antioxidant potential of all the synthesized compounds was assessed by measuring their ability to act as free radical scavengers or hydrogen donors, using the DPPH (2,2-diphenyl-1-picrylhydrazyl) method. The results of the antioxidant activity of

Table 3. The DPPH* scavenging activity of thiazolin-4-one derivatives.

Compound	EC ₅₀ (µg/mL) ^a
2	2177 ± 1.3
3a	–
3b	–
3c	2747 ± 2.2
3d	–
3e	20 ± 0.9
3f	–
3g	2524 ± 1.1
3h	2498 ± 1.5
5	590 ± 1.0
6a	2604 ± 1.2
6b	–
6c	2634 ± 1.6
6d	–
6e	12 ± 0.8
8	–
9a	4685 ± 1.9
9b	–
9c	885 ± 2.0
9d	> 5000
9e	24 ± 1.4
10	665 ± 0.7
11	923 ± 1.3
BHT	47 ± 0.5
Trolox	65 ± 1.2
Ascorbic acid	25 ± 0.3

^aMean ± SD (n = 3).

– indicates no free radical scavenging activity. The values obtained for the most active compounds are marked in bold.

thiazolin-4-one derivatives in comparison with those of the antioxidants (BHT, trolox, and ascorbic acid) used as references are presented in Table 3.

Of the 23 thiazolin-4-one derivatives tested, 15 showed a modest to good inhibitory activity, the rest being inactive compounds. The most active compounds were the thiazolin-4-one derivatives **3e**, **6e** and **9e**. They exhibited better antioxidant activity than the reference compounds used (ascorbic acid, trolox and BHT), suggesting that the presence of a chromonyl rest in their structure enhances the antiradical activity of the compounds by increasing their capacity to act as hydrogen donors.

3.2.2. The reducing power by FRAP test

The electron donating capacity of thiazolin-4-one derivatives was determined spectrophotometrically using the FRAP assay. This assay is based on the reduction of ferric ions to ferrous ions by the tested molecules. The resulted ferrous ions form a blue-coloured complex (Fe²⁺-TPTZ) at pH = 3.6 with tripyridyltriazine (2,4,6-Tris(2-pyridyl)-s-triazine). The amount of blue complex resulted is proportional with the reducing capacity of Fe³⁺ by the tested compounds. The results obtained are presented in Table 4.

All the compounds presented lower reducing capacities than those of the reference antioxidants (trolox, ascorbic acid, and BHT) used in the assay. The compounds with the best reducing abilities were the thiazolin-4-one derivatives **3e**, **6e** and **9e** that have a chromonyl moiety in their structure.

3.2.3. The phosphomolybdate assay for TAC

The assay is based on the reduction of Mo⁶⁺ to Mo⁵⁺ in the presence of a reducing agent (antioxidant), involving one electron transfer mechanism with the formation of a green phosphate

Table 4. The ferric reducing capacity of thiazolin-4-ones by FRAP test^a.

Compound	% of trolox reducing power (mg/mg)	% of ascorbic acid reducing power (mg/mg)	% of BHT reducing power (mg/mg)	Fe ²⁺ equivalents generated
2	5.97	6.21	8.87	0.1221
3a	5.73	5.96	8.51	0.1183
3b	7.93	8.25	11.78	0.1536
3c	9.51	9.90	14.13	0.1790
3d	5.77	6.01	8.57	0.1189
3e	24.61	25.61	36.55	0.4214
3f	12.76	13.28	18.96	0.2312
3g	11.98	12.47	17.79	0.2186
3h	7.94	8.26	11.79	0.1538
5	7.74	8.05	11.49	0.1505
6a	16.20	16.86	24.06	0.2864
6b	5.52	5.75	8.20	0.1149
6c	7.23	7.53	10.74	0.1424
6d	7.75	8.07	11.51	0.1507
6e	35.86	37.32	53.26	0.6022
8	5.84	6.08	8.68	0.1200
9a	8.16	8.50	12.13	0.1573
9b	5.07	5.28	7.53	0.1076
9c	9.59	9.99	14.25	0.1803
9d	10.12	10.54	15.04	0.1888
9e	46.15	48.03	68.55	0.7675
10	10.04	10.45	14.00	0.1875
11	16.79	17.47	24.93	0.2958
Trolox	N/A	N/A	N/A	1.6323
Ascorbic acid	N/A	N/A	N/A	1.5694
BHT	N/A	N/A	N/A	1.1076

N/A: not available/assigned. The values obtained for the most active compounds are marked in bold.

^aAll determinations were performed in triplicate (n = 3) and the average thereof was the final value.

Table 5. The total antioxidant capacity of the thiazolin-4-one derivatives^a.

Compound	% of trolox antioxidant power (mg/mg)	% of ascorbic acid antioxidant power (mg/mg)	% of BHT antioxidant power (mg/mg)
2	5.75	3.34	17.69
3a	5.13	2.97	15.76
3b	8.47	4.91	26.03
3c	10.36	6.01	31.85
3d	4.61	2.67	14.17
3e	9.48	5.50	29.13
3f	10.83	6.28	33.30
3g	10.62	6.16	32.65
3h	5.13	2.97	15.76
5	6.44	3.73	19.78
6a	22.51	13.05	69.17
6b	10.27	5.95	31.56
6c	22.69	13.16	69.74
6d	6.91	4.01	21.25
6e	55.84	32.38	171.63
8	5.61	3.25	17.25
9a	6.72	3.90	20.66
9b	9.01	5.23	27.70
9c	13.84	8.03	42.54
9d	5.93	3.44	18.21
9e	13.28	7.70	40.82
10	9.25	5.36	28.42
11	9.14	5.30	28.10

^aAll determinations were performed in triplicate ($n=3$) and the average thereof was the final value. The values obtained for the most active compounds are marked in bold.

Mo⁵⁺ complex at acidic pH, which can be monitored spectrophotometrically at 695 nm. A higher absorbance value indicates a better antioxidant power of the compound, when compared to a standard antioxidant.

The results of the compounds' TAC are presented in Table 5. Compounds **6a**, **6c**, **9c** and **9e** exhibited good total antioxidant capacities. The most active thiazolin-4-one derivative was **6e**, which presented a total antioxidant activity equivalent to 171.63% of BHT's antioxidant power.

3.2.4. The reducing power assay

In this assay, the reduction of ferricyanide to ferrocyanide gave the Perl's Prussian blue, in the presence of ferric ions. The resulted blue compound has an absorption peak at $\lambda=700$ nm. The absorbance measured is directly proportional with the percent of compound's reducing power when compared to a reference antioxidant. The results obtained in this experiment are presented in Table 6. All compounds exhibited lower reducing power than the antioxidants used as standards, and of these, compounds **3e**, **6a**, **6e** and **9e** presented the best reducing properties.

3.3. Molecular docking studies

All the investigated molecules (the thiazolin-4-one derivatives and indolmycin) were virtually subjected to docking, against the designated bacterial target (TrpRS) in order to investigate the potential binding mode and BA of these compounds. Docked ligand conformations (poses) were analyzed in terms of BA (expressed in kcal/mol) and polar interactions between the best poses and their target protein. Detailed analyses of the ligand-receptor interactions were carried out and final possible orientations of the ligands and receptors were saved.

Table 6. The reducing power of thiazolin-4-ones^a.

Compound	% of trolox reducing power (mg/mg)	% of ascorbic acid reducing power (mg/mg)	% of BHT reducing power (mg/mg)
2	0.44	0.44	0.50
3a	2.16	2.15	2.43
3b	3.71	3.68	4.18
3c	1.13	1.12	1.27
3d	6.35	6.30	7.14
3e	10.55	10.47	11.87
3f	7.81	7.75	8.79
3g	1.90	1.88	2.13
3h	0.18	0.18	0.20
5	6.56	6.51	7.38
6a	21.04	20.87	23.67
6b	3.25	3.22	3.65
6c	7.59	7.53	8.54
6d	5.50	5.45	6.18
6e	10.13	10.05	11.40
8	0.87	0.86	0.98
9a	1.21	1.20	1.36
9b	3.40	3.37	3.82
9c	0.40	0.40	0.45
9d	6.72	6.66	7.56
9e	17.13	16.99	19.26
10	0.57	0.57	0.65
11	4.83	4.79	5.43

^aAll determinations were performed in triplicate ($n=3$) and the average thereof was the final value. The values obtained for the most active compounds are marked in bold.

3.3.1. Docking against bacterial tryptophanyl-tRNA synthetase

Sequence alignment performed between *S. aureus* TrpRS's primary sequence P67592 and the sequence of the template PDB 1I6K structure, used in the homology modelling, suggested a common origin of both proteins. Multiple blocks or individual conserved residues were found between these two sequences (Figure S2, in Supplementary Materials). Based on these preliminary results, we considered that with the use of these two structures, we can develop the chimeric tridimensional structure of the corresponding missing TrpRS for *S. aureus*.

There are many validated primary structures of TrpRS isolated from various strains of *S. aureus* deposited in UniProt: P67593 – (strain N315), P67592 – strain Mu50/ATCC 700699, Q5HH88 – strain COL, Q6GI89 – strain MRSA252, Q6GAT0 – strain MSSA476, P67594 – strain MW2, T1Y8L7 from *S. aureus* subsp. *aureus* CN1, A0A0E0VMI8 from *S. aureus* subsp. *aureus* 71193, A0A0E1AGS6 from *S. aureus* subsp. *aureus* Z172, Q2FZQ7 – strain NCTC 8325, A0A0E1VIN1 from *S. aureus* subsp. *aureus* USA300_TCH959, A0A0E1X8M2 from *S. aureus* subsp. *aureus* MN8, A0A0H3KFE9 – strain Newman, A0A0H2XGX6 – strain USA300, A0A2H5AMI2 – strain 046. Studying these primary structures of the enzyme it was observed that, with the exception of the last one, which has a mutation, they are identical, thus the tryptophanyl-tRNA ligase of *S. aureus* is a highly conserved protein, without mutations, that can be considered a very attractive target for new antibiotics because along the way, during evolution, has not undergone evolution's pressure and did not develop mutations over time.

Compounds **2**, **3a–h**, **5**, **6a–e**, **8**, **9a–e**, **10**, **11** and indolmycin were docked *in silico* into the catalytic site of both TrpRSs (1I6K_P67592 and 5V0I). The predicted BA of the top binding conformation of the tested compounds to the catalytic sites of the enzymes and the consequent computed inhibition constant (K_i) of the best poses are presented in Table 7. The binding manner of all compounds in the catalytic sites of both enzymes is depicted

Table 7. The top binding affinity of compounds to *E. coli* TrpRS and *S. aureus* TrpRS, the computed inhibition constant and the mean binding affinities of compounds' conformations in the 2 Å cluster.

Compound	116K_P67592 (<i>S. aureus</i>)				PDB 5V01 (<i>E. coli</i>)			
	BA (kcal/mol)	K_i (nM)	2 Å cluster		BA (kcal/mol)	K_i (nM)	2 Å cluster	
			No. conf	Mean BA (kcal/mol)			No. conf	Mean BA (kcal/mol)
2	-5.13	173642.86	16	-4.88	-5.09	185770.75	25	-8.20
3a	-7.96	1462.98	21	-7.72	-8.15	1061.61	22	-7.88
3b	-8.11	1135.76	21	-7.92	-8.12	1116.75	14	-7.87
3c	-9.33	144.88	42	-8.96	-7.56	2873.70	7	-7.25
3d	-9.15	196.32	33	-9.10	-8.9	299.37	12	-8.42
3e	-8.94	279.83	31	-8.61	-8.89	304.47	2	-8.87
3f	-7.77	2016.09	39	-7.66	-8.42	673.06	35	-8.32
3g	-7.63	2553.47	5	-7.56	-8.19	992.31	36	-8.04
3h	-7.62	2596.94	10	-7.56	-7.86	1731.96	43	-7.81
5	-6.1	33778.23	47	-5.96	-6.79	10540.46	50	-6.77
6a	-8.59	505.17	23	-8.50	-9.79	66.65	18	-9.41
6b	-8.97	266.01	21	-8.68	-9.82	63.36	13	-9.37
6c	-10.11	38.84	28	-9.99	-8.86	320.28	10	-8.75
6d	-10.57	17.87	48	-10.41	-9.33	144.88	14	-9.11
6e	-10.34	26.34	35	-10.20	-10.31	27.71	3	-10.17
8	-7.88	1674.47	50	-7.83	-8.58	513.77	46	-8.46
9a	-10.51	19.77	33	-10.22	-11.12	7.06	32	-10.77
9b	-10.82	11.72	21	-10.48	-11.84	2.09	22	-11.32
9c	-11.24	5.77	22	-10.87	-10.87	10.77	2	-10.48
9d	-11.36	4.71	40	-10.97	-10.82	11.72	1	-10.82
9e	-12.1	1.35	37	-11.55	-12.2	1.14	3	-11.95
10	-5.73	63074.05	17	-5.71	-6.48	17786.60	47	-6.45
11	-4.34	658771.95	48	-4.33	-4.37	626245.74	35	-4.36
Indolmycin	-7.67	2386.77	5	-7.48	-8.65	456.52	25	-8.20

Bold values: The best binding affinities (higher than those of the reference compound).

BA: binding affinity (expressed in kcal/mol); No. conf: number of conformations; K_i : inhibition constant.

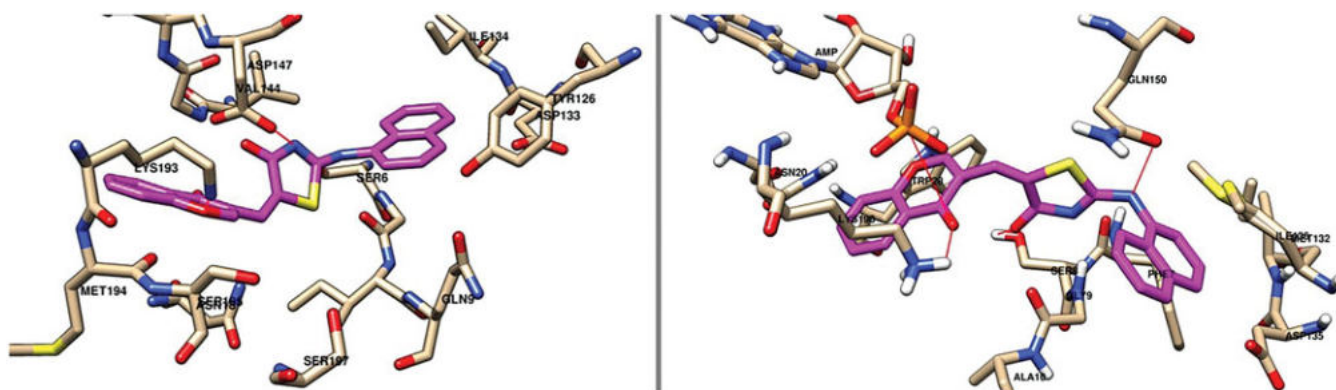


Figure 2. Docking pose of compound 9e in the active site of *S. aureus* TrpRS (left image) and *E. coli* TrpRS (right image) – the target is depicted as nude thin sticks, meanwhile the ligand is figured as pink sticks.

in Figure S3 (*S. aureus*) and Figure S4 (*E. coli*) in Supplementary Materials. The docking pose of the compound with the best BA toward the two targets, the thiazolin-4-one derivative **9e**, is presented in Figure 2.

For the top binding conformation of each compound, the number of other conformations out of the 50 predicted found in the 2 Å cluster inclusion limit are presented in Table 7.

There is an obvious increase in the interaction with the biological targets for the compounds functionalised in position 5 of the thiazolin-4-one nucleus, compared to the unsubstituted ones (the thiazolin-4-ones **2**, **5**, **8** vs. the 5-arylidene-thiazolin-4-ones **3a–h**, **6a–e**, **9a–e**). The best binding energies were obtained for the compounds that have a bulky residue such as phenylamino (compounds **6a–e**) or alpha-naphthylamino (compounds **9a–e**) in position 2 of the thiazolin-4-one nucleus. The presence of a smaller residue such as allylamino leads to diminished binding energies.

An increase in the BA towards the target is found also if the residue introduced in position 5 of the thiazolin-4-one ring by Knoevenagel condensation is a bulky, binuclear one (2-phenylthiazolyl, chromonyl), to the detriment of mononuclear ones (phenyl or substituted phenyl).

Considering the top binding conformations of thiazolin-4-one derivatives to the active site of the TrpRSs, we further focused on specific AA binding interactions. For each compound, the main polar interactions made by the compounds' best docking pose to the amino acids residues from the catalytic site of each enzyme are presented in Table 8.

A global difference regarding the binding mode of all the compounds between the two targets has been found. Noting the significant binding differences in the active sites of the compounds tested between the two targets, both in terms of interaction and binding homogeneity, we proceeded to analyze the sequence and the catalytic sites of the two enzymes. The results of the catalytic

Table 8. Polar contacts made by the top binding conformation of each compound to the catalytic site of TrpRS.

Compound	116K_P67592 (<i>S. aureus</i>)		PDB 5V0I (<i>E. coli</i>)	
	AA residue (s)	Interacting atom(s)	AA residue (s)	Interacting atom(s)
2	Tyr126 Gly7	C=O (tz4one) N-H	Gly9	C=O (tz4one)
3a	Gly145	N-H	Gly9 Gly147	C=O (tz4one) N-H
3b	Asn18	N-H	Gly9	N-H
3c	Tyr126 Ile8 Lys196 Ser195 Lys193	S (tz4one) C=O (tz4one) C=O (carboxyl) C=O (carboxyl) C=O (carboxyl)	Gly9 Asn20	N (tz4one) N=O
3d	Asn18 Gly145 Gln9	N (th) S (th) C=O (tz4one)	Gly9 PO ₄ PO ₄	N (th) S (th) N-H
3e	Tyr126 Gly145 Gly7	N-H C-O-C (chr) N-H	Asp135 Tyr128 Gln150	C-O-C (chr) N-H S (th)
3f	Gly145	N-H	Gln11	N-H
3g	Asn18 Gly145 Gly7 Thr126	Ph-OH C-O-C S (tz4one) C=O (tz4one)	Met132 Gln11	Ph-OH N (tz4one)
3h	Asn18 Tyr126 Gly7	Ph-OH N-H C=O (tz4one)	Met132 Gln11	Ph-OH N (tz4one)
5	Gln9	C=O (tz4one)	Gly9	N-H
6a	Thr126 Gly145	S (tz4one) N-H	Gly147 Gly9 Gly147	C=O (tz4one) N-H C=O (tz4one)
6b	Gly145	N-H	Gly9 Gly147	N-H C=O (tz4one)
6c	Lys193 Lys196 Gly7 Tyr126	N=O N=O N-H C=O (tz4one)	Gly9 Gly147	N-H C=O (tz4one)
6d	Gly7	N (th)	Phe7 Gly9 His45	S (th) N (th) NH
6e	N/A	N/A	N/A	N/A
8	Gln9	C=O (tz4one)	Gly147 Gly9	C=O (tz4one) N-H
9a	Gly145	C=O (tz4one)	N/A	N/A
9b	Asn18	N-H	Gly9	N (tz4one)
9c	Lys193 Gly7	N=O N-H	Gly9	N (tz4one)
9d	Asn18 Gly7	N-H N (th)	N/A	N/A
9e	Asn18	N-H	Gly9	N (tz4one)
10	Asn18	N (tz4one)	Gly9	N (tz4one)
11	Tyr126 Gly7	C=O (tz4one) N-H	Gly9	N (tz4one)
Indolmycin	Asp133	N-H (indole)	Met132 His45 Gln11	N-H (indole) N-H (exoc) N (oz4one)

Tz4one: thiazolin-4-one; oz4one: oxazolin-4-one; th: thiazole; chr: chromone; exoc: exocyclic.

site analysis is presented in the [Figures S5 and S6](#), and [Table T1 in Supplementary Materials](#). TrpRSs are known to have very flexible structures, with significantly different conformations depending on the ligand bound¹³. The homology model 116K_P67592 was based on a crystal structure with tryptophanyl-adenylate bound and the PDB 5V0I is a crystal structure with tryptophanyl + AMP. Besides the discrepancies between the targets' primary sequences, the different ligands bound could also be responsible for the differences observed between the active sites of the two enzymes, the two targets having different conformational states.

4. Conclusions

Twenty-three previously synthesized thiazolin-4-one derivatives and indolmycin have been investigated *in vitro* for their antibacterial potential against a gram-positive (*S. aureus*) and a gram-negative (*E. coli*) bacterial strain with the help of two different assays: the cup-plate agar diffusion method and the broth microdilution method. Compounds **3a-c**, **3e-h**, **6b-c** and **9a-c** were the most active against *S. aureus*, with MIC values similar or better than those of moxifloxacin. All compounds displayed antibacterial activity against *E. coli*, but inferior to that of moxifloxacin, used as reference antibiotic. The results of the inhibition zone diameter determination and MBC values determination were in agreement with the results obtained. The MBC/MIC ratio calculated for these compounds suggested a bactericidal effect.

The possible interactions with the TrpRSs were evaluated *in silico*. The molecular docking study, performed on TrpRS from *S. aureus* and *E. coli*, revealed that the thiazolin-4-ones have a common binding pattern to the enzyme, involving polar contacts between exocyclic secondary amine group, the C=O group from the thiazolin-4-one ring with AA residues from the active site of the enzyme. Sixteen thiazolin-4-ones presented better binding affinities to 116K_P67592 from *S. aureus* and twelve presented better binding energies to PDB 5V0I from *E. coli* than indolmycin. The substitution of position 2 of the thiazolin-4-one ring with a voluminous moiety seemed to enhance the BAs to the target enzymes, leading to compounds that mimic better indolmycin. Further *in vitro* studies are needed to confirm that the compounds actually bind to the TrpRSs and to establish the mechanism of action of the synthesized thiazolin-4-ones.

The antioxidant potential of the thiazolin-4-ones was also evaluated by four different assays, in one of these, the radical scavenging properties were tested (the DPPH[•] radical scavenging activity method) and the other three were based on the compounds' ability to act as reducing agents or to participate in electron transfer reactions (the FRAP method, the reducing power assay and the phosphomolybdate assay for TAC). Compounds **3e**, **6e** and **9e** bearing a chromonyl moiety presented the best antioxidant properties, comparable to the reference antioxidants.

From all compounds synthesized, compound **9e** was the most active compound regarding both biological activities, antibacterial and antioxidant, and also displayed the best BAs towards the bacterial TrpRSs *in silico*. This suggests that the presence of an α -naphthylamino rest in position 2 of the thiazolin-4-one ring and a chromonyl moiety in the structure is favourable for obtaining dual-targeting, antibacterial and antioxidant compounds. These moieties also seem to be important for bacterial targeting, as they enhanced the BA of the molecule towards the bacterial TrpRS.

These preliminary results obtained from the *in vitro* antibacterial and antioxidant activity evaluation and the molecular docking study may serve as a starting point for designing new heterocyclic compounds with antioxidant potential and antibacterial activity, acting as TrpRS inhibitors.

Disclosure statement

No potential conflict of interest was reported by the authors.

Funding

This research was supported by the "Iuliu Hațieganu" University of Medicine and Pharmacy Cluj-Napoca under internal research grant no. 4945/24/2016.

ORCID

Anca Stana  <http://orcid.org/0000-0002-8453-3642>

References

1. Stana A, Tipericiu B, Duma M, et al. Synthesis and antimicrobial activity of some new N-(aryl-oxo-alkyl)-5-arylidene-thiazolidine-2,4-diones. *J Serb Chem Soc* 2014;79:115–23.
2. Stana A, Vodnar DC, Tamaian R, et al. Design, synthesis and antifungal activity evaluation of new thiazolin-4-ones as potential lanosterol 14 α -demethylase inhibitors. *Int J Mol Sci* 2017;18:1–25.
3. Insuasty A, Ramírez J, Raimondi M, et al. Synthesis, antifungal and antitumor activity of novel (Z)-5-hetarylmethylidene-1,3-thiazol-4-ones and (z)-5-ethylidene-1,3-thiazol-4-ones. *Molecules* 2013; 18:5482–97.
4. Shaveta MS, Singh P. Hybrid molecules: the privileged scaffolds for various pharmaceuticals. *Eur J Med Chem* 2016;124: 500–36.
5. Jukić M, Đorđević A, Lazarević J, et al. Antimicrobial activity and cytotoxicity of some 2-amino-5-alkylidene-thiazol-4-ones. *Mol Divers* 2013;17:773–80.
6. Saundaneanand R, Kirankumar NM, Annapurna H. Synthesis of novel N-(aryl)diazenyl thiazol-2-amines and benzylidene-thiazolidin-4-ones linked to indole nucleus as antioxidant, antimicrobial, antimycobacterial and cytotoxic agents. *Int J Pharm Pharm Sci* 2014;6:141–7.
7. Al-Ansary GH, Ismail MAH, Abou El Ella DA, et al. Molecular design and synthesis of HCV inhibitors based on thiazolone scaffold. *Eur J Med Chem* 2013;68:19–32.
8. Zvezdanovic J, Daskalova L, Yancheva D, et al. 2-Amino-5-alkylidenethiazol-4-ones as promising lipid peroxidation inhibitors. *Monatsh Chem* 2014;145:945–52.
9. Mony L, Triballeau N, Paoletti P, et al. Identification of a novel NR2B-selective NMDA receptor antagonist using a virtual screening approach. *Bioorg Med Chem Lett* 2010;20: 5552–8.
10. Barzen S, Rödl CB, Lill A, et al. Synthesis and biological evaluation of a class of 5-benzylidene-2-phenyl-thiazolinones as potent 5-lipoxygenase inhibitors. *Bioorg Med Chem* 2012; 20:3575–83.
11. Ferri M, Ranucci E, Romagnoli P, Giaccone V. Antimicrobial resistance: A global emerging threat to public health systems. *Crit Rev Food Sci Nutr* 2017;57:2857–76.
12. Wu Y, Yu K, Xu B, et al. Potent and selective inhibitors of *Staphylococcus epidermidis* tryptophanyl-tRNA synthetase. *J Antimicrob Chemother* 2007;60:502–9.
13. Williams TL, Yin YW, Carter CW. Selective inhibition of bacterial tryptophanyl-tRNA synthetases by indolmycin is mechanism-based. *J Biol Chem* 2016;291:255–65.
14. Du Y-L, Alkhalaf LM, Ryan KS. In vitro reconstitution of indolmycin biosynthesis reveals the molecular basis of oxazolinone assembly. *Proc Natl Acad Sci USA* 2015;112: 2717–22.
15. Kanamaru T, Nakano Y, Toyoda Y, et al. In vitro and in vivo antibacterial activities of TAK-083, an agent for treatment of *Helicobacter pylori* infection. *Antimicrob Agents Chemother* 2001;45:2455–9.
16. Werner RG, Thorpe LF, Reuter W, Nierhaus KH. Indolmycin Inhibits Prokaryotic tryptophanyl-tRNA ligase. *Eur J Biochem* 1976;68:1–3.
17. Hybertson BM, Gao B, Bose SK, McCord JM. Oxidative stress in health and disease: the therapeutic potential of Nrf2 activation. *Mol Aspects Med* 2011;32:234–46.
18. Thorat ID, Jagtap DD, Mohapatra D, Joshi DC. Antioxidants, their properties, uses in food products and their legal implications. *Int J Food Stud* 2013;2:81–104.
19. Abu-Melha S. Synthesis, modeling study and antioxidants activity of new heterocycles derived from 4-antipyrinyl-2-chloroacetamidothiazoles. *Appl Sci* 2018;8:2128.
20. Csepányi E, Szabados-Furjesi P, Kiss-Szikszai A, et al. Antioxidant properties and oxidative transformation of different chromone derivatives. *Molecules* 2017;22:1–12.
21. Martelli G, Giacomini D. Antibacterial and antioxidant activities for natural and synthetic dual-active compounds. *Eur J Med Chem* 2018;158:91–105.
22. Clinical and Laboratory Standards Institute (CLSI). Performance standards for antimicrobial disk susceptibility tests. Approved Standard-Twelfth Edition. CLSI document M02-A12. 12th ed. Wayne (PA): Clinical and Laboratory Standards Institute, USA, 2015. ISBN 1-56238-986-6.
23. Clinical and Laboratory Standards Institute (CLSI). Performance standards for antimicrobial susceptibility testing. CLSI supplement M100. 27th ed. Wayne (PA): Clinical and Laboratory Standards Institute, USA, 2017. ISBN 1-56238-1-56238-805-3.
24. Nastasă C, Vodnar D, Ionuț I, et al. Antibacterial evaluation and virtual screening of new thiazolyl-triazole Schiff bases as potential DNA-gyrase inhibitors. *Int J Mol Sci* 2018;19:222.
25. Koppireddi S, Komsani JR, Avula S, et al. Novel 2-(2,4-dioxo-1,3-thiazolidin-5-yl)acetamides as antioxidant and/or anti-inflammatory compounds. *Eur J Med Chem* 2013;66:305–13.
26. Lupascu FG, Dragostin OM, Foia L, et al. The synthesis and the biological evaluation of new thiazolidin-4-one derivatives containing a xanthine moiety. *Molecules* 2013;18: 9684–703.
27. Benzie IFF, Strain JJ. Ferric reducing/antioxidant power assay: direct measure of total antioxidant activity of biological fluids and modified version for simultaneous measurement of total antioxidant power and ascorbic acid concentration. *Methods Enzymol* 1999;299:15–27.
28. Ahmed D, Khan M, Saeed R. Comparative analysis of phenolics, flavonoids, and antioxidant and antibacterial potential of methanolic, hexanic and aqueous extracts from *Adiantum caudatum* leaves. *Antioxidants (Basel)* 2015;4: 394–409.
29. Alam MN, Bristi NJ, Rafiquzzaman M. Review on in vivo and in vitro methods evaluation of antioxidant activity. *Saudi Pharm J* 2013;21:143–52.
30. Prieto P, Pineda M, Aguilar M. Spectrophotometric quantitation of antioxidant capacity through the formation of a phosphomolybdenum complex: specific application to the determination of vitamin E. *Anal Biochem* 1999;269:337–41.
31. Baig H, Ahmed D, Zara SA, et al. In Vitro evaluation of antioxidant properties of different solvent extracts of *Rumex acetosella* leaves. *Orient J Chem* 2011;27:1509–16.

32. Marc G, Ionuț I, Pirnau A, et al. Microwave assisted synthesis of 3,5-disubstituted thiazolidine-2,4-diones with antifungal activity. Design, synthesis, virtual and in vitro antifungal screening. *Farmacia* 2017;65:414–22.
33. O'Boyle NM, Banck M, James CA, et al. Open Babel: An open chemical toolbox. *J Cheminform* 2011;3:33.
34. Morris GM, Huey R, Lindstrom W, et al. AutoDock4 and AutoDockTools4: automated docking with selective receptor flexibility. *J Comput Chem* 2009;30:2785–91.
35. Arnold K, Bordoli L, Kopp J, Schwede T. The SWISS-MODEL workspace: a web-based environment for protein structure homology modelling. *Bioinformatics* 2006;22:195–201.
36. Biasini M, Bienert S, Waterhouse A, et al. SWISS-MODEL: modelling protein tertiary and quaternary structure using evolutionary information. *Nucleic Acids Res* 2014;42:W252–8.
37. Altschul SF, Madden TL, Schaffer AA, et al. Gapped BLAST and PSI-BLAST: a new generation of protein database search programs. *Nucleic Acids Res* 1997;25:3389–402.
38. Volkamer A, Kuhn D, Rippmann F, Rarey M. DoGSiteScorer: a web server for automatic binding site prediction, analysis and druggability assessment. *Bioinformatics* 2012;28:2074–5.
39. Pettersen EF, Goddard TD, Huang CC, et al. UCSF Chimera—a visualization system for exploratory research and analysis. *J Comput Chem* 2004;25:1605–12.
40. Chua SL, Ding Y, Liu Y, et al. Reactive oxygen species drive evolution of pro-biofilm variants in pathogens by modulating cyclic-di-GMP levels. *Open Biol* 2016;6(11):160162.



Article

Antibacterial Evaluation and Virtual Screening of New Thiazolyl-Triazole Schiff Bases as Potential DNA-Gyrase Inhibitors

Cristina Nastasă^{1,*} , Dan C. Vodnar^{2,*}, Ioana Ionuț¹, Anca Stana¹ , Daniela Benedec³, Radu Tamaian^{4,5,*} , Ovidiu Oniga¹ and Brîndușa Tiperciuc¹

¹ Department of Pharmaceutical Chemistry, “Iuliu Hațieganu” University of Medicine and Pharmacy, 41 Victor Babeș Street, RO-400012 Cluj-Napoca, Romania; ionut.ioana@umfcluj.ro (I.I.); teodora_anca@yahoo.com (A.S.); onigao65@yahoo.com (O.O.); brandu32@yahoo.com (B.T.)

² Department of Food Science and Technology, University of Agricultural Sciences and Veterinary Medicine, 3-5 Mănăștur Street, RO-400372 Cluj-Napoca, Romania

³ Department of Pharmacognosy, “Iuliu Hațieganu” University of Medicine and Pharmacy, 12 Ion Creangă Street, RO-400010 Cluj-Napoca, Romania; dani_67ro@yahoo.com

⁴ National Institute for Research and Development for Cryogenic and Isotopic Technologies, 4th Uzinei Street, RO-240050 Râmnicu Vâlcea, Romania

⁵ SC Biotech Corp SRL, 4th Uzinei Street, RO-240050 Râmnicu Vâlcea, Romania

* Correspondence: cmoldovan@umfcluj.ro (C.N.); dan.vodnar@usamvcluj.ro (D.C.V.); radu.tamaian@icsi.ro (R.T.); Tel.: +40-745-264-393 (C.N.); +40-747-341-881 (D.C.V.); +40-740-228-119 (R.T.)

Received: 23 November 2017; Accepted: 9 January 2018; Published: 11 January 2018

Abstract: The global spread of bacterial resistance to drugs used in therapy requires new potent and safe antimicrobial agents. DNA gyrases represent important targets in drug discovery. Schiff bases, thiazole, and triazole derivatives are considered key scaffolds in medicinal chemistry. Fifteen thiazolyl-triazole Schiff bases were evaluated for their antibacterial activity, measuring the growth inhibition zone diameter, the minimum inhibitory concentration (MIC), and the minimum bactericidal concentration (MBC), against Gram-positive (*Staphylococcus aureus*, *Listeria monocytogenes*) and Gram-negative (*Escherichia coli*, *Salmonella typhimurium*, *Pseudomonas aeruginosa*) bacteria. The inhibition of *S. aureus* and *S. typhimurium* was modest. Compounds **B1**, **B2**, and **B9** showed a similar effect as ciprofloxacin, the antimicrobial reference, against *L. monocytogenes*. **B10** displayed a better effect. Derivatives **B1**, **B5–7**, **B9**, and **B11–15** expressed MIC values lower than the reference, against *L. monocytogenes*. **B5**, **B6**, and **B11–15** strongly inhibited the growth of *P. aeruginosa*. All compounds were subjected to an in silico screening of the ADMET (absorption, distribution, metabolism, elimination, toxicity) properties. Molecular docking was performed on the gyrA and gyrB from *L. monocytogenes*. The virtual screening concluded that thiazolyl-triazole Schiff base **B8** is the best drug-like candidate, satisfying requirements for both safety and efficacy, being more potent against the bacterial gyrA than ciprofloxacin.

Keywords: Schiff base; thiazole; triazole; antibacterial activity; ADMET; molecular docking; DNA-gyrase

1. Introduction

The alarming worldwide spread of the bacterial resistance, to most of the drugs available nowadays in therapy [1–3], urgently requires the development of new effective antibacterial agents.

The DNA topoisomerases manage the topological state of the DNA in the cell, being involved in replication, transcription, recombination, and chromatin remodeling. In the bacterial proteome, there are various types of topoisomerases, the most common being type I topoisomerases, type II topoisomerases (DNA gyrases), and type IV topoisomerases [4].

One of the major targets of antibacterial compounds is represented by DNA gyrase (Type II topoisomerase), an enzyme playing an essential role in bacterial replication [5]. Structurally, the DNA gyrase is built of two A subunits (gyrA) and two B subunits (gyrB) that form an A₂B₂ heterotetramer. Topoisomerase IV consists of two constitutive subunits: parE (homologous to DNA gyrase subunit B–gyrB) and parC (homologous to DNA gyrase subunit A–gyrA) [6]. DNA gyrase has four functional domains (GO (Gene Ontology) terms) [7,8]. Domain 1, the N-terminal of domain gyrB, harbors the ATPase activity. The type II topoisomerases use the hydrolysis of ATP, in the presence of Mg²⁺, to simultaneously cut both strands of the double-helix, in order to manage DNA tangles and supercoils. Domain 2, the C-terminal domain of gyrB, which consists of a Toprim structural motif and a tail region, contributes to the binding of DNA, via the interaction with the gyrA subunit [9,10]. Domain 3, the N-terminal domain of gyrA, is responsible for the breaking-rejoining function, through its capacity to form protein-DNA bridges; meanwhile, Domain 4, the C-terminal domain of gyrA (TOP4c), is able to non-specifically bind DNA [11]. The Toprim domain (also known as the Rao-Rossmann fold) is a structural motif found in DNA primases, topoisomerases, and some enzymes involved in phosphotransfers or able to hydrolyze phosphodiester bonds [10]. The central DNA-binding core of gyrA contains the active site tyrosine residues located in the catabolite-activator-protein-like (CAP-like) domain which includes the DNA binding helix-turn-helix (HTH) motif. The CAP-like tyrosine residues are crucial for the breakage and religation of the DNA, by forming an ester with the 5'phosphate of the DNA [12]. The Toprim domain of subunit B is adjacent to the catalytic tyrosine in the CAP domain of subunit A and both form an active site, essential for the DNA-cleavage [10].

Quinolones are the only class of DNA gyrase inhibitors that are clinically used. Their effect is based on the inhibition of the gyrA subunit, therefore perturbing the DNA cleavage and the introduction of negative supercoils into the bacterial DNA [13]. Cyclothialidines [14] and aminocoumarins [15] are studied for their inhibition of the ATP-binding site of the gyrB subunit. Because of the bacterial resistance to fluoroquinolones used in therapy and also of their side effects and limitations, there are gyrase inhibitors searched, from different chemical classes: benzimidazoles, benzoxazole, benzothiazole, oxazolopyridines [16], aminopyrazinamides [17], thiazole derivatives [18–20], and triazole derivatives [21,22], which differently bind the biological target.

Schiff bases are a group of compounds which have gained popularity as biologically active scaffolds due to their ease of synthesis, their versatility, and their large spectra of activities, such as their antimicrobial [23,24], anti-inflammatory, anticonvulsant, and antioxidant [25] properties. Schiff bases have sufficient water solubility and are stable in vitro and in vivo [26]. The imine bond in Schiff bases provides binding opportunities with different nucleophiles and electrophiles, inhibiting enzymes or DNA replication. The isosteric replacement of the quinolones' 3-carboxyl group, essential for gyrase binding, with an amino-thiazolic fragment [27] or other azoles (thiazoles, triazoles), led to molecules with improved antimicrobial effects and a wider spectrum of activity. These compounds express fewer side effects and have a better capacity in overcoming bacterial resistance [28,29].

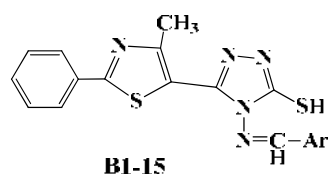
Even if research efforts are continuously made, there still remains the challenge to discover new drugs of a high potential, large spectrum of activity, and with a good safety profile. As a continuation of our efforts in discovering new heterocyclic Schiff bases with potent antimicrobial properties [30], we synthesized a series of new Schiff bases of thiazolyl-triazole [31]. Prompted by the aspects described above, the work presented here focuses on the investigation of the antibacterial potential of the new azolyl-Schiff bases against Gram-positive and Gram-negative bacteria. A molecular docking study was realized on DNA gyrases of *Listeria monocytogenes*. ADMET profiling for risks and safety risks was also conducted for the new series of compounds.

2. Result and Discussion

2.1. Antibacterial Activity

2.1.1. Determination of the Inhibition Zone Diameters

The antimicrobial activity was tested in vitro using the disk diffusion method, by measuring the diameters of the inhibition zones. The synthesized compounds **B1–15** (Figure 1) [31] were screened against two Gram-positive (*Listeria monocytogenes* ATCC 35152, *Staphylococcus aureus* ATCC 25923) and three Gram-negative (*Escherichia coli* ATCC 25922, *Salmonella typhimurium* ATCC 13311, *P. aeruginosa* ATCC 27853) bacterial strains (Table 1).



- | | |
|-------------------------------|-----------------------------------------------------------|
| B1) Ar=2,4-diCl-phenyl | B9) Ar=4-OH-phenyl |
| B2) Ar=2,6-diCl-phenyl | B10) Ar=3-NO ₂ -phenyl |
| B3) Ar=2,3-diCl-phenyl | B11) Ar=4-NO ₂ -phenyl |
| B4) Ar=3-Cl-phenyl | B12) Ar=2-OCH ₃ -phenyl |
| B5) Ar=4-Br-phenyl | B13) Ar=3-OCH ₃ -phenyl |
| B6) Ar=4-F-phenyl | B14) Ar=2-thienyl |
| B7) Ar=2-OH-phenyl | B15) Ar=4-(CH ₃) ₂ N-phenyl |
| B8) Ar=3-OH-phenyl | |

Figure 1. Structures of the Schiff bases **B1–15**.

Table 1. The antibacterial activity of compounds **B1–15**.

Cp.	Gram-Positive Bacteria				Gram-Negative Bacteria					
	<i>Staphylococcus aureus</i> ATCC 25923		<i>Listeria monocytogenes</i> ATCC 35152		<i>Escherichia coli</i> ATCC 25922		<i>Salmonella typhimurium</i> ATCC 13311		<i>P. aeruginosa</i> ATCC 27853	
	Diameter (mm)	%AI	Diameter (mm)	%AI	Diameter (mm)	%AI	Diameter (mm)	%AI	Diameter (mm)	%AI
B1	14	50	18	100	14	51.8	16	72.7	19	73
B2	14	50	18	100	14	51.8	18	81.8	19	73
B3	14	50	16	88.8	14	51.8	18	81.8	16	61.5
B4	14	50	14	77.7	14	51.8	18	81.8	18	69.2
B5	14	50	14	77.7	14	51.8	18	81.8	21	80.7
B6	14	50	14	77.7	14	51.8	16	72.7	21	80.7
B7	16	57.1	12	66.6	14	51.8	16	72.7	18	69.2
B8	12	42.8	12	66.6	14	51.8	16	72.7	18	69.2
B9	14	50	18	100	16	59.2	16	72.7	20	76.9
B10	18	64.2	20	111.1	16	59.2	18	81.8	18	69.2
B11	12	42.8	8	44.4	16	59.2	18	81.8	21	80.7
B12	12	42.8	14	77.7	14	51.8	18	81.8	21	80.7
B13	12	42.8	12	66.6	14	51.8	18	81.8	21	80.7
B14	12	42.8	16	88.8	16	59.2	18	81.8	21	80.7
B15	16	57.1	10	55.5	14	51.8	18	81.8	21	80.7
CIP	28	100	18	100	27	100	22	100	26	100

The values obtained for the most active compounds are marked in bold. Cp.: Compounds; CIP: ciprofloxacin; %AI = percentage activity index ((Zone of the inhibition of synthetic compound/Zone of the inhibition of reference drug) × 100).

For evaluating the antimicrobial activity, 100 µg/disk of the synthesized compounds and also of the reference substance, ciprofloxacin, were used. The solvent for the preparation of the solutions, dimethylsulfoxide (DMSO), exhibited no inhibitory activity on the bacterial strains considered for this study.

Regarding the activity against the Gram-positive bacteria, the strain of *Listeria monocytogenes* was more sensible to the tested compounds, three of them (**B1**, **B2**, and **B9**) showing a similar effect to

ciprofloxacin, with an 18 mm inhibition zone and an AI value of 100%. **B10** (3-nitro-phenyl) proved to be more active than the antibacterial reference, displaying a 20 mm diameter and an AI of 111.1%. The second Gram-positive bacterium, *Staphylococcus aureus*, was moderately inhibited by the new molecules, with inhibition zones ranging from 12 to 18 mm, respectively, and AI between 42.8 and 64.2%. In the case of both strains, compound **B10** exhibited the most pronounced effect.

The inhibitory activity against *Escherichia coli*, *Salmonella typhimurium*, and *Pseudomonas aeruginosa* was modestly related to ciprofloxacin. The compounds determined zones of 14–16 mm (AI 51.8–59.2%) against *Escherichia coli*. The values registered on *Salmonella typhimurium* ranged between 16–18 mm (AI 72.7–81.8%). The percentage activity index against *Pseudomonas aeruginosa* was between 61.5%, corresponding to a 16 mm inhibitory zone diameter, and 80.7%, corresponding to a 21 mm zone diameter. The most potent derivatives were **B5**, **B6**, and **B11–15**.

From the results obtained, it can be observed that Schiff base **B10** expressed the most pronounced antibacterial effect.

2.1.2. Determination of MIC and MBC Values

The broth microdilution method was employed for the minimum inhibitory concentration test. All synthesized compounds were tested against two Gram-positive bacterial strains (*Staphylococcus aureus* ATCC 49444, *Listeria monocytogenes* ATCC 19115) and two Gram-negative bacterial strains (*Pseudomonas aeruginosa* ATCC 27853, *Salmonella typhimurium* ATCC 14028). Stock solutions (1 mg/mL) were prepared by dissolving the test compounds and the reference antimicrobial, ciprofloxacin, in sterile DMSO. The results are presented in Table 2 (MIC and MBC).

Table 2. Minimum Inhibitory Concentration (MIC) and Minimum Bactericidal Concentration (MBC) (in µg/mL) of compounds **B1–15**.

Cp.	<i>S. aureus</i> ATCC 49444		<i>L. monocytogenes</i> ATCC 19115		<i>P. aeruginosa</i> ATCC 27853		<i>S. typhimurium</i> ATCC 14028	
	MIC	MBC	MIC	MBC	MIC	MBC	MIC	MBC
B1	31.25	31.25	1.95	3.9	7.81	15.62	62.5	125
B2	31.25	31.25	3.9	7.8	7.81	15.62	62.5	62.5
B3	62.5	62.5	3.9	7.8	15.62	31.25	62.5	62.5
B4	31.25	62.5	3.9	7.8	7.81	15.62	62.5	62.5
B5	31.25	31.25	1.95	3.9	1.95	3.9	62.5	62.5
B6	31.25	62.5	1.95	3.9	1.95	3.9	62.5	62.5
B7	31.25	31.25	1.95	3.9	7.81	15.62	62.5	125
B8	62.5	62.5	3.9	3.9	7.81	15.62	62.5	125
B9	31.25	31.25	1.95	3.9	3.9	7.8	62.5	125
B10	31.25	31.25	3.9	7.8	7.81	15.62	62.5	62.5
B11	62.5	62.5	1.95	3.9	1.95	3.9	62.5	62.5
B12	31.25	62.5	1.95	3.9	1.95	1.95	62.5	125
B13	31.25	62.5	1.95	3.9	1.95	3.9	31.25	62.5
B14	15.62	31.25	1.95	3.9	1.95	3.9	62.5	125
B15	31.25	62.5	1.95	3.9	1.95	3.9	62.5	62.5
Ciprofloxacin	1.95	3.9	3.9	7.8	3.9	7.8	0.97	1.95
Inoculum Control	+++		+++		+++		+++	
Broth control	No growth		No growth		No growth		No growth	

Cp.: Compounds; +++ Indicates growth in all concentrations. The values obtained for the most active compounds are marked in bold.

Analyzing the results obtained, it can be seen that the growth inhibitory activity against the Gram-positive bacteria was more pronounced against the strain of *Listeria monocytogenes*, where 10 of the compounds (**B1**, **B5–7**, **B9**, **B11–15**) expressed MIC values lower than that of ciprofloxacin. The others showed the same effect as the reference. The strain of *Staphylococcus aureus* was less sensitive to the activity of the new molecules.

Growth of *Pseudomonas aeruginosa* was strongly inhibited by most of the compounds. It can be observed that **B5**, **B6**, and **B11–15** had MICs lower than the antibacterial used as the reference, while **B9** had the same active concentration, in agreement with the inhibitory zone diameters. The inhibition of *Salmonella typhimurium* was modest for all the tested derivatives.

Determination of MBC confirmed the results previously obtained, when MIC was investigated. The MBC value of Schiff base **B8** (meta-hydroxy) against *L. monocytogenes* ATCC 19115 was inferior to that of ciprofloxacin. For this compound, MIC was equal to the antibacterial reference. Also, the MBC of 1.95 µg/mL should be noted, registered for **B12** (ortho-methoxy-phenyl), against the strain of *P. aeruginosa*, which is much smaller than that for ciprofloxacin. The MBC/MIC ratio (Table S1) is one or two for all the tested compounds, suggesting that they may exert bactericidal activity [32,33].

2.2. Virtual Screening

Virtual screening (VS) emerged as an adaptive response of cheminformatics to organic chemistry requirements, in order to prioritize the synthesis of the most promising drug candidates [34–37]. In this respect, various cheminformatics tools can be used to filter the candidate compounds, based on their absorption, distribution, metabolism, excretion, toxicity (ADMET) [38–40], and their spatial interaction with the targets and their binding affinity (BA) via molecular docking [40,41]. Development of novel antimicrobials as DNA gyrase inhibitors (validated drugs targets) has been exploited in both computational and wet-lab strategies [5,20,42].

In our VS setup, we assessed the activity and potency of the newly synthesized Schiff bases, via molecular docking, on the two subunits of topoisomerases II (gyrA and gyrB) from *Listeria monocytogenes*, comparing the results with ciprofloxacin, chosen as the reference drug. We also evaluated the safety-related concerns by the means of ADMET profiling. An academic license of MarvinSketch was used for the drawing and displaying of 2D structures, 3D optimization of all ligands, and also for generating the input SDF files for ADMET profiling and Tripos MOL2 files for docking, MarvinSketch 17.6.0, 2017, ChemAxon, Budapest, Hungary [43].

2.2.1. ADMET Profiling

ADMET profiling provides helpful guidance on the absorption, plasma clearance, tissue distribution, metabolic effects, and both acute and later toxicity. The results of the ADME study previously conducted and presented [31] showed that the thiazolyl-triazole Schiff bases **B1–15** displayed good pharmacokinetic properties and that all new molecules passed the drug-likeness criteria.

Toxicity studies are mandatory for a new product, due to the fact that a drug has to not only manifest its efficacy, but also have good tolerability and a low toxicity rate. Considering the above aspects as a good starting point, we continued the analysis of the newly synthesized compounds (Table 3).

Table 3. ADMET profiling—risks and safety concerns.

Cp.	MW (Da)	logP	tPSA (Å ²)	PPIs	UMSs	CIs	PAINS Filters			PPDI	Med Chem	GSK 4/400	Pfizer 3/75
							A	B	C				
B1	446.38	5.69	104.1	Yes	thiol hal.	thiol	ND	ND	ND	NI	hydr.	bad	warn.
B2	446.38	5.69	104.1	Yes	thiol hal.	thiol	ND	ND	ND	NI	hydr.	bad	warn.
B3	446.38	5.69	104.10	Yes	thiol hal.	thiol	ND	ND	ND	NI	hydr.	bad	warn.
B4	411.93	5.06	123.00	Yes	thiol hal.	thiol	ND	ND	ND	NI	hydr.	bad	warn.
B5	456.38	5.13	123.00	Yes	hal.	thiol	ND	ND	ND	NI	hydr.	bad	warn.
B6	395.48	4.53	123.00	Yes	thiol hal. F	thiol	ND	ND	ND	NI	hydr.	good	warn.
B7	393.49	4.08	143.23	Yes	thiol phenol	thiol	¹⁴⁷⁹ _{1479b}	ND	ND	NI	hydr.	good	warn.

Table 3. Cont.

Cp.	MW (Da)	logP	tPSA (Å ²)	PPIs	UMSs	CIs	PAINS Filters			PPDI	Med Chem	GSK 4/400	Pfizer 3/75
							A	B	C				
B8	393.49	4.08	143.23	Yes	thiol phenol	thiol	ND	ND	ND	NI	hydr.	good	warn.
B9	393.49	4.08	143.23	Yes	thiol phenol	thiol	I ²¹⁵	ND	ND	NI	hydr.	good	warn.
B10	422.48	4.26	149.92	Yes	thiol nitro	thiol	ND	ND	ND	NI	hydr.	bad	warn.
B11	422.48	4.26	149.92	Yes	thiol nitro	thiol	ND	ND	ND	NI	hydr.	bad	warn.
B12	407.51	4.41	132.23	Yes	thiol	thiol	ND	ND	ND	NI	hydr.	bad	warn.
B13	407.51	4.41	132.23	Yes	thiol	thiol	ND	ND	ND	NI	hydr.	bad	warn.
B14	383.51	4.45	151.24	Yes	thiol thp.	thiol	ND	ND	ND	NI	hydr.	good	warn.
B15	420.55	4.56	126.24	Yes	thiol	thiol	ND	ND	ND	NI	hydr.	bad	warn.
CIP	331.34	0.28	81.98	Not	hal. F	ND	I ²¹⁵	ND	ND	NI	ND	good	bad

Cp.: Compounds; MW: molecular weight; logP: logarithm of compound partition coefficient between n-octanol and water; tPSA: topological polar surface area; PPIs: protein-protein interactions; UMSs: undesirable moieties and substructures; hal.: halogenure; hal. F: halogenure with Fluorine; thp.: thiophene; CIs: covalent inhibitors; PAINS: Pan-Assay Interference Compounds; ND: none detected (compound is free of problematic sub-structures for the corresponding risk criteria). I⁴⁷⁹: intermediate compound which embeds a low-risk structural PAINS alert with a number of occurrences below the threshold, according to the PAINS filter more150_hzone_phenol_A. I^{479b}: intermediate compound which embeds a low-risk structural PAINS alert with a number of occurrences below the threshold, according to the PAINS filter more150_hzone_phenol_A_bis. I²¹⁵: intermediate compound which embeds a low-risk structural PAINS alert with a number of occurrences below the threshold, according to the PAINS filter more150_hzone_phenol_B. PPDI: phospholipidosis induction; NI: non-inducer of phospholipidosis; hydr.: hydrazine; warn.: warning (have to be used with caution as blindly applying such recipes can discard from development many interesting molecules)

The risks and safety profiling of the investigated compounds (Table 3) indicates that all compounds are non-inducers of phospholipidosis. On the other hand, ciprofloxacin (CIP) was classified as not PPI friendly, despite its approved drug status; meanwhile, all the Schiff bases successfully complied with this safety criterion. Referring to the problematic moieties, CIP is free of covalent inhibitors; meanwhile, all Schiff bases have in their framework structure the thiol (–SH) group, which is considered responsible for covalent binding [44,45]. Moreover, all compounds contain at least one low risk UMSs substructure: a halogenure in the case of CIP, respectively the aforementioned –SH group in the case of Schiff bases. Compounds B1–6 also have a secondary low risk halogenure. Meanwhile, other low risk groups are present as follows: phenol (B7–9), nitro (B10–11), and thiophene (B14). PAINS groups were detected only in the structure of B7, B9, and CIP (Table 3).

It can be observed that only five Schiff bases (B6–9 and B14) and CIP have good predictions from GSK 4/400 rules, which say that substances with clogP < 4 and a molecular weight <400 Da have better drug-like properties [46]. Schiff bases, due to their hydrazone moiety, may have, according to the MedChem rules [47], potentially reactive or promiscuous behavior and also received a warning from the Pfizer 3/75 rule (substances with clogP > 3 and tPSA < 75 Å² are more likely to have in vivo toxicity), due to the likelihood of promiscuous binding [48].

2.2.2. Molecular Docking

The DNA gyrase is built of two A subunits (gyrA) and two B subunits (gyrB) that form an A2B2 heterotetramer. Topoisomerase IV consists of two constitutive subunits: parE (homologous to DNA gyrase subunit B–gyrB) and parC (homologous to DNA gyrase subunit A–gyrA) [6].

Fluoroquinolones act by inhibiting the gyrA subunit and also as competitive inhibitors of the ATP-binding site on the gyrB subunit [5].

The best antibacterial activity for our Schiff bases was displayed against the Gram-positive *Listeria monocytogenes*. In this view, we selected as docking targets the two DNA gyrases (DNA gyrase

subunit A–gyrA and DNA gyrase subunit B–gyrB) from *L. monocytogenes*, since these are validated drug targets, currently used in drug design [5,21,42].

The results of the two molecular docking runs are presented briefly in Tables 4 and 5, in terms of binding affinity (BA) for the best docking poses—using as scoring criteria a root-mean-square deviation equal to zero. A graphical depiction of the docking results is illustrated in Figures 2 and 3. Detailed binding patterns and the total energetic interactions are shown in Table S2.

Table 4. Predicted binding affinity, interaction domain, and polar interactions between compounds B1–15 and the DNA gyrase A from *Listeria monocytogenes*.

Compound	gyrA BA (kcal/mol)	Atom ID of Ligand	Interacting AA Residue
B1	−8.9	N (2)	Ser112
		N (4)	Val113
		N (21)	Ser98
B2	−7.6	N (2)	Ser112, Val113
		N (4)	Val113
		N (21)	Ser98
		S (32)	Val268
B3	−8.1	N (2)	Val113
		N (4)	Val113, Val268
		N (21)	Ser98
		S (32)	Val268
B4	−8.5	N (2)	Val113
		N (4)	Val113, Val268
		N (21)	Ser98
B5	−8.8	N (2)	Val113
		N (4)	Val113, Val268
		N (21)	Ser98
		S (32)	Val268
B6	−8.8	N (2)	Val113
		N (4)	Val113, Val268
		N (21)	Ser98
B7	−8.1	N (2)	Val113
		N (4)	Val113, Val268
		N (21)	Ser98
		Phenolic O	Gln95, Ser98
B8	−8.7	N (2)	Val113
		N (4)	Val113, Val268
		N (21)	Ser98
		Phenolic O	Tyr266
B9	−8.5	N (2)	Val113
		N (4)	Val113, Val268
		N (21)	Ser98
		S (32)	Val268
B10	−9.1	N (2)	Val113
		N (4)	Val113, Val 268
		N (21)	Ser98
		Nitro N	Tyr266
		Nitro O	Gln267

Backbone of the Compounds B1–15

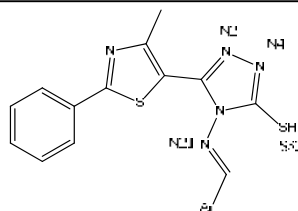


Table 4. Cont.

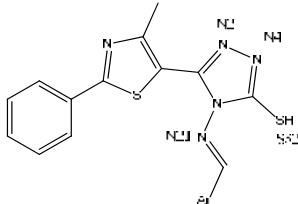
Backbone of the Compounds B1–15			
Compound	gyrA BA (kcal/mol)	Atom ID of Ligand	Interacting AA Residue
B11	−8.8	N (2)	Val113
		N (4)	Val113, Val268
		N (21)	Ser98
		S (32)	Val268
B12	−8	N (4)	Val113, Val268
		N (21)	Ser98
		Methoxy O	Ser98
		S (32)	Val268
B13	−8.8	N (2)	Val113
		N (4)	Val113, Val268
		N (21)	Ser98
		Methoxy O	Tyr266
B14	−7.9	N (2)	Val113
		N (4)	Val113, Val268
		N (21)	Ser98
		S (32)	Val268
B15	−8.8	N (2)	Val113
		N (4)	Val113, Val268
		N (21)	Ser98
CIP	−7.1	O (24)	Ser172
		O (25)	Gly171

Table 5. Predicted binding affinity, interaction domain, and polar interactions between compounds B1–15 and the DNA gyrase B from *Listeria monocytogenes*.

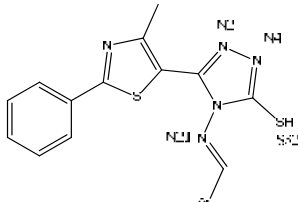
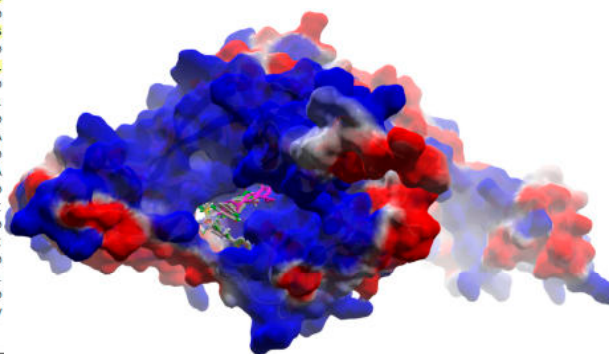
Backbone of the compounds B1–15			
Compound	gyrB BA (kcal/mol)	Atom ID of Ligand	Interacting AA Residue
B1	−6.3	N (4)	Asp611
		S (32)	Asp614
B2	−6.7	NA	NA
B3	−6.6	NA	NA
B4	−7.3	NA	NA
B5	−6.3	N (2)	Asp614, Thr618
B6	−7.2	NA	NA
B7	−6.3	N (4)	Asp611
		Phenolic O (30)	Thr618
		Thiazole S (16)	Asp614
B8	−7.3	Phenolic O (30)	Lys610, Asp611
B9	−7.2	N (21)	Asn608
		Phenolic O (30)	Asp611, Ala615

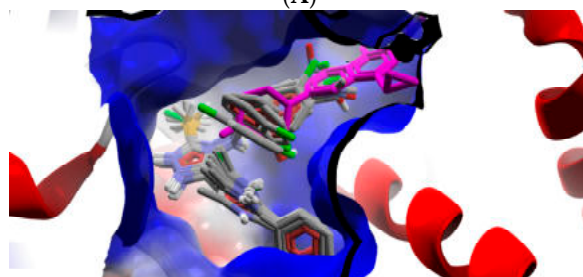
Table 5. Cont.

Compound	gyrB BA (kcal/mol)	Atom ID of Ligand	Interacting AA Residue
B10	-6.8	Nitro O (31,32)	Arg518
B11	-6.8	Nitro N (30) Nitro O (32) S (33)	Arg518 Arg518 Gln542
B12	-6.4	NA	NA
B13	-6.6	N (21) Methoxy O (30)	Gln542 Arg518
B14	-6.5	NA	NA
B15	-6.2	N (4)	Asp611
CIP	-6.5	O (25)	Ala510

10	20	30	40	50
MAETPNQRIT	EINLNKENRT	SFLDYAMSVI	VARALPDVRD	GLKPVHRRIL
60	70	80	90	100
YAMNDLGMTS	DKAYKKSARI	VGEVIGKYHP	HGDTAVYFTH	VRMAQDFSYSR
110	120	130	140	150
NMLVDGHGNF	GSDVGDMAAA	MRYTEARMSK	ISMELLRDIN	KDTIDYADNY
160	170	180	190	200
DGSEREPVI	PARFPNLLVN	GSSGIAGVMA	TNIPTHLGGE	VIDQVLALSH
210	220	230	240	250
DPEITIRDLN	EYIPGPDFPT	AGHIMGRSGI	RRAYESGRGS	ITVGRVDIE
260	270	280	290	300
EKKNGKETIV	ITEIPYQVNK	ARLVERIAEL	AREKKIDGIT	SLNDESDRSG
310	320	330	340	350
MRIVIEVRD	ISASVIVNNL	FKMTALQTFE	GINMLALVDN	HPKVLNLKEI
360	370	380	390	400
LYYYLEHQKV	VIRRRTEFEL	RKAEARAHIL	EGLRIALDNI	DAIKLIRGS
410	420	430	440	450
KTSOVAKEGL	MTQFNLSKQ	AQAILDMRLQ	RLTGLEREKI	EEEYQNLVAL
460	470	480	490	500
INDLKAILAD	DERILEIIRE	ELEEIKVKYA	DKRREILAG	DLVSLDEDL
510	520	530	540	550
IPEEEVAITL	TKRGYIKRLP	LSTYRSQRGG	GRGIQGMSTH	EDDFVEHLVA
560	570	580	590	600
TSHDTLLFF	TNTGKVRYSK	GVEVPEYGR	AKGIPIINLL	GIESQEQWIA
610	620	630	640	650
VINLSEFTDD	SYLFFTTKHG	VKRTTLSQF	AKIRQSGLRA	VELRENDELI
660	670	680	690	700
SVQMTDGSKN	MIATKHGQS	IYFPEEHIRV	MGRTAAGVRG	IRLREDEVI
710	720	730	740	750
GHEVLEDEEK	VLVTEKGYG	KQTPASQYPL	RNRGGMGVKT	VTITEKNGNL
760	770	780	790	800
VAMKTVTSEE	DLMMLTVSGV	LIRFEIDTVS	QTGRSAMGVK	LIRLDEDEKV
810	820	830	840	
ATVAKVPKEE	DEVELEEEID	ETLITQVPEE	SFEDAPGSDI	EE



(A)



(B)

Figure 2. General view (A) and detail (B) of the best docking poses of ligands against gyrA. Target is depicted as thin sticks with a secondary structure drawn as a cartoon backbone and semi-transparent electrostatic molecular surface (cropped in the detailed view), where ligands are figured as ball-and-stick (Schiff bases are CPK colored, meanwhile CIP is pink-magenta).

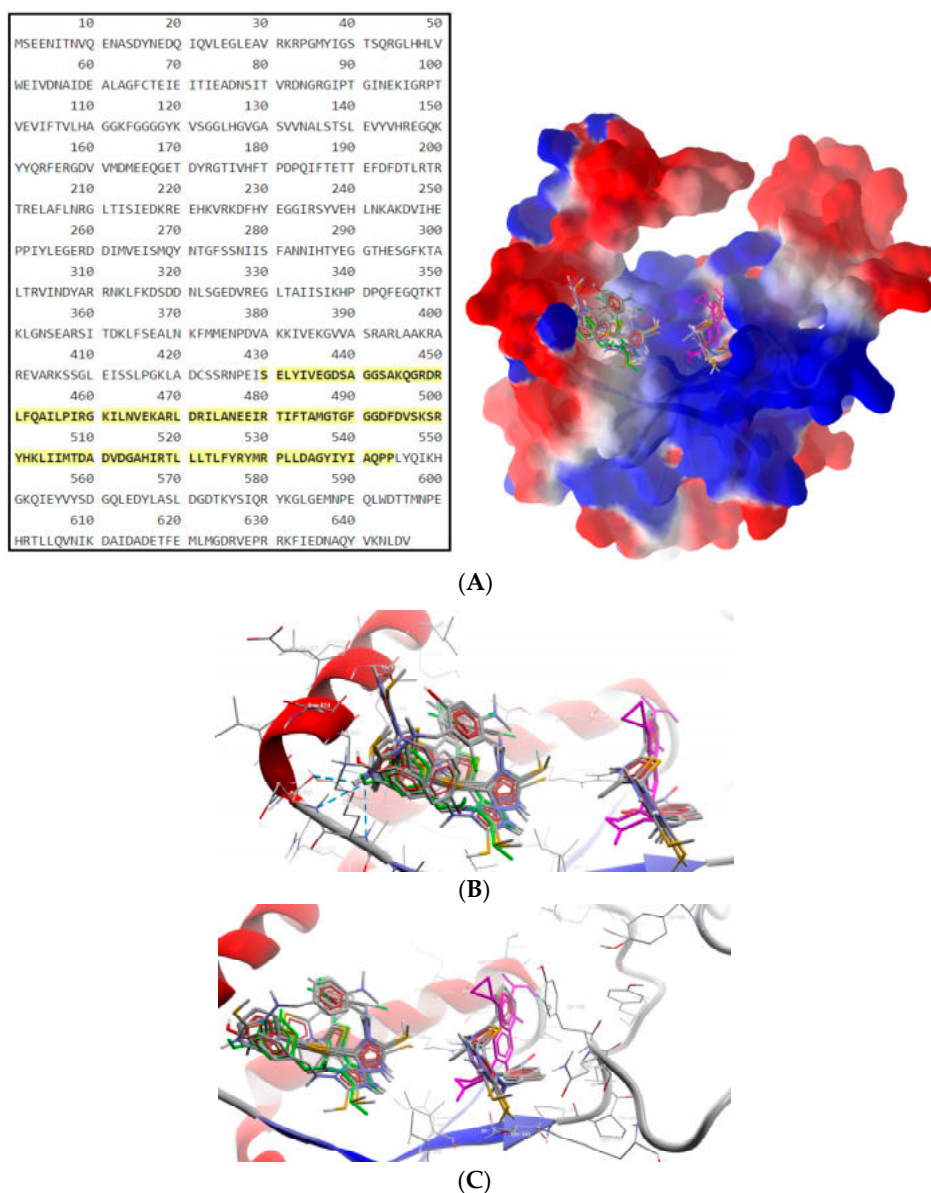


Figure 3. General view (A) and details (B,C) of the best docking poses of ligands against gyrB. Target is depicted as thin sticks with a secondary structure drawn as a cartoon backbone and semi-transparent electrostatic molecular surface (cropped in the detailed view), where ligands are figured as ball-and-stick (CIP is pink-magenta, B8 is green, meanwhile the rest of the Schiff bases are CPK colored). In the general view (A), the right group is made from CIP, B10, B11, and B13; meanwhile, the left group is made of the rest of the Schiff bases (including here B8); Detail (B) shows the left group (B8 group), image being focused on B8 (green) binding mode, emphasizing the three H-bonds established with Lys610 and Asp611 (2 H-bonds) (cropped view showing only the nearest AAs residues—until a 7.5 Å distance from B8); Detail (C) shows the right group (CIP group), image being focused on the CIP (pink-magenta) binding mode, emphasizing the H-bond established with Ala510 (cropped view showing only the nearest AAs residues—until a 7.5 Å distance from CIP).

From Table 4, it can be easily observed that all Schiff bases are stronger binders than CIP (used as the control inhibitor) to gyrA; meanwhile, on gyrB, all compounds are considerably weaker binders. For CIP, the docking results are consistent with the data included in DrugBank [49,50]. From the supplementary data (Table S2), it can be observed that Schiff bases have a common binding pattern (also illustrated in Figure 2) against gyrA within the TOP4c domain (located between positions 12–465

in *Listeria monocytogenes*, according with the UniProtKB ID: Q8YAV6), in the region described between Phe88 and Lys270; meanwhile, **CIP** binds slightly differently, between Gly41 and Gln267. The TOP4c domain or DNA topoisomerase, type IIA, subunit A/C-terminal domain, has been described as having DNA-binding activity (according to Simple Modular Architecture Research Tool–SMART accession number: SM00434) [51,52]. In medallions, the canonical sequence of *gyrA* with the TOP4c domain (positions 12–465) (Figure 2A) and the canonical sequence of *gyrB* with the Toprim domain (positions 430–544) (Figure 3A), marked with yellow, are depicted.

CIP formed two H-bonds, between the carboxyl group from position 3 (O24, O25) with Gly171 and Ser172 of the TOP4c domain (Figure 4A). All Schiff bases formed at least three H-bonds between the azomethine nitrogen (N21) and serine (Ser98) and between the triazole nitrogens (N2 and N4) and the valine residues (Val113, Val268). Additional H-bonds are formed by **B7** (with Gln95), **B8** (with Tyr266—Figure 4B, Figure 5), **B10** (with Tyr266 and Gln267), and **B13** (with Tyr266). Even though the Schiff bases and ciprofloxacin bind differently to the target, but in the same subunit A (C-terminal domain of DNA topoisomerase IIA, (TOP4c)), both binding patterns competitively block the access of *O*-(5'-phospho-DNA)-tyrosine intermediate at its binding site, located in position 123 (according UniProtKB ID: Q7BSI9), in *Listeria monocytogenes*. This confirms the importance of the imine functional group for the binding mode of the Schiff bases.

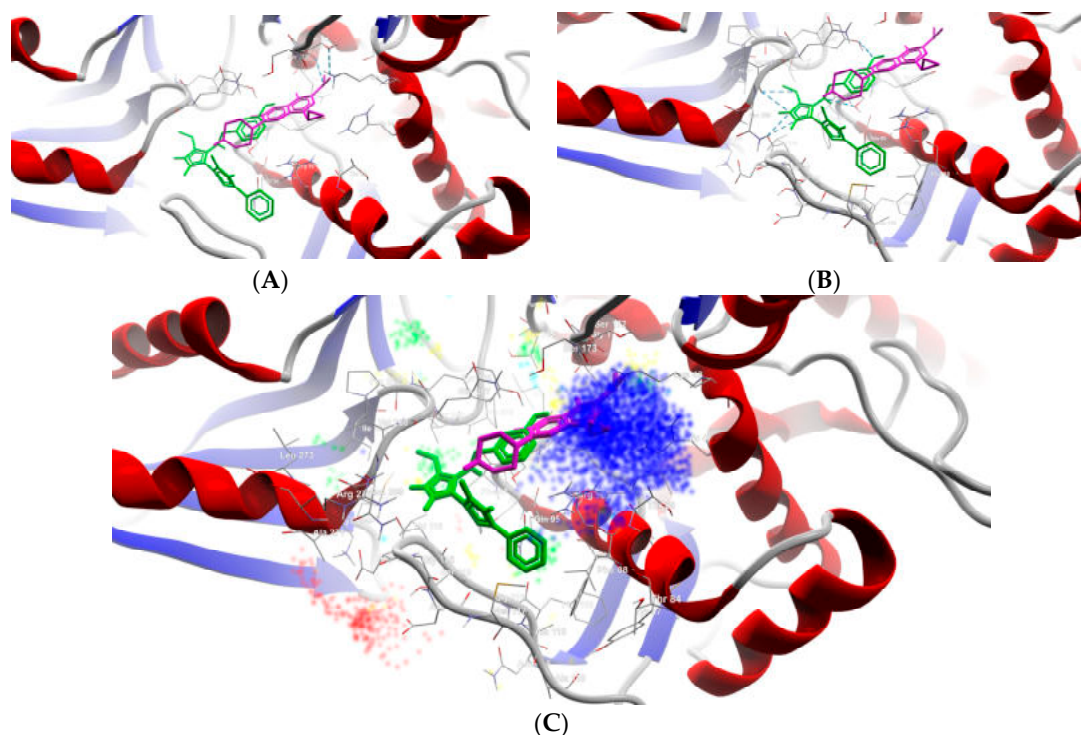


Figure 4. Details of the best docking poses of **CIP** (pink-magenta) and **B8** (green) against *gyrA* (target is depicted as thin sticks with a secondary structure drawn as a cartoon backbone, where ligands are figured as sticks and H-bonds are depicted as dashed blue lines). In detail (A), the image is focused on the **CIP** binding mode, emphasizing the two H-bonds established with Ser172 and Gly171 (in order to simplify the image, only the nearest AAs residues—until a 5.0 Å distance from **CIP**, are shown); In detail (B), the image is focused on the **B8** binding mode, emphasizing the six H-bonds established with Val113 (2 H-bonds), Val268 (2 H-bonds), Ser98, and Tyr266 (to simplify the image are shown only the nearest AAs residues—until a 5.0 Å distance from **B8**); Detail (C) illustrates the energy grid: green—steric favorable; light blue—hydrogen acceptor favorable; yellow—hydrogen donor favorable; red and dark blue—electrostatic interactions (cropped view showing only the nearest AAs residues—until a 7.5 Å distance from **B8**).

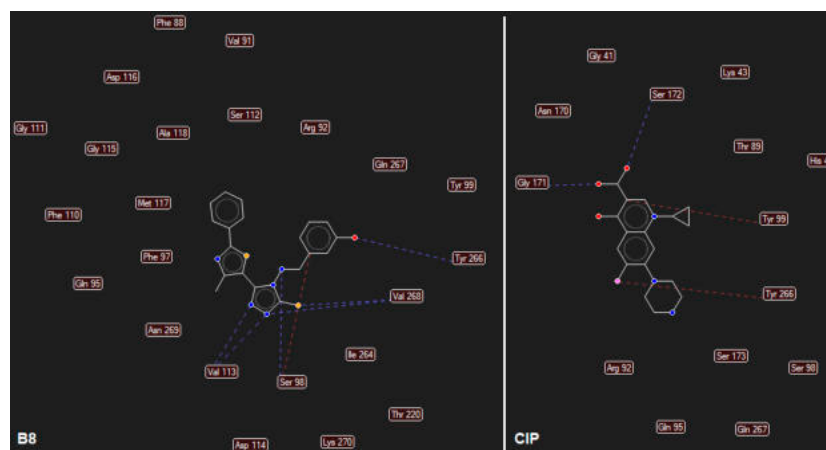


Figure 5. Mapping of H-bonds and steric interactions between ligands (case of **B8** and **CIP**) and gyrA (H-bonds are illustrated as blue dashed lines, strong steric interactions are represented as red dashed lines, the weak steric interaction are not figured, only the corresponding AAs are depicted).

Analyzing the docking results (Table 5), it can be observed that all screened compounds are weaker binders of gyrB than of gyrA. Moreover, the binding patterns indicate the lack of pharmacological relevance since the interacting region is placed partially outside the Toprim domain (Table S2, Figure 3B,C). Moreover, the H-bonds are scarce, and only **B1**, **B5**, **B7–11**, **B13**, **B15**, and **CIP** are able to establish such a type of interactions with gyrB (Table S2).

Analyzing the docking output, respectively, focusing on the best binders to gyrA, combined with the ADMET profiling, the best drug-like candidates are **B6–9** and **B14**, which comply with the GSK 4/400 rule (**CIP** also falls in the same category). Moreover, two of these drug candidates (**B8** and **B14**) are also free of PAINS, which make them the most balanced compounds, in terms of potency (being more potent than **CIP**) vs. safety (lacking of PAINS, meanwhile **CIP** being classified as an intermediate compound in terms of safety concerns).

B8 is a stronger binder than **B14** (Table 4), interacting with the TOP4c domain of gyrA in a binding pocket described between Phe88 and Lys270 (Table S2, Figures 4 and 5).

From Figures 4 and 5, and data presented in Table S2, it can be observed that compound **B8** forms six H-bonds with gyrA (one between azomethine N21 and Ser98, two between Val113 and the triazolic nitrogens N2 and N4, two between Val268 and triazolic N4 and thiolic S32, and one between hydroxy-phenol substituent from meta position and Tyr266), and multiple steric interactions with surrounding AAs.

The competitive binding pattern of **B8** prevents both ATP and DNA binding to gyrA, with the formation of *O*-(5'-phospho-DNA)-tyrosine intermediate in the active site (located at position 123) being competitively blocked, resulting in the inhibition of its GO functions: ATP binding function (GO:0005524), ATP-hydrolyzing activity (GO:0003918), and DNA binding (GO:0003677). Such a binding pattern prevents the topological transformation of bacterial DNA. Due to the homology of the subunit A (gyrA) of the bacterial DNA gyrase and parC domain of topoisomerase IV, it is also expected that the GO functions of topoisomerase IV will be inhibited.

3. Materials and Methods

3.1. Antibacterial Activity Assay

3.1.1. Determination of the Inhibition Zone Diameters

The *in vitro* antimicrobial activity was evaluated using the cup-plate agar diffusion method, according to the Clinical and Laboratory Standards Institute (CLSI) guidelines [53]. For the antibacterial

testing, Mueller-Hinton agar medium was used. The cell density was adjusted to the density of a 0.5 McFarland standard. A volume of 20 μL of each compound solution (5 mg/mL in dimethyl sulfoxide-DMSO) was delivered into the wells (100 μg /well). Ciprofloxacin (100 μg /well) was used as the standard drug. The controls were performed with sterile broth, overnight culture, and 20 μL of DMSO. The plates were incubated at 35 $^{\circ}\text{C}$. Zone diameters were measured after 24 h. Tests were repeated three times. The solvent used for the stock solutions (5 mg/mL), DMSO (Merck, Germany), did not express inhibitory activity against the tested bacterial strains.

3.1.2. Calculation of the Percentage Activity Index (% AI)

Percentage activity index (% AI) was determined using the mathematical formula [54]:

$$\% \text{ AI} = (\text{Zone of the inhibition of synthetic compound} / \text{Zone of the inhibition of reference drug}) \times 100$$

3.1.3. Determination of MIC and MBC Values

The microorganisms used for the antimicrobial activity evaluation were obtained from the University of Agricultural Sciences and Veterinary Medicine Cluj-Napoca, Romania. The Gram-positive bacteria (*Staphylococcus aureus* ATCC 49444, *Listeria monocytogenes* ATCC 19115) and Gram-negative bacteria (*Pseudomonas aeruginosa* ATCC 27853, *Salmonella typhimurium* ATCC 14028) were maintained on plate count agar slants, at 4 $^{\circ}\text{C}$. The cultures were maintained on Mueller Hinton agar (bioMérieux, Marcy l'Etoile, France). The bacteria were cultured overnight in 5 mm Mueller Hinton broth (bioMérieux, Marcy l'Etoile, France) in a shaker incubator (Heidolph Inkubator 1000 coupled with Heidolph Unimax 1010, Germany), at 37 $^{\circ}\text{C}$, 150 rpm, until the culture reached an OD_{550} of 0.02 (Nanodrop Spectrophotometer ND-1000, USA), corresponding to 10^8 CFU mL^{-1} . Before the incubation with materials, the cultures were diluted to 10^5 CFU mL^{-1} .

Stock solutions (1 mg/mL) were prepared by dissolving the test compounds and the reference antibiotic (ciprofloxacin), respectively, in sterile DMSO. These solutions were stored at 4 $^{\circ}\text{C}$. Series of double diluting solutions of the above compounds were prepared in RPMI 1640 medium, obtaining final concentrations in the range of 500 $\mu\text{g}/\text{mL}$ to 0.015 $\mu\text{g}/\text{mL}$.

The broth microdilution method was employed for the minimum inhibitory concentration (MIC) test [53]. The growth control, sterility control, and control of antibacterial compounds were used. Plates were incubated at 37 $^{\circ}\text{C}$, for 24 h, and next, MICs were determined, by adding resazurin (20 μL , 0.02%), followed by a 2 h incubation. For determining the minimum bactericidal concentration (MBC), a 0.01 mL aliquot of the medium drawn from the culture tubes, showing no macroscopic growth after 24 h, was subcultured on nutrient agar/potato dextrose agar plates, to determine the number of the vital organisms and was incubated further at 37 $^{\circ}\text{C}$, for 24 h. All MIC and MBC tests were repeated three times.

3.2. Virtual Screening

3.2.1. ADMET Predictions

FAF-Drugs4 [55,56] was used to screen all ligands in order to predict their ADME-Tox properties. The input files (previously generated SDF files) were formatted according to FAF-Drugs4's requirements using Bank-Formatter [55]. XLOGP3 [54] was chosen as the logP computation program to estimate lipophilicity and the derived ADMET descriptors. ADMET screening was carried out using a series of FAF-Drugs4's built-in filters for drug-likeness. The *Drug-Like Soft filter* of FAF-Drugs4 is based on the physicochemical and molecular properties and the bioavailability rules used widely for drug discovery [57–61]. The *Drug-Like Soft filter* uses a built-in statistical analysis of drugs [55] extracted from the *e-Drugs3D library* [62] for the threshold values of computed descriptors. Additional filters were used for the detection of the non-peptidic inhibitors of protein-protein interactions (PPIs) [63], the detection of the undesirable moieties and substructures (UMSs) involved in toxicity problems [46,63–65], covalent inhibitors (CIs) [32,33], and Pan-Assay Interference Compounds (PAINS) [66,67]. The detection of

PAINS was done using a set of three filters [55,67,68]. Finally, a series of ADMET filters, currently used by pharmaceutical companies, were used to assess the safety profiling: MedChem rules [47], the GSK 4/400 rule [46], the Pfizer 3/75 rule [48], and the estimation of phospholipidosis induction (PPDI) [69]. The MedChem is a package of 275 rules developed by Eli Lilly and Company (Indianapolis, IN, USA) to identify compounds that may interfere with the biological assays—we chose in our VS run a 100-demerit cutoff (the regular setting of FAF-Drugs4).

3.2.2. Molecular Docking

The molecular docking was performed on DNA gyrase subunit A—gyrA and DNA gyrase subunit B—gyrB from *L. monocytogenes*. A cross-search between The Universal Protein Resource—UniProt [70] and RCSB Protein Data Bank—RCSB-PDB [71] did not reveal any experimental structure for DNA gyrases from *L. monocytogenes*; consequently, there were constructed homologue models for both of them, using SWISS-MODEL [72], via the ExPASy web server [73].

The previously optimised Tripos MOL2 files of corresponding Schiff bases were docked against each of the two gyrases, in two separate runs, with PyRx—Python Prescription 0.9.5 [74] using AutoDock Vina [75] as the docking algorithm. AutoDock Vina is able to automatically calculate the grid maps and use an X-score inspired scoring function [76] to predict the noncovalent binding of ligands and to cluster the results. Since Autodock Vina is able to automatically calculate the grid maps, both runs were performed as blind docking [77] in order to detect all the possible binding sites and binding patterns. The exhaustiveness of each docking run was set to 80 (increased 10 times from the default value of software), in order to improve the accuracy of the predictions [75,78]. Supplementary, Molegro Molecular Viewer v2.5—MMV v2.5 (Molegro, A CLC Bio Company, Aarhus N, Denmark) was used for data extraction (binding patterns, energy contribution) and high-resolution renderings.

4. Conclusions

Fifteen thiazolyl-triazole Schiff bases, previously synthesized, have been investigated for their antibacterial potential, against Gram-positive and Gram-negative bacterial strains. The determination of the inhibitory zone diameters showed that compounds **B1**, **B2**, **B9**, and **B10** were the most potent against Gram-positive *L. monocytogenes*, with an equal or a superior effect (**B10**), compared to ciprofloxacin. MICs and MBCs were in agreement with the results obtained. Regarding the activity against the Gram-negative strains, most of the compounds inhibited the growth of *P. aeruginosa*, but MICs were smaller than the reference (**B5**, **B6**, **B11–15**) or equal to ciprofloxacin (**B9**). The calculated MBC/MIC ratio suggested a bactericidal effect for the new molecules.

The molecular docking study, performed on DNA-gyrA and gyrB from *L. monocytogenes*, revealed that the thiazolyl-triazole Schiff bases have a common binding pattern to gyrA and competitively block the access of O-(5'-phospho-DNA)-tyrosine intermediate at its binding site. All Schiff bases make at least three H-bonds between the azomethine nitrogen, the triazole nitrogens (N2 and N4), respectively, with AA residues from the TOP4c domain of gyrA. All screened compounds are weaker binders to gyrB than gyrA and the binding patterns indicate the lack of pharmacological relevance, since the interacting region is placed partially outside the Toprim domain.

The ADMET profiling revealed that all Schiff bases are non-inducers of phospholipidosis. The virtual screening selected the thiazolyl-triazole derivative **B8** as the best *drug-like* candidate, which complied with the safety rules (GSK 4/400, PAINS), and was more efficient than **CIP**, on gyrA. Plus, its binding pattern prevents both ATP and DNA binding to gyrA, and consequently, prevents the topological transformation of bacterial DNA.

All data collected from the in vitro antibacterial evaluation and the virtual screening, may be considered as a structural basis for the design of new antibacterial drugs, acting as DNA-gyrase inhibitors, without severe side effects.

Supplementary Materials: Supplementary materials can be found at www.mdpi.com/1422-0067/19/1/222/s1.

Acknowledgments: This study was supported by “Iuliu Hațieganu” University of Medicine and Pharmacy Cluj-Napoca internal research grant No. 4944/7/08.03.2016.

Author Contributions: All the authors participated in the research steps and/or the manuscript preparation: Cristina Nastasă participated in the microbiological assay, the ADMET profiling of the compounds, the molecular docking, and the preparation of the manuscript; Dan C. Vodnar, Ioana Ionuț, and Anca Stana were involved in the microbiological screening of the molecules; Radu Tamaian and Daniela Benedec participated in the ADMET profiling of the compounds and the molecular docking; Ovidiu Oniga and Brîndușa Tiperciuc designed the study, analyzed all the data, and participated in the preparation of the manuscript.

Conflicts of Interest: The authors declare no conflict of interest.

References

1. Tang, S.S.; Apisarnthanarak, A.; Hsu, L.Y. Mechanisms of β -lactam antimicrobial resistance and epidemiology of major community- and healthcare-associated multidrug-resistant bacteria. *Adv. Drug Deliv. Rev.* **2014**, *78*, 3–13. [[CrossRef](#)] [[PubMed](#)]
2. Dodds, D.R. Antibiotic resistance: A current epilogue. *Biochem. Pharmacol.* **2017**, *134*, 139–146. [[CrossRef](#)] [[PubMed](#)]
3. Johani, K.; Abualsaud, D.; Costa, D.M.; Hu, H.; Whiteley, G.; Deva, A.; Vickery, K. Characterization of microbial community composition, antimicrobial resistance and biofilm on intensive care surfaces. *J. Infect. Public Health.* **2017**. [[CrossRef](#)] [[PubMed](#)]
4. Zawadzki, P.; Stracy, M.; Ginda, K.; Zawadzka, K.; Lesterlin, C.; Kapanidis, A.N.; Sherratt, D.J. The Localization and Action of Topoisomerase IV in *Escherichia coli* Chromosome Segregation Is Coordinated by the SMC Complex, MukBEF. *Cell Rep.* **2015**, *13*, 2587–2596. [[CrossRef](#)] [[PubMed](#)]
5. Collin, F.; Karkare, S.; Maxwell, A. Exploiting bacterial DNA gyrase as a drug target: Current state and perspectives. *Appl. Microbiol. Biotechnol.* **2011**, *92*, 479–497. [[CrossRef](#)] [[PubMed](#)]
6. Corbett, K.D.; Schoeffler, A.J.; Thomsen, N.D.; Berger, J.M. The Structural Basis for Substrate Specificity in DNA Topoisomerase IV. *J. Mol. Biol.* **2005**, *351*, 545–561. [[CrossRef](#)] [[PubMed](#)]
7. Ashburner, M.; Ball, C.A.; Blake, J.A.; Botstein, D.; Butler, H.; Cherry, J.M.; Davis, A.P.; Dolinski, K.; Dwight, S.S.; Eppig, J.T.; et al. Gene ontology: Tool for the unification of biology. The Gene Ontology Consortium. *Nat. Genet.* **2000**, *25*, 25–29. [[CrossRef](#)] [[PubMed](#)]
8. The Gene Ontology Consortium. Expansion of the Gene Ontology knowledgebase and resources. *Nucleic Acids Res.* **2017**, *45*, D331–D338. [[CrossRef](#)]
9. Watt, P.M.; Hickson, I.D. Structure and function of type II DNA topoisomerases. *Biochem. J.* **1994**, *303*, 681–695. [[CrossRef](#)] [[PubMed](#)]
10. Champoux, J.J. DNA topoisomerases: Structure, function, and mechanism. *Annu. Rev. Biochem.* **2001**, *70*, 369–413. [[CrossRef](#)] [[PubMed](#)]
11. Mun Huang, W. Bacterial diversity based on type II DNA topoisomerase genes. *Annu. Rev. Genet.* **1996**, *30*, 79–107. [[CrossRef](#)] [[PubMed](#)]
12. Morais Cabral, J.H.; Jackson, A.P.; Smith, C.V.; Shikotra, N.; Maxwell, A.; Liddington, R.C. Crystal structure of the breakage-reunion domain of DNA gyrase. *Nature* **1997**, *388*, 903–906. [[CrossRef](#)] [[PubMed](#)]
13. Higgins, P.G.; Fluit, A.C.; Schmitz, F.J. Fluoroquinolones: Structure and target sites. *Curr. Drug Targets* **2003**, *4*, 181–190. [[CrossRef](#)] [[PubMed](#)]
14. Nakada, N.; Shimada, H.; Hirata, T.; Aoki, Y.; Kamiyama, T.; Watanabe, J.; Arisawa, M. Biological characterization of cyclothialidine, a new DNA gyrase inhibitor. *Antimicrob. Agents Chemother.* **1993**, *37*, 2656–2661. [[CrossRef](#)] [[PubMed](#)]
15. Gellert, M.; O’Dea, M.H.; Itoh, T.; Tomizawa, J. Novobiocin and coumeromycin inhibit DNA supercoiling catalyzed by DNA gyrase. *Proc. Natl. Acad. Sci. USA* **1976**, *73*, 4474–4478. [[CrossRef](#)] [[PubMed](#)]
16. Pinar, A.; Yurdakul, P.; Yildiz, I.; Temiz-Arpaci, O.; Acan, N.L.; Aki-Sener, E.; Yalcin, I. Some fused heterocyclic compounds as eukaryotic topoisomerase II inhibitors. *Biochem. Biophys. Res. Commun.* **2004**, *317*, 670–674. [[CrossRef](#)] [[PubMed](#)]
17. Shirude, P.S.; Madhavapeddi, P.; Tucker, J.A.; Murugan, K.; Patil, V.; Basavarajappa, H.; Raichurkar, A.V.; Humnabadkar, V.; Hussein, S.; Sharma, S.; et al. Aminopyrazinamides: Novel and Specific GyrB Inhibitors

- that Kill Replicating and Nonreplicating *Mycobacterium tuberculosis*. *ACS Chem. Biol.* **2013**, *8*, 519–523. [[CrossRef](#)] [[PubMed](#)]
18. Jeankumar, V.U.; Renuka, J.; Santosh, P.; Soni, V.; Sridevi, J.P.; Suryadevara, P.; Yogeewari, P.; Sriram, D. Thiazole–aminopiperidine hybrid analogues: Design and synthesis of novel *Mycobacterium tuberculosis* GyrB inhibitors. *Eur. J. Med. Chem.* **2013**, *70*, 143–153. [[CrossRef](#)] [[PubMed](#)]
 19. Tomašič, T.; Katsamakos, S.; Hodnik, Ž.; Ilaš, J.; Brvar, M.; Solmajer, T.; Montalvão, S.; Tammela, P.; Banjanac, M.; Ergović, G.; et al. Discovery of 4,5,6,7-Tetrahydrobenzo[1,2-D]thiazoles as Novel DNA Gyrase Inhibitors Targeting the ATP-Binding Site. *J. Med. Chem.* **2015**, *58*, 5501–5521. [[CrossRef](#)] [[PubMed](#)]
 20. Brvar, M.; Perdih, A.; Oblak, M.; Mašič, L.P.; Solmajer, T. In silico discovery of 2-amino-4-(2,4-dihydroxyphenyl)thiazoles as novel inhibitors of DNA gyrase B. *Bioorg. Med. Chem. Lett.* **2010**, *20*, 958–962. [[CrossRef](#)] [[PubMed](#)]
 21. Plech, T.; Kaproń, B.; Paneth, A.; Kosikowska, U.; Malm, A.; Strzelczyk, A.; Stączek, P.; Świątek, L.; Rajtar, B.; Polz-Dacewicz, M. Determination of the Primary Molecular Target of 1,2,4-Triazole-Ciprofloxacin Hybrids. *Molecules* **2015**, *20*, 6254–6272. [[CrossRef](#)] [[PubMed](#)]
 22. East, S.P.; White, C.B.; Barker, O.; Barker, S.; Bennett, J.; Brown, D.; Boyd, E.A.; Brennan, C.; Chowdhury, C.; Collins, I.; et al. DNA gyrase (GyrB)/topoisomerase IV (ParE) inhibitors: Synthesis and antibacterial activity. *Bioorg. Med. Chem. Lett.* **2009**, *19*, 894–899. [[CrossRef](#)] [[PubMed](#)]
 23. Saini, R.P.; Kumar, V.; Gupta, G.K. Synthesis, characterization, and antibacterial activity of a novel heterocyclic Schiff's base and its metal complexes of first transition series. *Med. Chem. Res.* **2014**, *23*, 690–698. [[CrossRef](#)]
 24. Khan, K.M.; Ambreen, N.; Karim, A.; Saied, S.; Aryn, A.; Ahmed, A.; Perveen, S. Schiff Bases of Thiazole as Antibacterial and Antifungal Agents. *J. Pharm. Res.* **2012**, *5*, 651–656.
 25. Kajal, A.; Bala, S.; Kamboj, S.; Sharma, N.; Shaini, V. Schiff bases: A versatile pharmacophore. *J. Catal.* **2013**, *2013*, 1–14. [[CrossRef](#)]
 26. Hameed, A.; al-Rashida, M.; Uroos, M.; Ali, S.A.; Khan, K.M. Schiff bases in medicinal chemistry: A patent review (2010–2015). *Expert Opin. Ther. Pat.* **2017**, *27*, 63–79. [[CrossRef](#)] [[PubMed](#)]
 27. Cui, S.-F.; Addla, D.; Zhou, C.-H. Novel 3-Aminothiazolquinolones: Design, Synthesis, Bioactive Evaluation, SARs and Preliminary Antibacterial Mechanism. *J. Med. Chem.* **2016**, *59*, 4488–4510. [[CrossRef](#)] [[PubMed](#)]
 28. Brvar, M.; Perdih, A.; Renko, M.; Anderluh, G.; Turk, D.; Solmajer, T. Structure-based discovery of substituted 4,5'-bithiazoles as novel DNA gyrase inhibitors. *J. Med. Chem.* **2012**, *55*, 6413–6426. [[CrossRef](#)] [[PubMed](#)]
 29. Wang, Y.; Damu, G.L.V.; Lv, J.S.; Geng, R.X.; Yang, D.C.; Zhou, C.H. Design, synthesis and evaluation of clinafloxacin triazole hybrids as a new type of antibacterial and antifungal agents. *Bioorg. Med. Chem. Lett.* **2012**, *22*, 5363–5366. [[CrossRef](#)] [[PubMed](#)]
 30. Nastasă, C.; Tipericiu, B.; Duma, M.; Benedec, D.; Oniga, O. New Hydrazones Bearing Thiazole Scaffold: Synthesis, Characterization, Antimicrobial, and Antioxidant Investigation. *Molecules* **2015**, *20*, 17325–17338. [[CrossRef](#)] [[PubMed](#)]
 31. Stana, A.; Enache, A.; Vodnar, D.C.; Nastasă, C.; Benedec, D.; Ionuț, I.; Login, C.; Marc, G.; Oniga, O.; Tipericiu, B. New Thiazolyl-triazole Schiff Bases: Synthesis and Evaluation of the Anti-Candida Potential. *Molecules* **2016**, *21*, 1595. [[CrossRef](#)] [[PubMed](#)]
 32. Levison, M.E.; Levison, J.H. Pharmacokinetics and Pharmacodynamics of Antibacterial Agents. *Infect. Dis. Clin. N. Am.* **2009**, *23*, 791–815. [[CrossRef](#)] [[PubMed](#)]
 33. Hafidh, R.R.; Abdulmir, A.S.; Vern, L.S.; Abu Bakar, F.; Abas, F.; Jahanshiri, F.; Sekawi, Z. Inhibition of Growth of Highly Resistant Bacterial and Fungal Pathogens by a Natural Product. *Open Microbiol. J.* **2011**, *5*, 96–106. [[CrossRef](#)] [[PubMed](#)]
 34. McInnes, C. Virtual screening strategies in drug discovery. *Curr. Opin. Chem. Biol.* **2007**, *11*, 494–502. [[CrossRef](#)] [[PubMed](#)]
 35. Ramírez, D. Computational Methods Applied to Rational Drug Design. *Open Med. Chem. J.* **2016**, *10*, 7–20. [[CrossRef](#)] [[PubMed](#)]
 36. Beesu, M.; Caruso, G.; Salyer, A.C.D.; Khetani, K.K.; Sil, D.; Weerasinghe, M.; Tanji, H.; Ohto, U.; Shimizu, T.; David, S.A. Structure-Based Design of Human TLR8-Specific Agonists with Augmented Potency and Adjuvanticity. *J. Med. Chem.* **2015**, *58*, 7833–7849. [[CrossRef](#)] [[PubMed](#)]

37. Beesu, M.; Caruso, G.; Salyer, A.C.D.; Shukla, N.M.; Khetani, K.K.; Smith, L.J.; Fox, L.M.; Tanji, H.; Ohto, U.; Shimizu, T.; et al. Identification of a Human Toll-Like Receptor (TLR) 8-Specific Agonist and a Functional Pan-TLR Inhibitor in 2-Aminoimidazoles. *J. Med. Chem.* **2016**, *59*, 3311–3330. [[CrossRef](#)] [[PubMed](#)]
38. Varnek, A.; Tropsha, A. *Chemoinformatics Approaches to Virtual Screening*; Royal Society of Chemistry: Cambridge, UK, 2008; pp. 1–338. ISBN 978-0-85404-144-2.
39. Trosset, J.-Y.; Carbonell, P. Synthetic biology for pharmaceutical drug discovery. *Drug Des. Dev. Ther.* **2015**, *9*, 6285–6302. [[CrossRef](#)] [[PubMed](#)]
40. Oprea, T.I.; Matter, H. Integrating virtual screening in lead discovery. *Curr. Opin. Chem. Biol.* **2004**, *8*, 349–358. [[CrossRef](#)] [[PubMed](#)]
41. Meng, X.-Y.; Zhang, H.-X.; Mezei, M.; Cui, M. Molecular docking: A powerful approach for structure-based drug discovery. *Curr. Comput. Aided Drug Des.* **2011**, *7*, 146–157. [[CrossRef](#)] [[PubMed](#)]
42. Rahimi, H.; Najafi, A.; Eslami, H.; Negahdari, B.; Moghaddam, M.M. Identification of novel bacterial DNA gyrase inhibitors: An in silico study. *Res. Pharm. Sci.* **2016**, *11*, 250–258. [[PubMed](#)]
43. ChemAxon. Available online: <https://chemaxon.com>.
44. Potashman, M.H.; Duggan, M.E. Covalent Modifiers: An Orthogonal Approach to Drug Design. *J. Med. Chem.* **2009**, *52*, 1231–1246. [[CrossRef](#)] [[PubMed](#)]
45. Roberts, D.W.; Natsch, A. High Throughput Kinetic Profiling Approach for Covalent Binding to Peptides: Application to Skin Sensitization Potency of Michael Acceptor Electrophiles. *Chem. Res. Toxicol.* **2009**, *22*, 592–603. [[CrossRef](#)] [[PubMed](#)]
46. Gleeson, M.P. Generation of a Set of Simple, Interpretable ADMET Rules of Thumb. *J. Med. Chem.* **2008**, *51*, 817–834. [[CrossRef](#)] [[PubMed](#)]
47. Bruns, R.F.; Ian, A.W. Rules for Identifying Potentially Reactive or Promiscuous Compounds. *J. Med. Chem.* **2012**, *55*, 9763–9772. [[CrossRef](#)] [[PubMed](#)]
48. Hughes, J.D.; Blagg, J.; Price, D.A.; Bailey, S.; DeCrescenzo, G.A.; Devraj, R.V.; Ellsworth, E.; Fobian, Y.M.; Gibbs, M.E.; Gilles, R.W.; et al. Physicochemical Drug Properties Associated with In Vivo Toxicological Outcomes. *Bioorg. Med. Chem. Lett.* **2008**, *18*, 4872–4875. [[CrossRef](#)] [[PubMed](#)]
49. Wishart, D.S.; Knox, C.; Guo, A.C.; Shrivastava, S.; Hassanali, M.; Stothard, P.; Chang, Z.; Woolsey, J. DrugBank: A comprehensive resource for in silico drug discovery and exploration. *Nucleic Acids Res.* **2006**, *34*, D668–D672. [[CrossRef](#)] [[PubMed](#)]
50. Drugbank. Available online: <https://www.drugbank.ca/drugs/DB00537>.
51. Letunic, I.; Bork, P. 20 years of the SMART protein domain annotation resource. *Nucleic Acids Res.* **2017**. [[CrossRef](#)] [[PubMed](#)]
52. Letunic, I.; Doerks, T.; Bork, P. SMART: Recent updates, new developments and status in 2015. *Nucleic Acids Res.* **2015**, *43*, D257–D260. [[CrossRef](#)] [[PubMed](#)]
53. National Committee for Clinical Laboratory Standards/Clinical and Laboratory Standards Institute (NCCLS/CLSI). *Methods for Dilution Antibacterial Susceptibility Test for Bacteria That Grow Aerobically: Approved Standard*, 8th ed.; CLSI Document M07-A8; Clinical and Laboratory standards Institute: Wayne, PA, USA, 2009.
54. Ahmed, M.; Qadir, M.A.; Shafiq, M.I.; Muddassar, M.; Samra, Z.Q.; Hameed, A. Synthesis, characterization, biological activities and molecular modeling of Schiff bases of benzene sulfonamides bearing curcumin scaffold. *Arab. J. Chem.* **2016**. [[CrossRef](#)]
55. Lagorce, D.; Sperandio, O.; Baell, J.B.; Miteva, M.A.; Villoutreix, B.O. FAF-Drugs3: A Web Server for Compound Property Calculation and Chemical Library Design. *Nucleic Acids Res.* **2015**, *43*, W200–W207. [[CrossRef](#)] [[PubMed](#)]
56. Lagorce, D.; Douguet, D.; Miteva, M.A.; Villoutreix, B.O. Computational Analysis of Calculated Physicochemical and ADMET Properties of Protein-Protein Interaction Inhibitors. *Sci. Rep.* **2017**, *7*, 46277. [[CrossRef](#)] [[PubMed](#)]
57. Cheng, T.; Zhao, Y.; Li, X.; Lin, F.; Xu, Y.; Zhang, X.; Li, Y.; Wang, R.; Lai, L. Computation of Octanol-Water Partition Coefficients by Guiding an Additive Model with Knowledge. *J. Chem. Inf. Model.* **2007**, *47*, 2140–2148. [[CrossRef](#)] [[PubMed](#)]
58. Lipinski, C.A.; Lombardo, F.; Dominy, B.W.; Feeney, P.J. Experimental and Computational Approaches to Estimate Solubility and Permeability in Drug Discovery and Development Settings. *Adv. Drug Deliv. Rev.* **2001**, *46*, 3–26. [[CrossRef](#)]

59. Veber, D.F.; Johnson, S.R.; Cheng, S.-Y.; Smith, B.R.; Ward, K.W.; Kopple, K.D. Molecular Properties That Influence the Oral Bioavailability of Drug Candidates. *J. Med. Chem.* **2002**, *45*, 2615–2623. [CrossRef] [PubMed]
60. Irwin, J.J.; Shoichet, B.K. ZINC—A Free Database of Commercially Available Compounds for Virtual Screening. *J. Chem. Inf. Model.* **2004**, *45*, 177–182. [CrossRef] [PubMed]
61. Egan, W.J.; Merz, K.M.; Baldwin, J.J. Prediction of Drug Absorption Using Multivariate Statistics. *J. Med. Chem.* **2000**, *43*, 3867–3877. [CrossRef] [PubMed]
62. Pihan, E.; Colliandre, L.; Guichou, J.-F.; Douguet, D. E-Drug3D: 3D Structure Collections Dedicated to Drug Repurposing and Fragment-Based Drug Design. *Bioinformatics* **2012**, *28*, 1540–1541. [CrossRef] [PubMed]
63. Reynès, C.; Host, H.; Camproux, A.-C.; Laconde, G.; Leroux, F.; Mazars, A.; Deprez, B.; Fahraeus, R.; Villoutreix, B.O.; Sperandio, O. Designing Focused Chemical Libraries Enriched in Protein-Protein Interaction Inhibitors Using Machine-Learning Methods. *PLoS Comput. Biol.* **2010**, *6*, e1000695.
64. Horvath, D.; Lisurek, M.; Rupp, B.; Kühne, R.; Specker, E.; Von Kries, J.; Rognan, D.; Andersson, C.D.; Almgvist, C.; Elofsson, M.; et al. Design of a General-Purpose European Compound Screening Library for EU-OPENSREEN. *ChemMedChem* **2014**, *9*, 2309–2326. [CrossRef] [PubMed]
65. Cumming, J.G.; Davis, A.M.; Muresan, S.; Haeberlein, M.; Chen, H. Chemical Predictive Modelling to Improve Compound Quality. *Nat. Rev. Drug Discov.* **2013**, *12*, 948–962. [CrossRef] [PubMed]
66. Mok, N.Y.; Maxe, S.; Brenk, R. Locating Sweet Spots for Screening Hits and Evaluating Pan-Assay Interference Filters from the Performance Analysis of Two Lead-like Libraries. *J. Chem. Inf. Model.* **2013**, *53*, 534–544. [CrossRef] [PubMed]
67. Baell, J.B.; Holloway, G.A. New Substructure Filters for Removal of Pan Assay Interference Compounds (PAINS) from Screening Libraries and for Their Exclusion in Bioassays. *J. Med. Chem.* **2010**, *53*, 2719–2740. [CrossRef] [PubMed]
68. Lagorce, D.; Sperandio, O.; Galons, H.; Miteva, M.A.; Villoutreix, B.O. FAF-Drugs2: Free ADME/tox Filtering Tool to Assist Drug Discovery and Chemical Biology Projects. *BMC Bioinform.* **2008**, *9*, 396. [CrossRef] [PubMed]
69. Przybylak, K.R.; Alzahrani, A.R.; Cronin, M.T.D. How Does the Quality of Phospholipidosis Data Influence the Predictivity of Structural Alerts? *J. Chem. Inf. Model.* **2014**, *54*, 2224–2232. [CrossRef] [PubMed]
70. Uniprot. Available online: <http://www.uniprot.org>.
71. RCSB Protein Data Bank. Available online: <http://www.rcsb.org>.
72. Biasini, M.; Bienert, S.; Waterhouse, A.; Arnold, K.; Studer, G.; Schmidt, T.; Kiefer, F.; Cassarino, T.G.; Bertoni, M.; Bordoli, L.; et al. SWISS-MODEL: Modelling protein tertiary and quaternary structure using evolutionary information. *Nucleic Acids Res.* **2014**, *42*, W252–W258. [CrossRef] [PubMed]
73. SWISS-MODEL. Available online: <https://swissmodel.expasy.org>.
74. Dallakyan, S.; Olson, A.J. Small-molecule library screening by docking with PyRx. *Methods Mol. Biol.* **2015**, *1263*, 243–250. [PubMed]
75. Trott, O.; Olson, A.J. AutoDock Vina: Improving the speed and accuracy of docking with a new scoring function, efficient optimization, and multithreading. *J. Comput. Chem.* **2010**, *31*, 455–461. [CrossRef] [PubMed]
76. Wang, R.; Lai, L.; Wang, S. Further development and validation of empirical scoring functions for structure-based binding affinity prediction. *J. Comput. Aided Mol. Des.* **2002**, *16*, 11–26. [CrossRef] [PubMed]
77. Hetényi, C.; Van der Spoel, D. Blind docking of drug-sized compounds to proteins with up to a thousand residues. *FEBS Lett.* **2006**, *580*, 1447–1450. [CrossRef] [PubMed]
78. Feinstein, W.P.; Brylinski, M. Calculating an optimal box size for ligand docking and virtual screening against experimental and predicted binding pockets. *J. Cheminform.* **2015**, *7*, 18. [CrossRef] [PubMed]



Article

Lipophilicity Evaluation of Some N^1 -Arylidene-Thiosemicarbazones and 1,3,4-Thiadiazolines with Antimicrobial Activity

Ioana Ionuț, Brîndușa Tiperciuc*, and Ovidiu Oniga

Pharmaceutical Chemistry Department, Iuliu Hațieganu University of Medicine and Pharmacy, 41 Victor Babeș Street, 400012 Cluj-Napoca, Romania

*Author to whom correspondence should be addressed. Email: brandu32@yahoo.com

Received 21 September 2015; Revised 7 October 2016; Editorial Decision 27 November 2016

Abstract

The lipophilic character of 20 previously reported compounds—derivatives of N^1 -arylidene-thiosemicarbazone (series **A**) and their corresponding 1,3,4-thiadiazolines (series **B**)—has been determined by reversed-phase thin-layer chromatography, using *i*-propanol–water mixtures as eluents. Principal component analysis (PCA) allowed an objective estimation of the retention behavior of the tested compounds and also afforded to obtain a 2D scatterplot, described by the first two principal components, which had the effect of separating the compounds from each other most effectively. With the use of clustering methods (*K*-means clustering) based on PCA data, the studied compounds were grouped into two congeneric classes. When comparing the obtained lipophilicity parameters' values with the antibacterial properties of the tested compounds, we noticed that the lipophilic character had no significant influence on their growth inhibitory activity.

Introduction

Some physico-chemical properties of biologically active compounds, such as solubility, stability, lipophilicity, and the acid-base character, must be determined in early stages of drug development (1). Of these properties, lipophilicity (affinity of a molecule or moiety for a lipophilic environment) is of principal importance in drug discovery and development, because it affects three phases (pharmaceutical, pharmacokinetic and pharmacodynamic) of the drug activity (2–5).

Even if lipophilicity is one of many factors involved in the biological activity of a drug, it is often one of the most influential. This property pertains to many stages of the drug's action. Prior to reaching a pharmacological target, lipophilicity determines the solubility, reactivity and degradation of drugs. The absorption of substances, from the site of administration to the site of action, involves transporting them through various biomembranes, such as skin, cornea, intestinal mucosa, blood–brain barrier (BBB) and placenta. In general, all these biomembranes are lipid bilayers containing phospholipids, cholesterol and integral proteins. Most molecules cross cell membranes by passive diffusion, while their lipophilic character has a decisive impact on this process (1, 2, 6).

The biological activity of the molecules may be linked to their lipophilic character by means of some quantitative parameters. These parameters are known as lipophilicity evaluation parameters, and they include those values (calculated by means of theoretical methods or determined experimentally) that give the interaction between the cell membranes and the molecules of biological interest (6, 7).

The lipophilicity of a compound is commonly measured by its distribution behavior in a biphasic system, either liquid–liquid (e.g., partition coefficient in octanol/water) or solid–liquid (e.g., retention on reversed-phase high-performance liquid chromatography or thin-layer chromatography system) (2, 8, 9).

As a continuation of our research on bioactive molecules' lipophilicity determination (6, 10, 11), in the present paper, we report the lipophilic character of some N^1 -arylidene-thiosemicarbazones (TSCs) as well as of their corresponding 1,3,4-thiadiazoline (TDZ) derivatives that were obtained by cyclization under acetylating condition. These compounds were previously reported (12) for their antimicrobial properties. The purpose of this research was to investigate the feasibility of the scores, obtained by principal component

analysis (PCA) based on RP-TLC retention data, as a measure of the lipophilic character, in correlation with the biological activity of the tested compounds. PCA also affords a useful graphical tool, since scatterplots of the scores onto a plane, described by the first two or three principal components, have the effect of separating the compounds most effectively.

The clustering of the compounds into groups was possible through PCA-guided search for *K*-means.

Experimental

Chemicals and reagents

Twenty compounds—ten arylidene-TSCs (A1–10) and their corresponding 1,3,4-TDZs (B1–10)—were assessed for their lipophilic character. The synthesis and physico-chemical characterization of these compounds, along with their *in vitro* antimicrobial effects, were previously reported (12). The chemical structures of the tested compounds are compiled in Table I.

Principal component analysis

The lipophilicity of the 20 studied compounds was evaluated by PCA based on RP-TLC data. It was performed in order to explore and visualize the similarities and differences among the tested compounds.

PCA is a technique used to summarize all the information contained in a matrix (retention data, resulted from all compounds' and all mobile phases' combination) in a form that is understandable by a simple performance. It works by decomposing as a product of two smaller matrices, which are called loadings (eigenvectors) and scores (linear combinations of retention indices). The best way to extract information from PCA is by graphically plotting the matrices in order to obtain 2D or 3D plots and loading scores. In order to get an overview of the data, one should look at the scores plot of the

most important principal components (in our case, the first two). These plots represent a relative position of the objects in the 2D or 3D space of the principal components. The loadings define the size of the contribution of each original variable to the principal components. In addition, the loadings plot will provide an overview of the importance of the original variables (4, 6).

By using PCA (also known as eigenvector analysis), it represents an economic way to find the location of the objects in a reduced coordinate system. Instead of *n*-axes (corresponding to *n* variables) only *P* ($P < n$) can usually be used to describe the data set, with a maximum possible information. The new variables are called principal components and they are given by the linear combination of the *n* real variables (13).

PCA was performed on the retention data by the use of XL-STAT extension. It displayed objects (the tested compounds) in a reduced space by finding a direction (first principal component) that best preserves the scatter of the observations ($100 \times R_f$ values) in a multidimensional space. PCA gave both the coordinates (scores) of the studied compounds and the loadings of the variables (solvents) on the principal components.

K-means clustering

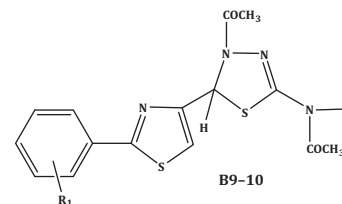
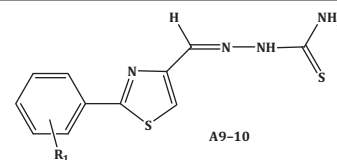
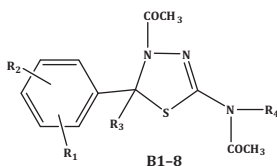
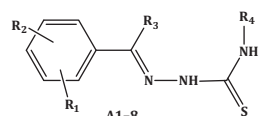
Since PCA only permits visualization of the similarities and differences of the tested compounds, dividing them into groups is only possible through clustering methods.

Data clustering is a method of creating groups of objects or clusters in such a way that all objects within a single cluster are very similar, while objects in different clusters are quite distinct. *K*-means algorithm is one of the most widely used clustering methods, being simple and easy to understand. *K*-means clustering models ball-shaped clusters using simple squared distances as distortion (14).

K-means clustering was performed based on PCA data, using the XL-STAT extension.

Table I. The Chemical Structures of the Investigated Compounds

Compound	R ₁	R ₂	R ₃	R ₄	
A1	B1	4-Br	H	CH ₃	H
A2	B2	2-OCOCH ₃	H	CH ₃	H
A3	B3	2-Cl	6-Cl	H	H
A4	B4	2-Cl	4-Cl	H	H
A5	B5	2-OCH ₃	H	H	H
A6	B6	3-NO ₂	H	H	CH ₃
A7	B7	2-Cl	4-Cl	H	C ₆ H ₅
A8	B8	3-NO ₂	H	H	C ₆ H ₅
A9	B9	H	H	H	H
A10	B10	4-Br	H	H	H



Chromatographic procedure

The lipophilicity of the 20 investigated compounds was evaluated using PCA based on thin-layer chromatographic retention data.

The chromatographic behavior of the test compounds (Table I) was studied on C₁₈ silicagel bonded 60 RP-180F₂₅₄S TLC (20 × 20 cm) plates, purchased from Merck (Darmstadt, Germany). The compounds were dissolved in DMSO (Merck) in order to achieve a 1-mg/mL concentration. Three microliters of each solution was manually spotted at 10 mm from the base and 5 mm from the edge of the plate, while the distance between successive spots was 10 mm. Chromatography was performed in a normal developing chamber, at room temperature (~20°C), and a developing distance of 8.5 cm. The mobile phase consisted of a water-*i*-propanol mixture. The organic modifier's (*i*-propanol) concentration ranged between 45 and 70% (v/v), with 5% increments. Before development, the chamber was saturated with mobile phase for 15 min. After being developed, the dried plates were visually inspected under UV light ($\lambda = 254$ nm). Each spot was clearly marked and its distance was manually measured, in order to calculate the R_f values.

Chromatographic lipophilicity parameters

Based on the R_f values, we were able to calculate one of the most common lipophilic estimators, the isocratic retention factor R_M , using the Bate-Smith and Westall equation (15).

The use of RP-TLC provides retention data in the form of R_f and corresponding R_M (1) values, that can be used to derive chromatographic descriptors for the estimation of lipophilicity: R_{M0} , b and PCA.

The use of RP-TLC is based on the assumed linear relationship between the molecular parameter (1) and $\log P$ (the logarithm of the *n*-octanol-water partition coefficient), the standard measure of lipophilicity (6, 13):

$$R_M = \log \left[\frac{1}{R_f} - 1 \right] \quad (1)$$

The R_M value (related to the molecular lipophilicity) generally depends linearly on the concentration of the organic component of the mobile phase. To increase the accuracy of the lipophilicity determination, the R_M values that were extrapolated to zero organic modifier concentration (R_{M0}) have been calculated from the linear correlation between the R_M values and the concentration of the organic component of the mobile phase:

$$R_M = R_{M0} + bc \quad (2)$$

where R_{M0} = lipophilicity estimation parameter, R_M = retention of the solute, b = slope and c = concentration of the mobile phase organic modifier (*i*-propanol).

The intercept (R_{M0}) in Equation (2) represents the extrapolated R_M values at 0% organic solvent. In other words, the intercept determined using this equation can be considered as an estimation of the compounds' partitioning between a non-polar stationary phase and the aqueous system. Hence, all the studied compounds can be compared on the basis of their lipophilicity determined this way (6, 13).

The lipophilic properties of the investigated compounds were evaluated by PCA (XL-STAT). For a better interpretation of the results obtained, these were correlated with $c\text{Log}P$ values of the tested compounds, which were generated using the ChemBioDraw 11.0 software.

Results

The lipophilicity of the 20 studied compounds was evaluated using PCA based on RP-TLC data.

Table II lists the eigenvalues of the covariance matrix, ordered from the largest to the smallest; the third column shows the difference between each eigenvalue and the next smallest one. The fourth column shows the proportion. These results suggested two component model that explained 98.993% of the total variance (information). The first component (P_1) explained 96.890% of the total variance, while the second one (P_2) only 2.103%.

Table III displays the eigenvectors associated with the first two principal components. The first eigenvector goes with the first eigenvalue and so on. The results obtained confirmed that the six solvents (mobile phases) are strongly related to each other, so they could be reduced. This shows that, for most of the investigated compounds, there was generally a regular increase in R_f values with the increasing *i*-propanol content.

The results of the regression analysis using Equation (2) are compiled in Table IV. The statistics obtained illustrate that the linear equation fits in a good way the experimental data, the linear model explaining ~98% of the total variance (see R^2 values), in the majority of cases.

Discussion

A good correlation was also found between the intercept's (R_{M0} , lipophilicity) and slope's (b , specific hydrophobic surface area) values of Equation (2). This finding suggested that the studied N¹-arylidene-TSCs A1–10 and their corresponding 1,3,4-TDZs B1–10 might form a "homologous series" of compounds, as has been suggested by some authors (16, 17).

Moreover, a high correlation ($R^2 = 0.946$) was obtained between R_{M0} and the scores on the first principal component (P_1), as it is described by the linear Equation (3).

$$R_{M0} = 1.699 - 0.168P_1 \quad (3)$$

Table II. The Eigenvalue of the Five Components (Mobile Phases)

Component	Eigenvalue	Difference	Proportion, %	Cumulative
1	5.813	5.687	96.890	96.890
2	0.126	0.084	2.103	98.993
3	0.042	0.031	0.698	99.691
4	0.011	0.006	0.183	99.874
5	0.005	0.003	0.089	99.963
6	0.002		0.037	100.000

Table III. Eigenvectors Associated with the First Two Principal Components

Component	Eigenvector	
	P_1	P_2
1	0.402	0.570
2	0.403	0.502
3	0.413	0.050
4	0.411	-0.268
5	0.410	-0.428
6	0.410	-0.407

On the basis of these findings, and as it can be seen in data provided in Table IV, the scores on the first principal component can efficiently replace the R_{M0} values in the estimation experiments of the lipophilicity of these compounds. In addition, as it is shown in Figure 1, score plots are very useful as a display tool for examining the relationships between compounds by looking for trends, groupings or outliers. By graphing scores onto the plane described by P_1 and P_2 , we obtained a “congeneric lipophilicity chart” (in which a strongly lipophilic compound is characterized by a low value of the P_1 parameter). It appears that A1–10 TSCs, as well as their

corresponding TDZ derivatives B1–10, obtained by cyclization in the presence of acetic anhydride, had a similar behavior. We can conclude that the lipophilicity is not significantly changed by cyclization.

The 2D graphic display of the scores described by P_1 and P_2 (Figure 1) afforded a good visualization of the similarities and differences between the compounds tested in the present study and supports that they might practically form two distinct congeneric classes, in a very good agreement with the selected eigenvectors and their chemical structures.

K-means clustering based on PCA data grouped the tested compounds into two congeneric classes (clusters)—1: compounds A1, A3, A4, A7, A8, A9, A10, B1, B4, B7, B8, B10 and 2: A2, A5, A6, B2, B3, B5, B6, B9. It can be noticed that, with the exception of A3, A9, B3 and B9, in each of the two classes, the compounds are found in pairs—TSCs and their corresponding TDZs.

Analysis of all retention parameters showed that the lipophilic character did not significantly change after cyclization of TSCs A1–10 to TDZs B1–10. The highest values of the lipophilicity parameters were obtained for compounds B7, A7, A10, B8, A8, A3 and A4, while the lowest belonged to compounds A5, B5, B2 and A6. The presence of electron-withdrawing substituents on the benzene ring in Position 5 of the TDZ system (Cl, Br, NO_2) increased lipophilicity, while the introduction of electron-donating substituents (OH, OCH_3) leads to a decrease in lipophilic character.

Further on, for all TDZs investigated, we decided to establish (when possible), a correlation between their biological effects and their lipophilicity (12). We considered the results (diameter of the inhibition zone) obtained for the antibacterial screening against *Bacillus cereus*. In order to compare values of similar orders of magnitude, the logarithm of the diameter of the inhibition zones (logDIZ) was calculated, and the comparison was made after a hierarchization of these compounds based on logDIZ values (Table V). We remind that the smaller the value of P_1 is, the more lipophilic a compound is.

Table IV. Regression Data and Scores on the Two First Principal Components for the Investigated Compounds and $\text{cLog}P$ values for the Studied Compounds

Compound	R_{M0}	b	R^2	P_1	P_2	$\text{cLog}P$
A1	1.741	-3.024	0.983	-0.185	-0.169	3.348
A2	1.194	-2.552	0.983	3.205	0.291	2.264
A3	1.796	-3.124	0.970	-0.142	-0.354	3.593
A4	1.894	-3.051	0.964	-1.905	0.006	3.593
A5	1.381	-2.671	0.995	1.757	0.173	1.920
A6	1.445	-2.650	0.967	0.808	0.096	1.614
A7	1.891	-2.985	0.964	-2.356	0.172	5.386
A8	2.247	-3.503	0.969	-2.927	-0.177	3.703
A9	1.855	-3.123	0.976	-0.886	-0.205	3.083
A10	2.064	-3.446	0.909	-1.097	-0.658	3.953
B1	1.593	-2.806	0.981	0.075	-0.014	3.187
B2	0.905	-2.217	0.968	4.312	0.662	1.673
B3	1.472	-2.724	0.984	0.996	0.035	3.231
B4	1.672	-2.920	0.981	-0.080	-0.117	3.231
B5	1.199	-2.574	0.982	3.284	0.217	1.724
B6	1.375	-2.638	0.982	1.600	0.098	2.304
B7	2.859	-3.906	0.978	-6.840	0.923	5.422
B8	1.873	-3.233	0.980	-0.308	-0.393	3.739
B9	1.569	-2.951	0.984	1.441	-0.191	2.247
B10	1.966	-3.330	0.980	-0.750	-0.395	3.116

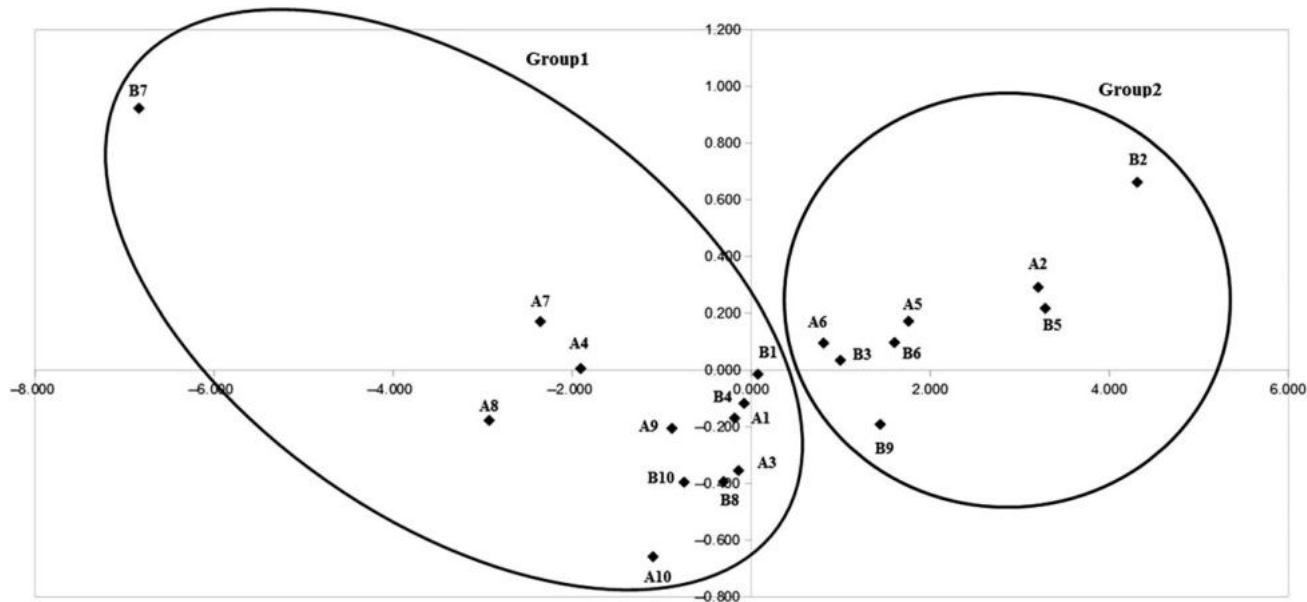



Figure 1. Congeneric lipophilicity chart (2D plot) obtained by plotting scores corresponding to P_1 and P_2 . *Groups (classes, clusters) were established via K-means clustering.

Table V. Correlation Between the Lipophilicity Parameter P_1 and the Antibacterial Activity of TDZ Derivatives **B1–10**


Compound	R ₁	R ₂	R ₃	R ₄	logDIZ	P_1
B5	2-OCH ₃	H	H	H	1.20412	3.284
B7	2-Cl	4-Cl	H	C ₆ H ₅	1.20412	-6.840
B8	3-NO ₂	H	H	C ₆ H ₅	1.20412	-0.308
B1	4-Br	H	CH ₃	H	1.255273	0.075
L2	2-OCOCH ₃	H	CH ₃	H	1.255273	4.312
B3	2-Cl	6-Cl	H	H	1.255273	0.996
B4	2-Cl	4-Cl	H	H	1.255273	-0.080
B6	3-NO ₂	H	H	CH ₃	1.255273	1.600
B9	H				1.255273	1.441
B10	4-Br				1.255273	-0.750

Data analysis showed that there is no proportionality (direct or reversed) relationship between the lipophilic character and the inhibitory activity against *Bacillus cereus* of these compounds, since their inhibitory effects were very similar, regardless of their lipophilicity.

Conclusions

In summary, 20 previously reported compounds, derivatives of N¹-arylidene-TSC and their corresponding TDZs, were investigated for their lipophilic character. After applying the PCA method based on chromatographic data (RP-TLC) and K-means clustering based on PCA data, the compounds were finally grouped into two classes, based on the influence of certain substituents on the lipophilic character of the whole molecule. In general, cyclization of TSCs to their corresponding TDZs did not have a significant influence on the lipophilic character of these compounds. The results obtained showed how a particular substituent attached to a pharmacophore (thiazole, TDZ) influences the chromatographic retention of a compound. Electron-withdrawing substituents (Br, Cl, NO₂) increased lipophilicity, whereas the presence of electron-donating groups (OH, OCH₃) leads to lower lipophilicity parameters' values. The results obtained also showed that the hydrophobic character of the investigated compounds does not significantly influence their antibacterial activity.

Funding

This work was supported by The Executive Agency for Higher Education Research Development and Innovation Funding—UEFISCDI, Romania, Contract 210/2014—Project PN-II-PT-PCCA-2013-4-2075.

References

- Janicka, M., Sztanke, M., Sztanke, K.; Reversed phase liquid chromatography with octadecylsilyl, immobilized artificial membrane and cholesterol columns in correlation studies with in silico biological descriptors of newly synthesized antiproliferative and analgesic active compounds; *Journal of Chromatography A*, (2013); 1318: 92–101.
- Rutkowska, E., Pająk, K., Józwiak, K.; Lipophilicity - Methods of determination and its role in medicinal chemistry; *Acta Poloniae Pharmaceutica - Drug Research*, (2013); 70: 3–18.
- Toma, A., Hapău, D., Casoni, D., Zaharia, V.; Heterocycles 33: lipophilicity of a new class of thioethers estimated by reversed-phase thin-layer chromatography and different computational methods; *Journal of Chromatographic Science*, (2014); 52: 1302–1307.
- Casoni, D., Kot-Wasik, A., Namieśnik, J., Sârbu, C.; Lipophilicity data for some preservatives estimated by reversed-phase liquid chromatography and different computation methods; *Journal of Chromatography A*, (2009); 1216: 2456–2465.
- Casoni, D., Sârbu, C.; Comprehensive evaluation of lipophilicity of biogenic amines and related compounds using different chemically bonded phases and various descriptors; *Journal of Separation Science*, (2012); 35: 915–921.
- Palage, M., Tipericiu, B., Oniga, S., Aranciu, C., Benedec, D., Oniga, O.; The evaluation of the lipophilic properties of some thiazolyl-oxadiazolines with antiinflammatory activity; *Farmacia*, (2011); 59: 347–357.
- Zydek, G., Brzezińska, E.; Normal and reversed phase thin layer chromatography data in quantitative structure-activity relationship study of compounds with affinity for serotonin (5-HT) receptors; *Journal of Chromatography B*, (2011); 879: 1764–1772.
- Sârbu, C., Kuhajda, K., Kevresan, S.; Evaluation of the lipophilicity of bile acids and their derivatives by thin-layer chromatography and principal component analysis; *Journal of Chromatography A*, (2001); 917: 361–366.
- Komsta, L., Skibiński, R., Berecka, A., Gumieniczek, A., Radkiewicz, B., Radoń, M.; Revisiting thin-layer chromatography as a lipophilicity determination tool - A comparative study on several techniques with a model solute set; *Journal of Pharmaceutical and Biomedical Analysis*, (2010); 53: 911–918.
- Sârbu, C., Tipericiu, B.; Modeling, by multivariate regression methods, of the chromatographic retention (lipophilicity) of new oxadiazoline derivatives; *Journal of Planar Chromatography - Modern TLC*, (2007); 19: 342–347.
- Tipericiu, B., Sârbu, C.; Prediction of the chromatographic retention (lipophilicity) of some new methyl-thiazole-oxadiazoline derivatives by multivariate regression methods; *Journal of Liquid Chromatography and Related Technologies*, (2006); 29: 2257–2270.
- Ionuț, I., Nastasă, C., Tipericiu, B., Oniga, S., Pirnău, A., Vlase, L., et al.; Synthesis and antimicrobial activity evaluation of some N¹-arylidene-thiosemicarbazone and 1,3,4-thiadiazoline derivatives; *Chujul Medical*, (2013); 86: 27–33.
- Sârbu, C., Todor, S.; Determination of lipophilicity of some non-steroidal anti-inflammatory agents and their relationships by using principal

- component analysis based on thin-layer chromatographic retention data; *Journal of Chromatography A*, (1998); 822: 263–269.
14. Xu, Q., Ding, C., Liu, J., Luo, B.; PCA-guided search for *K*-means; *Pattern Recognition Letters*, (2015); 54: 50–55.
 15. Bate-Smith, E.C., Westall, R.G.; Chromatographic behavior and chemical structure. I. Some naturally occurring phenolic substances; *Biochimica et Biophysica Acta*, (1950); 4: 427–440.
 16. Cserhádi, T.; Lipophilicity determination of non-homologous series of non-ionic surfactants by means of reversed-phase thin-layer chromatography; *Journal of Biochemical and Biophysical Methods*, (1993); 27: 133–142.
 17. Darwish, Y., Cserhati, T., Forgacs, E.; Relationship between lipophilicity and specific hydrophobic surface area of non-homologous series of pesticides; *Journal of Planar Chromatography - Modern TLC*, (1993); 6: 458–462.



Article

Design, Synthesis and Antifungal Activity Evaluation of New Thiazolin-4-ones as Potential Lanosterol 14 α -Demethylase Inhibitors

Anca Stana¹, Dan C. Vodnar^{2,*}, Radu Tamaian^{3,4}, Adrian Pîrnău⁵, Laurian Vlase⁶,
Ioana Ionuț^{1,*}, Ovidiu Oniga¹ and Brîndușa Tipericiu¹

¹ Department of Pharmaceutical Chemistry, “Iuliu Hațieganu” University of Medicine and Pharmacy, 41 Victor Babeș Street, RO-400012 Cluj-Napoca, Romania; teodora_anca@yahoo.com (A.S.); onigao65@yahoo.com (O.O.); brandu32@yahoo.com (B.T.)

² Department of Food Science and Technology, University of Agricultural Sciences and Veterinary Medicine, 3-5 Manăștur Street, RO-400372 Cluj-Napoca, Romania

³ National Institute for Research and Development for Cryogenic and Isotopic Technologies, 4th Uzinei Street, RO-240050 Râmnicu Vâlcea, Romania; radu.tamaian@icsi.ro

⁴ SC Biotech Corp SRL, 4th Uzinei Street, RO-240050 Râmnicu Vâlcea, Romania

⁵ National Institute for Research and Development of Isotopic and Molecular Technologies, RO-400293 Cluj-Napoca, Romania; adrian.pirnaeu@itim-cj.ro

⁶ Department of Pharmaceutical Technology and Biopharmaceutics, “Iuliu Hațieganu” University of Medicine and Pharmacy, 41 Victor Babeș Street, RO-400012 Cluj-Napoca, Romania; vlaselaur@yahoo.com

* Correspondence: dan.vodnar@usamvcluj.ro (D.C.V.); ionut.ioana@umfluj.ro (I.I.); Tel.: +40-747-341-881 (D.C.V.); +40-747-507-629 (I.I.)

Academic Editor: Christo Christov

Received: 22 November 2016; Accepted: 9 January 2017; Published: 17 January 2017

Abstract: Twenty-three thiazolin-4-ones were synthesized starting from phenylthioamide or thiourea derivatives by condensation with α -monochloroacetic acid or ethyl α -bromoacetate, followed by substitution in position 5 with various arylidene moieties. All the synthesized compounds were physico-chemically characterized and the IR (infrared spectra), ¹H NMR (proton nuclear magnetic resonance), ¹³C NMR (carbon nuclear magnetic resonance) and MS (mass spectrometry) data were consistent with the assigned structures. The synthesized thiazolin-4-one derivatives were tested for antifungal properties against several strains of *Candida* and all compounds exhibited efficient anti-*Candida* activity, two of them (**9b** and **10**) being over 500-fold more active than fluconazole. Furthermore, the compounds' lipophilicity was assessed and the compounds were subjected to in silico screening for prediction of their ADME-Tox properties (absorption, distribution, metabolism, excretion and toxicity). Molecular docking studies were performed to investigate the mode of action towards the fungal lanosterol 14 α -demethylase, a cytochrome P450-dependent enzyme. The results of the in vitro antifungal activity screening, docking study and ADME-Tox prediction revealed that the synthesized compounds are potential anti-*Candida* agents that might act by inhibiting the fungal lanosterol 14 α -demethylase and can be further optimized and developed as lead compounds.

Keywords: thiazolin-4-one; antifungal activity; lipophilicity; lanosterol 14 α -demethylase; molecular docking; ADME-Tox predictors

1. Introduction

Of the five-membered heterocyclic rings containing sulfur and nitrogen, the thiazolin-4-ones are considered biologically privileged molecules and enjoy special attention from researchers in the

field of medicinal chemistry due to their multifarious biological activities and good tolerability in humans [1,2].

Thiazolin-4-ones and their derivatives have great biological importance because they were found to have valuable pharmacological activities, such as antibacterial [1,3], antifungal [1,4], antiviral [5], anti-inflammatory (through COX inhibition) [6], hypoglycemic [7], antioxidant [8], neuroprotective and anticonvulsant [9], antitubercular [10] and antitumor [2,4,11] activities.

Despite the numerous antifungals approved for the treatment of infections, the emergence of fungal infectious diseases and the dramatically increasing number of pathogens resistant to different classes of currently available antimycotic agents resulted in the acute need to implement new strategies for developing new antifungal chemotherapeutics towards which there is little antimicrobial resistance or no cross-resistance [12]. The lanosterol 14 α -demethylase (or CYP51A1) is a key enzyme in the synthesis of ergosterol, an essential component of the fungal cell membrane and constitutes an important biological target for the most popular class of antifungals (the azoles) [13]. This enzyme catalyzes the conversion of lanosterol into ergosterol through C14-demethylation. Fluconazole, a triazole derivative, and ketoconazole, an imidazole derivative, from the azole class of antifungals inhibit CYP51A1 by forming a coordinate bond between the nucleophilic nitrogen of the azole heterocycle (N3 of imidazole and N4 of triazole) and the heme iron in the ferric state from the active site of enzyme. Inhibition of lanosterol 14 α -demethylase leads to accumulation of 14 α -methylsterols on the fungal surface and alteration of plasma membranes' permeability and rigidity, which results in arrest of fungal growth. Because this enzyme is found in all eukaryotes (including humans) and because the azoles interact also with other cytochrome P450 dependent enzymes (CYP3A4), a selective inhibition towards the fungal CYP51A1 is essential for an increased therapeutic index [13].

The pharmacological activity of some compounds is strictly related to their lipophilicity as for the manifestation of therapeutic properties they must pass through a series of biological barriers, from the administration site to the site of action. Therefore, from the physicochemical properties of biologically active compounds, lipophilicity is of great importance and should be determined from the early stages of drug development because it affects basic steps of a drug's pharmacokinetics and pharmacodynamics, such as absorption, distribution, metabolism, excretion and toxicity (ADME-Tox) [14].

Virtual screening (VS) is an important tool for the identification of good leads as one of the first essential steps in the drug discovery process. Therefore, the VS output allows prioritizing the development of the most promising compounds (drug-like or lead-like molecules) prior to high throughput screening (HTS) [15]. Computational prediction of lipophilicity, as a critical aspect of VS, is crucial for the improvement of ADME-Tox properties of the most promising drug/lead candidates, from the first steps. Suboptimal pharmacokinetic properties and increased toxicity are some of the most important reasons for a drug's failure in the development phases. In silico prediction of ADME-Tox properties of new drug candidates is more economic and time sparing compared to the in vivo experimental determination of these parameters and could be useful for eliminating the molecules that are likely to fail in the early stage of drug discovery.

In order to predict the binding affinity (BA), the activity and the potential mechanism of action of a molecule, molecular docking predicts the binding orientation of small molecule drug candidates to their biological targets [16].

Based on the proven biological potential of the compounds with thiazolin-4-one core in their structure and as a continuation to our increased interest in the chemistry of thiazole and its derivatives [17], herein we report the synthesis of new thiazolin-4-ones diversely substituted in positions 2 and 5, with structures that include, in addition to the thiazolin-4-one ring, other heterocycles with known biological potential such as thiazole [18] and chromone [19]. The synthesized compounds were evaluated for their antifungal potential and, furthermore, lipophilicity studies, in silico ADME-Tox predictions and molecular docking studies were conducted in order to establish their affinity towards the biological target and a potential mechanism of action. Considering the numerous data from

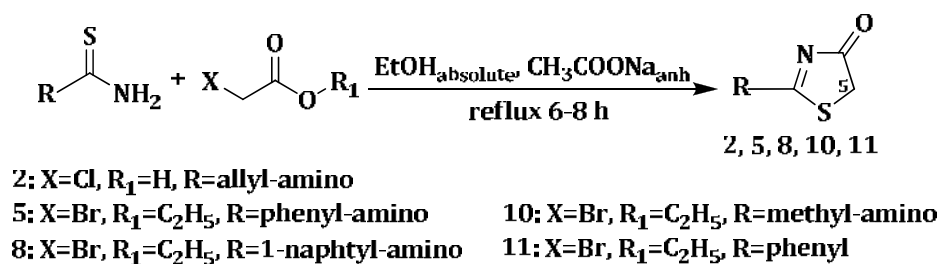
the literature that attest the ability to inhibit the fungal lanosterol 14 α -demethylase of antifungal azoles (fluconazole, a triazole; ketoconazole, an imidazole; and ravuconazole and isavuconazole, both triazoles with a thiazole moiety in their structure) [20], thiazolidine-4-one [21] and rhodanine derivatives [22], the fungal CYP51A1 was chosen as biological target in the docking study.

2. Results and Discussion

2.1. Chemistry

A series of new 2-(allyl-amino)-5-arylidene-thiazol-4(5H)-ones, 2-(phenyl-amino)-5-arylidene-thiazol-4(5H)-ones and 2-(1-naphthyl-amino)-5-arylidene-thiazol-4(5H)-ones were synthesized starting from various thiourea derivatives.

The synthetic route for the synthesis of thiazolin-4-ones, substituted in position 2 with phenyl, alkyl-amino or aryl-amino radicals is illustrated in Scheme 1. The thiazolin-4-one derivatives **2**, **5**, **8**, **10** and **11** were synthesized through the condensation of various thiourea derivatives or phenylthioamide with α -monochloroacetic acid or ethyl α -bromoacetate, in refluxing absolute ethanol, in the presence of anhydrous sodium acetate. The 2-substituted thiazolin-4-ones **2**, **5**, **8**, **10** and **11** were previously reported in the literature [23–27].



Scheme 1. Synthesis of 2-substituted thiazolin-4-ones.

Subsequently, the position 5 of the substituted 2-amino-thiazolin-4-ones was modulated through Knoevenagel condensation of the obtained intermediates **2**, **5** and **8**, with various aromatic or heteroaromatic aldehydes, in absolute ethanol and in the presence of anhydrous sodium acetate, in order to obtain, in good yields (59%–94%) the 2-(allyl/aryl-amino)-5-arylidene-thiazolin-4-ones **3a–h**, **6a–e** and **9a–e** (Scheme 2).

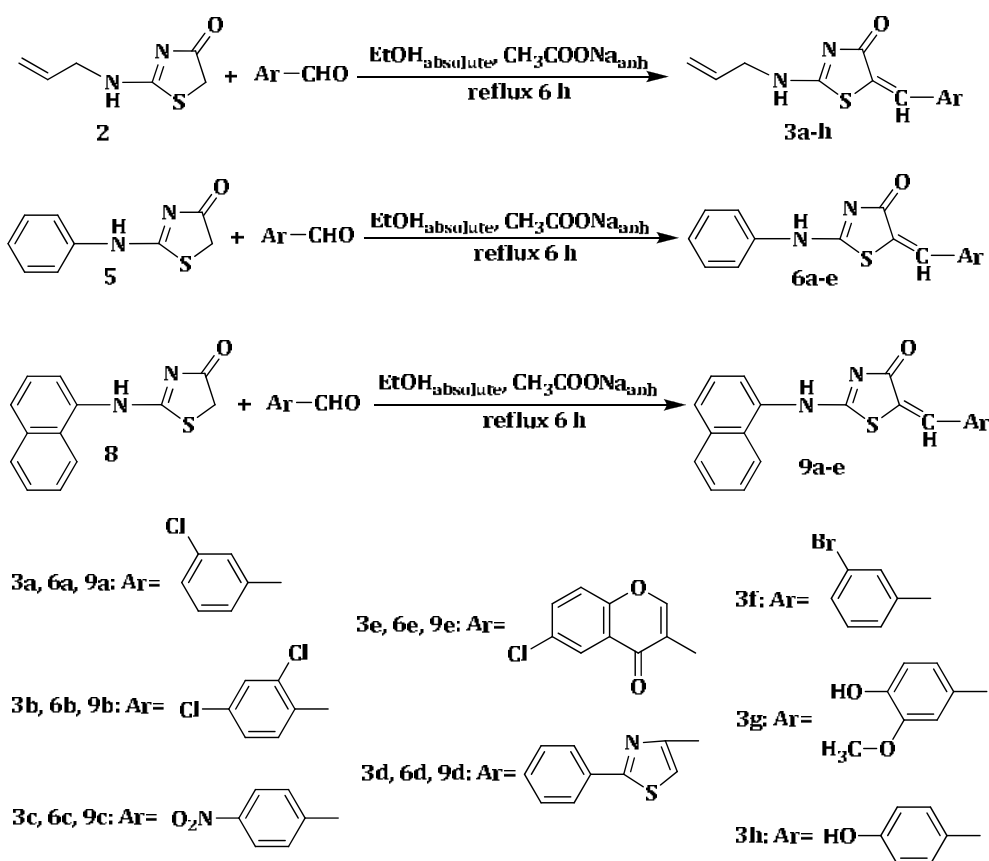
The results of the C, H, N, S quantitative elemental analysis of the synthesized compounds were consistent with the calculated values, within $\pm 0.4\%$ of the theoretical values.

The structural confirmation of the synthesized compounds was performed using spectral analysis by recording infrared spectra, mass spectra and nuclear magnetic resonance spectra. All spectral and analytical data were in accordance with the assumed structures. Details of the synthetic procedures, yields, physical, analytical and spectral data for the synthesized compounds are presented in the Experimental Section.

Mass spectra were recorded for both the 5-unsubstituted thiazolin-4-one derivatives **2**, **5**, **8**, **10**, and **11** and the 5-arylidene-thiazolin-4-ones **3a–h**, **6a–e** and **9a–e**, which gave information regarding the fragmentation of the compounds with their corresponding mass and, in all cases, revealed the correct molecular ion peaks (M^+ or M^{+1}), as suggested by their molecular formulas.

In the IR spectra of compounds **3a–h**, **6a–e** and **9a–e**, there is a strong absorption band at 1728–1681 cm^{-1} due to the stretching vibration of the C=O group from the thiazolin-4-one ring and a low intensity absorption band at 3438–3427 cm^{-1} due to valence vibration of the NH bond of the secondary amine. The IR spectra of 5-((6-chloro-4-oxo-4H-chromen-3-yl)methylene) thiazolin-4-ones **3e**, **6e** and **9e**, displayed, in addition, a high intensity absorption band at 1653–1647 cm^{-1} , characteristic to $\nu\text{C}=\text{O}$ stretching vibration, two strong absorption bands at 1273–1270 and 1045–1041 cm^{-1} , characteristic to the stretching vibration of the C–O group and a high intensity absorption band at

1173–1167 cm^{-1} , characteristic to the $\nu\text{C}-\text{Cl}$ stretching vibration of the 6-chloro-4-oxo-4*H*-chromen-3-yl rest. The absorption bands at 1523–1519 and 1330–1326 cm^{-1} in the IR spectra of compounds **3c**, **6c** and **9c** are due to the anti-symmetric and symmetric stretching vibration of the nitrogen-oxygen bonds of the aromatic NO_2 group. The IR spectra of the compounds **3a–b**, **6a–b** and **9a–b** presented high intensity absorption bands at 1158–1093 cm^{-1} , due to the valence vibrations of the $\text{C}-\text{Cl}$ bonds. Compound **3g** exhibited in the IR spectrum two strong absorption bands at 1046 and 1019 cm^{-1} due to the $\nu\text{C}-\text{O}$ stretching vibration of the phenyl-methyl-ether group. In the IR spectra of compounds **3g** and **3h**, the phenolic OH group registered an absorption band at 1336–1331 cm^{-1} corresponding to the $\nu\text{C}-\text{O}$ valence vibration and an absorption band at 3289–3285 cm^{-1} corresponding to the $\nu\text{O}-\text{H}$ stretching vibration.



In the ^1H NMR spectra of compounds **3a–h**, **6a–e** and **9a–h** were recorded the signal characteristic for the methine proton ($=\text{CH}-$) as a singlet in the 7.50–7.74 ppm region, which confirmed the success of the Knoevenagel condensation between the 2-amino substituted thiazolin-4-ones and the corresponding aromatic aldehydes, with the formation of 2-(aryl/allyl-amino)-5-arylidene-thiazolin-4-ones. The absence of a singlet signal, corresponding to the methylene protons from the 5th position of the thiazolin-4-one core, at 3.97–4.12 ppm in the ^1H NMR spectra of all the newly synthesized compounds, further confirmed the formation of the 5-substituted derivatives. In the 7.04–8.91 ppm region of the ^1H NMR spectra, the aromatic protons resonated as characteristic doublets, triplets and multiplets, that appeared as split signals based on the presence of other protons in their immediate vicinity. The phenolic OH group proton appeared as a singlet at 9.31–9.35 ppm. The protons of the methoxy group resonated as a singlet in the 3.83 ppm region of the spectrum. The ^{13}C NMR spectra of the synthesized compounds were consistent with the proposed structures.

2.2. Antifungal Activity

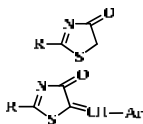
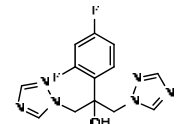
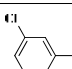
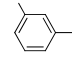
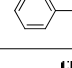
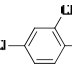
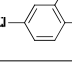
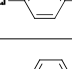
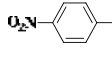
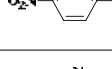
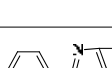
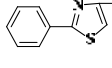
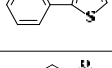
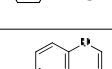
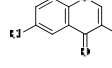
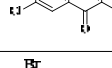
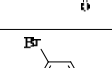
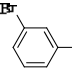
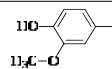
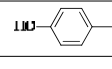
2.2.1. Determination of Inhibition Zone Diameters

All synthesized compounds were initially subjected to in vitro antifungal screening using the cup-plate agar diffusion method, against a fungal strain of *Candida albicans* ATCC 10231.

Fluconazole is an antifungal triazole that belongs to the well represented azole class and it is currently used to treat a wide variety of fungal infections. It acts by inhibiting the fungal lanosterol 14 α -demethylase, its mechanism of action involving the nucleophilic nitrogen of the azole heterocycle coordinating as the sixth ligand of the heme iron in the ferric state of the enzyme [13]. It was chosen as positive control due to the presence of two triazole rings in its structure that are essential for the biological activity.

The results of the antimicrobial activity testing of the 2-substituted-thiazolin-4-ones **2**, **5**, **8**, **10**, and **11** (1 mg/mL), and of the 2-(allyl/aryl-amino)-5-arylidene-thiazolin-4-ones **3a-h**, **6a-e** and **9a-e** (1 mg/mL) in comparison with those of the reference compound, fluconazole (1 mg/mL), are given in Table 1.

Table 1. The antifungal activity of the synthesized thiazolin-4-one derivatives (inhibition zone diameters (mm)).

			
2, 5, 8, 10, 11	Fluconazole	3a-h, 6a-e, 9a-e	
Compound	R	Ar	<i>C. albicans</i> ATCC 10231
2	CH ₂ =CH-CH ₂ -NH-	-	20 ± 0.2
5	C ₆ H ₅ -NH-	-	22 ± 0.5
8	α -C ₁₀ H ₇ -NH-	-	24 ± 1
10	CH ₃ -NH-	-	22 ± 1
11	C ₆ H ₅ -	-	18 ± 1
3a	CH ₂ =CH-CH ₂ -NH-		20 ± 0.5
6a	C ₆ H ₅ -NH-		20 ± 0.5
9a	α -C ₁₀ H ₇ -NH-		18 ± 1
3b	CH ₂ =CH-CH ₂ -NH-		20 ± 0.5
6b	C ₆ H ₅ -NH-		20 ± 1
9b	α -C ₁₀ H ₇ -NH-		18 ± 0.2
3c	CH ₂ =CH-CH ₂ -NH-		18 ± 1
6c	C ₆ H ₅ -NH-		20 ± 1
9c	α -C ₁₀ H ₇ -NH-		20 ± 0.5
3d	CH ₂ =CH-CH ₂ -NH-		20 ± 0.2
6d	C ₆ H ₅ -NH-		20 ± 1
9d	α -C ₁₀ H ₇ -NH-		20 ± 1
3e	CH ₂ =CH-CH ₂ -NH-		20 ± 0.5
6e	C ₆ H ₅ -NH-		16 ± 1
9e	α -C ₁₀ H ₇ -NH-		22 ± 0.5
3f	CH ₂ =CH-CH ₂ -NH-		22 ± 0.2
3g	CH ₂ =CH-CH ₂ -NH-		22 ± 0.2
3h	CH ₂ =CH-CH ₂ -NH-		20 ± 0.5
Fluconazole			22 ± 0.5

The value obtained for each compound represents the mean of three independent measurements \pm SD. The values obtained for the most active compounds are marked in bold.

All the synthesized compounds showed moderate to good inhibitory activity against *C. albicans* ATCC 10231 (16–22 mm inhibition zone diameters) (Table 1). Of these, compounds **5**, **3f**, **3g**, **8**, **9e** and **10** exhibited similar or better antifungal activities than that of fluconazole, used as reference antimycotic ($p < 0.05$). The 5-unsubstituted 2-(alkyl/aryl-amino)-thiazolin-4-ones **5**, **8**, and **10** and the 2-(allylamino)-5-arylidene-thiazolin-4-ones **3a–h** were generally more active than the rest of the compounds against *C. albicans* ATCC 10231 at tested concentration, suggesting that the presence of an allyl substituent at the exocyclic amine from position 2 of the thiazolin-4-one core is favorable to the antifungal activity.

2.2.2. Determination of Minimum Inhibitory Concentration (MIC) and Minimum Fungicidal Concentration (MFC) Values

The incidence of fungal infections has increased significantly over the past decades, thus contributing to morbidity and mortality through microbial infections. *Candida* species are the major human fungal pathogens that cause both mucosal and deep tissue infections and over 90% of invasive infections are caused by *Candida albicans*, *Candida glabrata*, *Candida parapsilosis*, *Candida tropicalis* and *Candida krusei* [28].

Prompted by the results obtained in the antimicrobial screening using the agar diffusion method, minimum inhibitory concentrations and fungicidal concentrations were determined, employing the broth microdilution method. All the synthesized compounds were tested against four strains of fungi (*Candida albicans* ATCC 10231, *Candida albicans* ATCC 18804, *Candida krusei* ATCC 6258 and *Candida parapsilosis* ATCC 22019). As reference antifungals, fluconazole (a systemic use azole, also used as positive control in the previous study) and ketoconazole (a topical azole) were chosen.

The results of the minimum inhibitory concentration test and those of the minimum fungicidal concentration assay are depicted in Table 2.

Table 2. Minimum Inhibitory Concentration (MIC) ($\mu\text{g}/\text{mL}$) and Minimum Fungicidal Concentration (MFC) ($\mu\text{g}/\text{mL}$) of the thiazolin-4-one derivatives.

Samples	<i>C. albicans</i> ATCC 10231		<i>C. albicans</i> ATCC 18804		<i>C. krusei</i> ATCC 6258		<i>C. parapsilosis</i> ATCC 22019	
	MIC	MFC	MIC	MFC	MIC	MFC	MIC	MFC
2	0.12	0.24	0.24	0.48	0.24	0.48	0.12	0.24
5	0.24	0.48	0.12	0.24	0.06	0.12	0.06	0.12
8	0.12	0.24	0.12	0.24	0.06	0.12	0.03	0.12
10	0.015	0.03	0.015	0.03	0.015	0.015	0.015	0.015
11	0.24	0.48	0.12	0.24	0.12	0.48	0.06	0.12
3a	31.25	31.25	15.62	31.25	15.62	31.25	7.81	15.62
3b	31.25	31.25	15.62	15.62	15.62	31.25	7.81	15.62
3c	31.25	31.25	31.25	31.25	15.62	15.62	15.62	31.25
3d	31.25	62.5	31.25	62.5	15.62	31.25	7.81	15.62
3e	31.25	62.5	15.62	31.25	15.62	31.25	7.81	15.62
3f	1.95	3.9	7.81	15.62	3.9	7.81	1.95	3.9
3g	0.48	1.95	0.48	0.97	0.48	1.95	0.24	0.48
3h	0.24	0.48	0.48	0.97	0.24	0.97	0.12	0.97
6a	15.62	31.25	7.81	15.62	7.81	3.9	3.9	3.9
6b	15.62	31.25	15.62	31.25	7.81	7.81	3.9	3.9
6c	0.97	1.95	1.95	3.9	0.97	1.95	0.97	1.95
6d	3.9	7.81	7.81	15.62	7.81	15.62	3.9	7.81
6e	1.95	3.9	0.97	3.9	0.97	3.9	0.48	0.97
9a	3.9	7.81	1.95	7.81	0.48	0.97	0.48	0.97
9b	0.015	0.03	0.015	0.03	0.015	0.015	0.015	0.015
9c	1.95	3.9	1.95	3.9	0.97	1.95	0.03	0.06
9d	7.81	15.62	3.9	3.9	0.24	0.48	0.12	0.24
9e	7.81	15.62	1.95	3.9	1.95	3.9	1.95	3.9
Fluconazole	15.62	31.25	15.62	31.25	15.62	31.25	7.81	15.62
Ketoconazole	7.81	15.62	7.81	15.62	7.81	15.62	3.9	7.81
Inoculum control	+++	-	+++	-	+++	-	+++	-
Broth control	No growth	-	No growth	-	No growth	-	No growth	-

- indicates the compound has no inhibitory activity; +++ indicates growth in all concentrations. The values obtained for the most active compounds are marked in bold.

The antifungal activity against two strains of *C. albicans*, one *C. krusei* strain and one strain of *C. parapsilosis* showed MIC values ranging from 0.015 µg/mL (compounds **10** and **9b**) to 31.25 µg/mL and MFC values ranging from 0.015 µg/mL (compounds **10** and **9b**) to 62.5 µg/mL. Most of the compounds exhibited similar or much higher MIC and MFC values than those of fluconazole (MIC = 7.81–15.62 µg/mL, MFC = 15.62–31.25 µg/mL) and ketoconazole (MIC = 3.9–7.81 µg/mL, MFC = 7.81–15.62 µg/mL). All the compounds displayed similar or much better antifungal activity than fluconazole ($p \ll 0.05$), and of these, 16 were more active than ketoconazole ($p \ll 0.05$) against *C. krusei* ATCC 6258. In addition, 16 compounds presented better inhibitory activity than fluconazole ($p \ll 0.05$) and 15 displayed better antifungal potential than ketoconazole ($p \ll 0.05$) against the *C. albicans* strains used in the assay. All the compounds except **3c** exhibited similar or much higher MIC and MFC values against *C. parapsilosis* ATCC 22019 than fluconazole ($p \ll 0.05$) and of these, 18 were as active as or even more active than ketoconazole ($p \ll 0.05$).

Overall, the synthesized thiazolin-4-ones presented good to excellent antifungal activities. The MFC/MIC ratio for all tested compounds ranged from 1 to 4, suggesting that the synthesized thiazolin-4-one derivatives could act as fungicidal agents [29]. The most active compounds were the 2-(methylamino)thiazol-4(5H)-one **10** and the 5-(2,4-dichlorobenzylidene)-2-(naphthalen-1-ylamino)thiazol-4(5H)-one **9b**, being over 250 times more active than ketoconazole.

2.3. Lipophilicity Evaluation

The lipophilicity of the synthesized compounds was assessed using PCA based on RP-TLC data. Compounds **3f**, **10** and **11** were not included in this study because their R_f could not be calculated due to the lack of their spots' visibility in UV light.

In Table 3 are presented from the largest to the smallest, the eigenvalues of the covariance matrix, the proportion and also the difference between each eigenvalue and the next smallest one. The obtained results suggested a one component model as the first principal component (P_1) explained 96.609% of the total initial information (variance).

Table 3. The eigenvalues of the five components (*i*-propanol concentration).

Component	Eigenvalue	Difference	Variability (%)	Cumulative (%)
1	4.830	4.671	96.609	96.609
2	0.159	0.153	3.175	99.784
3	0.006	0.002	0.123	99.907
4	0.004	0.003	0.071	99.978
5	0.001	-	0.022	100.000

For a better interpretation and a better graphical representation of the obtained results, we took into consideration the scores of the first two principal components obtained for the tested compounds. The eigenvectors associated with the first two principal components are displayed in Table 4. The results obtained confirmed that the five mobile phases used are strongly related to each other so they could be reduced. This shows that for all the investigated compounds there was a regular increase in R_f values with the increasing concentration of the organic modifier (*i*-propanol).

Table 4. Eigenvectors associated with the first two principal components.

Component	Eigenvector	
	P_1	P_2
1	0.437	0.693
2	0.450	0.361
3	0.452	-0.240
4	0.451	-0.310
5	0.446	-0.485

The results of the regression analysis are compiled in Table 5. The statistics obtained are in accordance with the experimental data, the linear model explaining approximately 95% of the total variance (see R^2 values) in most of the cases.

A good correlation ($R^2 = 0.9507$) was found between the intercept's— R_{M0} (lipophilicity)—and the slope's— b (specific hydrophobic surface area)—values (Table 5). This suggested that the compounds used in this study might form a homologous series. In addition, a very good correlation ($R^2 = 0.901$) was observed between R_{M0} and the scores of the first principal component (P_1) as described by the following equation (Equation (1)):

$$R_{M0} = 1.9864 - 0.3317 \times P_1 \quad (1)$$

Table 5. Regression data, scores of the two first principal components and cLogP values for the studied compounds.

Compound	R_{M0}	b	R^2	P_1	P_2	cLogP
2	0.0414	−1.1059	0.9014	4.335	0.879	0.779
3a	2.0801	−3.6152	0.9413	−0.090	−0.268	3.725
3b	2.2398	−3.6102	0.9716	−1.263	−0.062	4.438
3c	1.7553	−3.314	0.9537	1.049	−0.259	2.755
3d	2.2119	−3.7366	0.9427	−0.549	−0.241	3.454
3e	2.2869	−3.9184	0.9455	−0.349	−0.354	2.965
3g	0.6734	−1.9546	0.9598	3.365	0.453	2.1942
3h	1.1465	−2.6897	0.9407	2.905	0.056	2.345
5	0.9459	−2.2931	0.9239	2.796	0.238	0.851
6a	2.1738	−3.9258	0.9316	0.485	−0.534	4.86
6b	2.4679	−4.0118	0.9544	−1.253	−0.186	5.573
6c	1.7388	−3.3696	0.9487	1.394	−0.304	3.89
6d	2.1996	−3.8092	0.9346	−0.168	−0.359	4.589
6e	2.22	−3.9066	0.9518	0.079	−0.443	4.1
8	1.6225	−3.0931	0.9344	1.125	−0.163	2.025
9a	2.5309	−4.1292	0.9555	−1.227	−0.239	6.034
9b	2.9283	−4.3675	0.9661	−2.876	0.232	6.747
9c	2.7789	−4.1555	0.9654	−2.722	0.228	5.264
9d	3.287	−4.6935	0.8744	−3.746	0.618	5.763
9e	2.3983	−3.319	0.9422	−3.292	0.708	5.274

Based on these findings and as can be seen in data provided in Table 5, the scores of the first principal component can efficiently replace the R_{M0} values in the estimation experiments of these compounds' lipophilicity. It can be observed that R_{M0} and P_1 profiles (Figure 1) are well correlated with the profile of the computed cLogP values, all describing similar patterns. Furthermore, scores plots are very useful as a display tool for observing the relationship between compounds, looking for trends, groupings or outliers, as shown in Figure 2. Therefore, by graphing scores onto the plane described by the first two principal components, P_1 and P_2 , a "congeneric lipophilicity chart" was obtained, where a highly lipophilic compound was characterized by a low value of the P_1 parameter.

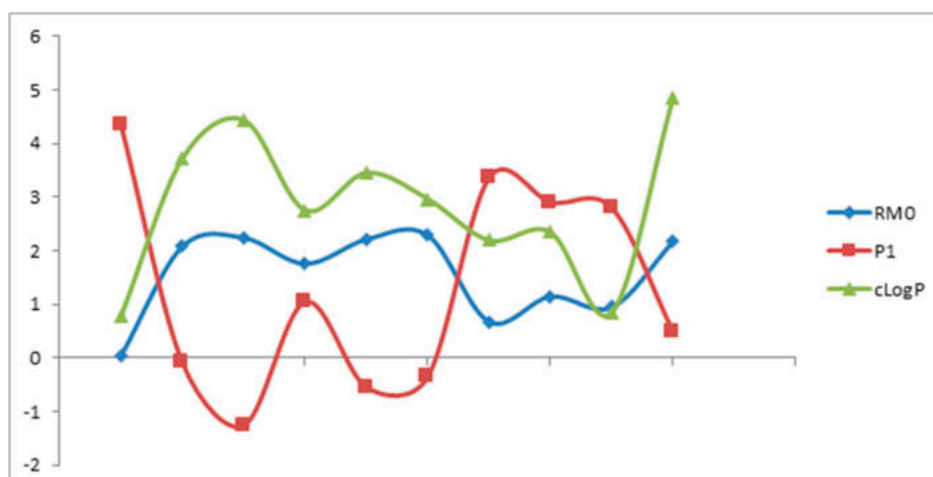


Figure 1. The relationship between experimental lipophilicity indices (R_{M0} , P_1) and computed cLogP values.

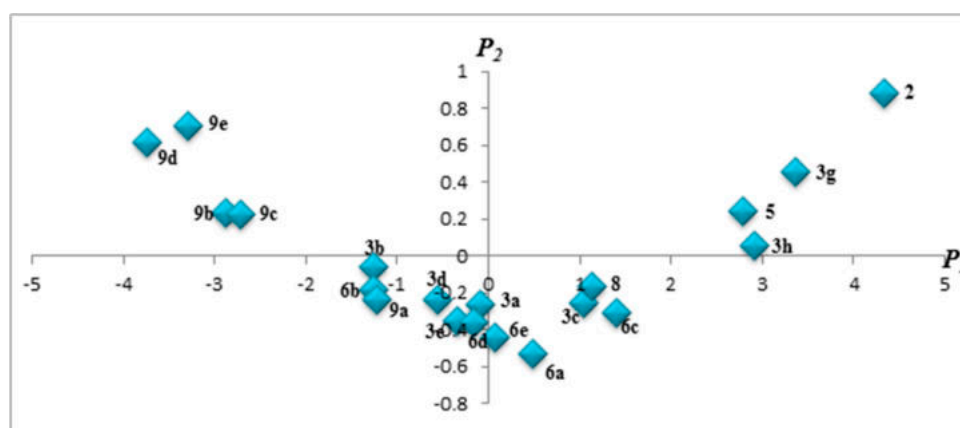


Figure 2. Congeneric lipophilicity chart (2D plot) obtained by plotting the scores corresponding to P_1 and P_2 .

The highest values of the lipophilicity parameters were obtained for compounds **9d**, **9e**, **9b**, **9c**, **3b**, **6b** and **9a** while the lowest values were characteristic for compounds **2**, **3g**, **3h**, **5**, **6c**, **8** and **3c**. By analyzing the relationships between the compounds' chemical structures and P_1 values as a parameter used for estimating lipophilicity it was observed that the lipophilic character of the compounds was significantly influenced by both substituents from position 2 and 5 of the thiazolin-4-one ring. Regarding the 5-unsubstituted thiazolin-4-one derivatives, the substituent in position 2 caused an increase in lipophilicity with the increase of its molecular mass; thereby the most lipophilic 5-unsubstituted thiazolin-4-one derivatives were the 2- α -naphthylamino-thiazolin-4-one **8**, followed by the less lipophilic 2-phenylamino-thiazolin-4-one **5** and then by the least lipophilic 2-allylamino-thiazolin-4-one **2**.

For all the studied compounds it was observed that the substitution in position 5 of the thiazolin-4-one heterocycle led to an increase in lipophilicity.

The lowest lipophilicity was registered for the compounds with an allylamino rest in position 2 of the thiazolin-4-one moiety. By introducing an arylidene or hetarylidene rest in position 5, a lipophilicity augmentation was noticed. The presence of a polar group (OH, OCH₃) on the phenyl rest from position 5 determined a less pronounced lipophilicity raise. Moreover, the introduction of one or two chloride atoms on the aromatic or heteroaromatic ring generally resulted in an increase of the compound's lipophilicity.

2.4. Virtual Screening

All thiazolin-4-one derivatives and the reference compounds (fluconazole (Flu), and ketoconazole (Ket)) were virtually screened for prediction of the ADME-Tox properties and docked against fungal lanosterol 14 α -demethylase, the biological target of the antifungals used as positive control in the previous studies.

2.4.1. ADME-Tox Predictions

The results of VS carried out with FAF-Drugs3 [30] are presented subsequently for lead-likeness, drug-likeness descriptors and penetration of the blood–brain barrier (Table 6). Additional data are presented in Table S1, referring to protein–protein interactions (PPIs), undesirable moieties and substructures involved (UMSs) in toxicity problems, respectively in Table S2 referring to covalent inhibitors and PAINS (Pan Assay Interference Compounds) moieties. In Table S3 are presented the results of VS using the customized filters developed by well-known pharmaceutical companies for drug safety profiling.

Table 6. The results of VS carried out for lead-like and drug-like descriptors.

ID	MW (Da)	LogP	H _{BA}	H _{BD}	tPSA (Å ²)	RtB	RiB	R _s	M _{xS}	C _s	HA	H/C	Crg	T _{Crg}	SC
2	156.21	0.79	3	1	66.76	3	7	1	5	6	4	0.67	1	-1	0
3a	278.76	3.54	3	1	66.76	4	14	2	6	13	5	0.38	0	0	0
3b	313.20	<u>4.17</u>	3	1	66.76	4	14	2	6	13	6	0.46	0	0	0
3c	289.31	2.74	6	1	112.58	5	16	2	6	13	7	0.54	0	0	0
3d	327.42	3.64	4	1	107.89	5	19	3	6	16	6	0.38	0	0	0
3e	346.79	3.18	5	1	96.97	4	20	2	10	16	7	0.44	0	0	0
3f	323.21	3.61	3	1	66.76	4	14	2	6	13	5	0.38	0	0	0
3g	290.34	2.53	5	2	96.22	5	14	2	6	14	6	0.43	0	0	0
3h	260.31	2.56	4	2	86.99	4	14	2	6	13	5	0.38	0	0	0
5	192.24	1.70	3	1	73.08	2	12	2	6	9	4	0.44	1	-1	0
6a	314.79	<u>4.46</u>	3	1	66.76	3	19	3	6	16	5	0.31	0	0	0
6b	349.23	<u>5.09</u>	3	1	66.76	3	19	3	6	16	6	0.38	0	0	0
6c	325.34	3.66	6	1	112.58	4	21	3	6	16	7	0.44	0	0	0
6d	363.46	<u>4.56</u>	4	1	107.89	4	24	4	6	19	6	0.32	0	0	0
6e	382.82	<u>4.09</u>	5	1	96.97	3	25	3	10	19	7	0.37	0	0	0
8	242.30	2.95	3	1	73.08	2	17	2	10	13	4	0.31	1	-1	0
9a	364.85	<u>5.71</u>	3	1	66.76	3	24	3	10	20	5	0.25	0	0	0
9b	399.29	6.34 *	3	1	66.76	3	24	3	10	20	6	0.30	0	0	0
9c	375.40	<u>4.91</u>	6	1	112.58	4	26	3	10	20	7	0.35	0	0	0
9d	413.51	<u>5.81</u>	4	1	107.89	4	29	4	10	23	6	0.26	0	0	0
9e	432.88	<u>5.34</u>	5	1	96.97	3	30	3	10	23	7	0.30	0	0	0
10	<u>130.17</u>	0.15	3	1	66.76	1	6	1	5	4	4	1.00	1	-1	0
11	177.22	1.98	2	0	54.73	1	12	2	6	9	3	0.33	0	0	0
Flu	306.27	0.52	7	1	81.65	5	16	3	6	13	9	0.69	0	0	1
Ket	<u>531.43</u>	3.26	8	0	69.06	7	30	5	6	26	10	0.38	0	0	2
DLS _{tv}	100–600	-3–6	≤12	≤5	≤180	≤11	≤30	≤6	≤18	3–35	1–15	0.1–1.1	≤3	-2–2	-
LLS _{tv}	150–400	-3–4	≤7	≤4	≤160	≤9	≤30	≤4	≤18	3–35	1–15	0.1–1.1	≤3	-2–2	≤2
CNS _{tv}	135–582	-0.2–6.1	≤5	≤3	3–118	-	-	-	-	-	-	-	-	-	-

DLS_{tv}: Threshold values of the *Drug-Like Soft* filter; LLS_{tv}: Threshold values of the *Lead-Like Soft* filter; CNS_{tv}: Threshold values of the *CNS* filter; Underlined values: Overpass the thresholds for lead-likeness filters; * **bold, italic values**: Overpass the thresholds for drug-likeness filters; Red values: Overpass the thresholds for CNS activity filters (penetration of BBB).

The results of VS, carried out with FAF-Drugs3, are summarized in Table 6. These were carried out for the following lead-likeness and drug-likeness descriptors: molecular weight (MW, expressed in Daltons), the logarithm of the partition coefficient between *n*-octanol and water (LogP) characterizing lipophilicity, hydrogen bond donors (H_{BD}, sum of all –OHs and –NHs, according to Lipinski’s rule of five (RO5) definition [31]), hydrogen bond acceptors (H_{BA}, sum of all oxygen and nitrogen atoms, according to RO5 definition [31]), topological Polar Surface Area (tPSA, summation of tabulated surface contributions of polar fragments—topologically calculated), number of rotatable bonds (RtB, number of any single non-ring bond, bounded to non-terminal heavy atom—amide C–N bonds are not considered because of their high rotational energy barrier [32]), number of rigid bonds (RiB, number of non-flexible

bonds—e.g., double and triple bonds, bonds involved in ring systems and additionally amide bonds), number of the smallest set of smallest rings (R_s , the smallest ring building blocks necessary to form other ring systems), maximum size of the biggest ring system (M_xS , number of atoms involved in the biggest ring system), number of carbon atoms (C_s), number of heteroatoms (HA , number of non-carbon atoms—hydrogen atoms are not included), the ratio between the number of non-carbon atoms and the number of carbon atoms (H/C), number of charged groups (C_{rg}), formal total charge of the compound ($T_{C_{rg}}$) and stereo centers (SC —computed only for leads, the presence of stereo centers and the number of chiral centers, are descriptors of complexity). The activity at the central nervous system level (CNS), respectively the penetration of blood–brain barrier (BBB) were evaluated only based on the values predicted for MW, LogP, H_{BA} , H_{BD} and tPSA, as specified in the literature [33].

As it can be observed in Table 6, more than half of the synthesized thiazolin-4-one derivatives (**2**, **3a**, **3c–h**, **5**, **6c**, **8** and **11**) were qualified as potential leads. Only one thiazolin-4-one derivative (**10**) cannot be qualified as a good lead due its way too low MW, meanwhile the rest of rejected thiazolin-4-one derivatives exhibited higher values than upper thresholds for LogP (**3b**, **6a**, **6b**, **6d**, **6e**, and **9a–e**). Except **9b**, all thiazolin-4-one derivatives were accepted as drug-like compounds. In addition, the predictions made for **9b** and four of the drug-like thiazolin-4-one derivatives (**3c**, **6c**, **9c** and **10**) indicated their inability to penetrate the BBB. Therefore, for those compounds, a CNS level inactivity is forecasted. Additionally, from Table S1 it can be observed that all thiazolin-4-one derivatives comply with Veber's rule [32] and Egan's rule [34] regarding the molecular properties that influence oral bioavailability. In addition, all thiazolin-4-one derivatives fit into RO5 for oral bioavailability [31], even though the computations for five compounds (**6b**, **9a**, **9b**, **9d** and **9e**) slightly overpassed the threshold values for LogP considered by Christopher A. Lipinski and coworkers [31], this being only one violation of the rule, while the predictions for their oral bioavailability are considered good.

Table S1 summarizes the results of VS carried out with FAF-Drugs3 for detection of non-peptidic inhibitors of PPI and UMSs involved in toxicity problems. It can be observed that only eight thiazolin-4-one derivatives (**6c–e**, and **9a–e**) are PPI friendly, same as **Ket**, the rest of compounds requiring further structural optimization prior to their use as possible “hits” in the drug development process. Moreover, those PPI friendly derivatives and three compounds which require further structural optimization (**2**, **6a–b**) should be refined in order to decrease even more their toxicity predictions generated by the presence of Michael acceptors (double bonds)—a “warhead” moiety present in the structure of all those compounds, together with other low risk UMSs: terminal vinyl from the structure of derivative **2**, thiazole found in **6d** and **9d**, respectively nitro and nitrobenzene present in **6c** and **9c**. In the case of eight 2-(allyl-amino)-5-arylidene-thiazolin-4-ones (**3a–h**) the prediction is bad, the compounds being rejected by the imposed filter, due the presence of high risk Michael acceptors in their structure combined with some low risk moieties: terminal vinyl (detected also in all of those derivatives), nitro and nitrobenzene (found in **3c**), thiazole (found in **3d**), and phenol (found in the structure of **3g** and **3h**). Four of the not so PPI friendly derivatives were found free of UMSs: **5**, **8**, **10** and **11** (all are 5-unsubstituted thiazolin-4-one derivatives).

Table S2 summarizes the results of VS carried out with FAF-Drugs3, in order to detect the problematic groups involved in covalent binding with biological macromolecules and structural alerts for PAINS, compounds that appear as frequent hitters in HTS. The results presented in Table S2 indicated that the same UMSs-free 5-unsubstituted thiazolin-4-one derivatives, as shown in Table S1 (**5**, **8**, **10** and **11**), do not contain any covalent inhibitor group—the reference compounds are all free of this kind of substructures. The rest of the thiazolin-4-one derivatives have Michael acceptors (double bonds) in their structure, functional groups responsible for both electrophilic protein-reactive false positives in HTS [35,36] and covalent binding with peptides. Moreover, with the exception of derivative **2**, the rest of thiazolin-4-one derivatives contain a second covalent inhibitor: α , β -unsaturated carbonyl, substructure with possible undesirable effects [37]. According to two PAINS filters (A and C), all 5-unsubstituted thiazolin-4-one derivatives are free of “promiscuous

substructures”, meanwhile the filter B detected a low-risk structural alert at compounds **3a–h**, **6a–e** and **9a–e**.

Table S3 shows the results of VS using the customized filters for drug safety profiling: the GSK 4/400 rule, the Pfizer 3/75 rule, phospholipidosis induction and the MedChem rules (for identifying potentially reactive or promiscuous compounds) [35].

The integrated analysis of various rules taken into consideration for drug safety profiling (Table S3) indicates possible safety issues at the administration of **9d–e**, according to GSK 4/400 rule (this rule is based on lowering the MW and LogP area of physicochemical property space to obtain improved ADME-Tox parameters), the rest of the screened compounds having a good prediction. On the other hand, according to the Pfizer 3/75 rule, compounds **3a–b**, **3f**, **6a–b** are likely to cause toxicity and experimental promiscuity, because they have LogP > 3 and tPSA < 75 Å² (as shown in Table 6).

None of the thiazolin-4-one derivatives were classified as phospholipidosis inducers, meanwhile **Ket** is considered as being one.

Compound **11** successfully overpassed the thresholds of MedChem rules; meanwhile the rest of thiazolin-4-one derivatives and the reference compound (**Ket**) may exhibit some safety issues due to the presence of various flagged substructures. A flagged interference, the amino_naphthalene rule, is related to possible lack of druggability attendant on excessive lipophilicity and flexibility due to the number of successive methylenes (C4 through C7) detected in compounds **8** and **9a–e**. Moreover, some problematic substructures were also detected in one of the reference compounds (**Ket**), but, according to the MedChem rules, 19 drugs out of 123 best-selling drugs failed the rules as an outright rejection, and another 18 failed on demerits.

2.4.2. Docking against the Fungal Lanosterol-14- α -demethylase

Lanosterol 14- α demethylase is a cytochrome P450 enzyme that plays a crucial role in sterol biosynthesis in eukaryotes because it catalyzes the C14-demethylation of lanosterol which is critical for ergosterol biosynthesis, a fundamental component of fungal membranes. The azole antifungal drugs selectively inhibit the fungal lanosterol 14 α -demethylase, their mechanism of action involving the nucleophilic nitrogen of the azole heterocycle coordinating as the sixth ligand of the heme iron in the ferric state and the azole drug side chains interacting with the polypeptide structure [13].

All investigated molecules (the thiazolin-4-one derivatives and the reference compounds) were virtually subjected to docking, against the designated fungal target (lanosterol 14- α demethylase) in order to investigate the potential binding mode and binding affinity of these inhibitors. Docked ligand conformations (poses) were analyzed in terms of binding affinity (BA, expressed in kcal/mol) and hydrogen bonding between the best poses and their target protein. Detailed analyses of the ligand–receptor interactions were carried out, and final possible orientations of the ligands and receptors were saved.

All thiazolin-4-one derivatives and the antifungal reference compounds (**Flu** and **Ket**) were docked against the generated homology model for lanosterol-14 α -demethylase and the results are presented in Table 7 and Figure 3 and Figure S1.

Table 7. Binding affinity of the tested compounds (best poses) towards lanosterol-14 α -demethylase.

ID	BA (kcal/mol)	H-Bonds: Best Pose Interaction(s) with Lanosterol-14 α -demethylase	
		AA Residue(s) of Target	Interacting Atom(s) of the Ligand (#atom)
2	−5.4	Asn440	Oxygen (#6)
3a	−8.1	Asn440	Nitrogen (#2)
3b	−7.9	N/A	N/A(N/A)
3c	−7.9	Asn440	Nitrogen (#2)
3d	−8.4	N/A	N/A(N/A)
3e	−8.4	Met508	Nitrogen (#2)
3f	−8.0	Asn440	Nitrogen (#2)
3g	−7.6	Asn440	Nitrogen (#2)
3h	−7.6	Asn440	Nitrogen (#2)

Table 7. Cont.

ID	BA (kcal/mol)	H-Bonds: Best Pose Interaction(s) with Lanosterol-14 α -demethylase	
		AA Residue(s) of Target	Interacting Atom(s) of the Ligand (#atom)
5	-7.4	Tyr460 Ser436	Hydrogen (#16) Oxygen (#6)
6a	-9.5	Ile304	Hydrogen (#22)
6b	-8.8	N/A	N/A(N/A)
6c	-8.8	N/A	N/A(N/A)
6d	-10.1	N/A	N/A(N/A)
6e	-10.3	N/A	N/A(N/A)
8	-9.4	Asn440	Oxygen (#6)
9a	-10.0	N/A	N/A(N/A)
9b	-10.3	His468	Nitrogen (#2)
9c	-10.2	N/A	N/A(N/A)
9d	-11.2	N/A	N/A(N/A)
9e	-11.4	N/A	N/A(N/A)
10	-4.6	Asn440	Oxygen (#6)
11	-6.9	N/A	N/A(N/A)
Flu	-7.6	Thr311	Nitrogen (#8)
Ket	-10.0	N/A	N/A(N/A)

N/A: Not available/assigned; #atom: Atoms numbering; **Bold values**: The best binding affinities (similar to or higher than those of the reference compounds).

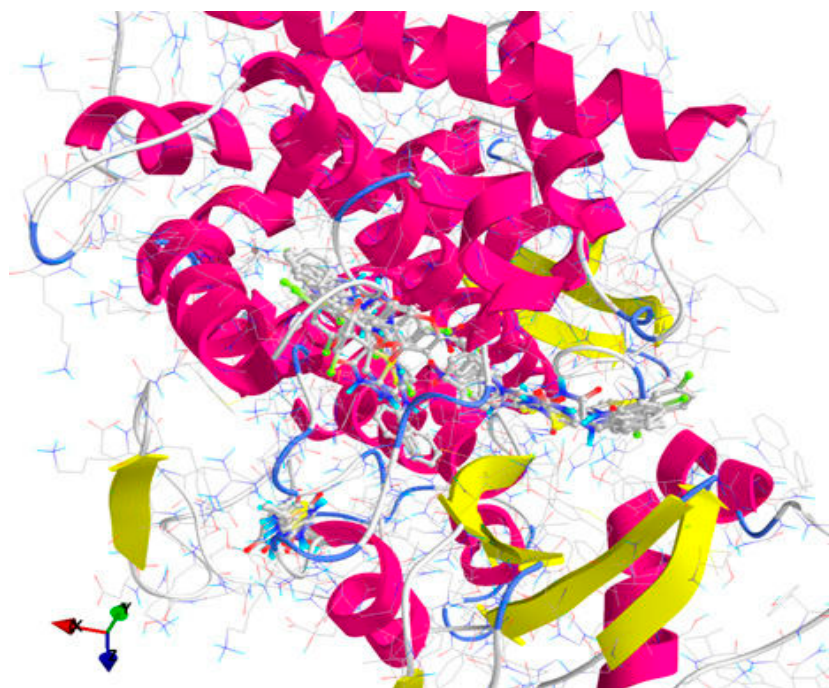


Figure 3. General view of docking poses of the screened compounds in the active site of lanosterol-14 α -demethylase (target is depicted as thin sticks with secondary structure drawn as cartoon backbone, meanwhile ligands are figured as sticks): there can be described three binding patterns—Group A (left): 2, 3a, 3c, 3f–h, 5, 8, 10 and 11; Group B (right): 3b, 3d–e, 6d, 9a–9c and Ket; and Group C (center): 6a–c, 6e and Flu.

The results of docking against lanosterol-14 α -demethylase (Table 7) indicated that most of the screened derivatives and Flu make H-bonds especially with amino acids residues with polar uncharged side chains (asparagine, serine and threonine), meanwhile 10 derivatives (3b, 3d, 6b–e and 9c–e) and Ket do not interact with their target by hydrogen bonding. Three derivatives (3e, 5 and 6a) bind to

amino acids residues with hydrophobic side chains and only one compound (**9b**) binds to histidine, an amino acid residue with an electropositively charged side chain. Moreover, compound **5** binds both to amino acids residues with polar uncharged side chains (Ser436) and hydrophobic side chains (Tyr460). Some of the tested derivatives (**2**, **10** and **11**) are weaker inhibitors than **Flu** (the weakest inhibitor from the two reference compounds), meanwhile compounds **6d**, **6e** and **9a–e** are stronger inhibitors than **Ket**.

3. Materials and Methods

3.1. Chemistry

All chemicals (reagent grade) were obtained from commercial sources and were used as supplied, without further purification.

Melting points were determined with an MPM-H1 Electrothermal melting point meter using the open glass capillary method and are uncorrected. The reaction progress and purity of the synthesized compounds were monitored by analytical thin layer chromatography (TLC) using Merck precoated Silica Gel 60F₂₅₄ sheets (Darmstadt, Germany), heptane–ethyl-acetate 3:7 elution system and UV light for visualization. Elemental analysis was registered with a Vario El CHNS instrument (Hanau, Germany) and the results obtained for all synthesized compounds were in agreement with the calculated values within $\pm 0.4\%$ range. MS analyses were performed at 70 eV with an Agilent gas chromatograph 6890 (Darmstadt, Germany) equipped with an apolar Macherey Nagel Permabond SE 52 capillary column (Dueren, Germany) and with an LC-MS Shimadzu Mass Spectrometer (Shimadzu Corporation, Torrance, CA, USA). IR spectra were recorded using the ATR technique (Attenuated Total Reflectance) on a JASCO FT-IR—4100 spectrometer (Cremella, Italy). Nuclear magnetic resonance (¹H NMR) spectra were recorded on a Bruker Avance NMR spectrometer (Karlsruhe, Germany) operating at 400 and 500 MHz, at room temperature, using tetramethylsilane (TMS) as internal standard. Chemical shifts were reported in ppm (δ). The samples were prepared by dissolving the compounds in DMSO-*d*₆ ($\delta_{\text{H}} = 2.51$ ppm) as solvent and the spectra were recorded using a single excitation pulse of 12 μs (¹H NMR). Spin multiplets are given as *s* (singlet), *d* (doublet), *t* (triplet) and *m* (multiplet). ¹³C NMR spectra were recorded on Bruker Avance NMR spectrometer (Karlsruhe, Germany) operating at 125 MHz in DMSO-*d*₆, using a waltz-16 decoupling scheme. All spectral analyses data were in accordance with the assigned structures.

3.1.1. General Procedure for the Synthesis of 2-Substituted Thiazol-4(5*H*)-ones **2**, **5**, **8**, **10** and **11**

To a solution of 20 mmol of the appropriate thiourea derivative or phenylthioamide in absolute ethanol (15 mL) were added 40 mmol (3.28 g) of anhydrous sodium acetate and 20 mmol ethyl α -bromoacetate or α -monochloroacetic acid. The obtained reaction mixture was refluxed for 6–8 h and, after cooling, it was poured into ice-cold water. Subsequently, the resulted precipitate was isolated by filtration and washed on filter with a mixture of ethanol and distilled water. Afterwards, the crude product was purified by recrystallization from absolute ethanol in order to obtain the pure 2-substituted thiazol-4(5*H*)-one.

Compounds **2**, **5**, **8**, **10** and **11** were previously reported in the literature [23–27] and were synthesized following the procedure described above.

2-(allylamino)thiazol-4(5*H*)-one **2**: yield 60%, m.p. 90–91 °C (lit [23], m.p. 89–90 °C).

2-(phenylamino)thiazol-4(5*H*)-one **5**: yield 75%, m.p. 179 °C (lit [24], m.p. 178–179 °C).

2-(naphthalen-1-ylamino)thiazol-4(5*H*)-one **8**: yield 89%, m.p. 213 °C (lit [25], m.p. 213–214 °C).

2-(methylamino)thiazol-4(5*H*)-one **10**: yield 78%, m.p. 196–197 °C (lit [26], m.p. 196–199 °C).

2-phenylthiazol-4(5*H*)-one **11**: yield 59%, m.p. 108–110 °C (lit [27], m.p. 107 °C).

3.1.2. General Procedure for the Synthesis of 2-(Allyl/aryl-amino)-5-arylidene-thiazolin-4-ones **3a-h**, **6a-e** and **9a-e**

2 mmol of the appropriate 2-(allyl/aryl-amino)-thiazolin-4-one were suspended in 8 mL of absolute ethanol and then, to the obtained suspension were added 8 mmol (0.656 g) of anhydrous sodium acetate and 2 mmol of the corresponding aromatic aldehyde. The reaction mixture was refluxed for 6 h, and, after the reaction was completed, it was dropwise poured into ice-cold water. The resulting precipitate was filtered off and washed on the filter with distilled water and ethanol. The obtained compound was recrystallized from an appropriate solvent (absolute ethanol or absolute methanol).

2-(Allylamino)-5-(3-chlorobenzylidene)thiazol-4(5H)-one (3a). Yield 87% (0.485 g); light yellow powder; m.p. 198 °C; IR (ATR, ν (cm⁻¹)): 3437 (N-H_{amine}), 1726 (C=O_{TZ}), 1155 (C-Cl); ¹H NMR (500 MHz, DMSO-*d*₆, δ /ppm): 7.74 (t, 1H, NH), 7.50 (s, 1H, -CH=), 7.36–7.50 (m, 4H, Ar-H), 6.03 (m, 1H, CH=), 5.23 (d, 2H, =CH₂), 3.98 (m, 2H, CH₂); ¹³C NMR (125 MHz, DMSO-*d*₆, δ /ppm): 168.12 (C=O), 157.23 (C), 139.54 (CH), 136.75 (C), 135.62 (C), 133.81 (C), 131.05 (CH), 130.55 (CH), 129.11 (CH), 128.33 (CH), 126.27 (CH), 118.44 (CH₂), 50.15 (CH₂); MS (EI, 70 eV) *m/z* (%): 279 (M + 1, 100), 280 (M + 2, 10.6), 281 (M + 3, 36.8), 252 (29.0), 226 (6.7), 209 (22.6), 195 (100), 176 (19.0); Anal. Calcd. for C₁₃H₁₁ClN₂OS (278.76): C, 56.01; H, 3.98; N, 10.05; S, 11.50; Found: C, 56.32; H, 3.79; N, 10.12; S, 11.52.

2-(Allylamino)-5-(2,4-dichlorobenzylidene)thiazol-4(5H)-one (3b). Yield 65% (0.407 g); white powder; m.p. 238 °C; IR (ATR, ν (cm⁻¹)): 3438 (N-H_{amine}), 1714 (C=O_{TZ}), 1158 (C-Cl), 1093 (C-Cl); ¹H NMR (500 MHz, DMSO-*d*₆, δ /ppm): 7.93 (t, 1H, NH), 7.56 (s, 1H, -CH=), 7.10–7.12 (m, 3H, Ar-H), 6.31 (m, 1H, CH=), 5.34 (d, 2H, =CH₂), 3.66 (m, 2H, CH₂); ¹³C NMR (125 MHz, DMSO-*d*₆, δ /ppm): 166.20 (C=O), 158.42 (C), 138.94 (CH), 137.77 (C), 135.31 (C), 133.15 (C), 131.56 (C), 130.99 (CH), 129.78 (CH), 126.63 (CH), 124.88 (CH), 117.08 (CH₂), 49.94 (CH₂); MS (EI, 70 eV) *m/z* (%): 313 (M + 1, 100), 314 (M + 2, 13.3), 315 (M + 3, 95.5), 316 (M + 4, 17.3), 317 (M + 5, 19.2), 277 (100), 256 (7.2), 208 (14.1), 185 (5.9), 149 (5.1); Anal. Calcd. for C₁₃H₁₀Cl₂N₂OS (313.20): C, 49.85; H, 3.22; N, 8.94; S, 10.24; Found: C, 49.93; H, 3.35; N, 8.98; S, 10.36.

2-(Allylamino)-5-(4-nitrobenzylidene)thiazol-4(5H)-one (3c). Yield 89% (0.514 g); pale yellow powder; m.p. 265 °C; IR (ATR, ν (cm⁻¹)): 3431 (N-H_{amine}), 1705 (C=O_{TZ}), 1523 (NO₂ asymmetric), 1326 (NO₂ symmetric); ¹H NMR (500 MHz, DMSO-*d*₆, δ /ppm): 7.98 (t, 1H, NH), 7.62 (s, 1H, -CH=), 7.13–7.84 (m, 4H, Ar-H), 5.98 (m, 1H, CH=), 5.25 (d, 2H, =CH₂), 3.84 (m, 2H, CH₂); ¹³C NMR (125 MHz, DMSO-*d*₆, δ /ppm): 175.30 (C=O), 161.57 (C), 148.11 (C), 142.59 (C), 138.72 (CH), 134.09 (C), 131.25 (2CH), 129.44 (CH), 125.22 (2CH), 117.45 (CH₂), 50.11 (CH₂); MS (EI, 70 eV) *m/z* (%): 290 (M + 1, 100), 291 (M + 2, 17.2), 292 (M + 3, 6.3), 248 (97.0), 245 (100), 203 (7.3), 174 (10.2), 141 (17.9); Anal. Calcd. for C₁₃H₁₁N₃O₃S (289.31): C, 53.97; H, 3.83; N, 14.52; S, 11.08; Found: C, 53.88; H, 3.97; N, 14.67; S, 11.23.

2-(Allylamino)-5-((2-phenylthiazol-4-yl)methylene)thiazol-4(5H)-one (3d). Yield 80% (0.523 g); white powder; m.p. 339 °C; IR (ATR, ν (cm⁻¹)): 3435 (N-H_{amine}), 1728 (C=O_{TZ}); ¹H NMR (500 MHz, DMSO-*d*₆, δ /ppm): 8.02 (s, 1H, NH), 8.00 (s, 1H, C5-thiazole-H), 7.70 (s, 1H, -CH=), 7.42–7.71 (m, 5H, Ar-H), 6.05 (m, 1H, CH=), 5.32 (d, 2H, =CH₂), 4.15 (m, 2H, CH₂); ¹³C NMR (125 MHz, DMSO-*d*₆, δ /ppm): 172.20 (C=O), 169.85 (C), 158.33 (C), 150.08 (C), 140.88 (CH), 138.63 (C), 134.66 (CH), 133.19 (C), 130.97 (2CH), 129.14 (2CH), 128.93 (CH), 127.51 (CH), 117.68 (CH₂), 50.42 (CH₂); MS (EI, 70 eV) *m/z* (%): 328 (M + 1, 100), 329 (M + 2, 11.7), 330 (M + 3, 11.5), 301 (5.1), 287 (28.7), 261 (22.5), 246 (39.6), 218 (100), 155 (14.1); Anal. Calcd. for C₁₆H₁₃N₃OS₂ (327.42): C, 58.69; H, 4.00; N, 12.83; S, 19.59; Found: C, 58.82; H, 4.21; N, 12.99; S, 19.68.

2-(Allylamino)-5-((6-chloro-4-oxo-4H-chromen-3-yl)methylene)thiazol-4(5H)-one (3e). Yield 91% (0.631 g); pale pink powder; m.p. 299–301 °C; IR (ATR, ν (cm⁻¹)): 3432 (N-H_{amine}), 1684 (C=O_{TZ}), 1647 (C=O_{chromone}), 1273 (C-O_{chromone}), 1167 (C-Cl), 1045 (C-O_{chromone}); ¹H NMR (500 MHz, DMSO-*d*₆, δ /ppm): 7.93 (t, 1H, NH), 7.74 (s, 1H, -CH=), 7.11–8.74 (m, 4H, Ar-H), 6.27 (m, 1H, CH=), 5.27 (d, 2H, =CH₂), 3.73 (m, 2H, CH₂); ¹³C NMR (125 MHz, DMSO-*d*₆, δ /ppm): 178.55 (C=O), 167.64 (C=O), 159.21 (C), 155.82 (C), 153.03 (CH), 149.43 (CH), 136.97 (C), 136.16 (CH), 134.68 (CH), 130.74 (CH), 128.42 (C),

125.55 (C), 119.25 (C), 119.01 (CH), 118.14 (CH₂), 51.26 (CH₂); MS (EI, 70 eV) *m/z* (%): 347 (M + 1, 100), 348 (M + 2, 19.9), 349 (M + 3, 33.8), 330 (9.8), 305 (36.5), 290 (14.8), 277 (20.3), 265 (74.2), 237 (100), 213 (1.9), 205 (1.8), 155 (26.7); Anal. Calcd. for C₁₆H₁₁ClN₂O₃S (346.79): C, 55.41; H, 3.20; N, 8.08; S, 9.25; Found: C, 55.65; H, 3.33; N, 8.31; S, 9.34.

2-(Allylamino)-5-(3-bromobenzylidene)thiazol-4(5H)-one (**3f**). Yield 75% (0.485 g); white powder; m.p. 330 °C; IR (ATR, ν (cm⁻¹)): 3429 (N-H_{amine}), 1689 (C=O_{TZ}), 1035 (C-Br); ¹H NMR (500 MHz, DMSO-*d*₆, δ /ppm): 7.96 (t, 1H, NH), 7.58 (s, 1H, -CH=), 7.44–7.86 (m, 4H, Ar-H), 6.30 (m, 1H, CH=), 5.29 (d, 2H, =CH₂), 3.86 (m, 2H, CH₂); ¹³C NMR (125 MHz, DMSO-*d*₆, δ /ppm): 168.74 (C=O), 158.62 (C), 138.42 (CH), 136.33 (C), 135.10 (C), 133.96 (C), 131.14 (CH), 130.27 (CH), 129.19 (CH), 128.45 (CH), 126.47 (CH), 118.21 (CH₂), 51.17 (CH₂); MS (EI, 70 eV) *m/z* (%): 323 (M + 1, 100), 324 (M + 2, 52.1), 325 (M + 3, 50.1), 306 (9.0), 279 (17.6), 259 (13.6), 240 (20.8), 235 (11.0), 177 (17.7), 161 (22.6), 145 (9.3), 121 (12.7); Anal. Calcd. for C₁₃H₁₁BrN₂OS (323.21): C, 48.31; H, 3.43; N, 8.67; S, 9.92; Found: C, 48.45; H, 3.55; N, 8.54; S, 9.85.

2-(Allylamino)-5-(4-hydroxy-3-methoxybenzylidene)thiazol-4(5H)-one (**3g**). Yield 77% (0.447 g); pale yellow powder; m.p. 240 °C; IR (ATR, ν (cm⁻¹)): 3435 (N-H_{amine}), 3285 (O-H_{phenol}), 1705 (C=O_{TZ}), 1336 (C-O_{phenol}), 1046 (C-O_{methoxy}), 1019 (C-O_{methoxy}); ¹H NMR (500 MHz, DMSO-*d*₆, δ /ppm): 9.31 (s, 1H, OH), 8.06 (t, 1H, NH), 7.72 (s, 1H, -CH=), 7.13–7.74 (m, 3H, Ar-H), 6.31 (m, 1H, CH=), 5.34 (d, 2H, =CH₂), 4.01 (m, 2H, CH₂), 3.83 (s, 3H, -OCH₃); ¹³C NMR (125 MHz, DMSO-*d*₆, δ /ppm): 187.08 (C=O), 174.77 (C), 159.42 (C), 152.06 (CH), 148.20 (C), 134.12 (CH), 132.66 (C), 129.01 (C), 122.81 (CH), 117.30 (CH₂), 116.57 (CH), 111.96 (CH), 55.13 (CH₃), 50.56 (CH₂); MS (EI, 70 eV) *m/z* (%): 291 (M + 1, 100), 292 (M + 2, 12.8), 293 (M + 3, 13.2), 265 (5.1), 238 (3.1), 180 (6.6), 138 (10.6); Anal. Calcd. for C₁₄H₁₄N₂O₃S (290.34): C, 57.92; H, 4.86; N, 9.65; S, 11.04; Found: C, 57.87; H, 4.83; N, 9.61; S, 11.17.

2-(Allylamino)-5-(4-hydroxybenzylidene)thiazol-4(5H)-one (**3h**). Yield 59% (0.307 g); pale yellow powder; m.p. 338 °C; IR (ATR, ν (cm⁻¹)): 3428 (N-H_{amine}), 3289 (O-H_{phenol}), 1695 (C=O_{TZ}), 1331 (C-O_{phenol}); ¹H NMR (500 MHz, DMSO-*d*₆, δ /ppm): 9.35 (s, 1H, OH), 7.88 (t, 1H, NH), 7.67 (s, 1H, -CH=), 7.35–7.71 (m, 4H, Ar-H), 6.29 (m, 1H, CH=), 5.31 (d, 2H, =CH₂), 3.85 (m, 2H, CH₂); ¹³C NMR (125 MHz, DMSO-*d*₆, δ /ppm): 184.14 (C=O), 162.56 (C), 159.13 (C), 152.47 (CH), 134.75 (CH), 132.86 (C), 129.91 (2CH), 127.50 (C), 117.49 (CH₂), 116.04 (2CH), 50.32 (CH₂); MS (EI, 70 eV) *m/z* (%): 261 (M + 1, 100), 262 (M + 2, 8.7), 263 (M + 3, 3.3), 209 (1.9), 183 (1.4), 158 (1.3), 138 (5.0); Anal. Calcd. for C₁₃H₁₂N₂O₂S (260.31): C, 59.98; H, 4.65; N, 10.76; S, 12.32; Found: C, 59.79; H, 4.76; N, 10.93; S, 12.36.

5-(3-Chlorobenzylidene)-2-(phenylamino)thiazol-4(5H)-one (**6a**). Yield 74% (0.466 g); light brown powder; m.p. 278–280 °C; IR (ATR, ν (cm⁻¹)): 3427 (N-H_{amine}), 1721 (C=O_{TZ}), 1157 (C-Cl); ¹H NMR (500 MHz, DMSO-*d*₆, δ /ppm): 11.95 (s, 1H, NH), 7.57 (s, 1H, -CH=), 7.04–7.84 (m, 9H, Ar-H); ¹³C NMR (125 MHz, DMSO-*d*₆, δ /ppm): 187.52 (C=O), 176.43 (C), 142.15 (CH), 139.42 (C), 136.01 (C), 134.28 (C), 132.98 (C), 130.21 (CH), 129.68 (2CH), 128.77 (CH), 126.79 (CH), 126.30 (CH), 122.84 (CH), 120.71 (2CH); MS (EI, 70 eV) *m/z* (%): 315 (M + 1, 100), 316 (M + 2, 20.0), 317 (M + 3, 53.4), 286 (1.7), 196 (1.0), 169 (0.9), 118 (0.9); Anal. Calcd. for C₁₆H₁₁ClN₂OS (314.79): C, 61.05; H, 3.52; N, 8.90; S, 10.19; Found: C, 61.09; H, 3.65; N, 8.94; S, 10.27.

5-(2,4-Dichlorobenzylidene)-2-(phenylamino)thiazol-4(5H)-one (**6b**). Yield 61% (0.426 g); light brown powder; m.p. 204–206 °C; IR (ATR, ν (cm⁻¹)): 3434 (N-H_{amine}), 1717 (C=O_{TZ}), 1156 (C-Cl), 1096 (C-Cl); ¹H NMR (500 MHz, DMSO-*d*₆, δ /ppm): 11.97 (s, 1H, NH), 7.61 (s, 1H, -CH=), 7.06–7.80 (m, 8H, Ar-H); ¹³C NMR (125 MHz, DMSO-*d*₆, δ /ppm): 188.02 (C=O), 177.67 (C), 140.30 (CH), 139.15 (C), 135.45 (C), 133.36 (C), 131.63 (C), 130.33 (CH), 129.52 (2CH), 128.82 (CH), 127.94 (CH), 125.66 (C), 123.74 (CH), 120.78 (2CH); MS (EI, 70 eV) *m/z* (%): 349 (M + 1, 100), 350 (M + 2, 13.2), 351 (M + 3, 87.6), 352 (15.8), 353 (27.0), 315 (12.0), 313 (100), 138 (0.9); Anal. Calcd. for C₁₆H₁₀Cl₂N₂OS (349.23): C, 55.03; H, 2.89; N, 8.02; S, 9.18; Found: C, 55.12; H, 2.91; N, 8.15; S, 9.34.

5-(4-Nitrobenzylidene)-2-(phenylamino)thiazol-4(5H)-one (**6c**). Yield 87% (0.566 g); yellow powder; m.p. 347 °C; IR (ATR, ν (cm⁻¹)): 3436 (N-H_{amine}), 1710 (C=O_{TZ}), 1519 (NO₂ asymmetric), 1330 (NO₂ symmetric); ¹H NMR (500 MHz, DMSO-*d*₆, δ /ppm): 11.99 (s, 1H, NH), 7.69 (s, 1H, -CH=), 7.23–7.91

(m, 9H, Ar-H); ^{13}C NMR (125 MHz, DMSO- d_6 , δ /ppm): 187.65 (C=O), 176.13 (C), 148.62 (C), 143.23 (CH), 141.85 (C), 139.99 (C), 132.44 (C), 130.09 (2CH), 129.27 (2CH), 123.95 (2CH), 122.11 (CH), 120.74 (2CH); MS (EI, 70 eV) m/z (%): 326 (M + 1, 100), 327 (M + 2, 14.2), 328 (M + 3, 6.0), 313 (8.8), 281 (100), 280 (93.0), 180 (13.4), 119 (40.9); Anal. Calcd. for $\text{C}_{16}\text{H}_{11}\text{N}_3\text{O}_3\text{S}$ (325.34): C, 59.07; H, 3.41; N, 12.92; S, 9.86; Found: C, 59.19; H, 3.53; N, 12.98; S, 9.89.

2-(Phenylamino)-5-((2-phenylthiazol-4-yl)methylene)thiazol-4(5H)-one (**6d**). Yield 89% (0.647 g); light brown powder; m.p. 287–289 °C; IR (ATR, ν (cm^{-1})): 3430 (N-H_{amine}), 1719 (C=O_{TZ}); ^1H NMR (500 MHz, DMSO- d_6 , δ /ppm): 11.92 (s, 1H, NH), 8.11 (s, 1H, C5-thiazole-H), 7.73 (s, 1H, -CH=), 7.34–8.01 (m, 10H, Ar-H); ^{13}C NMR (125 MHz, DMSO- d_6 , δ /ppm): 187.24 (C=O), 171.76 (C), 156.61 (C), 149.98 (C), 143.85 (CH), 139.48 (C), 138.53 (C), 132.07 (C), 130.69 (2CH), 129.78 (2CH), 129.15 (2CH), 128.66 (CH), 126.31 (CH), 122.54 (CH), 120.35 (2CH); MS (EI, 70 eV) m/z (%): 364 (M + 1, 100), 365 (M + 2, 22.4), 366 (M + 3, 10.5), 338 (18.4), 261 (95.5), 243 (10.4), 246 (58.9), 219 (22.0), 218 (100), 201 (12.2); Anal. Calcd. for $\text{C}_{19}\text{H}_{13}\text{N}_3\text{O}_2\text{S}_2$ (363.46): C, 62.79; H, 3.61; N, 11.56; S, 17.64; Found: C, 62.84; H, 3.73; N, 11.67; S, 17.77.

5-((6-Chloro-4-oxo-4H-chromen-3-yl)methylene)-2-(phenylamino)thiazol-4(5H)-one (**6e**). Yield 94% (0.720 g); brown powder; m.p. 356 °C; IR (ATR, ν (cm^{-1})): 3429 (N-H_{amine}), 1699 (C=O_{TZ}), 1653 (C=O_{chromone}), 1270 (C-O_{chromone}), 1173 (C-Cl), 1041 (C-O_{chromone}); ^1H NMR (500 MHz, DMSO- d_6 , δ /ppm): 11.98 (s, 1H, NH), 7.71 (s, 1H, -CH=), 7.12–8.86 (m, 9H, Ar-H); ^{13}C NMR (125 MHz, DMSO- d_6 , δ /ppm): 188.58 (C=O), 170.33 (C=O), 158.46 (C), 156.02 (C), 151.65 (CH), 149.39 (CH), 139.87 (C), 136.43 (C), 136.05 (CH), 130.58 (CH), 129.81 (2CH), 129.17 (C), 126.01 (C), 122.22 (CH), 120.75 (2CH), 119.30 (C), 119.12 (CH); MS (EI, 70 eV) m/z (%): 383 (M + 1, 100), 384 (M + 2, 20.2), 385 (M + 3, 31.9), 386 (M + 4, 11.3), 326 (30.03), 312 (12.7), 259 (7.8), 205 (5.9), 183 (5.5), 138 (4.8); Anal. Calcd. for $\text{C}_{19}\text{H}_{11}\text{ClN}_2\text{O}_3\text{S}$ (382.82): C, 59.61; H, 2.90; N, 7.32; S, 8.38; Found: C, 59.66; H, 2.97; N, 7.41; S, 8.47.

5-(3-Chlorobenzylidene)-2-(naphthalen-1-ylamino)thiazol-4(5H)-one (**9a**). Yield 81% (0.591 g); yellow powder; m.p. 140 °C; IR (ATR, ν (cm^{-1})): 3430 (N-H_{amine}), 1686 (C=O_{TZ}), 1151 (C-Cl); ^1H NMR (500 MHz, DMSO- d_6 , δ /ppm): 12.01 (s, 1H, NH), 7.71 (s, 1H, -CH=), 7.05–7.92 (m, 11H, Ar-H); ^{13}C NMR (125 MHz, DMSO- d_6 , δ /ppm): 175.20 (C=O), 161.05 (C), 154.43 (CH), 144.60 (C), 135.89 (C), 134.38 (C), 134.07 (C), 132.10 (C), 130.24 (CH), 128.41 (CH), 128.11 (CH), 127.57 (CH), 126.89 (CH), 126.45 (CH), 126.26 (CH), 124.81 (CH), 123.47 (C), 121.35 (CH), 116.43 (CH), 105.63 (CH); MS (EI, 70 eV) m/z (%): 365 (M + 1, 100), 366 (M + 2, 2.5), 367 (M + 3, 19.7), 368 (M + 4, 7.7), 369 (M + 5, 1.4), 336 (3.3), 322 (2.2), 252 (4.9), 210 (2.1), 197 (64.5), 171 (10.3), 169 (100), 134 (52.2); Anal. Calcd. for $\text{C}_{20}\text{H}_{13}\text{ClN}_2\text{O}_2\text{S}$ (364.85): C, 65.84; H, 3.59; N, 7.68; S, 8.79; Found: C, 65.90; H, 3.66; N, 7.63; S, 8.84.

5-(2,4-Dichlorobenzylidene)-2-(naphthalen-1-ylamino)thiazol-4(5H)-one (**9b**). Yield 63% (0.503 g); yellow powder; m.p. 185 °C; IR (ATR, ν (cm^{-1})): 3433 (N-H_{amine}), 1713 (C=O_{TZ}), 1155 (C-Cl), 1099 (C-Cl); ^1H NMR (500 MHz, DMSO- d_6 , δ /ppm): 12.06 (s, 1H, NH), 7.62 (s, 1H, -CH=), 7.11–8.08 (m, 10H, Ar-H); ^{13}C NMR (125 MHz, DMSO- d_6 , δ /ppm): 175.74 (C=O), 161.42 (C), 154.35 (CH), 143.89 (C), 135.94 (C), 134.51 (C), 132.68 (C), 131.33 (C), 130.12 (CH), 128.60 (CH), 128.19 (CH), 127.76 (CH), 126.81 (CH), 126.40 (CH), 125.53 (C), 124.99 (CH), 123.93 (C), 121.17 (CH), 118.32 (CH), 105.25 (CH); MS (EI, 70 eV) m/z (%): 399 (M + 1, 90.5), 400 (M + 2, 22.2), 401 (M + 3, 100), 402 (M + 4, 17.0), 365 (31.6), 363 (100), 297 (1.0), 168 (13.2), 159 (3.4); Anal. Calcd. for $\text{C}_{20}\text{H}_{12}\text{Cl}_2\text{N}_2\text{O}_2\text{S}$ (399.29): C, 60.16; H, 3.03; N, 7.02; S, 8.03; Found: C, 60.35; H, 3.08; N, 7.11; S, 8.05.

2-(Naphthalen-1-ylamino)-5-(4-nitrobenzylidene)thiazol-4(5H)-one (**9c**). Yield 72% (0.540 g); yellow powder; m.p. 152 °C; IR (ATR, ν (cm^{-1})): 3426 (N-H_{amine}), 1706 (C=O_{TZ}), 1521 (NO₂ asymmetric), 1328 (NO₂ symmetric); ^1H NMR (500 MHz, DMSO- d_6 , δ /ppm): 12.23 (s, 1H, NH), 7.68 (s, 1H, -CH=), 7.13–8.18 (m, 11H, Ar-H); ^{13}C NMR (125 MHz, DMSO- d_6 , δ /ppm): 174.88 (C=O), 161.31 (C), 154.10 (CH), 147.66 (C), 141.41 (C), 140.73 (C), 134.56 (C), 132.46 (C), 129.41 (2CH), 128.57 (CH), 127.32 (CH), 126.18 (CH), 125.86 (CH), 124.91 (C), 123.77 (2CH), 121.05 (CH), 118.81 (CH), 105.95 (CH); MS (EI, 70 eV) m/z (%): 376 (M + 1, 100), 378 (M + 2, 16.4), 379 (M + 3, 9.3), 330 (30.6), 316 (5.7), 208 (10.7), 180 (21.3), 170 (22.3),

169 (100), 150 (3.8), 134 (37.7); Anal. Calcd. for $C_{20}H_{13}N_3O_3S$ (375.40): C, 63.99; H, 3.49; N, 11.19; S, 8.54; Found: C, 63.78; H, 3.52; N, 11.24; S, 8.64.

2-(Naphthalen-1-ylamino)-5-((2-phenylthiazol-4-yl)methylene)thiazol-4(5H)-one (**9d**). Yield 86% (0.711 g); pale yellow powder; m.p. 312 °C; IR (ATR, ν (cm^{-1})): 3429 (N-H_{amine}), 1728 (C=O_{TZ}); ¹H NMR (500 MHz, DMSO-*d*₆, δ /ppm): 12.31 (s, 1H, NH), 7.69 (s, 1H, -CH=), 7.12–8.91 (m, 13H, Ar-H + C5-thiazole-H); ¹³C NMR (125 MHz, DMSO-*d*₆, δ /ppm): 174.67 (C=O), 169.54 (C), 161.11 (C), 149.69 (C), 142.33 (CH), 140.61 (C), 138.89 (C), 134.54 (C), 131.26 (C), 130.97 (2CH), 129.38 (2CH), 128.88 (CH), 128.79 (CH), 127.64 (CH), 126.78 (CH), 125.99 (CH), 125.07 (CH), 124.76 (C), 121.13 (CH), 118.92 (CH), 105.86 (CH); MS (EI, 70 eV) *m/z* (%): 414 (M + 1, 100), 415 (M + 2, 22.2), 416 (M + 3, 15.7), 387 (4.1), 261 (30.1), 246 (10.5), 218 (100), 213 (6.8), 174 (4.5), 158 (7.9), 130 (2.5); Anal. Calcd. for $C_{23}H_{15}N_3OS_2$ (413.51): C, 66.80; H, 3.66; N, 10.16; S, 15.51; Found: C, 66.66; H, 3.74; N, 10.19; S, 15.44.

5-((6-Chloro-4-oxo-4H-chromen-3-yl)methylene)-2-(naphthalen-1-ylamino)thiazol-4(5H)-one (**9e**). Yield 90% (0.779 g); orange powder; m.p. 266–268 °C; IR (ATR, ν (cm^{-1})): 3434 (N-H_{amine}), 1701 (C=O_{TZ}), 1649 (C=O_{chromone}), 1271 (C-O_{chromone}), 1170 (C-Cl), 1044 (C-O_{chromone}); ¹H NMR (500 MHz, DMSO-*d*₆, δ /ppm): 12.51 (s, 1H, NH), 7.70 (s, 1H, -CH=), 7.11–8.74 (m, 11H, Ar-H); ¹³C NMR (125 MHz, DMSO-*d*₆, δ /ppm): 174.21 (C=O), 160.63 (C=O), 154.38 (2C), 135.15 (CH), 134.36 (C), 131.09 (CH), 128.45 (2C), 127.49 (CH), 127.03 (C), 126.56 (CH), 126.49 (C), 125.06 (C), 124.95 (2CH), 124.49 (CH), 123.48 (2CH), 121.78 (C), 121.48 (CH), 118.76 (CH), 116.60 (CH); MS (EI, 70 eV) *m/z* (%): 433 (M + 1, 100), 434 (M + 2, 17.8), 435 (M + 3, 52.6), 436 (M + 4, 10.9), 413 (5.6), 401 (100), 376 (28.4), 290 (34.2), 299 (3.5), 267 (32.8), 265 (100), 237 (85.8), 205 (22.2), 165 (21.1); Anal. Calcd. for $C_{23}H_{13}ClN_2O_3S$ (432.88): C, 63.82; H, 3.03; N, 6.47; S, 7.41; Found: C, 63.70; H, 3.01; N, 6.50; S, 7.53.

3.2. Antifungal Activity Assay

3.2.1. Determination of Inhibition Zone Diameters

The in vitro antifungal activity was determined using the cup-plate agar diffusion method according to the Clinical and Laboratory Standards Institute (CLSI) guidelines [38].

Mueller-Hinton medium supplemented with 2% glucose (providing adequate growth of yeasts) and 0.5 mg/mL methylene blue (providing a better definition of the inhibition zone diameter) was used. The inoculum was prepared by suspending five representative colonies, obtained from an 18–24 h culture on non-selective nutritive agar medium, in sterile distilled water. The cell density was adjusted to the density of a 0.5 McFarland standard by spectrophotometrically measuring the absorbance at 530 nm and adding sterile distilled water as required (corresponding to a population of 1 to 5 × 10⁶ CFU/mL). A sterile swab was soaked in the suspension and then the Mueller-Hinton agar plates were inoculated by streaking the entire surface. After drying for 10–15 min, six-millimeter diameter wells were cut from the agar using a sterile cork-borer and a volume of 20 μ L of each compound solution (1 mg/mL in dimethyl sulfoxide (DMSO)) were delivered into the wells (20 μ g/well). Fluconazole (20 μ g/well) was used as standard drug. The controls were performed with only sterile broth, overnight culture and 20 μ L of DMSO. The plates were incubated at 35 °C. Zone diameters were measured to the nearest whole millimeter at a point in which there was no visible growth after 24–48 h. Results were obtained in triplicate. The solvent used for the preparation of each compound stock solution (1 mg/mL), DMSO (Merck, Darmstadt, Germany) presented no inhibitory activity against the tested fungal strains.

3.2.2. Determination of MIC and MFC Values

The microorganisms used for the antimicrobial activity evaluation were obtained from the University of Agricultural Sciences and Veterinary Medicine Cluj-Napoca, Romania. The antifungal activity was evaluated against cultures of *Candida albicans* ATCC 10231, *Candida albicans* ATCC 18804, *Candida krusei* ATCC 6258, *Candida parapsilosis* ATCC 22019. The cultures were store on potato dextrose

agar (Sifin, Berlin, Germany). Prior to antifungal susceptibility testing, each strain was inoculated on potato dextrose agar plates to ensure optical growth characteristics and purity. Then, yeast cells were suspended in saline and adjusted spectrophotometrically to RPMI 1640 medium.

Stock solutions (1 mg/mL) were prepared by dissolving the test compounds and the reference antifungals (ketoconazole and fluconazole) in sterile DMSO. These solutions were stored at 4 °C. Series of double diluting solutions of the above compounds were prepared in RPMI 1640 medium obtaining final concentrations in the range of 500 to 0.015 µg/mL.

The broth microdilution method (according to the CLSI guidelines [39]) was employed for minimum inhibitory concentration test. Media was placed into each 96 wells of the microplates. Sample solutions at high concentration (100 µg/mL) were added into the first rows of the microplates and two-fold dilutions of the compounds were made by dispensing the solutions into the remaining wells. Ten-microliter culture suspensions were inoculated into all the wells. The sealed microplates were incubated at 37 °C for 18 h. The initial density of *Candida* sp. was approximately 2×10^6 colony forming units (CFU)/mL. Inoculums (density of 0.5 in McFarland scale) were prepared in a sterile solution of 0.9% NaCl. Then the tested strains were suspended in nutrient broth and RPMI 1640 media to give a final density of 2×10^5 CFU/mL. Solutions of the test compounds and suspensions of fungi were inoculated onto 96 wells microplates. Growth control, sterility control and control of antifungal compounds were used. Plates were incubated under normal atmospheric conditions 25 °C for 48 h (*Candida albicans* ATCC 10231, *Candida albicans* ATCC 18804, *Candida krusei* ATCC 6258, *Candida parapsilosis* ATCC 22019), and next minimum inhibitory concentration (MIC) values have been determined by recording the optical density at 600 nm using a spectroscopically method with a microplate reader Biotek Synergy HT. The MIC was defined as the lowest concentration required arresting the growth of the fungi. For determination of minimum fungicidal concentration (MFC), a 0.01 mL aliquot of the medium drawn from the culture tubes showing no macroscopic growth at the end of the 24 h culture was subcultured on nutrient agar/potato dextrose agar plates to determine the number of vital organisms and incubated further at 37 °C for 24 h, respectively 25–30 °C for 48 h. The MFC was defined as the lowest concentration of the agent at which no colonies are observed. All MIC and MFC experiments were repeated three times.

3.2.3. Statistical Analysis

The results obtained in the determination of the inhibition zone diameters assay were expressed as mean \pm standard deviation (SD) of three independent experiments. Statistical comparisons between the groups were made using one-way analysis of variance (ANOVA) test. A value of $p < 0.05$ was considered to be statistically significant. Analysis was performed using standard software (Excel for Windows, version 14.0 included in Microsoft Office Professional Plus 2010).

3.3. Lipophilicity Assay

The lipophilic character of twenty thiazolin-4-one derivatives was assessed with the help of the principal component analysis (PCA) based on the reversed-phase thin-layer chromatography (RP-TLC) data.

3.3.1. Chromatographic Procedure

The chromatographic behavior of the test compounds was studied on C₁₈ silicagel bonded 60 RP-180F₂₅₄S TLC (20 × 20 cm) plates, purchased from Merck (Darmstadt, Germany). The test compounds' solutions (1 mg/mL) were prepared by dissolving the samples in DMSO (Merck, Darmstadt, Germany). The plates were manually spotted with 3 µL aliquots of each solution at 10 mm from the base and 5 mm from the edge of the plate, leaving a 10 mm distance between successive spots, and developed by the ascending technique, without preconditioning. Chromatography was performed in a normal developing chamber at room temperature (~24 °C), the developing distance being of 9 cm. The solvent system used as mobile phase consisted of a water-*i*-propanol mixture,

with a varying content of organic modifier (*i*-propanol—concentration ranged between 45% and 65% (*v/v*), with 5% vol. increments). Before the development, the chamber was saturated with the mobile phase for 15 min. After being developed, the dried plates were visually inspected under the UV light ($\lambda = 254$ nm), each spot was clearly marked and its distance was manually measured in order to calculate the R_f values. The spots of the compounds **3f**, **10** and **11** were not visible in UV light, thus their R_f values could not be calculated, therefore they were excluded from this assay.

3.3.2. Chromatographic Lipophilicity Parameters

Based on the R_f values, one of the most common lipophilic estimator, meaning the isocratic retention factor R_M was calculated using the Bate-Smith and Westall equations [40].

RP-TLC provides retention data in the form of R_f and the corresponding R_M values (Equation (2)) that can be used to derive chromatographic descriptors for estimating lipophilicity: R_{M0} , b and PCA. The most popular lipophilicity descriptor estimated by this method is R_M and it is derived from the retention factor (R_f) according to the following formula:

$$R_M = \log[(1/R_f) - 1] \quad (2)$$

where R_f is calculated on the basis of migration distance of a compound and the solvent front.

The use of RP-TLC is based on the assumed linear relationship between the molecular parameter (Equation (2)) and the standard measure of lipophilicity, $\log P$ (the logarithm of the *n*-octanol-water partition coefficient).

As R_M value (related to the molecular lipophilicity) depends linearly on the concentration of the organic modifier in the mobile phase, the value is extrapolated to pure water as mobile phase. In order to increase the accuracy of the lipophilicity determination, the R_M values extrapolated to zero organic modifier concentration (R_{M0}) have been calculated from the linear correlation between the R_M values and the concentration of the organic component of the mobile phase:

$$R_M = R_{M0} + bc \quad (3)$$

where R_{M0} is the lipophilicity estimation parameter, R_M is the retention of the solute, b is the slope, and c is the concentration of the mobile phase organic modifier (*i*-propanol).

The intercept (R_{M0}) in Equation (3) represents the extrapolated R_M values at 0% organic modifier. In other words, the intercept determined using this equation can be considered an estimation of the partitioning of compounds between the nonpolar stationary phase and the aqueous system, hence all compounds studied can be compared on the basis of their lipophilicity determined this way [41].

The lipophilic properties of the investigated compounds were evaluated by using the principal component analysis (PCA, XL-STAT). For a better interpretation of the obtained results, these were correlated with $c\text{LogP}$ values of the tested compounds, which were generated by the ChemBioDraw 11.0 software.

3.3.3. Principal Component Analysis (PCA)

PCA, also known as eigenvector analysis, is a statistical procedure used to represent in an economic way the location of the objects in a reduced coordinate system where instead of n -axes (corresponding to n variables) only p ($p \leq n$) can usually be used to describe the data set with maximum possible information. The new variables are called principal components and they are given by the linear combination of the n real variables [42].

PCA was performed on the obtained retention parameters with the help of XL-STAT extension. It displayed objects (the tested compounds) in a reduced space by finding a direction (first principal component) that best preserved the scatter of the observations ($100 \times R_f$ values) in the multidimensional space. PCA gave the coordinates (scores) of the studied compounds and also the loadings of the variables (solvents) on the principal components.

3.4. Virtual Screening

Identification of good “hits” (lead/drug-like molecules) is the first critical step in the drug discovery and development process. The qualities of the “hits” may dramatically set the stage for subsequent efforts to improve their therapeutic efficacy through potency against their designated target, their selectivity against related targets (including here protein binding specificity versus promiscuity), adequate pharmacokinetics, and lowering toxicity and their side effects [43].

The synthesized thiazolin-4-one derivatives and the reference compounds (fluconazole and ketoconazole) were screened in silico for both prediction of ADME-Tox properties (including here lipophilicity) and the binding modes with their designated targets. An academic license of MarvinSketch was used for drawing, displaying of 2D structures and 3D optimization of all screened compounds and generations of input files (SDF and Tripos MOL2 file formats) for virtual screening, MarvinSketch 15.1.5.0, 2015, ChemAxon (<https://www.chemaxon.com/>).

3.4.1. ADME-Tox Predictions

Achieving the desired specificity and activity alone is not a self-sufficient goal to produce high-quality leads or drug candidates. Therefore, pharmacokinetic and metabolic characteristics should be taken into consideration as early as possible hence the major reasons preventing many candidates from reaching market are the side effects, respectively the inappropriate ADME-Tox properties. Therefore, from an economical point-of-view, it is desirable that compounds with inappropriate ADME-Tox properties are optimized or removed from the early discovery phase rather than during the expensive drug development phases.

The use of cheminformatics to predict the ADME-Tox properties can provide helpful guidance on absorption, plasma clearance and tissue distribution, activity at the level of central nervous system (penetration of compounds through the BBB), various metabolic effects and toxicity aspects. In this respect, FAF-Drugs3 [30], a web-based software, hosted on the public domain of *The Ressource Parisienne en Bioinformatique Structurale (RPBS)* (<http://fafdrugs3.mti.univ-paris-diderot.fr/>), was used to screen all thiazolin-4-one derivatives and the reference compounds for ADME-Tox properties.

Prior to screening, the input SDF files were formatted according to the software’s requirements using Bank Formatter (the files formatter service of FAF-Drugs3) and XLOGP3 was chosen as method to estimate lipophilicity (and the derived ADME-Tox descriptors) due to its prediction accuracy. VS was carried out using a series of FAF-Drugs3’s built-in filters for lead-likeness, drug-likeness, activity at CNS level [33], detection of non-peptidic inhibitors of protein–protein interactions, detection of undesirable moieties and substructures involved in toxicity problems [35,36], covalent inhibitors, PAINS and customized filters for safety profiling [35].

The chosen *Lead-Like Soft filter* uses well-known lead-like descriptors, while the *Drug-Like Soft filter* is based on physico-chemical, molecular properties and bioavailability rules, widely used for drug discovery—both *soft filters* use a built-in statistical analysis of drugs [30] extracted from the *e-Drugs3D library* for the threshold values of descriptors.

PPIs are essential to a healthy life, but aberrant PPIs contribute to many diseases and therefore represent a very populated class of essentially untouched targets for rational drug design. In this respect, FAF-Drugs3 uses a decision tree constructed with the help of two trained Dragon descriptors (*Ui* and *RDF070m*).

For the detection of the undesirable moieties and substructures involved in toxicity problems, the FAF-Drugs3 built-in filters based on a comprehensive literature data were used. As a particular threshold of the software, with direct interest for our work, is the acceptance of up to 3 nitro groups, otherwise well-known structural alerts, because several approved and experimental drugs (e.g., nitroimidazole antibiotics) have at least one nitro group and because this group can be replaced during the optimization process. Similar to the detection of UMSs, FAF-Drugs3 uses built-in filters to identify covalent inhibitors.

The detection of the possible frequent hitters, compounds that appear in many biochemical high throughput screens—PAINS moieties, was done using three filters (A, B and C), in order to detect problematic compound classes in the **WEHI (The Walter and Eliza Hall Institute of Medical Research, Parkville, Australia) 93K HTS library** that contain over 150 analogs (filter A), from 15 to 149 analogs (filter B), respectively, 1 to 14 analogs (filter C) [30].

A series of customized filters developed by pharmaceutical companies were used to assess the safety profiling: the GSK 4/400 rule, the Pfizer 3/75 rule, estimation of phospholipidosis induction (directly linked with the molecular substructure of compounds) and the MedChem rules rating [35]. The MedChem rules is a set of 275 rules developed by Eli Lilly and Company (Indianapolis, IN, USA), to identify compounds that may interfere with biological assays, allowing their removal from screening sets. For this particular VS run, the MedChem rules were used with the regular settings (100-demerit cutoff).

3.4.2. Molecular Docking Studies

The thiazolin-4-one derivatives and the corresponding reference compounds (generated as Tripos MOL2 files) were docked in silico against their corresponding target (the same species used for determination of MIC and MFC values were considered): a fungal enzyme (lanosterol 14- α demethylase). Due to the lack of experimentally determined high-resolution crystal structures from *Research Collaboratory for Structural Bioinformatics—Protein Data Bank* (RCSB-PDB: <http://www.rcsb.org/>), as best recommended for docking [44], a homology model was used for the target protein.

The homology model for lanosterol-14 α -demethylase was generated with *SWISS-MODEL* (a fully automated protein structure homology-modeling server, accessible via ExPASy web server: <http://www.expasy.org/>) [45] starting from the corresponding amino acid sequence (Accession Code: P10613) of the enzyme for *Candida albicans* (strain SC5314/ATCC MYA-2876) obtained from the *Universal Protein Resource (UniProt)* (<http://www.uniprot.org/>) and using as template a validated experimental structure from *Saccharomyces cerevisiae* (PDB ID: 4WMZ) [45].

Lanosterol 14- α demethylase (cytochrome P450 14 α -lanosterol-demethylase) catalyzes the C14-demethylation of lanosterol which is critical for ergosterol biosynthesis (transforms lanosterol into 4,4'-dimethyl cholesta-8,14,24-triene-3- β -ol). Therefore, lanosterol 14- α demethylase is an enzyme with a crucial role in sterol biosynthesis in eukaryotes, being thus a druggable protein for antifungal design and development of new inhibitors. The active site of enzyme includes a triazole ring perpendicularly positioned to the porphyrin plane with a ring nitrogen atom coordinated to the Hem iron. Docking of thiazolin-4-one derivatives and reference compounds (fluconazole and ketoconazole) against the generated homology model for lanosterol-14 α -demethylase was carried out setting an extended search space (X:26.610; Y:18.853; Z:19.715), with a volume bigger than 27.000 Å³ and manually increasing the exhaustiveness to 80 in order to improve docking accuracy.

4. Conclusions

Twenty-three thiazoline-4-ones were synthesized, of which 18 are new 5-arylidene-thiazoline-4-one derivatives. The newly synthesized compounds were characterized by quantitative elemental analysis, IR, ¹H NMR, ¹³C NMR and MS. All compounds were evaluated for their antifungal activity against four strains of *Candida* and the compounds' lipophilicity was assessed. Most of the compounds presented excellent anti-*Candida* properties, two of them (**10** and **9b**) being 250-fold more active than ketoconazole and over 500-fold more active than fluconazole. For all the studied compounds, it was observed a lipophilicity augmentation with the increase of the molar mass of the substituent from position 2 of the thiazolin-4-one core, and also, by introducing an arylidene or hetarylidene rest in position 5. A comprehensive VS was carried out for ADME-Tox profiling of the thiazolin-4-one derivatives and it can be concluded that based on the predicted values of physico-chemical descriptors, almost all derivatives are drug-like small-molecules (except **9b**), non-inducer of phospholipidosis

and with good predictions for oral bioavailability according to RO5, Veber's rule and Egan's rule, thus making them suitable for systemic use. Most of the drug-like derivatives forecasted good activity at CNS level (except **3c**, **6c**, **9b**, **9c** and **10**), but all require further structural optimization due multiple safety alerts. Therefore, compound **11** appears to be the safest drug-like derivative since it has only two alerts (PPI unfriendly and a warning from Pfizer 3/75 rule).

On the other hand, some of thiazolin-4-one derivatives were also qualified as potential leads (**2**, **3a**, **3c–h**, **5**, **6c**, **8** and **11**) able to penetrate BBB (except **3c** and **6c**) and with good predictions for oral bioavailability. However, all those lead-like compounds require further optimization in the drug development process. In regards to this aspect, we can identify as "hits" compounds **5** and **8** (both free of UMSs, covalent inhibitors and PAINS—according to all three PAINS's filters, but PPI unfriendly and with different safety concerns according to the MedChem rules); compound **6c** (the only lead compound which is PPI friendly), and compound **11** (with the already discussed safety concerns as drug candidate).

Regarding the thiazolin-4-one derivatives inhibitory activity as antifungals we can summarize that from the identified "hits", two derivatives (**5** and **11**) are weaker inhibitors than both reference drugs (**Flu** and **Ket**), meanwhile **6c** and **8** have a better binding affinity than **Flu**, but with lesser safety concerns than **Ket**—both virtually predicted and referred in the literature [46]. Moreover, three of the identified "hits" (**5**, **8** and **11**) block the same entry of the active site of lanosterol 14 α -demethylase, while only **6c** binds deeply inserted in the active site.

Supplementary Materials: Supplementary materials can be found at www.mdpi.com/1422-0067/18/1/177/s1.

Acknowledgments: This research was financed by the "Iuliu Hațieganu" University of Medicine and Pharmacy Cluj-Napoca internal research grant no. 4945/24/2016 and by the Executive Agency for Higher Education Research Development and Innovation Funding—UEFISCDI, Romania, on the Contract 210/2014—Project PN-II-PT-PCCA-2013-4-2075.

Author Contributions: All authors have materially participated in the research and/or article preparation, as follows: Anca Stana has participated in chemical synthesis, compounds' characterization, lipophilicity assessment and article preparation; Dan C. Vodnar was responsible for the antifungal activity studies and article preparation; Radu Tamaian was responsible for ADME-Tox studies, molecular docking and article preparation; Adrian Pîrnău performed the NMR spectral analysis of compounds; Laurian Vlase recorded the MS spectra of the synthesized compounds; Ioana Ionuț participated in the lipophilicity study and article preparation; Ovidiu Oniga participated in quantitative elemental analysis, chemical synthesis and study design; and Brîndușa Tipericiu participated in IR analysis, study design and article preparation.

Conflicts of Interest: The authors declare no conflict of interest.

References

1. Devprakash, A.; Udaykumar, A.B. A complete review of thiazolidine-4-ones. *J. Pharm. Res.* **2011**, *4*, 2436–2440.
2. Lv, P.C.; Zhou, C.F.; Chen, J.; Liu, P.G.; Wang, K.R.; Mao, W.J.; Li, H.Q.; Yang, Y.; Xiong, J.; Zhu, H.L. Design, synthesis and biological evaluation of thiazolidinone derivatives as potential EGFR and HER-2 kinase inhibitors. *Bioorg. Med. Chem.* **2010**, *18*, 314–319. [[CrossRef](#)] [[PubMed](#)]
3. Yang, Y.S.; Zhang, F.; Gao, C.; Zhang, Y.B.; Wang, X.L.; Tang, J.F.; Sun, J.; Gong, H.B.; Zhu, H.L. Discovery and modification of sulfur-containing heterocyclic pyrazoline derivatives as potential novel class of β -ketoacyl-acyl carrier protein synthase III (FabH) inhibitors. *Bioorg. Med. Chem. Lett.* **2012**, *22*, 4619–4624. [[CrossRef](#)] [[PubMed](#)]
4. Insuasty, A.; Ramírez, J.; Raimondi, M.; Echeverry, C.; Quiroga, J.; Abonia, R.; Nogueras, M.; Cobo, J.; Rodríguez, M.V.; Zacchino, S.A.; et al. Synthesis, antifungal and antitumor activity of novel (Z)-5-hetarylmethylidene-1,3-thiazol-4-ones and (Z)-5-ethylidene-1,3-thiazol-4-ones. *Molecules* **2013**, *18*, 5482–5497. [[CrossRef](#)] [[PubMed](#)]
5. Al-Ansary, G.H.; Ismail, M.A.H.; Abou El Ella, D.A.; Eid, S.; Abouzid, K.A.M. Molecular design and synthesis of HCV inhibitors based on thiazolone scaffold. *Eur. J. Med. Chem.* **2013**, *68*, 19–32. [[CrossRef](#)] [[PubMed](#)]

6. Barzen, S.; Rödl, C.B.; Lill, A.; Steinhilber, D.; Stark, H.; Hofmann, B. Synthesis and biological evaluation of a class of 5-benzylidene-2-phenyl-thiazolinones as potent 5-lipoxygenase inhibitors. *Bioorg. Med. Chem.* **2012**, *20*, 3575–3583. [[CrossRef](#)] [[PubMed](#)]
7. Verspohl, E.J. Novel pharmacological approaches to the treatment of type 2 diabetes. *Pharmacol. Rev.* **2012**, *64*, 188–237. [[CrossRef](#)] [[PubMed](#)]
8. Zvezdanovic, J.; Daskalova, L.; Yancheva, D.; Cvetkovic, D.; Markovic, D.; Anderluh, M.; Smelcerovic, A. 2-Amino-5-alkylidenethiazol-4-ones as promising lipid peroxidation inhibitors. *Monatshfte fur Chemie* **2014**, *145*, 945–952. [[CrossRef](#)]
9. Mony, L.; Triballeau, N.; Paoletti, P.; Acher, F.C.; Bertrand, H.-O. Identification of a novel NR2B-selective NMDA receptor antagonist using a virtual screening approach. *Bioorg. Med. Chem. Lett.* **2010**, *20*, 5552–5558. [[CrossRef](#)] [[PubMed](#)]
10. Saundaneanand, R.; Kirankumar, N.M.; Annapurna, H. Synthesis of novel N-(aryl)diazenyl thiazol-2-amines and benzylidene-thiazolidin-4-ones linked to indole nucleus as antioxidant, antimicrobial, antimycobacterial and cytotoxic agents. *Int. J. Pharm. Pharm. Sci.* **2014**, *6*, 141–147.
11. Sarkis, M.; Ngan, D.; Kolb, S.; Miteva, M.A.; Villoutreix, B.O.; Garbay, C.; Braud, E. Bioorganic & Medicinal Chemistry Letters Design and synthesis of novel bis-thiazolone derivatives as micromolar CDC25 phosphatase inhibitors: Effect of dimerisation on phosphatase inhibition. *Bioorg. Med. Chem. Lett.* **2012**, *22*, 7345–7350. [[PubMed](#)]
12. Sanglard, D. Emerging threats in antifungal-resistant fungal pathogens. *Front. Med.* **2016**, *3*, 1–10. [[CrossRef](#)] [[PubMed](#)]
13. Becher, R.; Wirsal, S.G.R. Fungal cytochrome P450 sterol 14 α -demethylase (CYP51) and azole resistance in plant and human pathogens. *Appl. Microbiol. Biotechnol.* **2012**, *95*, 825–840. [[CrossRef](#)] [[PubMed](#)]
14. Arnott, J.A.; Planey, S.L. The influence of lipophilicity in drug discovery and design. *Expert Opin. Drug Discov.* **2012**, *7*, 863–875. [[CrossRef](#)] [[PubMed](#)]
15. Lionta, E.; Spyrou, G.; Vassilatis, D.K.; Cournia, Z. Structure-based virtual screening for drug discovery: principles, applications and recent advances. *Curr. Top. Med. Chem.* **2014**, *14*, 1923–1938. [[CrossRef](#)] [[PubMed](#)]
16. Meng, X.-Y.; Zhang, H.-X.; Mezei, M.; Cui, M. Molecular docking: A powerful approach for structure-based drug discovery. *Curr. Comput. Aided Drug Des.* **2011**, *7*, 146–157. [[CrossRef](#)] [[PubMed](#)]
17. Stana, A.; Tipericiuc, B.; Duma, M.; Vlase, L.; Crişan, O.; Pîrnău, A.; Oniga, O. Synthesis and Antimicrobial Activity of Some New N-substituted-5-arylidene-thiazolidine-2,4-diones. *J. Heterocycl. Chem.* **2014**, *51*, 411–417. [[CrossRef](#)]
18. Kant, V.; Gupta, V. A review on biological activity of imidazole and thiazole moieties and their derivatives. *Sci. Int.* **2013**, 253–260.
19. Gaspar, A.; Matos, M.J.; Garrido, J.; Uriarte, E.; Borges, F. Chromone: A valid scaffold in medicinal chemistry. *Chem. Rev.* **2014**, *114*, 4960–4992. [[CrossRef](#)] [[PubMed](#)]
20. Sheng, C.; Miao, Z.; Ji, H.; Yao, J.; Wang, W.; Che, X.; Dong, G.; Lu, J. Three-dimensional model of lanosterol 14 α -demethylase from *Cryptococcus neoformans*: Active-site characterization and insights into azole binding. *Antimicrob. Agents Chemother.* **2009**, *53*, 3487–3495. [[CrossRef](#)] [[PubMed](#)]
21. De Monte, C.; Carradori, S.; Bizzarri, B.; Bolasco, A.; Caprara, F.; Mollica, A.; Rivanera, D.; Mari, E.; Zicari, A.; Akdemir, A.; et al. Anti-*Candida* activity and cytotoxicity of a large library of new N-substituted-1,3-thiazolidin-4-one derivatives. *Eur. J. Med. Chem.* **2016**, *107*, 82–96. [[CrossRef](#)] [[PubMed](#)]
22. Chauhan, K.; Sharma, M.; Singh, P.; Kumar, V.; Shukla, P.K.; Siddiqi, M.I.; Chauhan, P.M.S. Discovery of a new class of dithiocarbamates and rhodanine scaffolds as potent antifungal agents: Synthesis, biology and molecular docking. *Med. Chem. Commun.* **2012**, *3*, 1104–1110. [[CrossRef](#)]
23. Studzińska, R.; Karczmarzka-Wódzka, A.; Kozakiewicz, A.; Kołodziejka, R.; Paprocka, R.; Wróblewski, M.; Augustyńska, B.; Modzelewska-Banachiewicz, B. 2-Allylaminothiazole and 2-allylamino-dihydrothiazole derivatives: Synthesis, characterization, and evaluation of bioactivity. *Monatshfte fur Chemie* **2015**, *146*, 1673–1679. [[CrossRef](#)] [[PubMed](#)]
24. Adhikari, A.; Kalluraya, B.; Sujith, K.V.; Gouthamchandra, K.; Mahmood, R. Microwave assisted synthesis of novel thiazolidinone analogues as possible bioactive agents. *J. Adv. Res.* **2012**, *3*, 325–330. [[CrossRef](#)]
25. Desai, R.D.; Hunter, R.F.; Koppar, L.G. The condensation of thiocarbamides with monochloroacetic acid and the conversion of Arylformamidinethiolacetic acids into ψ -thiohydantoin derivatives. *Recl. Trav. Chim. Pays-Bas* **1935**, *54*, 118–121. [[CrossRef](#)]

26. Bellus, D.; Boyd, G.V.; Fanghänel, E.; Gudat, D.; Kikelj, D.; Pedersen, C.T.; Perst, H.; Pfeiffer, W.-D.; Sainsbury, M.; Schaumann, E.; et al. *Science of Synthesis: Houben-Weyl Methods of Molecular Transformations*; Georg Thieme Verlag: Stuttgart, Germany, 2002; Volume 11.
27. Kerdesky, F.A.J.; Holms, J.H.; Moore, J.L.; Bell, R.L.; Dyer, R.D.; Carter, G.W.; Brooks, D.W. 4-Hydroxythiazole inhibitors of 5-lipoxygenase. *J. Med. Chem.* **1991**, *34*, 2158–2165. [[CrossRef](#)] [[PubMed](#)]
28. Sardi, J.; Scorzoni, L.; Bernardi, T.; Fusco-Almeida, A.; Giannini, M.M. Candida species: Current epidemiology, pathogenicity, biofilm formation, natural antifungal products and new therapeutic options. *J. Med. Microbiol.* **2013**, *62*, 10–24. [[CrossRef](#)] [[PubMed](#)]
29. Movahed, E.; Tan, G.M.; Munusamy, K.; Yeow, T.C.; Tay, S.T.; Wong, W.F.; Looi, C.Y. Triclosan demonstrates synergic effect with amphotericin B and fluconazole and induces apoptosis-like cell death in *Cryptococcus neoformans*. *Front. Microbiol.* **2016**, *7*, 1–10. [[CrossRef](#)] [[PubMed](#)]
30. Lagorce, D.; Sperandio, O.; Baell, J.B.; Miteva, M.A.; Villoutreix, B.O. FAF-Drugs3: A web server for compound property calculation and chemical library design. *Nucleic Acids Res.* **2015**, *43*, W200–W207. [[CrossRef](#)] [[PubMed](#)]
31. Lipinski, C.A.; Lombardo, F.; Dominy, B.W.; Feeney, P.J. Experimental and computational approaches to estimate solubility and permeability in drug discovery and development settings. *Adv. Drug Deliv. Rev.* **2012**, *64*, 4–17. [[CrossRef](#)]
32. Veber, D.F.; Johnson, S.R.; Cheng, H.-Y.; Smith, B.R.; Ward, K.W.; Kopple, K.D. Molecular properties that influence the oral bioavailability of drug candidates. *J. Med. Chem.* **2002**, *45*, 2615–2623. [[CrossRef](#)] [[PubMed](#)]
33. Jeffrey, P.; Summerfield, S. Assessment of the blood–brain barrier in CNS drug discovery. *Neurobiol. Dis.* **2010**, *37*, 33–37. [[CrossRef](#)] [[PubMed](#)]
34. Egan, W.J.; Merz, K.M.; Baldwin, J.J. Prediction of drug absorption using multivariate statistics. *J. Med. Chem.* **2000**, *43*, 3867–3877. [[CrossRef](#)] [[PubMed](#)]
35. Bruns, R.F.; Watson, I.A. Rules for identifying potentially reactive or promiscuous compounds. *J. Med. Chem.* **2012**, *55*, 9763–9772. [[CrossRef](#)] [[PubMed](#)]
36. Blagg, J. Structural Alerts for Toxicity. In *Burger's Medicinal Chemistry and Drug Discovery*; Abraham, D.J., Ed.; John Wiley & Sons, Inc.: Hoboken, NJ, USA, 2010; pp. 301–334.
37. Pérez-Garrido, A.; Helguera, A.M.; López, G.C.; Cordeiro, M.N.D.S.; Escudero, A.G. A topological substructural molecular design approach for predicting mutagenesis end-points of α , β -unsaturated carbonyl compounds. *Toxicology* **2010**, *268*, 64–77. [[CrossRef](#)] [[PubMed](#)]
38. Clinical and Laboratory Standards Institute (CLSI). *Performance Standards for Antimicrobial Disk Susceptibility Tests*; CLSI: Wayne, PA, USA, 2012; Volume 32.
39. Clinical and Laboratory Standards Institute (CLSI). *Reference Method for Broth Dilution Antifungal Susceptibility Testing of Yeasts*; Third Informational Supplement—M27-S3; CLSI: Wayne, PA, USA, 2008; Volume 28.
40. Bate-Smith, E.C.; Westall, R.G. Chromatographic behavior and chemical structure. I. Some naturally occurring phenolic substances. *Biochim. Biophys. Acta* **1950**, *4*, 427–440. [[CrossRef](#)]
41. Rutkowska, E.; Pająk, K.; Józwiak, K. Lipophilicity—Methods of determination and its role in medicinal chemistry. *Acta Pol. Pharm. Drug Res.* **2013**, *70*, 3–18.
42. Sârbu, C.; Todor, S. Determination of lipophilicity of some non-steroidal anti-inflammatory agents and their relationships by using principal component analysis based on thin-layer chromatographic retention data. *J. Chromatogr. A* **1998**, *822*, 263–269. [[CrossRef](#)]
43. Kell, D.B.; Dobson, P.D.; Bilsland, E.; Oliver, S.G. The promiscuous binding of pharmaceutical drugs and their transporter-mediated uptake into cells: What we (need to) know and how we can do so. *Drug Discov. Today* **2013**, *18*, 218–239. [[CrossRef](#)] [[PubMed](#)]
44. Varnek, A. *Cheminformatics Approaches to Virtual Screening*; Royal Society of Chemistry: Cambridge, UK, 2008.
45. Biasini, M.; Bienert, S.; Waterhouse, A.; Arnold, K.; Studer, G.; Schmidt, T.; Kiefer, F.; Cassarino, T.G.; Bertoni, M.; Bordoli, L.; et al. SWISS-MODEL: Modelling protein tertiary and quaternary structure using evolutionary information. *Nucleic Acids Res.* **2014**, *42*, W252–W258. [[CrossRef](#)] [[PubMed](#)]
46. Aronson, J.K. *Meyler's Side Effects of Drugs. The International Encyclopedia of Adverse Drug Reactions and Interactions*, 16th ed.; Elsevier: Oxford, UK, 2016.



CHEMICAL, ANTIOXIDANT AND ANTIBACTERIAL STUDIES OF ROMANIAN *HERACLEUM SPHONDYLIIUM*

DANIELA BENEDEC^{1#}, DANIELA HANGANU^{1#}, LORENA FILIP^{1#}, ILIOARA ONIGA^{1*}, BRÎNDUȘA TIPERCIUC^{1#}, NELI-KINGA OLAH^{2#}, ANA-MARIA GHELDIU¹, OANA RAITA³, LAURIAN VLASE¹

¹"Iuliu Hațieganu" University of Medicine and Pharmacy, 8 V. Babeș Street, Cluj-Napoca, Romania

²"Vasile Goldiș" Western University of Arad, Faculty of Pharmacy, 86 L. Rebreanu Street, Arad and SC PlantExtrakt SRL, Rădaia, Cluj, Romania

³National Institute for Research and Development of Isotopic and Molecular Technologies, 67-103 Donath Street, Cluj-Napoca, Romania

*corresponding author: ilioara4@yahoo.com

#These authors contributed equally to this work.

Manuscript received: August 2016

Abstract

In order to obtain a chemical and biological characterization of *Heracleum sphondylium* subsp. *sphondylium*, we proposed the qualitative and quantitative analysis of polyphenolic compounds from roots, stems, leaves, flowers and fruits, as well as the antioxidant and antibacterial potential evaluation. For the identification and quantification of the phenolic compounds, chromatographic and spectrophotometric methods were employed. The antioxidant activity was evaluated using DPPH (2,2-diphenyl-1-picrylhydrazyl) radical scavenging, FRAP (ferric reducing antioxidant power) and EPR (electron paramagnetic resonance) methods. The antibacterial test was performed by means of agar diffusimetric method. The HPLC (high performance liquid chromatography) phenolic profile has revealed high amounts of rutin in flowers (983.88 mg/100 g) and in leaves (477.08 mg/100 g), other flavonoids: quercitrin (15.60 mg/100 g leaves), quercetin (13.38 mg/100 g flowers) and phenol acids: ferulic acid (13.04 mg/100 g) and chlorogenic acid (4.32 mg/100 g) in roots. The flowers and leaves extracts showed the highest antioxidant capacity, according to the phenolic content. The antimicrobial tests revealed a good inhibitory activity against *S. aureus* and *L. monocytogenes* for all samples. The results of the present investigation showed both qualitative and quantitative differences between the parts of *H. sphondylium*, so it is recommended to use in practice the extract obtained from a specific organ that furnishes the higher yield of active constituents.

Rezumat

În vederea caracterizării chimice și biologice a speciei *Heracleum sphondylium* subsp. *sphondylium*, ne-am propus analiza calitativă și cantitativă a compușilor polifenolici din rădăcini, tulpini, frunze, flori și fructe, precum și evaluarea potențialului lor antioxidant și antibacterian. Identificarea și dozarea compușilor fenolici s-a realizat prin metode cromatografice și spectrofotometrice. Activitatea antioxidantă a fost evaluată prin metodele DPPH (2,2-difenil-1-picrilhidrazil), FRAP (activitatea antioxidantă totală prin reducerea fierului) și EPR (rezonanța electronică paramagnetică), iar cea antibacteriană prin metoda difuzimetrică. Profilul fenolic a pus în evidență cantități mari de rutozidă în flori (983,88 mg/100 g) și în frunze (477,08 mg/100 g), dar și alte flavonoide: quercitrină în frunze (15,60 mg/100 g), quercetol în flori (13,38 mg /100 g) și acizi fenolici: acid ferulic (13,04 mg/100 g) și acid clorogenic (4,32 mg/100 g) în rădăcini. Extractele obținute din flori și frunze au avut cea mai mare capacitate antioxidantă, în concordanță cu conținutul în compuși fenolici. Testele antimicrobiene au evidențiat o activitate antibacteriană bună pe *S. aureus* și *L. monocytogenes*, pentru toate probele. Rezultatele acestui studiu au arătat diferențe calitative și cantitative semnificative între cele cinci produse naturale medicinale, care stau la baza unei utilizări corecte în practică a extractelor obținute din organele care conțin cele mai multe principii active.

Keywords: *Heracleum sphondylium*, plant parts, polyphenols, antioxidant, antibacterial

Introduction

The genus *Heracleum* L. from the *Apiaceae* family contains 3 species, 3 subspecies and a hybrid, spread in Romania. Among them, *Heracleum sphondylium* L. (hogweed) is an herbaceous plant with stem hollow, leaves pinnate, often with 5 broad, lobed and toothed segments, upper leaves with large inflated bases, white flowers, 5 to 10 mm in large

umbels up to 15 cm across with 12 to 25 rays and petals of outer flowers very unequal [1, 2, 13]. The roots and aerial parts are widely used in traditional food and medicine for its tonic, aphrodisiac, vasodilator, antihypertensive, sedative, digestive properties, in the treatment of digestive disorders (dyspepsia, diarrhoea), hypertension, healing wounds, menstrual problems [1, 2]. In Romania, the extract of aerial parts is reputed to be aphrodisiac and antihypertensive

and to treat the male and female sterility, impotence, frigidity, hypertension etc. [14]. Modern biological studies have shown that *H. sphondylium* has a vaso-relaxant action, *H. sphondylium* subsp. *artvinense* is antimicrobial, *H. sphondylium* subsp. *ternatum* is antioxidant, anti-bacterial, cytotoxic and the extract of *H. sphondylium* subsp. *sphondylium* upper aerial part revealed anti-oxidant, antifungal and germination inhibitory activity [3-5, 9-11, 14]. Phytochemical investigations on this species showed the predominance of furocoumarins (bergapten, isopimpinellin, heraclenin,) in fruits, seeds and roots and the presence of essential oil (with octyl acetate, octyl butanoate, *n*-octanol, apiol, *ar*-curcumene) [8-12, 14].

The present studies carried out on roots, stems, leaves, flowers and fruits harvested from Romanian (north-west area) *H. sphondylium* subsp. *sphondylium* are the first report in terms of the phenolic chemical composition and the evaluation of the biological potential for possible therapeutic applications in modern medicine.

Materials and Methods

Plant materials consisted of roots, stems, leaves, flowers and fruits of *H. sphondylium* subsp. *sphondylium* (Voucher No. 37), identified and harvested in 2015 from the spontaneous flora from Ciucea (Bihor, Romania) by Prof. Dr. biologist Mircea Tămaş. The samples preparation: 5 g of plant material powder were extracted with 50 mL of 70% ethanol (Merck), for 30 min on water bath, at 60°C. The samples were then cooled down and centrifuged at 4500 rpm for 15 min. and the supernatants were recovered [6, 7, 16].

Chemicals: All necessary substances were purchased from Sigma-Aldrich (Steinheim, Germany), Merck (Darmstadt, Germany) and Alfa-Aesar (Karlsruhe, Germany).

HPLC analysis. HPLC-MS analysis was performed using the chromatographic conditions previously described [6, 7, 16]. Quantitative determinations were performed using an external standard method. The polyphenolic compounds of the extracts were identified based on their retention time, UV and MS spectra as compared to the standards. Calibration curves in the 0.5 - 50 mg/mL range with good linearity ($R^2 > 0.999$) for a five points plot were used to determine the concentration of polyphenols.

Determination of polyphenolic compounds. Quantitative determinations of total polyphenols (TPC), flavonoids and caffeic acid derivatives were carried out using spectrophotometric methods. Gallic acid, rutin and caffeic acid reagents were used as standards [6, 7, 16].

Evaluation of the antioxidant activity. The extracts were screened for antioxidant activity using three *in vitro* assay models, the DPPH (2,2-diphenyl-1-

picrylhydrazyl), FRAP (ferric reducing/antioxidants power) and EPR (electron paramagnetic resonance) assays [6, 7, 15, 16]. The DPPH· scavenging activity assay is based on the spectrophotometric measurement of the DPPH concentration change, resulting from the reaction with an antioxidant. The FRAP method is based on the change in the colour of a complex with iron (III) ion of the 2,4,6-tri(2-pyridyl)-1,3,5-triazine (TPTZ) radical, due to the reduction of the ferric ion to the ferrous iron in this complex. As antioxidant standard Trolox was used. An absorbance curve was built in function of Trolox mass, the correlation coefficient (R^2) for this curve being 0.992. The final results were converted to μM Trolox equivalents/100 mL extract. EPR measurements for the DPPH test have been made on a Bruker EPR spectrometer which is equipped with X-band (9.54 GHz) Microwave Bridge; EPR spectra have been registered at various time points. The relative concentration changes of the paramagnetic species have been achieved with double integration of the spectra (Integral intensity) using X EPR software [6, 7].

Determination of the antibacterial activity

The extracts were investigated concerning the activity on the most common human pathogenic microbial strains: *S. aureus* (ATCC 49444), *L. monocytogenes* (ATCC 13076), *S. typhimurium* (ATCC 14028), *E.coli* (ATCC 25922), using a disc-diffusion assay previously described [16].

Results and Discussion

The concentrations of the identified polyphenolic compounds by HPLC method in all the five analysed samples are presented in Table I and the HPLC chromatograms are shown in Figures 1 and 2. Gentisic acid was identified only in *H. sphondylium* flowers while the caffeic acid was also found in leaves and fruits. Chlorogenic acid was identified in all the parts of the plant, but it was quantified only in the roots and stems extracts (about 4.5 mg/100 g). The *p*-coumaric acid was found in roots, leaves, flowers and fruits extracts, but in small quantities. Ferulic acid was present in flowers and leaves and in higher quantity in roots (13.04 mg/100 g). Three flavonoid glycosides (isoquercitrin, rutin, quercitrin) were found in high concentrations in leaves and flowers (eg. Iso-quercitrin: 14.37 mg/100 g flowers and 15.60 mg/ 100 g leaves; quercitrin 15.60 mg/100 g leaves). The levels of rutin in the five samples have dropped in the order: flowers > leaves > stems > fruits > roots, the flowers extracts being the richest in rutin (983.88 mg/100 g). Four flavonoid aglycones (luteolin, quercetin, kaempferol and apigenin) were identified, but only quercetin was present in all samples, the flowers containing the greatest amount (13.38 mg/ 100 g). Our results showed that the

extracts of leaves, flowers and fruits are rich in flavonoids, especially rutin, whereas the extract of

roots contains phenol acids, especially ferulic acid.

Table I

Phenolic compounds in different organs of *H. sphondylium* (mg polyphenols/100 g plant material)

Phenolic compounds	RT ± SD (min)	H. roots	H. stems	H. leaves	H. flowers	H. fruits
Caffeic acid	5.60 ± 0.04			< 0.2	< 0.2	< 0.2
Chlorogenic acid	5.62 ± 0.05	4.32 ± 1.12	4.70 ± 0.20	< 0.2	< 0.2	< 0.2
Gentisic acid	6.52 ± 0.04				< 0.2	
<i>p</i> -Coumaric acid	9.48 ± 0.08	1.22 ± 0.04		< 0.2	2.06 ± 0.23	0.38 ± 0.04
Ferulic acid	12.8 ± 0.10	13.04 ± 0.95		< 0.2	1.06 ± 0.15	
Isoquercitrin	19.60 ± 0.10		0.81 ± 0.13	15.60 ± 0.59	14.37 ± 0.62	
Rutin	20.20 ± 0.15	0.11 ± 0.02	40.79 ± 3.20	477.08 ± 7.93	983.88 ± 15.11	11.99 ± 0.65
Quercitrin	23.64 ± 0.13			15.60 ± 2.39	0.92 ± 0.07	
Quercetin	26.80 ± 0.15	< 0.2	< 0.2	0.61 ± 0.08	13.38 ± 1.11	0.11 ± 0.03
Luteolin	29.10 ± 0.19					0.88 ± 0.11
Kaempferol	32.48 ± 0.17				1.27 ± 0.06	
Apigenin	33.10 ± 0.15				< 0.2	

Notes: H, *Heracleum*; SD, standard deviation. Values are the mean ± SD (n = 3).

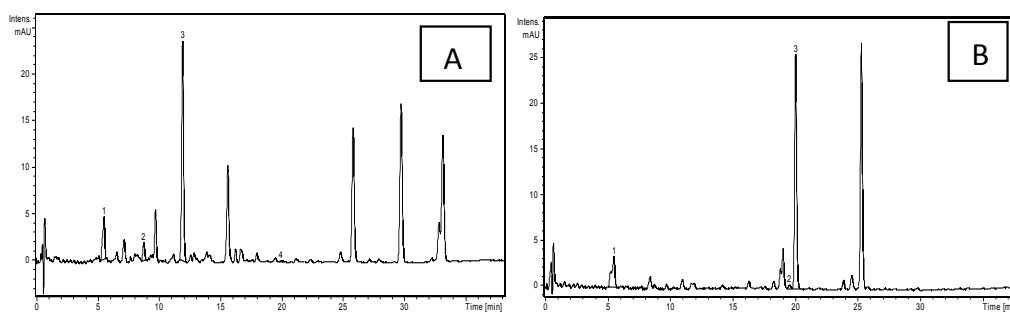


Figure 1.

HPLC chromatograms of *H. sphondylium* roots (A) and stems (B)

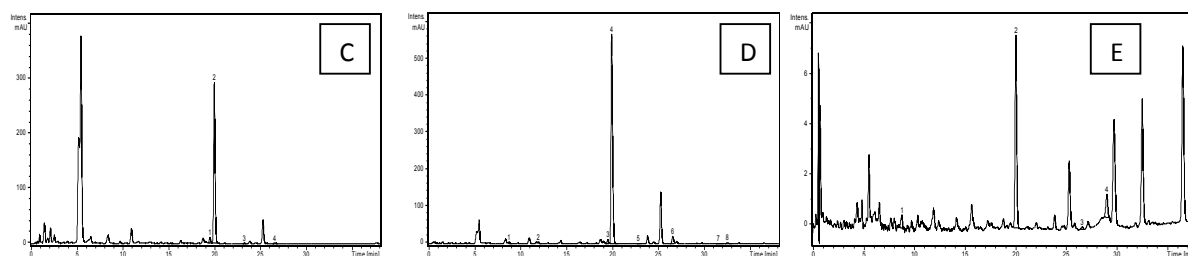


Figure 2.

HPLC chromatograms of *H. sphondylium* leaves (C), flowers (D) and fruits (E)

Table II

Polyphenolic contents and antioxidant activity of *H. sphondylium* extracts

<i>Heracleum</i> samples	TPC (g GAE/100 g)	Flavonoids (g RE/100 g)	Caffeic acid derivatives (g CAE/100 g)	DPPH IC ₅₀ µg/mL	FRAP µM Trolox/100 mL	EPR Integral intensity
roots (H ₁)	0.56 ± 0.08	0.02 ± 0.005	-	> 200	153 ± 7.00	115 ± 5
stems (H ₂)	0.18 ± 0.01	0.10 ± 0.01	-	> 200	63 ± 6.00	113 ± 7
leaves (H ₃)	3.48 ± 0.51	1.03 ± 0.06	2.26 ± 0.23	116.22 ± 2.78	1128 ± 12.00	101 ± 9
flowers (H ₄)	3.32 ± 0.27	2.84 ± 0.35	0.43 ± 0.05	168.94 ± 6.05	710 ± 9.00	59 ± 4
fruits (H ₅)	0.69 ± 0.10	-	0.26 ± 0.03	> 200	48 ± 2.00	104 ± 6
Trolox	-	-	-	11.20 ± 0.20	2073.91 ± 14.09	
DPPH						543 ± 37

Notes: Each value is the mean ± SD of three independent measurements. GAE, RE, CAE: gallic acid, rutin, caffeic acid equivalents; IC₅₀: half maximal inhibitory concentration.

The levels of TPC in the five samples decreased in the order: leaves > flowers > fruits > roots > stems.

The flowers contain a large amount of flavonoids (2.84%). The highest level of caffeic acid derivatives

was found in leaves (2.26%), while in roots and stems were not found. Similar results to ours were obtained for the aerial parts of *H. sphondylium* from Serbia [11].

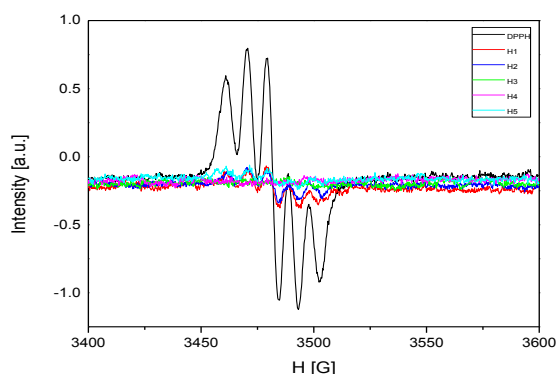


Figure 3.

EPR - the rate of interaction between the extracts and DPPH radical

The antioxidant potential was determined by three methods. The antioxidant properties values obtained by DPPH and FRAP revealed a great antioxidant activity of the tested leaves and flowers extracts, while the roots, stems and fruits extracts revealed a weak antioxidant capacity ($IC_{50} > 200 \mu\text{g/mL}$). Other authors reported a good antioxidant activity

of *H. sphondylium* aerial parts extract (Pitești, Romania) [5]. Concerning the EPR method, as expected, the integral intensity of DPPH is notably reduced by the antioxidant extracts with the integral intensity values of the five extracts (Table II, Figure 3). Thus the flowers extract exhibited an antioxidant effect by two times higher than the other samples. The EPR measurement are in line with the DPPH and FRAP assays results.

The results of the *in vitro* activity of *H. sphondylium* extracts against bacteria are summarized in Table III. The results showed a variation in the antimicrobial properties of the five extracts. Gram-negative bacteria tested did not show any sensitivity to all extracts (inhibition diameter - 6 mm), while all samples demonstrated some activity against gram-positive strains. The most pronounced activity on *S. aureus* (inhibition diameter - 18 mm) was shown by the leaves and flowers extracts, quite similar with the gentamicin. The roots and fruits extracts showed a moderate antibacterial activity against *L. monocytogenes* (roots) and *S. aureus* (fruit) and low activity against the other tested bacterial pathogens. The results of the present investigation suggested that the extracts obtained from different parts of *H. sphondylium*, the leaves and flowers extracts especially, exhibited activity against Gram-positive bacteria.

Table III

Antibacterial activity of *H. sphondylium* extracts

<i>Heracleum</i> samples	Zone of inhibition (mm)			
	<i>Staphylococcus aureus</i>	<i>Listeria monocytogenes</i>	<i>Escherichia coli</i>	<i>Salmonella typhimurium</i>
roots	10 ± 1.50	16 ± 1.00	6 ± 0.00	6 ± 0.00
stems	8 ± 0.50	12 ± 0.50	6 ± 0.00	6 ± 0.00
leaves	18 ± 2.00	12 ± 0.30	6 ± 0.00	6 ± 0.00
flowers	18 ± 0.00	14 ± 0.10	6 ± 0.00	6 ± 0.00
fruits	16 ± 0.02	10 ± 0.00	6 ± 0.00	6 ± 0.00
Gentamicin	19 ± 0.60	18 ± 1.00	22 ± 0.50	18 ± 0.00

Each value is the mean ± SD of four independent measurements. Gentamicin (10 $\mu\text{g/well}$) was used as positive control.

Conclusions

In the present investigation, it was determined the phenolic composition, the antioxidant and anti-bacterial activities for Romanian *Heracleum sphondylium* subsp. *Sphondylium*, with the aim of better phytochemical and biological assessments. The comparative phytochemical study on roots, stems, leaves, flowers and fruits, showed large qualitative and quantitative differences between the organs of the plant. The leaves and flowers extracts were rich in active principles (TPC, flavonoids and caffeic acid derivatives). The antioxidant activity evaluated by the DPPH, FRAP and EPR methods indicated that the leaves and flowers extracts were more antioxidant, related with the polyphenolic total content. Concerning the antibacterial effect, *H. sphondylium* aerial parts extracts (leaves, flowers) could be used as agents especially against *S. aureus* strains.

Therefore, our results highlight that the leaves and flowers of *H. sphondylium* subsp. *sphondylium* may be used as a source of antioxidant flavonoids, as well as antibacterial agents in pharmaceuticals and food chains.

References

1. Bahadori B.M., Dinparast L., Zengin G., The genus *Heracleum*: a comprehensive review on its phytochemistry, pharmacology, and ethnobotanical values as a useful herb. *Compr. Rev. Food Sci. Food Saf.*, 2016; 15: 1018-1039.
2. Ciesla L., Bogucka-Kocka A., Hajnos M., Petruczynik A., Waksmundzka-Hajnos M., Two-dimensional thin-layer chromatography with adsorbent gradient as a method of chromatographic fingerprinting of furanocoumarins for distinguishing selected varieties and forms of *Heracleum* spp. *J. Chromatogr. A*, 2008; 1207(1-2): 160-168.

3. Dusko B.L., Comic L., Soluji C., Sukdolak S., Antibacterial activity of some plants from family *Apiaceae* in relation to selected phytopathogenic bacteria. *Kragujevac J. Sci.*, 2006; 28: 65-72.
4. Ergene A., Guler P., Tan S., Mrc S., Hamzaoglu E., Duran A., Antibacterial and antifungal activity of *Heracleum sphondylium* subsp. *artvinens*. *Afr. J. Biotechnol.*, 2006; 5: 1087-1089.
5. Fierascu R.C, Padure I.M., Avramescu S.M, Ungureanu C, Bunghez R.I., Ortan A., Dinu-Pirvu C., Fierascu I., Soare L.C., Preliminary assessment of the antioxidant, antifungal and germination inhibitory potential of *Heracleum sphondylium* L. (*Apiaceae*). *Farmacia*, 2016; 64(3): 403-408.
6. Hanganu D., Benedec D., Vlase L., Popica I., Bele C, Raita O, Gheldiu A.M., Mihali C.V., Țărmure V., Polyphenolic content and antioxidant activity of *Chrysanthemum parthenium* extract. *Farmacia*, 2016; 64(4): 498-501.
7. Ivănescu B., Vlase L., Corciovă A., Lazăr M.I., Artemisinin evaluation in Romanian *Artemisia annua* wild plants using a new HPLC/MS method. *Natural product research*, 2011; 25(7): 716-722.
8. Iscan G., Demirci F., Kurkcuoğlu M., Kivanc M., Baser K.H., The bioactive essential oil of *Heracleum sphondylium* L. subsp. *ternatum* (Velen.) Brummitt. *Z. Naturforsch C*, 2003; 58(3-4): 195-200.
9. Karuppusamy S., Muthuraja G., Chemical composition and antioxidant activity of *Heracleum sprengeianum* (Wight and Arnott) essential oils growing wild in Peninsular India. *Iran J. Pharm. Res.*, 2011; 10(4): 769-775.
10. Maggi F., Quassinti L., Bramucci M., Lupidi G., Petrelli D., Vitali L.A., Papa F., Vittori S., Composition and biological activities of hogweed (*Heracleum sphondylium* L. subsp. *ternatum* (Velen.) Brummitt) essential oil and its main components octyl acetate and octyl butyrate. *Nat. Prod. Res.*, 2014; 28(17): 1354-1363.
11. Matejic J.S., Dzamic A.M., Mihajilov-Krstev T., Ristic M.S., Ranelovic V.N., Krivošej Z.Đ., Marin D.P., Chemical composition, antioxidant and antimicrobial properties of essential oil and extracts from *Heracleum sphondylium* L. *J. Essent. Oil-Bear. Plants*, 2016; 19(4): 944-953.
12. Ozek T., Demirci B., Baser K., Comparative study of the essential oils of *Heracleum sphondylium* ssp. *ternatum* obtained by micro-and hydro-distillation methods. *Chem. Nat. Compd.*, 2002; 38: 48-50.
13. Sarbu I., Stefan N., Oprea A., Vascular plants from Romania. Ed. Victor B Victor, 2013; 444, (available in Romanian).
14. Senejoux F., Demougeot C., Cuciureanu M., Miron A., Cuciureanu R., Berthelot A., Girard-Thernier C., Vasorelaxant effects and mechanisms of action of *Heracleum sphondylium* L. (*Apiaceae*) in rat thoracic aorta. *J. Ethnopharmacol.*, 2013; 147(2): 536-539.
15. Tero-Vescan A., Vari C.E., Muntean D.L., Dogaru M.T., Filip C., Imre S., Determination of genistein in rat liver and kidney by a HPLC/UV method. Possible extrapolation from animals to humans. *Rev Romana Med Lab.*, 2014; 22(1): 119-127.
16. Vlase L., Benedec D., Hanganu D., Damian G., Csillag I., Sevastre B., Mot A.C., Silaghi-Dumitrescu R., Tilea I. Evaluation of antioxidant and antimicrobial activities and phenolic profile for *Hyssopus officinalis*, *Ocimum basilicum* and *Teucrium chamaedrys*. *Molecules*, 2014; 19(5): 5490-5507.

Article

New Thiazolyl-triazole Schiff Bases: Synthesis and Evaluation of the Anti-*Candida* Potential

Anca Stana ¹, Alexandra Enache ¹, Dan Cristian Vodnar ², Cristina Nastasă ^{1,*}, Daniela Benedec ³, Ioana Ionuț ¹, Cezar Login ⁴, Gabriel Marc ¹, Ovidiu Oniga ¹ and Brîndușa Tiperciuc ¹

¹ Department of Pharmaceutical Chemistry, "Iuliu Hațieganu" University of Medicine and Pharmacy, 41 Victor Babeș Street, RO-400012 Cluj-Napoca, Romania; teodora_anca@yahoo.com (A.S.); ale.enache@yahoo.de (A.E.); ionut.ioana@umfcluj.ro (I.I.); marc.gabriel@umfcluj.ro (G.M.); onigao65@yahoo.com (O.O.); brandu32@yahoo.com (B.T.)

² Department of Food Science, University of Agricultural Sciences and Veterinary Medicine, 3-5 Mănăstur Street, RO-400372 Cluj-Napoca, Romania; dan.vodnar@usamvcluj.ro

³ Department of Pharmacognosy, "Iuliu Hațieganu" University of Medicine and Pharmacy, 12 Ion Creangă Street, RO-400010 Cluj-Napoca, Romania; dani_67ro@yahoo.com

⁴ Department of Physiology, "Iuliu Hațieganu" University of Medicine and Pharmacy, 1 Clinicilor Street, RO-400006 Cluj-Napoca, Romania; cezar.login@umfcluj.ro

* Correspondence: cmoldovan@umfcluj.ro or cris.moldovan@yahoo.com; Tel.: +40-745-264393

Academic Editor: Panayiotis A. Koutentis

Received: 31 October 2016; Accepted: 17 November 2016; Published: 22 November 2016

Abstract: In the context of the dangerous phenomenon of fungal resistance to the available therapies, we present here the chemical synthesis of a new series of thiazolyl-triazole Schiff bases **B1–B15**, which were in vitro assessed for their anti-*Candida* potential. Compound **B10** was found to be more potent against *Candida* spp. when compared with the reference drugs Fluconazole and Ketoconazole. A docking study of the newly synthesized Schiff bases was performed, and results showed good binding affinity in the active site of co-crystallized Itraconazole-lanosterol 14 α -demethylase isolated from *Saccharomyces cerevisiae*. An in silico ADMET (absorption, distribution, metabolism, excretion, toxicity) study was done in order to predict some pharmacokinetic and pharmacotoxicological properties. The Schiff bases showed good drug-like properties. The results of in vitro anti-*Candida* activity, a docking study and ADMET prediction revealed that the newly synthesized compounds have potential anti-*Candida* activity and evidenced the most active derivative, **B10**, which can be further optimized as a lead compound.

Keywords: Schiff base; triazole; fungicidal activity; docking; ADME

1. Introduction

Over the last years, invasive fungal infections caused by *Candida* have become a major cause of morbidity and mortality in immunocompromised patients. In clinic, the number of antifungal agents that are available is limited. These drugs belong to major classes of azoles, allylamines, polyenes, fluopyrimidines, and thiocarbamates. The azole molecules are the most widely used [1]. They act by inhibiting CYP51 (lanosterol-14 α -demethylase), an enzyme that catalyzes the demethylation of lanosterol into ergosterol. Due to the inhibition, the steroid accumulates and alters the permeability and rigidity of plasma membranes. Azole antifungal agents inhibit the enzyme by forming a bond between the heterocyclic nitrogen atom (N-3 of imidazole and N-4 of triazole) and the heme iron atom in the binding site of CYP51. Because of the existence of CYP51 in fungi and mammals and because of the effects of these compounds on CYP3A4 (Cytochrome P450 3A4), the selective inhibition of fungal CYP51 is very important and results in an increased therapeutic index [2].

Unfortunately, the extensive use of azole molecules as antifungals has led to the appearance of severe fungal resistance. The majority of candidiasis is caused by *Candida albicans*, followed by *C. glabrata*, *C. tropicalis*, *C. parapsilosis* and *C. krusei*. Some types of *Candida* became resistant to the first and second line of antifungal treatment (fluconazole, echinocandins). Most of the isolated strains are of *C. glabrata*. A growing concern worldwide is represented by the multidrug-resistant *Candida* infections, which no longer respond to the treatment with fluconazole or echinocandins. The number of drugs available is surpassed by the large spread of fungal infections. Furthermore, they present a series of disadvantages, such as reduced bioavailability, marked hepatotoxicity and many drug interactions, which limit their use. Due to the facts presented above, the resistance and the toxicity of available antifungals, and the development of new antifungal molecules, which can act by a different mechanism of action, have a better pharmacokinetic and safety profile and are efficient against the resistant strains, are urgently required.

Schiff bases, key intermediates in organic synthesis and also as common ligands in the coordination chemistry [3], have been shown to exhibit a broad range of biological activities, including antifungal, antibacterial [4], antiviral, antihelminthic, antiproliferative [5], antioxidant [6]. The imine group present in such compounds has been shown to be essential for their biological activities [7]. Thiazoles, triazoles and their derivatives play an important part in heterocyclic chemistry due to their biological activity [8–10]. Fluconazole and voriconazole, broad spectrum antifungals, contain these heterocyclic systems incorporated into their structures. The ample evidence reported in the literature on the biological potential of Schiff bases containing thiazole and triazole moieties in their structure [11] led us to the synthesis, physico-chemical characterization and antifungal evaluation of new Schiff bases containing both heterocycles.

The pharmacokinetic and pharmacodynamic behavior of molecules inside the human body is influenced by their molecular properties, molecular size, flexibility and the presence of different pharmacophore features. Almost one half of the drug failures in development phases are due to suboptimal pharmacokinetic properties and unacceptable toxicity [12]. The in vivo experimental determination of pharmacokinetic parameters of newly synthesized compounds is uneconomical and time consuming. From this point of view, computational methods which can predict the ADMET (absorption, distribution, metabolism, excretion, toxicity) properties of the new compounds could help to eliminate the molecules likely to fail in the early stage of drug discovery. In order to predict some pharmacokinetic and pharmacotoxicological properties, an in silico ADME-Tox (absorption, distribution, metabolism, excretion, toxicity) study was realized on the newly synthesized compounds.

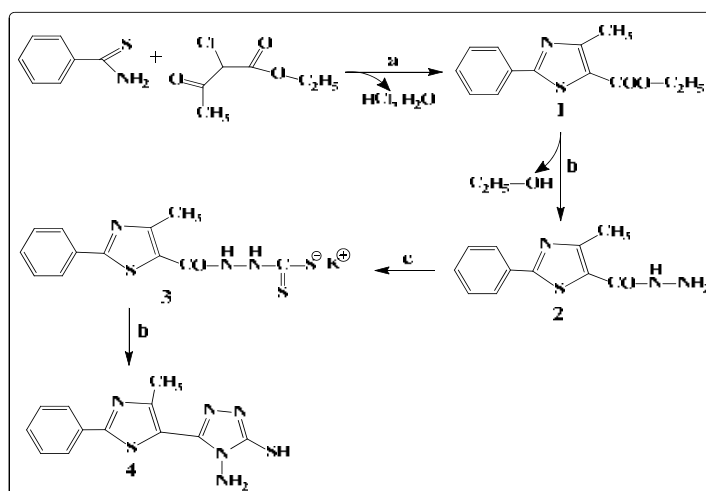
Docking studies are useful in drug discovery to predict the docked structure of the ligand-receptor complex and to rank the ligand molecules based on their binding energy. Docking protocols help elucidating the most energetically favorable binding pose of a ligand to its receptor. The new derivatives were docked into the active site of lanosterol-14 α -demethylase from *Saccharomyces cerevisiae*, to facilitate the understanding of the antifungal mechanism of action of the synthesized Schiff bases.

2. Results and Discussion

2.1. Chemistry

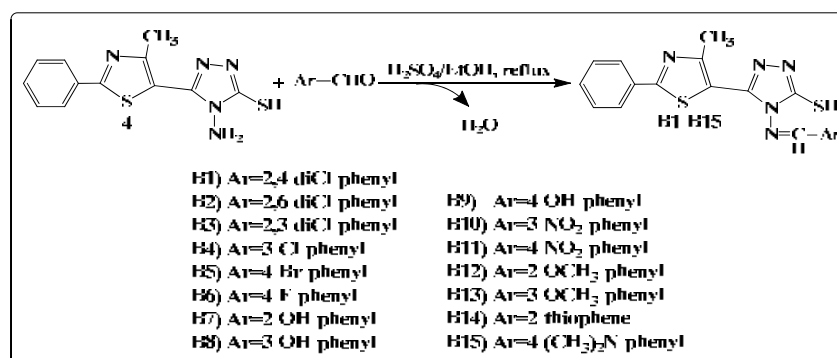
The general synthetic route for the synthesis of 4-amino-5-(4-methyl-2-phenylthiazol-5-yl)-4H-1,2,4-triazole-3-thiol is illustrated in Scheme 1. The general method known as Hantzsch condensation has been used for the synthesis in good yields (85%–90%) of 4-methyl-2-phenylthiazole carboxylate 1. The 4-methyl-2-phenylthiazole-5-carbohydrazide 2 was obtained by treating compound 1 with hydrazine hydrate, under reflux, in a water bath, for 3 h. Then, compound 2 was treated with CS₂ and KOH, at room temperature, to give the potassium 2-(4-methyl-2-phenylthiazole-5-carbonyl)hydrazine-carbodithioate 3. Finally, the 4-amino-5-(4-methyl-2-phenylthiazol-5-yl)-4H-1,2,4-triazole-3-thiol 4 was obtained, in good yields (80%), by treating compound 3 with hydrazine hydrate, under reflux, for 2 h. Schiff bases B1–B15 were synthesized in good yields by the condensation of compound

4 with various aromatic or heteroaromatic aldehydes, in the presence of concentrated H_2SO_4 , used as a catalyst (Scheme 2).



Scheme 1. The synthesis of 4-amino-5-(4-methyl-2-phenylthiazol-5-yl)-4H-1,2,4-triazole-3-thiol.

^a EtOH, reflux; ^b $\text{H}_2\text{N-NH}_2/\text{EtOH}$, reflux; ^c CS_2/KOH , room temperature.



Scheme 2. Synthesis of Schiff bases.

The structures of thiazolyl-triazole Schiff bases were established by elemental analysis and on the basis of their mass spectra (MS), infrared spectra (IR), nuclear magnetic resonance ($^1\text{H-NMR}$ and $^{13}\text{C-NMR}$) spectra. The results of the C, H, N, S quantitative elemental analysis of all synthesized compounds were in accordance with the calculated values, within $\pm 0.4\%$ of the theoretical values. The spectral data confirmed the formation of the **B1–B15** Schiff bases. Details of the synthetic procedures, the yields and the physical, analytical and spectral data of the synthesized compounds are presented in the Experimental Section. Compounds **1–3** were previously reported in the literature [13,14].

Mass spectra recorded for the final products **B1–B15** gave an idea about the fragmentation of the compounds with their corresponding mass and, in all cases, revealed the correct molecular ion peaks ($M + 1$), as suggested by their molecular formulas. The absence of the NH_2 asymmetric and symmetric stretching vibrations at 3281 cm^{-1} and 3186 cm^{-1} and also the presence of $\text{N}=\text{CH}$ stretch absorption bands at $1635\text{--}1618\text{ cm}^{-1}$ in the final compounds' IR spectra provided strong evidences for the formation of Schiff bases **B1–B15**.

In the $^1\text{H-NMR}$ spectrum of compound **4**, a signal was recorded, characteristic for the amino protons, as a singlet, at 5.73 ppm. The absence of this signal from the $^1\text{H-NMR}$ spectra of the new synthesized compounds (**B1–B15**), and also the presence of a singlet characteristic to the $\text{N}=\text{CH}$ proton at 9.36–9.52 ppm further confirmed the condensation between the 4-amino-5-(4-methyl-2-phenylthiazol-5-yl)-4H-1,2,4-triazole-3-thiol **4** and the corresponding aromatic aldehydes. The 3-mercapto-

1,2,4-triazoles could exist in two tautomeric forms (Figure 1), because the labile hydrogen may be attached either to the nitrogen (the thione form) or to the sulphur atom (the thiol form) [15].

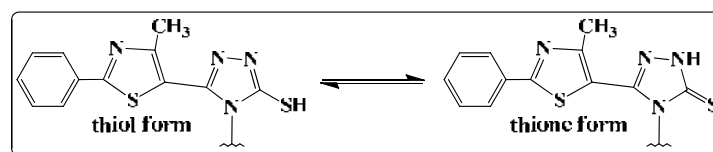


Figure 1. Thiol-thione tautomerism shown by the synthesized Schiff bases.

In the IR spectra of compounds **4** and **B1–B15**, absorption peaks were observed at 3131–3086 cm^{-1} ; due to the stretching vibration of the N-H group from the triazole ring, the absorption bands were at 1288–1257 cm^{-1} , corresponding to C=S stretching vibrations and the absence of the thiol SH absorption band at about 2600–2550 cm^{-1} (characteristic for the thiol form), proving that the compounds were in thione form, in solid state. Furthermore, in the 13.91–14.18 ppm region of the $^1\text{H-NMR}$ spectra of compounds **4** and **B1–B15**, the NH proton resonated as a singlet, indicating that the crystal structures of the compounds correspond to the thione form. The $^{13}\text{C-NMR}$ spectra of the newly synthesized compounds were consistent with the proposed structures and exhibited only the presence of thionic tautomeric form (C=S) through the presence of the exocyclic C=S peaks, at 169.88–170.25 ppm. The spectral investigations performed by us proved that thiazolyl-triazole Schiff bases **B1–B15** exist in their thione form, in solid state.

2.2. Antifungal Activity

2.2.1. Determination of Inhibition Zone Diameters

The anti-*Candida* activity was tested in vitro using the disk diffusion method, by measuring the diameters of the inhibition zones. The synthesized compounds **B1–B15** were screened against the fungal strain of *Candida albicans* ATCC 90028. The concentrations used for evaluating the antimicrobial activity were 100 $\mu\text{g}/\text{disk}$ for the synthesized compounds and for the reference substance used, fluconazole. Because the compounds are not soluble in water, the solvent used to prepare the solutions of the synthesized compounds, dimethylsulfoxide (DMSO), exhibited no inhibitory activity on the fungal strain used in the study. The obtained results are presented in Table 1, compared to fluconazole.

Table 1. The inhibition zone diameters on *Candida albicans*.

Cp	Inhibition Zone Diameter (mm)
	<i>Candida albicans</i> ATCC 90028
B1	16
B2	18
B3	18
B4	18
B5	20
B6	18
B7	18
B8	18
B9	18
B10	20
B11	20
B12	18
B13	18
B14	18
B15	18
Fluconazole	25

The values obtained for the most active compounds are marked in bold.

Analyzing the results obtained, we can observe that all the tested compounds showed zone inhibition diameters inferior to Fluconazole, used as an antifungal reference drug. Concerning the relationships between the structure of the compounds and the anti-*Candida* activity, we observed that the compounds substituted on the phenyl bound to the azomethinic group with *para*-Br (**B5**), *meta*-nitro (**B10**) and *para*-nitro (**B11**) showed the biggest zone inhibition diameters (20 mm). The other compounds, with the exception of the 2,4-dichloro substituted compound **B1** (16 mm), showed the same diameter (18 mm).

2.2.2. Determination of Minimum Inhibitory Concentration (MIC) and Minimum Fungicidal Concentration (MFC) Values

In the first screening test, we observed that the compounds showed similar anti-*Candida* activity, eleven Schiff bases having the same inhibition zone diameters (Table 1). In order to analyze the relationships between the structure of the **B1–B15** compounds and their anti-*Candida* activity, we used two less virulent *Candida albicans* strains (*C. albicans* ATCC 10231 and *C. albicans* ATCC 18804) and a non-*albicans Candida* strain (*Candida krusei*) [16–18], for the minimum inhibitory concentration (MIC) and for the minimum fungicidal concentration (MFC) tests.

The broth microdilution method was employed for the MIC test. All the synthesized compounds were tested against three strains of fungi (*Candida albicans* ATCC 10231, *Candida albicans* ATCC 18804 and *Candida krusei* ATCC 6258). Stock solutions (1 mg/mL) were prepared by dissolving the test compounds and the reference antimicrobials (fluconazole, ketoconazole) in sterile DMSO. The results are presented in Tables 2 and 3.

Table 2. Minimum Inhibitory Concentration—MIC (in $\mu\text{g/mL}$) of compounds **B1–B15**.

Cp	<i>C. albicans</i> ATCC 10231	<i>C. albicans</i> ATCC 18804	<i>C. krusei</i> ATCC 6258
B1	62.5	62.5	62.5
B2	62.5	62.5	62.5
B3	62.5	62.5	62.5
B4	62.5	62.5	62.5
B5	62.5	62.5	31.25
B6	62.5	62.5	62.5
B7	62.5	62.5	62.5
B8	62.5	31.25	62.5
B9	62.5	62.5	62.5
B10	15.62	31.25	31.25
B11	62.5	62.5	62.5
B12	62.5	62.5	62.5
B13	62.5	62.5	62.5
B14	62.5	31.25	62.5
B15	62.5	62.5	62.5
Fluconazole	62.5	62.5	62.5
Ketoconazole	31.25	31.25	31.25
Inoculum control	+++	+++	+++
Broth control	No growth	No growth	No growth

+++ indicates growth in all concentrations; the values obtained for the most active compounds are marked in bold.

From the obtained results, we can observe that all the tested compounds showed MIC values equal or inferior to systemic antifungal reference drug, Fluconazole (Table 2). The Schiff base **B10** (*meta*-nitro) is 4-fold more active than Fluconazole and 2-fold more active than the other reference local antifungal drug, Ketoconazole, respectively, on *Candida albicans* ATCC 10231. On *C. albicans* ATCC 18804, compounds **B8** (*meta*-hydroxy), **B10** and **B14** (substituted with thiophene heterocycle) were 2-fold more active than Fluconazole and equal, as potential, with Ketoconazole. Concerning the non-*albicans Candida* strain, compounds **B5** (*para*-Br) and **B10** were 2-fold more active than Fluconazole and with the same activity as Ketoconazole.

Table 3. Minimum Fungicidal Concentration—MFC (in µg/mL) of compounds **B1–B15**.

Cp.	<i>C. albicans</i> ATCC 10231	<i>C. albicans</i> ATCC 18804	<i>C. krusei</i> ATCC 6258
B1	125	125	125
B2	125	125	125
B3	125	125	125
B4	125	125	125
B5	125	125	62.5
B6	125	125	125
B7	125	125	125
B8	125	62.5	125
B9	125	62.5	125
B10	31.25	62.5	62.5
B11	125	125	125
B12	125	125	125
B13	125	125	125
B14	125	62.5	125
B15	125	125	62.5
Fluconazole	125	125	125
Ketoconazole	62.5	62.5	62.5

The values obtained for the most active compounds are marked in bold.

Determination of MFC confirmed the results previously obtained when MIC was investigated. Supplementary, we observed that Schiff bases **B8** (*meta*-hydroxy), **B9** (*para*-hydroxy) and **B10** presented the same activity against *C. albicans* ATCC 18804.

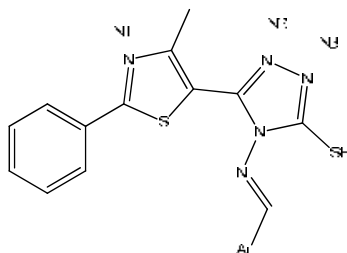
Finally, we remarked that the thiazolyl-triazole Schiff base **B10** can be considered the most promising anti-*Candida* candidate, the compound being more active than Fluconazole and with similar activity as Ketoconazole, on the three tested *Candida* strains. The MFC/MIC ratio for all tested compounds was 2, suggesting that the synthesized Schiff bases could act as fungicidal agents [19].

2.3. Molecular Docking

With the aim of elucidating the mechanism of action of synthesized Schiff bases, molecular docking studies were performed on lanosterol-14 α -demethylase from *Saccharomyces cerevisiae*. To check the settings and the accuracy of the docking method, we performed a re-docking of itraconazole, the former co-crystallized ligand with CYP51 in its active site. The root mean square deviation (RMSD) value between the top ranked predicted conformation and the observed X-ray crystal structure of the Protein Data Bank (PDB) deposited structure, was 0.324 Å. A value being below 2 Å the docking protocol was validated.

The synthesized compounds **B1–B15** and fluconazole, as a control inhibitor, were docked into the active site of lanosterol 14 α -demethylase. The predicted binding affinity of Schiff bases into the active site of the enzyme and the predicted polar contacts between them, are presented in Table 4.

Our studies showed that all of our thiazolyl-triazoles Schiff bases **B1–B15** did not covalently interact with the heme from the active site of lanosterol 14 α -demethylase, like classic antifungal azoles. They interact with the amino acids in the access channel to the active site of the lanosterol 14 α -demethylase (Figure 2, Table 4). All the compounds form hydrogen bonds between the thiazole nitrogen (N1) with Met509 or Ser382 and between the triazole nitrogens (N2, N3) with the residues Phe506 and Ser508. We also observed that the Schiff bases carrying a hydroxy-phenol substituent in *meta* position (**B8**) and the corresponding *meta*- and *para*-substituted nitro-derivatives (**B10**, **B11**) form supplementary bonds with the Arg98 from the access groove (Figure 2).

Table 4. Predicted binding affinity and polar contacts between compounds **B1–B15** and the active site of CYP51.Backbone of the compounds **B1–15**

Samples	Binding Affinity (kcal/mol)	Atom ID of Ligand	Interacting AA Residue	Bond Length (Å)
B1	−11.39	N1	Met509	3.0
		N2	Ser508	3.5
		N3	Phe506	2.6
B2	−11.85	N2	Ser508	3.5
		N3	Phe506	2.6
B3	−11.59	N1	Met509	2.9
		N2	Ser508	4.4
		N3	Phe506	2.6
B4	−11.08	N1	Ser382	3.1
		N2	Ser508	2.9
		N3	Ser508	3.2
		N3	Phe506	2.5
B5	−11.22	N1	Met509	3.2
		N2	Ser508	2.9
		N3	Phe506	2.5
B6	−10.30	N1	Met509	2.9
		N2	Phe506	2.7
		N3	Phe506	2.7
B7	−10.92	N1	Met509	2.9
		N2	Ser508	3.6
		N3	Phe506	2.6
B8	−11.25	N1	Ser382	3.1
		N2	Phe506	3.0
		N3	Phe506	2.7
		Phenolic O	Arg98	3.1
B9	−10.84	N1	Ser382	3.0
		N2	Ser508	2.9
		N3	Ser508	3.2
		N3	Phe506	2.6
B10	−12.92	N1	Met509	2.6
		N2	Ser508	3.3
		N2	Phe506	2.5
		N3	Phe506	2.5
		Nitro O	Arg98	3.0
		Nitro O	Arg98	3.2
B11	−11.70	N1	Met509	2.9
		N2	Ser508	3.5
		N3	Phe506	2.6
		Nitro O	Arg98	3.4

Table 4. Cont.

Samples	Binding Affinity (kcal/mol)	Atom ID of Ligand	Interacting AA Residue	Bond Length (Å)
B12	−11.17	N1	Ser382	2.8
		N2	Ser508	2.9
		N3	Ser508	3.0
		N3	Phe506	2.5
B13	−10.93	N1	Ser382	3.3
		N2	Ser508	3.2
		N3	Phe506	2.8
B14	−10.45	N1	Ser382	3.1
		N2	Ser508	2.8
		N3	Ser508	3.2
		N3	Phe506	2.6
B15	−11.18	N1	Met509	2.8
		N2	Ser508	3.4
		N3	Phe506	2.6
Fluconazole	−7.03	N/A	N/A	N/A

Despite the role of the azole as an important pharmacophore for the antimycotic activity, it represents also a key toxicophore for the hepatotoxicity of azole antifungal drugs, due to the coordination binding of its nitrogen atom to the iron atom of heme [20]. Because the affinity of our Schiff bases for CYP51 was attributed to the non-covalent interaction with the aminoacids from the access channel to the active site, the studies presented here can be exploited to develop new antifungal agents that specifically interact with the residues from the active site, avoiding the serious toxicity of classic azoles, which arises from coordination binding with the heme of mammalian CYTP450s.

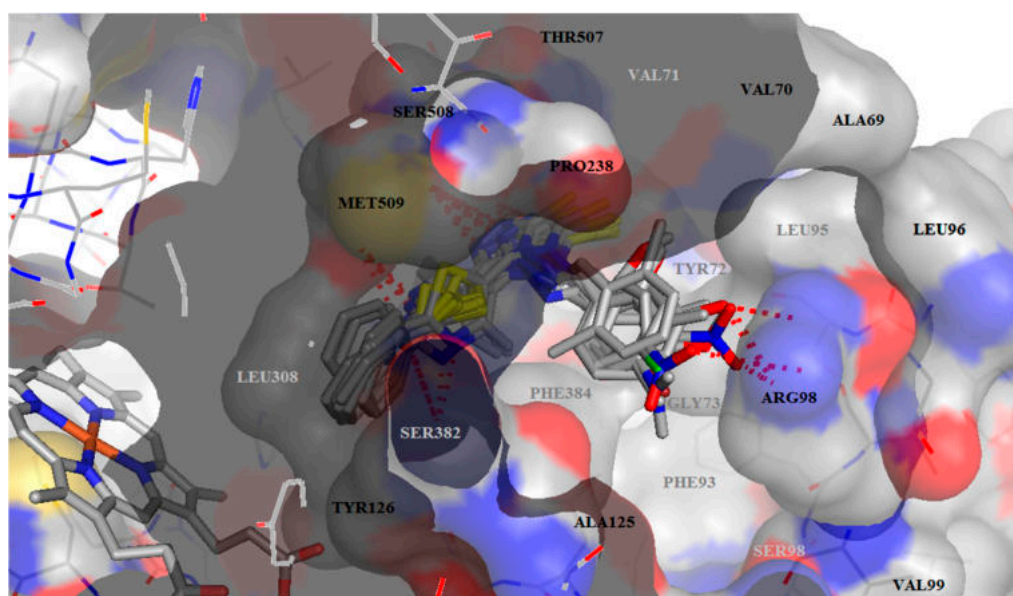


Figure 2. Docking results—A general view with all ligands inserted in the active site of CYP51. The active site and the ligands are depicted as sticks. The hydrogen bonds are depicted as dashed red lines. The foreground amino acids are in grey.

The data obtained from docking shows that all the Schiff bases have higher binding interaction energy, ranging from −10.45 to −12.92 kcal/mol relative to fluconazole (−7.03 kcal/mol) (Table 4). Figure 3 shows the representation of the binding patterns into the active site of CYP51 for the

fluconazole (green), used as the reference antifungal drug and for the Schiff base **B10** (pink) which showed the highest inhibition capacity. Non-interacting amino acids in the foreground were removed for clarity. The thiole group is not supposed to interact with amino acids from the enzyme. Our future studies will be directed towards optimizing the structure, in order to obtain compounds with a superior binding affinity and with better anti-*Candida* activity. Modulation of thiole by introducing one polar substituent, may improve the inhibition ability, because of the possible supplementary interaction with Tyr72.

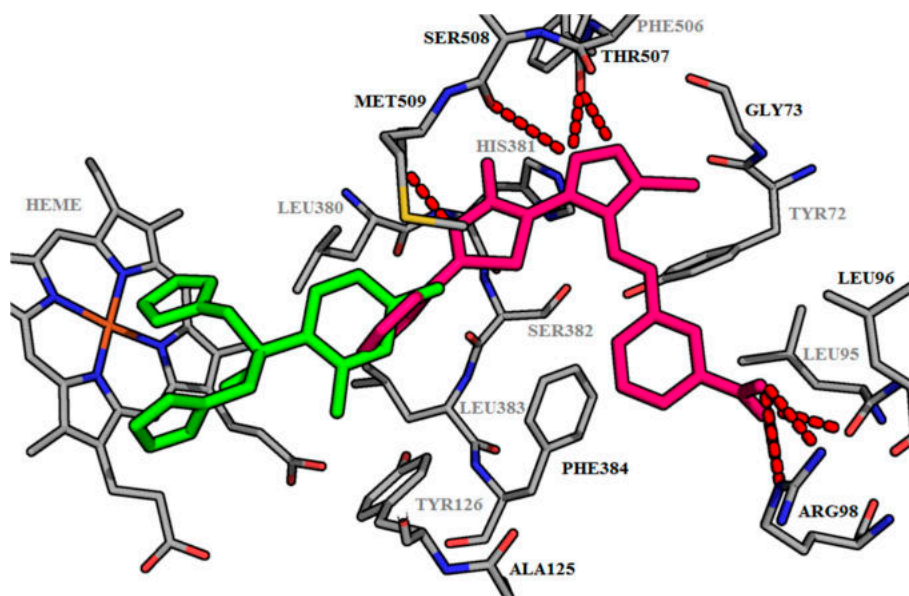


Figure 3. Binding mode of Fluconazole and **B10**. The active site of lanosterol 14 α -demethylase is depicted as sticks. The Fluconazole is depicted in green; the Schiff base **B10** in pink. The hydrogen bonds are depicted as dashed red lines. The foreground amino acids are in grey.

2.4. ADME and Molecular Property Prediction

High oral bioavailability is an important factor for the development of bioactive compounds as therapeutic agents [21]. The predictors for this are represented by a good intestinal absorption, a reduced molecular flexibility, low polar surface area and hydrogen-bonding capacity [22]. All our compounds pass Lipinski's "Rule of 5" (Table 5). Number of rotatable bonds is important for conformational changes of molecules and consequently, for the binding of receptors or channels. All tested compounds pass one of the oral bioavailability criteria, having less than 10 rotatable bonds and no chirality center, therefore exhibiting low conformational flexibility. All compounds have molar refractivity under 130.

Topological polar surface area (tPSA), that is the surface belonging to polar atoms, is a descriptor that correlates well with passive molecular transport through membranes, including the blood–brain barrier [23]. Compounds **B1–6**, **B12**, **B13** and **B15** have tPSA values less than 140 Å², passing the criteria for gastro-intestinal absorption, after oral administration (Table 5). The other compounds—**B7–11** with hydroxyl, nitro groups and thiophene substituted compound **B14**—violate this rule. The absorption percent of all the Schiff bases ranges from 50% to 66%, which is an indication of an acceptable bioavailability by oral route (>50%). On the other hand, all the compounds were predicted to have a low blood–brain barrier penetration (tPSA > 90 Å²), so, the risks of central nervous system (CNS) side effects are reduced or absent. Water solubility of our compounds is poor, for all compounds—logS value being between -6 and -10 . The compounds **B1–B5** are considered "poorly soluble" and the rest are "moderately soluble".

Table 5. Virtual ADME (absorption, distribution, metabolism, excretion) and molecular property prediction of the Schiff bases **B1–B15**.

Comp.	tPSA ^a	%Abs ^b	MW ^c	RoB ^d	HBD ^e	HBA ^f	MR ^g	logP ^h (MlogP)	LogS ⁱ	CYP2D6 Inhibitor
Rule	≤140 Å ²	-	≤1500	≤110	≤15	≤110	40–130	<5	>−4	
B1	123	66.57	446.38	4	0	4	118.24	3.77 (4.12)	−8.19	No
B2	123	66.57	446.38	4	0	4	118.24	3.69 (4.12)	−8.19	No
B3	123	66.57	446.38	4	0	4	118.24	3.42 (4.12)	−8.19	No
B4	123	66.57	411.93	4	0	4	113.23	3.86 (3.89)	−7.60	No
B5	123	66.57	456.38	4	0	4	115.92	3.35 (4.01)	−7.80	No
B6	123	66.57	395.48	4	0	5	108.18	3.3 (3.78)	−7.28	No
B7	143.23	59.59	393.49	4	1	5	110.24	3.09 (2.85)	−6.43	No
B8	143.23	59.59	393.49	4	1	5	110.24	3.12 (2.85)	−6.43	No
B9	143.23	59.59	393.49	4	1	5	110.24	3.24 (2.85)	−6.43	No
B10	168.82	50.76	422.48	5	0	6	117.04	2.78 (2.42)	−6.84	No
B11	168.82	50.76	422.48	5	0	6	117.04	2.75 (2.42)	−6.84	No
B12	132.23	63.38	407.51	5	0	5	114.71	3.98 (3.08)	−7.12	No
B13	132.23	63.38	407.51	5	0	5	114.71	3.84 (3.08)	−7.12	No
B14	151.24	56.82	383.51	4	0	4	106.09	3.26 (2.96)	−6.28	No
B15	126.24	65.45	420.55	5	0	4	122.42	3.82 (3.3)	−7.09	No

Abbreviations: ^a Topological polar surface area; ^b Absorption; ^c Molecular weight; ^d Number of rotatable bonds; ^e Number of hydrogen bond donors; ^f Number of hydrogen bonds acceptors; ^g Molar refractivity; ^h Logarithm of compound partition coefficient between *n*-octanol and water; ⁱ Logarithm of water solubility.

All Schiff bases are predicted as noninhibitors of CYP2D6, therefore the side effects (i.e., liver dysfunction) are not expected upon the administration of these compounds. Also, all are predicted to be metabolized by CYP2C9 [24,25], due to the presence of the acidic thiol group.

P-glycoprotein (P-gp) is a member of the ATP-binding cassette (ABC) transporter family involved in intestinal absorption, drug metabolism, and brain penetration, and its inhibition can seriously alter a drug's bioavailability and safety [26]. The drug induced phospholipidosis is a disorder characterized by the excess accumulation of phospholipids in tissues and is associated with drug induced toxicity [27]. The results obtained showed that none of our Schiff bases is a substrate for P-gp and none induce phospholipidosis.

According to the above ADME and toxicity results, the thiazolyl-triazole Schiff bases **B1–15** show good pharmacokinetic properties, but with some limitations, such as moderate gastrointestinal absorption and no blood–brain barrier penetration. All molecules are accepted as drug-like, passing Lipinski's "Rule of five". The predicted parameters are within the range of accepted values. However, further optimization should be performed on tested compounds, in order to achieve better ADME properties. A mandatory improvement for the properties of the newly synthesized derivatives would be to increase their bioavailability. Small chemical modulations on the molecules could improve the ADME properties. Potential chemical modulations, such as alkylation, on the ionisable thiol moiety, would severely change the ADME properties of the resulted molecules, in order to extend the potential oral administration.

3. Materials and Methods

3.1. Chemistry

All chemicals and reagents were obtained from commercial sources and were used as supplied, without further purification. Compounds **1–3** were previously reported and were synthesized by us according to methodologies described in the literature [13,14].

Melting points were determined with an Electrothermal melting point meter in the open glass capillary method and are uncorrected. The reaction progress and purity of the synthesized compounds were monitored by analytical thin layer chromatography (TLC) using Merck precoated Silica Gel 60F₂₅₄ sheets (Darmstadt, Germany), heptane–ethyl-acetate 3:7 elution system and ultraviolet UV light (254 nm) for visualization. MS analyses were performed at 70 eV with an Agilent gas chromatograph

6890 (Darmstadt, Germany) equipped with an apolar Macherey Nagel Permabond SE 52 capillary column (Dueren, Germany) and with an LCMS Shimadzu Mass Spectrometer (Shimadzu Corporation, Columbia, MD, USA). Elemental analysis was registered with a Vario El CHNS instrument (Hanau, Germany). IR spectra were recorded on a JASCO FT-IR-4100 spectrometer (Cremella, Italy) using the ATR technique (Attenuated Total Reflectance). Nuclear magnetic resonance ($^1\text{H-NMR}$) spectra were recorded at room temperature on a Bruker Avance NMR spectrometer (Karlsruhe, Germany) operating at 400 and 500 MHz, using tetramethylsilane (TMS) as an internal standard (chemical shift in δ ppm) and were in accordance with the assigned structures. The samples were prepared by dissolving the compounds in $\text{DMSO-}d_6$ ($\delta_{\text{H}} = 2.51$ ppm) as a solvent and spectra were recorded using a single excitation pulse of 12 μs ($^1\text{H-NMR}$). Spin multiplets are given as *s* (singlet), *d* (doublet), *t* (triplet) and *m* (multiplet). $^{13}\text{C-NMR}$ spectra were recorded on a Bruker Avance NMR spectrometer (Karlsruhe, Germany), operating at 125 MHz, in $\text{DMSO-}d_6$, using a waltz-16 decoupling scheme.

General procedure for the synthesis of ethyl 4-methyl-2-phenylthiazole-5-carboxylate (1) [13]. An amount of 1 mmol (0.137 g) of thiobenzamide was dissolved in 10 mL of ethanol and 0.20 mL of ethyl 2-chloroacetoacetate was added. The reaction mixture was refluxed for 3 h on a water bath. After cooling, the reaction mixture was poured onto a mixture of ice and water. The formed precipitate was filtered, then washed with distilled water, to remove traces of the remaining halocarbonyl and then vacuum dried.

General procedure for the synthesis of 4-methyl-2-phenylthiazole-5-carbohydrazide (2) [14]. An amount of 117.4 mmol (5.87 g) of hydrazine hydrate was added to the alcoholic solution of the carboxylate of 4-methyl-2-phenylthiazole (**1**) (58.7 mmol in 100 mL absolute ethanol). The resulting reaction mixture was refluxed on a water bath, at 100 °C, for 4 h, and then it was concentrated under reduced pressure. Distilled water was added to the obtained precipitate and then the mixture was subjected to low pressure filtration, washed with distilled water, dried and recrystallized from absolute ethanol.

General procedure for the synthesis of potassium 2-(4-methyl-2-phenylthiazole-5-carbonyl)hydrazinecarbodithioate (3) [14]. To the alcoholic solution of 4-methyl-2-phenylthiazol-5-carbohydrazide **2** (20 mmol in 40 mL of alcohol) was added a suspension of 30 mmol (1.68 g) of KOH in 60 mL of absolute ethanol and 30 mmol (3.04 g) CS_2 . The reaction mixture was stirred for 3 h at room temperature to obtain a quantitative precipitation. The reaction mass was filtered, washed with diethyl ether and dried in order to yield a bright yellow precipitate.

General procedure for the synthesis of 4-amino-5-(4-methyl-2-phenylthiazol-5-yl)-4H-1,2,4-triazole-3-thiol (4). The alcoholic solution of potassium 2-(4-methyl-2-phenylthiazole-5-carbonyl) hydrazinecarbodithioate **3** (10 mmol in 40 mL of absolute ethanol) was treated with 10 mmol of hydrazine hydrate (80%). The reaction mixture was refluxed for 2 h. After cooling, the reaction mass was poured onto water and then acidified with a HCl (10%) solution. The reaction mixture was allowed to stand for 2 h for quantitative precipitation and evolution of H_2S . The obtained precipitate was filtered and washed with ethanol. The obtained compound was recrystallized from absolute ethanol. Yield 80.0% (0.23 g); m.p. 165 °C; light yellow powder; Anal. Calcd for $\text{C}_{12}\text{H}_{11}\text{N}_5\text{S}_2$ (289.38): C, 49.81; H, 3.83; N, 24.20; S, 22.16; Found: C, 49.83; H, 3.85; N, 24.24; S, 22.13; IR (ATR, cm^{-1}): 3281 (ν NH_2 asym), 3186 (ν NH_2 sym), 3110 (ν $\text{NH}_{\text{triazole}}$), 1268 (ν C=S); $^1\text{H-NMR}$ (500 MHz, $\text{DMSO-}d_6$, δ /ppm): 14.09 (*s*, 1H, NH), 7.92 (*d*, 2H, ArH), 7.68 (*m*, 2H, ArH), 7.59 (*m*, 1H, ArH), 5.73 (*s*, 2H, NH_2), 2.54 (*s*, 3H, CH_3); $^{13}\text{C-NMR}$ (125 MHz, $\text{DMSO-}d_6$, δ /ppm): 170.16 (C=S), 159.34 (C), 153.51 (C), 151.07 (C), 144.12 (C), 143.81 (C), 131.12 (2CH), 129.41 (2CH), 127.85 (CH), 16.05 (CH_3); MS (EI, 70 eV) *m/z* (%): 290.08 (M + 1).

General procedure for the synthesis of Schiff bases B1–B15. An amount of 2 mmol (0.578 g) of 4-amino-5-(4-methyl-2-phenylthiazol-5-yl)-4H-1,2,4-triazole-3-thiol **4** was suspended in 10 mL of absolute ethanol. To the resulting suspension was added an alcoholic solution of 2 mmol of aldehyde (aromatic or heteroaromatic) in 5 mL of absolute ethanol and 2–3 drops of concentrated H_2SO_4 as a catalyst.

The reaction mixture was refluxed for 6 h. The obtained precipitate was filtered hot and washed with absolute ethanol, and then it was dried and recrystallized from DMSO.

4-(2,4-Dichlorobenzylideneamino)-5-(4-methyl-2-phenylthiazol-5-yl)-4H-1,2,4-triazole-3-thiol (B1). Yield 67.4% (0.300 g); m.p. 247–249 °C; light yellow powder; Anal. Calcd for C₁₉H₁₃Cl₂N₅S₂ (446.38): C, 51.12; H, 2.31; N, 15.68; S, 14.33; Found: C, 51.32; H, 2.32; N, 15.61; S, 14.36; IR (ATR, cm⁻¹): 3095 (ν NH_{triazole}), 1633 (ν -N=CH-), 1260 (ν C=S); 1165 (ν C-Cl), 1098 (ν C-Cl); ¹H-NMR (500 MHz, DMSO-*d*₆, δ/ppm): 14.15 (s, 1H, NH), 9.42 (s, 1H, -N=CH-), 7.93–8.01 (d, 3H, ArH), 7.72 (s, 1H, ArH), 7.50 (d, 1H, ArH), 7.35–7.42 (m, 3H, ArH), 2.33 (s, 3H, CH₃); ¹³C-NMR (125 MHz, DMSO-*d*₆, δ/ppm): 170.25 (C=S), 159.14 (C), 157.73 (CH=N), 154.01 (C), 150.98 (C), 144.11 (C), 132.44 (C), 131.09 (C), 130.89 (2CH), 129.33 (2CH), 129.15 (CH), 129.03 (CH), 128.82 (CH), 128.41 (2C), 126.01 (CH), 15.93 (CH₃); MS (EI, 70 eV) *m/z* (%): 446.3 (M + 1).

4-(2,6-Dichlorobenzylideneamino)-5-(4-methyl-2-phenylthiazol-5-yl)-4H-1,2,4-triazole-3-thiol (B2). Yield 70.5% (0.314 g); m.p. 300 °C; light yellow powder; Anal. Calcd for C₁₉H₁₃Cl₂N₅S₂ (446.38): C, 51.12; H, 2.31; N, 15.68; S, 14.33; Found: C, 50.9; H, 2.32; N, 15.61; S, 14.27; IR (ATR, cm⁻¹): 3092 (ν NH_{triazole}), 1635 (ν -N=CH-), 1265 (ν C=S); 1161 (ν C-Cl), 1095 (ν C-Cl); ¹H-NMR (500 MHz, DMSO-*d*₆, δ/ppm): 14.11 (s, 1H, NH), 9.41 (s, 1H, -N=CH-), 7.95–8.03 (d, 2H, ArH), 7.54–7.59 (m, 4H, ArH), 2.39 (s, 3H, CH₃); ¹³C-NMR (125 MHz, DMSO-*d*₆, δ/ppm): 170.09 (C=S), 159.16 (C), 157.61 (CH=N), 153.97 (C), 151.04 (C), 144.01 (C), 133.72 (2C), 132.19 (C), 130.96 (2CH), 129.37 (2CH), 129.11 (CH), 128.75 (CH), 128.64 (C), 128.32 (2CH), 15.86 (CH₃); MS (EI, 70 eV) *m/z* (%): 446.3 (M + 1).

4-(2,3-Dichlorobenzylideneamino)-5-(4-methyl-2-phenylthiazol-5-yl)-4H-1,2,4-triazole-3-thiol (B3). Yield 77.1% (0.687 g); m.p. 285–290 °C; light yellow powder; Anal. Calcd for C₁₉H₁₃Cl₂N₅S₂ (446.38): C, 51.12; H, 2.31; N, 15.68; S, 14.33; Found: C, 51.32; H, 2.32; N, 15.61; S, 14.27; IR (ATR, cm⁻¹): 3096 (ν NH_{triazole}), 1632 (ν -N=CH-), 1263 (ν C=S); 1159 (ν C-Cl), 1091 (ν C-Cl); ¹H-NMR (500 MHz, DMSO-*d*₆, δ/ppm): 14.06 (s, 1H, NH), 9.48 (s, 1H, -N=CH-), 7.89–8.93 (d, 2H, ArH), 7.71 (d, 1H, ArH), 7.54 (d, 1H, ArH), 7.35–7.48 (m, 4H, ArH), 2.36 (s, 3H, CH₃); ¹³C-NMR (125 MHz, DMSO-*d*₆, δ/ppm): 170.04 (C=S), 159.11 (C), 157.75 (CH=N), 153.97 (C), 151.04 (C), 144.01 (C), 142.88 (C), 134.65 (C), 132.19 (CH), 130.98 (2CH), 130.44 (C), 129.33 (2CH), 128.88 (CH), 128.61 (C), 128.33 (CH), 125.12 (CH), 15.79 (CH₃); MS (EI, 70 eV) *m/z* (%): 446.3 (M + 1).

4-(3-Chlorobenzylideneamino)-5-(4-methyl-2-phenylthiazol-5-yl)-4H-1,2,4-triazole-3-thiol (B4). Yield 82.92% (0.781 g); m.p. 275 °C; light yellow powder; Anal. Calcd for C₁₉H₁₄ClN₅S₂ (411.9): C, 55.34; H, 3.39; N, 16.99; S, 15.53; Found: C, 55.6; H, 3.37; N, 17.05; S, 15.59; IR (ATR, cm⁻¹): 3091 (ν NH_{triazole}), 1630 (ν -N=CH-), 1271 (ν C=S); 1132 (ν C-Cl); ¹H-NMR (500 MHz, DMSO-*d*₆, δ/ppm): 14.18 (s, 1H, NH), 9.52 (s, 1H, -N=CH-), 7.97–8.06 (d, 2H, ArH), 7.92 (s, 1H, ArH), 7.77 (d, 1H, ArH), 7.59 (d, 1H, ArH), 7.47–7.54 (m, 4H, ArH), 2.41 (s, 3H, CH₃); ¹³C-NMR (125 MHz, DMSO-*d*₆, δ/ppm): 170.12 (C=S), 159.15 (C), 157.66 (CH=N), 153.81 (C), 151.07 (C), 143.96 (C), 135.16 (C), 134.51 (C), 131.21 (CH), 130.93 (2CH), 130.29 (CH), 129.29 (2CH), 128.94 (CH), 128.68 (C), 127.36 (CH), 127.14 (CH), 15.92 (CH₃); MS (EI, 70 eV) *m/z* (%): 412.04 (M + 1).

4-(4-Bromobenzylideneamino)-5-(4-methyl-2-phenylthiazol-5-yl)-4H-1,2,4-triazole-3-thiol (B5). Yield 75.3% (0.343 g); m.p. 296–298 °C; yellow powder; Anal. Calcd for C₁₉H₁₄BrN₅S₂ (456.38): C, 49.89; H, 3.06; N, 15.33; S, 14.02; Found: C, 50.1; H, 3.07; N, 15.33; S, 14.07; IR (ATR, cm⁻¹): 3104 (ν NH_{triazole}), 1618 (ν -N=CH-), 1274 (ν C=S); 1055 (ν C-Br); ¹H-NMR (500 MHz, DMSO-*d*₆, δ/ppm): 14.12 (s, 1H, NH), 9.40 (s, 1H, -N=CH-), 7.98–8.04 (d, 2H, ArH), 7.81–7.83 (d, 2H, ArH), 7.60 (d, 2H, ArH), 7.44–7.49 (m, 3H, ArH), 2.35 (s, 3H, CH₃); ¹³C-NMR (125 MHz, DMSO-*d*₆, δ/ppm): 170.02 (C=S), 159.16 (C), 157.64 (CH=N), 153.61 (C), 151.17 (C), 143.67 (C), 131.85 (2CH), 131.11 (C), 130.89 (2CH), 129.29 (2CH), 128.93 (CH), 128.71 (C), 128.30 (2CH), 125.59 (C), 15.77 (CH₃); MS (EI, 70 eV) *m/z* (%): 456.3 (M + 1).

4-(4-Fluorobenzylideneamino)-5-(4-methyl-2-phenylthiazol-5-yl)-4H-1,2,4-triazole-3-thiol (B6). Yield 67.8% (0.268 g); m.p. 294–296 °C; yellow powder; Anal. Calcd for C₁₉H₁₄FN₅S₂ (395.48): C, 57.65; H, 3.54; N, 17.7; S, 16.18; Found: C, 57.9; H, 3.55; N, 17.62; S, 16.11; IR (ATR, cm⁻¹): 3107 (ν NH_{triazole}), 1620

(ν -N=CH-), 1270 (ν C=S); 1215 (ν C-F); $^1\text{H-NMR}$ (500 MHz, DMSO- d_6 , δ /ppm): 13.99 (s, 1H, NH), 9.47 (s, 1H, -N=CH-), 7.96–8.01 (d, 2H, ArH), 7.79–7.82 (d, 2H, ArH), 7.46–7.54 (m, 3H, ArH), 7.31 (d, 2H, ArH), 2.29 (s, 3H, CH₃); $^{13}\text{C-NMR}$ (125 MHz, DMSO- d_6 , δ /ppm): 169.96 (C=S), 165.22 (C), 159.20 (C), 157.58 (CH=N), 153.65 (C), 151.18 (C), 143.53 (C), 130.98 (2CH), 130.81 (2CH), 129.33 (2CH), 128.95 (CH), 128.68 (C), 127.77 (C), 115.59 (2CH), 15.83 (CH₃); MS (EI, 70 eV) m/z (%): 396.3 (M + 1).

2-((3-Mercapto-5-(4-methyl-2-phenylthiazol-5-yl)-4H-1,2,4-triazol-4-ylimino) methyl)phenol (**B7**). Yield 46.8% (0.356 g); m.p. 269 °C; yellow powder; Anal. Calcd for C₁₉H₁₅N₅OS₂ (393.49): C, 57.94; H, 3.81; N, 17.78; S, 16.26; Found: C, 58.2; H, 3.82; N, 17.85 S, 16.19; IR (ATR, cm⁻¹): 3348 (ν O-H), 3115 (ν NH_{triazole}), 1626 (ν -N=CH-), 1284 (ν C=S); 1243 (ν C-O); $^1\text{H-NMR}$ (500 MHz, DMSO- d_6 , δ /ppm): 13.97 (s, 1H, NH), 9.82 (s, 1H, OH), 9.43 (s, 1H, -N=CH-), 7.99–8.05 (d, 2H, ArH), 7.68 (d, 1H, ArH), 7.44–7.46 (m, 4H, ArH), 7.15 (m, 1H, ArH), 7.01 (d, 1H, ArH), 2.27 (s, 3H, CH₃); $^{13}\text{C-NMR}$ (125 MHz, DMSO- d_6 , δ /ppm): 169.99 (C=S), 161.31 (C), 159.23 (C), 157.88 (CH=N), 153.57 (C), 151.21 (C), 143.51 (C), 132.53 (CH), 132.15 (CH), 130.85 (2CH), 129.41 (2CH), 128.90 (CH), 128.59 (C), 121.76 (CH), 118.18 (C), 116.99 (CH), 15.88 (CH₃); MS (EI, 70 eV) m/z (%): 394.2 (M + 1).

3-((3-Mercapto-5-(4-methyl-2-phenylthiazol-5-yl)-4H-1,2,4-triazol-4-ylimino) methyl)phenol (**B8**). Yield 65.3% (0.496 g); m.p. 295–297 °C; light yellow powder; Anal. Calcd for C₁₉H₁₅N₅OS₂ (393.49): C, 57.94; H, 3.81; N, 17.78; S, 16.26; Found: C, 58.2; H, 3.82; N, 17.85 S, 16.19; IR (ATR, cm⁻¹): 3344 (ν O-H), 3112 (ν NH_{triazole}), 1622 (ν -N=CH-), 1281 (ν C=S); 1245 (ν C-O); $^1\text{H-NMR}$ (500 MHz, DMSO- d_6 , δ /ppm): 13.92 (s, 1H, NH), 9.78 (s, 1H, OH), 9.39 (s, 1H, -N=CH-), 8.01–8.04 (d, 2H, ArH), 7.54 (s, 1H, ArH), 7.48–7.56 (m, 3H, ArH), 7.39 (d, 1H, ArH), 7.23 (m, 1H, ArH), 6.98 (d, 1H, ArH), 2.34 (s, 3H, CH₃); $^{13}\text{C-NMR}$ (125 MHz, DMSO- d_6 , δ /ppm): 169.92 (C=S), 159.09 (C), 158.83 (C), 157.67 (CH=N), 153.46 (C), 151.24 (C), 143.44 (C), 135.33 (C), 130.87 (2CH), 130.27 (CH), 129.30 (2CH), 128.92 (CH), 128.64 (C), 121.74 (CH), 118.26 (CH), 115.01 (CH), 15.93 (CH₃); MS (EI, 70 eV) m/z (%): 394.2 (M + 1).

4-((3-Mercapto-5-(4-methyl-2-phenylthiazol-5-yl)-4H-1,2,4-triazol-4-ylimino) methyl)phenol (**B9**). Yield 68.15% (0.518 g); m.p. 285 °C; light yellow powder; Anal. Calcd for C₁₉H₁₅N₅OS₂ (393.49): C, 57.94; H, 3.81; N, 17.78; S, 16.26; Found: C, 57.7; H, 3.82; N, 17.7 S, 16.19; IR (ATR, cm⁻¹): 3341 (ν O-H), 3118 (ν NH_{triazole}), 1623 (ν -N=CH-), 1285 (ν C=S); 1249 (ν C-O); $^1\text{H-NMR}$ (500 MHz, DMSO- d_6 , δ /ppm): 14.07 (s, 1H, NH), 9.83 (s, 1H, OH), 9.38 (s, 1H, -N=CH-), 7.78–7.95 (d, 4H, ArH), 7.41–7.47 (m, 3H, ArH), 6.98 (d, 2H, ArH), 2.32 (s, 3H, CH₃); $^{13}\text{C-NMR}$ (125 MHz, DMSO- d_6 , δ /ppm): 169.94 (C=S), 160.39 (C), 158.88 (2C), 158.42 (C), 157.97 (CH=N), 143.74 (C), 130.97 (2CH), 130.52 (2CH), 129.36 (2CH), 128.94 (CH), 126.33 (C), 116.11 (2CH), 106.06 (C), 16.24 (CH₃); MS (EI, 70 eV) m/z (%): 394.2 (M + 1).

5-(4-Methyl-2-phenylthiazol-5-yl)-4-(3-nitrobenzylideneamino)-4H-1,2,4-triazole-3-thiol (**B10**). Yield 80.8% (0.682 g); m.p. 270 °C; light yellow powder; Anal. Calcd for C₁₉H₁₄N₆O₂S₂ (422.48): C, 53.96; H, 3.31; N, 19.88; S, 15.14; Found: C, 53.7; H, 3.32; N, 19.8; S, 15.2; IR (ATR, cm⁻¹): 3131 (ν NH_{triazole}), 1521 (ν N-O asy), 1629 (ν -N=CH-), 1324 (ν N-O sy), 1257 (ν C=S); $^1\text{H-NMR}$ (500 MHz, DMSO- d_6 , δ /ppm): 14.04 (s, 1H, NH), 9.34 (s, 1H, -N=CH-), 8.52 (s, 1H, ArH), 8.01–8.22 (d, 4H, ArH), 7.49–7.59 (m, 4H, ArH), 2.45 (s, 3H, CH₃); $^{13}\text{C-NMR}$ (125 MHz, DMSO- d_6 , δ /ppm): 169.88 (C=S), 159.03 (C), 157.76 (CH=N), 153.45 (C), 151.19 (C), 148.88 (C), 143.66 (C), 135.44 (CH), 134.58 (C), 130.83 (2CH), 129.71 (CH), 129.38 (2CH), 128.83 (CH), 128.55 (C), 126.36 (CH), 121.65 (CH), 16.12 (CH₃); MS (EI, 70 eV) m/z (%): 423.2 (M + 1).

5-(4-Methyl-2-phenylthiazol-5-yl)-4-(4-nitrobenzylideneamino)-4H-1,2,4-triazole-3-thiol (**B11**). Yield 50% (0.412 g); m.p. 275 °C; orange powder; Anal. Calcd for C₁₉H₁₄N₆O₂S₂ (422.48): C, 53.96; H, 3.31; N, 19.88; S, 15.14; Found: C, 53.7; H, 3.29; N, 19.95; S, 15.2; IR (ATR, cm⁻¹): 3129 (ν NH_{triazole}), 1525 (ν N-O asym), 1625 (ν -N=CH-), 1320 (ν N-O sym), 1259 (ν C=S); $^1\text{H-NMR}$ (500 MHz, DMSO- d_6 , δ /ppm): 13.93 (s, 1H, NH), 9.36 (s, 1H, -N=CH-), 8.02–8.29 (d, 6H, ArH), 7.45–7.51 (m, 3H, ArH), 2.34 (s, 3H, CH₃); $^{13}\text{C-NMR}$ (125 MHz, DMSO- d_6 , δ /ppm): 169.91 (C=S), 159.09 (C), 157.78 (CH=N), 153.35 (C), 151.16 (C), 150.13 (C), 143.59 (C), 138.54 (C), 130.91 (2CH), 129.25 (2CH), 128.90 (CH), 128.57 (C), 127.89 (2CH), 124.16 (2CH), 16.16 (CH₃); MS (EI, 70 eV) m/z (%): 423.2 (M + 1).

4-(2-Methoxybenzylideneamino)-5-(4-methyl-2-phenylthiazol-5-yl)-4H-1,2,4-triazole-3-thiol (**B12**). Yield 71.7% (0.603 g); m.p. 285 °C; yellow powder; Anal. Calcd for C₂₀H₁₇N₅OS₂ (407.51): C, 58.89; H, 4.17; N, 17.17; S, 15.7; Found: C, 58.7; H, 4.15; N, 17.23; S, 15.63; IR (ATR, cm⁻¹): 3093 (ν NH_{triazole}), 1628 (ν -N=CH-), 1272 (ν C=S); 1254 (ν C-O), 1038 (ν C-O); ¹H-NMR (500 MHz, DMSO-*d*₆, δ/ppm): 13.95 (s, 1H, NH), 9.45 (s, 1H, -N=CH-), 7.92–8.05 (d, 2H, ArH), 7.71 (d, 1H, ArH), 7.47–7.55 (m, 4H, ArH), 7.29 (d, 1H, ArH), 7.09 (m, 1H, ArH), 3.86 (s, 3H, OCH₃), 2.41 (s, 3H, CH₃); ¹³C-NMR (125 MHz, DMSO-*d*₆, δ/ppm): 169.97 (C=S), 159.10 (C), 157.88 (CH=N), 157.43 (C), 153.40 (C), 151.17 (C), 143.43 (C), 132.10 (CH), 131.81 (CH), 130.79 (2CH), 129.21 (2CH), 128.93 (CH), 128.72 (C), 121.39 (CH), 117.02 (C), 111.22 (CH), 55.69 (CH₃), 15.91 (CH₃); MS (EI, 70 eV) *m/z* (%): 408.49 (M + 1).

4-(3-Methoxybenzylideneamino)-5-(4-methyl-2-phenylthiazol-5-yl)-4H-1,2,4-triazole-3-thiol (**B13**). Yield 80.6% (0.680 g); m.p. 270 °C; yellow powder; Anal. Calcd for C₂₀H₁₇N₅OS₂ (407.51): C, 58.89; H, 4.17; N, 17.17; S, 15.7; Found: C, 58.7; H, 4.18; N, 17.23; S, 15.63; IR (ATR, cm⁻¹): 3089 (ν NH_{triazole}), 1621 (ν -N=CH-), 1283 (ν C=S); 1257 (ν C-O), 1034 (ν C-O); ¹H-NMR (500 MHz, DMSO-*d*₆, δ/ppm): 13.91 (s, 1H, NH), 9.44 (s, 1H, -N=CH-), 7.99–8.05 (d, 2H, ArH), 7.58 (s, 1H, ArH), 7.38–7.52 (m, 4H, ArH), 7.38 (d, 1H, ArH), 7.14 (d, 1H, ArH), 3.93 (s, 3H, OCH₃), 2.43 (s, 3H, CH₃); ¹³C-NMR (125 MHz, DMSO-*d*₆, δ/ppm): 169.95 (C=S), 160.75 (C), 159.14 (C), 157.88 (CH=N), 153.37 (C), 151.09 (C), 143.41 (C), 134.80 (C), 130.85 (2CH), 129.86 (CH), 129.25 (2CH), 128.83 (CH), 128.66 (C), 121.62 (CH), 116.66 (CH), 111.28 (CH), 55.75 (CH₃), 15.89 (CH₃); MS (EI, 70 eV) *m/z* (%): 408.49 (M + 1).

5-(4-Methyl-2-phenylthiazol-5-yl)-4-(thiophen-2-ylmethyleneamino)-4H-1,2,4-triazole-3-thiol (**B14**). Yield 79.3% (0.536 g); m.p. 280 °C; yellow powder; Anal. Calcd for C₁₇H₁₃N₅S₃ (383.51): C, 53.19; H, 3.38; N, 18.25; S, 25.03; Found: C, 53.4; H, 3.38; N, 18.32; S, 24.92; IR (ATR, cm⁻¹): 3088 (ν NH_{triazole}), 1627 (ν -N=CH-), 1288 (ν C=S); ¹H-NMR (500 MHz, DMSO-*d*₆, δ/ppm): 14.10 (s, 1H, NH), 9.46 (s, 1H, -N=CH-), 7.94–7.99 (d, 2H, ArH), 7.74–7.78 (d, 2H, ArH), 7.40–7.51 (m, 4H, ArH), 2.42 (s, 3H, CH₃); ¹³C-NMR (125 MHz, DMSO-*d*₆, δ/ppm): 170.08 (C=S), 159.13 (C), 157.95 (CH=N), 153.29 (C), 151.09 (C), 144.96 (C), 143.27 (C), 130.98 (2CH), 130.11 (CH), 129.27 (2CH), 128.91 (CH), 128.77 (C), 128.55 (CH), 127.30 (CH), 16.01 (CH₃); MS (EI, 70 eV) *m/z* (%): 384.4 (M + 1).

4-(4-(Dimethylamino)benzylideneamino)-5-(4-methyl-2-phenylthiazol-5-yl)-4H-1,2,4-triazole-3-thiol (**B15**). Yield 77.3% (0.653 g); m.p. 260 °C; Anal. Calcd for C₂₁H₂₀N₆S₂ (420.55): C, 59.92; H, 4.75; N, 19.97; S, 15.21; Found: C, 59.7; H, 4.76; N, 19.89; S, 15.27; yellow powder; IR (ATR, cm⁻¹): 3086 (ν NH_{triazole}), 1619 (ν -N=CH-), 1331 (ν C-N), 1258 (ν C=S); ¹H-NMR (500 MHz, DMSO-*d*₆, δ/ppm): 14.01 (s, 1H, NH), 9.51 (s, 1H, -N=CH-), 7.96–7.98 (d, 2H, ArH), 7.45–7.53 (m, 3H, ArH), 6.99–7.34 (d, 4H, ArH), 3.31 (s, 6H, 2CH₃), 2.47 (s, 3H, CH₃); ¹³C-NMR (125 MHz, DMSO-*d*₆, δ/ppm): 170.03 (C=S), 159.09 (C), 157.63 (CH=N), 153.53 (C), 153.28 (C), 151.06 (C), 138.27 (C), 130.97 (2CH), 129.33 (2CH), 128.81 (CH), 128.37 (2CH), 127.94 (C), 121.86 (C), 111.99 (2CH), 43.31 (2CH₃), 16.09 (CH₃); MS (EI, 70 eV) *m/z* (%): 421.12 (M + 1).

3.2. Antifungal Activity Assay

3.2.1. Determination of Inhibition Zone Diameters

The *in vitro* antifungal activity was determined using the cup-plate agar diffusion method according to the Clinical and Laboratory Standards Institute (CLSI) guidelines [28]. For antifungal testing, Mueller-Hinton medium supplemented with 2% glucose (providing adequate growth of yeasts) and 0.5 mg/mL methylene blue (providing a better definition of the inhibition zone diameter) was used. The inoculum was prepared by suspending five representative colonies, obtained from an 18–24 h culture on non-selective nutritive agar medium, in sterile distilled water. The cell density was adjusted to the density of a 0.5 McFarland standard by measuring the absorbance in a spectrophotometer at a wavelength of 530 nm and adding sterile distilled water as required (corresponding to a population of 1–5 × 10⁶ CFU/mL). A sterile swab was soaked in suspension and then the Mueller-Hinton agar plates were inoculated by streaking the entire surface. After drying for 10–15 min, six-millimeter diameter

wells were cut from the agar using a sterile cork-borer, and a volume of 20 μL of each compound solution (5 mg/mL in dimethyl sulfoxide-DMSO) was delivered into the wells (100 μg /well).

Fluconazole (100 μg /well) was used as the standard drugs. The controls were performed with only sterile broth, overnight culture and 20 μL of DMSO. The plates were incubated at 35 °C. Zone diameters were measured to the nearest whole millimeter at a point in which there will be no visible growth after 24–48 h. Results were obtained in triplicate. The solvent used for the preparation of each compound stock solution (5 mg/mL), DMSO (Merck, Darmstadt, Germany) exhibited no inhibitory activity against the tested fungal strain.

3.2.2. Determination of MIC and MFC Values

The microorganisms used for antifungal activity evaluation were obtained from the University of Agricultural Sciences and Veterinary Medicine Cluj-Napoca Romania. The antifungal activity was evaluated against cultures of *Candida albicans* ATCC 10231, *Candida albicans* ATCC 18804, *Candida krusei* ATCC 6258. The cultures were stored on potato dextrose agar (Sifin, Germany). Prior to antifungal susceptibility testing, each strain was inoculated on potato dextrose agar plated to ensure optical growth characteristics and purity. Then, yeast cells were suspended in saline and adjusted spectrophotometrically to RPMI (Roswell Park Memorial Institute) 1640 medium to a final concentration of 10^6 CFU/mL.

Stock solutions (1 mg/mL) were prepared by dissolving the test compounds, the reference antifungals (fluconazole and ketoconazole) in sterile DMSO. These solutions were stored at 4 °C. A series of double diluting solutions of the above compounds were prepared in RPMI 1640 medium obtaining final concentrations in the range of 500 μg /mL to 0.015 μg /mL. The broth microdilution method was employed for the minimum inhibitory concentration test. Media were placed into each of the 96 wells of the microplates. Sample solutions at high concentration (100 μg /mL) were added into the first rows of the microplates and two-fold dilutions of the compounds were made by dispensing the solutions into the remaining wells. Culture suspensions of 10 μL were inoculated into all the wells. The sealed microplates were incubated at 37 °C for 18 h. Antifungal activity was tested by using the broth microdilution method according to the Clinical and Laboratory Standard Institute (CLSI) guidelines [28]. The medium used for susceptibility testing was nutrient broth for bacteria and RPMI 1640 with L-glutamine, to pH 7.0 with 3-(*n*-morpholino)propanesulfonic acid. The initial density of *E. coli* and *S. aureus* was 10^5 CFU/mL and *Candida sp* was approximately 2×10^6 colony forming units (CFU)/mL. Inoculums (density of 0.5 in McFarland scale) were prepared in a sterile solution of 0.9% NaCl solution. Then, tested strains were suspended in nutrient broth and RPMI 1640 media to give a final density of 2×10^5 CFU/mL. Solutions of the test compounds and suspensions of bacteria and fungi were inoculated onto 96-well microplates. The growth control, sterility control and control of antibacterial/antifungal compounds were used. Plates were incubated under normal atmospheric conditions at 30 °C for 48 h (*Candida albicans* ATCC 10231, *Candida albicans* ATCC 18804, *Candida krusei* ATCC 6258), and next minimum inhibitory concentration (MIC) values have been determined by adding resazurin (20 μL , 0.02%) followed by incubation for 2 h. The MIC was defined as the lowest concentration required to arrest the growth of the bacteria/fungi. For determination of minimum fungicidal concentration (MFC), a 0.01 mL aliquot of the medium drawn from the culture tubes showing no macroscopic growth at the end of the 24 h culture was subcultured on nutrient agar/potato dextrose agar plates to determine the number of vital organisms and incubated further at 30 °C for 48 h. The MFC was defined as the lowest concentration of the agent at which no colonies are observed. All MIC and MFC experiments were repeated three times.

3.3. Molecular Docking

A molecular docking study was carried out using AutoDock 4.2 [29], in order to investigate the possible interactions with cytochrome P450 14 α -sterol demethylase (CYP51) from *Saccharomyces cerevisiae* and to predict the binding mode of our synthesized compounds. The crystallographic structure of the

complex between the three-dimensional (3D) structure of the enzyme, with the intact transmembrane domain, and co-crystallized itraconazole (PDB:5EQB), was used for the docking study. The crystal structure of the enzyme obtained by X-ray diffraction was taken from Protein Data Bank [30].

A dataset of 3D thiazolyl-triazole Schiff bases **B1–B15** was generated using HyperChem 6, with geometry optimization and minimized energy conformation. Further, all input files were prepared using AutoDock Tools 1.5.6 [29]. Ligand preparation included addition of Gasteiger charges and merging non-polar hydrogen atoms. Fluconazole, a drug known to inhibit cytochrome P450 lanosterol 14 α -demethylase [31], was taken as the positive control.

Using AutoDock Tools, co-crystallized ligand (itraconazole) and water were removed from the active site of the enzyme, polar hydrogen atoms were added, non-polar hydrogen atoms merged, rotatable bonds were defined, amide bonds were set non-rotatable, carboxylic moieties deprotonated and Gasteiger partial charges were assigned. The grid box was defined as $x = y = z = 28 \text{ \AA}$ in dimension with $x = 19.692$, $y = 14.168$, $z = 16.077$ center coordinates. Grid maps were generated using AutoGrid 4 with 0.375 grid points size space.

AutoDock searched for the best conformers poses, based on the Lamarkian genetic algorithm. For each compound, AutoDock searched for 10 conformers. The maximum number of evaluation was set at 9×10^4 , rate of mutation at 0.02, rate of crossover at 0.8, step size for translations at 2 \AA and cluster tolerance at 2 \AA .

3.4. ADME and Molecular Property Prediction

In this present investigation, the new thiazolyl-triazole Schiff bases were subjected to a theoretical in silico ADME and toxicity prediction study, under Lipinski's "Rule of five" [32]. Lipinski's parameters were calculated using web tool Swiss ADME [33]. We have also assessed tPSA (topological polar surface area), a descriptor that allows prediction of bioavailability and the transport of an active compound by the blood–brain barrier [23]. Bioavailability is highly multifactorial, but is primarily driven by gastrointestinal absorption [34]. The percentage of the absorption was calculated according to the equation: $\%ABS = 109 - 0.345 \times TPSA$ [35]. Also, water solubility, CYP2D6, CYP2D9, P-glycoprotein inhibition and phospholipidosis (PLD) induction were predicted.

4. Conclusions

Synthesis of Schiff bases **B1–B15** followed several steps. The 4-amino-5-(4-methyl-2-phenylthiazol-5-yl)-4H-1,2,4-triazole-3 thiol **4** was obtained by treating potassium 2-(4-methyl-2-phenylthiazole-5-carbonyl)hydrazine-carbodithioate **3**, previously obtained, with hydrazine hydrate. The final derivatives were synthesized in good yields by the condensation of compound **4** with various aromatic or heteroaromatic aldehydes.

Schiff bases were investigated for their anti-*Candida* potential. The in vitro methods used were the disk diffusion disk, the determination of MIC and MFC, respectively. The activity of the new derivatives was reported to reference drugs, already used in therapy. Some of the Schiff bases showed MICs inferior to those of the references used. Compound **B10** showed to be the most promising anti-*Candida* candidate, inhibiting the growth of all three *Candida* strains used and being more potent than fluconazole. The obtained results suggest that the new series bearing thiazole and triazole scaffolds may be considered for further investigation and optimization, in designing anti-*Candida* drugs.

A docking study of the thiazolyl-triazole Schiff bases was performed on compounds **B1–B15** and presented a rationale for the activity of these compounds. Performed on CYP51 enzyme, this study showed that the thiazolyl-triazole Schiff bases interact with the amino acids in the access channel to the active site of the lanosterol 14 α -demethylase with higher binding affinity energy than fluconazole. Moreover, the compounds do not interact with the heme.

Furthermore, a virtual study was performed to predict the ADME and the toxicity of the derivatives. The studied compounds showed an acceptable gastro-intestinal absorption and a low to moderate water solubility. We could predict the absence of toxicity at CNS level, due to the fact that the compounds do not pass the blood–brain barrier. All of the newly synthesized compounds were predicted as noninhibitors of CYP2D6, noninducers of phospholipidosis, and they are not a substrate for P-glycoprotein. All these observations will be helpful in designing newer anti-*Candida* agents with good pharmacokinetic properties and without severe side effects.

Acknowledgments: This study was supported by “Iuliu Hațieganu” University of Medicine and Pharmacy Cluj-Napoca internal research grant No. 1493/14/2014, No. 4944/7/08.03.2016, No. 4944/23/08.03.2016 and by The Executive Agency for Higher Education Research Development and Innovation Funding (UEFISCDI), Bucharest, Romania, on the Contract No. 210/2014-Project PN-II-PT-PCCA-2013-4-2075.

Author Contributions: B.T. and O.O. conceived and designed the experiments; A.S., A.E., C.N., I.I. performed the chemical synthesis and the characterization of the compounds; D.V. performed the antifungal investigation; G.M. contributed to the docking study; B.T. has performed the ADMET study; D.B. and C.L. contributed to the analysis of the data. All authors contributed to writing this paper.

Conflicts of Interest: The authors declare no conflict of interest.

References

1. Chai, X.; Zhang, J.; Cao, Y.; Zou, Y.; Wu, Q.; Zhang, D.; Jiang, Y.; Sun, Q. Design, synthesis and molecular docking studies of novel triazole as antifungal agent. *Eur. J. Med. Chem.* **2011**, *46*, 3167–3176. [[CrossRef](#)] [[PubMed](#)]
2. Jiang, Y.; Zhang, J.; Cao, Y.; Chai, X.; Zou, Y.; Wu, Q.; Zhang, D.; Jiang, Y.; Sun, Q. Synthesis, in vitro evaluation and molecular docking studies of new triazole derivatives as antifungal agents. *Bioorg. Med. Chem. Lett.* **2011**, *21*, 4471–4475. [[CrossRef](#)] [[PubMed](#)]
3. Tidwell, T.T. Hugo (Ugo) Schiff, Schiff Bases, and a Century of β -Lactam Synthesis. *Angew. Chem. Int. Ed.* **2008**, *47*, 1016–1020. [[CrossRef](#)] [[PubMed](#)]
4. Li, Y.; Zhao, C.P.; Ma, H.P.; Zhao, M.Y.; Xue, Y.R.; Wang, X.M. Design, synthesis and antimicrobial activities evaluation of Schiff base derived from secnidazole derivatives as potential FabH inhibitors. *Bioorg. Med. Chem.* **2013**, *21*, 3120–3126. [[CrossRef](#)] [[PubMed](#)]
5. Chazin, E.L.; Sanches, P.S.; Lindgren, E.B.; Vellasco, W.T.; Pinto, L.C.; Burbano, R.M.; Yoneda, J.D.; Leal, K.Z.; Gomes, C.R.; Wardell, J.L.; et al. Synthesis and Biological Evaluation of Novel 6-Hydroxybenzo[d][1,3]oxathiol-2-one Schiff Bases as Potential Anticancer Agents. *Molecules* **2015**, *20*, 1968–1983. [[CrossRef](#)] [[PubMed](#)]
6. Barbuceanu, S.F.; Ilies, D.C.; Saramet, G.; Uivarosi, V.; Draghici, C.; Radulescu, V. Synthesis and Antioxidant Activity Evaluation of New Compounds from Hydrazinecarbothioamide and 1,2,4-Triazole Class Containing Diarylsulfone and 2,4-Difluorophenyl Moieties. *Int. J. Mol. Sci.* **2014**, *15*, 10908–10925. [[CrossRef](#)] [[PubMed](#)]
7. De Souza, A.O.; Galetti, F.C.S.; Silva, C.L.; Bicalho, B.; Parma, M.M.; Fonseca, S.F.; Andrade-Neto, M. Antimycobacterial and cytotoxicity activity of synthetic and natural compounds. *Quim. Nova* **2007**, *30*, 1563–1566. [[CrossRef](#)]
8. Hanif, M.; Chohan, Z.H. Design, spectral characterization and biological studies of transition metal(II) complexes with triazole Schiff bases. *Spectrochim. Acta A* **2013**, *104*, 468–476. [[CrossRef](#)] [[PubMed](#)]
9. Aouad, M.R. Synthesis, Characterization and Antimicrobial Evaluation of Some New Schiff, Mannich and Acetylenic Mannich Bases Incorporating a 1,2,4-Triazole Nucleus. *Molecules* **2014**, *19*, 18897–18910. [[CrossRef](#)] [[PubMed](#)]
10. Aswathanarayanappa, C.; Bheemappa, E.; Bodke, Y.D.; Krishnegowda, P.S.; Venkata, S.P.; Ningegowda, R. Synthesis and Evaluation of Antioxidant Properties of Novel 1,2,4-Triazole-Based Schiff Base Heterocycles. *Arch. Pharm.* **2013**, *346*, 922–930. [[CrossRef](#)] [[PubMed](#)]
11. Anand, P.; Patil, V.M.; Sharma, V.K.; Khosa, R.L.; Masand, N. Schiff bases: A Review on Biological Insights. *Int. J. Drug Des. Discov.* **2012**, *3*, 851–868.
12. Johnson, D.E.; Wolfgang, G.H. Predicting human safety: Screening and computational approaches to estimate solubility and permeability in drug discovery and development settings. *Drug Discov. Today* **2000**, *5*, 445–454. [[CrossRef](#)]

13. Simiti, I.; Mureşan, A. Application of the Sommelet reaction in the series of 2-aryl-4methyl-5-chlormethyl-thiazole. *Roum. Chim.* **1976**, *7*, 1078.
14. Tiperciuc, B.; Colosi, I.; Moldovan, C.; Crişan, O.; Pîrnău, A.; Vlase, L.; Duma, M.; Oniga, O. Synthesis and Evaluation of Antimicrobial Activity of Some New Hetaryl-Azoles Derivatives Obtained from 2-Aryl-4-methylthiazol-5-carbohydrazides and Isonicotinic Acid Hydrazide. *J. Heterocycl. Chem.* **2012**, *49*, 1407–1414. [[CrossRef](#)]
15. Pinto, D.C.; Santos, C.M.; Silva, A.M. Advanced NMR Techniques for Structural Characterization of Heterocyclic Structures. *Recent Res. Dev. Heterocycl. Chem.* **2007**, *37/661*, 397–475.
16. Alnuaimi, A.D.; O'Brien-Simpson, N.M.; Reynolds, E.C.; McCullough, M.J. Clinical isolates and laboratory reference *Candida* species and strains have varying abilities to form biofilms. *FEMS Yeast Res.* **2013**, *13*, 689–699. [[CrossRef](#)] [[PubMed](#)]
17. Schmidt, A.; Geschke, U. Comparative virulence of *Candida albicans* strains in CFW1 mice and Sprague-Dawley rats. *Mycoses* **1996**, *39*, 157–160. [[CrossRef](#)] [[PubMed](#)]
18. Deorukhkar, S.C.; Saini, S.; Mathew, S. Non-*albicans Candida* Infection: An Emerging Threat. *Interdiscip. Perspect. Infect. Dis.* **2014**, *2014*, 615958. [[PubMed](#)]
19. Movahed, E.; Yi Tan, G.M.; Munusamy, K.; Yeow, T.C.; Tay, S.T.; Wong, W.F.; Looi, C.Y. Triclosan Demonstrates Synergic Effect with Amphotericin B and Fluconazole and Induces Apoptosis-Like Cell Death in *Cryptococcus neoformans*. *Front. Microbiol.* **2016**, *7*. [[CrossRef](#)] [[PubMed](#)]
20. Sheehan, D.J.; Hitchcock, C.A.; Sibley, C.M. Current and emerging azole antifungal agents. *Clin. Microbiol. Rev.* **1999**, *12*, 40–79. [[PubMed](#)]
21. Newby, D.; Freitas, A.A.; Ghafourian, T. Decision trees to characterise the roles of permeability and solubility on the prediction of oral absorption. *Eur. J. Med. Chem.* **2015**, *90*, 751–765. [[CrossRef](#)] [[PubMed](#)]
22. Azam, F.; Madi, A.M.; Ali, H.I. Molecular Docking and Prediction of Pharmacokinetic Properties of Dual Mechanism Drugs that Block MAO-B and Adenosine A2A Receptors for the Treatment of Parkinson's Disease. *J. Young Pharm.* **2012**, *4*, 184–192. [[CrossRef](#)] [[PubMed](#)]
23. Ertl, P.; Rohde, B.; Selzer, P. Fast calculation of molecular polar surface area as a sum of fragment-based contributions and its application to the prediction of drug transport properties. *J. Med. Chem.* **2000**, *43*, 3714–3717. [[CrossRef](#)] [[PubMed](#)]
24. Mo, S.L.; Zhou, Z.W.; Yang, L.P.; Wei, M.Q.; Zhou, S.F. New insights into the structural features, and functional relevance of human cytochrome P4502C9. Part I. *Curr. Drug Metab.* **2009**, *10*, 1075–1126. [[CrossRef](#)] [[PubMed](#)]
25. Mo, S.L.; Zhou, Z.W.; Yang, L.P.; Wei, M.Q.; Zhou, S.F. New insights into the structural features, and functional relevance of human cytochrome P4502C9. Part II. *Curr. Drug Metab.* **2009**, *10*, 1127–1150. [[CrossRef](#)] [[PubMed](#)]
26. Fromm, M.F. P-glycoprotein: A defense mechanism limiting oral bioavailability and CNS accumulation of drugs. *Int. J. Clin. Pharmacol. Ther.* **2000**, *38*, 69–74. [[CrossRef](#)] [[PubMed](#)]
27. Nonoyama, T.; Fukuda, R. Drug induced phospholipidosis pathological aspects and its prediction. *J. Toxicol. Pathol.* **2008**, *21*, 9–24. [[CrossRef](#)]
28. *Reference Method for Broth Dilution Antifungal Susceptibility Testing of Yeast*; Third Informational Supplement, CLSI Document M27-S3; Clinical and Laboratory Standards Institute (CLSI): Wayne, PA, USA, 2008.
29. Morris, G.M.; Huey, R.; Lindstrom, W.; Sanner, M.F.; Belew, R.K.; Goodsell, D.S.; Olson, A.J. AutoDock4 and AutoDockTools4: Automated Docking with Selective Receptor Flexibility. *J. Comput. Chem.* **2009**, *30*, 2785–2791. [[CrossRef](#)] [[PubMed](#)]
30. Monk, B.C.; Tomasiak, T.M.; Keniya, M.V.; Huschmann, F.U.; Tyndall, J.D.; O'Connell, J.D.; Cannon, R.D.; McDonald, J.G.; Rodriguez, A.; Finer-Moore, J.S.; et al. Architecture of a single membrane spanning cytochrome P450 suggests constraints that orient the catalytic domain relative to a bilayer. *Proc. Natl. Acad. Sci. USA* **2014**, *111*, 3865–3870. [[CrossRef](#)] [[PubMed](#)]
31. Podust, L.M.; Poulos, T.L.; Waterman, M.R. Crystal structure of cytochrome P450 14alpha-sterol demethylase (CYP51) from *Mycobacterium tuberculosis* in complex with azole inhibitors. *Proc. Natl. Acad. Sci. USA* **2001**, *98*, 3068–3073. [[CrossRef](#)] [[PubMed](#)]
32. Lipinski, C.A.; Lombardo, F.; Dominy, B.W.; Feeney, P.J. Experimental and computational approaches to estimate solubility and permeability in drug discovery and development settings. *Adv. Drug Deliv. Rev.* **2001**, *46*, 3–26. [[CrossRef](#)]

33. Swiss ADME. Available online: <http://www.swissadme.ch> (accessed on 20 November 2016).
34. Daina, A.; Zoete, V. A BOILED-Egg To Predict Gastrointestinal Absorption and Brain Penetration of Small Molecules. *ChemMedChem* **2016**, *11*, 1117–1121. [[CrossRef](#)] [[PubMed](#)]
35. Zhao, Y.; Abraham, M.H.; Lee, J.; Hersey, A.; Luscombe, N.C.; Beck, G.; Cooper, I. Rate-limited steps of human oral absorption and QSAR studies. *Pharm. Res.* **2002**, *19*, 1446–1457. [[CrossRef](#)] [[PubMed](#)]

Sample Availability: Samples of the compounds **B1–B15** are available from the authors.



© 2016 by the authors; licensee MDPI, Basel, Switzerland. This article is an open access article distributed under the terms and conditions of the Creative Commons Attribution (CC-BY) license (<http://creativecommons.org/licenses/by/4.0/>).

Article

Study of the Relationships between the Structure, Lipophilicity and Biological Activity of Some Thiazolyl-carbonyl-thiosemicarbazides and Thiazolyl-azoles

Radu Tamaian^{1,2,3}, Augustin Mot^{4,*}, Radu Silaghi-Dumitrescu⁴, Ioana Ionuț⁵, Anca Stana⁵, Ovidiu Oniga⁵, Cristina Nastasă⁵, Daniela Benedec⁶ and Brîndușa Tiperciuc⁵

Received: 20 October 2015 ; Accepted: 3 December 2015 ; Published: 11 December 2015

Academic Editor: Derek J. McPhee

¹ National Research and Development Institute for Cryogenic and Isotopic Technologies, 4th Uzinei Street, Râmnicu Vâlcea 240050, Romania; radu.tamaian@icsi.ro

² 3Nano-SAE Research Centre, Faculty of Physics, University of Bucharest, P. O. Box MG-38, Bucharest-Măgurele RO-077125, Romania

³ SC Biotech Corp SRL, 4th Uzinei Street, Office C52, 2 Râmnicu Vâlcea 40050, Romania

⁴ Department of Chemistry and Chemical Engineering, Babeș-Bolyai University, 1st Mihail Kogălniceanu Street, Cluj-Napoca RO-400084, Romania; rsilaghi@chem.ubbcluj.ro

⁵ Department of Pharmaceutical Chemistry, Faculty of Pharmacy, Iuliu Hațieganu University of Medicine and Pharmacy, 41 Victor Babeș Street, Cluj-Napoca RO-400012, Romania; ionut.ioana@umfcluj.ro (I.I.); teodora_anca@yahoo.com (A.S.); onigao65@yahoo.com (O.O.); cmoldovan@umfcluj.ro (C.N.); brandu32@yahoo.com (B.T.)

⁶ Department of Pharmacognosy, Faculty of Pharmacy, Iuliu Hațieganu University of Medicine and Pharmacy, 12 Ion Creangă Street, Cluj-Napoca RO-400010, Romania; dani_67ro@yahoo.com

* Correspondence: augustinmot@chem.ubbcluj.ro

Abstract: Lipophilicity, as one of the most important physicochemical parameters of bioactive molecules, was investigated for twenty-two thiazolyl-carbonyl-thiosemicarbazides and thiazolyl-azoles. The determination was carried out by reversed-phase thin-layer chromatography, using a binary isopropanol-water mobile phase. Chromatographically obtained lipophilicity parameters were correlated with calculated log P and log D and with some biological parameters, determined in order to evaluate the anti-inflammatory and antioxidant potential of the investigated compounds, by using principal component analysis (PCA). The PCA grouped the compounds based on the nature of their substituents (X, R and Y), indicating that their nature, electronic effects and molar volumes influence the lipophilicity parameters and their anti-inflammatory and antioxidant effects. Also, the results of the PCA analysis applied on all the experimental and computed parameters show that the best anti-inflammatory and antioxidant compounds were correlated with medium values of the lipophilicity parameters. On the other hand, the knowledge of the grouping patterns of the tested variables allows the reduction of the number of parameters, determined in order to establish the biological activity.

Keywords: thiosemicarbazide; thiazolyl-azole; lipophilicity; PCA; anti-inflammatory; antioxidant

1. Introduction

Lipophilicity is an important physicochemical property of bioactive compounds affecting their biological activity with a determinant role in the transport of compounds through biological membranes and in the formation of the ligand-receptor complex. The lipophilic character of an active molecule, defined as the ability of a compound to penetrate through hydrophobic barriers in order

to get from the delivery point to the site of action [1,2], is usually quantitatively characterized as the logarithmic forms of the *n*-octanol-water partition coefficient P_{ow} ($\text{Log}P_{ow}$) and *n*-octanol-water distribution coefficient D_{ow} ($\text{Log}D_{ow}$)—experimentally determined [3] or calculated by using a series of mathematical models [4]. Due to experimental limitations of the classical “shake-flask” method [5], the most widely used techniques for the measurement of the lipophilic properties of different chemical molecules are nowadays the chromatographic techniques in reversed-phase systems (RP-TLC and RP-HPLC) [6,7].

Some of the parameters resulting from a RP-TLC may be associated to the lipophilic character of the analytes [8,9]. The retention parameters (R_M) are calculated by means of well-known Batte-Smith and Westall Equation (1):

$$R_M = \log(1/R_F - 1) \quad (1)$$

Generally, the R_M values determined by RP-TLC are linearly dependent on the concentration of the organic modifier (C) in the mobile phase Equation (2):

$$R_M = R_{M0} + bC \quad (2)$$

where b and R_{M0} are, respectively, the slope and the intercept of Equation (2). Extrapolation of the R_M value to pure water, leads to determination of R_{M0} , which can be considered as an estimation of the partitioning of compounds between nonpolar stationary phase and the aqueous system, and hence a way to estimate the lipophilicity of the compounds (Soczewinski-Wachtmeister model) [9,10]. Additionally, it has been stated that not only the R_{M0} , but also the slope, b , as a characteristic of the specific hydrophobic surface area of the compounds, can be used as an estimation of lipophilicity [6,11,12]. The advantages of TLC methods consist in the small quantity of compounds needed for the determination, and the rapidity and simplicity of the method. Also, they are inexpensive, rapid and easy to perform [13].

Principal Component Analysis (PCA) is a chemometric tool designed to transform a set of original variables into new uncorrelated variables (axes), which are called principal components. The new variables are linear combinations of the original variables and the new axes lie along the directions of maximum variance. PCA provides an objective way of finding indices of this type, so that the variation in the data can be accounted for, as concisely as possible. By applying PCA to the matrix formed by the retardation factors (R_F) of all compounds in all mobile phases, it is possible to obtain a new lipophilicity scale where the linear combinations of retention indices (the scores) corresponding to the first component (PC1) appears to be a new parameter capable to quantitatively assess the lipophilic character of the compounds [6,14–16].

Based on our experience in the field of heterocyclic compounds [17–19], we synthesized and evaluated *in vivo*, in term of anti-inflammatory and antioxidant activity, a new series of thiazolyl-carbonyl-thiosemicarbazides and hybrid thiazolyl-1,3,4-oxadiazoles, thiazolyl-1,3,4-triazoles and thiazolyl-1,3,4-triazoles [20,21]. The results demonstrated that the new thiazole compounds exhibit anti-inflammatory effects, lowering the acute-phase response of bone marrow and the oxidative stress. Based on the virtual screening and on the obtained results, the activity may be due to their capacity to reduce NO synthesis by blocking the binding of L-arginine at the active site of inducible nitric oxide synthase (iNOS) [21].

The goal of the present study was to determine the relationships between the computed lipophilicity coefficients and RP-TLC retention parameters of new thiazolyl-carbonyl-thiosemicarbazides and thiazolyl-azoles with the anti-inflammatory/antioxidant potential and their structural parameters obtained by molecular modeling calculations, applying the PCA method.

2. Results and Discussion

2.1. Chemistry

Twenty two thiazolyl-carbonyl-thiosemicarbazides and hybrid thiazolyl-1,3,4-oxadiazoles, thiazolyl-1,3,4-triazoles, and thiazolyl-1,3,4-triazoles (**Th1–Th22**), synthesized in our laboratory, according to a previously described procedure [20], were investigated. The structures of the compounds used in this study are presented in Figure 1. All components of the mobile phases used were of analytical grade purity.

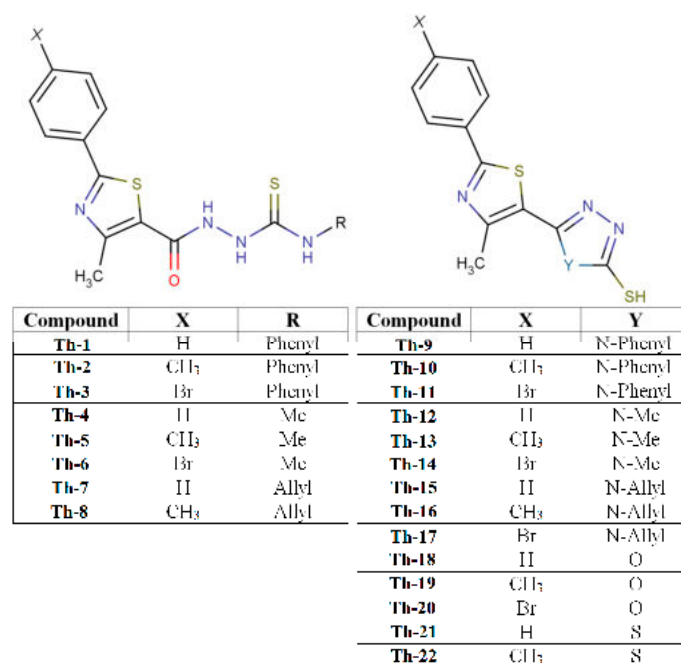


Figure 1. Structures of the studied thiazolyl-carbonyl-thiosemicarbazides and thiazolyl-azole compounds—Marvin was used for drawing and displaying of chemical structures (MarvinSketch 6.3.1, 2014, ChemAxon Kft., Budapest, Hungary, <http://www.chemaxon.com>).

2.2. Lipophilicity Evaluation of the Studied Compounds

In all instances, it was found that the retention of the investigated compounds increased with increasing concentration of the organic modifier in the mobile phase. The change of the retardation factor with increasing the organic solvent content in the binary mobile phase, correlates well with the polarity, the substituents (phenyl, allyl, methyl, hydrogen and bromine). The R_M values obtained from Equation (1) decrease linearly as the concentration of the organic modifier in the mobile phase increases, and therefore they might be used to assess lipophilicity. The profiles of the R_M values present regular changes as the organic modifier content increases, indicating that the same mechanism of lipophilic interaction is dominant (Figure 2). Nevertheless, minor changes of these systematic regularities can be observed with compounds **Th-11–17**, most probably due to their more rigid molecular structures compared to compounds **Th-1–8**.

The results of regression analyses using Equation (2) (intercept values (R_{M0}), slopes (b) and correlation coefficient (r) are presented in Table 1. These values afford a quantitative estimation for the distribution of the investigated compounds between a non-polar phase (a chemically bound reversed stationary phase) that represents the biological membranes, and a polar phase that represents the extracellular aqueous environment. As expected, it can be observed that there is a linear dependence between the values of R_{M0} (lipophilic parameter) and the values of b (specific hydrophobic surface) for the majority of these compounds. This linear dependence shows that thiazolyl derivatives might

form a homologous series of compounds, as has been suggested by some authors [22]. Once more, it can be observed that compound **Th-1-8** has a mean correlation coefficient of 0.979 ± 0.005 , while compounds **Th-9-17** and **Th-18-22** have 0.927 ± 0.034 and 0.925 ± 0.018 , respectively. In addition, similar significant differences ($p < 0.0003$, $12.56 < f < 25.34$, ANOVA test) could be observed between these three groups, for R_{M0} and b values (Table 1). Based on these observations and together with structural aspects (Table 1), the studied compounds have been divided in three groups: compounds **Th-1-8** form group A, while compounds **Th-9-17** and **Th-18-22** form group B and group C, respectively. This classification will be used in further observations and discussions (*vide infra*).

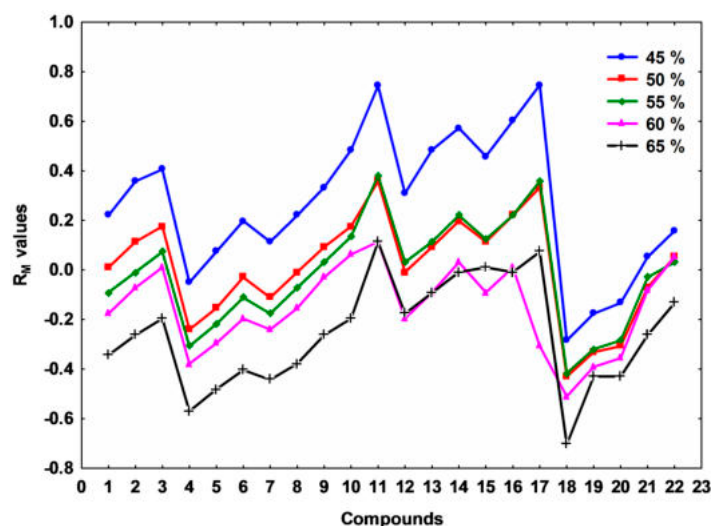


Figure 2. Profiles of R_M values at all mobile binary phase composition (% of organic modifier) for all studied compounds.

Table 1. Retention parameters obtained from equation $R_M = R_{M0} + bC$.

Group	Compd.	R_{M0}	Mean \pm SD	b	Mean \pm SD	r^a	Mean \pm SD
A	Th-1	1.369		-2.627		0.987	
	Th-2	1.595		-2.853		0.980	
	Th-3	1.600		-2.739		0.979	
	Th-4	0.986	1.338 ± 0.213	-2.355	-2.623 ± 0.165	0.979	0.979 ± 0.005
	Th-5	1.161		-2.502		0.976	
	Th-6	1.398		-2.740		0.981	
	Th-7	1.195		-2.484		0.972	
	Th-8	1.398		-2.685		0.975	
B	Th-9	1.479		-2.630		0.965	
	Th-10	1.754		-2.948		0.954	
	Th-11	2.020		-3.133		0.912	
	Th-12	1.305		-2.463		0.899	
	Th-13	1.565	1.779 ± 0.435	-2.672	-3.012 ± 0.680	0.898	0.927 ± 0.034
	Th-14	1.630		-2.659		0.876	
	Th-15	1.664		-2.905		0.943	
	Th-16	1.783		-2.962		0.921	
	Th-17	2.808		-4.737		0.974	
C	Th-18	0.540		-1.840		0.951	
	Th-19	0.286		-1.134		0.920	
	Th-20	0.393	0.508 ± 0.168	-1.283	-1.354 ± 0.279	0.921	0.925 ± 0.018
	Th-21	0.620		-1.286		0.900	
	Th-22	0.701		-1.227		0.931	

^a bold = correlation coefficients > 0.95 . R_{M0} = lipophilicity estimation parameter; b = slope.

Besides the well-known R_{M0} values which are the experimentally-determined indices for the lipophilicity of the studied compounds, PC1 values, which are obtained by applying PCA to the matrix of the R_F values for all mobile phases for all compounds, can be successfully used for quantifying the lipophilicity and may bring complementary information to the R_{M0} [14,15]. The variation of these two parameters for the studied compounds, along with the computed LogP and LogD values, is presented in Figure 3. It can be observed that the R_{M0} and PC1 profiles are well correlated with the profiles of the computed LogP and LogD values, all describing similar patterns. Regarding the experimental lipophilicity parameters, R_{M0} and PC1, the compounds present expected variations of the lipophilicity, as the functional groups are modified (both R and X groups).

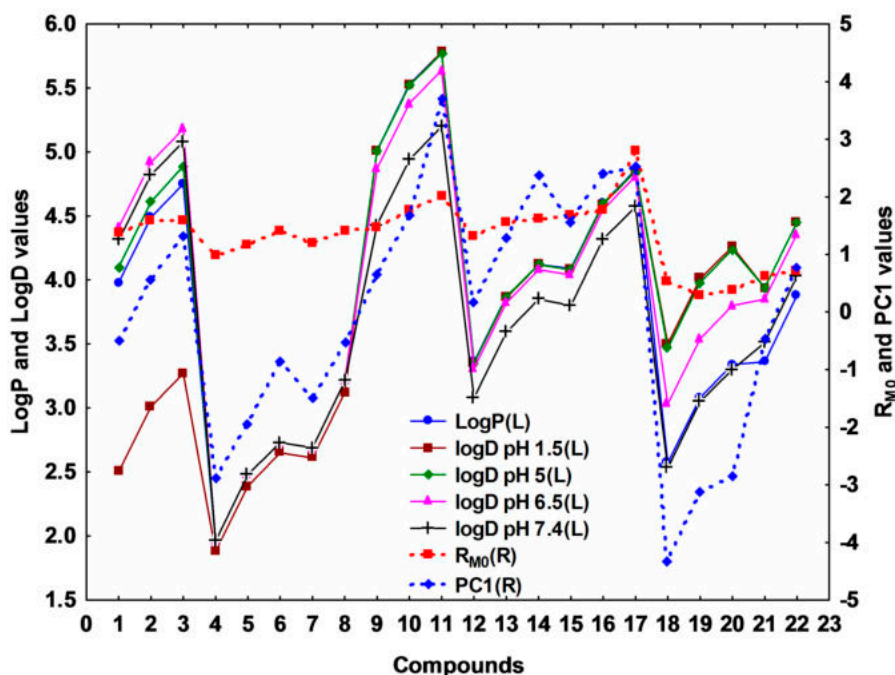


Figure 3. Relationship between computed LogP and LogD (calculated by the equally weighted calculation algorithm combining the three methods described in the [Experimental Section](#)) values profiles and experimental lipophilicity indices R_{M0} and PC1. The L or R information in the brackets refers to either left or right disposition of the values on the y axis.

Analyzing the values obtained for PC1, it was noticed that the cyclisation of thiosemicarbazides **Th-1-8** to the corresponding thiazolyl-triazoles **Th-9-17** increased the lipophilicity, probably as result of a decrease of the polar character of the former, due to the $-\text{CO}-\text{NH}-\text{NH}-\text{CS}-\text{NH}-$ fragment. Concerning the nature of the Y substituent, it can be observed that the presence of an electron withdrawing substituent (phenyl) increases the lipophilicity, while electron donating groups decrease it (**Th-11** > **Th-14** > **Th-17**) (Figure 3). Regarding the X substituent and the whole molecules, as expected in these homologous series, the lipophilicity increases with the molecular volume, the bromo substituted derivatives being the most lipophilic compounds. Also, the *N*-substituted thiazolyl-triazoles (**Th-9-17**) are more lipophilic than the corresponding thiadiazoles (**Th-21-22**) and oxadiazoles (**Th-18-20**), the molecular volume decreasing in the order: group B > group C (S > O) (Figure 3).

According to their structure (Figure 1), the studied compounds can be involved in acid-base equilibria, and are hence ionizable, so that the analysis of the distribution coefficient (LogD) at several physiological relevant pH levels is adequate. Figure 3 also presents the profiles of the LogD values at four pH levels (stomach (1.5), duodenum (5), jeuno-ileum (6.5) and blood serum (7.4) pH levels). The compounds from group A (**Th-1-8**) have slightly basic behavior; the LogD values increase as the

pH increases, with a more pronounced effect, thus a much wider interval of distribution, for the first three compounds—which can be explained by the electron withdrawing inductive effect of the phenyl group. Mainly due to the presence of the thiol group, the compounds from groups B and C (**Th-9-22**) present rather an acidic behavior, which is more evident for compounds **Th-9-11** and in group C (**Th-18-22**). This may suggest that compounds **Th-1-3** are better absorbed in intestine than in stomach, while compounds **Th-9-11** and **Th-18-22** are better absorbed in stomach and less in intestine, due to their higher uncharged population of molecules in the first mentioned compartments. The other compounds (**Th-4-9**, **Th-12-17**) are to a lesser extent affected by pH variation at the studied interval (*i.e.*, 1.5–7.4).

Applying PCA on both experimentally and computed lipophilicity indices on all studied compounds, 2D plot of the loadings (circle correlation) showed a regular increase of the correlation between LogD values and experimentally determined lipophilicity indices (PC1, R_{M0}) as the pH increases (Figure 4 and Figure S1). However, since the compounds behaved differently according to their group, a PCA application on two separated groups: A (basic compounds) and B and C (acidic compounds) revealed interesting results (Figure 5 and Figure S2). As expected, in both groups, PC1 and R_{M0} positively correlate with each other ($r = 0.804$) and these indices present a strong negative correlation with b ($r = -0.965$ with R_{M0} and $r = -0.621$ with PC1) since it is the characteristic of the specific hydrophobic surface area [6,11,12]. LogP and LogD values afford a relatively moderate correlation with the experimentally determined indices, most probably due to the limitation of estimation of computed indices for complex compounds, since none of the available methods can take into consideration all the effects of molecular conformation. However, as can be observed from Figure 5, LogD at acidic pH in the case of group A and LogD at basic pH in the case of groups B and C are more correlated with R_{M0} and PC1 values.

The scatterplot of the scores of the first three principal components after applying PCA on all the previously discussed lipophilicity indices reveals an obvious clustering of the compounds, according to their properties and structural aspects, in very good agreement with the grouping performed in Table 1 (Figure 6). Group A and group B overlap to some extent but group C forms a distinct cluster despite the high scattering within it, most probably due to numerous changes caused by the presence of the heteroatom (Y substituent, Table 1). Compound **Th-17** appeared as an outlier due to its distinct higher R_{M0} value.

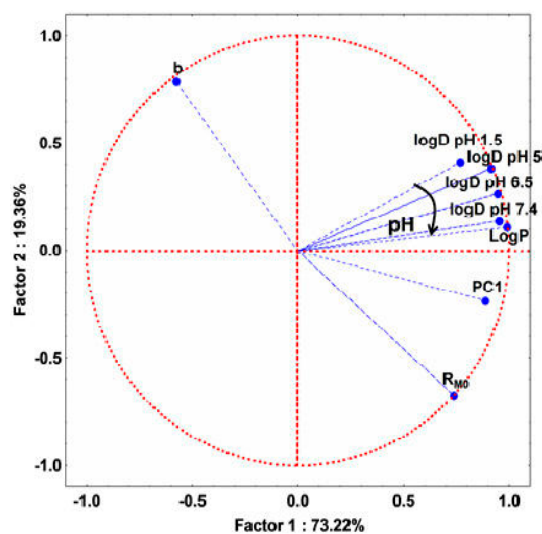


Figure 4. Loadings (circle correlation) for the experimental lipophilicity indices (R_{M0} , PC1, b) and computed (logD and logP—calculated by the equally weighted calculation algorithm combining the three methods described in the [Experimental Section](#)) lipophilicity indices for all the studied compounds.

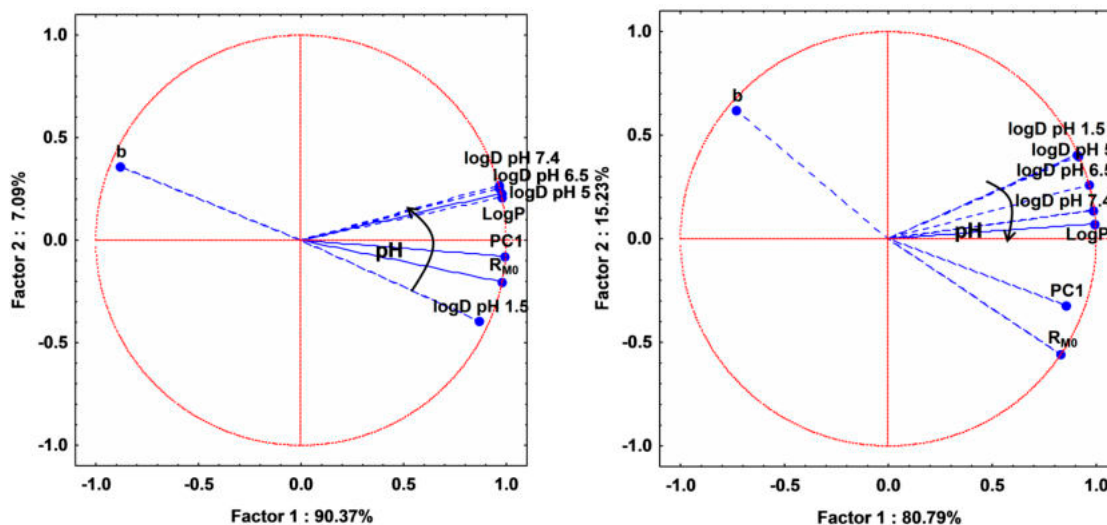


Figure 5. Loadings (circle correlation) for the experimental lipophilicity indices (R_{M0} , PC1, b) and computed (LogD and LogP—calculated by the equally weighted calculation algorithm combining the three methods described in the [Experimental Section](#)) lipophilicity indices for compounds in group A (left) and for compounds in groups B and C (right).

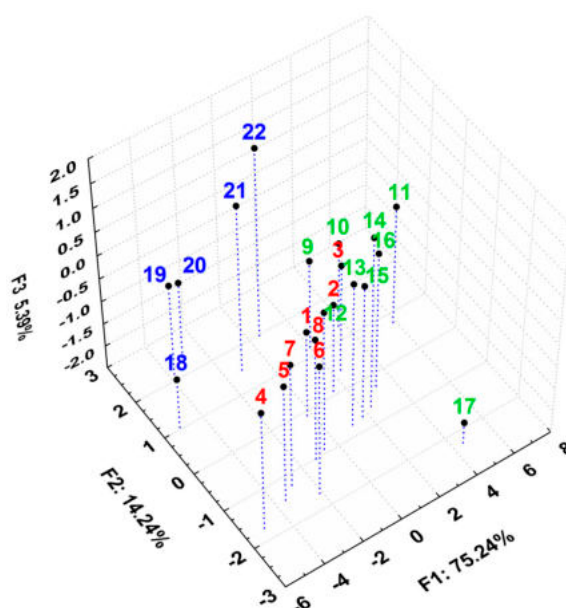


Figure 6. 3D plot of the scores for first three principal components after applying PCA on all the discussed parameters, describing lipophilicity for all the studied compounds.

2.3. Antioxidant and Anti-Inflammatory Effects of the Studied Compounds

The new thiazole compounds have anti-inflammatory effects by lowering the acute-phase response of bone marrow (L and PMN), phagocytic capacity (PI and PA) and oxidative stress [21]. The best anti-inflammatory and antioxidant effects were found for thiazolyl-carbonyl-thiosemicarbazides **Th-1-8** (Group A) and for the oxadiazoles **Th-18-20** and thiadiazole **Th-21** (Group C). Also, the virtual screening of thiazole derivatives revealed that all twenty-two compounds bind the active site of iNOS [21]. Based on the virtual screening and on the obtained results, the activity may be due to their capacity to reduce NO synthesis by blocking the active site of iNOS [21].

In order to obtain a model with less variables, we applied PCA on determined biological parameters (L, PMN, PA, PI, NO, TOS, TAR, OSI) (Table 2).

Table 2. Effect of thiazolyl-carbonyl-thiosemicarbazides and thiazolyl-azoles on the determined biological parameters for anti-inflammatory and antioxidant activities.

Comp.	Leukocytes	PMN	PA	PI	NO	TOS	TAR	OSI
Th-1	5587.5 ± 455	60.4 ± 4.1	18.5 ± 1.8	21.5 ± 4.6	50.479 ± 5.7	51.622 ± 6.2	1.108 ± 0.003	4.66 ± 2.2
Th-2	6543 ± 271	60.6 ± 3.1	22.5 ± 2.8	21.5 ± 2.8	51.827 ± 6.3	63.265 ± 5.4	1.099 ± 0.003	5.76 ± 5.3
Th-3	4987 ± 133	63.6 ± 3.9	31 ± 1.8	21.5 ± 0.9	52.838 ± 8.9	39.601 ± 7.9	1.095 ± 0.003	3.62 ± 2.9
Th-4	12,218.8 ± 1341	82.8 ± 4.1	29 ± 1.8	22.5 ± 3.5	47.501 ± 2.8	49.823 ± 3.6	1.109 ± 0.006	4.49 ± 3.6
Th-5	11,633.3 ± 154	59.8 ± 3.6	22.5 ± 0.9	19.5 ± 2.3	47.024 ± 8.9	51.557 ± 17.1	1.096 ± 0.001	4.7 ± 3.1
Th-6	6056.25 ± 862	70.4 ± 2.9	18 ± 1.5	13 ± 3.2	50.591 ± 9.1	43.108 ± 5.6	1.097 ± 0.006	3.93 ± 2.6
Th-7	6356.25 ± 66	73.2 ± 4.0	53.5 ± 3.5	20.5 ± 0.9	54.355 ± 6.2	44.073 ± 3.8	1.107 ± 0.003	3.98 ± 3.8
Th-8	5718.75 ± 104	66.6 ± 1.0	21 ± 1.1	21.5 ± 0.9	48.793 ± 5.5	55.664 ± 4.2	1.107 ± 0.002	5.03 ± 4.1
Th-9	9000 ± 428	67.4 ± 3.0	20.5 ± 0.9	21 ± 7.0	65.479 ± 4.8	68.780 ± 16.2	1.101 ± 0.001	6.25 ± 5.2
Th-10	5606.25 ± 154	61.2 ± 3.4	23 ± 1.1	20.5 ± 0.9	65.142 ± 5.3	54.164 ± 5.4	1.095 ± 0.003	4.95 ± 5.4
Th-11	11,137.5 ± 483	86.4 ± 2.6	19.75 ± 2.4	21 ± 1.1	66.799 ± 5.9	66.394 ± 8.9	1.092 ± 0.003	6.08 ± 4.9
Th-12	8456.25 ± 565	78.6 ± 1.0	20 ± 1.5	22.5 ± 3.5	70.029 ± 6.4	90.592 ± 4.2	1.095 ± 0.004	8.27 ± 4.2
Th-13	10,172 ± 331	80.8 ± 3.0	27.5 ± 0.9	25.5 ± 2.8	75.451 ± 6.9	50.886 ± 5.6	1.1 ± 0.012	4.63 ± 3.6
Th-14	10,172 ± 520	75.4 ± 4.5	23.5 ± 0.9	28 ± 2.1	86.04 ± 2.9	66.876 ± 9.7	1.097 ± 0.006	6.1 ± 4.7
Th-15	9982.5 ± 81	77.4 ± 5.1	29 ± 3.2	24 ± 4.3	71.630 ± 5.9	69.171 ± 4.4	1.094 ± 0.006	6.32 ± 4.4
Th-16	9225 ± 333	77.4 ± 1.9	27 ± 1.1	21.2 ± 1.0	63.091 ± 5.1	66.681 ± 9.1	1.103 ± 0.009	6.04 ± 4.1
Th-17	10,147.5 ± 528	75.4 ± 5.2	19.5 ± 0.9	15 ± 3.5	60.479 ± 11.8	69.962 ± 5.2	1.093 ± 0.003	6.38 ± 5.2
Th-18	4575 ± 805	63.7 ± 2.4	56 ± 8.6	17 ± 1.9	43.23 ± 3.9	78.089 ± 14.1	1.118 ± 0.006	6.98 ± 4.1
Th-19	7443.75 ± 1172	72.8 ± 5.0	13.5 ± 2.78	20 ± 1.5	45.198 ± 2.2	79.849 ± 12	1.119 ± 0.009	7.13 ± 5.9
Th-20	4837.5 ± 1305	59.2 ± 5.6	20 ± 1.5	16 ± 3.0	43.288 ± 5.0	81.022 ± 13.2	1.106 ± 0.003	7.32 ± 3.2
Th-21	3000 ± 241	52.6 ± 2.1	23 ± 1.9	14.5 ± 4.6	43.737 ± 6.2	67.137 ± 10.6	1.114 ± 0.007	6.03 ± 4.5
Th-22	5812.5 ± 399	66.4 ± 0.8	23.5 ± 0.9	35 ± 8.2	52.08 ± 8.1	56.694 ± 7.9	1.105 ± 0.001	5.13 ± 4.9

After applying PCA only on these biological activity parameters, an acceptable model was obtained, the first three principal components containing 75.87% of total variance (Figure S3). However, it is interesting that the 3D scatterplot of the first three principal components revealed a pattern of clustering of the studied compounds, similar to the one of their lipophilicity (Figure 7). The three groups are well and distinctly grouped, with compound **Th-22** as an exception. Here, groups A and B are better separated than in case of the lipophilicity (Figure 6), indicating their more distinct behavior in case of their biological activities.

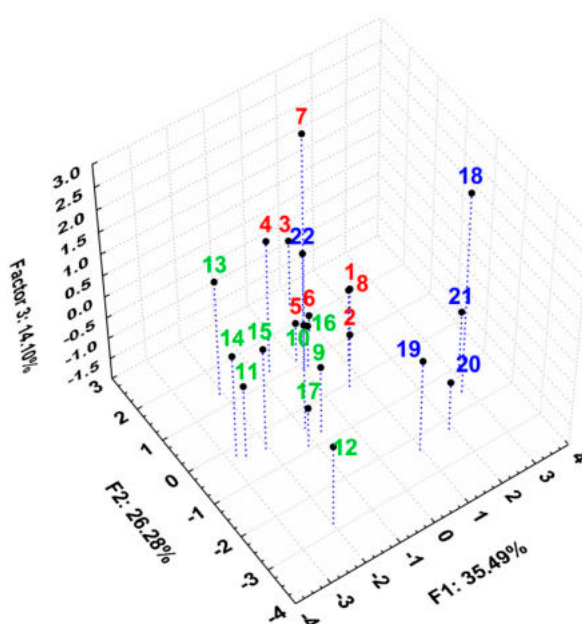


Figure 7. 3D scatterplot of the scores for the first three principal components after applying PCA on all the discussed parameters, describing biological activity for all the studied compounds.

2.4. Comparative Evaluation of Both Lipophilicity Indices and Antioxidant and Anti-Inflammatory Activities Evaluation for the Studied Compounds

A similar clustering of the compounds to the one seen in the case of their lipophilicity indicates that there are some possible correlations between their lipophilicity and their biological activity. In this regard, PCA was applied on all the studied variables, describing lipophilicity and the anti-inflammatory and antioxidant activities. After applying PCA, an acceptable model was obtained—the first three principal components containing 74.96% of total variance (Figure S4). Analyzing the loadings of the variables and the matrix correlation of the original variables, we observed that NO parameter is positively correlated with the lipophilicity, and TAR activities are negatively correlated with the lipophilicity indices (Figure 8, Table 3).

Table 3. Correlation matrix of the lipophilicity indices and antioxidant and anti-inflammatory effects for all the studied compounds. Values greater than 0.5 are in bold face characters.

	L	PMN	PA	PI	NO	TOS	TAR	OSI	R _{M0}	b	PC1
L	1.000	0.735	−0.175	0.250	0.522	0.025	−0.455	0.043	0.453	−0.469	0.313
PMN		1.000	0.016	0.281	0.576	0.086	−0.305	0.098	0.398	−0.384	0.354
PA			1.000	−0.008	−0.111	−0.162	0.291	−0.174	−0.166	0.071	−0.318
PI				1.000	0.443	−0.105	−0.127	−0.098	−0.009	0.153	0.320
NO					1.000	0.109	−0.629	0.135	0.600	−0.474	0.741
TOS						1.000	0.178	0.999	−0.206	0.208	−0.091
TAR							1.000	0.142	−0.782	0.704	−0.741
OSI								1.000	−0.178	0.184	−0.063
R _{M0}									1.000	−0.965	0.804
b										1.000	−0.621
PC1											1.000

L = leukocytes; PMN = polymorphonuclear leukocytes; PA = phagocytic activity; PI = phagocytosis index; NO = nitric oxide; TOS = total oxidative status; TAR = total antioxidant response; OSI = oxidative stress index; R_{M0} = lipophilicity estimation parameter; b = slope; PC1 = first principal component.

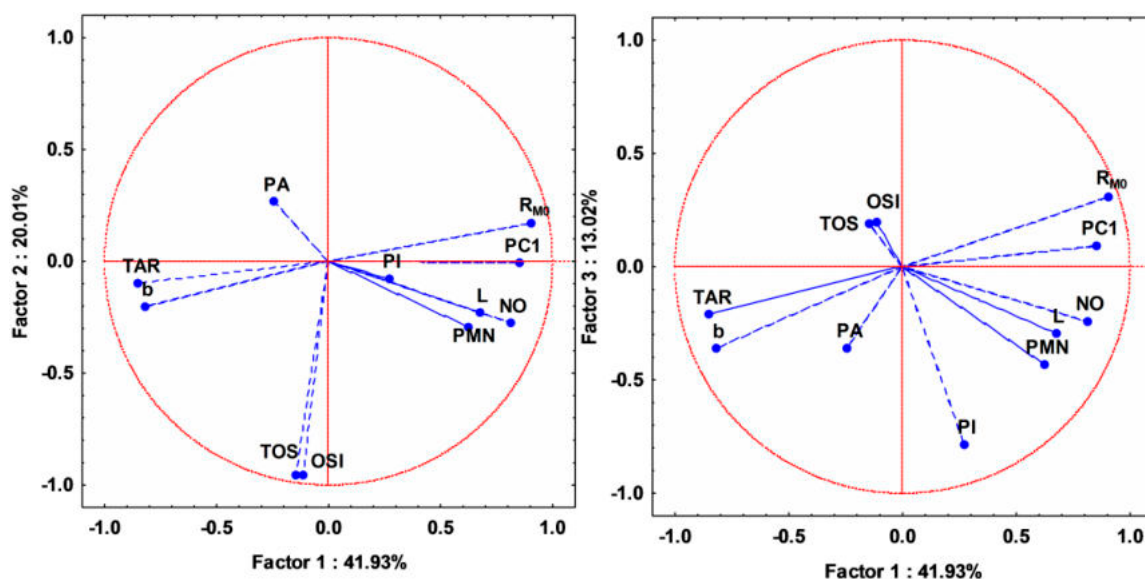


Figure 8. Loadings (circle correlation) for the assessed biological activity (left panel) and lipophilicity indices (right panel) for all studied compounds. L = leukocytes; PMN = polymorphonuclear leukocytes; PA = phagocytic activity; PI = phagocytosis index; NO = nitric oxide; TOS = total oxidative status; TAR = total antioxidant response; OSI = oxidative stress index; R_{M0} = lipophilicity estimation parameter; b = slope; PC1 = first principal component.

Besides this, PA, PI, TOS and OSI have statistically no correlation, while PMN and L have low correlation with any lipophilicity indices. However, the two previously mentioned variables (TAR and NO) have distinctly higher correlation with all lipophilicity indices. Activation and stimulation of phagocytes in the inflammatory process is dependent on membrane-derived lipid mediators (e.g., arachidonic acid derivatives) [23,24]. This may explain the positive correlation between the reactive nitrogen intermediates (RNIs) (*i.e.*, NO), produced by phagocytes, and lipophilicity (Figures 8 and 9). On the other hand, as a consequence of oxidative stress increase by reactive oxygen intermediates (ROIs) and RNIs, the antioxidant defense capacity is reduced. This justifies the negative correlation between TAR and lipophilicity (Figures 8 and 9).

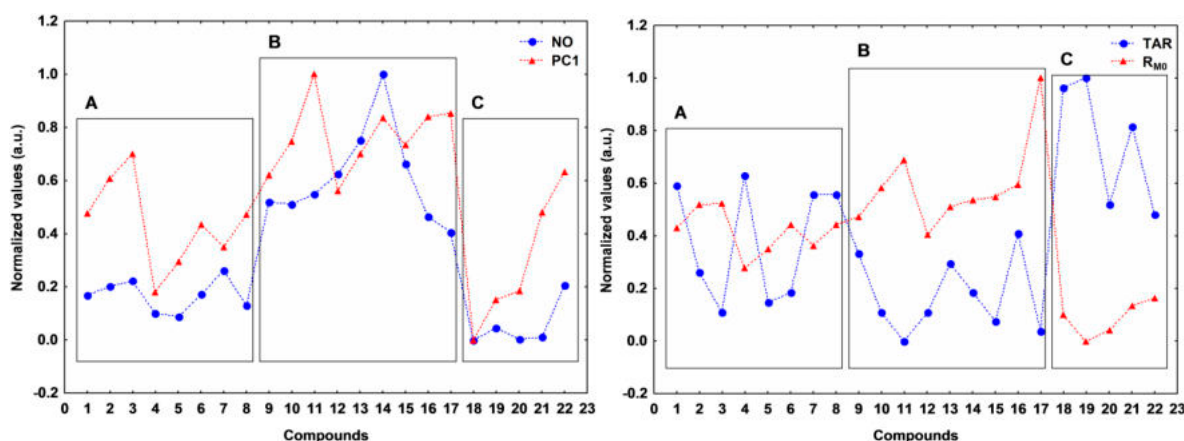


Figure 9. Profiles of NO *vs.* PC1 (left panel) and TAR *vs.* R_{MO} (right panel) for all studied compounds.

The 3D scatterplot of the scores for the first three principal components reported in Figure 10 reveals an even better and more compact clustering for the studied compounds forming the three distinct groups: the thiosemicarbazides Th-1-8 from group A with the best anti-inflammatory and antioxidant effects [21], the triazoles Th-9-17 from group B and the oxadiazoles and thiadiazoles Th-18-22 from group C.

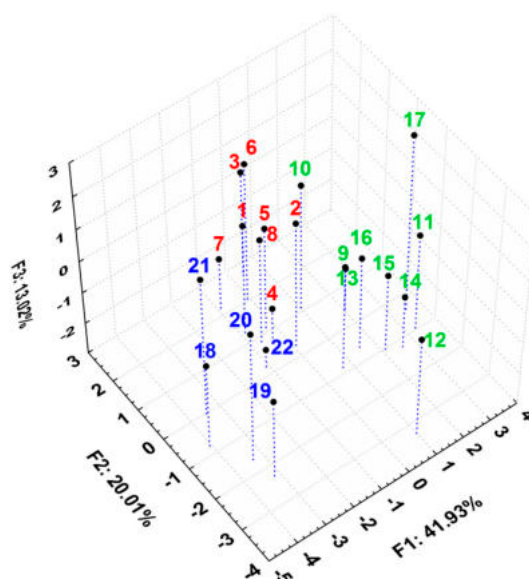


Figure 10. 3D scatterplot of the scores for the first three principal components after applying PCA on all the discussed parameters describing biological activity and lipophilicity for all studied compounds.

The knowledge of the grouping patterns of the tested variables allows for the reduction of experimental determined parameters, the variables which are close to each other in PCA results describing similar properties of the substances. For this reason, it is not necessary to measure and evaluate all variables to achieve the same characterization—thus reducing the amount of experimental work required [25].

The pattern of the profiles of both NO and TAR *vs.* PC1 and R_{M0} respectively, clearly sustain the positive and negative correlation (Figure 9). For the first case (NO *vs.* PC1), the A and C groups present a distinctly higher similarity of the pattern than the B group (Figure 9 left), and the NO synthesis increases with the lipophilicity in agreement with the previous observations. Thus, best anti-inflammatory compounds **Th-1-8** have the medium values for the lipophilicity parameters. For the second case, the negative correlation profiles between TAR and R_{M0} (Figure 9 right) is salient for group A and for some compounds from groups B and C. The negative correlation might be explained by the fact that the increase in hydrophobicity of a given compound may imply an increase in redox potential, thus decreasing its antioxidant ability [26].

3. Experimental Section

3.1. Chromatographic Procedure

Chromatography was performed on 20 × 20 cm RP-18F_{254s} TLC precoated silica plates (Merck; Darmstadt, Germany). Solutions (1 mg/mL) of the tested compounds were prepared in *iso*-propanol, and 3 µL aliquots were spotted in duplicate on the plates by hand, 10 mm from the bottom edge and 20 mm apart. The mobile phases were composed of the *iso*-propanol-water binary mixtures, with a varying content of organic modifier between 45% and 65% (*v/v*) in 5% increments, as the study compounds differed considerably in their retention. Chromatography was performed in a normal developing chamber at room temperature, the developing distance being 10 cm. The chromatography chamber was saturated with the mobile phase for 30 min before use. After the development (30–60 min), the plates were air dried at room temperature and examined under a UV lamp ($\lambda = 254$ nm), and the R_F (retardation factor) values were measured manually by a digital caliper. The experiments were performed in triplicate.

3.2. Prediction of Partitioning and Distribution Coefficients

The lipophilicity effects of compounds were predicted as log P and log D using the partitioning module of MarvinSketch 5.5.0.1, 2011 (ChemAxon Kft., Budapest, Hungary, <http://www.chemaxon.com>). Calculations for log D were estimated for the implicit reference values: log D_{1.5} (log D calculated at the physiological pH of stomach), log D_{5.0} (log D calculated at the physiological pH of duodenum), log D_{6.5} (log D calculated at the physiological pH of jejunum-ileum) and log D_{7.4} (log D calculated at the physiological pH of blood serum). Both calculations for log P and log D were performed using four different methods: a calculation algorithm developed by ChemAxon Kft. based on the publication of Viswanadhan and coworkers [27], one based on method developed by Klopman and coworkers [28], another one using the log P data from PHYSPROP© database and an equally weighted calculation algorithm combining the three methods. Supplementary, the software was set to take in account, for each set of calculations/algorithm, the major tautomeric forms of each compound.

3.3. Biological Activity Measurements

The synthesized thiazolyl-carbonyl-thiosemicarbazides and thiazolyl-azoles **Th-1-Th-22** were previously evaluated *in vivo* for their anti-inflammatory activity in a turpentine oil-induced inflammation model [21]. Their anti-inflammatory activity was assessed by evaluating the acute-phase response of bone marrow by leukocytes count (L) and by differential leucocyte count, expressed as a percentage (PMN) and by phagocytes' capacity (PI%-phagocytosis index,

PA-phagocytic activity), nitric oxide (NO) synthesis and antioxidant capacity (TOS-total oxidative status, TAR-total antioxidant response and OSI-oxidative stress index [21]).

3.4. Statistical Analysis

All results were expressed as mean \pm standard deviation (SD) of three independent experiments. Statistical comparisons between the groups were performed using one-way analysis of variance (ANOVA) test. A value of $p < 0.05$ was considered to be statistically significant.

4. Conclusions

The applied PCA method of multivariate analysis allowed us to compare the chromatographic retention data, the lipophilic parameters and the biological parameters of the investigated thiazolyl-carbonyl-thiosemicarbazides and thiazolyl-azoles.

The obtained results illustrate how the nature of the substituents attached to a pharmacophore (thiazole for group A, thiazolyl-azole for groups B and C) influences the chromatographic retention, *i.e.*, the lipophilic behavior and the determined biological parameters of the investigated compounds.

The PCA method could be used to group the studied compounds based on the influence of the substituents on the lipophilic character of the whole molecule. Also, the results of the PCA analysis applied on all the experimental and computed lipophilic parameters and on the biological parameters show, as expected, that the best anti-inflammatory and antioxidant compounds are correlated with medium values for the lipophilicity parameters (an optimum hydrophilic-lipophilic balance). The knowledge of the grouping patterns of the tested variables offers the possibility to reduce the number of determined parameters, needed for predicting biological activity.

Supplementary Materials: Supplementary materials can be accessed at: <http://www.mdpi.com/1420-3049/20/12/19841/s1>.

Acknowledgments: This study was supported by The Executive Agency for Higher Education Research Development and Innovation Funding (UEFISCDI), Bucharest, Romania, on the Contract no. 210/2014—Project PN-II-PT-PCCA-2013-4-2075 “Synthesis, screening and controlled release of some novel thiazole, bithiazole and thiazolidin-4-one compounds with antioxidant, antiproliferative and antimicrobial activity”.

Author Contributions: Radu Tamaian was responsible of virtual prediction of the lipophilicity parameters, using computer software. Augustin Moț and Radu Silaghi-Dumitrescu have done the correlations between the biological parameters and lipophilicity and chemical structures. Brîndușa Tipericiuc conducted the design of this study and supervised all the steps of the project. Ovidiu Oniga, Brîndușa Tipericiuc, Ioana Ionuț, Anca Stana, Cristina Nastasă, Daniela Benedec were responsible for the experimental determination of lipophilicity parameters, the analyze of the results from the biological investigation, collecting data, interpreting correlation partial results and writing the manuscript.

Conflicts of Interest: The authors declare no conflict of interest.

References

1. Testa, B.; Crivori, P.; Reist, M.; Carrupt, P.-A. The influence of lipophilicity on the pharmacokinetic behavior of drugs: Concepts and examples. *Perspect. Drug Discov. Des.* **2000**, *19*, 179–211. [CrossRef]
2. Van de Waterbeemd, H. Calculation of drug lipophilicity—The hydrophobic fragmental constant approach. *Quant. Struct. Act. Relatsh.* **1993**, *12*. [CrossRef]
3. Sangster, J. *Octanol-Water Partition Coefficients: Fundamentals and Physical Chemistry*, 1st ed.; John Wiley & Sons Ltd.: Hoboken, NJ, USA, 1997.
4. Mannhold, R.; Poda, G.I.; Ostermann, C.; Tetko, I.V. Calculation of molecular lipophilicity: State-of-the-art and comparison of log *P* methods on more than 96,000 compounds. *J. Pharm. Sci.* **2009**, *98*, 861–893. [CrossRef] [PubMed]
5. Leo, A.; Hansch, C.; Elkins, D. Partition coefficients and their uses. *Chem. Rev.* **1971**, *71*, 525–616. [CrossRef]
6. Tipericiuc, B.; Sârbu, C. Prediction of the chromatographic retention (lipophilicity) of some new methyl-thiazole-oxadiazoline derivatives by multivariate regression methods. *J. Liq. Chromatogr. Relat. Technol.* **2006**, *29*, 2257–2270. [CrossRef]

7. Durcekova, T.; Boronova, K.; Mocak, J.; Lehotay, J.; Cizmarik, J. QSRR models for potential local anaesthetic drugs using high performance liquid chromatography. *J. Pharm. Biomed. Anal.* **2012**, *59*, 209–216. [[CrossRef](#)] [[PubMed](#)]
8. Pyka, A.; Miszczyk, M. Chromatographic evaluation of the lipophilic properties of selected pesticides. *Chromatographia* **2005**, *61*, 37–42. [[CrossRef](#)]
9. Biagi, G.L.; Barbaro, A.M.; Sapone, A.; Recanatini, M. Determination of lipophilicity by means of reversed-phase thin-layer chromatography I. Basic aspects and relationship between slope and intercept of TLC equations. *J. Chromatogr. A* **1994**, *662*, 341–361. [[CrossRef](#)]
10. Soczewiński, E.; Wachtmeister, C.A. The relation between the composition of certain ternary two-phase solvent systems and RM values. *J. Chromatogr. A* **1962**, *7*, 311–320. [[CrossRef](#)]
11. Sârbu, C.; Casoni, D.; Darabantu, M.; Maioreanu, C. Quantitative structure—Retention activity relationship of some 1,3-oxazolidine systems by RP-HPTLC and PCA. *J. Pharm. Biomed. Anal.* **2004**, *35*, 213–219. [[CrossRef](#)] [[PubMed](#)]
12. Alvarez-Coque, M.C.G.; Lapasió, J.R.T. Quantitation of hydrophobicity in micellar liquid chromatography. *TrAC Trends Anal. Chem.* **1999**, *18*, 533–543. [[CrossRef](#)]
13. Fuchs, B.; Süß, R.; Teuber, K.; Eibisch, M.; Schiller, J. Lipid analysis by thin-layer chromatography—A review of the current state. *J. Chromatogr. A* **2011**, *1218*, 2754–2774. [[CrossRef](#)] [[PubMed](#)]
14. Maćkiewicz, A.; Ratajczak, W. Principal components analysis. *Comput. Geosci.* **1993**, *19*, 303–342. [[CrossRef](#)]
15. Mannhold, R.; Cruciani, G.; Dross, K.; Rekker, R.F. Multivariate analysis of experimental and calculative descriptors for molecular lipophilicity. *J. Comput. Aided Mol. Des.* **1998**, *12*, 573–581. [[CrossRef](#)] [[PubMed](#)]
16. Casoni, D.; Kot-Wasik, A.; Namieśnik, J.; Sârbu, C. Lipophilicity data for some preservatives estimated by reversed-phase liquid chromatography and different computation methods. *J. Chromatogr. A* **2009**, *1216*, 2456–2465. [[CrossRef](#)] [[PubMed](#)]
17. Oniga, O.; Grosu, I.; Mager, S.; Simiti, I. Heterocycles LXXVIII. Electrophilic substitution 2'-phenyl-4R-2,4'-bisthiazoles. *Monatsh. Chem.* **1998**, *129*, 661–669. [[CrossRef](#)]
18. Zaharia, V.; Ignat, A.; Palibroda, N.; Ngameni, B.; Kuete, V.; Fokunang, C.N.; Mounang, M.L.; Ngadjui, B.T. Synthesis of some *p*-toluenesulfonyl-hydrazinotiazoles and hydrazino-*bis*-thiazoles and their anticancer activity. *Eur. J. Med. Chem.* **2010**, *45*, 5080–5085. [[CrossRef](#)] [[PubMed](#)]
19. Moldovan, C.M.; Oniga, O.; Pârnu, A.; Tipericiu, B.; Verité, P.; Pîrnău, A.; Crişan, O.; Bojiţă, M.; Pop, R. Synthesis and anti-inflammatory evaluation of some new acyl-hydrazones bearing 2-aryl-thiazole. *Eur. J. Med. Chem.* **2011**, *46*, 526–534. [[CrossRef](#)] [[PubMed](#)]
20. Tipericiu, B.; Zaharia, V.; Colosi, I.; Moldovan, C.; Crişan, O.; Pîrnău, A.; Vlase, L.; Duma, M.; Oniga, O. Synthesis and evaluation of antimicrobial activity of some new hetaryl-azoles derivatives obtained from 2-aryl-4-methylthiazol-5-carbohydrazides and isonicotinic acid hydrazide. *J. Heterocycl. Chem.* **2012**, *49*, 1407–1414. [[CrossRef](#)]
21. Tipericiu, B.; Pârnu, A.; Tamaian, R.; Nastasă, C.; Ionuţ, I.; Oniga, O. New anti-inflammatory thiazolyl-carbonyl-thiosemicarbazides and thiazolyl-azoles with antioxidant properties as potential iNOS inhibitors. *Arch. Pharm. Res.* **2013**, *36*, 702–714. [[CrossRef](#)] [[PubMed](#)]
22. Horváth, C.; Melander, W.; Molnár, I. Solvophobic interactions in liquid chromatography with nonpolar stationary phases. *J. Chromatogr. A* **1976**, *125*, 129–156. [[CrossRef](#)]
23. Apostolova, N.; Garcia-Bou, R.; Hernandez-Mijares, A.; Herance, R.; Rocha, M.; Victor, V.M. Mitochondrial antioxidants alleviate oxidative and nitrosative stress in a cellular model of sepsis. *Pharm. Res.* **2011**, *28*, 2910–2919. [[CrossRef](#)] [[PubMed](#)]
24. Asadollahi, K.; Beeching, N.J.; Gill, G.V. Leukocytosis as a predictor for non-infective mortality and morbidity. *QJM* **2010**, *103*, 285–292. [[CrossRef](#)] [[PubMed](#)]
25. Vastag, G.; Apostolov, S.; Perišić-Janjić, N.; Matijević, B. Multivariate analysis of chromatographic retention data and lipophilicity of phenylacetamide derivatives. *Anal. Chim. Acta* **2013**, *767*, 44–49. [[CrossRef](#)] [[PubMed](#)]
26. De Faria, C.M.Q.G.; Nazaré, A.C.; Petrônio, M.S.; Paracatu, L.C.; Zeraik, M.L.; Regasini, L.O.; Silva, D.H.S.; da Fonseca, L.M.; Ximenes, V.F. Protocatechuic acid alkyl esters: Hydrophobicity as a determinant factor for inhibition of NADPH oxidase. *Curr. Med. Chem.* **2012**, *19*, 4885–4893. [[CrossRef](#)] [[PubMed](#)]

27. Viswanadhan, V.N.; Ghose, A.K.; Revankar, G.R.; Robins, R.K. Atomic physicochemical parameters for three dimensional structure directed quantitative structure-activity relationships. 4. Additional parameters for hydrophobic and dispersive interactions and their application for an automated superposition of certain naturally occurring nucleoside antibiotics. *J. Chem. Inf. Model.* **1989**, *29*, 163–172.
28. Klopman, G.; Li, J.-Y.; Wang, S.; Dimayuga, M. Computer automated log *P* calculations based on an extended group contribution approach. *J. Chem. Inf. Model.* **1994**, *34*, 752–781. [[CrossRef](#)]

Sample Availability: Samples of the compounds **Th-1–22** are available from the authors.



© 2015 by the authors; licensee MDPI, Basel, Switzerland. This article is an open access article distributed under the terms and conditions of the Creative Commons by Attribution (CC-BY) license (<http://creativecommons.org/licenses/by/4.0/>).

New anti-inflammatory thiazolyl-carbonyl-thiosemicarbazides and thiazolyl-azoles with antioxidant properties as potential iNOS inhibitors

Brîndușa Tipericiuc, Alina Pârvu, Radu Tamaian, Cristina Nastasă, Ioana Ionuț & Ovidiu Oniga

Archives of Pharmacal Research

ISSN 0253-6269

Volume 36

Number 6

Arch. Pharm. Res. (2013) 36:702-714

DOI 10.1007/s12272-013-0083-9



Your article is protected by copyright and all rights are held exclusively by The Pharmaceutical Society of Korea. This e-offprint is for personal use only and shall not be self-archived in electronic repositories. If you wish to self-archive your article, please use the accepted manuscript version for posting on your own website. You may further deposit the accepted manuscript version in any repository, provided it is only made publicly available 12 months after official publication or later and provided acknowledgement is given to the original source of publication and a link is inserted to the published article on Springer's website. The link must be accompanied by the following text: "The final publication is available at link.springer.com".

New anti-inflammatory thiazolyl-carbonyl-thiosemicarbazides and thiazolyl-azoles with antioxidant properties as potential iNOS inhibitors

Brîndușa Tiperçiuc · Alina Pârvu · Radu Tamaian ·
Cristina Nastasă · Ioana Ionuț · Ovidiu Oniga

Published online: 16 March 2013
© The Pharmaceutical Society of Korea 2013

Abstract The objective of this study was to investigate the anti-inflammatory and antioxidant activity of new thiazolyl-carbonyl-thiosemicarbazides and thiazolyl-azole derivatives as potential iNOS inhibitors. The *in vivo* anti-inflammatory effects of the new thiazole compounds were studied in a turpentine oil induced inflammation model. Their anti-inflammatory activity was assessed by evaluating the acute phase bone marrow response, phagocytes' activity, NO synthesis and antioxidant capacity. The new thiazole compounds have anti-inflammatory effects by lowering bone marrow acute phase response and oxidative stress. The best anti-inflammatory and antioxidant effect was found for thiazolyl-carbonyl-thiosemicarbazides **Th-1-8**, thiazolyl-1,3,4-oxadiazole **Th-20** and thiazolyl-1,3,4-thiadiazole **Th-21**. Virtual screening of thiazole derivatives against the oxygenase domain of chain A from 2Y37 revealed that all twenty-two compounds bind the active site of inducible nitric oxide synthase (iNOS). Based on the virtual screening and on the results obtained above,

the activity may be due to their capacity to reduce the NO synthesis by blocking the bind of L-Arg in the active site of iNOS, the compounds binding the synthase by hydrogen bonds between the NH (2 and/or 4) of thiosemicarbazide fragment (**Th-2-8**) or N2/N3 from azole cycles and by the thiol function (**Th-9-22**).

Keywords Thiazole · Thiosemicarbazides · Anti-inflammatory · Oxidative stress · Nitric oxide · Virtual screening · iNOS

Introduction

The inflammatory response prepares the organism to act against intruding agents. A large array of inflammatory mediators induces local vascular and cellular changes and a systemic acute phase response (SAPR) (Jain et al. 2011) or immune phase, that comprises a series of events that lead to migration of leukocytes to the inflammatory site. Upon activation, phagocytes produce reactive oxygen intermediates (ROIs) and nitric oxide (NO) (Silva 2010). The production of ROIs is kept to minimum by antioxidant mechanisms (Palmieri and Sblendorio 2010; Wink et al. 2001). ROIs may combine with NO and form reactive nitrogen intermediates (RNIs). Excessive production of ROIs and RNIs can lead to oxidative stress. This occurs in biological systems when there is an overproduction of ROIs and/or there is a deficiency of antioxidants. The excess ROIs induce cellular damage that can lead to apoptosis or necrosis, can damage cellular lipids, proteins and DNA. Assessment of oxidative stress and development of disease-specific antioxidant therapies are based upon mechanisms of specific disruption of redox processes (Jones 2006; Espey et al. 2000; Valko et al. 2007).

B. Tiperçiuc, A. Pârvu and R. Tamaian contributed equally to this work.

B. Tiperçiuc (✉) · C. Nastasă · I. Ionuț · O. Oniga
Department of Pharmaceutical Chemistry, Faculty of Pharmacy,
Iuliu Hațieganu University of Medicine and Pharmacy,
400010 Cluj-Napoca, Romania
e-mail: brandu32@yahoo.com

A. Pârvu
Department of Physiopathology, Faculty of Medicine,
Iuliu Hațieganu University of Medicine and Pharmacy,
Cluj-Napoca, Romania

R. Tamaian
Research and Development Department, National Institute
for Research and Development for Cryogenic and Isotopic
Technologies, 240050 Ramnicu Valcea, Romania

NO is produced by the nitric oxide synthase (NOS) from L-arginine (L-Arg) in a reaction that requires molecular oxygen and electrons. There are three isoforms of NOS: neuronal NOS (nNOS or NOS1) and endothelial cell NOS (eNOS or NOS3), both constitutively expressed, whereas inducible NOS (iNOS or NOS2) is calcium independent and induced by inflammatory cytokines such as TNF- α and IFN- γ . All three isoforms are multi-domain hemeproteins consisting in a N-terminal oxygenase domain linked by a CaM binding site to a C-terminal reductase domain (Daff 2010). The oxygenase domain of NOS contains the binding sites for the substrate (L-Arg), the heme (iron protoporphyrin IX) and the redox cofactor (6*R*)-5,6,7,8-tetrahydrobiopterin (BH₄).

The active sites of the three isoforms are almost identical, so the designing of new drugs capable to block or inhibit only one of the three forms (especially iNOS) is a major challenge for the medicinal chemists (Goodsell 2011). At all isoforms, the heme is buried in the active site and forms Van der Waals interactions with aliphatic and hydrophobic side chains. The BH₄ cavity is located near the dimer interface, but the cofactor is deeply buried in the protein and inaccessible to the solvent (Gautier et al. 2004). Crystallographic researches showed some small structural differences between iNOS and constitutively expressed synthases that can be exploited in order to develop very specific drugs. The active site of mouse iNOS is smaller by 13 Å³ compared with nNOS, respectively, by 8.4 Å³ compared with eNOS (Fedorov et al. 2003). This small difference appears because iNOS possesses a bulkier Asn364 residue in the place of a Ser585 residue, both found in eNOS and nNOS, that pushes the side wall (the β -strand S15) deeper in the active site approaching Gly-365 residue, closer to the heme (Fedorov et al. 2003; Li and Poulos 2005). In the structure of iNOS oxygenase domain, L-Arg makes two hydrogen bonds with the two carboxy oxygens of glutamic acid residue: Glu377 residue in human iNOS, respectively Glu371 in murine iNOS (Crane et al. 1998). Moreover, the Glu371 residue has been found to be critical for L-Arg binding to murine iNOS (Gachhui et al. 1997). L-Arg, the synthase substrate, binds the catalytic site of iNOS with additional hydrogen bonds formed with Tyr367 residue and Asp376 residue, which is replaced by an asparagine residue in eNOS (Crane et al. 2000).

Thiazole derivatives are found to be associated with various biological activities such as anti-inflammatory (Haviv et al. 1988), anticonvulsant (Ergenc and Capan 1994), antihypertensive (Patt et al. 1992), antimicrobial (Tsuji and Ishikawa 1994; Wilson et al. 2001; Kumar et al. 1993a, b; Metzger 1984), anti-HIV (Bell et al. 1995), including here the inhibition of iNOS (Ueda et al. 2004). Heterocyclic compounds containing 1,3,4-oxadiazole, 1,3,4-thiadiazole or 1,3,4-triazole moiety serve both as

biomimetic and reactive pharmacophores and many are key compounds in obtaining molecules with potential biological activities (Boschelli et al. 1993; Amir and Shahani 1998; Rajak et al. 2007; Shiradkar et al. 2007; Joshi et al. 2008).

As a continuation of our research in this area (Oniga et al. 1998; Simiti et al. 1995; Zaharia et al. 2010), and an attempt to achieve new safe and potent compounds for treatment of inflammatory diseases, we recently synthesized new series of thiazole-carbonyl-thiosemicarbazides and hybrid thiazolyl-1,3,4-oxadiazoles, thiazolyl-1,3,4-triazoles and thiazolyl-1,3,4-triazoles, according to a previously described procedure (Tipericiu et al. 2012). The aim of this study was to evaluate *in vivo* the anti-inflammatory activity of these new compounds, in terms of their effects on phagocytosis, ROIs and NO production. In addition, a docking study using a model of iNOS was performed in order to rationalize the pharmacological results and to investigate how the potential ligands interact with the enzyme.

Materials and methods

Virtual screening of thiazole derivatives

The virtual screening of thiazole derivatives against a high-resolution crystal structure (Varnek and Tropsha 2008) for mouse iNOS (PDB ID: 2Y37, resolution: 2.60 Å) was done with a free trial version of Molegro Virtual Docker 5.0, 2011 (MVD5) (Molegro ApS, Aarhus C, DK, <http://www.molegro.com>) which uses the MolDock docking algorithm (Storn and Price 1997, Thomsen and Christensen 2006). MolDock Score was chosen as scoring function (Thomsen and Christensen 2006; Friesner et al. 2004). Ligands were prepared with MarvinSketch 5.5.0.1, 2011 and prior to docking, the cavities prediction algorithm of MVD5 was run against the oxygenase domain (chain A) of synthase to detect the potential binding sites. The binding site was set with the origin in the center of the major detected cavity with a radius of 15 Å. MolDock Optimizer was chosen as search algorithm and was set to perform 20 runs for each ligand (Thomsen and Christensen 2006). Poses were constrained to detected cavity, the energy minimization and the optimization of hydrogen bonds were imposed as compulsory post-docking operations. Finally, the clustering of poses was set to be made according to a virtual screening procedure by imposing that only the top ranked pose for each ligand to be returned as successful. After the virtual screening was finished, the binding affinity (BA) was subsequently used to predict the strongest ligands (Thomsen and Christensen 2006).

Chemicals

Sulfanilamide (SULF), *N*-(1-Naphthyl) ethylenediamine dihydrochloride (NEDD), Vanadium (III) chloride (VCl₃) methanol, diethylether, xylenol orange [o-cresosulfonphthalein-3,3-bis(sodium methyliminodiacetate)], ortho dianisidine dihydrochloride (3-3'-dimethoxybenzidine), ferrous ammonium sulfate, hydrogen peroxide (H₂O₂), sulfuric acid, hydrochloric acid, glycerol, trichloroacetic acid (TCA), trolox (6-hydroxy-2,5,7,8-tetramethylchroman-2-carboxylic acid), were purchased from Merck (Darmstadt, Germany) and Sigma-Aldrich (Taufkirchen, Germany). All chemicals were ultra pure grade, and type I reagent grade deionized water was used.

Thiazole Compounds

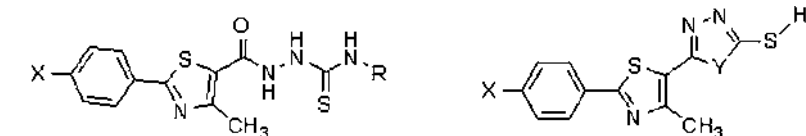
Twenty-two thiazole derivatives with the structures shown in Fig. 1: 4-alkyl/aryl-1-(2-aryl-4-methylthiazole-5-carbonyl)-thiosemicarbazides (**Th-1-8**), 4-alkyl/aryl-3-(2-aryl-4-methylthiazole-5-yl)-1H-1,2,4-triazole-5(4H)-thiones (**Th-9-17**), 5-(2-aryl-4-methylthiazole-5-yl)-1,3,4-oxadiazole-2(3H)-thiones (**Th-18-20**), and 5-(2-aryl-4-methylthiazole-5-yl)-1,3,4-thiadiazole-2(3H)-thiones (**Th-21-22**), synthesized

according to a previous procedure (Tipericiu et al. 2012), were used in this study.

Animals

Experiments were carried out on male 200 ± 50 g Wistar rats received from the breeding colony of University of Medicine and Pharmacy Cluj Napoca. The animals were kept in plastic cages in a 12-h light/dark cycle and maintained on standard rat laboratory chow and tap water ad libitum. All procedures conformed to the European Convention for the protection of vertebrate animals used for experimental and other scientific purposes. The study was approved by the Institutional Animal Ethical Committee of University of Medicine and Pharmacy Cluj-Napoca. Rats were randomly allocated to one of 25 groups (*n* = 8 per group): (i) a negative control group of healthy rats without any treatment (C) (ii) an inflammation control group (I), treated with 1 mL of vehicle saline 2 % carboxymethylcellulose solution (CMC); (iii) an inflammation group, treated with Tenoxicam (T) (20 mg/kg b.w., equivalent to 0.05928 mmol/kg b.w.), as a reference NSAID; (iv) 22 groups of inflammation (**Th-1-22**), treated with the newly synthesized thiazole compounds. The test

Fig. 1 Structure of thiazolyl-carbonyl-thiosemicarbazides and thiazolyl-azole compounds



Compound	X	R
Th-1	H	Phenyl
Th-2	CH ₃	Phenyl
Th-3	Br	Phenyl
Th-4	H	Me
Th-5	CH ₃	Me
Th-6	Br	Me
Th-7	H	Allyl
Th-8	CH ₃	Allyl

Compound	X	Y
Th-9	H	N-Phenyl
Th-10	CH ₃	N-Phenyl
Th-11	Br	N-Phenyl
Th-12	H	N-Me
Th-13	CH ₃	N-Me
Th-14	Br	N-Me
Th-15	H	N-Allyl
Th-16	CH ₃	N-Allyl
Th-17	Br	N-Allyl
Th-18	H	O
Th-19	CH ₃	O
Th-20	Br	O
Th-21	H	S
Th-22	CH ₃	S

compounds were suspended in 1 mL CMC to a final concentration of 0.05928 mmol/kg b.w., to be injected intraperitoneally.

Acute inflammation was induced by intramuscular injection of 6 mL/kg b.w. turpentine oil (Plesca-Manea et al. 2002). After 24 h, blood samples were collected into tubes with EDTA for leukocytes count (WCC) and the in vitro phagocytes test, and without anticoagulant for serum tests. Samples were run immediately or stored at $-80\text{ }^{\circ}\text{C}$ until analysis. Experiments were performed in triplicate. After the experiment, the animals were sacrificed by cervical dislocation.

Measurement of acute phase bone marrow response

The acute phase bone marrow response was measured by WCC with an optical microscope (Olympus) on a Bürcker-Türk counting-chamber, and by differential leukocyte count, expressed as a percentage, on May-Grünwald-Giemsa stained smears (Moldovan et al. 2011).

In vitro phagocytes test

In vitro phagocytes test was performed as previously described (Moldovan et al. 2011; Hrabák et al. 2008) with slight modifications. Blood samples were incubated in siliconated tubes with *E. coli* suspension at $37\text{ }^{\circ}\text{C}$ for 30 min and smears stained with May-Grunwald Giemsa were observed at an optic microscope (Olympus). Phagocytic capacity was evaluated in terms of phagocytosis index (PI) (% of phagocytic cells with at least one phagocytosed germ) and phagocytic activity (PA) (number of germs phagocytosed by 100 leukocytes).

Measurement of total oxidative status

Total oxidative status (TOS) of serum was measured using a colorimetric method (Erel 2005). The assay is based on the oxidation of ferrous ion to ferric ion in the presence of various oxidant species in acidic medium and the measurement of the ferric ion by xylenol orange. The assay is calibrated with H_2O_2 and the results are expressed in $\mu\text{mol H}_2\text{O}_2$ equiv./L.

Measurement of total antioxidant response

Measurement of serum total antioxidant response (TAR) was performed using a colorimetric method (Erel 2004), in which the hydroxyl radical is produced by Fenton reaction and the rate of the process is monitored by following the absorbance of colored dianisidyl radicals. Upon addition of a serum sample, the oxidative reactions initiated by the hydroxyl radicals present in the reaction medium are

suppressed by the antioxidant components of the serum, preventing the color change and thereby providing an effective measure of the total antioxidant capacity of the serum. The assay is calibrated with Trolox, a water-soluble derivative of vitamin E, and the results are expressed as mmol Trolox equiv./L.

Measurement of oxidative stress index

Oxidative stress index (OSI) as the ratio of TOS and TAR (Harma and Erel 2003) was calculated with the formula: $\text{OSI (Arbitrary Unit)} = \text{TOS } (\mu\text{mol H}_2\text{O}_2 \text{ equiv./L})/\text{TAR (mmol Trolox equiv./L)}$.

Measurement of serum nitrites and nitrates

The serum samples were deproteinized by methanol/diethylether (3/1, v/v) (sample: methanol/diethylether, 1:9, v/v) (Ghasemi et al. 2007). The Griess reaction was used as an indirect assay to determine the total nitrite and nitrate (NO_x) as an indicator of intracellular NO production. In brief, 100 $\mu\text{L VCl}_3$ (8 mg/mL) was added for the reduction of nitrate to nitrite to 100 μL of supernatant and this was followed by the addition of the Griess reagents, 50 μL SULF (2 %) and 50 μL NEDD (0.1 %). After 30 min of incubation at $37\text{ }^{\circ}\text{C}$, the absorbance was read at 540 nm. Serum NO_x level was expressed in nitrite/nitrate ($\mu\text{mol/L}$) (Miranda et al. 2001).

Statistical analysis

All results were expressed as mean \pm standard deviation (SD) of three independent experiments. Statistical comparisons between the groups were made using one-way analysis of variance (ANOVA) test. A value of $p < 0.05$ was considered to be statistically significant. Pearson's and Spearman's correlation analyses were used to calculate statistical relationships between parameters. Analysis was performed using standard software (SPSS for Windows, version 16.0).

Results

Virtual screening of the thiazole derivatives against mouse iNOS

Virtual screening of thiazole derivatives against the oxygenase domain of chain A from 2Y37 performed with MVD5 revealed that all twenty-two compounds bind the active site of synthase (Table 1; Fig. 2).

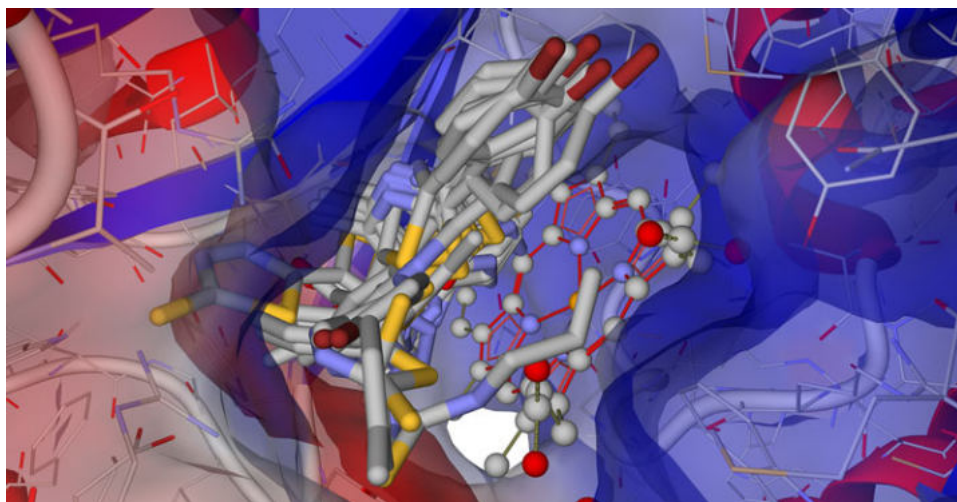
The re-rank scoring function of MVD5 was used to increase the docking accuracy and to identify the highest ranked pose for each thiazole derivative. Therefore,

Table 1 Virtual screening results: docking and re-ranking scores with ligand efficiency (LE) after scoring (LE1) and re-ranking (LE3); estimation of BA of synthase–ligand complex

Ligand	MolDock score	LE1 ^a	Re-rank score	LE3 ^b	BA (kcal/mol)
Th-1	-170.314	-6.81256	-112.9430	-4.51771	-26.5515
Th-2	-173.069	-6.65650	-110.4740	-4.24902	-25.7833
Th-3	-170.366	-6.55255	-112.6820	-4.33391	-30.2230
Th-4	-136.529	-6.82645	-76.9715	-3.84858	-26.6469
Th-5	-138.686	-6.60408	-92.9335	-4.42541	-39.9672
Th-6	-135.474	-6.45115	-78.5821	-3.74201	-57.4721
Th-7	-150.278	-6.83082	-100.8800	-4.58547	-49.0535
Th-8	-150.899	-6.56081	-107.4220	-4.67054	-24.1512
Th-9	-173.008	-7.20866	-116.4800	-4.85334	-28.2735
Th-10	-174.563	-6.98253	-115.2830	-4.61131	-27.5967
Th-11	-173.700	-6.94798	-114.0980	-4.56394	-31.6084
Th-12	-134.771	-7.09320	-59.6017	-3.13693	-30.6296
Th-13	-132.320	-6.61602	-58.8486	-2.94243	-33.6308
Th-14	-130.806	-6.54032	-72.9158	-3.64579	-37.3478
Th-15	-144.350	-6.87380	-96.3147	-4.58641	-25.3617
Th-16	-147.447	-6.70212	-98.1764	-4.46256	-28.7951
Th-17	-146.396	-6.65438	-97.1527	-4.41603	-32.9367
Th-18	-132.529	-7.36274	-89.7746	-4.98748	-31.6848
Th-19	-132.343	-6.96542	-93.2967	-4.91035	-32.4708
Th-20	-129.810	-6.83213	-91.8006	-4.83161	-36.4724
Th-21	-117.039	-6.50219	-25.0671	-1.39262	-30.1832
Th-22	-115.858	-6.09780	-81.5966	-4.29456	-27.7077

LE1 MolDock score divided by heavy atoms count, LE3 re-rank score divided by heavy atoms count

Fig. 2 Docking results—a general view with all ligands deeply inserted in the active site of iNOS. The active site of iNOS is showed with the electrostatic potential molecular surface, the synthase is depicted as *thin sticks* with secondary structure drawn as cartoon backbone, heme is drawn as *balls and sticks*, meanwhile ligands are figured as *sticks*



because re-rank scoring function is not calibrated in chemical units and it does not take complex contributions into consideration, the BA build-in model of MVD5 was used subsequently to roughly estimate the strongest ligands of iNOS as being **Th-6** (BA = -57.4721 kcal/mol) and **Th-7** (BA = -49.0535 kcal/mol). All other thiazole derivatives have a moderate BA for the synthase comparing with **Th-6** and **Th-7** (Table 1).

From Fig. 2 it can be observed that all ligands bind in the major cavity detected, corresponding to the active site of the synthase, blocking the access of the substrate (L-Arg) to the binding site of oxygenase domain. Moreover, in Table 2 there are presented the most important energetic interactions: the hydrogen bonds established between the high-ranked poses and the target macromolecule.

Table 2 Detailed information about hydrogen bonds between ligands and the oxygenase domain of iNOS—chain A of 2Y37

Ligand	Atom ID of ligand	Interacting AA residue of iNOS or cofactor	Energy donor	Energy (kcal/mol)	Bond length (Å)
Th-1	N/A	N/A	N/A	N/A	N/A
Th-2	15: O	Tyr367	Target	-2.5	2.84334
Th-3	15: O	Tyr367	Target	-2.5	2.99086
	18: N	Trp366	Ligand	-0.61234	3.45872
Th-4	14: O	Tyr367	Target	-2.5	2.84636
	15: N	Glu371	Ligand	-2.02805	2.87228
	17: N	Glu371	Ligand	-1.28549	2.64489
Th-5	16: N	38: N Heme	Ligand	-2.5	2.85854
	16: N	39: N Heme	Ligand	-0.466843	3.50663
	18: N	40: N Heme	Ligand	-1.93632	3.21274
Th-6	16: N	38: N Heme	Ligand	-2.5	3.09042
	16: N	40: N Heme	Ligand	-1.3651	3.32698
	16: N	41: N Heme	Ligand	-2.5	2.94137
	18: N	39: N Heme	Ligand	-2.5	2.92243
Th-7	15: N	Glu371	Ligand	-2.5	2.60008
	13: N	12: O Heme	Ligand	-2.5	3.04752
	17: N	12: O Heme	Ligand	-2.5	3.09750
	17: N	5: O BH4	Ligand	-1.95803	3.20839
Th-8	14: O	Tyr367	Target	-1.54228	3.29154
Th-9	17: S	Trp366	Ligand	-2.5	3.01602
Th-10	17: S	Trp366	Ligand	-2.5	2.60062
Th-11	17: S	Trp366	Ligand	-2.5	2.60012
Th-12	16: N	Gly365	Target	-0.848071	2.95178
	17: S	40: N Heme	Ligand	-1.49754	3.30049
Th-13	16: N	Gly365	Target	-1.0382	2.90967
	17: S	40: N Heme	Ligand	-2.5	3.09968
Th-14	16: N	Gly365	Target	-0.933556	3.07364
	17: S	40: N Heme	Ligand	-2.38668	3.12266
Th-15	17: S	Trp366	Ligand	-2.5	2.65829
Th-16	17: S	Trp366	Ligand	-2.5	2.72144
	17: S	39: N Heme	Ligand	-1.04099	3.39180
Th-17	17: S	Trp366	Ligand	-2.5	2.73772
	17: S	39: N Heme	Ligand	-1.07232	3.38554
Th-18	16: N	Gly365	Target	-0.878546	3.09852
	17: S	40: N Heme	Ligand	-1.14029	3.37194
Th-19	16: N	Gly365	Target	-0.939771	3.09926
	17: S	40: N Heme	Ligand	-1.49078	3.30184
Th-20	16: N	Gly365	Target	-0.887684	3.16040
	17: S	40: N Heme	Ligand	-1.49082	3.30184
Th-21	13: N	Gln257	Target	-2.5	2.84096
	13: N	Tyr341	Target	-1.75112	3.24978
	13: N	Tyr367	Target	-1.76437	2.51172
	16: N	Gln257	Target	-2.5	2.66435
	16: N	Tyr341	Target	0.101867	2.28829
	16: N	Tyr367	Target	-2.5	2.81539
	17: S	Tyr341	Ligand	-0.731108	3.45378
	17: S	Asp376	Ligand	-2.5	2.60005
Th-22	13: N	Arg382	Target	-1.79507	3.24099
	16: N	Arg382	Target	-2.44411	2.59329

Analyzing the binding mode shown in Table 2, it can be observed that the strongest binder of synthase, **Th-6**, makes four donor hydrogen bonds only with the heme, meanwhile the next strong ligand, **Th-7**, binds preferentially the same cofactor of iNOS (two donor hydrogen bonds) but also interacts with the cofactor BH4 and with Glu371, a critical residue for substrate binding of murine iNOS. From the other six thiosemicarbazides, only **Th-5** binds the heme, meanwhile **Th-1** does not interact at all with AA residues from active site of iNOS by hydrogen bonds, but only through electrostatic interactions (Fig. 3). **Th-2-4** and **Th-8** bind with Tyr367, another critical residue for substrate binding of murine iNOS. In the same time, **Th-3** makes an additional hydrogen bond with a back-wall AA residue with uncharged polar side chain (Trp366).

Six of the thiazolyl-1,2,4-triazole-thiones strongly bind by a hydrogen bond a back-wall AA residue: Trp366 (**Th-9-11**, **Th-15-17**), **Th-16-17**, making an additional weaker hydrogen bond with the heme (Table 2). The *N*-methyl substituted thiazolyl-1,2,4-triazole-thiones (**Th-12-14**) make, each of them, hydrogen bonds with heme and Gly365, a conserved AA residue at all NOSs, but closer to the heme at iNOS comparatively with constitutive NOSs. The thiazolyl-1,3,4-oxadiazole-thiones (**Th-18-20**) make similar hydrogen bonds with iNOS as triazole derivatives **Th-12-14**.

The high-ranked poses of thiazolyl-1,3,4-thiadiazole-thiones (**Th-21-22**) bind quite different from all ligands in the active site of oxygenase domain. **Th-21** strongly binds, two critical AA residues for L-Arg binding of murine iNOS: Tyr367 and Asp376. Supplementary, **Th-21** binds AA residues with two uncharged polar side chain, reported as key residues in the design of selective murine iNOS inhibitors: Gln257 (two hydrogen bonds) and Tyr341 (three hydrogen bonds) (Table 2; Fig. 4). **Th-22** makes two strong hydrogen bonds with Arg382, reported also as key residue in the design of selective murine iNOS inhibitors.

Effects of thiazole compounds on acute phase bone marrow response

A series of new thiazolyl-carbonyl-thiosemicarbazides and thiazolyl-azoles were tested for their ability to reduce the cellular inflammatory response. Compared to the inflammation group, 21 from a total of 22 compounds, reduced WCC significantly (Table 3) ($p < 0.05$), and only the compound **Th-4** had no significant effect ($p = 0.1$). In the differential leukocytes count, it was found that substances **Th-1**, **Th-20-21** caused an important decrease of the polymorphonuclear cells (PMN) percentage ($p < 0.01$), and substances **Th-2-3**, **Th-5**, **Th-8-10**, **Th-18** and **Th-22** just a small reduction ($p < 0.05$). All the thiazole compounds had a lower inhibitory effect than Tenoxicam on both WCC and differential leukocyte count ($p < 0.01$).

Effects of thiazole compounds on in vitro phagocytosis test

All tested substances reduced significantly the phagocytic capacity by decreasing PI and PA (Table 4) ($p < 0.001$), and these results were positively correlated with WCC ($r = 0.69-0.85$). For the compounds that decreased PMN, PI and PA were positively correlated with PMN reduction, too ($r = 0.72$, $r = 0.98$). Compared to Tenoxicam, substances **Th-5**, **Th-17**, **Th-18** and **Th-20** had almost similar inhibitory effects on PI ($p > 0.05$), **Th-6** and **Th-21** caused a stronger inhibition ($p < 0.01$) and the rest of the compounds had less inhibitory effects ($p < 0.01$). Only one compound, **Th-19**, was a more powerful inhibitor of PA than Tenoxicam ($p < 0.001$).

Effects of thiazole compounds on TOS

TOS measures all oxidized molecules. As shown in Fig. 5, TOS was significantly decreased by all the tested compounds ($p < 0.01$). The inhibitory effects on TOS were stronger than those of Tenoxicam ($p < 0.01$), excepting for compound **Th-12** ($p < 0.05$). ROIs reduction was positively correlated with the decrease of the phagocytic capacity (PI, PA) ($r = 0.76$, $r = 0.97$).

Effects of thiazole compounds on total antioxidant response

TAR measures all antioxidants and therefore can reflect the oxidative status of the organism (Serefhanoglu et al. 2009). In our study, we found that TAR level was significantly increased by all the substances (Fig. 6) compared to the inflammation group, and these effects were similar to that of Tenoxicam ($p > 0.05$).

Effects on oxidative stress index

Because oxidative stress is a matter of balance between oxidants and anti-oxidants, we calculated OSI. In the present study, OSI was significantly lower in the test groups than inflammation group (Fig. 7). Compared to Tenoxicam, three compounds (**Th-12**, **Th-19-20**) had similar effects (Fig. 7), and the rest of the thiazole compounds had a better inhibitory effect on OSI.

Effects of thiazole compounds on serum nitrites and nitrates

Upon activation, phagocytes release important quantities of NO with cytotoxic effects. Serum nitrites and nitrates levels, the indirect test for NO synthesis, were significantly reduced by eight thiazole compounds (**Th-1**, **Th-4-5**, **Th-8**,

Fig. 3 The **Th-1**-iNOS complex. **a** The electrostatic interactions between **Th-1** and synthase presented as *blue spheres* (positive charges) and *red spheres* (negative charges). **b** The electrostatic interactions between **Th-1** and synthase presented as electrostatic potential surface

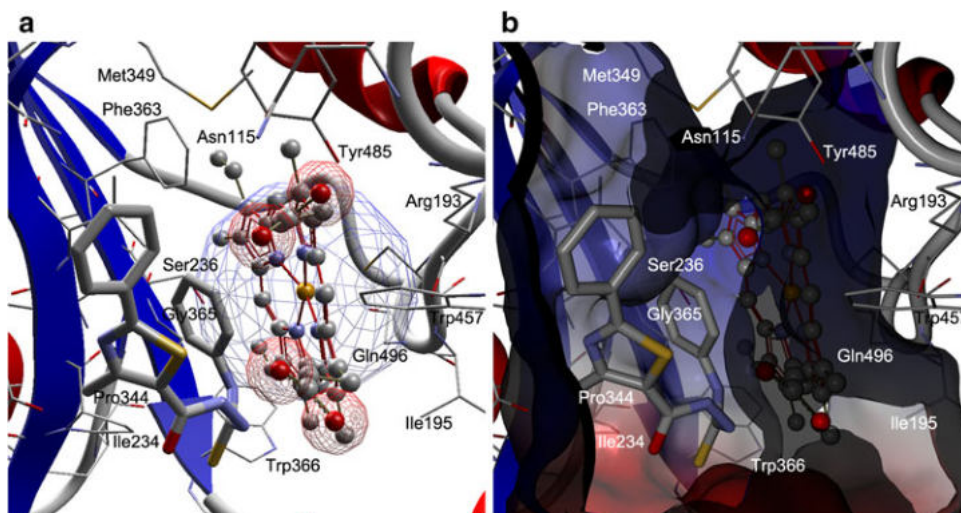
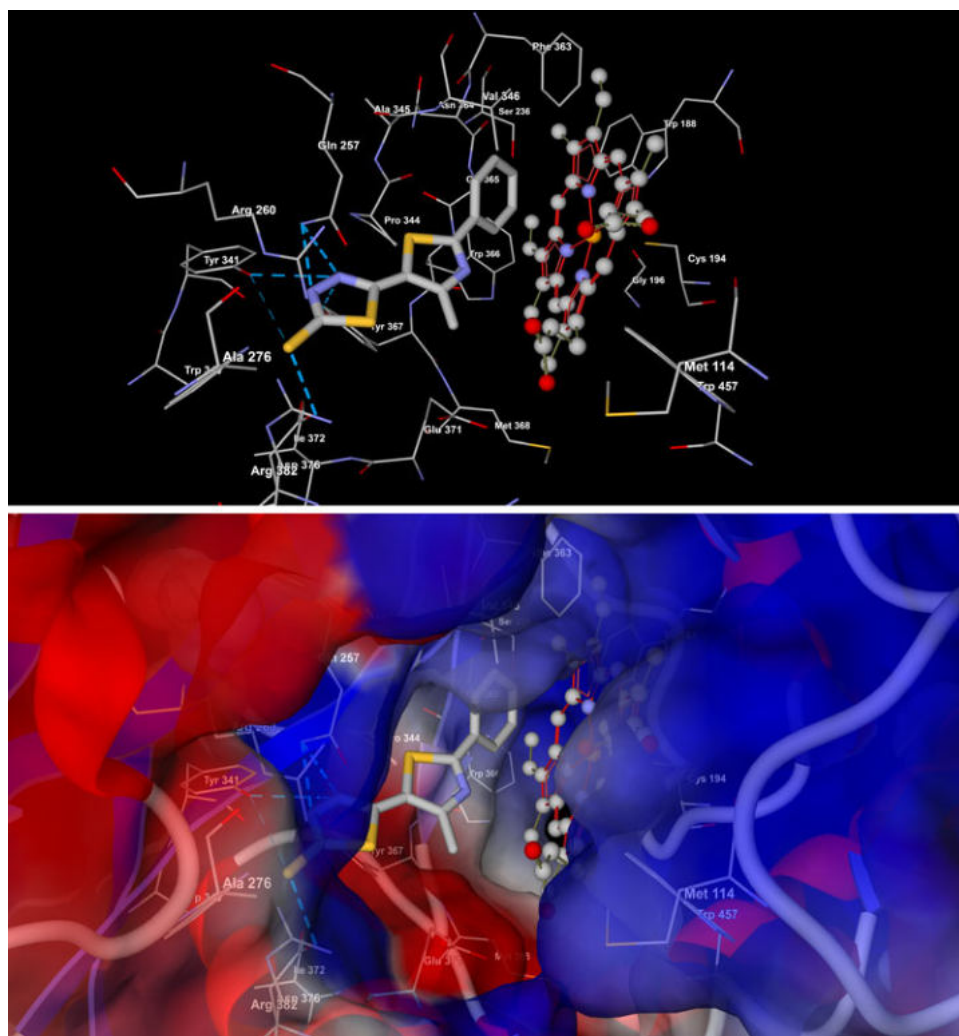


Fig. 4 Binding mode of **Th-21**. The synthase is depicted as *thin sticks* with secondary structure drawn as cartoon backbone, heme is drawn as *balls and sticks*, meanwhile ligands are figured as *sticks*. The hydrogen bonds are depicted as *dashed blue lines*. In the *left side* of the figure, there is a schematic representation of ligand–protein complex, meanwhile in the *right side* the ligand is depicted more realistic, inserted in the active site of iNOS



Th-18-21) (Table 4, $p < 0.001$). Substances **Th-2**, **Th-6**, **Th-7**, **Th-17** and **Th-22** had a lower inhibitory effect ($p < 0.05$) and the rest of the substances did not influence

NO synthesis ($p > 0.05$). Compared to Tenoxicam, all the substances had a lower inhibitory activity on NO synthesis ($p < 0.01$).

Table 3 Effect of thiazolyl-carbonyl-thiosemicarbazides and thiazolyl-azoles on the acute medullar response

Compound ^a	Leukocytes (no/mm ³)	Neutrophils (%)
Control	4,952 ± 436	55 ± 8.30
Inflammation	13,528 ± 1,077.11	71 ± 3.50
Tenoxicam	2,344 ± 291.16	48 ± 2.90
Th-1	5,588 ± 455.33 ^b	60 ± 4.09 ^c
Th-2	6,543 ± 271.09 ^b	61 ± 3.13 ^d
Th-3	4,988 ± 132.96 ^b	64 ± 3.86 ^d
Th-4	12,219 ± 1,341.29	83 ± 4.13 ^c
Th-5	11,633 ± 153.97 ^b	60 ± 3.58 ^d
Th-6	6,056 ± 862.38 ^b	70 ± 2.95
Th-7	6,356 ± 66.48 ^b	73 ± 4.02
Th-8	5,719 ± 104.15 ^b	67 ± 0.97 ^d
Th-9	9,000 ± 428.04 ^b	67 ± 2.99 ^d
Th-10	5,606 ± 153.97 ^b	61 ± 3.43 ^d
Th-11	11,138 ± 482.74 ^b	86 ± 2.63
Th-12	8,456 ± 565.17 ^b	79 ± 0.97
Th-13	10,172 ± 331.29 ^b	81 ± 3.01
Th-14	10,172 ± 520.47 ^b	75 ± 4.53
Th-15	9,983 ± 808.82 ^b	77 ± 5.17
Th-16	9,225 ± 332.74 ^b	77 ± 1.90
Th-17	10,148 ± 527.82	75 ± 5.17
Th-18	4,575 ± 805.78	64 ± 2.45 ^d
Th-19	7,444 ± 1,172.05	73 ± 5.01
Th-20	4,838 ± 1,304.59	59 ± 5.67 ^c
Th-21	3,000 ± 240.54	53 ± 2.12 ^c
Th-22	5,813 ± 398.88	66 ± 0.84 ^d

Each experiment was run three times, and the results are presented as average values ± SD ($n = 8$)

^a Detailed structures of the compounds are given in Fig. 1

^b $p < 0.05$ versus inflammation group

^c $p < 0.01$ versus inflammation group

^d $p < 0.01$ versus Tenoxicam

Discussion

In the inflammatory processes, the acute phase bone marrow response leads to leukocytosis with neutrophilia. Initially it reflects the increased release of leukocytes from the storage pool and later the increased production by the bone marrow.

In the groups treated with thiazole compounds, bone marrow acute phase response was reduced by lowering both WCC and PMN (Table 3). Because leukocytosis may represent an acute phase marker analogous to C-reactive protein (CRP) or the erythrocyte sedimentation rate (ESR) (Asadollahi et al. 2010), these results revealed anti-inflammatory effects for the tested compounds. Analyzing the chemical structures of these compounds, it can be observed that the thiazole-1,3,4-oxadiazole-thiones **Th-18-**

Table 4 Effect of thiazolyl-carbonyl-thiosemicarbazides and thiazolyl-azoles on in vitro phagocytosis test and on nitrite/nitrate levels

Compound ^a	Phagocytosis test		Nitrites/nitrates (μmol/L)
	PI (%) ^a	PA ^a	
Control	20.8 ± 4.87	24.4 ± 5.5	4.25 ± 1.03
Inflammation	51.2 ± 6.2	119 ± 8.49	70.99 ± 7.76
Tenoxicam	16.5 ± 3.16	16.5 ± 2.33	39.86 ± 4.75
Th-1	21.5 ± 4.63 ^b	18.5 ± 1.77	50.48 ± 5.68 ^d
Th-2	21.5 ± 2.78 ^b	22.5 ± 2.78	51.83 ± 6.3 ^e
Th-3	21.5 ± 0.93 ^b	31 ± 1.85	52.84 ± 4.91
Th-4	22.5 ± 3.51 ^b	29 ± 1.85	47.50 ± 2.75 ^d
Th-5	19.5 ± 2.33	22.5 ± 0.89	47.02 ± 5 ^d
Th-6	13 ± 3.21 ^b	18 ± 1.51	50.59 ± 5.14 ^c
Th-7	20.5 ± 0.93 ^b	53.5 ± 3.51	54.36 ± 6.2 ^e
Th-8	21.5 ± 0.93 ^b	21 ± 1.07	48.79 ± 5.51 ^d
Th-9	21 ± 4.01 ^b	20.5 ± 0.93	65.48 ± 4.79
Th-10	20.5 ± 0.93 ^b	23 ± 1.07	65.14 ± 5.31
Th-11	21 ± 1.07 ^b	19.75 ± 2.43	66.80 ± 5.91
Th-12	22.5 ± 3.51 ^b	20 ± 1.51	70.03 ± 5.37
Th-13	25.5 ± 2.78 ^b	27.5 ± 0.93	75.45 ± 7
Th-14	28 ± 2.14 ^b	23.5 ± 0.93	86.04
Th-15	24 ± 4.28 ^b	29 ± 3.21	71.63 ± 5.86
Th-16	21.25 ± 1.04 ^b	27 ± 1.07	63.09 ± 5.05
Th-17	15 ± 3.55	19.5 ± 0.93	60.48 ± 7.75 ^c
Th-18	17 ± 1.85	56 ± 8.55	43.23 ± 3.97 ^d
Th-19	20 ± 1.51 ^b	13.5 ± 2.78 ^c	45.20 ± 2.22 ^d
Th-20	16 ± 3.02	20 ± 1.51	43.29 ± 5.03 ^d
Th-21	14.5 ± 4.63 ^b	23 ± 1.85	43.74 ± 6.2 ^d
Th-22	35 ± 5.21 ^b	23.5 ± 0.93	52.08 ± 6.09 ^c

Each experiment was run three times, and the results are presented as average values ± SD ($n = 8$)

^a $p < 0.001$ **Th-1-22** versus inflammation group

^b $p < 0.01$ versus Tenoxicam

^c $p < 0.001$ versus Tenoxicam

^d $p < 0.001$ versus inflammation group

^e $p < 0.05$ versus inflammation group

20 and the thiazole-1,3,4-triazole-thiones **Th-21-22** had the best influence on the acute phase bone marrow response (Table 3).

Phagocytes are reported to play a crucial role in the development of local inflammatory response (Apostolova et al. 2011). Their function was evaluated using the in vitro phagocytosis test (Hrabák et al. 2008; Strom et al. 2011). The tested thiazole compounds inhibited phagocytes activity and the effects were as important as those of Tenoxicam. These effects represent one more mechanism for the anti-inflammatory activity. The PI and PA were highly correlated for the compounds **Th-3**, **Th-11**, **Th-14**, **Th-17**, **Th-20** and **Th-21** (Table 4). Analyzing the chemical structures, it can be observed that the substitution of

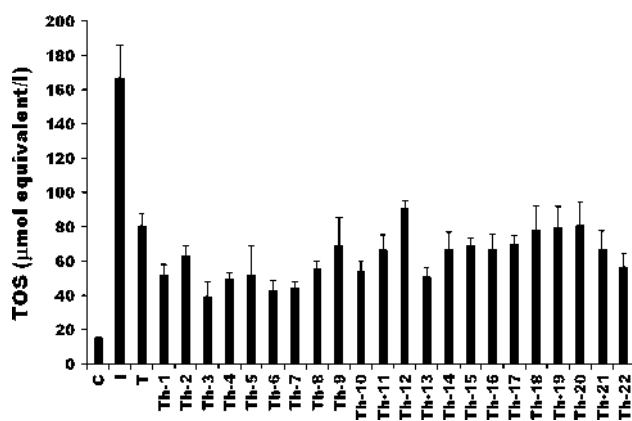


Fig. 5 The effect of the thiazole compounds on TOS. After treatment with 59.3 mmol/kg of **Th-1-22**, the TOS decreased significantly compared with inflammation group; Each experiment was run three times, and the results are presented as average values \pm SD ($n = 8$); $p < 0.01$ versus inflammation group, $p < 0.05$ versus Tenoxicam group

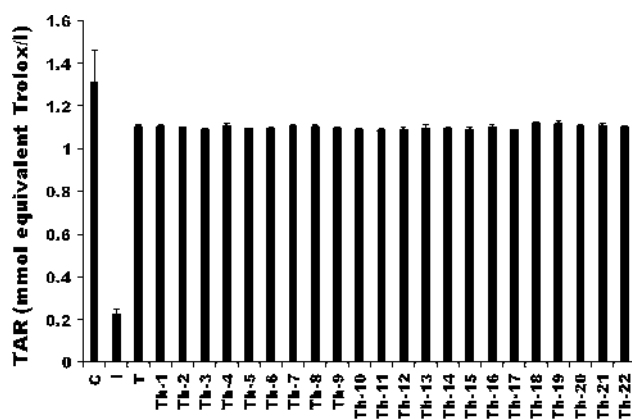


Fig. 6 The effect of the thiazole compounds on TAR. The TAR represent the total antioxidant response produced by the plasma antioxidant, and the tested compounds. Each experiment was run three times, and the results are presented as average values \pm SD ($n = 8$); $p < 0.001$ versus inflammation group, $p > 0.05$ versus Tenoxicam group

phenyl from position 2 of thiazole with a bromine atom in 4 had a good influence on the anti-inflammatory activity.

Activated phagocytes can generate large amounts of highly toxic ROIs. In excess, ROIs may harm host tissue through oxidative stress (Serefhanoglu et al. 2009; Paino et al. 2005; Edeas 2011). When the generation of ROS exceeds the counterbalance of antioxidant cellular mechanism, it results in oxidative stress, finally leading to many pathological outcomes (Edeas 2011). The increase in TOS and diminished TAR were reversed by the treatments with the thiazole compounds (Figs. 5, 6). Based on the results obtained above, we hypothesized that the effects were protective against oxidative stress due to their efficacy to scavenge ROIs by the thiosemicarbazide moiety and by the

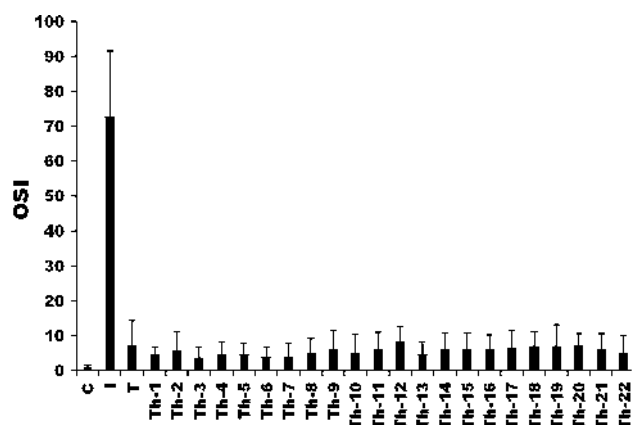


Fig. 7 The effect of the thiazole compounds on OSI. OSI calculation after the treatment with the new thiazole compounds revealed their antioxidant activity. The results are presented as average values \pm SD ($n = 8$); $p < 0.001$ versus inflammation group, $p < 0.05$ versus Tenoxicam

thiol function. The antioxidant activity may be due to their capacity of metal chelating. Thus, the thiazole compounds may inhibit free-radical formation and the consequent free radical tissue damage (Horackova et al. 2000). Another possible mechanism for TAR increase could be that the radical-scavenging antioxidants were not consumed due to the initial decrease of ROIs.

It has been suggested that OSI may reflect the state of oxidative status more accurately than TOS or TAR alone (Serefhanoglu et al. 2009). Most compounds were better antioxidants than Tenoxicam (Fig. 7). The thiazolyl-carbonyl-thiosemicarbazides **Th-1-8** had the best antioxidant effect by the inhibition of TOS. By their cyclisation to the thiazolyl-1,2,4-triazole-thione derivatives (**Th-9-17**), the antioxidant potential decreases (Figs. 5–7). The antioxidant activity is not significantly modified by the replacement of triazole heterocycle with 1,3,4-oxadiazole (**Th-18-20**) or with 1,3,4-thiadiazole ring (**Th-21-22**). Analyzing all the tested compounds, it can be observed that the best antioxidant compounds are represented by the thiazole derivatives substituted in position 2 of thiazole ring with a para-brom-phenyl substituent. This fact could be explained by the strongest chemical interactions with the biological substrate due to their electronegativity and electron withdrawing inductive effects and to their lipophilic character.

When stimulated by inflammatory mediators, phagocytes not only displayed increased ROIs generation but also manifested enhanced release of NO (Apostolova et al. 2011). When released in excess, it reacts with ROIs and the resulting RNIs may be used as an oxidative stress marker, too. This latter effect was abolished significantly by eight of the new compounds (**Th-1, Th-4-5, Th-8, Th-18-22**) (Table 4). Also, it can be observed that the best inhibitory effect on the NO species is expressed by all the tested

thiazolyl-carbonyl-thiosemicarbazides, the thiazolyl-1,3,4-oxadiazole-thiones **Th-18-20** and the thiazolyl-1,3,4-thiadiazole-thione **Th-21**.

Comparing the results of indirect test for NO synthesis (Table 4) with the virtual screening (Table 1), it can be observed that the thiazolyl-thiosemicarbazides **Th-1**, **Th-4-5** and **Th-8**, the thiazolyl-1,3,4-oxadiazole-thiones **Th-18-20** and the thiazolyl-1,3,4-thiadiazole-thione **Th-21**, who significantly reduced the serum nitrites and nitrates, showed a moderate BA for iNOS compared with the strongest ligands, thiosemicarbazides **Th-6-7**. The lower inhibitory effect of **Th-6** and **Th-7** could be explained based on their binding mode. Their strong BA for the heme, according to Table 2, suggests a non-selective affinity for hemoproteins (oxygen transport proteins, peroxidases, cytochrome C oxidase, cytochromes, soluble guanylyl cyclase, catalase), especially for those with larger binding site, iNOS having a smaller active site than constitutive NOSs. The significant inhibitory effect on the NO species of the eight thiazole compounds could be explained by the fact that the thiosemicarbazides **Th-4**, **Th-8** and thiazolyl-1,3,4-thiadiazole-thione **Th-21** do not bind the heme, the thiosemicarbazide **Th-5** and thiazolyl-1,3,4-oxadiazole-thiones **Th-18-20** binding the heme weakly comparative with **Th-6** and **Th-7** (Table 2).

The binding to the active site of iNOS is achieved by hydrogen bonds with the participation of the N2 and/or N4 from the thiosemicarbazide fragment of **Th-2-8** or the N2 of 1,2,4-triazole cycles, respectively, N3 of 1,3,4-oxa(thia)diazole cycles, thiadiazole and/or thiol group of **Th-9-22** (Table 2).

Based on these findings, it is also reasonable to assume that inhibition of iNOS expression is another possible mechanism by which the compounds exert an anti-inflammatory and antioxidative action. However, which one of the possible mediators actually participates should be resolved by future studies.

Overall, our results demonstrated that the new thiazole compounds have anti-inflammatory effects by lowering bone marrow acute phase response and oxidative stress. Oxidative stress reduction is the consequence of associated TOS and NOs decrease and TAR increase. The best anti-inflammatory and antioxidant effect was found for the thiazolyl-carbonyl-thiosemicarbazides **Th-1-8**, thiazolyl-1,3,4-oxadiazole **Th-20** and thiazolyl-1,3,4-thiadiazole **Th-21**.

We believe that the evidence reported here can contribute to a better general understanding of the cellular mechanisms involved in the anti-inflammatory effects of the new compounds. Further studies are needed in order to make them promising candidates for therapeutic applications.

Acknowledgments This work was financially supported by the National University Research Council, Romania (Project PNII-ID No. 1348/2008). This support is gratefully acknowledged.

References

- Amir, M., and S. Shahani. 1998. Synthesis and anti-inflammatory of naphthylmethyl oxadiazoles, thiadiazoles and triazoles. *Indian Journal of Heterocyclic Chemistry* 8: 107–110.
- Apostolova, N., R. Garcia-Bou, A. Hernandez-Mijares, R. Herance, M. Rocha, and V.M. Victor. 2011. Mitochondrial antioxidants alleviate oxidative and nitrosative stress in a cellular model of sepsis. *Pharmaceutical Research* 28: 2910–2919.
- Asadollahi, K., N.J. Beeching, and G.V. Gill. 2010. Leukocytosis as a predictor for non-infective mortality and morbidity. *QJM* 103: 285–292.
- Bell, F.W., A.S. Cantrell, M. Hoegberg, S.R. Jaskunas, N.G. Johansson, J. Jordan, M.D. Kinnick, P. Lind, and J.M. Morin. 1995. Phenethylthiazolethiourea (PETT) compounds, a new class of HIV-1 reverse transcriptase inhibitors. 1. Synthesis and basic structure–activity relationship studies of PETT analogs. *Journal of Medicinal Chemistry* 38: 4929–4936.
- Boschelli, D.H., D.T. Connor, D.A. Bornemeier, R.D. Dyer, J.A. Kennedy, P.J. Kuipers, G.C. Okonkwo, D.J. Schrier, and C.D. Wright. 1993. 1,3,4-oxadiazole, 1,3,4-thiadiazole, and 1,2,4-triazole analogs of the fenamates: In vitro inhibition of cyclooxygenase and 5-lipoxygenase activities. *Journal of Medicinal Chemistry* 36: 1802–1810.
- Crane, B.R., A.S. Arvai, D.K. Ghosh, E.D. Getzoff, D.J. Stuehr, and J.A. Tainer. 2000. Structures of the N^ω-hydroxy-L-arginine complex of inducible nitric oxide synthase oxygenase dimer with active and inactive pterins. *Biochemistry* 39: 4608–4621.
- Crane, B.R., A.S. Arvai, D.K. Ghosh, C. Wu, E.D. Getzoff, D.J. Stuehr, and J.A. Tainer. 1998. Structure of nitric oxide synthase oxygenase dimer with pterin and substrate. *Science* 279: 2121–2126.
- Daff, S. 2010. NO synthase: Structures and mechanisms. *Nitric Oxide* 23: 1–11.
- Edeas, M. 2011. Strategies to target mitochondria and oxidative stress by antioxidants: Key points and perspectives. *Pharmaceutical Research* 28: 2771–2779.
- Erel, O. 2005. A new automated colorimetric method for measuring total oxidant status. *Clinical Biochemistry* 38: 1103–1111.
- Erel, O. 2004. A novel automated method to measure total antioxidant response against potent free radical reactions. *Clinical Biochemistry* 37: 112–119.
- Ergenc, N., and G. Capan. 1994. Synthesis and anticonvulsant activity of new 4-thiazolidinone and 4-thiazoline derivatives. *II Farmaco* 49: 449–451.
- Espey, M.G., K.M. Miranda, M. Feelisch, J. Fukuto, M.B. Grisham, M.P. Vitek, and D.A. Wink. 2000. Mechanisms of cell death governed by the balance between nitrosative and oxidative stress. *Annals of the New York Academy of Sciences* 899: 209–221.
- Fedorov, R., E. Hartmann, D.K. Ghosh, and I. Schlichting. 2003. Structural basis for the specificity of the nitric-oxide synthase inhibitors W1400 and N^ω-propyl-L-Arg for the inducible and neuronal isoforms. *Journal of Biological Chemistry* 278: 45818–45825.
- Friesner, R.A., J.L. Banks, R.B. Murphy, T.A. Halgren, J.J. Klicic, D.T. Mainz, M.P. Repasky, E.H. Knoll, M. Shelley, J.K. Perry, D.E. Shaw, P. Francis, and P.S. Shenkin. 2004. Glide: A new approach for rapid accurate docking and scoring. 1. Method and

- assessment of docking accuracy. *Journal of Medicinal Chemistry* 47: 1739–1749.
- Gachhui, R., D.K. Ghosh, C. Wu, J. Parkinson, B.R. Crane, and D.J. Stuehr. 1997. Mutagenesis of acidic residues in the oxygenase domain of inducible nitric-oxide synthase identifies a glutamate involved in arginine binding. *Biochemistry* 36: 5097–5103.
- Gautier, C., M. Négrerie, Z.Q. Wang, J.C. Lambry, D.J. Stuehr, F. Collin, J.L. Martin, and A. Slama-Schwok. 2004. Dynamic regulation of the inducible nitric-oxide synthase by NO: Comparison with the endothelial isoform. *Journal of Biological Chemistry* 279: 4358–4365.
- Ghaseemi, A., M. Hedayati, and H. Biabani. 2007. Protein precipitation methods evaluated for determination of serum nitric oxide end products by the Griess assay. *Journal of Medical Sciences Research* 2: 29–32.
- Goodsell, D. Nitric oxide synthase molecule of the month. RCSB PDB Protein Data Bank. <http://www.rcsb.org/pdb/101/motm.do?momID=133>. Last accessed 30 Nov 2011.
- Harma, M., and O. Erel. 2003. Increased oxidative stress in patients with hydatidiform mole. *Swiss Medical Weekly* 133: 563–566.
- Haviv, F., R.J. Ratajczyk, R.W. DeNet, F.A. Kerdesky, R.L. Walters, S.P. Schmidt, J.H. Holms, P.R. Young, and G.W. Carter. 1988. 3-[1-(2-Benzoxazolyl)hydrazino]propanenitrile derivatives: Inhibitors of immune complex induced inflammation. *Journal of Medicinal Chemistry* 31: 1719–1728.
- Horackova, M., P. Ponka, and Z. Byczko. 2000. The antioxidant effects of a novel iron chelator salicylaldehyde isonicotinoyl hydrazone in the prevention of H₂O₂ injury in adult cardiomyocytes. *Cardiovascular Research* 47: 529–536.
- Hrabák, A., T. Bajor, and I. Csuka. 2008. The effects of various inflammatory agents on the phagocytosis and cytokine profile of mouse and rat macrophages. *Inflammation Research* 57: 75–83.
- Jain, S., V. Gautam, and S. Naseem. 2011. Acute-phase proteins: As diagnostic tool. *Journal of Pharmacy and Bioallied Sciences* 3: 118–127.
- Jones, D.P. 2006. Redefining oxidative stress. *Antioxidants & Redox Signaling* 8: 1865–1879.
- Joshi, S.D., H.M. Vagdevi, V.P. Vaidya, and G.S. Gadaginamath. 2008. Synthesis of new 4-pyrrol-1-yl benzoic acid hydrazide analogs and some derived oxadiazole, triazole and pyrrole ring systems: A novel class of potential antibacterial and antitubercular agents. *European Journal of Medicinal Chemistry* 43: 1989–1996.
- Kumar, Y., R. Green, K.Z. Borysko, D.S. Wise, L.L. Wotring, and L.B. Townsend. 1993a. Synthesis of 2,4-disubstituted thiazoles and selenazoles as potential antitumor and antifilarial agents. 1. Methyl 4-(isothiocyanatomethyl)-thiazole-2-carbamates, selenazole-2-carbamates, and related derivatives. *Journal of Medicinal Chemistry* 36: 3843–3848.
- Kumar, Y., R. Green, D.S. Wise, L.L. Wotring, and L.B. Townsend. 1993b. Synthesis of 2,4-disubstituted thiazoles and selenazoles as potential antifilarial and antitumor agents. 2. 2-Arylamido and 2-alkylamido derivatives of 2-amino-4-(isothiocyanatomethyl)-thiazole and 2-amino-4-(isothiocyanatomethyl)-selenazole. *Journal of Medicinal Chemistry* 36: 3849–3852.
- Li, H., and T.L. Poulos. 2005. Structure-function studies on nitric oxide synthases. *Journal of Inorganic Biochemistry* 99: 293–305.
- Metzger, J.V. 1984. *Comprehensive heterocyclic chemistry I*, vol. 6. New York: Pergamon.
- Miranda, K.M., M.G. Espey, and D.A. Wink. 2001. A rapid, simple spectrophotometric method for simultaneous detection of nitrate and nitrite. *Nitric Oxide* 5: 62–71.
- Moldovan, C.M., O. Oniga, A. Pârvu, B. Tipericiu, P. Verite, A. Pîrnău, O. Crișan, M. Bojiță, and R. Pop. 2011. Synthesis and anti-inflammatory evaluation of some new acyl-hydrazones bearing 2-aryl-thiazole. *European Journal of Medicinal Chemistry* 46: 526–534.
- Oniga, O., I. Grosu, S. Mager, and I. Simiti. 1998. Heterocycles LXXVIII. Electrophilic substitution of 2'-phenyl-4R-2,4'-bis-thiazoles. *Monatshefte fuer Chemie* 129: 661–669.
- Paino, I.M.M., V.F. Ximenes, L.M. Da Fonseca, M.P.P. Kanegae, N.M. Khalil, and I.L. Brunetti. 2005. Effect of therapeutic plasma concentrations of non-steroidal anti-inflammatory drugs on the production of reactive oxygen species by activated rat neutrophils. *Brazilian Journal of Medical and Biological Research* 38: 543–551.
- Palmieri, B., and V. Sblendorio. 2010. Current status of measuring oxidative stress. *Methods in Molecular Biology* 594: 3–17.
- Patt, W.C., H.W. Hamilton, M.D. Taylor, M.J. Ryan, D. Taylor, C.J. Connolly, A.M. Doherty, S.R. Klutchko, and I. Sircar. 1992. Structure-activity relationships of a series of 2-amino-4-thiazole-containing renin inhibitors. *Journal of Medicinal Chemistry* 35: 2562–2572.
- Pleşca-Manea, L., A.E. Pârvu, M. Pârvu, M. Tămaș, R. Buia, and M. Puia. 2002. Effects of melilotus officinalis on acute inflammation. *Phytotherapy Research* 16: 316–319.
- Rajak, H., M.D. Kharya, and P. Mishra. 2007. Synthesis of some novel oxadiazole and oxadiazoline analogue for their anti-inflammatory activity. *Yakugaku Zasshi* 127: 1757–1764.
- Serephanoglu, K., A. Taskin, H. Turan, F.E. Timurkaynak, H. Arslan, and O. Erel. 2009. Evaluation of oxidative status in patients with brucellosis. *Brazilian Journal of Infectious Diseases* 13: 249–251.
- Shiradkar, M.R., K.K. Murahari, H.R. Gangadasu, T. Suresh, C.A. Kalyan, D. Panchal, R. Kaur, P. Burange, J. Ghogare, V. Mokale, and M. Raut. 2007. Synthesis of new S-derivatives of clubbed triazolyl thiazole as anti-Mycobacterium tuberculosis agents. *Bioorganic & Medicinal Chemistry* 15: 3997–4008.
- Silva, M.T. 2010. When two is better than one: Macrophages and neutrophils work in concert in innate immunity as complementary and cooperative partners of a myeloid phagocyte system. *Journal of Leukocyte Biology* 87: 93–106.
- Simiti, I., O. Oniga, V. Zaharia, and M. Horn. 1995. Hantzsch reaction intermediates as a means to obtain bisthiazoles and 5-acetyl-bisthiazoles. *Die Pharmazie* 50: 794–796.
- Storn, R., and K. Price. 1997. Differential evolution—A simple and efficient heuristic for global optimization over continuous spaces. *Journal of Global Optimization* 11: 341–359.
- Strom, T.S., P. Anur, and A. Prislovsky. 2011. A numerical analysis model for interpretation of flow cytometric studies of ex vivo phagocytosis. *PLoS ONE* 6: 26657.
- Thomsen, R., and M.H. Christensen. 2006. MolDock: A new technique for high-accuracy molecular docking. *Journal of Medicinal Chemistry* 49: 3315–3321.
- Tipericiu, B., V. Zaharia, I. Colosi, C. Moldovan, O. Crisan, A. Pirnau, L. Vlase, M. Duma, and O. Oniga. 2012. Synthesis and evaluation of antimicrobial activity of some new heteraryl-azoles derivatives obtained from 2-aryl-4-methylthiazol-5-carbohydrazides and isonicotinic acid hydrazide. *Journal of Heterocyclic Chemistry* 49: 1407–1414.
- Tsuji, K., and H. Ishikawa. 1994. Synthesis and anti-pseudomonal activity of new 2-isocephems with a dihydroxypyridone moiety at C-7. *Bioorganic & Medicinal Chemistry Letters* 4: 1601–1606.
- Ueda, S., H. Terauchi, M. Kawasaki, A. Yano, and M. Ido. 2004. Structure-activity relationships of 2-aminothiazole derivatives as inducible nitric oxide synthase inhibitor. *Chemical & Pharmaceutical Bulletin* 52: 634–637.
- Valko, M., D. Leibfritz, J. Moncol, M.T. Cronin, M. Mazur, and J. Telser. 2007. Free radicals and antioxidants in normal physiological functions and human disease. *International Journal of Biochemistry & Cell Biology* 39: 44–84.

- Varnek, A., and A. Tropsha. 2008. *Chemoinformatics approaches to virtual screening*, 1st ed. Cambridge: Royal Society of Chemistry.
- Wilson, K.J., C.R. Illig, N. Subasinghe, J.B. Hoffman, M.J. Rudolph, R. Soll, C. Molloy, R. Bone, D. Green, T. Randall, M. Zhang, F.A. Lewandowski, Z. Zhou, C. Sharp, D. Maguire, B. Grasberger, R.L. DesJarlais, and O. Spurlino. 2001. Synthesis of thiophene-2-carboxamidines containing 2-aminothiazoles and their biological evaluation as urokinase inhibitors. *Journal of Bioorganic & Medicinal Chemistry Letters* 11: 915–918.
- Wink, D.A., K.M. Miranda, and M.G. Espey. 2001. Cytotoxicity related to oxidative and nitrosative stress by nitric oxide. *Experimental Biology and Medicine (Maywood)* 226: 621–623.
- Zaharia, V., A. Ignat, N. Palibroda, B. Ngameni, V. Kuete, K.N. Fokunang, M.L. Mounang, and B.T. Ngadjui. 2010. Synthesis of some *p*-toluenesulfonyl-hydrazinothiazoles and hydrazino-bis-thiazoles and their anticancer activity. *European Journal of Medicinal Chemistry* 45: 5080–5085.

QSPR STUDY ON THE CHROMATOGRAPHIC BEHAVIOR OF A SET OF THIAZOLE DERIVATIVES BY AUTO-CORRELATION ANALYSIS

RALUCA MATIES^a, BEATA SZEFLER^b, IOANA IONUT^c,
BRANDUSA TIPERCIUC^{c,*}

ABSTRACT. A set of twenty six thiazole derivatives, synthesized in our laboratory and measured for chromatographic retention, was submitted to a QSPR study by auto-correlation analysis on the hypermolecule model. As predictor variables, mass fragments, Cluj indices and the HOMO energy, computed at the Hartree-Fock level of theory, are used. Several QSPR models were derived while the leave-one-out procedure was used to evaluate the predictive ability of the main model.

Key words: *thiazoles, hypermolecules, QSPR, topological descriptors*

INTRODUCTION

Quantitative structure-property relations (QSPR) have become a fundamental tool for property prediction in various scientific fields including chemistry, biology, pharmacology, and chemical engineering. Accordingly, relations between molecular structure and macroscopic quantities have been established in diverse areas ranging from thermophysics [1–7] carcinogenicity and toxicity, [8–10] and catalytic activity [11] up to combustion kinetic properties [12–15] and lubricity [16] of biofuels. Quantitative structure-activity relations (QSAR) are employed in drug design to identify molecules with high binding affinity to receptors in order to maximize biological activity.[17–20] A recent review about theory and applications of QSPR was provided by Katritzky et al. [21].

Any QSPR and QSAR approach assumes that a macroscopic property of a chemical compound depends on the molecular structure, as described,

^a Faculty of Chemistry and Chemical Engineering, Babeş-Bolyai University, 400028 Cluj, Romania.

^b Department of Physical Chemistry, Collegium Medicum, Nicolaus Copernicus University, Kurpińskiego 5, 85-950, Bydgoszcz, Poland.

^c Department of Pharmaceutical Chemistry, Faculty of Pharmacy, Iuliu Hatieganu University of Medicine and Pharmacy, Cluj-Napoca, Romania. * brandu32@yahoo.com

e.g. by the topological indices TIs, which are derived from the molecular topology or geometry. In the last years, thousands of TIs have been proposed and used in predicting various molecular properties. Among these, the Cluj indices play an important role [22], even we cannot hide a sentimental relation with them. They have been defined by Diudea at the end of the 2nd millennium [23,24], as shown below.

A Cluj fragment $CJ_{i,j,p}$ collects vertices v lying closer to i than to j , the endpoints of a path $p(i,j)$. Such a fragment collects the vertex proximities of i against any vertex j , joined by the path p , with the distances measured in the subgraph $D_{(G-p)}$, as shown in the following equation:

$$CJ_{i,j,p} = \left\{ v \mid v \in V(G); D_{(G-p)}(i, v) < D_{(G-p)}(j, v) \right\} \quad (1)$$

In graphs containing rings, more than one path could join the pair (i, j) , thus resulting more than one fragment related to i (with respect to j and a given path p). The entries in the Cluj matrix are taken, by definition, as the maximum cardinality among all such fragments:

$$[UCJ]_{i,j} = \max_p |CJ_{i,j,p}| \quad (2)$$

Indices I_e and I_p are calculated, from the Cluj topological matrices UCJ_e , and UCJ_p , respectively (see above), as half sum of matrix entries. In the above symbols, e refers to edge-calculated matrix while p refers to the path-calculated ones.

The chromatographic behavior of a molecule reflects its interaction with two phases: a mobile phase (i.e., the eluent) and a stationary one. This interaction is a function of more than one factor, polarity, lipophylicity and the size of the molecule being included. Lipophilicity is related to the chromatographic behavior and controls the passive transport of a medicinal molecule through the cell membranes (of lipidic nature) [25].

AUTO-CORRELATION METHOD

In order to achieve the QSPR, the structure is encoded in a numerical form. The arrangement of substituent groups, on the Thiazole derivatives herein discussed, can be accounted for by the *hypermolecule* HM concept [26], viewed as the union of the molecules forming the correlating space. In the construction of the hypermolecule, a property *row-vector* P_i is attached to each molecule i :

$$P_i = \{ P_{ij}; j = 1, 2, \dots, n_{HM} \} \quad (3)$$

where n_{HM} is the number of vertices in the hypermolecule. The molecules of the set are superimposed according to their maximal common substructures.

This superposition is indicated by an associated vector X_i , in which the matching positions take $X_{ij} = 1$ while for the non-matching ones $X_{ij} = 0$.

The molecules under study can be numerically described by using a global molecular descriptor AD_i , calculated as a linear combination of the property descriptors $P_{ij}X_{ij}$, multiplied by the regression coefficients b_j performed on the all or most important positions j in the hypermolecule HM:

$$AD_i = \sum_j b_j P_{ij} X_{ij} \quad (4)$$

The above AD_i are called *auto-correlation* descriptors [27,28] and they are *ad-hoc* ones, depending on the chosen set of molecules.

The general regression equations are of the form:

$$Y_i = a + \sum_{j=1}^m b_j \cdot Z_{ij} \quad (5)$$

where Y_i is the dependent variable, Z_{ij} are the predictor variables, $m < n$, n being the number of structures in the set.

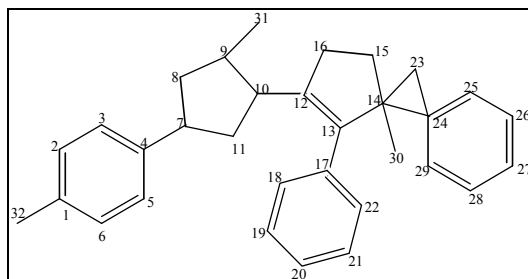
The correlating algorithm followed the steps:

1. generate the *hypermolecule*
2. calculate the molecular descriptors by using a chosen property P_i
3. find the best regression equations
4. test the predictive capability of the model

In this paper, the property P_i was taken the mass fragment M_i while the correlated property was the measured chromatographic retention.

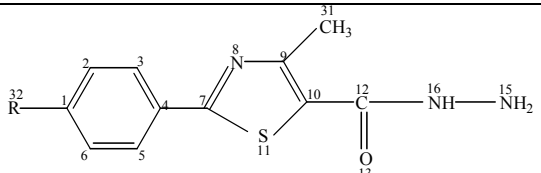
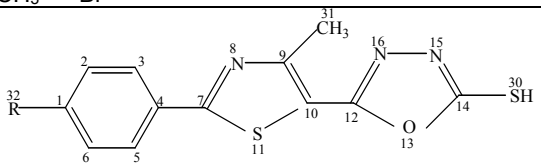
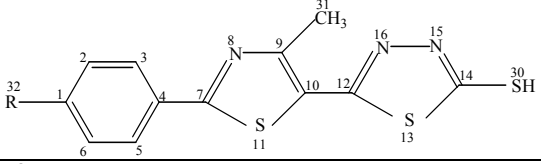
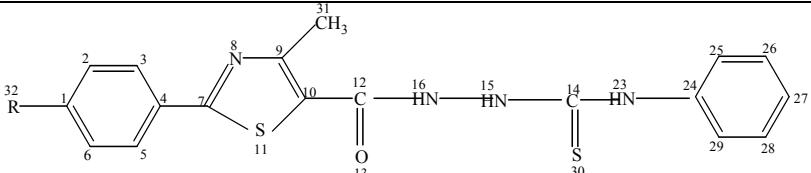
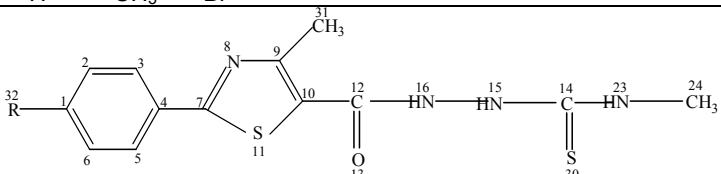
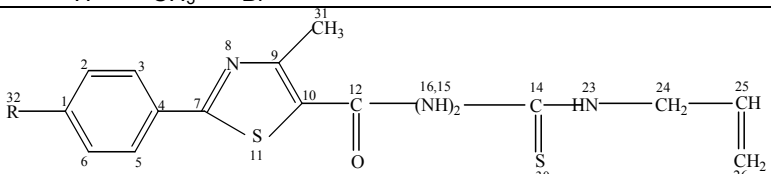
STRUCTURAL DATA

Statistics were done on the set of 26 thiazole derivatives illustrated in Table 1 (see also the experimental part). Numbering refers to the numbering of the hypermolecule, built up as the union of all molecules in the studied set. Chromatographic retention index is listed in Table 2, for each faze F_k , $k=1$ to 5. Details are given in the Experimental section.



Hypermolecule

Table 1. Structural formulas for the studied thiazoles

	Formulas			
1				
Struct.	R	1 H	2 CH ₃	3 Br
2				
Struct.	R	4 H	5 CH ₃	6 Br
3				
Struct.	R	7 H	8 CH ₃	
4				
Struct.	R	9 H	10 CH ₃	11 Br
5				
Struct.	R	12 H	13 CH ₃	14 Br
6				
Struct.	R	15 H	16 CH ₃	17 Br

Formulas				
7				
Struct.	R	18 H	19 CH ₃	20 Br
8				
Struct.	R	21 H	22 CH ₃	23 Br
9				
Struct.	R	24 H	25 CH ₃	26 Br

Table 2. Chromatographic retention values R_f for the Thiazoles in five mobile fazes F_i

Structure	i-propanol:water ratio				
	45:55:00	50:50:00	55:45:00	60:40:00	65:35:00
	F_1	F_2	F_3	F_4	F_5
1	0.400	0.510	0.588	0.552	0.694
2	0.352	0.482	0.529	0.576	0.670
3	0.247	0.376	0.458	0.470	0.611
4	0.658	0.729	0.723	0.764	0.835
5	0.600	0.682	0.676	0.711	0.729
6	0.576	0.670	0.658	0.694	0.729
7	0.470	0.540	0.517	0.547	0.647
8	0.410	0.470	0.482	0.470	0.576
9	0.376	0.494	0.552	0.600	0.688

Structure	i-propanol:water ratio				
	45:55:00	50:50:00	55:45:00	60:40:00	65:35:00
	F_1	F_2	F_3	F_4	F_5
10	0.305	0.435	0.505	0.541	0.647
11	0.282	0.400	0.458	0.494	0.611
12	0.529	0.635	0.670	0.705	0.788
13	0.458	0.588	0.623	0.664	0.752
14	0.388	0.517	0.564	0.611	0.717
15	0.435	0.564	0.600	0.635	0.735
16	0.376	0.505	0.541	0.588	0.705
17	0.329	0.447	0.482	0.529	0.658
18	0.317	0.447	0.482	0.517	0.647
19	0.247	0.400	0.423	0.464	0.611
20	0.153	0.305	0.294	0.435	0.435
21	0.329	0.505	0.482	0.611	0.600
22	0.247	0.447	0.435	0.552	0.553
23	0.211	0.388	0.376	0.482	0.505
24	0.258	0.435	0.429	0.552	0.494
25	0.200	0.376	0.376	0.494	0.505
26	0.152	0.317	0.305	0.670	0.458

RESULTS AND DISCUSSION

The local property P_{ij} chosen here was the hydride fragment mass M_{ij} (listed in Table 3, for each j -position of the hypermolecule). It will be used in the calculation of the auto-correlation property descriptor AD (see below).

Table 3. Hydride fragment mass M_{ij} , for each j -position of the hypermolecule

j	1	2	3	4	5	6	7	8	9	10	11	12	13	14	15	16	17	18	19	20	21	22	23	24	25	26
1	12	12	12	12	12	12	12	12	12	12	12	12	12	12	12	12	12	12	12	12	12	12	12	12	12	12
2	12	12	12	12	12	12	12	12	12	12	12	12	12	12	12	12	12	12	12	12	12	12	12	12	12	12
3	12	12	12	12	12	12	12	12	12	12	12	12	12	12	12	12	12	12	12	12	12	12	12	12	12	12
4	12	12	12	12	12	12	12	12	12	12	12	12	12	12	12	12	12	12	12	12	12	12	12	12	12	12
5	12	12	12	12	12	12	12	12	12	12	12	12	12	12	12	12	12	12	12	12	12	12	12	12	12	12
6	12	12	12	12	12	12	12	12	12	12	12	12	12	12	12	12	12	12	12	12	12	12	12	12	12	12
7	12	12	12	12	12	12	12	12	12	12	12	12	12	12	12	12	12	12	12	12	12	12	12	12	12	12
8	14	14	14	14	14	14	14	14	14	14	14	14	14	14	14	14	14	14	14	14	14	14	14	14	14	14
9	12	12	12	12	12	12	12	12	12	12	12	12	12	12	12	12	12	12	12	12	12	12	12	12	12	12
10	12	12	12	12	12	12	12	12	12	12	12	12	12	12	12	12	12	12	12	12	12	12	12	12	12	12
11	32	32	32	32	32	32	32	32	32	32	32	32	32	32	32	32	32	32	32	32	32	32	32	32	32	32
12	12	12	12	12	12	12	12	12	12	12	12	12	12	12	12	12	12	12	12	12	12	12	12	12	12	12
13	16	16	16	16	16	16	32	32	16	16	16	16	16	16	16	16	16	14	14	14	14	14	14	14	14	14
14	0	0	0	12	12	12	12	12	12	12	12	12	12	12	12	12	12	12	12	12	12	12	12	12	12	12

<i>j</i>	1	2	3	4	5	6	7	8	9	10	11	12	13	14	15	16	17	18	19	20	21	22	23	24	25	26
15	14	14	14	14	14	14	14	14	14	14	14	14	14	14	14	14	14	14	14	14	14	14	14	14	14	14
16	14	14	14	14	14	14	14	14	14	14	14	14	14	14	14	14	14	14	14	14	14	14	14	14	14	14
17	0	0	0	0	0	0	0	0	0	0	0	0	0	0	0	0	0	12	12	12	12	12	12	12	12	12
18	0	0	0	0	0	0	0	0	0	0	0	0	0	0	0	0	0	12	12	12	0	0	0	12	12	12
19	0	0	0	0	0	0	0	0	0	0	0	0	0	0	0	0	0	12	12	12	0	0	0	12	12	12
20	0	0	0	0	0	0	0	0	0	0	0	0	0	0	0	0	0	12	12	12	0	0	0	0	0	0
21	0	0	0	0	0	0	0	0	0	0	0	0	0	0	0	0	0	12	12	12	0	0	0	0	0	0
22	0	0	0	0	0	0	0	0	0	0	0	0	0	0	0	0	0	12	12	12	0	0	0	0	0	0
23	0	0	0	0	0	0	0	0	14	14	14	14	14	14	14	14	14	0	0	0	0	0	0	0	0	0
24	0	0	0	0	0	0	0	0	12	12	12	12	12	12	12	12	12	0	0	0	0	0	0	0	0	0
25	0	0	0	0	0	0	0	0	12	12	12	0	0	0	12	12	12	0	0	0	0	0	0	0	0	0
26	0	0	0	0	0	0	0	0	12	12	12	0	0	0	12	12	12	0	0	0	0	0	0	0	0	0
27	0	0	0	0	0	0	0	0	12	12	12	0	0	0	0	0	0	0	0	0	0	0	0	0	0	0
28	0	0	0	0	0	0	0	0	12	12	12	0	0	0	0	0	0	0	0	0	0	0	0	0	0	0
29	0	0	0	0	0	0	0	0	12	12	12	0	0	0	0	0	0	0	0	0	0	0	0	0	0	0
30	0	0	0	32	32	32	32	32	32	32	32	32	32	32	32	32	32	32	32	32	32	32	32	32	32	32
31	12	12	12	12	12	12	12	12	12	12	12	12	12	12	12	12	12	12	12	12	12	12	12	12	12	12
32	0	12	80	0	12	80	0	12	0	12	80	0	12	80	0	12	80	0	12	80	0	12	80	0	12	80

Topological Cluj descriptors were computed by TOPOCLUJ software and listed in Table 4 along with the number of atoms *N* in molecules and the energy of the highest occupied molecular orbital HOMO, computed on the optimized molecules, at the Hartree-Fock level of theory (see the experimental part).

Table 4. Topological and energetic descriptors of the optimized molecules at the Hartree-Fock level of theory

Molecule	<i>N</i>	<i>I_e</i>	<i>I_p</i>	HOMO (au)
1	16	310	1400	-1778.65
2	17	380	1800	-1817.691
3	17	380	1800	-4347.955
4	18	430	2500	-1588.141
5	19	520	3000	-1627.187
6	19	520	3000	-4157.45
7	18	430	2500	-1665.028
8	19	520	3000	-1704.068
9	25	1100	7500	-1702.554
10	26	1300	8600	-1741.595
11	26	1300	8600	-4271.859
12	20	570	3000	-1512.092
13	21	670	3600	-1551.132
14	21	670	3600	-4081.396

Molecule	N	I_e	I_p	HOMO (au)
15	22	740	4200	-1588.973
16	23	860	5000	-1628.013
17	23	860	5000	-4158.278
18	24	930	6700	-1492.878
19	25	1100	7800	-1531.919
20	25	1100	7800	-4062.183
21	19	480	2900	-1815.518
22	20	580	3500	-1854.559
23	20	580	3500	-4234.319
24	21	620	3900	-1891.562
25	22	720	4600	-1930.602
26	22	720	4600	-1058.682

The best QSPR model, without auto-correlation descriptors are listed in Table 5. The descriptors named by numbers represent the mass fragments in the given positions of the hypermolecule. Even the models are statistically significant, the number of predictor variables is too large for the set of 26 thiazole derivatives, according to [29]. By this reason, we calculated the auto-correlation descriptors AD, cf. [4] (see below).

Table 5. Regressions without auto-correlation; the descriptors named by numbers represent the mass fragments in the given positions of the hypermolecule

Descriptors	F_1			
	R^2	Adjus. R^2	St. Error	F
IE, 13, 17, 24, 25, 30, 32	0.957	0.940	0.033	56.592
IE, IP, 13, 17, 25, 30, 32, HOMO	0.969	0.955	0.029	67.008
IE, 13, 17, 24, 30, 32	0.941	0.922	0.037	50.464
IE, IP, 13, 17, 25, 30, HOMO	0.954	0.936	0.034	53.425
F_2				
IE, 13, 17, 24, 30, 32, HOMO	0.949	0.929	0.029	47.577
IE, 13, 17, 24, 30, 32	0.943	0.926	0.030	52.806
IP, 13, 17, 24, 30, 32	0.937	0.917	0.031	47.162
F_3				
IE, 13, 17, 25, 30, 32, HOMO	0.947	0.926	0.030	45.614
IE, 13, 17, 25, 30, 32	0.938	0.919	0.032	48.169
IP, 13, 17, 25, 30, 32	0.932	0.911	0.033	43.432
F_4				
IE, IP, 13, 17, 22, 25, 30, 32, HOMO	0.957	0.932	0.023	39.275
IE, 13, 17, 22, 25, 30, 32, HOMO	0.913	0.872	0.031	22.359
IE, 13, 17, 25, 30, 32, HOMO	0.913	0.879	0.031	27.044
F_5				
IE, 13, 17, 22, 29, 30, 32	0.933	0.906	0.031	35.598
IP, 13, 17, 22, 29, 30, 32	0.937	0.913	0.030	38.378
IE, 13, 17, 22, 29, 30, HOMO	0.918	0.885	0.035	28.619

Table 6 lists the global auto-correlating descriptor $AD_{(13, 17, 19, 24, 25, 30, 32)}$ calculated cf (4) (on the positions 13, 17, 19, 24, 25, 30, 32 of the hypermolecule), the F_1 values, observed and estimated, the corresponding residuals (i.e., the difference between the experimental and calculated F-values) for eq. (6) and the predicted *leave-one-out* $F_{1,loo}$ -values cf (7).

$$F_1 = 0.575 + AD(F_1); n=26; R^2=0.950; s=0.031; F=454.567 \quad (6)$$

$$F_{1,loo} = 0.002 + 0.994 AD(F_1)_{loo}; n=25; R^2=0.942; s=0.033; F=391.815 \quad (7)$$

One can see a good predictive ability of the $AD(F_1)_{loo}$ descriptors by the small drop of the correlation coefficient R^2 in a monovariate regression (eqs. 6 and 7). The subscript numbers in AD_i symbols represent the positions in hypermolecule and suggest these are responsible of the chromatographic retention. The large values of Fischer ratio F in (6) in comparison to the multivariate regressions listed in Table 5 suggest a higher level of (statistical) significance for the monovariate regression in comparison to that of multivariate ones. Table 7 lists the best model using the auto-correlating descriptors and some other molecular: Cluj indices and the energy of HOMO, for all the 5 mobile phases F_i . One can see a similar chromatographic behavior in all the phases except F_4 , which is the worst one.

It is noteworthy the adjusted R^2 speaks clearly that the additional variables (i.e., Cluj indices and HOMO) are not necessary, thus proving the utility of the auto-correlating descriptors.

Table 6. Auto-correlating descriptors $AD_{(13, 17, 19, 24, 25, 30, 32)}$ in the learning (calcd) and predicting (*loo*) steps, respectively

Molecule <i>i</i>	AD_i	$F_{1,obs}$	$F_{1,calcd.}$	$Resid_{calcd}$	$F_{1,loo}$
1	-0.203	0.4	0.372	0.028	0.371
2	-0.218	0.352	0.357	-0.005	0.357
3	-0.305	0.247	0.270	-0.023	0.271
4	0.075	0.658	0.651	0.007	0.648
5	0.060	0.6	0.635	-0.035	0.645
6	-0.027	0.576	0.548	0.028	0.544
7	-0.128	0.47	0.448	0.022	0.446
8	-0.143	0.41	0.432	-0.022	0.434
9	-0.185	0.376	0.390	-0.014	0.39
10	-0.201	0.305	0.374	-0.069	0.377
11	-0.288	0.282	0.287	-0.005	0.288
12	-0.078	0.529	0.498	0.031	0.495
13	-0.093	0.458	0.482	-0.024	0.484
14	-0.180	0.388	0.395	-0.007	0.395
15	-0.185	0.435	0.390	0.045	0.388
16	-0.201	0.376	0.374	0.002	0.374

Molecule <i>i</i>	AD_i	$F_{1,obs}$	$F_{1,calcd.}$	$Resid_{calcd}$	$F_{1,loo}$
17	-0.288	0.329	0.287	0.042	0.285
18	-0.315	0.317	0.260	0.057	0.257
19	-0.330	0.247	0.245	0.002	0.245
20	-0.417	0.153	0.158	-0.005	0.159
21	-0.274	0.329	0.302	0.027	0.300
22	-0.289	0.247	0.286	-0.039	0.288
23	-0.376	0.211	0.199	0.012	0.198
24	-0.315	0.258	0.260	-0.002	0.261
25	-0.330	0.200	0.245	-0.045	0.248
26	-0.417	0.152	0.158	-0.006	0.159

Table 7. Regressions with auto-correlation descriptors

Descriptors	F_1			
	R^2	Adjust. R^2	St. Error	F
$AD_{(13, 17, 19, 24, 25, 30, 32)}$	0.950	0.948	0.031	454.567
IE, AD	0.952	0.948	0.031	228.094
IE, IP, AD	0.952	0.946	0.031	146.168
IE, AD, HOMO	0.952	0.946	0.031	146.705
IE, IP, AD, HOMO	0.953	0.944	0.032	106.068
F_2				
$AD_{(13, 17, 18, 24, 26, 30, 32)}$	0.944	0.942	0.026	403.468
AD, HOMO	0.944	0.939	0.027	194.442
IE, IP, AD	0.949	0.943	0.026	137.740
IP, AD, HOMO	0.950	0.943	0.026	138.406
IE, IP, AD, HOMO	0.950	0.940	0.027	99.095
F_3				
$AD_{(13, 17, 24, 25, 30, 32)}$	0.940	0.937	0.028	372.732
AD, HOMO	0.942	0.937	0.028	186.190
IE, IP, AD	0.945	0.937	0.028	125.169
IE, AD, HOMO	0.947	0.940	0.027	131.604
IE, IP, AD, HOMO	0.947	0.937	0.028	94.370
F_4				
$AD_{(13, 17, 22, 24, 25, 30, 32)}$	0.776	0.766	0.943	82.981
IE, IP, AD	0.781	0.751	0.044	26.084
AD, HOMO	0.805	0.788	0.041	47.424
IP, AD, HOMO	0.809	0.783	0.041	31.037
IE, IP, AD, HOMO	0.809	0.773	0.042	22.294
F_5				
$AD_{(13, 17, 18, 22, 26, 29, 30, 32)}$	0.926	0.923	0.029	298.865
AD, HOMO	0.926	0.919	0.029	143.519
IE, AD, HOMO	0.926	0.916	0.030	92.332
IE, IP, AD	0.929	0.919	0.029	95.325
IE, IP, AD, HOMO	0.929	0.915	0.030	68.276

EXPERIMENTAL

Twenty six thiazole derivatives (thiazolyl-carbonyl-thiosemicarbazides and hybrid thiazolyl-1,3,4-oxadiazoles, thiazolyl-1,3,4-triazoles, and thiazolyl-1,3,4-triazoles - Table 1), synthesized in our laboratory, according to a previously described procedure [30,31], were investigated for chromatographic behavior. Chromatography was performed on 20 X 20 cm RP-18F_{254s} TLC precoated silica plates (Merck; Darmstadt, Germany). Solutions (1 mg mL⁻¹) of the tested compounds were prepared in *iso*-propanol, and 3 μ l in duplicate were spotted on the plates by hand, 10 mm from the bottom edge and 20 mm apart. The mobile phases were composed of the *iso*-propanol-water binary mixtures, with a varying content of organic modifier between 45-65% (v/v) in 5% increments, as the study compounds differed considerably in their retention. Chromatography was performed in a normal developing chamber at room temperature, the developing distance being 10 cm. The chromatography chamber was saturated with the mobile phase for 30 minutes before use. After the development (30-60 minutes), the plates were air dried at room temperature and examined under UV lamp ($\lambda = 254$ nm) and the R_f (retardation factor) values were measured manually by a digital caliper. The experiments were made in triplicate. All components of the mobile phases used were of the analytical grade of purity. Table 2 lists the data for each faze F_k , $k=1$ to 5. The results were addressed to statistical correlational analysis.

Topological indices were computed by the TOPOCLUJ [32] software while the HOMO energy was computed by single point on the optimized molecules at the Hartree-Fock HF/6-31G(d,p) level of theory.

CONCLUSIONS

A set of twenty six thiazole derivatives, synthesized in the laboratory of Faculty of Pharmacy, "Iuliu Hatieganu" University of Medicine and Pharmacy, and measured for chromatographic retention was submitted to a QSPR study by auto-correlation analysis within the hypermolecule model. As predictor variables, mass fragments, Cluj indices and the HOMO energy, computed at the Hartree-Fock level of theory, have been used. Several QSPR models were derived while the leave-one-out procedure was used to prove the predictive ability of the main model. The auto-correlation descriptors behaved statistically better than the normal descriptors, according to the parameters of regression equations.

ACKNOWLEDGEMENTS

The authors acknowledge to Prof. Mircea V. Diudea for useful discussions.

REFERENCES

1. W. Herndon, P. Biedermann, I. Agranat, *J. Org. Chem.*, **1998**, 63, 7445.
2. N. Zefirov, V. Palyulin, A. Oliferenko, A. Ivanova, A. Ivanov, *Dokl. Chem.*, **2001**, 381, 356.
3. N. Brauner, M. St. Shacham, G. Cholakov, R. Stateva, *Chem. Eng. Sci.*, **2005**, 60, 5458.
4. A. Vatani, M. Mehrpooya, F. Gharagheizi, *Int. J. Mol. Sci.*, **2007**, 8, 407.
5. G.S. Cholakov, R. Stateva, N. Brauner, M. Shacham, *J. Chem. Eng.*, **2008**, 53, 2510.
6. M. Shacham, G. Cholakov, R. Stateva, N. Brauner, *Ind. Eng. Chem. Res.*, **2010**, 49, 900.
7. A. Katritzky, I. Stoyanova-Slavova, K. Tämm, T. Tamm, M. Karelson, *J. Phys. Chem. A*, **2011**, 115, 3475.
8. S. Sixt, J. Altschuh, R. Brüggemann, *Chemosphere*, **1995**, 30, 2397.
9. A. Helguera, M. Cordeiro, D. Natalia, M. Perez, R. Combes, M. Gonzalez, *Bioorg. Med. Chem.*, **2008**, 16, 3395.
10. I. Shamovsky, L. Ripa, L. Börjesson, C.D. Mee, B. Norden, P. Hansen, C. Hasselgren, M. O'Donovan, P. Sjö, *J. Am. Chem. Soc.*, **2011**, 133, 16168.
11. G. Occhipinti, H. Bjørsvik, V. Jensen, *J. Am. Chem. Soc.*, **2006**, 128, 6952.
12. B. Creton, C. Dartiguelongue, T. de Bruin, H. Toulhoat, *Energy Fuels*, **2010**, 24, 5396.
13. Y. Pan, J. Jiang, X. Ding, R. Wang, J. Jiang, *AIChE J.*, **2010**, 56, 690.
14. M. Hechinger, W. Marquardt, *Comput. Chem. Eng.*, **2010**, 34, 1507.
15. A. Katritzky, D. Fara, *Energy Fuels*, **2005**, 19, 922.
16. K. Masuch, A. Fatemi, H. Murrenhoff, K. Leonhard, *Lubrication*, **2011**, 23, 249.
17. H. Kubinyi, *Drug Discovery Today*, **1997**, 2, 457.
18. S. Jonsdottir, F. Jorgensen, S. Brunak, *Bioinformatics*, **2005**, 21, 2145.
19. R. Perkins, H. Fang, W. Tong, W. Welsh, *Environ. Toxicol. Chem.*, **2003**, 22, 1666.
20. M. Devereux, P. Popelier, I. McLay, *J. Chem. Inf. Model*, **2009**, 49, 1497.
21. A. Katritzky, M. Kuanar, S. Slavov, C. Hall, *Chem. Rev.*, **2010**, 110, 5714.
22. D. Janežič, A. Miličević, S. Nikolić, and N. Trinajstić, *Graph Theoretical Matrices in Chemistry*, Math. Chem. Monographs, Univ. Kragujevac, **2007**.
23. M.V. Diudea, *MATCH Commun. Math. Comput. Chem. (MATCH)*, **1997**, 35, 169.
24. M.V. Diudea, *J. Chem. Inf. Comput. Sci.*, **1997**, 37, 300.
25. H. Kubinyi, *Quant. Struct.-Act. Relat.*, **1994**, 13, 285

26. A.T. Balaban, A. Chiriac, I. Motoc, and Z. Simon, *Steric Fit in QSAR (Lectures Notes in Chemistry, Vol. 15)*, Springer, Berlin, **1980**, Chap. 6.
27. M. Wagener, J. Sadowski, and J. Gasteiger, *J. Am. Chem. Soc.*, **1995**, *117*, 7769.
28. A.A. Toropov, and A.P. Toropova, *Internet El. J. Molec. Design*, **2002**, *1*, 108.
29. J.G. Topliss and R.P. Edwards, *J. Med. Chem.* **1979**, *22*, 1238.
30. B. Tipericiuc, V. Zaharia, I. Colosi, C. Moldovan, O. Crisan, A. Parnau, L. Vlase, M. Duma, O. Oniga, *J. Het. Chem.*, **2012**, *49(6)*, 1407.
31. B. Tipericiuc, C. Sârbu, *Journal of Liquid Chromatography & Related Technologies*, **2006**, *29:15*, 2257.
32. O. Ursu, M.V. Diudea, "TOPOCLUJ software program", Babes-Bolyai University, Cluj, **2005**.

Brîndușă Tiperciuc,^{a*} Valentin Zaharia,^a Ioana Colosi,^b Cristina Moldovan,^a
Ovidiu Crișan,^a Adrian Pîrmau,^c Laurian Vlase,^a Mihaela Duma,^d
and Ovidiu Oniga^a

^aDepartment of Pharmaceutical Chemistry, Faculty of Pharmacy, University of Medicine and Pharmacy,
400010 Cluj-Napoca, Romania

^bDepartment of Microbiology, Faculty of Medicine, University of Medicine and Pharmacy,
400010 Cluj-Napoca, Romania

^cNational Institute for Research and Development of Isotopic and Molecular Technologies,
400293 Cluj-Napoca, Romania

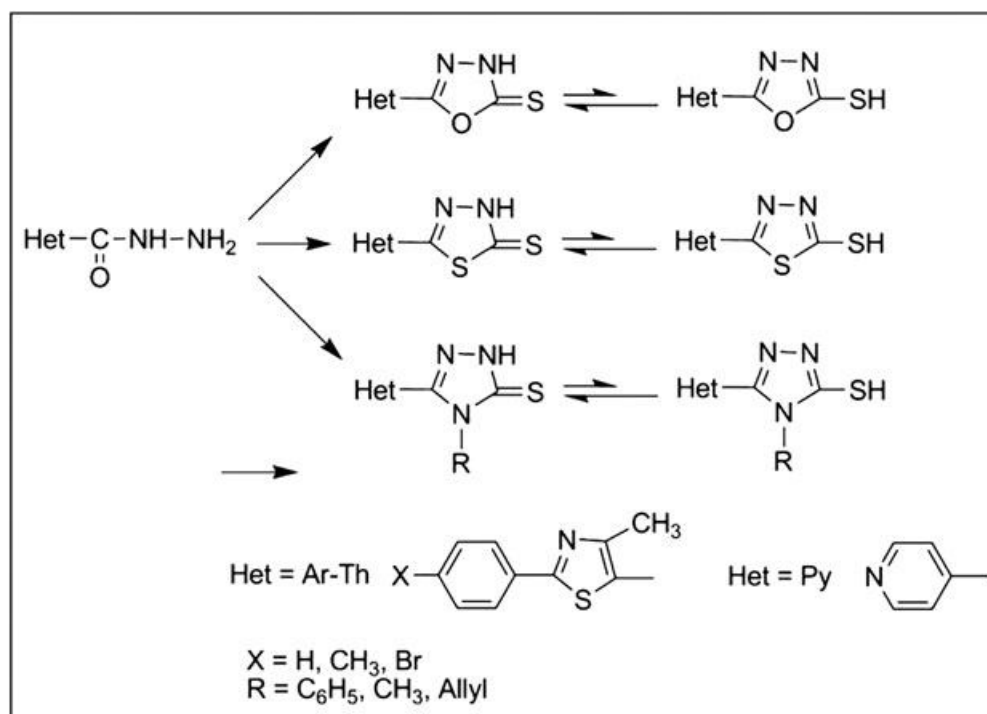
^dState Veterinary Laboratory for Animal Health and Food Safety, 400572 Cluj-Napoca, Romania

*E-mail: brandu32@yahoo.com

Received April 5, 2011

DOI 10.1002/jhet.1060

View this article online at wileyonlinelibrary.com.



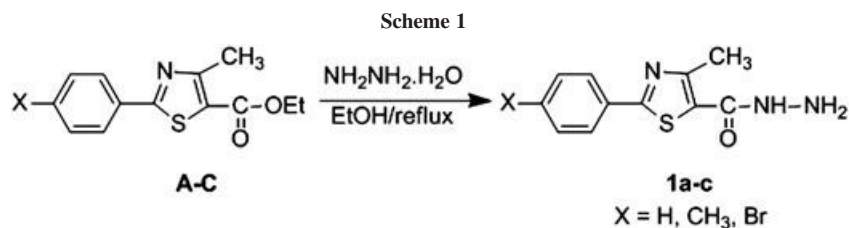
A series of new 1,3,4-oxadiazole/thiadiazole and 1,2,4-triazole derivatives have been synthesized starting from 2-aryl-4-methylthiazol-5-carbohydrazides and isonicotinic acid hydrazide. All the newly synthesized compounds were characterized by IR, ¹H NMR, ¹³C NMR, and mass spectrometry. The synthesized compounds were screened for their antibacterial and antifungal activity, assessed as growth inhibition diameter. Some of them showed good antibacterial activity against gram positive *Staphylococcus aureus*, while the antibacterial activity against *Listeria monocytogenes*, *Escherichia coli*, and *Salmonella typhimurium* and antifungal activity against *Candida albicans* was modest. None of the tested compounds showed inhibitory activity against gram positive bacteria *Enterococcus faecalis* and *Bacillus cereus* and against gram negative bacteria *Pseudomonas aeruginosa*.

J. Heterocyclic Chem., **49**, 1407 (2012).

INTRODUCTION

The problem of multidrug resistant microorganisms has reached an alarming level around the world in the past decades, and represents a challenge for the development

of new antimicrobial agents, with novel mechanisms and a broadened spectrum of activity. In the past years, some azole derivatives were developed as new antimicrobial agents, for instance, Linezolid and Eperezolid are currently used for the treatment of multidrug-resistant gram positive



infections [1–3]. There is some important antifungal drugs containing thiazole or 1,2,4-triazole ring in their structures, such as Ravuconazole, Fluconazole, Voriconazole, and Itraconazole, [4]. Also, thiazole derivatives are found to be associated with various biological activities such as antibacterial [5], antifungal [6], antiinflammatory [7], anti-hypertensive [8], anti-HIV [9], antitumor [10–13], antifilarial [12, 13], anticonvulsant [14], herbicidal, insecticidal, schistosomicidal, and anthelmintic [15]. Heterocyclic compounds containing 1,3,4-oxadiazole, 1,3,4-thiadiazole or 1,2,4-triazole moiety present a wide spectrum of biological activities such as antimicrobial, antiviral, anti-inflammatory, and antitumoral [16–21]. Acid hydrazides were documented as important compounds, due to their high reactivity in heterocycles synthesis, as key starting materials for 1,2,4-triazole, 1,3,4-oxadiazole or 1,3,4-thiadiazole synthesis [22, 23].

In view of the wide interest in the biological activity of these compounds and as a continuation of our research in this area [24–26], our aim was to synthesize new isolated heterocyclic systems, as antimicrobial agents, that comprise both the thiazole/pyridine and the 1,2,4-triazole,

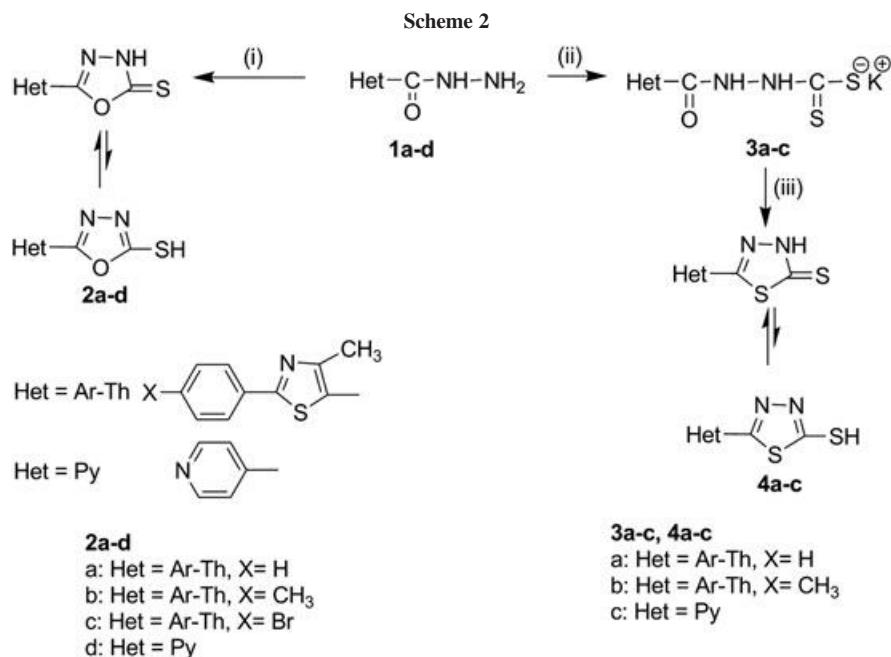
1,3,4-oxadiazole or 1,3,4-thiadiazole rings, using 2-aryl-4-methylthiazol-5-carbohydrazides and isonicotinic acid hydrazide as starting materials. The compounds were designed to investigate the effect of such structural variation on the anticipated antimicrobial activities.

RESULTS AND DISCUSSION

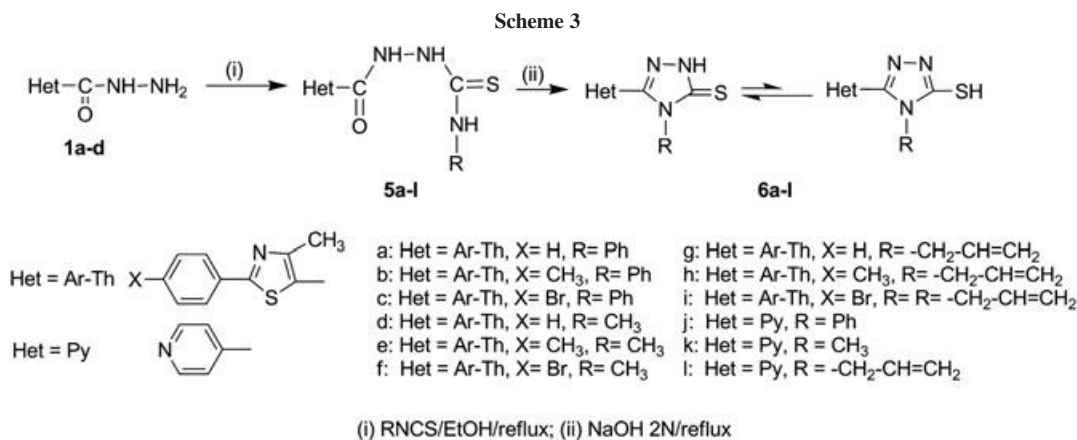
Chemistry. The reaction sequences used for the synthesis of target compounds are shown in Schemes 1–3. The structures of the newly synthesized compounds were confirmed by analytical and spectral data (IR, ¹H NMR, ¹³C NMR, and MS).

The key intermediates 2-aryl-4-methylthiazol-5-carbohydrazides **1a–c** (X H, CH₃, and Br) were prepared by the reaction of ethyl-2-aryl-4-methylthiazol-5-carboxylates (**A–C**) with hydrazine hydrate in absolute ethanol, according to the literature [27] (Scheme 1).

The 1,3,4-oxadiazole derivatives **2a–d** were obtained in good yield, by the reaction of the carbohydrazides **1a–c** and isonicotinic acid hydrazide **1d** with CS₂ and KOH in



(i) CS₂/KOH/EtOH/reflux; (ii) CS₂/KOH/EtOH/10⁰C; (iii) H₂SO₄/rt;



refluxing ethanol, followed by hydrochloric acid work up. Reaction of **1a–b**, respectively, **1d** with CS_2 and KOH in absolute ethanol below 10°C resulted in the formation of potassium dithiocarbazates **3a–c**. Dehydrative cyclization of compounds **3a–c** using sulfuric acid at room temperature yielded the 1,3,4-thiadiazoles **4a–c** (Scheme 2).

4-Alkyl/aryl-1-(2-aryl-4-methylthiazol-5-carbonyl)-thiosemicarbazides **5a–i** and 4-alkyl/aryl-1-(pyridin-4-carbonyl)-thiosemicarbazide **5j–l** were obtained from hydrazides **1a–d** and the corresponding alkyl/arylisothiocyanates. The thiosemicarbazides **5a–l**, on heating with NaOH 2 N in ethanol, underwent cyclization through dehydration to afford 4-alkyl/aryl-3-(2-aryl-4-methylthiazol-5-yl)-1H-1,2,4-triazol-5(4H)-thiones **6a–i** and 4-alkyl/aryl-3-(pyridin-4-yl)-1H-1,2,4-triazol-5(4H)-thiones **6j–l** (Scheme 3), respectively.

IR spectra of thiosemicarbazides **5a–l** displayed absorption peaks at $3115\text{--}3308\text{ cm}^{-1}$ for NH, $1650\text{--}1682\text{ cm}^{-1}$ for C O, and $1214\text{--}1265\text{ cm}^{-1}$ corresponding to C S stretching vibrations. ^1H NMR spectra showed the three signals for the CONH, CSNH, and NH protons, as singlets at 10–10.3, 9.3–9.85, and 8.1–8.8 ppm, respectively, confirming the formation of thiosemicarbazide.

IR spectra of **2a–d**, **4a–c**, and **6a–l** exhibited NH bands in $3448\text{--}3463$, $3438\text{--}3400$, and $3070\text{--}3187\text{ cm}^{-1}$, respectively. The absorption bands at $1597\text{--}1616$, $1541\text{--}1599$, and $1538\text{--}1614\text{ cm}^{-1}$ are due to the presence of C N stretch of the oxadiazole, thiadiazole, and triazole ring system, respectively. The absence of the C O absorption in **2a–d**, **4a–c**, and **6a–l** provided strong evidences for the formation of the new products. Also, the presence of bands for the C S group in the $1232\text{--}1275$, $1242\text{--}1258$, and $1214\text{--}1286\text{ cm}^{-1}$ proved that the compounds were in thione form in the solid state. In the ^1H NMR spectra of **1a–c**, the NH proton appeared in the 9.56–9.72 ppm region, whereas in compounds **2a–d**, **3a–c**, and **6a–l**, the NH signal was shifted to 14.1–14.4 ppm, indicating the thiol–thione tautomerism in solution. In the ^{13}C NMR spectra of **2a–d**, **3a–c**, and **6a–l**, the C S gave a peak at 169.9–172.9, 182.9–183.6, 168.6–171.4 ppm, respectively, indicating that the

crystal structures of the compounds correspond to the thione form. The mass spectra of the prepared compounds showed the correct molecular ions (M^+ or $\text{M} + 1$) as suggested by their molecular formulas.

Antibacterial and antifungal activity. The newly synthesized compounds were tested for their antimicrobial activity, at a concentration of 10 mg/mL, against four gram positive bacterial strains: *Staphylococcus aureus* (ATCC 49444), *Enterococcus faecalis* (ATCC 29211), *Bacillus cereus* (ATCC 11778), *Listeria monocytogenes* (ATCC 13076); three gram negative bacterial strains: *Escherichia coli* (ATCC 25922), *Salmonella typhimurium* (ATCC 14028), *Pseudomonas aeruginosa* (ATCC 27853); and one fungal strain: *Candida albicans* (ATCC 10231), by the cup-plate agar diffusion method [28]. Each microorganism was suspended in Mueller Hinton (MH) broth and diluted approximately to 10^6 colony forming unit (cfu)/mL. They were “flood inoculated” onto the surface of MH agar and MH dextrose agar (MDA) and then dried. For *C. albicans*, MDA was used. Six millimeter diameter wells were cut from the agar using a sterile cork-borer, and 10 μL of each compound solution were delivered into the wells. The plates were incubated at 37°C , and the diameters of the growth inhibition zones were measured after 24 h in case of bacteria and after 48 h in case of *C. albicans*. Stock solution of each compound (10 mg/mL) was prepared in dimethyl sulfoxide (DMSO; Merck, Germany). Gentamicin (10 μg per well) and Fluconazole (25 μg per well) were used as standard drugs. The controls were performed with only sterile broth and with only overnight culture and 10 μL of DMSO. Results were obtained in duplicate. The results of the antimicrobial screening are summarized in Table 1.

All the tested compounds were inactives against *E. faecalis*, *B. cereus*, and *P. aeruginosa*. Some of the compounds are active and showed moderate-to-good activity against *S. aureus*: thiazolyl-1,3,4-oxadiazoles **2a–c**, potassium dithiocarbazates **3a–c**, thiazolyl-1,3,4-thiadiazoles **4a–b**, and thiazolyl-thiosemicarbazides **5a–d** and **5g–h**. As it can be seen in Table 1,

Table 1
Antimicrobial activity of the synthesized compounds.^a

Compound	Gram positive bacteria		Gram negative bacteria		Fungi
	<i>S. aureus</i>	<i>L. monocytogenes</i>	<i>E. coli</i>	<i>S. typhimurium</i>	<i>C. albicans</i>
1a	-	5	4	5	10
1b	-	4	4	4	12
1c	-	4	4	4	-
2a	16	3	4	-	-
2b	20	3	3	-	-
2c	22	4	4	-	-
3a	15	3	4	-	6
3b	15	3	4	-	-
3c	20	-	-	-	9
4a	7	-	3	-	-
4b	15	3	4	-	-
5a	7	3	4	-	-
5b	10	3	4	-	-
5c	9	3	3	-	-
5d	6	3	4	-	-
5e	-	3	4	-	15
5f	-	3	4	-	10
5g	6	3	4	-	-
5h	6	-	4	-	-
5i	4	-	4	-	-
6a	4	-	4	-	-
6b	-	-	4	-	-
6c	-	-	4	-	-
6d	-	-	4	-	-
6e	-	-	4	-	-
6f	-	-	4	-	-
6g	-	-	4	-	-
6h	-	-	4	-	-
6i	4	-	4	-	-
Gentamicin	19	18	22	18	-
Fluconazole	-	-	-	-	25

Gentamycin (10 µg per well) and Fluconazole (25 µg per well) were used as standard drugs.

- Indicates the compound has no activity.

^aZones of inhibition in millimeter.

oxadiazole derivatives **2a–c** were more active than the thiadiazole derivatives **4a–b**. The most active compound was **2c** with a 4-bromophenyl group in position 2 of the thiazole ring, the inhibitory activity being more powerful than that of Gentamicin (10 µg per well), used as standard drug. All the synthesized compounds were slightly sensitive against gram positive *B. cereus* and *L. monocytogenes* and gram negative bacteria *E. coli*. The antifungal screening data reveal that most of the new compounds are inactive, only six compounds displayed weak inhibitory activity against *C. albicans*: acid hydrazides **1a**, **1b**, potassium dithiocarbazates **3a**, **3c**, and thiazolyl-thiosemicarbazides **5e**, **5f**.

In conclusion, a series of new thiazolo/pyridin-1,3,4-oxadiazole, thiazolo/pyridin-1,3,4-thiadiazole, and thiazolo/pyridin-1,2,4-triazole derivatives have been synthesized starting from 2-aryl-4-methylthiazol-5-carbohydrazides and isonicotinic acid hydrazide and evaluated for their antibacterial and antifungal activity against various gram positive, gram negative bacteria, and *C. albicans*.

EXPERIMENTAL

Reagents were commercial grade and were used as supplied. Thin layer chromatography was used to analyze the reaction progress and purity of the synthesized compounds and was carried out on precoated Silica Gel 60F254 sheets using heptan-ethyl acetate 1:1 system and ultraviolet light for visualization. Melting points were determined in open glass capillary method with an electrothermal melting point meter and were uncorrected. IR spectra were obtained in KBr disks on a Nicolet 210 FT-IR spectrometer. The ¹H NMR spectra were recorded at room temperature on a Bruker Avance NMR spectrometer (500 MHz) using TMS as internal standard. The samples were prepared by dissolving the compounds in DMSO-d₆ (δH = 2.51ppm) as solvent and the spectra were recorded using a single excitation pulse of 12 µs. ¹³C NMR spectra were recorded on Bruker spectrometer (125 MHz) in DMSO-d₆. Mass spectra were recorded by Agilent 1100, type SL spectrometer (positive ionization) and with a Varian MAT CH-5 spectrometer (70 eV). Elemental analysis was registered with a Vario El CHNS instrument, results were found to be in good agreement (±0.4%) with the calculated

values. The hydrazides **1a–c** were already published [27], but they were characterized only by elemental analysis and melting points.

2-Aryl-4-methylthiazol-5-carbohydrazides (1a–c) [27]. To a solution of ethyl 2-aryl-2-methylthiazol-5-carboxylates **A–C** (58.7 mmol) in absolute ethanol (100 mL), hydrazine hydrate (5.87 g, 117.4 mmol) was added and the resulting mixture was heated to 100°C for 4 h. The mixture was concentrated under reduced pressure. Water was added to the residue and the resulting solid was filtered, washed with water, and recrystallized from ethanol to give compounds **1a–c**, as white crystals.

4-Methyl-2-phenylthiazol-5-carbohydrazide (1a). Yield 13 g, 55.8 mmol, (95%), mp 168–169°C [27]; IR (KBr): ν 1620 (C N), 1670 (C O) cm^{-1} ; $^1\text{H NMR}$ (DMSO- d_6): δ 2.77 (s, 3H, CH₃), 4.21 (s, 2H, NH₂), 7.46–7.96 (m, 5H, Ar H), 9.72 (s, 1H, NH) ppm; MS: m/z (%) 233 (M⁺, 100). Anal. Calcd. for C₁₁H₁₁N₃OS: C, 56.63; H, 4.75; N, 18.01; S, 13.74. Found: C, 56.59; H, 4.77; N, 17.94; S, 13.67.

4-Methyl-2-p-tolylthiazol-5-carbohydrazide (1b). Yield 13.63g, 55.18 mmol, (94%), mp 186–187°C (Ref. [27] 182–183°C); IR (KBr): ν 1625 (C N), 1675 (C O) cm^{-1} ; $^1\text{H NMR}$ (DMSO- d_6): δ 2.36 (s, 3H, CH₃), 2.59 (s, 3H, CH₃), 4.64 (s, 2H, NH₂), 7.32–7.83 (m, 4H, Ar H), 9.56 (s, 1H, NH) ppm; MS: m/z (%) 247 (M⁺, 100). Anal. Calcd. for C₁₂H₁₃N₃OS: C, 58.28; H, 5.30; N, 16.99; S, 12.97. Found: C, 58.21; H, 5.33; N, 16.92; S, 12.95.

2-(4-Bromophenyl)-4-methylthiazol-5-carbohydrazide (1c). Yield 16.85g, 54 mmol, (92%), mp 218–219°C (Ref. [27] 215–216°C); IR (KBr): ν 1615 (C N), 1677 (C O) cm^{-1} ; $^1\text{H NMR}$ (DMSO- d_6): δ 2.7 (s, 3H, CH₃), 4.13 (s, 2H, NH₂), 7.68–7.73 (m, 4H, Ar H), 9.67 (s, 1H, NH) ppm; MS: m/z (%) 312 (M⁺, 100). Anal. Calcd. for C₁₁H₁₀BrN₃OS: C, 42.32; H, 3.23; N, 13.46; S, 10.27. Found: C, 42.35; H, 3.28; N, 13.41; S, 10.22.

5-(2-Aryl-4-methylthiazol-5-yl)-1,3,4-oxadiazol-2(3H)-thione (2a–c); 5-(pyridin-4-yl)-1,3,4-oxadiazol-2(3H)-thione (2d). To a solution of **1a–d** (10 mmol) in absolute ethanol (100 mL), carbon disulfide (20 mmol) and potassium hydroxide (12.5 mmol) were added and the resulting solution was heated to reflux for 24 h. The reaction mixture was concentrated and the residue was dissolved in water and acidified with diluted hydrochloric acid. The resulting solid was filtered, dried, and recrystallized from ethanol to afford compounds **2a–d** as yellow solids.

5-(4-Methyl-2-phenylthiazol-5-yl)-1,3,4-oxadiazol-2(3H)-thione (2a). Yield 2.13 g, 7.73 mmol, (77.3%), mp 243–244°C; IR (KBr): ν 1155 (C O C), 1271 (C S), 1612 (C N), 3448 (NH) cm^{-1} ; $^1\text{H NMR}$ (DMSO- d_6): δ 2.48 (s, 3H, CH₃), 7.54–8.0 (m, 5H, Ar H), 14.17 (s, 1H, NH) ppm; $^{13}\text{C NMR}$ (DMSO- d_6): δ 17.01 (CH₃), 115.8 (CH), 126.17 (CH), 129.71 (CH), 132.3 (C), 134.7 (C), 144.5 (C), 156.9 (C), 167.5 (C), 169.9 (C S) ppm; MS: m/z (%) 276 (M + 1, 100). Anal. Calcd. for C₁₂H₉N₃OS₂: C, 52.34; H, 3.29; N, 15.26; S, 23.29. Found: C, 52.32; H, 3.26; N, 15.24; S, 23.26.

5-(4-Methyl-2-p-tolylthiazol-5-yl)-1,3,4-oxadiazol-2(3H)-thione (2b). Yield 2.46 g, 8.52 mmol, (85.2%), mp 247–248°C; IR (KBr): ν 1158 (C O C), 1267 (C S), 1596 (C N), 3463 (NH) cm^{-1} ; $^1\text{H NMR}$ (DMSO- d_6): δ 2.37 (s, 3H, CH₃), 2.43 (s, 3H, CH₃), 7.3–7.8 (m, 4H, Ar H), 14.26 (s, 1H, NH) ppm; $^{13}\text{C NMR}$ (DMSO- d_6): δ 16.9 (Th CH₃), 21.38 (Ar CH₃), 117.4 (CH), 126.5 (CH), 129.7 (C), 131.6 (C), 141.5 (C), 144.3 (C), 156.9 (C), 167.5 (C), 172.9 (C S) ppm; MS: m/z (%) 290 (M + 1, 100). Anal. Calcd. for C₁₃H₁₁N₃OS₂: C, 53.96; H, 3.83; N, 14.52; S, 22.16. Found: C, 53.93; H, 3.81; N, 14.49; S, 22.15.

5-(2-(4-Bromophenyl)-4-methylthiazol-5-yl)-1,3,4-oxadiazol-2(3H)-thione (2c). Yield 2.99 g, 8.45 mmol, (84.5%), mp 255–257°C;

IR (KBr): ν 1156 (C O C), 1275 (C S), 1608 (C N), 3452 (NH) cm^{-1} ; $^1\text{H NMR}$ (DMSO- d_6): δ 2.68 (s, 3H, CH₃), 7.73–7.96 (m, 4H, Ar H), 14.93 (s, 1H, NH) ppm; $^{13}\text{C NMR}$ (DMSO- d_6): δ 17.63 (CH₃), 114.3 (C), 125.45 (CH), 128.89 (CH), 131.42 (C), 132.9 (C), 156.2 (C), 156.9 (C), 167.2.5 (C), 183.9 (C S) ppm; MS: m/z (%) 354 (M + 1, 100). Anal. Calcd. for C₁₂H₈BrN₃OS₂: C, 40.69; H, 2.28; N, 11.86; S, 18.1. Found: C, 40.68; H, 2.27; N, 11.83; S, 18.02.

5-(Pyridin-4-yl)-1,3,4-oxadiazol-2(3H)-thione (2d) [29]. Yield 1.46 g, 7.49 mmol, (75%); mp 264–265°C; IR (KBr): ν 1232 (C S), 1352 (C O C), 1616 (C N), 3450 (NH) cm^{-1} ; $^1\text{H NMR}$ (DMSO- d_6): δ 7.63 (dd, 2H, J = 5, 3-Py), 8.76 (dd, 2H, J = 5, 2-Py), 14.73 (s, 1H, NH) ppm; $^{13}\text{C NMR}$ (DMSO- d_6): δ 121.9 (2CH), 139.8 (C), 149.1 (C), 150.1 (2CH), 182.7 (C S) ppm; MS: m/z (%) 179 (M⁺, 20). Anal. Calcd. for C₇H₅N₃OS: C, 46.92; H, 2.81; N, 23.45; S, 17.89. Found: C, 46.78; H, 2.70; N, 23.25; S, 17.76.

Potassium 2-(2-aryl-4-methylthiazol-5-carbonyl)-hydrazinecarbodithioate (3a–c). To a solution of **1a–b** and **1d** (20 mmol) in 40 mL ethanol refrigerated below 10°C, a solution of 1.68 g potassium hydroxide (30 mmol) in 60 mL ethanol and 3.04 g carbon disulfide (30 mmol) were added and the reaction mixture was refrigerated 3 h. The resulting solid was filtered, washed with ether, and dried to afford compounds **3a–c** as yellow–orange solids.

Potassium 2-(4-methyl-2-phenylthiazol-5-carbonyl)-hydrazinecarbodithioate (3a). Yield 4.6 g, 13.3 mmol, (66.5%); IR (KBr): ν 3444, 3228 (2NH), 1647 (C O) cm^{-1} .

Potassium 2-(4-methyl-2-p-tolylthiazol-5-carbonyl)-hydrazinecarbodithioate (3b). Yield 6.6 g, 18.28 mmol, (91.4%); IR (KBr): ν 3443, 3223 (2NH), 1652 (C O) cm^{-1} .

Potassium pyridin-4-carbonyl-hydrazinecarbodithioate (3c). Yield 3.91 g, 15.57 mmol, (78%); IR (KBr): ν 3370, 3309 (2NH), 1675 (C O) cm^{-1} .

5-(2-Aryl-4-methylthiazol-5-yl)-1,3,4-tiadiazol-2(3H)-thione (4a–b); 5-(pyridin-4-yl)-1,3,4-thiadiazol-2(3H)-thione (4c). Potassium hydrazinecarbodithioates **3a–c** (10 mmol) were added portion wise to 98% sulfuric acid (25 mL) and the resulted clear solution was stirred at room temperature for 24 h. The mixture was cautiously added to crushed ice, stirred for 1h, refrigerated for 4 h, and the separated precipitate was filtered, washed with water, and dried and crystallized from ethanol to afford compounds **4a–c**, as yellow solids.

5-(4-Methyl-2-phenylthiazol-5-yl)-1,3,4-tiadiazol-2(3H)-thione (4a). Yield 1.98 g, 6.8 mmol, (68.1%), mp 204–205°C; IR (KBr): ν 1242 (C S), 1541 (C N), 3438 (NH) cm^{-1} ; $^1\text{H NMR}$ (DMSO- d_6): δ 2.6 (s, 3H, CH₃), 7.5–8.1 (m, 5H, Ar H), 14.2 (s, 1H, NH) ppm; $^{13}\text{C NMR}$ (DMSO- d_6): δ 17.2 (CH₃), 120.1 (CH), 126.2 (CH), 128.9 (CH), 133.3 (C), 143.7 (C), 153.6 (C), 156.7 (C), 161.2 (C), 182.9 (C S) ppm; MS: m/z (%) 292 (M + 1, 100). Anal. Calcd. for C₁₂H₉N₃S₃: C, 49.46; H, 3.11; N, 14.42; S, 33.01. Found: C, 49.42; H, 3.10; N, 14.41; S, 33.04.

5-(4-Methyl-2-p-tolylthiazol-5-yl)-1,3,4-tiadiazol-2(3H)-thione (4b). Yield 2.9 g, 5.28 mmol, (52.8%), mp 250–251°C; IR (KBr): ν 1243 (C S), 1558 (C N), 3410 (NH) cm^{-1} ; $^1\text{H NMR}$ (DMSO- d_6): δ 2.44 (s, 3H, CH₃), 2.58 (s, 3H, CH₃), 7.32–7.92 (m, 4H, Ar H), 14.92 (s, 1H, NH) ppm; $^{13}\text{C NMR}$ (DMSO- d_6): δ 17.67 (Th CH₃), 21.55 (Ar CH₃), 120.8 (CH), 126.7 (CH), 126.9 (C), 129.8 (C), 130.3 (C), 141.9 (C), 154.8 (C), 167.8 (C), 183.6 (C S) ppm; MS: m/z (%) 306 (M + 1, 100). Anal. Calcd. for C₁₃H₁₁N₃S₃: C, 51.12; H, 3.63; N, 13.76; S, 31.49. Found: C, 51.13; H, 3.61; N, 13.76; S, 31.50.

5-(Pyridin-4-yl)-1,3,4-thiadiazol-2(3H)-thione (4c). Yield 1.10g, 5.63 mmol (56.5%); mp 280–282°C; IR (KBr): ν 1258 (C S), 1599 (C N), 3400 (NH) cm^{-1} ; ^1H NMR (DMSO- d_6): δ 7.66 (dd, 2H, $J = 5$, 3-Py), 8.78 (dd, 2H, $J = 5$, 2-Py), 14.68 (s, 1H, NH) ppm; ^{13}C NMR (DMSO- d_6): δ 122.1 (2CH), 139.7 (C), 148.8 (C), 150.5 (2CH), 183.1 (C S) ppm; MS: m/z (%) 195 (M^+ , 36). Anal. Calcd. for $\text{C}_7\text{H}_5\text{N}_3\text{S}_2$: C, 43.06; H, 2.58; N, 21.52; S, 32.84. Found: C, 43.19; H, 2.54; N, 21.44; S, 32.64.

4-Alkyl/aryl-1-(2-aryl-4-methylthiazol-5-carbonyl)-thiosemicarbazides (5a–i); 4-alkyl/aryl-1-(pyridin-4-yl-carbonyl)-thiosemicarbazides (5j). To a solution of 4 mmol **1a–d** in 30 mL ethanol, 4 mmol of the appropriate isothiocyanate were added. The resulting mixture was heated under reflux for 3 h. After cooling the precipitate was separated and recrystallized from methanol/acetone to afford thiosemicarbazides **5a–l**.

1-(4-Methyl-2-phenylthiazol-5-carbonyl)-4-phenylthiosemicarbazide (5a). This was obtained as yellow crystal; Yield 1.35 g, 3.68 mmol, (92%), mp 184–185°C; IR (KBr): ν 1231 (C S), 1532 (C N), 1672 (C O), 3115 (NH) cm^{-1} ; ^1H NMR (DMSO- d_6): δ 2.67 (s, 3H, CH_3), 7.16–7.32 (m, 5H, Ar H), 7.95–7.97 (m, 5H, Ar H), 8.3 (s, 1H, NH C S), 9.6 (s, 1H, NH C S), 10.13 (s, 1H, NH C O) ppm; ^{13}C NMR (DMSO- d_6): δ 17.9 (CH_3), 123.1 (2CH), 126.2 (4CH), 129.6 (4CH), 130.3 (C), 131.5 (C), 132.7 (C), 157.8 (C O), 160.7 (C), 167.1 (C), 182.9 (C S) ppm; MS: m/z (%) 369 ($M + 1$, 100). Anal. Calcd. for $\text{C}_{18}\text{H}_{16}\text{N}_4\text{OS}_2$: C, 58.67; H, 4.38; N, 15.21; S, 17.4. Found: C, 58.65; H, 4.36; N, 15.18; S, 17.38.

1-(4-Methyl-2-p-tolylthiazol-5-carbonyl)-4-phenylthiosemicarbazide (5b). This was obtained as yellow solid; Yield 1.4 g, 3.66 mmol, (91%), mp 179–180°C; IR (KBr): ν 1234 (C S), 1534 (C N), 1615 (C O), 3317 (NH) cm^{-1} ; ^1H NMR (DMSO- d_6): δ 2.37 (s, 3H, CH_3), 2.69 (s, 3H, CH_3), 7.24–7.52 (m, 5H, Ar H), 7.35 (d, 2H, $J = 8.5$ Hz, Ar), 7.85 (d, 2H, $J = 8.5$ Hz, Ar), 8.7 (s, 1H, NH C S), 9.8 (s, 1H, NH C S), 10.3 (s, 1H, NH C O) ppm; ^{13}C NMR (DMSO- d_6): δ 17.95 (Th CH_3), 21.5 (Ar CH_3), 126.7 (4CH), 127.2 (CH), 128.5 (4CH), 130.2 (C), 130.4 (C), 139.7 (C), 141.6 (C), 160.4 (C O), 167.1 (C), 182.1 (C S) ppm; MS: m/z (%) 383 ($M + 1$, 100). Anal. Calcd. for $\text{C}_{19}\text{H}_{18}\text{N}_4\text{OS}_2$: C, 59.66; H, 4.74; N, 14.65; S, 16.77. Found: C, 59.63; H, 4.71; N, 14.63; S, 16.78.

1-(2-(4-bromophenyl)-4-methylthiazol-5-carbonyl)-4-phenylthiosemicarbazides (5c). This was obtained as yellow crystal; Yield 1.7 g, 3.8 mmol, (95%), mp 254–256°C; IR (KBr): ν 1214 (C S), 1567 (C N), 1670 (C O), 3300 (NH) cm^{-1} ; ^1H NMR (DMSO- d_6): δ 2.5 (s, 3H, CH_3), 7.17–7.36 (m, 5H, Ar H), 7.74 (d, 2H, $J = 9$ Hz, ar), 7.90 (d, 2H, $J = 8.5$ Hz, ar), 8.3 (s, 1H, NH C S), 9.5 (s, 1H, NH C S), 10.1 (s, 1H, NH C O) ppm; ^{13}C NMR (DMSO- d_6): δ 17.4 (Th CH_3), 124.7 (C), 128.2 (2CH), 129.4 (C), 129.9 (3CH), 130.5 (2CH), 131.2 (2CH), 132.6 (C), 134.3 (C), 156.1 (C), 159.9 (C O), 164 (C), 180.8 (C S) ppm; MS: m/z (%) 448 ($M + 1$, 100). Anal. Calcd. for $\text{C}_{18}\text{H}_{15}\text{BrN}_4\text{OS}_2$: C, 48.33; H, 3.38; N, 12.52; S, 14.33. Found: C, 48.32; H, 3.36; N, 12.49; S, 14.34.

1-(4-Methyl-2-phenylthiazol-5-carbonyl)-4-methylthiosemicarbazide (5d). This was obtained as white solid; Yield 0.95 g, 2.58 mmol, (64.5%), mp 205–207°C; IR (KBr): ν 1265 (C S), 1527 (C N), 1660 (C O), 3113 (NH) cm^{-1} ; ^1H NMR (DMSO- d_6): δ 2.6 (s, 3H, CH_3), 2.8 (d, 3H, $J = 4.5$ Hz, NCH_3), 7.11–7.28 (m, 5H, Ar H), 8.1 (s, 1H, NH C S), 9.7 (s, 1H, NH C S), 10.11 (s, 1H, NH C O) ppm; ^{13}C NMR (DMSO- d_6): δ 17.9 (CH_3), 31.48 (NCH_3), 125.2 (CH), 126.8 (2CH), 129.9 (2CH), 130.7 (C), 131.6 (C), 132.8 (C), 157.9 (C O), 161.6 (C), 167.2 (C), 183.4 (C S) ppm; MS: m/z (%) 307 ($M + 1$, 100). Anal. Calcd. for

$\text{C}_{13}\text{H}_{14}\text{N}_4\text{OS}_2$: C, 50.96; H, 4.61; N, 18.29; S, 20.93. Found: C, 50.92; H, 4.59; N, 18.24; S, 20.90.

1-(4-Methyl-2-p-tolylthiazol-5-carbonyl)-4-methylthiosemicarbazide (5e). This was obtained as white solid; Yield 1.2 g, 3.75 mmol, (64.5%), mp 208–209°C; IR (KBr): ν 1233 (C S), 1540 (C N), 1650 (C O), 3315 (NH) cm^{-1} ; ^1H NMR (DMSO- d_6): δ 2.43 (s, 3H, CH_3), 2.58 (s, 3H, CH_3), 2.9 (d, 3H, $J = 4.5$ Hz, NCH_3), 7.54 (d, 2H, $J = 8.5$ Hz, Ar), 7.97 (d, 2H, $J = 8.5$ Hz, Ar), 8.81 (s, 1H, NH C S), 9.85 (s, 1H, NH C S), 10.31 (s, 1H, NH C O) ppm; ^{13}C NMR (DMSO- d_6): δ 17.7 (Th CH_3), 21.4 (Ar CH_3), 31.24 (NCH_3), 124.5 (2CH), 127.3 (2CH), 131.5 (C), 136.6 (C), 138.8 (C), 159.9 (C O), 161.2 (C), 166.7 (C), 182.1 (C S) ppm; MS: m/z (%) 321 ($M + 1$, 100). Anal. Calcd. for $\text{C}_{14}\text{H}_{16}\text{N}_4\text{OS}_2$: C, 52.48; H, 5.03; N, 17.48; S, 20.01. Found: C, 52.47; H, 5.04; N, 17.45; S, 20.05.

1-(2-(4-Bromophenyl)-4-methylthiazol-5-carbonyl)-4-methylthiosemicarbazides (5f). This was obtained as yellow solid; Yield 1.25 g, 3.25 mmol, (81.2%), mp 220–221°C; IR (KBr): ν 1232 (C S), 1567 (C N), 1658 (C O), 3307 (NH) cm^{-1} ; ^1H NMR (DMSO- d_6): δ 2.43 (s, 3H, CH_3), 2.88 (d, 3H, $J = 4.5$ Hz, NCH_3), 7.48 (d, 2H, $J = 8.5$ Hz, Ar), 7.90 (d, 2H, $J = 8.5$ Hz, Ar), 8.4 (s, 1H, NH C S), 9.5 (s, 1H, NH C S), 10.2 (s, 1H, NH C O) ppm; ^{13}C NMR (DMSO- d_6): δ 17.61 (CH_3), 31.14 (NCH_3), 126.2 (2CH), 129.1 (2CH), 133.4 (C), 138.2 (C), 139.8 (C), 160.1 (C O), 163.4 (C), 168.2 (C), 181.9 (C S) ppm; MS: m/z (%) 386 ($M + 1$, 100). Anal. Calcd. for $\text{C}_{13}\text{H}_{13}\text{BrN}_4\text{OS}_2$: C, 40.52; H, 3.40; N, 14.54; S, 16.64. Found: C, 40.49; H, 3.41; N, 14.52; S, 16.6.

4-Allyl-1-(4-methyl-2-phenylthiazol-5-carbonyl)-thiosemicarbazide (5g). This was obtained as white solid; Yield 1.22 g, 3.68 mmol, (92%), mp 185–188°C; IR (KBr): ν 1235 (C S), 1530 (C N), 1660 (C O), 3302 (NH) cm^{-1} ; ^1H NMR (DMSO- d_6): δ 2.7 (s, 3H, CH_3), 4.11 (m, 2H, CH_2), 5.06 (d, 2H, CH_2), 5.8 (m, 1H, CH), 7.17–7.36 (m, 5H, Ar H), 8.3 (s, 1H, NH C S), 9.4 (s, 1H, NH C S), 10.1 (s, 1H, NH C O) ppm; ^{13}C NMR (DMSO- d_6): δ 17.9 (CH_3), 46.3 (CH_2), 114.9 (CH_2), 125.7 (CH), 126.6 (2CH), 128.4 (CH), 129.4 (2CH), 130.1 (C), 131.9 (C), 132.6 (C), 157.4 (C O), 161.2 (C), 166.9 (C), 181.8 (C S) ppm; MS: m/z (%) 333 ($M + 1$, 100). Anal. Calcd. for $\text{C}_{15}\text{H}_{16}\text{N}_4\text{OS}_2$: C, 54.19; H, 4.85; N, 16.85; S, 19.29. Found: C, 54.16; H, 4.84; N, 16.81; S, 19.27.

4-Allyl-1-(4-methyl-2-p-tolylthiazol-5-carbonyl)-thiosemicarbazide (5h). This was obtained as white solid; Yield 1.06 g, 3.07 mmol, (76.7%), mp 199–200°C; IR (KBr): ν 1226 (C S), 1545 (C N), 1662 (C O), 3125 (NH) cm^{-1} ; ^1H NMR (DMSO- d_6): δ 2.38 (s, 3H, CH_3), 2.69 (s, 3H, CH_3), 4.1 (m, 2H, CH_2), 5.05 (d, 2H, CH_2), 5.82 (m, 1H, CH), 7.41 (d, 2H, $J = 8$ Hz, Ar), 7.89 (d, 2H, $J = 8$ Hz, Ar), 8.4 (s, 1H, NH C S), 9.3 (s, 1H, NH C S), 10.06 (s, 1H, NH C O) ppm; ^{13}C NMR (DMSO- d_6): δ 17.4 (Th CH_3), 21.25 (Ar CH_3), 46.1 (CH_2), 115.2 (CH_2), 124.6 (C), 124.4 (2CH), 128.9 (2CH), 128.7 (CH), 131.2 (C), 132.2 (C), 136.7 (C O), 161.9 (C), 165.9 (C), 181.7 (C S) ppm; MS: m/z (%) 347 ($M + 1$, 100). Anal. Calcd. for $\text{C}_{16}\text{H}_{18}\text{N}_4\text{OS}_2$: C, 55.47; H, 5.24; N, 16.17; S, 18.51. Found: C, 55.44; H, 5.22; N, 16.14; S, 18.46.

4-Allyl-1-(2-(4-bromophenyl)-4-methylthiazol-5-carbonyl)-thiosemicarbazides (5i). This was obtained as yellow solid; Yield 1.35 g, 3.28 mmol, (82%), mp 224–225°C; IR (KBr): ν 1264 (C S), 1558 (C N), 1668 (C O), 3173 (NH) cm^{-1} ; ^1H NMR (DMSO- d_6): δ 2.67 (s, 3H, CH_3), 4.12 (m, 2H, CH_2), 5.12 (d, 2H, CH_2), 5.8 (m, 1H, CH), 7.74 (d, 2H, $J = 9$ Hz, Ar), 7.9 (d, 2H, $J = 9$ Hz, Ar), 8.36 (s, 1H, NH C S), 9.48 (s, 1H, NH C S), 10.19 (s, 1H, NH C O) ppm; ^{13}C NMR (DMSO- d_6): δ 17.89 (CH_3), 46.4 (CH_2), 115.7 (CH_2), 124.2 (C), 124.9 (2CH), 128.3 (2CH), 128.6 (CH), 131.9 (C), 132.9 (C), 135.9

(C O), 161.4 (C), 165.8 (C), 183.9 (C S) ppm; MS: *m/z* (%) 412 (M + 1, 100). Anal. Calcd. for C₁₅H₁₅BrN₄OS₂: C, 43.80; H, 3.68; N, 13.62; S, 15.59. Found: C, 43.81; H, 3.66; N, 13.59; S, 15.55.

4-Phenyl-1-(pyridin-4-yl-carbonyl)-thiosemicarbazide (5j).

This was obtained as white solid; Yield 0.84 g, 3.10 mmol (81%); mp 187–189°C (Ref. [30] 120°C); MS: *m/z* (%) 272 (M⁺, 18). Anal. Calcd. for C₁₃H₁₂N₄OS: C, 57.33; H, 4.44; N, 20.57; S, 11.77. Found: C, 57.44; H, 4.28; N, 20.65; S, 11.35.

4-Methyl-1-(pyridine-4-yl-carbonyl)-thiosemicarbazide (5k).

This was obtained as white solid; Yield 0.68 g, 3.22 mmol (80.5%); mp 265–267°C; IR (KBr): ν 1252(C S), 1553(C N), 1673(C O), 2971, 2975, 3114, 3263(3NH) cm⁻¹; ¹H NMR (DMSO-d₆): δ 2.8 (d, 3H, J = 5 Hz, NCH₃), 7.78 (dd, 2H, J = 5, 3-Py), 8.79 (dd, 2H, J = 5, 2-Py), 8.40 (s, 1H, NH C S), 9.48 (s, 1H, NH C S), 10.57 (s, 1H, NH C O) ppm; ¹³C NMR (DMSO-d₆): δ 32.2 (NCH₃), 121.8 (2CH), 138.6 (C), 148.9 (2CH), 164.7 (C O), 180.9 (C S) ppm; MS: *m/z* (%) 210 (M⁺, 40). Anal. Calcd. for C₈H₁₀N₄OS: C, 45.70; H, 4.79; N, 26.65; S, 15.25. Found: C, 45.94; H, 4.53; N, 26.32; S, 15.10.

4-Allyl-1-(pyridine-4-yl-carbonyl)-thiosemicarbazide (5l).

This was obtained as white solid; Yield 0.80 g, 3.4 mmol (85.8%); mp 210–211°C; IR (cm⁻¹): ν 1229 (C S), 1526 (C N), 1676 (C O), 3219, 3268, 3308 (3NH) cm⁻¹; ¹H NMR (DMSO-d₆): δ 4.11 (d, 2H, CH₂), 5.14 (dd, 2H, CH₂), 5.82 (m, 1H, CH), 7.83 (dd, 2H, J = 5, 3-Py), 8.77 (dd, 2H, J = 5, 2-Py), 8.42 (s, 1H, NH C S), 9.51 (s, 1H, NH C S), 10.69 (s, 1H, NH C O) ppm; ¹³C NMR (DMSO-d₆): δ 46.4 (CH₂), 115.7 (CH₂), 122.1 (2CH), 135.4 (CH), 140.0 (C), 150.6 (2CH), 164.9 (C O), 182.0 (C S) ppm; MS: *m/z* (%) 237 (M + 1, 100). Anal. Calcd. for C₁₀H₁₂N₄OS: C, 50.83; H, 5.12; N, 23.71; S, 13.57. Found: C, 50.99; H, 5.487; N, 23.40; S, 13.31.

4-Alkyl/aryl-3-(2-aryl-4-methylthiazol-5-yl)-1H-1,2,4-triazol-5(4H)-thione (6a–i); 4-alkyl/aryl-3-(pyridin-4-yl)-1H-1,2,4-triazol-5(4H)-thione (6j–l). A solution of corresponding thiosemicarbazide **5a–l** (3.5 mmol) in 20 mL NaOH 2N was refluxed for 2 h. The resulting solution was cooled to room temperature, diluted with water, and acidified to pH 5–6. The precipitate was filtered, washed with water, and recrystallized from ethanol to afford the triazolyl-thiones **6a–l** as white solids.

3-(4-Methyl-2-phenylthiazol-5-yl)-4-phenyl-1H-1,2,4-triazol-5(4H)-thione (6a). Yield 1.18 g, 3.4 mmol, (97%), mp 272–274°C; IR (KBr): ν 1265 (C S), 1531 (C N), 1570 (C N), 3110 (NH) cm⁻¹; ¹H NMR (DMSO-d₆): δ 2.48 (s, 3H, CH₃), 7.44–7.56 (m, 5H, Ar H), 7.6–7.99 (m, 5H, Ar H), 14.1 (s, 1H, NH) ppm; ¹³C NMR (DMSO-d₆): δ 17.04 (CH₃), 115.1 (C), 126.1 (CH), 126.3 (3CH), 129.9 (4CH), 131.2 (2CH), 132.3 (C), 142.5 (C), 144.5 (C), 156.8 (C), 160.7 (C), 165.1 (C), 168.9 (C S) ppm; MS: *m/z* (%) 350 (M⁺, 100). Anal. Calcd. for C₁₈H₁₄N₄S₂: C, 61.69; H, 4.03; N, 15.99; S, 18.30. Found: C, 61.65; H, 4.01; N, 15.94; S, 18.27.

3-(4-Methyl-2-p-tolylthiazol-5-yl)-4-phenyl-1H-1,2,4-triazol-5(4H)-thione (6b). Yield 0.92 g, 2.62 mmol, (75%), mp 267–269°C; IR (KBr): ν 1257 (C S), 1520 (C N), 1538 (C N), 3102 (NH) cm⁻¹; ¹H NMR (DMSO-d₆): δ 2.38 (s, 3H, CH₃), 2.44 (s, 3H, CH₃), 7.45–7.55 (m, 5H, Ar H), 7.34 (d, 2H, J = 8 Hz, Ar), 7.86 (d, 2H, J = 9 Hz, Ar), 14.2 (s, 1H, NH) ppm; ¹³C NMR (DMSO-d₆): δ 16.9 (Th CH₃), 21.5 (Ar CH₃), 117.2 (C), 124.8 (C), 126.2 (2CH), 127.8 (3CH), 128.8 (2CH), 132.1 (2CH), 130.4 (C), 140.1 (C), 142.6 (C), 144.4 (C), 157.1 (C), 170.2 (C S) ppm; MS: *m/z* (%) 364 (M⁺, 100). Anal. Calcd. for C₁₉H₁₆N₄S₂: C, 62.61; H, 4.42; N, 15.37; S, 17.59. Found: C, 62.58; H, 4.41; N, 15.32; S, 17.53.

3-(2-(4-Bromophenyl)-4-methylthiazol-5-yl)-4-phenyl-1H-1,2,4-triazol-5(4H)-thione (6c). Yield 1.39 g, 3.24 mmol, (92.5%), mp 295–296°C; IR (KBr): ν 1268 (C S), 1515 (C N), 1557 (C N), 3172 (NH) cm⁻¹; ¹H NMR (DMSO-d₆): δ 2.45 (s, 3H, CH₃), 7.44–7.56 (m, 5H, Ar H), 7.67 (d, 2H, J = 9 Hz, Ar), 7.7 (d, 2H, J = 9 Hz, Ar), 14.37 (s, 1H, NH) ppm; ¹³C NMR (DMSO-d₆): δ 17.42 (CH₃), 115.9 (C), 124.7 (C), 128.4 (2CH), 129.5 (3CH), 129.9 (2CH), 130.5 (2CH), 131.5 (C), 132.8 (C), 134.0 (C), 144.85 (C), 156.5 (C), 168.72 (C S) ppm; MS: *m/z* (%) 429 (M⁺, 100). Anal. Calcd. for C₁₈H₁₃BrN₄S₂: C, 50.33; H, 3.02; N, 13.01; S, 14.89. Found: C, 50.35; H, 3.05; N, 13.05; S, 14.94.

4-Methyl-3-(4-methyl-2-phenylthiazol-5-yl)-1H-1,2,4-triazol-5(4H)-thione (6d). Yield 0.92 g, 3.19 mmol, (91%), mp 228–229°C; IR (KBr): ν 1280 (C S), 1488 (C N), 1541 (C N), 3070 (NH) cm⁻¹; ¹H NMR (DMSO-d₆): δ 2.48 (s, 3H, CH₃), 3.48 (s, 3H, NCH₃), 7.54–7.99 (m, 5H, Ar H), 14.17 (s, 1H, NH) ppm; ¹³C NMR (DMSO-d₆): δ 17.04 (CH₃), 31.8 (NCH₃), 115.1 (C), 126.8 (CH), 129.9 (2CH), 131.6 (2CH), 132.6 (C), 144.8 (C), 156.3 (C), 167.9 (C), 168.8 (C S) ppm; MS: *m/z* (%) 289 (M + 1, 100). Anal. Calcd. for C₁₃H₁₂N₄S₂: C, 54.14; H, 4.19; N, 19.43; S, 22.24. Found: C, 54.13; H, 4.18; N, 19.39; S, 22.19.

4-Methyl-3-(4-methyl-2-p-tolylthiazol-5-yl)-1H-1,2,4-triazol-5(4H)-thione (6e). Yield 0.84 g, 2.77 mmol, (79%), mp 278–279°C; IR (KBr): ν 1279 (C S), 1522 (C N), 1540 (C N), 3092 (NH) cm⁻¹; ¹H NMR (DMSO-d₆): δ 2.37 (s, 3H, CH₃), 2.69 (s, 3H, CH₃), 3.42 (s, 3H, NCH₃), 7.35 (d, 2H, J = 8 Hz, Ar), 7.86 (d, 2H, J = 9 Hz, Ar), 14.31 (s, 1H, NH) ppm; ¹³C NMR (DMSO-d₆): δ 17.2 (Th CH₃), 21.38 (Ar CH₃), 31.6 (NCH₃), 116.2 (C), 124.7 (C), 126.6 (2CH), 129.7 (2CH), 131.9 (C), 138.6 (C), 144.8 (C), 154.9 (C), 169.7 (C S) ppm; MS: *m/z* (%) = 303 (M + 1, 100). Anal. Calcd. for C₁₄H₁₄N₄S₂: C, 55.6; H, 4.67; N, 18.53; S, 21.21. Found: C, 55.58; H, 4.65; N, 18.49; S, 21.18.

3-(2-(4-Bromophenyl)-4-methylthiazol-5-yl)-4-methyl-1H-1,2,4-triazol-5(4H)-thione (6f). Yield 1.24 g, 3.4 mmol, (97%), mp 283–285°C; IR (KBr): ν 1280 (C S), 1521 (C N), 1541 (C N), 3095 (NH) cm⁻¹; ¹H NMR (DMSO-d₆): δ 2.46 (s, 3H, CH₃), 3.5 (s, 3H, NCH₃), 7.6 (d, 2H, J = 9 Hz, Ar), 7.7 (d, 2H, J = 9 Hz, Ar), 14.37 (s, 1H, NH) ppm; ¹³C NMR (DMSO-d₆): δ 17.4 (Th CH₃), 31.9 (NCH₃), 115.6 (C), 124.9 (C), 128.2 (2CH), 129.4 (2CH), 131.2 (C), 132.9 (C), 144.5 (C), 156.5 (C), 171.4 (C S) ppm; MS: *m/z* (%) 367 (M⁺, 100). Anal. Calcd. for C₁₃H₁₁BrN₄S₂: C, 42.51; H, 3.02; N, 15.25; S, 17.46. Found: C, 42.52; H, 3.02; N, 15.21; S, 17.42.

4-Allyl-3-(4-methyl-2-phenylthiazol-5-yl)-1H-1,2,4-triazol-5(4H)-thione (6g). Yield 1.03 g, 3.3 mmol, (94%), mp 214–216°C; IR (KBr): ν 1267 (C S), 1533 (C N), 1573 (C N), 3099 (NH) cm⁻¹; ¹H NMR (DMSO-d₆): δ 2.48 (s, 3H, CH₃), 4.65 (m, 2H, CH₂), 4.85–5.16 (dd, 2H, CH₂), 5.82 (m, 1H, CH), 7.55–7.99 (m, 5H, Ar H), 14.21 (s, 1H, NH) ppm; ¹³C NMR (DMSO-d₆): δ 17.7 (CH₃), 46.2 (CH₂), 113.7 (CH₂), 115.9 (C), 126.6 (CH), 129.8 (2CH), 130.3 (2CH), 131.7 (CH), 140.2 (C), 144.4 (C), 156.2 (C), 162.9 (C), 170.8 (C S) ppm; MS: *m/z* (%) 314 (M + 1, 100). Anal. Calcd. for C₁₅H₁₄N₄S₂: C, 57.30; H, 4.49; N, 17.82; S, 20.40. Found: C, 57.27; H, 4.47; N, 17.78; S, 20.36.

4-Allyl-3-(4-methyl-2-p-tolylthiazol-5-yl)-1H-1,2,4-triazol-5(4H)-thione (6h). Yield 1.1 g, 3.3 mmol, (94%), mp 185–186°C; IR (KBr): ν 1279 (C S), 1522 (C N), 1540 (C N), 3187 (NH) cm⁻¹; ¹H NMR (DMSO-d₆): δ 2.37 (s, 3H, CH₃), 2.44 (s, 3H, CH₃), 4.66 (m, 2H, CH₂), 4.86–5.17 (dd, 2H, CH₂), 5.87 (m, 1H, CH), 7.34 (d, 2H, J = 8 Hz, Ar), 7.86 (d, 2H, J = 9 Hz, Ar), 14.26 (s, 1H, NH) ppm; ¹³C NMR (DMSO-d₆): δ 16.97 (Th CH₃), 21.48 (Ar CH₃),

46.27 (CH₂), 113.9 (CH₂), 117.7 (C), 126.7 (2CH), 129.9 (2CH), 130.4 (C), 131.89 (CH), 141.6 (C), 144.5 (C), 156.6 (C), 167.9 (C), 168.67 (C S) ppm; MS: *m/z* (%) 329 (M + 1, 100). Anal. Calcd. for C₁₆H₁₆N₄S₂: C, 58.51; H, 4.91; N, 17.06; S, 19.52. Found: C, 58.49; H, 4.90; N, 17.01; S, 19.49.

4-Allyl-3-(2-(4-bromophenyl)-4-methylthiazol-5-yl)-1H-1,2,4-triazol-5(4H)-thione (6i). Yield 1.34 g, 3.4 mmol, (98%), mp 259–260°C; IR (KBr): ν 1286 (C S), 1533 (C N), 1558 (C N), 3108 (NH) cm⁻¹; ¹H NMR (DMSO-d₆): δ 2.7 (s, 3H, CH₃), 4.13 (m, 2H, CH₂), 5.05–5.17 (dd, 2H, CH₂), 5.86 (m, 1H, CH), 7.66 (d, 2H, J = 9 Hz, Ar), 7.71 (d, 2H, J = 9 Hz, Ar), 14.4 (s, 1H, NH) ppm; ¹³C NMR (DMSO-d₆): δ 17.4 (Th CH₃), 46.7 (CH₂), 114 (CH₂), 116.7 (C), 128.9 (2CH), 131.2 (2CH), 131.9 (CH), 133.2 (C), 143.9 (C), 144.9 (C), 156.8 (C), 164.7 (C), 168.7 (C S) ppm; MS: *m/z* (%) 393 (M⁺, 100). Anal. Calcd. for C₁₅H₁₃BrN₄S₂: C, 45.80; H, 3.33; N, 14.24; S, 16.30. Found: C, 45.77; H, 3.32; N, 14.22; S, 16.27.

4-Phenyl-3-(pyridin-4-yl)-1H-1,2,4-triazol-5(4H)-thione (6j). Yield 0.66 g, 2.6 mmol (74.6%); mp 279–280°C (Ref. [30] 122°C); MS: *m/z* (%) = 254 (M⁺, 100). Anal. Calcd. for C₁₃H₁₀N₄S: C, 61.39; H, 3.96; N, 22.03; S, 12.61. Found: C, 61.30; H, 3.65; N, 21.86; S, 12.51.

4-Methyl-3-(pyridin-4-yl)-1H-1,2,4-triazol-5(4H)-thione (6k). Yield 0.50 g, 2.62 mmol, (75%); mp 283–284°C; IR (KBr): ν 1226 (C S), 1571 (C N), 1609 (C N), 3271 (NH) cm⁻¹; ¹H NMR (DMSO-d₆): δ 3.45 (s, 3H, NCH₃), 7.46 (dd, 2H, J = 5 Hz, 3-Py), 8.64 (dd, 2H, J = 5 Hz, 2-Py), 14.16 (s, 1H, NH) ppm; ¹³C NMR (DMSO-d₆): δ 31.64 (NCH₃), 123.1 (2CH), 133.6 (C), 149.5 (C N), 151.2 (2CH), 168.8 (C S) ppm; MS: *m/z* (%) 192 (M⁺, 100). Anal. Calcd. for C₈H₈N₄S: C, 49.98; H, 4.09; N, 29.14; S, 16.68. Found: C, 50.11; H, 3.93; N, 29.48; S, 16.41.

4-Allyl-3-(pyridin-4-yl)-1H-1,2,4-triazol-5(4H)-thione (6l). Yield 0.595 g, 2.73 mmol (78%); mp 210–212°C; IR (KBr): ν 1262 (C S), 1571 (C N), 1614 (C N), 3337 (NH) cm⁻¹; ¹H NMR (DMSO-d₆): δ 4.8 (d, 2H, CH₂), 5.01 (dd, 2H, CH₂), 5.86 (m, 2H, CH), 7.66 (dd, 2H, J = 5 Hz, 3-Py), 8.77 (dd, 2H, J = 5 Hz, 2-Py), 14.26 (s, 1H, NH) ppm; ¹³C NMR (DMSO-d₆): δ 46.7 (CH₂), 117.7 (CH₂), 122.6 (2CH), 130.4 (CH), 133.8 (C), 149.7 (C N), 150.8 (2CH), 168.6 (C S) ppm; MS: *m/z* (%) 218 (M⁺, 25). Anal. Calcd. for C₁₀H₁₀N₄S: C, 55.02; H, 4.62; N, 25.67; S, 14.69. Found: C, 55.05; H, 4.34; N, 25.94; S, 14.47.

Acknowledgments. This work was financially supported by the National University Research Council, Romania (Project PNII-ID No.1348/2008). This support is gratefully acknowledged.

REFERENCES AND NOTES

- [1] Akbas, E.; Berber, I.; Sener, A.; Hasanov, B. *Il Farmaco* 2005, 60, 23.
- [2] Bonde, C. G.; Gaikwad, N. J. *Bioorg Med Chem* 2004, 12, 2151.
- [3] Weidner-Wells, M. A.; Boggs, C. M.; Foleno, B. D.; Melton, J.; Bush, K.; Goldschmidt, R.; Hlasta, D. J. *Bioorg Med Chem* 2002, 10, 2345.
- [4] Castellano, S.; Stefancich, G.; Chillotti, A.; Poni, G. *Il Farmaco* 2003, 58, 568.
- [5] Tsuji, K.; Ishikawa, H. *Bioorg Med Chem Lett* 1994, 4, 1601.
- [6] Wilson, K. J.; Illig, C. R.; Subasinghe, N.; Hoffman, J. B.; Rudolph, M. J.; Soll, R.; Molloy, C.; Bone, R.; Green, D.; Randall, T.; Zhang, M.; Lewandowski, F. A.; Zhou, Z.; Sharp, C.; Maguire, D.; Grasberger, B.; DesJarlais, R. L.; Spurlino, O. *J Bioorg Med Chem Lett* 2001, 11, 915.
- [7] Haviv, F.; Ratajczyk, R. J.; DeNet, R. W.; Kerdesky, F. A.; Walters, R. L.; Schmidt, S. P.; Holms, J. H.; Young, P. R.; Carter, G. W. *J Med Chem* 1988, 31, 1719.
- [8] Patt, W. C.; Hamilton, H. W.; Taylor, M. D.; Ryan, M. J.; Taylor, D. Jr.; Connolly, C. J.; Doherty, A. M.; Klutchko, S. R.; Sircar, I. J. *J Med Chem* 1992, 35, 2562.
- [9] Bell, F. W.; Cantrell, A. S.; Hoegberg, M.; Jaskunas, S. R.; Johansson, N. G.; Jordan, J.; Kinnick, M. D.; Lind, P.; Morin, J. M. Jr. *J Med Chem* 1995, 38, 4929.
- [10] Gu, X. H.; Wan, X. Z.; Jiang, B. *Bioorg Med Chem Lett* 1999, 9, 569.
- [11] Jiang, B.; Gu, X. H. *Bioorg Med Chem* 2000, 8, 363.
- [12] Kumar, Y.; Green, R.; Borysko, K. Z.; Wise, D. S.; Wotring, L. L.; Townsend, L. B. *J Med Chem* 1993, 36, 3843.
- [13] Kumar, Y.; Green, R.; Wise, D. S.; Wotring, L. L.; Townsend, L. B. *J Med Chem* 1993, 36, 3849.
- [14] Medime, E.; Capan, G. *Il Farmaco* 1994, 49, 449.
- [15] Metzger, J. V. *Comprehensive Heterocyclic Chemistry I*; Pergamon: New York, NY, 1984; Vol.6, pp328.
- [16] Amir, M.; Kumar, H.; Javed, S. A. *Eur J Med Chem* 2008, 43, 2056.
- [17] Navidpour, L.; Shafaroodi, H.; Abdi, K.; Amini, M.; Ghahremani, M. H.; Dehpour, A. R.; Shafiee, A. *Bioorg Med Chem* 2006, 14, 2507.
- [18] Tehranchian, S.; Akbarzadeh, T.; Fazeli, M. R.; Jamalifar, H.; Shafiee, A. *Bioorg Med Chem Lett* 2005, 15, 1023.
- [19] Holla, B. S.; Poorjary, N. K.; Rao, S. B.; Shivananda, M. K. *Eur J Med Chem* 2002, 37, 511.
- [20] Shiradkar, M. R.; Murahari, K. K.; Gangadasu, H. R.; Suresh, T.; Kalyan, C. A.; Panchal, D.; Kaur, R.; Burange, P.; Ghogare, O. J. *Bioorg Med Chem* 2007, 42, 3997.
- [21] Joshi, S. D.; Vagdevi, H. M.; Vaidya, V. P.; Gadaginamath, G. S. *Eur J Med Chem* 2008, 43, 1989.
- [22] Cansiz, A.; Koparir, M.; Demirdag, A. *Molecules* 2004, 9, 204.
- [23] Rostom, S. A. F.; Shalaby, M. A.; EL-Demellawy, M. A. *Eur J Med Chem* 2003, 38, 959.
- [24] Oniga, O.; Grosu, I.; Mager, S.; Simiti, I. *Monatsh Chem* 1998, 129, 661.
- [25] Simiti, I.; Oniga, O.; Zaharia, V.; Horm, M. *Die Pharmazie* 1995, 50, 12, 794.
- [26] Zaharia, V.; Ignat, A.; Palibroda, N.; Ngameni, B.; Kuete, V.; Fokunang, K. N.; Mounang, M. L.; Ngadjui, B. T. *Eur J Med Chem* 2010, 45, 5080.
- [27] Simiti, I.; Muresan, A. *Rev Roumaine Chim* 1976, 7, 1078.
- [28] Reeves, D. S.; White, L. O. *Principles of Methods of Assaying Antibiotic in Pharmaceutical Microbiology*, 3rd ed.; Blackwell: Oxford, UK, 1983; p140.
- [29] Bayrak, H.; Demirbas, A.; Demirbas, N.; Karaoglu, S. A. *Eur J Med Chem* 2009, 44, 4362.
- [30] Bayrak, H.; Demirbas, A.; Karaoglu, S. A.; Demirbas, N. *Eur J Med Chem* 2009, 44, 1057.

ISOFLAVONOIDS FROM *GLYCYRRHIZA SP.* AND *ONONIS SPINOSA*

DANIELA BENEDEC^{1*}, LAURIAN VLASE², ILIOARA ONIGA¹, ANCA TOIU¹, MIRCEA TĂMAȘ³, BRÎNDUȘA TIPERCIUC⁴

¹Department of Pharmacognosy, Faculty of Pharmacy, "Iuliu Hațieganu" University of Medicine and Pharmacy, 12 I. Creanga Street, Cluj-Napoca, Romania

²Department of Pharmaceutical Technology and Biopharmaceutics, "Iuliu Hațieganu" University of Medicine and Pharmacy, 12 I. Creanga Street, Cluj-Napoca, Romania

³Department of Pharmaceutical Botany, Faculty of Pharmacy, "Iuliu Hațieganu" University of Medicine and Pharmacy, 12 I. Creanga Street, Cluj-Napoca, Romania

⁴Department of Pharmaceutical Chemistry, Faculty of Pharmacy, "Iuliu Hațieganu" University of Medicine and Pharmacy, Cluj-Napoca, Romania

*corresponding author: dani_67ro@yahoo.com

Abstract

In order to identify new sources of isoflavonoids, an analysis was carried out on three species of the *Fabaceae* family: *Glycyrrhiza glabra* L., *Glycyrrhiza echinata* L., *Ononis spinosa* L., harvested from the Romanian spontaneous flora. The HPLC-MS method was used to investigate the presence of isoflavonoids in the studied plants. In *Glycyrrhiza glabra* the isoflavonic glycosides like daidzin ($0.434 \times 10^{-3}\%$), genistin ($0.672 \times 10^{-3}\%$), ononin ($27.490 \times 10^{-3}\%$), and the aglycon formononetin ($16.607 \times 10^{-3}\%$) were found, while in *Glycyrrhiza echinata*, only formononetin ($0.864 \times 10^{-3}\%$) and ononin ($3.904 \times 10^{-3}\%$) were found. Formononetin was identified in both hydrolyzed solutions. *Ononis spinosa*, the richest species in isoflavonoids, contains daidzin ($0.944 \times 10^{-3}\%$), genistin ($1.173 \times 10^{-3}\%$), ononin ($175.7 \times 10^{-3}\%$), formononetin ($9.499 \times 10^{-3}\%$) and after hydrolysis, daidzein ($0.8196 \times 10^{-3}\%$), formononetin ($113.622 \times 10^{-3}\%$) and ononin ($18.939 \times 10^{-3}\%$) as residual glycosides.

Rezumat

În vederea identificării de noi surse de izoflavonoide, s-au analizat trei specii din familia *Fabaceae*: *Glycyrrhiza glabra* L., *Glycyrrhiza echinata* L., *Ononis spinosa* L., recoltate din flora spontană a României. A fost utilizată metoda HPLC-MS pentru a investiga prezența izoflavonoidelor în plantele studiate. *Glycyrrhiza glabra* conține heterozidele daidzină ($0,434 \times 10^{-3}\%$), genistină ($0,672 \times 10^{-3}\%$) și ononină ($27,490 \times 10^{-3}\%$) și agliconul formononetină, iar în *Glycyrrhiza echinata* au fost identificate numai formononetina ($0,864 \times 10^{-3}\%$) și ononina ($3,904 \times 10^{-3}\%$). În probele hidrolizate a fost identificată formononetina. Specia *Ononis spinosa*, cea mai bogată în aceste principii active, conține daidzină ($0,944 \times 10^{-3}\%$), genisteină ($1,173 \times 10^{-3}\%$), ononină ($175,7 \times 10^{-3}\%$), formononetină ($9,499 \times 10^{-3}\%$); după hidroliză s-au identificat daidzeina ($0,8196 \times 10^{-3}\%$), formononetina ($113,622 \times 10^{-3}\%$) și ononina ($18,939 \times 10^{-3}\%$).

Keywords: *Fabaceae*, isoflavonoids, HPLC-MS

Introduction

Isoflavonoids are plant secondary metabolites that have various biological functions and significant ecological impacts. It is known that they are frequently found in soybeans and other plants from *Fabaceae* family [1,2,12]. Isoflavones are a subgroup of phytoestrogens, natural plant substances with structures similar to 17- β -estradiol and capable of binding to estrogen receptors [2,3,9]. Recently, isoflavones have become of great interest due to several reports on their positive effect on human health, in particular, in the prevention of some forms of hormone-dependent cancers, cardiovascular diseases, osteoporosis, adverse menopausal manifestations and age-related cognitive decline [2,9,12].

Glycyrrhiza glabra L. (licorice) contains not only triterpene saponins (glycyrrhizin), flavonoids, polysaccharides, but also various isoflavonoids: glabrone, glyzaglabrin, glyzarin, formononetin, glycyrrhizaisoflavones; *Glycyrrhiza echinata* was less studied, its aerial parts contain formononetin [1,5,6]. In the roots of *Ononis spinosa* L. (spiny restharrow) the following compounds are present: onocerin, sitosterol, isoflavones (ononin, formononetin, genistein, biochanin A 7-glucoside), as well as small amounts of the essential oil with trans-anethole, carvone and menthol [2,7].

The purpose of this study was to evaluate the isoflavone profile in the roots of some *Fabaceae* species from the Romanian spontaneous flora, by HPLC-MS analysis, in order to obtain new sources of phytoestrogens.

Materials and Methods

The roots of *Glycyrrhiza glabra* L. (voucher No. 579), the roots of *Glycyrrhiza echinata* L. (voucher No. 580) and the roots of *Ononis spinosa* L. (voucher No. 682) were collected in September-October 2009 (Cluj, Romania). Voucher specimens were deposited in the Herbarium of the Department of Pharmaceutical Botany of the Faculty of Pharmacy ("Iuliu Hatieganu" University of Medicine and Pharmacy Cluj-Napoca, Romania). The hydroalcoholic extracts obtained from the roots (5% in 80% methanol, 60°C) were analyzed by HPLC-MS, before and after acid hydrolysis (2M HCl) [4,5,11].

Reagents

Standards: daidzin (daidzein 7-glucoside), genistin (genistein 7-glucoside), ononin (formononetin 7-glucoside), daidzein, glycitein,

genistein, formononetin from Merck (Germany). Methanol and hydrochloric acid used for the HPLC analyses were purchased from Merck (Germany). Methanolic stock solutions (100 g/mL) of the above standards were prepared and stored at 4°C, protected from daylight. They were properly diluted with ultrapurified water in order to obtain the standard concentrations for the calibration curves [4,5,11].

Equipment and Chromatographic Conditions

The experiment was carried out using an Agilent 1100 HPLC system equipped with a degasser, binary pump, autosampler and column thermostat. For the separation of the compounds it was used a reversed-phase Zorbax SB-C18 analytical column (100x3.0 mm i.d., 5 µm). The column thermostat operated at 48°C. The mobile phase used for the separation of isoflavones was a mixture of 0.1% acetic acid (V/V) in water (A) and methanol (B), in linear gradient mode, as follows: until 2 min, 20% B, at 10 min 40% B, at 10.5 min 40% B, at 11.5 min 45% B, hold 45% B until 17 min. The flow rate was 1 mL/min. For detection and quantification, the HPLC system was coupled with an Agilent 1100 Ion Trap SL mass spectrometer, operated with an electrospray (ESI) ion source in negative ion mode. The nebulisation gas used by the mass spectrometer was nitrogen at 65 psi; the dry gas was also nitrogen at a flow rate of 12 L/min and heated at 360°C. The capillary potential was set at +2500 V. The analysis mode of isoflavones was either in single ion monitoring mode (SIM) - for aglycons or in single reaction monitoring mode (SRM) – for glycosides [2, 5, 6, 8, 10,11]. The calibration curves for all isoflavones were built in the range of 40-4000 ng/mL. For fitting the calibration curves, a quadratic model and a 1/y weighing scheme were used. The accuracy of the calibration points, for each compound, was no more than ± 15% [4,5].

Results and Discussion

The retention time of isoflavones and their mass spectrometry detection parameters are presented in Table I. Generally, glycosides' ions lose the sugar group thus we can observe the aglycon ion, so all glycosides can be analyzed by the SRM mode. The aglycons ions were not efficiently fragmented, so for these compounds we applied a SIM mode analysis [4,11].

Table I
The retention time of isoflavones and their mass spectrometry detection parameters

Compounds	Retention time (min)	Detection mode*	Parent m/z ion [M-H] ⁻	Quantified m/z ion
Daidzin	3.7	SRM	415	253
Genistin	5.5	SRM	431	268, 269
Ononin	8.9	SRM	429	267
Daidzein	9.2	SIM	253	253
Glycitein	10.2	SIM	283	283
Genistein	11.0	SIM	269	269
Formononetin	14.4	SIM	267	267

*SRM= single reaction monitoring; SIM = single ion monitoring

The compounds (heterosides and aglycons of isoflavones) identified by HPLC and their levels are presented in Table II.

Table II
Content in isoflavones (mg/100g dry plant)

Isoflavones (standards)	<i>Glycyrrhiza glabra</i>		<i>Glycyrrhiza echinata</i>		<i>Ononis spinosa</i>	
	NH	H	NH	H	NH	H
daidzin	0.434	-	-	-	0.944	-
genistin	0.672	-	-	-	1.173	-
ononin	27.490	7.999	3.904	-	175.72	18.939
daidzein	-	-	-	-	-	0.819
glycitein	-	-	-	-	-	-
genistein	-	-	-	-	-	-
formononetin	16.607	27.856	0.864	5.218	9.499	113.622

NH – non hydrolyzed samples; H – hydrolyzed samples

The roots of *Glycyrrhiza glabra* contain daidzin ($0.434 \times 10^{-3}\%$), genistin ($0.672 \times 10^{-3}\%$), ononin ($27.490 \times 10^{-3}\%$) and formononetin ($16.607 \times 10^{-3}\%$). Only formononetin ($27.856 \times 10^{-3}\%$) and ononin ($7.999 \times 10^{-3}\%$) were identified after hydrolysis. The levels of isoflavones in our samples were smaller than in *Glycyrrhiza glabra* harvested from Syria [5]. Only ononin ($3.904 \times 10^{-3}\%$) and formononetin ($0.864 \times 10^{-3}\%$) were determined in the extract of *Glycyrrhiza echinata* roots. After acid hydrolysis the identified compound was formononetin ($5.218 \times 10^{-3}\%$).

The extract of *Ononis spinosa* roots contains daidzin ($0.944 \times 10^{-3}\%$), genistin ($1.173 \times 10^{-3}\%$), ononin ($175.7 \times 10^{-3}\%$) and formononetin ($9.499 \times 10^{-3}\%$). The hydrolysed solution contains two aglycons, daidzein ($0.819 \times 10^{-3}\%$) and formononetin ($113.622 \times 10^{-3}\%$) and ononin ($18.939 \times 10^{-3}\%$) as residual glycoside. *Ononis spinosa* was the richest species in isoflavonoids and it can be considered an important source of these active principles.

The isoflavonoids can be present in plants like glycosides or more complex combinations like ester-glycosides: acetyl-glycosides or malonyl-glycosides. The presence of ononin in the hydrolysed extracts could be explained by the fact that the acid hydrolysis was capable of cleaving ester bonds (malonyl- and acetyl-7-glycosides), but not sufficient for the quantitative cleavage of glycosidic bonds [8,10]. Increasing of formononetin levels after hydrolysis suggests the presence of its glycosides in the analyzed extracts.

The absence of daidzin and genistin from *Glycyrrhiza echinata* can be used for the differentiation of the two species, to avoid the substitution of *Glycyrrhiza glabra* with *Glycyrrhiza echinata*.

Conclusions

The extract of *Glycyrrhiza glabra* roots contain daidzin, genistin, ononin and formononetin, while the extract of *Glycyrrhiza echinata* roots contain small quantities of formononetin and ononin; that is why we cannot use both the roots of *Glycyrrhiza glabra* and *Glycyrrhiza echinata* as being the same therapeutical product.

The roots of *Ononis spinosa*, richer in isoflavonoids (daidzin, genistin, ononin, formononetin), represent an important natural source for oestrogenic therapy.

Ononin was the most abundant isoflavone glycoside and it was found in all samples; its aglycon, formononetin was present in all extracts, before and after hydrolysis.

Our results confirm the presence of isoflavones in the plants of *Fabaceae* family, compounds that belong to a class of substances known as non-steroidal phytoestrogens.

References

1. Ammsov AS., Litvinenko VI. Phenolic compounds of the genera *Glycyrrhiza* L. and *Meristotopis* Fisch. et Mey. *Pharmaceutical Chemistry Journal* 2007, 41(7), 3,72-395
2. Bruneton J. Pharmacognosie. Phytochimie. Plantes medicinales, 3e edition, Edition TEC et DOC, Paris, 1999, 347-35

3. Dragomirescu A., Antal D., Deheleanu C. Fitoestrogenii. Rolul izoflavonelor, *Farmacia*, 2003, 51(6), 15-24
4. Hanganu D., Vlase L., Olah N. LC/MS analysis of isoflavones from *Fabaceae* species extracts. *Farmacia*, 2010, 58(2), 177-183
5. Khalaf I., Vlase L., Lazăr D., Corciovă A., Ivănescu B., Lazăr MI. HPLC-MS study of phytoestrogens from *Glycyrrhiza glabra*. *Farmacia*, 2010, 58(1), 89-93
6. Khalaf I., Vlase L., Lazăr D., Corciovă A., Ivănescu B., Lazăr MI. HPLC-UV-MS study of polyphenols from *Glycyrrhiza glabra*. *Farmacia*, 2010, 58(4), 416-420
7. Klejdus B., Vacek J., Lojková L., Benesová L., Kubán V. Ultrahigh-pressure liquid chromatography of isoflavones and phenolic acids on different stationary phases. *J Chromatogr A*. 2008; 1195(1-2):52-9.
8. Penalvo JL., Nurmi T., Adlercreutz H. A simplified HPLC method for total isoflavones in soy product. *Food Chem*. 2004, 87 (2), 297-305
9. Ryu Y., Won B., Park H., Ghafoor K., Park J. Effects of the β -glycosidase reaction on bio-conversion of isoflavones and quality during tofu processing, *Journal of the Science of Food and Agriculture*, 2010, 90(5), 843-849
10. Schwartz H., Sontag G. Comparison of sample preparation methods for analysis of isoflavones in foodstuffs, *Analytica Chimica Acta*, 2009, 633(2), 204-215
11. Olah NK, Hanganu D., Vlase L., Cobzac C. The study of polyphenols from *Trifolium pretense* L. and *Medicago sativa* L. Hydroalcoholic extracts by HPLC-UV-MS, *Studia Universitatis Babeş-Bolyai-Chemia*, 2010, 45(2), 353-362
12. x x x Phytochemical Dictionary of the Leguminosae ILDIS (International Legume Database and Information Service), vol 1, Plants and their Constituents, Ed. Chapman & Hall, London, 1994, 327-328.

Manuscript received: October 2nd 2010

7. J.A. DiMasi, R.W. Hansen, H.G. Grabowski, The price of innovation: new estimates of drug development costs, *J. Health Econ.*, **2003**, *22*, 151-185.
8. P.M. Dean, Molecular Similarity in Drug Design, *Blackie Academic*, London, **1995**
9. P. Willet, Similarity and Clustering in Chemical Information Systems, *Research Studies Press Ltd*: Letchworth, U.K., **1987**.
10. J.M. Barnard, G.M. Downs, Clustering of Chemical Structures on the Basis of Two-Dimensional Similarity Measures, *J. Chem. Inf. Comput. Sci.*, **1992**, *32*, 644-649
11. D.J. Wild, C.J. Blankey, Comparison of 2D Fingerprints Types and Hierarchy Level Selection Methods for Structural Grouping Using Ward's Clustering, *J. Chem. Inf. Comput. Sci.*, **2000**, *40*, 155-162.
12. R.D. Brown, Y.C. Martin, Use of Structure-Activity Data To Compare Structure-Based Clustering Methods and Descriptors for Use in Compound Selection, *J. Chem. Inf. Comput. Sci.*, **1996**, *36*, 572-584.
13. M.A. Johnson, G.M. Maggiora, Eds., Concepts and Applications of Molecular Similarity, *John Wiley & Sons*, New York, **1990**.
14. P. Willett, Chemical Similarity Searching, *J. Chem. Inf. Comput. Sci.*, **1998**, *38*, 983-996.
15. N. Nikolova, J. Jaworska, Approaches to measure chemical similarity – a review. *QSAR & Combin. Sci.*, **2004**, *22*, 1006-1026.
16. Dragon Professional version 5.4, **2006** (http://www.taletе.mi.it/dragon_exp.htm).
17. StatSoft, Inc. STATISTICA (data analysis software system), version 6, **2001** (www.statsoft.com).
18. G. Katona and M. V. Diudea, CLUJSIMIL software, "Babes-Bolyai" University, 2001, Cluj, Romania.

A QSAR Study on Antimicrobial Activity of Some New Sulfonylhydrazinothiazoles

Brindusa Tiperciuc,^a V. Zaharia,^a R. Campean,^a Manuela Curticean,^b
Adina Costescu^c and M. V. Diudea^c

^aUniversity of Medicine and Pharmacy "Iuliu Hatieganu" Cluj-Napoca, Romania

^bUniversity of Medicine and Pharmacy Tg-Mures, Romania

^c"Babes-Bolyai" University, Faculty of Chemistry and Chemical Engineering,

Cluj, 400028, Romania

(Received May 12, 2008)

Abstracts

A quantitative structure-activity relationship QSAR study on antimicrobial activity of a series of newly synthesized sulfonylhydrazinothiazoles was performed by using the Free-Wilson and auto-correlating partial charges approaches. Several models were developed using stepwise multiple linear regression analysis and the results were further validated by leave-one-out method. They showed the most important contributors at the antimicrobial activity of sulfonylhydrazinothiazoles are the substituents on 4 and 5 position at the thiazole ring. Also, the main feature describing the activity of these compounds is a partial charge-based descriptor, a measure of the molecular electronic properties, used within an auto-correlation weighting scheme.

Introduction

Thiazole nucleus is known to be present in various molecules having a biological activity. They display antitumor, anti-inflammatory, antifungal and antibacterial activity against both Gram-positive and Gram-negative bacteria [1-3]. Compounds having sulfonylhydrazine moiety are also known to possess a wide range of biological and pharmacological activity: antimicrobial [4-5], antitumor [5-7], analgesic [8], anti-inflammatory, antipyretic [4]. Also thiosemicarbazides and hydrazinethiazoles with IMAO activity [9] and arylidenehydrazinethiazoles with antimicrobial and anti-inflammatory potential [10], have been reported.

Motivated by these facts and in pursuing our research in the field of synthesis and antimicrobial evaluation of heterocyclic compounds with thiazolic nucleus, we aimed to develop a QSAR model and to explain the antibacterial and antifungal activity of some newly synthesized benzensulfonylhydrazinethiazoles, for which antimicrobial activity has been evaluated experimentally [11].

To obtain additional information on structural requirements necessary for antimicrobial activity, we performed both a Free-Wilson and auto-correlating partial charges approaches on a set of 14 compounds [12, 13]. The data set includes substances with variations on the position 4 and 5 of the thiazolic ring and the hydrazine moiety.

Materials and Methods

The in vitro minimum inhibitory concentration (MIC) in $\mu\text{M/ml}$ required for inhibiting the growth of *Bacillus subtilis*, *Citrobacter*, *Escherichia coli* and *Candida albicans* was the property studied [11]. The $\log(1/\text{MIC})$ is being used as biological response, for QSAR analysis (Table 2).

The QSAR analysis consists of the following steps: (i) structure optimization by using semiempirical method PM3; (ii) calculation of molecular descriptors; (iii) correlation analysis by step-forward selection of descriptors; (iv) evaluation of the significance level of the model; (v) validation of the model (leave-one-out *loo* cross-validation procedure); (vi) interpretation of the model.

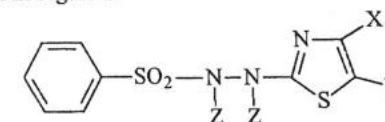
Most of the applications of molecular descriptors have been dedicated to studies because of the great importance for biology of the structure-activity relationship. The computation of such descriptors is accessible by using available software products. The complete set of molecular descriptors described in this study (some of them will be described below), was calculated by Dragon program package [16].

The structures were optimized by using the semiempirical PM3 Hamiltonian, available in HyperChem.

In order to build the regression models, we tried to fit a linear function, which was estimated by the squared correlation coefficient (R^2), the standard error of estimate, the Fischer ratio (F), chance statistics lower than 0.01 ($p < 0.01$) and the coefficient of variation ($CV\%$). The predicting ability of each model was estimated by the cross-validated squared correlation coefficient (R_{cv}^2), calculated by LOO method [14].

Free-Wilson Analysis

The chemical structure of all compounds studied and the descriptors for the Free-Wilson analysis are given in Figure 1.



X: X₁-X₃, Y: Y₁-X₄ Z: Z₁-Z₂

	X		Y		Z	
X ₁	CH ₃	Y ₁	H	Z ₁	H	H
X ₂	CH ₂ Cl	Y ₂	COCH ₃	Z ₂		CC
X ₃	C ₆ H ₅ Cl	Y ₃	COOC ₂ H ₅			
		Y ₄	Br			

Figure 1. General structure of 2-(2-benzensulfonyl-1,2-di-Z-hydrazino)-4X,5Y-thiazole antimicrobials considered.

Free and Wilson's model is based on the assumption that each substituent makes an additive and constant contribution to the biological activity regardless of its position in the rest of molecule. The values of individual contributions are calculated by regression analysis and the constant term obtained, is a theoretically predicted activity value of the unsubstituted compound (all R = H) [12].

The code for each compound and the matrix used in the Free-Wilson analysis are given in Table 1.

Table 1. The codes for S1-S14 compounds and the Free-Wilson matrix

Comp	Code	X			Y				Z	
		X ₁	X ₂	X ₃	Y ₁	Y ₂	Y ₃	Y ₄	Z ₁	Z ₂
S1	X ₁ Y ₁ Z ₁	1			1				1	
S2	X ₂ Y ₁ Z ₁		1		1				1	
S3	X ₃ Y ₁ Z ₁			1	1				1	
S4	X ₁ Y ₂ Z ₁	1				1			1	
S5	X ₁ Y ₃ Z ₁	1					1		1	
S6	X ₁ Y ₁ Z ₂	1			1					1
S7	X ₂ Y ₁ Z ₂		1		1					1
S8	X ₃ Y ₁ Z ₂			1	1					1
S9	X ₁ Y ₂ Z ₂	1				1				1
S10	X ₁ Y ₃ Z ₂	1					1			1
S11	X ₁ Y ₄ Z ₁	1						1	1	
S12	X ₃ Y ₄ Z ₁			1				1	1	
S13	X ₁ Y ₄ Z ₂	1						1		1
S14	X ₃ Y ₄ Z ₂			1				1		1

The matrix was solved by multiple linear regression analysis, using the Excel software package. The 95% confidence interval is given for each regression coefficient.

The correlation was sought between inhibitory activity and various substituent at position 4 (X₁₋₃) and 5 (Y₁₋₄) of the thiazolic ring and for the acetyl group on the hydrazinic moiety (Z₁₋₂).

Leave-one-out analysis was performed, in view of testing the predicting ability of the regression equation. The question of outliers was addressed for points which do not fall within a specified error limits (standard residual >2×s). These compounds were not included in the further analysis. With these outliers removed, we observed an improvement in correlation with the same descriptors.

Auto-correlating Partial Charges Analysis

A QSAR method is based on the comparison of a measured and calculated molecular activity and then relating a few of the most informative structural descriptors to the target bioactivity. The quantitative structure-activity relationships constructed this way provide a means of investigating and predicting antimicrobial activities.

The subset of electronic parameters includes molecular descriptors on partial charges.

Within TOPOCLUJ program, the partial charges Ch_i are calculated as follows [17]:

$$Ch_{i,j} = \log(S_j/S_i)^{1/d_{ij}^2}$$

$$Ch_i = \sum_j ch_{i,j}$$

In the above relations, S_i , S_j represent the Sanderson group electronegativity calculated for the hydride groups (*i.e.*, the heavy atoms with their surrounding hydrogens) in the molecule and d_{ij} is the Euclidean distance separating atoms i and j in a mini energy optimized chemical structure (HyperChem). For other topological partial charge calculations see refs. [18, 19]. Any sulfonylhydrazinethiazole compound can be describe these partial charges which characterize both the substituted/unsubstituted aromatic position and the heteroatom (nitrogen).

The partial charges are calculated for the positions marked by black points in Figure 2.

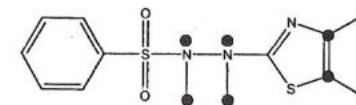


Figure 2. Partial charges selected for general structure of 2-(2-benzensulfonyl-1,2-dihydrazino)-4X,5Y-thiazole.

On this ground, a flexible global descriptor (CD), can be defined as an add function of correlation weights of the partial charges corresponding to each atom i :

$$CD_i = \sum_j c_j \cdot Ch_{i,j}$$

where c_j represents the regression coefficient (*i.e.*, the correlation weight) as given by multivariate regression $\log(A_{i,exp}) = f(Ch_i)$ (see Table 2). These "ad-hoc" weightings depend on the set of molecules in work as well as on the considered molecular (or local) property.

The *Dragon 5.4* software was used to calculate a total of 1600 molecular descriptors for each of the studied compounds. The descriptors chosen for the analysis are either *getaway* descriptors; 2) *whim* descriptors and 3) *2D autocorrelation* indices.

Getaway descriptors [16] are based on a leverage matrix similar to the defined statistics and usually used for regression diagnostics. These molecular descriptors try to model 3D-molecular geometry provided by the molecular influence matrix and the atom related

by molecular topology, with chemical information by using various atomic weights (atomic mass, polarizability, van der Waals volume and electronegativity, etc.).

The two descriptors which belong to this group are: R8m (R autocorrelation of lag 8/weighted by atomic masses) and ISH (standardized information content on the leverage equality).

WHIM [16] descriptors are 3-D descriptors based on the calculation of principal component axes calculated from a weighted covariance matrix obtained by the molecular geometric coordinates. Six different weighting schemes are used for the weighted covariance matrix: u (unweighted), m (atomic mass), p (atomic polarizability), v (van der Waals volume), e (atomic electronegativity) and s (atomic electrotopological state). They contain chemical information concerning: size, symmetry, shape and distribution of the molecule atoms.

WHIM descriptors used in our study are: G1e (1st component symmetry directional WHIM index/weighted by atomic Sanderson electronegativities), E2s (2nd component accessibility directional WHIM index/weighted by atomic electrotopological state) and E1m (1st component accessibility directional WHIM index/weighted by atomic masses).

The next group of descriptors is based on 2-D autocorrelation [16] functions applied to a molecular graph, which is a 2-dimensional structural representation of a molecule. This class of descriptors expresses a correlation between numerical values of the graph entries, which can be statistically weighted using various atomic properties, at intervals equal to the given lag value.

From this class of descriptors, the following indices gave good results: ATS8e (Broto-Moreau autocorrelation of a topological structure-lag 8/weighted by atomic Sanderson electronegativities) and GATS4m (Geary autocorrelation-lag 4/weighted by atomic masses).

Results and discussions

Free-Wilson Analysis

The Free-Wilson equations obtained describes the pharmacological activity of the compounds in a pretty good way ($R^2=0.626-0.831$). Table 2 presents the observed and calculated values of $\log(1/MIC)$ by the best obtained models.

The best model of antibacterial activity in *Bacillus subtilis*, with the coefficient of correlation $R=0.886$, is that given in eq 4 (see also Table 2). The data contain no outliers.

$$\text{Log}(1/MIC) = 1.35 - 0.091 \times X1 + 0.11 \times X2 - 0.375 \times Y1 - 0.162 \times Y2 - 0.277 \times Y3 - 0.358 \times Z1 \quad (4)$$

$n=14, R=0.886, R^2=0.785; s=0.174, F=4.274, R^2_{cv}=0.507$

Table 2. Observed and calculated $\log(1/MIC)$ and the squared correlation coefficient R^2 for *Bacillus subtilis*, *Citrobacter*, *Escherichia coli* and *Candida albicans*.

No.	Bacillus subtilis (log(1/MIC))		Citrobacter (log(1/MIC))			Escherichia coli (log(1/MIC))		Candida albicans (log(1/MIC))			
	Obs.	CalcEq 4	Obs.	Calc.	Calc. Eq 5	Obs.	Calc. Eq 6	Obs.	Calc.	Calc. Eq 7	
S1	0.652	0.526	0.652	0.682	0.632	1.430	1.380	1.731	1.79	1.622	
S2	0.703	0.727	0.703	0.871	0.937	1.481	1.581	1.481	1.728	1.560	
S3	0.742	0.616	0.742	0.447	0.629	1.520	1.621	1.821	1.955	1.788	
S4	0.715	0.737	1.016	1.032	1.098	1.493	1.644	2.396	1.388	-	
S5	0.755	0.623	1.357	1.068	1.134	1.533	1.085	2.436	2.376	2.208	
S6	0.77	0.884	0.770	1.054	0.873	1.548	1.781	1.849	2.005	2.173	
S7	1.111	1.086	1.412	1.244	1.178	1.889	1.983	2.19	1.944	2.111	
S8	0.84	0.975	0.840	0.820	0.870	1.919	2.023	2.521	2.171	2.339	
S9	1.12	1.096	1.421	1.404	1.339	2.199	2.046	0.597	1.604	-	
S10	0.850	0.982	1.151	1.440	1.374	1.628	1.487	2.532	2.592	2.760	
S11	0.723	0.901	1.325	1.183	1.364	1.501	1.506	1.501	1.788	1.620	
S12	0.835	0.991	0.437	0.948	-	1.613	1.747	1.613	1.954	1.786	
S13	1.427	1.259	1.728	1.555	1.605	1.904	1.908	2.506	2.004	2.172	
S14	1.518	1.350	1.518	1.321	1.602	2.296	2.149	2.296	2.17	2.338	
	$R^2=0.785$ $n=14$ no outliers		$R^2=0.626$ $n=14$			$R^2=0.825$ $n=13$ outlier: S12	$R^2=0.831$ $n=14$ no outliers		$R^2=0.306$ $n=14$		$R^2=0.776$ $n=12$ outliers: S4 and S9

In case of antibacterial activity on *Citrobacter*, for all data ($n = 14$), correlation explains about 62% of the variance in inhibitory activity (Table 2). S12 is an outlier and with this outlier removed, an improvement in correlation with the same descriptors (82.5%, eq 5) was observed.

$$\text{Log}(1/MIC) = 1.601 + 0.003 \times X1 + 0.308 \times X2 - 0.731 \times Y1 - 0.266 \times Y2 - 0.230 \times Y3 - 0.240 \times Z1 \quad (5)$$

$n=13, R=0.908, R^2=0.825; s=0.19, F=6.60, r^2_{cv}=0.752$

For *Escherichia coli*, correlation ($R=0.912$) is given in eq 6, which explains about 83% of the variance in inhibitory activity (see also Table 2). The data contain no outliers.

$$\text{Log}(1/MIC) = 2.149 - 0.241250 \times X1 - 0.039 \times X2 - 0.224 \times Y1 + 0.138 \times Y2 - 0.127 \times Y3 - 0.401 \times Z1 \quad (6)$$

$n=14, R=0.912, R^2=0.831, s=0.157, F=5.75, R^2_{cv}=0.753$

Finally, the statistically low correlation, with $R^2 = 0.306$, was considered a poor model for antifungal activity in *Candida albicans* (Table 2). After the elimination of two outliers, compounds: S4 and S9, which are not properly predicted by the model, the squared correlation coefficient increased at $R^2 = 0.776$ (eq 7).

$$\text{Log}(1/\text{MIC}) = 2.337 - 0.166 \times X1 - 0.228 \times X2 + 0.001 \times Y1 + 0.588 \times Y3 - 0.551 \times Z1 \quad (7)$$

n=12, R=0.881, R²=0.776, s=0.26, F=4.165, R²_{cv}=0.71

The descriptors which take into account the presence or the absence of the substituents in the selected positions are more significant in case of Citrobacter and Escherichia coli (82.5% and 83.1% respectively). Predicting abilities for Bacillus subtilis and Candida albicans are satisfactory (78.5% and 77.6%, respectively - Table 2)

Auto-correlating Partial Charges Analysis

The regression analysis was used to determine which of the available molecular descriptors were most relevant in modeling of some sulfonylhydrazinotiazoles antimicrobial activities. Several descriptors were selected in this respect. Definitely, the electronic descriptor (CD) is the best predictor in a monivariate regression (Table 3). All-together, this approach is superior to the Free-Wilson analysis, as can be seen from the results given below.

Table 3. Observed and calculated log(1/MIC), squared correlation coefficient R² and CV% in monivariate regression, for Bacillus subtilis, Citrobacter, Escherichia coli and Candida albicans.

No.	Bacillus subtilis (log(1/MIC))		Citrobacter (log(1/MIC))		Escherichia coli (log(1/MIC))		Candida albicans (log(1/MIC))	
	obs.	calc.=f(CD)	obs.	calc.=f(CD)	obs.	calc.=f(CD)	obs.	calc.=f(CD)
1	0.652	0.671	0.652	0.405	1.430	1.457	1.731	1.714
2	0.703	0.505	0.703	0.669	1.481	1.370	1.481	1.377
3	0.742	0.724	0.742	0.760	1.520	1.523	1.821	1.813
4	0.715	0.820	1.016	1.267	1.493	1.482	2.396	2.331
5	0.755	0.699	1.357	1.165	1.533	1.567	2.436	2.492
6	0.770	1.055	0.770	1.195	1.548	1.862	1.849	2.138
7	1.111	0.966	1.412	1.223	1.889	1.727	2.190	2.287
8	0.840	1.016	0.840	0.915	1.919	1.961	2.521	2.249
9	1.120	1.115	1.421	1.408	2.199	2.196	0.597	0.603
10	0.850	0.868	1.151	1.184	1.628	1.632	2.532	2.522
11	0.723	0.865	1.325	1.263	1.501	1.535	1.501	1.473
12	0.835	0.840	0.437	0.700	1.613	1.638	1.613	1.782
13	1.427	1.344	1.728	1.627	1.904	1.938	2.506	2.360
14	1.518	1.274	1.518	1.291	2.296	2.067	2.296	2.329
		R ² = 0.723		R ² = 0.738		R ² = 0.81		R ² = 0.94
		CV% = 12.23		CV% = 17.9		CV% = 4.28		CV% = 4.66

Bacillus subtilis

First molecule (S1) seems to be outlier and it was excluded from the analysis.

Bivariate regression

$$\text{Log}(1/\text{MIC}) = -0.240 + 0.675 \times \text{CD} + 1.573 \times \text{R8m}$$

n=13; R²=0.908; s=0.10; F=49.51; p=6.49E-06

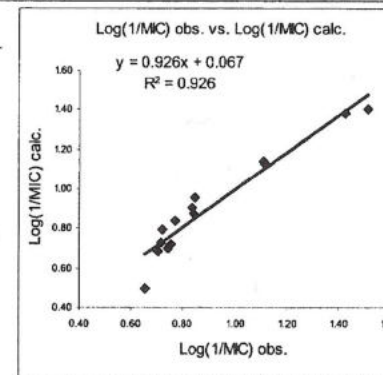
Trivariate regression

$$\text{Log}(1/\text{MIC}) = 0.722 + 0.629 \times \text{CD} + 1.615 \times \text{R8m} - 5.471 \times \text{G1e}$$

n=13; R²=0.962; s=0.06; F=77.0; p=1E-06; R²_{cv}=0.934

Table 4. Observed and calculated log(1/MIC), CV% in trivariate regression for Bacillus subtilis

	Bacillus subtilis (log(1/MIC))			CV%
	Obs	Calc.	Rez.	
S2	0.703	0.682	0.021	2.987
S3	0.742	0.701	0.041	5.530
S4	0.715	0.733	-0.018	2.497
S5	0.755	0.726	0.029	3.903
S6	0.770	0.842	-0.072	9.298
S7	1.111	1.140	-0.029	2.608
S8	0.840	0.879	-0.039	4.658
S9	1.120	1.127	-0.007	0.646
S10	0.850	0.957	-0.107	12.639
S11	0.723	0.793	-0.070	9.726
S12	0.835	0.906	-0.071	8.474
S13	1.427	1.377	0.050	3.471
S14	1.518	1.403	0.115	7.563
				7.010*



*CV% average

Citrobacter

Bivariate regression

$$\text{Log}(1/\text{MIC}) = 0.470 + 0.960 \times \text{CD} - 0.531 \times \text{GATS4m}$$

n=14; R²=0.824; s=0.17; F=25.84; p=7E-05;

Trivariate regression

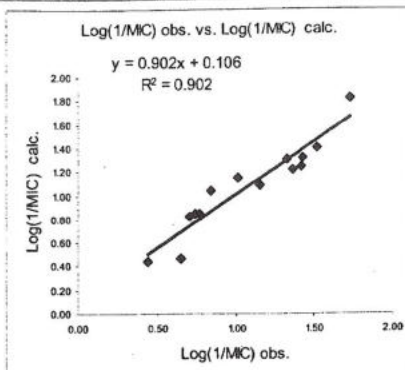
$$\text{Log}(1/\text{MIC}) = -0.007 + 0.832 \times \text{CD} - 0.983 \times \text{GATS4m} + 0.333 \times \text{ATS8e}$$

n=14; R²=0.901; s=0.13; F=30.58; p=24E-06; R²_{cv}=0.80

GATS4m and ATS8e belong to the 2D autocorrelation group of descriptors. It seems that partial charges descriptor (CD) associated with this type of indices (eq 10 and eq 11) show good correlations for Citrobacter antimicrobial activity.

Table 5. Observed and calculated log(1/MIC), CV% in trivariate regression for Citrobacter

	Citrobacter (log(1/MIC))			CV%
	Obs	Calc	Rez	
S1	0.652	0.471	0.181	27.698
S2	0.703	0.821	-0.118	16.768
S3	0.742	0.841	-0.099	13.407
S4	1.016	1.150	-0.134	13.238
S5	1.357	1.223	0.134	9.876
S6	0.770	0.847	-0.077	9.998
S7	1.412	1.253	0.159	11.230
S8	0.840	1.038	-0.198	23.537
S9	1.421	1.329	0.092	6.489
S10	1.151	1.094	0.057	4.987
S11	1.325	1.317	0.008	0.582
S12	0.437	0.447	-0.010	2.205
S13	1.728	1.828	-0.100	5.771
S14	1.518	1.413	0.105	6.945
				10.909*



*CV% average

Escherichia coli

Bivariate regression

$\text{Log}(1/\text{MIC}) = 0.034 + 0.785 \times \text{CD} + 1.008 \times \text{R8m}$ (12)

$n = 14; R^2 = 0.92; s = 0.08; F = 61.86; 1E-06;$

Trivariate regression

$\text{Log}(1/\text{MIC}) = -0.011 + 0.894 \times \text{CD} + 0.950 \times \text{R8m} - 0.349 \times \text{E2s}$ (13)

$n = 14; R^2 = 0.951; s = 0.07; F = 64.81; p = 1E-06; R^2_{cv} = 0.87$

Calculated values and residuals together with the coefficient of variance (CV%) for eq 13 are presented in Table 6.

Candida albicans

Bivariate regression

$\text{Log}(1/\text{MIC}) = 2.23 + 0.97 \times \text{CD} - 2.46 \times \text{ISH}$ (14)

$n = 14; R^2 = 0.975; s = 0.09; F = 216.41; p = 1.4E-09;$

Trivariate regression

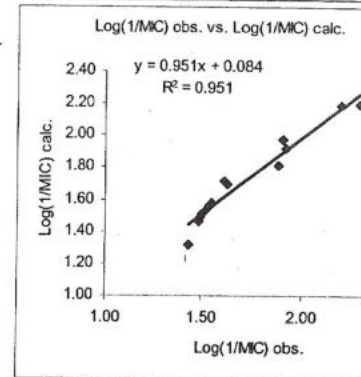
$\text{Log}(1/\text{MIC}) = 2.061 + 0.989 \times \text{CD} - 2.441 \times \text{ISH} + 0.261 \times \text{E1m}$ (15)

$n = 14; R^2 = 0.985; s = 0.07; F = 226.06; p = 1.7E-09; R^2_{cv} = 0.972$

Calculated values and residuals together with CV% for eq 15 are given in Table 7.

Table 6. Observed and calculated log(1/MIC), CV% in trivariate regression for Esche coli

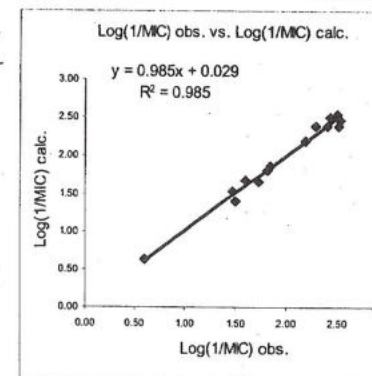
	Escherichia coli (log(1/MIC))			CV%
	Obs	Calc	Rez	
S1	1.430	1.317	0.113	7.901
S2	1.481	1.463	0.018	1.215
S3	1.520	1.534	-0.014	0.944
S4	1.493	1.486	0.007	0.485
S5	1.533	1.558	-0.025	1.610
S6	1.548	1.579	-0.031	1.994
S7	1.889	1.810	0.079	4.192
S8	1.919	1.923	-0.004	0.231
S9	2.199	2.196	0.003	0.148
S10	1.628	1.693	-0.065	3.979
S11	1.501	1.508	-0.007	0.459
S12	1.613	1.717	-0.104	6.478
S13	1.904	1.971	-0.067	3.520
S14	2.296	2.199	0.097	4.219
				2.670*



*CV% average

Table 7. Observed and calculated log(1/MIC), CV% in trivariate regression for Ca albicans

	Candida albicans (log(1/MIC))			CV%
	Obs	Calc	Rez	
S1	1.731	1.667	0.064	3.679
S2	1.481	1.521	-0.040	2.682
S3	1.821	1.815	0.006	0.306
S4	2.396	2.385	0.011	0.472
S5	2.436	2.497	-0.061	2.498
S6	1.849	1.881	-0.032	1.719
S7	2.190	2.203	-0.013	0.590
S8	2.521	2.392	0.129	5.111
S9	0.597	0.629	-0.032	5.421
S10	2.532	2.463	0.069	2.719
S11	1.501	1.398	0.103	6.854
S12	1.613	1.682	-0.069	4.305
S13	2.506	2.550	-0.044	1.771
S14	2.296	2.386	-0.090	3.907
				3.002*



*CV% average

Conclusions

The Free-Wilson analysis was performed on a set of 14 sulphonylhydrazino-thio on four microbial strains (Bacillus subtilis, Citrobacter, Escherichia coli and Ca albicans. Using Free-Wilson procedure, QSAR equations with moderate predictability obtained.

All four antimicrobial activities are favorable influenced by the presence of the following substituents at the thiazole ring: methyl, methyl chloride, acethyl and ethoxycarbonyl. The methyl chloride substituent on position 4 of the thiazole ring increases the activity on Escherichia while the ethoxycarbonyl substituent on position 5 of the thiazole ring increases the activity on Bacillus Subtilis and decreases the Escheria antimicrobial activities.

The auto-correlating partial charges descriptor CD is the best descriptor in monovariate regression. When this electronic index is combined with Ghetaway, WHIM or 2D autocorrelation descriptors, the correlations are significantly improved.

The models obtained show good estimating and predicting abilities, as can be seen from the CV%, lower than 10, up to 2.7. The models are stable, and statistically significant, despite the rather small set of (newly synthesized) molecules under discussion.

References

- [1]. Fahmy H.T.Y., *Pharmazie*, **1997**, *52*, 750-752;
- [2]. Gursog A., Demirayak S., Cesur Z., Reisch J., Otuk G., *Die Pharmazie*, **1990**, *45*, 246-249;
- [3]. Oniga O., Grosu I., Mager S., Simiti., *Monats. Chem.*, **1998**, *129*, 661-669;
- [4]. Silva L.L., Navakoski de Oliveira K., Nunes R.J., *Arkivoc*, **2006**, 124-129;
- [5]. Kamal A., Khan M. N. A., Reddy S., Rohini K., *Bioorg. Med. Chem.*, **2007**, *15*, 1004-1013;
- [6]. Finch R.A., Shyam K., Penketh P.G., Sartorelli A.C., *Cancer Res.*, **2001**, *61*, 3033-3038;
- [7]. Giles F., Verstovsek S., Thomas D., Gerson S., Cortes J., Fader S., Ferrajoli A., Ravandi F., Kornblau S., Garcia-Manero G., Jabbour E., O'Brien S., Karsten V., Cahill A., Yee K., Albitar M., Sznol M., Kantarjian H., *Clin. Cancer Res.*, **2005**, *11*, 7817-7824;
- [8]. Ariesan V., Marie M., Cuparencu B., Safta L., *Therapie*, **1972**, *27*, 309;
- [9]. Pignatello R., Mazzone S., Castelli I., Mazzone P., Racite G., Mazzone G., *Pharmazie*, **1994**, *49*, 272-276;
- [10]. Holla B. S., Maloni K. V., Rao B. S., Sarojini B. K., Kumari N. S., *Eur. J. Med. Chem.*, **2003**, *38*, 313-318;
- [11]. Zaharia V., Silvestru A., Manuela Curticapean, Palibroda N., Vlasa M., *Heterocycles* **21**, Synthesis, characterisation and evaluation of antimicrobial potential of some new sulfonylhydrazinothiazoles (*In press*);
- [12]. Kubinyi H., Kehrhn O.H., *J. Med. Chem.*, **1976**, *19*, 578-86;
- [13]. Tmej C., Chiba P., Huber M., Richter E., Hitzler M., Schaper K. J., Ecker G., *Arch. Pharm. Pharm. Med. Chem.*, **1998**, *331*, 233-240;
- [14]. Khan N., Soni L. K., Gupta A. K., Wakode S. R., Wagh R. D., Kaskhedikar S. G., *Indian J. Pharm. Sci.*, **2006**, *68*, 341-346;
- [15]. Basak S. C., In Practical Applications of Quantitative Structure-Activity Relationships QSAR in Environmental Chemistry and Toxicology, (Karcher W, Devillers J. Eds, Kluwer Academic Publishers: Dordrecht, The Netherlands), **1990**, 83;
- [16]. Dragon Professional version 5.4-2004, Copyright (c) TALETE srl;
- [17]. Diudea M. V., Ursu O., *TOPOCLUJ* (Copyright Babes-Bolyai Univ. Cluj), **2002**;
- [18]. Rios-Santamaria I., Garcia-Domenech R., Cortijo J., Santamaria P., Morcillo E. J., Galvez J., *Internet Elect. J. Molec. Des.*, **2002**, *1*, 70-79;
- [19]. Galvez J., Garcia-Domenech R., Salabert M. T., Soler R., *J. Chem. Inf. Comput. Sci.*, **1994**, *34*, 520-525.

QSPR STUDY OF PHOSPHORIC POLYESTER GLASS TRANSITION TEMPERATURE BY PLS

Simona Funar-Timofei*, Smaranda Iliescu

Institute of Chemistry, Romanian Academy, Bul. Mihai Viteazul 24,

Timisoara, 300223, Romania

(Received March 15, 2008)

Abstract. This paper presents a structure-property study for a series of polyphosphates and polyphosphonates. Structural parameters were derived from the structures of minimum energy obtained by molecular mechanics and the semiempirical molecular orbital PM6 calculations. The influence of monomer structural descriptors of polyphosphates and polyphosphonates on the glass transition temperature was accomplished by Partial Least Squares (PLS). Good correlations of the glass transition temperature with different structural parameters were obtained. Thus, increased number of sulfur atoms present in the molecule, the number of phosphite groups, the polymer polarity and aromaticity are favorable for the glass transition temperature. Increased polymer size, higher polymer flexibility and hydrophobicity decrease the glass transition temperature, in opposition to the hydrophilicity influence.

INTRODUCTION

Studies made on phosphorus containing polymers are steadily developed having view the polymer range diversification and characterization and their use in varied domains. Phosphoric polyesters, respectively polyphosphonates and polyphosphates are of interest because they confer low flammability on polymers [1].

Much attention has been drawn in recent years towards a new class of biodegradable polymers belonging to polyphosphates and polyphosphonates, which have been investigated as biomaterials in drug delivery, gene delivery, tissue engineering and agriculture [2, 3].

Structure-property study of polyester flexibility, of their capacity of order and of their glass transition temperature was studied by molecular modeling [4]. The semi-ri-

* Corresponding author: timofei@acad-icht.tm.edu.ro

Modeling, by Multivariate Regression Methods, of the Chromatographic Retention (Lipophilicity) of New Oxadiazoline Derivatives

Costel Sârбу* and Brîndușa Tîperciuc

Key Words:

Oxadiazoline derivatives

Lipophilicity

TLC

QSRR

MLR

PCA

PCR

PLS

Summary

A comparative QSAR and QSRR study has been conducted by multiple linear regression (MLR), principal-component regression (PCR), and partial least-squares (PLS) analysis. Comparisons based on these regression methods have been used to model the chromatographic retention (lipophilicity) of thirteen new oxadiazoline derivatives by means of descriptors obtained by use of the Alchemy software package. Retention indices were determined by reversed-phased high-performance thin-layer chromatography on C₁₈ plates. The retention indices predicted were quite satisfactory and in very good agreement with the molecular structure of the compounds investigated.

1 Introduction

Quantitative structure–activity relationships (QSAR) describe how molecular structure, in terms of lipophilic, electronic, and steric descriptors, affects the biological activity of a compound [1–4]. Similarly, quantitative structure–retention relationships (QSRR) relate the same descriptors to chromatographic retention. Finally, quantitative retention–activity relationships (QRAR) imply that conclusions about biological activity can be based on results from chromatographic experiments [5–11]. In this respect it is assumed the same basic intermolecular properties determine the behavior of chemical compounds in both biological and chromatographic environments. As a consequence, the chromatographic approach has been quite a successful means of duplicating partition coefficient (log *P*) data obtained by use of the traditional “shake-flask”

technique or by other procedures. The relationships themselves are usually obtained by correlation analysis.

Other forms of computational analysis used for correlation of chemical or biological activity and chromatographic retention with different molecular descriptors are multiple linear regression (MLR) [11–13], principal-component analysis (PCA) [14–16], partial least-squares (PLS) analysis [17–19], or use of artificial neural networks (ANN) [20–22]. In PCA and PLS, starting from a multidimensional space described by different variables a quantitative model is derived that transforms the axes of the hypersystem. The first principal component (PC1) defines as much of the variation in the data as possible. The second principal component (PC2) describes the maximum amount of residual variation after the first PC has been taken into consideration, and so on. By using a limited number of PCs only the dimensionality of the data space is reduced, thereby simplifying further analysis.

In this paper we compare the three multivariate regression methods for development of a QSAR-QSRR model for characterization and classification of some new oxadiazoline derivatives with potential biological activity.

2 Methods

2.1 Principal-Component Analysis

Principal-component analysis (PCA) is also known as eigenvector analysis, eigenvector decomposition, or *Karhunen–Loève* expansion. Many problems in chemistry and other technical fields can be treated effectively by use of PCA [23]. The main purpose of PCA is to represent economically the location of the samples in a reduced coordinate system in which instead

C. Sârбу, Babeș-Bolyai University, Faculty of Chemistry and Chemical Engineering, Arany Janos 11, 400028 Cluj-Napoca, Romania; and B. Tîperciuc, Iuliu Hatieganu University of Medicine and Pharmacy, Faculty of Pharmacy, Louis Pasteur 6, 400349 Cluj-Napoca, Romania.

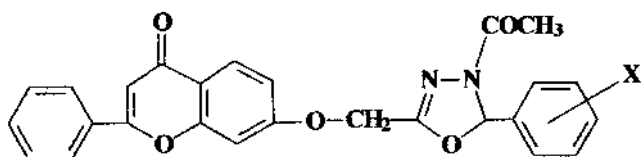


Figure 1

The chemical structures of the oxadiazoline derivatives.

of m axes corresponding to m characteristics p axes only ($p < m$) are used to describe the data set and provide the maximum possible information.

In practice principal-component analysis transforms the original data matrix ($\mathbf{X}_{n \times m}$) into a product of two matrices, $\mathbf{S}_{n \times m}$ and $\mathbf{V}_{m \times m}$, which contains the information about the objects and the variables, respectively. The \mathbf{S} matrix contains the scores of the n objects on m principal components (the scores are the projection of the objects on the principal components). The \mathbf{V} matrix is a square matrix and contains the loadings of the original variables on the principal components (the loadings are the weights of the original variables in each principal component). It is usually found that two or three principal components provide a good summary of all the original variables. Loadings and scores plots are very useful as a display tool for examining the relationships between characteristics and between compounds, and looking for trends, grouping, or outliers.

2.2 Multiple Linear Regression

Multiple linear regression (MLR) is an extension of simple linear regression to two or more independent variables (e.g. chemical descriptors) and a numeric dependent variable (e.g. chro-

matographic retention). MLR attempts to model the relationship between the independent variables and a response variable by fitting a linear equation to the observed data by use of the equation:

$$\mathbf{R} = a_0 + \sum_{i=1}^k a_i x_i, \quad (1)$$

where a_0 and a_i are the estimated terms.

2.3 Principal-Components Regression

Principal-components regression (PCR) is a two-step multivariate calibration method. In the first step principal-component analysis of the data matrix \mathbf{X} is performed. The measured or calculated variables (e.g. descriptors) are converted into new variables (scores on latent variables). This is followed by multiple linear regression, MLR, between the scores obtained in the PCA step and the characteristic \mathbf{R} to be modeled.

2.4 Partial Least-Squares Regression

Partial least-squares regression resolves matrices \mathbf{X} and \mathbf{R} into the product of the smaller matrices \mathbf{P} (the \mathbf{X} loading matrix, which contains the directions of the principal components or axes), \mathbf{T} (the scores matrix, which includes the coordinates of the new axes), and \mathbf{Q} (the \mathbf{R} loading matrix), where:

$$\mathbf{X} = \mathbf{TP} + \mathbf{E} \quad (2)$$

$$\mathbf{R} = \mathbf{TQ} + \mathbf{F} \quad (3)$$

In our work matrix \mathbf{X} (the descriptor matrix) was composed of compounds as rows (1, ..., 13) and variables as columns (1, ..., 17). Matrix \mathbf{R} (the retention matrix) consisted of the compounds

Table 1

Retention indices, associated regression data ($n = 5$)^{a)} and melting points of the oxadiazoline derivatives investigated in this work.

Compound	R_{M0} (\pm SD)	b (\pm SD)	r	F	s_e	mp [$^{\circ}$ C]
1	0.269 (\pm 0.057)	-1.23 (\pm 0.10)	0.9900	148	0.032	217–219
2	0.236 (\pm 0.060)	-1.11 (\pm 0.11)	0.9868	112	0.034	196.3–197.7
3	0.267 (\pm 0.093)	-1.19 (\pm 0.16)	0.9724	52	0.052	193.6–194.2
4	0.287 (\pm 0.093)	-1.23 (\pm 0.16)	0.9744	56	0.052	160.9
5	0.327 (\pm 0.125)	-1.33 (\pm 0.22)	0.9609	36	0.070	190–193.7
6	0.343 (\pm 0.110)	-1.39 (\pm 0.19)	0.9720	51	0.061	198–199
7	0.421 (\pm 0.122)	-1.54 (\pm 0.21)	0.9819	51	0.068	214.3–216.5
8	0.403 (\pm 0.153)	-1.55 (\pm 0.27)	0.9572	33	0.085	203.5
9	0.378 (\pm 0.137)	-1.50 (\pm 0.24)	0.9632	39	0.076	268–269
10	0.415 (\pm 0.194)	-1.60 (\pm 0.34)	0.9377	22	0.108	266.7–268.4
11	0.326 (\pm 0.130)	-1.36 (\pm 0.23)	0.9600	35	0.073	118.5
12	0.317 (\pm 0.115)	-1.35 (\pm 0.20)	0.9680	45	0.064	189.5
13	0.387 (\pm 0.141)	-1.51 (\pm 0.25)	0.9619	37	0.078	262–264

^{a)} n is the number of regression points (concentrations)

Table 2

The descriptors computed for the oxadiazoline derivatives investigated in this work.

Compound	log <i>P</i>	¹ χ	³ χ	⁰ χ ^v	¹ χ ^v	³ K _α	<i>W</i>	<i>V</i>	<i>M</i>	<i>DM</i>	<i>MP</i>	<i>SP</i>	<i>Q</i> ⁺	<i>SQ</i>	<i>SQ</i> _{NO}
1	3.32	16.08	12.33	17.80	10.43	4.43	3541	384.5	440.4	4.28	47.18	0.122	0.211	5.257	2.088
2	2.96	16.49	12.80	18.85	10.91	4.63	3812	397.8	474.9	4.61	49.11	0.123	0.212	5.303	2.086
3	3.58	16.47	12.66	18.85	10.91	4.77	3839	398.5	474.9	2.99	49.11	0.123	0.211	5.268	2.088
4	3.61	16.47	12.74	18.85	10.91	4.77	3866	398.5	474.9	2.81	49.11	0.123	0.212	5.260	2.087
5	2.87	16.49	12.80	19.68	11.33	4.70	3812	405.1	519.3	4.28	49.81	0.122	0.211	5.199	2.089
6	3.17	16.47	12.74	19.68	11.32	4.84	3866	406.2	519.3	3.83	49.81	0.122	0.211	5.154	2.089
7	3.70	16.47	12.74	18.10	10.53	4.66	3866	388.6	458.4	2.46	47.09	0.121	0.212	5.432	2.086
8	2.74	17.88	13.36	20.04	11.46	5.35	4799	427.8	498.4	2.83	51.58	0.120	0.212	6.243	2.732
9	2.94	17.86	13.31	20.04	11.45	5.50	4907	428.4	498.4	5.40	51.58	0.120	0.212	6.214	2.744
10	2.74	17.86	13.37	20.04	11.45	5.50	5015	428.2	498.4	2.24	51.58	0.120	0.212	6.186	2.738
11	2.93	17.02	13.11	19.13	10.96	4.74	4117	408.9	470.4	5.74	49.66	0.121	0.212	5.742	2.465
12	2.80	17.01	13.08	19.13	10.95	4.87	4171	409.5	470.4	4.75	49.66	0.121	0.211	5.697	2.469
13	2.81	17.01	13.15	19.13	10.95	4.87	4225	409.5	470.4	2.74	49.66	0.121	0.212	5.684	2.467

as rows and retention indices as columns (1, 2). Finally, matrices **E** and **F** (the residual matrices) contained the model error and random noise, respectively.

3 Experimental

3.1 Chromatography

The chromatographic behavior of the compounds was studied on the C₁₈ silica gel bonded HPTLC plates (20 cm × 20 cm), obtained as a gift from Macherey–Nagel (Düren, Germany). Methanol for chromatography was supplied by Reactivul (Bucharest, Romania). Each compound (**Figure 1**) was dissolved in methanol (1 mg mL⁻¹) and 3 μL of the solutions were spotted randomly on the plates. Methanol–water mixtures containing from 25 to 75% (v/v) methanol in steps of 10% were used as mobile phases because the compounds studied differed substantially in their retention. Chromatography was performed in duplicate. Plates were developed by the ascending technique at room temperature; the development distance was 10 cm. After development the dried plates were examined under a UV lamp (λ = 254 nm). *R_M* values of each compound were obtained by use of the well-known equation:

$$R_M = \log(1/R_F - 1) \quad (4)$$

Linear correlation between *R_M* values and the concentration of organic modifier in the mobile phase were calculated separately for each compound by use of the equation:

$$R_M = R_{M0} + bC \quad (5)$$

where *C* is the concentration of methanol in the mobile phase. *R_{M0}* and *b* values (related to molecular lipophilicity) and statistical data from regression analysis (correlation coefficients *r*,

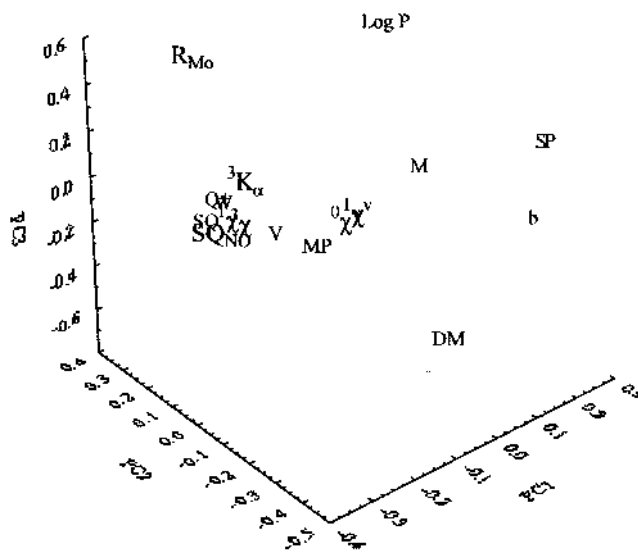


Figure 2

PC1, PC2, and PC3 loading plot of all the data in Table 1 (autoscaled data).

F-test values *F*, and the standard error of estimates *s*) are depicted in **Table 1**.

3.2 The Oxadiazolines

The oxadiazoline derivatives investigated were synthesized as described elsewhere [24]. The molecular structures of the oxadiazolines studied in this paper are shown in Figure 1, in which X stands for H (**1**), *o*-Cl (**2**), *m*-Cl (**3**), *p*-Cl (**4**), *o*-Br (**5**), *p*-Br (**6**), *p*-F (**7**), *o*-OCOCH₃ (**8**), *m*-OCOCH₃ (**9**), *p*-OCOCH₃ (**10**), *o*-OCH₃ (**11**), *m*-OCH₃ (**12**), and *p*-OCH₃ (**13**). The melting points (mp) of compounds are listed in Table 1.

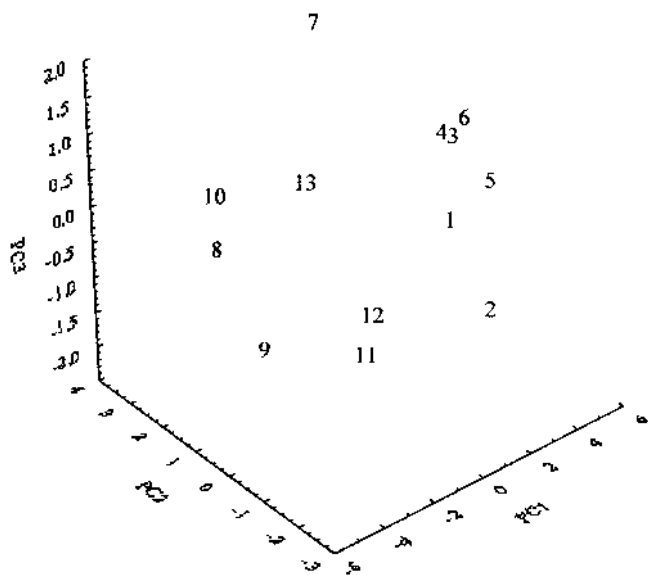


Figure 3
PC1, PC2, and PC3 score plot of all the data in Table 1 (autoscaled data).

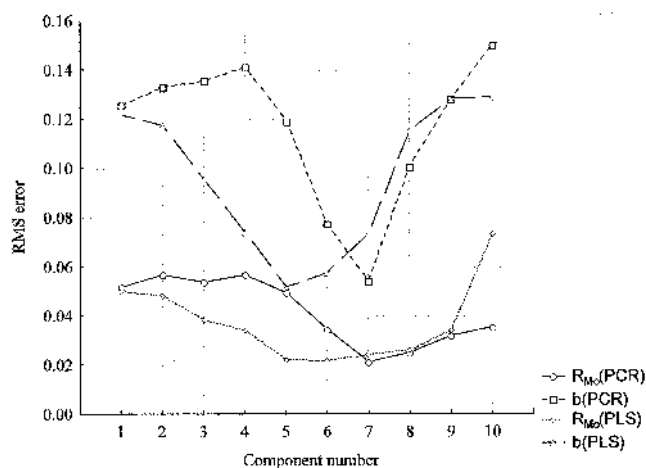


Figure 4
Cross-validated error for the oxadiazoline derivatives, for application of PCR and PLS.

To define the character of the compounds from their structures, descriptors available in the Alchemy 2000 software [25] were used as independent variables. The descriptors used were the partition coefficient ($\log P$), the first-order (${}^1\chi$) and third-order (${}^3\chi$) connectivity indexes, the zero-order (${}^0\chi^v$) and first-order (${}^1\chi^v$) valence order connectivity indexes, the third-order shape index for molecule (${}^3K_\omega$), the Wiener (W) index based on the graph of the molecule, the volume (V), the molar mass (M), the dipole moment (DM), the molecular polarizability (MP), the specific molar polarizability (SP), the largest positive charge over the atoms in a molecule, in electrons (Q^+), the sum of absolute values of the charges on each atom of the molecule, in electrons (SQ), and the sum of absolute values of the charges on the nitrogen and oxygen atoms in the molecule, in electrons

Table 3

Statistical data from evaluation of the linear correlation between observed retention indices and values predicted using three multiple regression methods (MLR, PCR, and PLS).

Variable	MLR		PCR		PLS	
	R_{M0}	b	R_{M0}	b	R_{M0}	b
R^2	0.9785	0.9833	0.8652	0.8668	0.8536	0.8858
F	502	647	71	78	64	85
p	0.0000	0.0000	0.0000	0.0000	0.0000	0.0000
s	0.0090	0.0212	0.0227	0.0576	0.0236	0.0554
a_0	0.0000	-0.0000	0.0007	-0.0790	-0.0049	0.0339
a_1	1.0000	1.0000	1.0076	0.9486	1.0256	1.0304

(SQ_{NO}). Before calculation Alchemy performs minimization of the potential energy (geometry optimization) for each molecule by the standard technique of the molecular mechanics method. The values obtained are presented in Table 2.

4 Results and Discussion

By reducing the number of features from 17 original descriptors (including also retention indices) to three principal components (latent variables), the information preserved is sufficient to enable primary examination of the similarities and differences between descriptors and oxadiazoline derivatives. The contribution of the first component represents 69.07% of the total variance and the second component 13.80%; a two-component model accounts for 82.87% of the total variance. The first three components reproduce almost 92% of the total variance and the first six reproduce as much as 99.17%, and the eigenvalues become negligible after the seventh component.

All these statements are well supported by the 2D and 3D representations of the loadings. The projection of the 3D representation (Figure 2) gives a more complete pattern. It is clear, for example, that most of the descriptors considered in this study form two well defined clusters: the first includes ${}^1\chi$, ${}^3\chi$, ${}^3K_\omega$, W , V , Q , SQ , and SQ_{NO} and the second encompasses MP , ${}^0\chi^v$, and ${}^1\chi^v$. $\log P$, R_{M0} , b , SP , DM , and M appear more or less as outliers.

The scatter plot of scores in the space described by PC1, PC2, and PC3 (Figure 3) reveals interesting results. Three clusters seem to be well defined and in good agreement with the compound structure – one corresponds to the halogen derivatives (right) the others include the group of methoxy derivatives (middle) and methyl acetate group (left).

Multivariate regression analysis was performed to describe the relationship between the chromatographic retention indices of the chemicals (R_{M0} and b values) and the calculated structural data. The high-quality regression equations below were obtained by stepwise regression analysis.

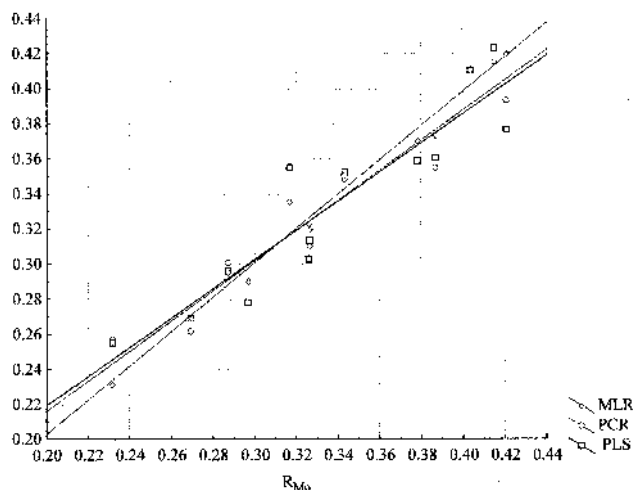


Figure 5

Linear correlation of observed R_{M0} values with values predicted by use of multivariate regression methods (MLR, PCR, and PLS).

$$R_{M0} = 7.628 - 62.582SP - 0.0182DM + 0.0013M + 0.0055^1\chi^v + 0.042\log P - 0.0837^3K_a \quad (6)$$

$$(R^2 = 0.9786, n = 13, F = 46, p < 0.0000, s = 0.0122)$$

$$b = -1.913 + 176.09SP + 0.034DM - 0.003M + 0.163^1\chi \quad (7)$$

$$(R^2 = 0.9800, n = 13, F = 98, p < 0.0000, s = 0.0272)$$

where n is the number of compounds, R^2 the determination coefficient, F the F -test value, p the significance level of the equation, and s is standard error of the estimate. The F and p values for eqs (6) and (7) show that the equations are very significant, because of the high determination coefficients and small s values. These results also suggest that the most significant descriptors in both models are SP and DM , i.e. the electronic term and the shape (volume) of the molecules. By eliminating the descriptors with statistically non-significant coefficients (according to the t -test), the simpler models below were obtained (eqs 8 and 9):

$$R_{M0} = 5.437 - 41.222SP - 0.0196DM \quad (8)$$

$$(R^2 = 0.8454, n = 13, F = 27, p < 0.0000, s = 0.0255)$$

$$b = -16.061 + 119.299SP + 0.0375DM \quad (9)$$

$$(R^2 = 0.8876, n = 13, F = 39, p < 0.0000, s = 0.0577)$$

For PCR and PLS the original 15 descriptors were used for selection of the optimum number of factors by using the cross-validation procedure. The prediction error was calculated as the root mean square (RMS) error, as described elsewhere [26]. The values of RMS are plotted in **Figure 4**. By use of the cross-validation procedure it is easy to observe that its numerical values were minimized by use of the first seven factors in PCR and five factors in PLS.

To compare MLR, PCR, and PLS as predictive models, linear regression was applied using observed and predicted values of the retention indices. Good correlations were obtained between observed retention indices and those predicted by use of the

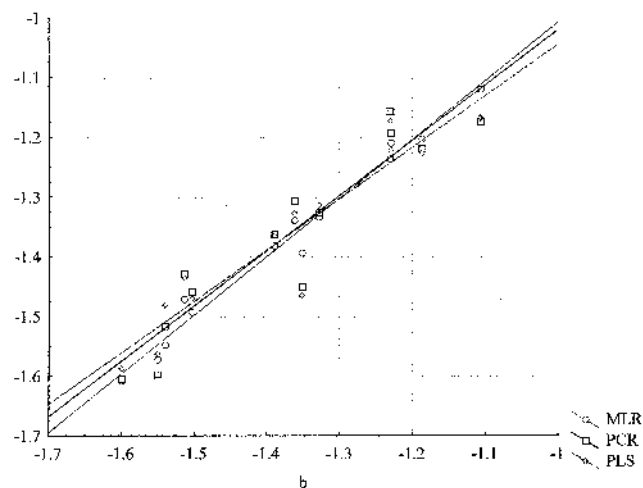


Figure 6

Linear correlation of observed b values with values predicted by use of multivariate regression methods (MLR, PCR, and PLS).

three methods, as is readily apparent from **Table 3** and **Figures 5** and **6**. The intercept a_0 is always statistically zero (t -test) and the slope a_1 is not statistically different from unity (t -test). As a direct consequence it can be concluded that all three straight lines are parallel and pass through the origin. In addition, high F values and very small s values were always obtained. It should be remarked that MLR seems to be the most effective method for estimation of retention indices.

5 Conclusion

Correlation obtained between chromatographic retention indices and structure descriptors for substituted oxadiazolines are highly significant and might be used to predict the retention behavior and, as a consequence, the lipophilicity of other members of the series. Of the multivariate regression methods compared in this study, MLR seemed to be most effective for predicting the retention indices of the compounds studied. The specific polarizability and dipole moment seem to be dominant in the retention mechanism, in good agreement with other reported results.

References

- [1] A. Leo, C. Hansch, and D. Elkins, *Chem. Rev.* **71** (1971) 525–616.
- [2] R.F. Rekker and R. Mannhold, *Calculation of Drug Lipophilicity*, VCH, Weinheim, 1992.
- [3] M. Karelson, *Molecular Descriptors in QSAR/QSPR*, Wiley and Sons, New York, 2000.
- [4] A. Chiriac, D. Ciubotariu, and Z. Simon, *QSAR – Quantitative Relationships*, Mirton Publishing House, Timișoara, 1996.
- [5] R. Kaliszan, *Anal. Chem.* **64** (1992) 619A–631A.

- [6] P. Gramatica, M. Vighi, F. Consolaro, R. Todeschini, A. Finizio, and M. Faust, *Chemosphere* **42** (2001) 873–883.
- [7] R. Kaliszan, *Trends Anal. Chem.* **18** (1999) 401–409.
- [8] Q.S. Wang and L. Zhang, *J. Liq. Chromatogr. Related Technol.* **22** (1999) 1–14.
- [9] M.C. Garcia Alvarez-Coque and J.R. Torres Lapasio, *Trends Anal. Chem.* **18** (1999) 533–543.
- [10] K. Valko, *Trends Anal. Chem.* **6** (1987) 214–219.
- [11] J. Dai, L. Jin, S. Yao, and L. Wang, *Chemosphere* **42** (2001) 899–907.
- [12] A. Detroyer, Y.V. Heyden, S. Carda-Broch, M. C. Garcia-Alvarez-Coque, and D.L. Massart, *J. Chromatogr. A* **912** (2001) 211–221.
- [13] C. Sârbu, D. Casoni, M. Dărăbanțu, and C. Maiereanu, *J. Pharm. Biomed. Anal.* **35** (2004) 213–219.
- [14] C. Sârbu and S. Todor, *J. Chromatogr. A* **822** (1998) 263–269.
- [15] C. Sârbu, K. Kuhajda, and S. Kevresan, *J. Chromatogr. A* **917** (2001) 361–366.
- [16] A. Detroyer, V. Schoonjans, F. Questier, Y.V. Heyden, A.P. Borosy, Q. Guo, and D.L. Massart, *J. Chromatogr. A* **897** (2000) 23–36.
- [17] H. Martens and T. Naes, *Multivariate Calibration*, Wiley, Chichester, 1991.
- [18] Y. Zhou, L. Xu, Y. Wu, and B. Liu, *Chemometr. Intell. Lab. Syst.* **45** (1999) 95–100.
- [19] T. Li, H. Mei, and P. Cong, *Chemometr. Intell. Lab. Syst.* **45** (1999) 177–184.
- [20] R. Zhang, A. Yan, M. Liu, H. Liu, and Z. Hu, *Chemometr. Intell. Lab. Syst.* **45** (1999) 113–120.
- [21] R.H. Zhao, B.F. Yue, J.Y. Ni, H.F. Zhou, and Y.K. Zhang, *Chemometr. Intell. Lab. Syst.* **45** (1999) 163–170.
- [22] Y. Chen, D. Chen, C. He, and S. Hu, *Chemometr. Intell. Lab. Syst.* **45** (1999) 267–276.
- [23] C. Sârbu and H. F. Pop, *Fuzzy Soft-Computing Methods and Their Applications in Chemistry*. In: K.B. Lipkowitz, D.B. Boyd, and T.R. Cundari (Eds) *Reviews in Computational Chemistry*, Wiley-VCH, 2004, Chapter 5, pp. 249–332.
- [24] B. Tipericiuc, I. Oniga, D. Benedec, and O. Oniga, *Farmacia* **4** (2002) 39–44.
- [25] <http://www.alchemysoftware.ie/index.html>
- [26] R.G. Brereton, *Chemometrics; data analysis for the laboratory and chemical plant*, Wiley and Sons, Chichester, 2003.

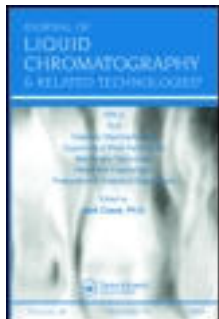
Ms received: February 10, 2006
Accepted by SN: August 14, 2006

This article was downloaded by: [Brandusa Tipericiuc]

On: 03 November 2011, At: 07:09

Publisher: Taylor & Francis

Informa Ltd Registered in England and Wales Registered Number: 1072954 Registered office: Mortimer House, 37-41 Mortimer Street, London W1T 3JH, UK



Journal of Liquid Chromatography & Related Technologies

Publication details, including instructions for authors and subscription information:

<http://www.tandfonline.com/loi/ljlc20>

Prediction of the Chromatographic Retention (Lipophilicity) of Some New Methyl-Thiazole-Oxadiazoline Derivatives by Multivariate Regression Methods

B. Tipericiuc^a & C. Sârbu^b

^a Iuliu Hatieganu University of Medicine and Pharmacy, Faculty of Pharmacy, Cluj-Napoca, Romania

^b Babeş-Bolyai University, Faculty of Chemistry and Chemical Engineering, Cluj-Napoca, Romania

Available online: 07 Feb 2007

To cite this article: B. Tipericiuc & C. Sârbu (2006): Prediction of the Chromatographic Retention (Lipophilicity) of Some New Methyl-Thiazole-Oxadiazoline Derivatives by Multivariate Regression Methods, *Journal of Liquid Chromatography & Related Technologies*, 29:15, 2257-2270

To link to this article: <http://dx.doi.org/10.1080/10826070600832939>

PLEASE SCROLL DOWN FOR ARTICLE

Full terms and conditions of use: <http://www.tandfonline.com/page/terms-and-conditions>

This article may be used for research, teaching, and private study purposes. Any substantial or systematic reproduction, redistribution, reselling, loan, sub-licensing, systematic supply, or distribution in any form to anyone is expressly forbidden.

The publisher does not give any warranty express or implied or make any representation that the contents will be complete or accurate or up to date. The accuracy of any instructions, formulae, and drug doses should be independently verified with primary sources. The publisher shall not be liable for any loss, actions, claims, proceedings, demand, or costs or damages whatsoever or howsoever caused arising directly or indirectly in connection with or arising out of the use of this material.

Prediction of the Chromatographic Retention (Lipophilicity) of Some New Methyl-Thiazole-Oxadiazoline Derivatives by Multivariate Regression Methods

B. Tipericiu

Iuliu Hatieganu University of Medicine and Pharmacy,
Faculty of Pharmacy, Cluj-Napoca, Romania

C. Sârbu

Babeş-Bolyai University, Faculty of Chemistry and Chemical
Engineering, Cluj-Napoca, Romania

Abstract: Retention indices for a new series of methyl-thiazole-oxadiazolines were determined by reversed phase high performance thin layer chromatography on C₁₈ plates with methanol-water in different volume proportions as mobile phase. Comparisons based on the multiple regression methods including multiple linear regression (MLR), principal component regression (PCR) and partial least squares (PLS) have been applied to the modelling of chromatographic lipophilicity (R_{M0} and b values) by means of 16 different descriptors obtained by using Alchemy package software. The results achieved concerning the prediction of retention indices are highly significant and are in very good agreement with the molecular structure of the compounds investigated. The largest positive charge over the atoms in a molecule (Q_+), the sum of absolute values of the charges on each atom of the molecule (SQ), and the sum of absolute values of the charges on the nitrogens and oxygens in the molecule (SQ_{NO}) seem to be dominant in the retention mechanism.

Keywords: Methyl-thiazole-oxadiazolines, Lipophilicity, TLC, QSRR, MLR, PCA, PCR, PLS

Address correspondence to C. Sârbu, Babeş-Bolyai University, Faculty of Chemistry and Chemical Engineering, Arany Janos 11, 400028 Cluj-Napoca, Romania. E-mail: csarbu@chem.ubbcluj.ro

INTRODUCTION

Quantitative structure-activity relations (QSAR) describe how the molecular structure, in terms of descriptors – lipophilic, electronic, and steric – affects the biological activity of a compound.^[1–4] Similarly, quantitative structure – retention relations (QSRR) relate these descriptors to chromatographic retention. Finally, the quantitative retention – activity relations (QRAR) imply that conclusions concerning biological activity can be based on chromatographic experiments.^[5–11] In this regard of QRAR, it is considered that the same basic intermolecular actions determine the behaviour of chemical compounds in both biological and chromatographic environments. As a consequence, the chromatographic approach has been quite successful in duplicating Log P data derived by the traditional “shake-flask” technique or other procedures. The relations themselves are usually based on correlation analysis.

Another form of computational analysis used for the correlation of chemical or biological activity and chromatographic retention with different molecular descriptors are Multiple Linear Regression (MLR),^[11–13] Principal Component Analysis (PCA),^[14–16] Partial Least Squares (PLS),^[17–19] or Artificial Neural Networks (ANN).^[20–22] In the case of PCA and PLS, for example, starting from a multidimensional space described by different variables, a quantitative model is derived that transforms the axes of the hypersystem. The first principal component (PC1) defines as much of the variation in the data as possible. The second principal component (PC2) describes the maximum amount of residual variation after the first PC has been taken into consideration, and so on. By using only a limited number of PCs, the dimensionality of the data space is reduced, thereby simplifying further analysis.

In this paper we discuss and apply three multivariate regression methods to develop comparative studies, and to provide a QSAR-QSRR model for the characterization and classification of some new methyl-thiazole-oxadiazoline derivatives with a potential antibacterial, antimycotic, and anti-inflammatory activity.

Principal Component Analysis

Principal components analysis (PCA) is also known as eigenvector analysis, eigenvector decomposition, or Karhunen-Loève expansion. Many problems from chemistry and other scientific fields are strongly related to PCA.^[23] The main purpose of PCA is to represent, in an economic way, the location of the samples in a reduced coordinate system where, instead of m -axes (corresponding to m characteristics), only p ($p < m$) can usually be used to describe the data set with maximum possible information.

Principal component analysis practically transforms the original data matrix ($X_{n \times m}$) into a product of two matrices, one of which contains the

information about the objects ($S_{n \times m}$) and the other about the variables ($V_{m \times m}$). The S matrix contains the scores of the n objects on m principal components (the scores are the projection of the objects on principal components). The V matrix is a square matrix and contains the loadings of the original variables on the principal components (the loadings are the weights of the original variables in each principal component).

Moreover, it may well turn out that usually two or three principal components provide a good summary of all the original variables. Loadings and scores plots, respectively, are very useful as a display tool for examining the relationships between characteristics as well as between compounds, looking for trends, groupings, or outliers.

Multiple Linear Regression

Multiple linear regression (MLR) is an extension of simple linear regression consisting of two or more independent variables (e.g., chemical descriptors) and a numeric dependent variable (e.g., chromatographic retention index). MLR attempts to model the relationship between the independent variables and a response variable by fitting a linear equation to observed data in the following equation:

$$R = a_0 + \sum_{i=1}^k a_i x_i \quad (1)$$

where a_0 , a_i are the estimated regression parameters.

Principal Component Regression

Principal component regression (PCR) is a two-step multivariate calibration method: in the first step, a principal component analysis of the data matrix X is performed. The measured or calculated variables (e.g., descriptors) are converted into new ones (scores on latent variables). This is followed by a multiple linear regression step, MLR, between the scores obtained in the PCA step and the characteristic R to be modelled.

Partial Least Squares Regression

Partial least squares (PLS) is a statistical multivariate regression procedure that is widely applied in chemistry and many other scientific fields. Being a multivariate procedure, PLS provides the ability to predict multiple components of interest simultaneously. The PLS procedure simultaneously estimates underlying factors (loading factors or eigenvectors) that represent

the variation patterns (trends) in both the descriptor data X (in our study) and the retention values R (R_{M0} and b in our study). These loading factors are used to define a subspace in X that better models R . This is accomplished by using the columns of R matrix to estimate the loading factors of X matrix. At the same time, the columns of X matrix are used to estimate the loading factors for R matrix. The resulting models are shown in Equation (2) and (3).

$$X = TP + E \quad (2)$$

$$R = TQ + F \quad (3)$$

PLS resolves matrices X and R into products of smaller matrices, namely P (the X loading matrix, which contains the directions of the principal components or axes) and T (the scores matrix, which includes the coordinates for the new axes) and Q (the R loading matrix). The factors for X and R are associated through the following relationship:

$$q = bt + \varepsilon \quad (4)$$

where q and t equal the column vectors of Q and T matrices, respectively, and ε equals errors associated with the u - t relationship.

Using both descriptor and retention information to determine the loading factors is the main difference between the PLS and other statistical multivariate procedures, such as multiple linear regression and principal component regression. This feature makes the PLS prediction models more robust for complex data. The number of loading factors used in the final regression model was selected through a cross-validation procedure.^[27]

EXPERIMENTAL

The chromatographic behavior of the compounds was studied on the C_{18} silica gel bonded plates. Glass HPTLC plates (20 × 20 cm) were obtained as a gift

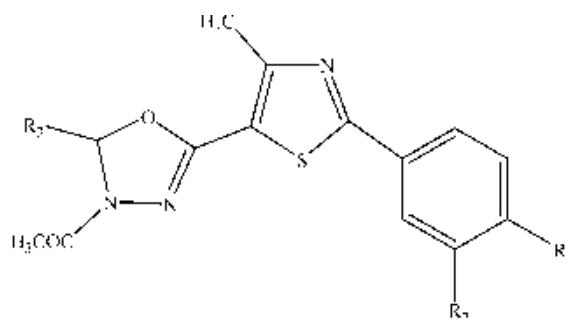
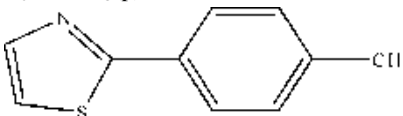
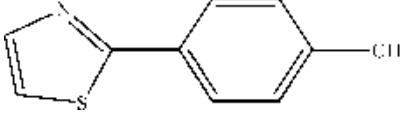
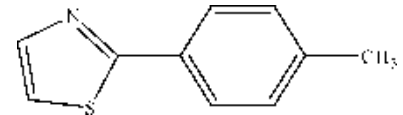


Figure 1. Chemical structure of methyl-thiazole-oxadiazolines.

from Macherey-Nagel (Düren, Germany). Methanol for chromatography was supplied from Reactivul (Bucharest, Romania). Methanolic solutions of each compound, in Table 1, were prepared at a concentration of 1 mg mL^{-1} . Chromatograms were developed by an ascending technique at room temperature; the developing distance being 10 cm. The mobile phase was a mixture of methanol–water with various content from 45 to 70% (v/v) in 5% steps, as the studied compounds differed considerably in their retention. After being developed, the dried plates were examined under a UV lamp ($\lambda = 254 \text{ nm}$). The R_M values of each compound were obtained by using the well known following equation:

$$R_M = \log(1/R_f - 1) \quad (5)$$

Table 1. The structures of the substituents in Figure 1

Compound	R ₁	R ₂	R ₃
1	CH ₃	H	C ₆ H ₄ Cl(o)
2	H	H	C ₆ H ₄ Cl(m)
3	H	CF ₃	C ₆ H ₄ Cl(p)
4	H	H	C ₆ H ₄ OCH ₃ (p)
5	H	CF ₃	
6	CH ₃	H	
7	CH ₃	H	C ₆ H ₄ OCH ₃ (o)
8	H	CF ₃	C ₆ H ₄ OCH ₃ (m)
9	H	CF ₃	C ₆ H ₄ OCOCH ₃ (p)
10	H	H	C ₆ H ₄ OCOCH ₃ (o)
11	CH ₃	H	C ₆ H ₄ OCOCH ₃ (m)
12	H	H	C ₆ H ₅
13	CH ₃	H	C ₆ H ₄ Cl(p)
14	H	H	
15	H	CF ₃	C ₆ H ₅
16	H	CF ₃	C ₆ H ₄ OCOCH ₃ (o)
17	H	H	C ₆ H ₄ Cl(o)
18	H	CF ₃	C ₆ H ₄ Cl(o)
19	H	CF ₃	C ₆ H ₄ OCH ₃ (o)
20	CH ₃	H	C ₆ H ₄ OCOCH ₃ (p)

Linear correlation between R_M values and the concentration of organic modifier in the mobile phase were calculated separately for each compound according to the equation:

$$R_M = R_{M_0} + bC, \quad (6)$$

where C is the concentration of methanol in the mobile phase. The R_{M_0} and b values (related to the molecular lipophilicity) are listed in Table 2.

Description of Methyl-Thiazole-Oxadiazolines

The investigated methyl-thiazole-oxadiazoline derivatives were synthesized by the procedure described earlier.^[24,25] The molecular structure of methyl-thiazole oxadiazoline series studied in this paper is depicted in Table 1.

In order to define the character of the compound structure, the following descriptors available in the ALCHEMY 2000 programs^[26] were taken into consideration and used as independent variables. The partition coefficient ($\log P$), the first-order ($^1\chi$) and the third-order ($^3\chi$) connectivity index, the zero-order ($^0\chi^v$) and the first-order ($^1\chi^v$) valence order connectivity index, the third-order shape index for molecule (3K_a), the Wiener (W) index based on the graph of the molecule, volume (V), molar mass (M), dipole moment (DM), molecular polarizability (MP), specific molar polarizability (SP), the largest positive charge over the atoms in a molecule, in electrons (Q_+), the largest negative charge over the atoms in a molecule, in electrons (Q_-), the sum of absolute values of the charges on each atom of the molecule, in electrons (SQ), and the sum of absolute values of the charges on the nitrogens and oxygens in the molecule, in electrons (SQ_{NO}). The values obtained are presented in Table 2.

RESULTS AND DISCUSSION

By reducing the number of features from 18 original descriptors (including retention indices) to three principal components (latent variables), the information preserved is enough to permit a primary examination of the similarities and differences between descriptors and methyl-thiazole-oxadiazoline derivatives. The contribution of the first component represents 55.71% of the total variance and 75.11% of the total variance. The first three components reproduce approximately 88% of the total variance and the first six even 99.31%, and the eigenvalues become negligible after seventh component.

All the statements above are well supported by the 2D- and 3D-representations of the loadings. The projection of the 3D-representation (Figure 2) gives a more complete pattern: it is clear, for example, that the majority of the descriptors considered in this study form two close clusters: the first one includes $^1\chi$, $^3\chi$, W , R_{M_0} , M , and the second one encompasses MP , $^0\chi^v$, $^1\chi^v$,

Table 2. The descriptors computed for the methyl-thiazole-oxadiazoline derivatives investigated in this paper

	Log P	$^1\chi$	$^3\chi$	$^0\chi^v$	$^1\chi^v$	$^3K_\alpha$	W	V	M	DM	MP	SP	Q ₊	Q ₋	SQ	SQ _{NO}	R _{Mo}	b
1	4.111	13.44	10.60	17.21	10.0	3.72	2059	348.84	411.91	3.80	43.86	0.126	0.215	-0.377	3.760	1.253	2.74	-4.35
2	3.941	13.02	10.04	16.29	9.6	3.61	1856	332.36	397.87	4.67	42.03	0.126	0.215	-0.376	3.683	1.256	2.63	-4.22
3	4.207	14.63	11.41	17.85	10.3	4.53	2782	361.07	465.88	4.28	43.59	0.121	0.424	-0.376	4.502	1.254	3.38	-5.33
4	3.335	13.56	10.53	16.56	9.6	3.73	2103	343.01	393.47	5.72	42.57	0.124	0.215	-0.382	4.099	1.635	2.54	-4.07
5	4.248	17.10	13.59	20.96	12.5	5.07	4327	424.07	528.58	5.45	51.97	0.122	0.424	-0.376	5.124	1.549	3.55	-5.32
6	4.637	15.88	12.72	20.33	12.2	4.39	3405	411.67	474.61	3.10	52.25	0.127	0.219	-0.376	4.338	1.549	3.06	-4.76
7	3.594	13.97	10.91	17.49	10.0	3.82	2260	359.52	407.49	3.13	44.41	0.123	0.215	-0.381	4.200	1.633	2.30	-3.88
8	3.563	15.17	11.75	18.12	10.3	4.64	3024	372.14	461.47	3.02	44.14	0.119	0.424	-0.382	4.939	1.637	2.71	-4.47
9	2.718	16.02	12.05	19.03	10.8	5.28	3718	390.11	489.48	8.03	46.06	0.118	0.424	-0.376	5.428	1.906	2.87	-4.66
10	2.558	14.43	10.75	17.47	10.1	4.20	2455	361.03	421.48	5.49	44.49	0.123	0.216	-0.375	4.657	1.900	1.78	-3.36
11	3.315	14.81	11.10	18.40	10.5	4.57	2806	377.26	435.51	3.74	46.33	0.123	0.215	-0.376	4.670	1.911	2.16	-3.77
12	3.302	12.63	9.71	15.23	9.1	3.30	1676	318.38	363.44	3.47	40.10	0.126	0.215	-0.376	3.672	1.256	2.04	-3.48
13	4.180	13.42	10.53	17.21	10.0	3.85	2101	349.16	411.91	5.26	43.86	0.126	0.215	-0.376	3.717	1.254	2.81	-4.50
14	4.606	15.49	12.30	19.41	11.8	4.17	3098	394.78	460.58	2.98	50.41	0.128	0.219	-0.376	4.296	1.549	2.70	-4.30
15	4.020	14.24	11.00	16.79	9.8	4.20	2523	346.99	431.44	5.04	41.66	0.120	0.424	-0.376	4.499	1.256	2.64	-4.33
16	3.171	16.04	12.04	19.03	10.8	5.13	3526	390.42	489.48	3.65	46.06	0.118	0.424	-0.376	5.487	1.900	2.29	-4.00
17	3.733	13.04	10.19	16.29	9.6	3.49	1836	331.85	397.89	3.66	42.03	0.127	0.215	-0.376	3.719	1.253	2.84	-4.55
18	4.188	14.65	11.48	17.85	10.3	4.39	2734	361.29	465.88	4.40	43.59	0.121	0.424	-0.376	4.546	1.253	3.10	-4.89
19	3.929	15.18	11.79	18.12	10.3	4.50	2976	372.31	461.47	5.65	44.14	0.118	0.424	-0.381	4.985	1.633	2.61	-4.33
20	2.675	14.81	11.17	18.40	10.5	4.57	2890	377.03	435.51	6.07	46.33	0.123	0.215	-0.376	4.642	1.906	2.20	-3.77

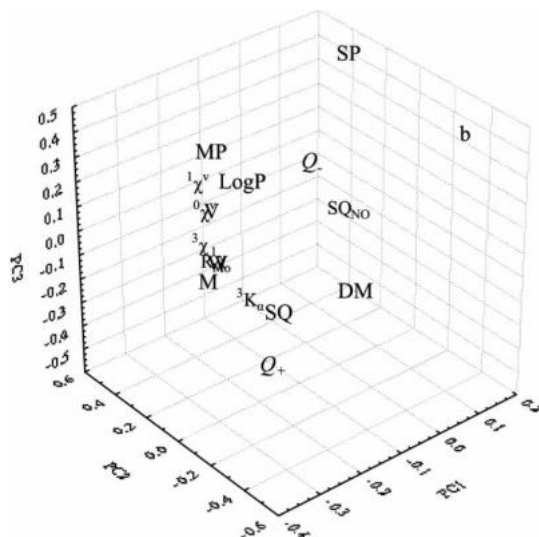


Figure 2. PC1, PC2, and PC3 loading plot of the autoscaled all data in Table 2.

$\text{Log } P$, V ; ${}^3K_{\alpha}$, SQ , Q_{+} , DM , SQ_{NO} , Q_{-} , SP , and b appear more or less as outliers and are the most discriminating.

The scatter plot of scores in the space described by PC1, PC2, and PC3 (see Figure 3) shows interesting results. Three clusters appear to be

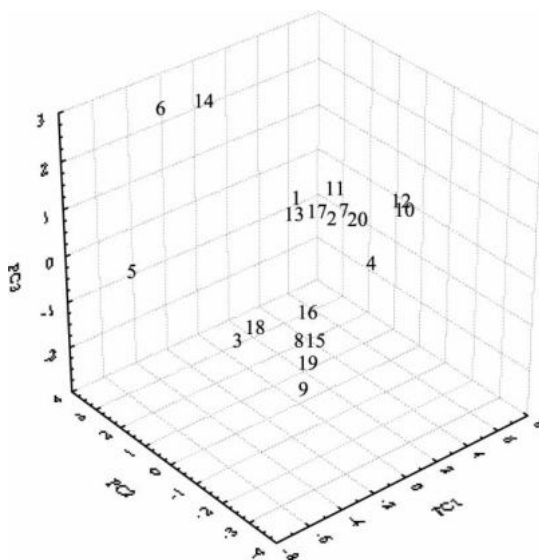


Figure 3. PC1, PC2, and PC3 score plot of the autoscaled all data in Table 2.

well defined and in good agreement to the structure of compounds: one of them corresponds to the compounds 5, 6, 14 (the largest molecules in the series) in the above left part of the graph, the second including the group of fluorine derivatives (3, 8, 9, 15, 16, 18, 19), with the exception of compounds 5, 6, and 16, is located in the middle bottom of the graph and the third group (1, 2, 4, 7, 10, 11, 12, 13, 17, 20), respectively (right).

In order to describe the relationship between the chromatographic retention indices of tested compounds (R_{M0} and b values) and the calculated structural descriptors, a multivariate regression analysis was performed. By forward stepwise multiple regression analysis, the following high quality regression equations were obtained:

$$R_{M0} = 3.365 - 0.203\text{LogP} + 0.021M + 3.268 \text{SQ}_{\text{NO}} - 4.094\text{SQ} + 10.937Q_+ + 0.0003W \quad (7)$$

$$(R^2 = 0.9438, n = 20, F = 36, p < 0.0000, s = 0.1260)$$

$$b = -2.477 - 0.203\text{LogP} + 0.029M - 3.625\text{SQ}_{\text{NO}} + 4.393\text{SQ} - 11.999Q_+ - 0.026\text{DM} - 2.094\text{SP}(8) \quad (8)$$

$$(R^2 = 0.9402, n = 20, F = 27, p < 0.0000, s = 0.1635)$$

where n is the number of compounds, R^2 the determination coefficient, F the F -test value, p is the significance level of all the equation, and s is standard error of estimates.

The F and p values of Equation (7) and (8) show that the equations are very significant, having a high determination coefficient and relatively small s values.

The results also suggest that the largest positive charge over the atoms in a molecule (Q_+), the sum of absolute values of the charges on each atom of the molecule (SQ) and the sum of absolute values of the charges on the nitrogens and oxygens in the molecule (SQ_{NO}), seem to be dominant in the retention mechanism and, as a consequence, control the lipophilicity.

By eliminating the descriptors having statistical non significant coefficients (according to t -test), the following simpler models may be obtained (Equation (9) and (10)):

$$R_{M0} = 1.132 - 0.021M + 3.112\text{SQ}_{\text{NO}} - 3.487\text{SQ} + 9.593Q_+ \quad (9)$$

$$(R^2 = 0.9191, n = 20, F = 43, p < 0.0000, s = 0.1408)$$

$$b = -2.369 - 0.025M - 3.777\text{SQ}_{\text{NO}} + 4.125\text{SQ} - 11.900Q_+ \quad (10)$$

$$(R^2 = 0.9196, n = 20, F = 43, p < 0.0000, s = 0.1696)$$

For PCR and PLS methods, the original 16 descriptors were used for the selection of the optimum number of factors by using the cross-validation procedure.

The prediction error was calculated as a root mean square (RMS) error according to ref. [27]. The values of RMS are graphed in Figure 4. By using the cross-validation procedure, it is easy to observe that its numerical values were minimized in the case of the first eight factors for PCR and seven factors for PLS, respectively.

In order to compare the MLR, PCR, and PLS predictive models, the linear regression was applied considering observed and predicted values of retention indices. Good correlations between observed and predicted retention indices of the three methods were found, as it is easy to observe in Table 3. In all cases, the intercept a_0 is statistically zero (t-test) and the slope a_1 is not statistically different from 1 (t-test). As a direct consequence, one can conclude that all three straight lines are parallel and pass through the origin (Figure 5 and 6). In addition, high F values and very small s values were obtained in all cases with a special remark in the case of MLR, which appears to be the most effective for the estimation of retention indices.

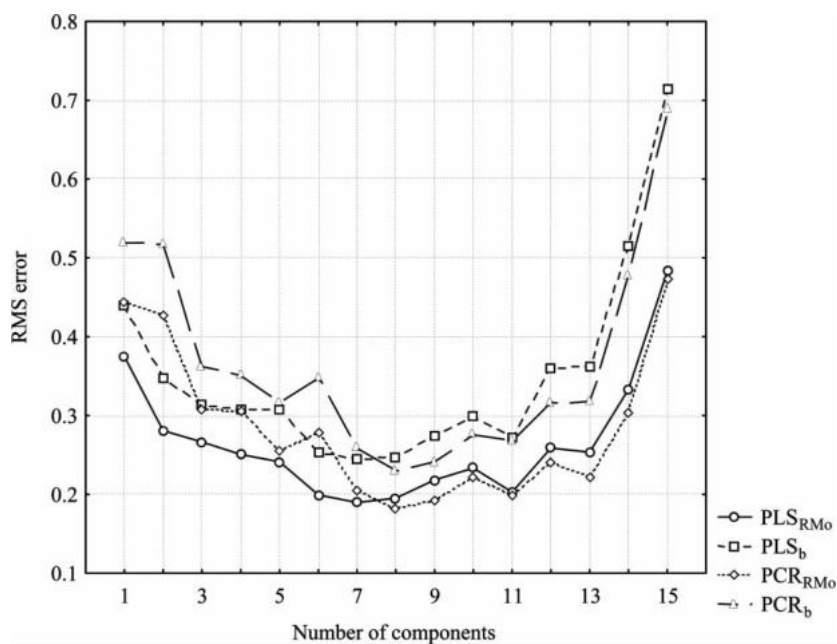


Figure 4. Root mean square errors of estimation of R_{M_0} and b using PCR and PLS.

Table 3. Statistical parameters to evaluate linear relation between observed and predicted retention indices considering all three multiple regression methods (MLR, PCR and PLS)

Statistical	MLR		PCR		PLS	
	R _{Mo}	b	R _{Mo}	b	R _{Mo}	b
R ²	0.9438	0.9402	0.8254	0.8099	0.8164	0.7926
F	302	283	85	77	80	69
p	0.0000	0.0000	0.0000	0.0000	0.0000	0.0000
s	0.1042	0.1294	0.1845	0.2311	0.1944	0.2493
a _o	0.1486	-0.2581	0.3145	-0.5708	0.2636	-0.4828
a ₁	0.9438	0.9402	0.8875	0.8737	0.9073	0.8930

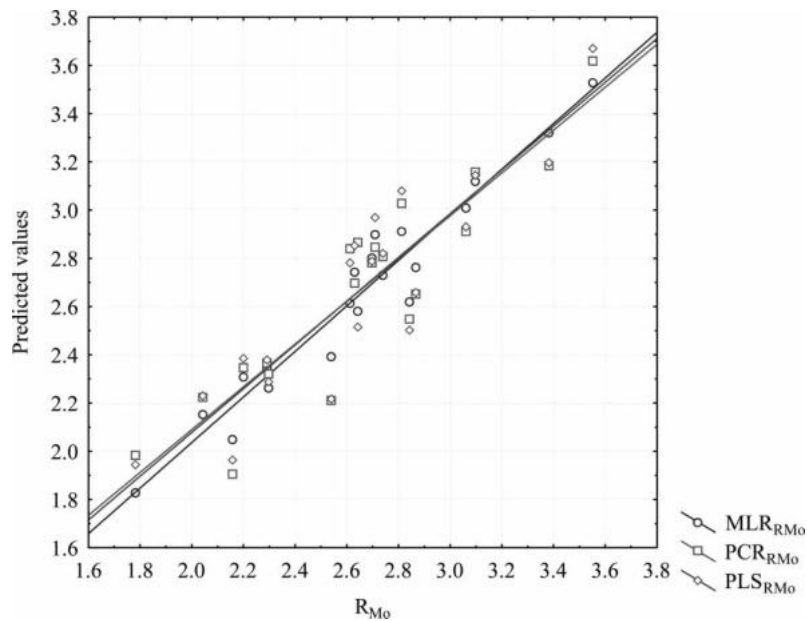


Figure 5. Correlation between R_{M0} determined by HPTLC and predicted values by MLR, PCR, and PLS.

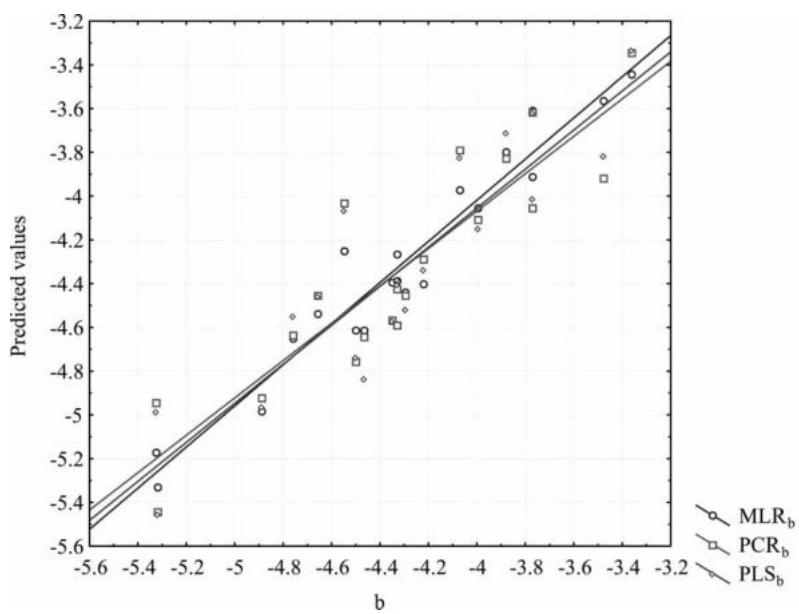


Figure 6. Correlation between b determined by HPTLC and predicted values by MLR, PCR, and PLS.

CONCLUSIONS

Correlation obtained between chromatographic retention indices and structure descriptors for substituted methyl-thiazole-oxadiazolines are highly significant and might be used to predict the retention behavior, and as a consequence, the lipophilicity of other members of the series. By comparing the multivariate regression methods used in this study, the forward stepwise MLR appeared to be the most effective in predicting retention indices for compounds investigated. The largest positive charge over the atoms in a molecule (Q_+), the sum of absolute values of the charges on each atom of the molecule (SQ), and the sum of absolute values of the charges on the nitrogens and oxygens in the molecule (SQ_{NO}) seem to be dominant in the retention mechanism and, hence, these descriptors control the lipophilicity.

REFERENCES

1. Leo, A.; Hansch, C.; Elkins, D. Partition coefficients and their uses. *Chem. Rev.* **1971**, *71*, 525–616.
2. Rekker, R.F.; Mannhold, R. *Calculation of Drug Lipophilicity*; VCH: Weinheim, 1992.
3. Karelson, M. *Molecular Descriptors in QSAR/QSPR*; Wiley & Sons: New York, 2000.
4. Chiriac, A.; Ciubotariu, D.; Simon, Z. *QSAR-Quantitative Relationships*; Mirton Publishing House: Timișoara, 1995.
5. Kaliszan, R. Quantitative structure retention relationships. *Anal. Chem.* **1992**, *64*, 619A–631A.
6. Pyka, A.; Miszczyk, M. Chromatographic evaluation of the lipophilic properties of selected pesticides. *Chromatographia* **2005**, *61*, 37–42.
7. Kaliszan, R. Chromatography and capillary electrophoresis in modelling the basic processes of drug action. *Trends Anal. Chem.* **1999**, *18*, 401–409.
8. Wang, Q.S.; Zhang, L. Review of research on quantitative structure-retention relationships in thin-layer chromatography. *J. Liq. Chromatogr. & Rel. Technol.* **1999**, *22*, 1–14.
9. Garcia Alvarez-Coque, M.C.; Torres Lapasio, J.R. Quantitation of hydrophobicity in micellar liquid chromatography. *Trends Anal. Chem.* **1999**, *18*, 533–543.
10. Djaković-Sekulić, T.L.J.; Sârbu, C.; Perišić-Janjić, N.U. A Comparative study of the lipophilicity of benzimidazole and benztriazole derivatives by RP-TLC. *J. Planar Chromatogr.* **2005**, *18*, 432–436.
11. Dai, J.; Jin, L.; Yao, S.; Wang, L. Prediction of partition coefficient and toxicity for benzaldehyde compounds by their capacity factors and various molecular descriptors. *Chemosphere* **2001**, *42*, 899–907.
12. Detroyer, A.; Heyden, Y.V.; Carda-Broch, S.; Garcia-Alvarez-Coque, M.C.; Massart, D.L. Quantitative structure-retention and retention-activity relationships of β -blocking agents by micellar liquid chromatography. *J. Chromatogr. A* **2001**, *912*, 211–221.
13. Sârbu, C.; Casoni, D.; Dărbăbanțu, M.; Maieranu, C. Quantitative structure-retention and retention-activity relationships of some 1,3-oxazolidine systems by RP-HPTLC and PCA. *J. Pharm. Biomed. Anal.* **2004**, *35*, 213–219.

14. Sârbu, C.; Todor, S. Determination of lipophilicity of some non-steroidal anti-inflammatory agents and their relationships by using principal component analysis based on thin-layer chromatographic retention data. *J. Chromatogr. A* **1998**, *822*, 263–269.
15. Sârbu, C.; Kuhajda, K.; Kevresan, S. Evaluation of lipophilicity of bile acids and their derivatives by Thin Layer Chromatography and Principal Component Analysis. *J. Chromatogr. A* **2001**, *917*, 361–366.
16. Detroyer, A.; Schoonjans, V.F.; Questier, F.; Heyden, Y.V.; Borosy, A.P.; Guo, Q.; Massart, D.L. Exploratory chemometric analysis of the classification of pharmaceutical substances based on chromatographic data. *J. Chromatogr. A* **2000**, *897*, 23–36.
17. Martens, H.; Naes, T. *Multivariate Calibration*; Wiley: Chichester, 1991.
18. Zhou, Y.; Xu, L.; Wu, Y.; Liu, B. A QSAR study of the antiallergic activities of some benzamides and their structures. *Chemometr. Intell. Lab. Syst.* **1999**, *45*, 95–100.
19. Li, T.; Mei, H.; Cong, P. Combining nonlinear PLS with the numeric genetic algorithm for QSAR. *Chemometr. Intell. Lab. Syst.* **1999**, *45*, 177–184.
20. Zhang, R.; Yan, A.; Liu, M.; Liu, H.; Hu, Z. Application of artificial networks for prediction of the retention indices of alkylbenzenes. *Chemometr. Intell. Lab. Syst.* **1999**, *45*, 113–120.
21. Zhao, R.H.; Yue, B.F.; Ni, J.Y.; Zhou, H.F.; Zhang, Y.K. Application of an artificial neural network in chromatography-retention behaviour prediction and pattern recognition. *Chemometr. Intell. Lab. Syst.* **1999**, *45*, 163–170.
22. Chen, Y.; Chen, D.; He, C.; Hu, S. Quantitative structure-activity relationships study of herbicides using neural networks and different statistical methods. *Chemometr. Intell. Lab. Syst.* **1999**, *45*, 267–276.
23. Sârbu, C.; Pop, H.F. Fuzzy Soft-Computing Methods and Their Applications in Chemistry. In *Reviews in Computational Chemistry*; Lipkowitz, K.B., Boyd, D.B., Cundari, T.R., Eds.; Wiley-VCH, 2004; 249–332.
24. Tipericiuc, B.; Oniga, O.; Palage, M.; Chiran, D.; Chirtoc, I. Heterocicli 81. Obținerea și caracterizarea unor 3-N-acetil-2-R-5-[2'-fenil-4'-metil-tiazol-5'-il]- Δ_2 -1,3,4-oxadiazoline. *Clujul Medical* **1999**, *LXXII*, 99–103.
25. Tipericiuc, B.; Parvu, A.; Palage, M.; Oniga, O.; Chirtan, D. Heterocycles 82. The synthesis and the study of the anti-inflammatory activity of some 3-N-acetyl-2-R-5-[2'-aryl-4'-methyl-thiazole-5'-yl]- Δ_2 -1,3,4-oxadiazoline. *Farmacia* **1999**, *XLVII*, 77–83.
26. <http://www.tripos.com/software/alchemy.html>.
27. Brereton, R.G. *Chemometrics; Data Analysis for the Laboratory and Chemical Plant*; Wiley & Sons: Chichester, 2003.

Received February 22, 2006

Accepted March 24, 2006

Manuscript 6848